

674P

5101-271
Flat-Plate
Solar Array Project

DOE/JPL-1012-119
Distribution Category UC-63b

Progress Report 25

for the Period October 1984 to June 1985

and Proceedings of the 25th Project Integration Meeting

(NASA-CR-176815) PROCEEDINGS OF THE 25TH
PROJECT INTEGRATION MEETING Progress
Report, Oct. 1984 - Jun. 1985 (Jet
Propulsion Lab.) 674 p

CSSL 10A

G3/44

N86-29347
THRU
N86-29408
Unclas
42916

Prepared for
U.S. Department of Energy
Through an Agreement with
National Aeronautics and Space Administration
by
Jet Propulsion Laboratory
California Institute of Technology
Pasadena, California

JPL Publication 86-4

5101-271
Flat-Plate
Solar Array Project

DOE/JPL-1012-119
Distribution Category UC-63b

Progress Report 25

for the Period October 1984 to June 1985

and Proceedings of the
25th Project Integration Meeting

Prepared for
U.S. Department of Energy
Through an Agreement with
National Aeronautics and Space Administration
by
Jet Propulsion Laboratory
California Institute of Technology
Pasadena, California

JPL Publication 86-4

Prepared by the Jet Propulsion Laboratory, California Institute of Technology, for the U.S. Department of Energy through an agreement with the National Aeronautics and Space Administration.

The JPL Flat-Plate Solar Array Project is sponsored by the U.S. Department of Energy and is part of the National Photovoltaics Program to initiate a major effort toward the development of cost-competitive solar arrays.

This report was prepared as an account of work sponsored by an agency of the United States Government. Neither the United States Government nor any agency thereof, nor any of their employees, makes any warranty, express or implied, or assumes any legal liability or responsibility for the accuracy, completeness, or usefulness of any information, apparatus, product, or process disclosed, or represents that its use would not infringe privately owned rights.

Reference herein to any specific commercial product, process, or service by trade name, trademark, manufacturer, or otherwise, does not necessarily constitute or imply its endorsement, recommendation, or favoring by the United States Government or any agency thereof. The views and opinions of authors expressed herein do not necessarily state or reflect those of the United States Government or any agency thereof.

This document reports on work done under NASA Task RE-152, Amendment 419, DOE/NASA IAA No. DE-AI01-85CE89008.

ABSTRACT

This report describes progress made by the Flat-Plate Solar Array Project during the period October 1984 to June 1985. It includes reports on silicon sheet growth and characterization, silicon material, process development, high-efficiency cells, environmental isolation, engineering sciences, and reliability physics. It includes a report on, and copies of visual presentations made at, the 25th Project Integration Meeting held at Pasadena, California, on June 19 and 20, 1985.

NOMENCLATURE

AC	alternating current
AE	acoustic emission
AM	air mass (e.g., AML = unit air mass)
AR	antireflective
ARAPS	Angular Resolved Auger Parameter Spectroscopy
ASEC	Applied Solar Energy Corp.
a-Si	amorphous silicon
ASME	American Society of Mechanical Engineers
ASTM	American Society for Testing and Materials
BA	butyl acrylate
B-E-T	Brunauer-Emmet-Teller
BIS	Bremstrahlung Isochromate Spectroscopy
BOS	balance of system (non-array elements of a PV system)
BSF	back-surface field
BSR	back-surface reflector
Caltech	California Institute of Technology
CEC	Commission of European Communities
CER	controlled-environment reactor
CIV	Corona Inception Voltage
CML	constant melt level
COSMIC	Computer Software Management Information Center
CPVC	chlorinated polyvinyl chloride
c-Si	single-crystal silicon
CSTR	continuous-flow, stirred reactor
CV	capacitance voltage
CVD	chemical vapor deposition

CVT	chemical vapor transport
Cz	Czochralski (classical silicon crystal growth method)
DAS	data acquisition system
DC	direct current
DCS	dichlorosilane
DI	deionized
DLTS	deep-level transient spectroscopy
DOE	U.S. Department of Energy
DT	double torsion
DTM	dendrite thickness monitor
EBIC	electron-beam-induced current
EDAX, EDX	electron-dispersive analysis of x-rays
EDS	electron-dispersion spectroscopy
EFG	edge-defined film-fed growth (silicon-ribbon growth method)
EMA	ethylene methyl acrylate
EPDM	ethylene-propylene-diene monomer
EPRI	Electric Power Research Institute
EPSDU	experimental process system development unit
ESP	edge-supported pulling (silicon-sheet production process)
ESR	Electron Spin Resonance
EVA	ethylene vinyl acetate
FBR	fluidized-bed reactor
FF	fill factor
FSA	Flat-Plate Solar Array Project
FSR	free-space reactor
FTIR	Fourier transform infrared
FZ	float-zone (silicon sheet growth method)

GC	gas chromatography
GFCI	ground-fault circuit interruptor
h	heat transfer coefficient; hour(s)
HEM	heat-exchange method (silicon-crystal ingot-growth method)
ICB	ion cluster beam
ID	inside diameter
IEEE	Institute of Electrical and Electronics Engineers, Inc.
IES	Institute of Environmental sciences
IIT	Illinois Institute of Technology
IITRI	IIT Research Institute
IPEG	Improved Price Estimation Guidelines
IR	infrared
ISES	International Solar Energy Society
ITO	indium-tin oxide
JPL	Jet Propulsion Laboratory
JRC	Joint Research Center
LAPSS	large-area pulsed solar simulator
LASS	low-angle silicon sheet growth method
LBIC	light-beam-induced current
LCP	Lifetime Cost and Performance
LED	light emitting diode
LPE	liquid-phase epitaxy
LVDT	linear voltage displacement transducer
MBE	molecular-beam epitaxy
MEPSDU	module experimental process system development unit
mgSi	metallurgical silicon
MINP	metal insulator, n-p

MIS	metal-insulator semiconductor (cell configuration)
MLB	modulated light beam
MOD	metallo-organic deposition
MSEC	Mobil Solar Energy Corp.
m-Si	microcrystalline silicon
NASA	National Aeronautics and Space Administration
NBS	National Bureau of Standards
NEC	National Electrical Code
NMA	non-mass analyzed
NOC	nominal operating conditions
NOCT	nominal operating cell temperature
OFHC	oxygen-free hard copper
O&M	operation and maintenance
OPTAR	Outdoor Photothermal Aging Device
PA&I	Project Analysis and Integration Area (of FSA)
PC	personal computer
PC	power conditioner
PCS	power-conditioning system
PC/TS	Performance Criteria/Test Standards (SERI)
PDU	process development unit
PE	polyethylene
PEBA	pulsed electron beam annealing
P/FR	problem/failure report
PIM	Project Integration Meeting
P_{max}	maximum power
PMMA	polymethyl methacrylate
PMR	Progress Management Report

PnBA	poly-n-butyl acrylate
PU	polyurethane
PV	photovoltaic(s)
PVB	polyvinyl butyral
PVC	polyvinyl chloride
PVD	physical vapor deposition
R&D	research and development
RES	Residential Experiment Station
RF	radio frequency
RH	relative humidity
RTV	room-temperature vulcanized
SAMICS	Solar Array Manufacturing Industry Costing Standards
SAMIS	Standard Assembly-Line Manufacturing Industry Simulation
SCAP1D	Solar-Cell Analysis Program in One Dimension
SCLS	solar-cell laser scanner
SEEMA	Solar-Cell Efficiency Estimation Methodology and Analysis
SEM	scanning electron microscope
SERI	Solar Energy Research Institute
SIMRAND	<u>S</u> IMulation of <u>R</u> esearch <u>A</u> ND <u>D</u> evelopment Projects
SIMS	secondary ion mass spectroscopy
SINDA	Systems Improved Numerical Differencing Analyzer
SMUD	Sacramento (California) Municipal Utility District
SOC	standard operating conditions (module performance)
SOLMET	solar radiation surface meteorological observations
SRH	Schockley-Reed-Hall
STC	silicon tetrachloride

STC standard test conditions
SUNYA State University of New York at Albany
TCM transparent conducting material
TCO transparent conducting oxide
TCS trichlorosilane
TEM transmission electron microscope
TMY typical meteorological year
TREI Texas Research and Engineering Institute
TTU Texas Technology University
UCC Union Carbide Corp.
UCP ubiquitous crystallization process
UL Underwriters Laboratories, Inc.
UV ultraviolet
VTE vertical thermal element
XPS x-ray photoemission spectroscopy

DEFINITION OF SYMBOLS

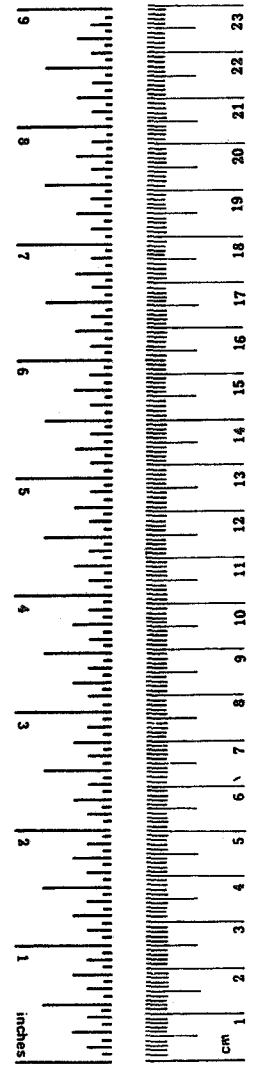
I_{sc}	short-circuit current
I-V	current-voltage
J_{sc}	short-circuit current density
k	equilibrium constant
L_D	minority carrier diffusion length
P	power
P_{max}	maximum power
S	incident solar energy density
T	temperature
U	superficial velocity
U_{mf}	minimum fluidization velocity
V_{oc}	open-circuit voltage
y	molecular percent silane
η	Greek letter eta: efficiency
σ_{xx}	Greek letter sigma: lateral stress
σ_{yy}	Greek letter sigma: longitudinal stress
Ω	Greek letter omega: resistance in ohms

METRIC CONVERSION FACTORS

Approximate Conversions to Metric Measures

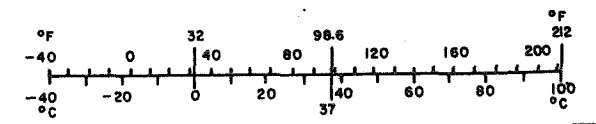
Symbol	When You Know	Multiply by	To Find	Symbol
LENGTH				
in	inches	2.5	centimeters	cm
ft	feet	30	centimeters	cm
yd	yards	0.9	meters	m
mi	miles	1.6	kilometers	km
AREA				
in ²	square inches	6.5	square centimeters	cm ²
ft ²	square feet	0.09	square meters	m ²
yd ²	square yards	0.8	square meters	m ²
mi ²	square miles	2.6	square kilometers	km ²
	acres	0.4	hectares	ha
MASS (weight)				
oz	ounces	28	grams	g
lb	pounds	0.45	kilograms	kg
	short tons (2000 lb)	0.9	tonnes	t
VOLUME				
tsp	teaspoons	5	milliliters	ml
Tbsp	tablespoons	15	milliliters	ml
fl oz	fluid ounces	30	milliliters	ml
c	cups	0.24	liters	l
pt	pints	0.47	liters	l
qt	quarts	0.95	liters	l
gal	gallons	3.8	liters	l
ft ³	cubic feet	0.03	cubic meters	m ³
yd ³	cubic yards	0.76	cubic meters	m ³
TEMPERATURE (exact)				
°F	Fahrenheit temperature	5/9 (after subtracting 32)	Celsius temperature	°C

*1 in = 2.54 (exactly). For other exact conversions and more detailed tables, see NBS Misc. Publ. 286, Units of Weights and Measures, Price \$2.25, SD Catalog No. C13.10:286.



Approximate Conversions from Metric Measures

Symbol	When You Know	Multiply by	To Find	Symbol
LENGTH				
mm	millimeters	0.04	inches	in
cm	centimeters	0.4	inches	in
m	meters	3.3	feet	ft
m	meters	1.1	yards	yd
km	kilometers	0.6	miles	mi
AREA				
cm ²	square centimeters	0.16	square inches	in ²
m ²	square meters	1.2	square yards	yd ²
km ²	square kilometers	0.4	square miles	mi ²
ha	hectares (10,000 m ²)	2.5	acres	
MASS (weight)				
g	grams	0.035	ounces	oz
kg	kilograms	2.2	pounds	lb
t	tonnes (1000 kg)	1.1	short tons	
VOLUME				
ml	milliliters	0.03	fluid ounces	fl oz
l	liters	2.1	pints	pt
l	liters	1.06	quarts	qt
l	liters	0.26	gallons	gal
m ³	cubic meters	35	cubic feet	ft ³
m ³	cubic meters	1.3	cubic yards	yd ³
TEMPERATURE (exact)				
°C	Celsius temperature	9/5 (then add 32)	Fahrenheit temperature	°F



xiii PRECEDING PAGE BLANK NOT FILMED

CONTENTS

PROGRESS REPORT

PROJECT SUMMARY 1

AREA REPORTS 7

 Materials and Devices Research Area 7

 Silicon Materials Task and
 Advanced Silicon Sheet Task 7

 Device Research Task 21

 Project Analysis and Integration Area 33

 Process Development Area 39

 Reliability and Engineering Sciences Area 41

PROCEEDINGS OF THE 25th PROJECT INTEGRATION MEETING

INTRODUCTION 63

AGENDA 65

PLENARY SESSIONS 67

 Summary 67

 FSA Future Directions

 Introduction (W. Callaghan, Jet Propulsion Laboratory) 73

 Reliability and Engineering Sciences FY 85-FY 86
 Activities and Plans (R. Ross, Jr.,
 Jet Propulsion Laboratory) 75

 FSA Technology Activities in FY 86 (M. Leipold,
 Jet Propulsion Laboratory) 83

 Summary of High-Efficiency Solar-Cell Research (R. Kachare,
 Jet Propulsion Laboratory) 87

 Overview of Processing Activities Aimed at Higher
 Efficiencies and Economical Production (D. Bickler,
 Jet Propulsion Laboratory) 93

 Summary of Process Research Analysis Efforts (D. Burger,
 Jet Propulsion Laboratory) 99

PLENARY SESSIONS (Cont'd)

Metallo-Organic Decomposition Films (B. Gallagher, Jet Propulsion Laboratory)	105
Directed-Energy Process Technology Efforts (P. Alexander, Jet Propulsion Laboratory)	111
Crystal Growth for High-Efficiency Silicon Solar Cells Workshop: Summary (K. Dumas, Jet Propulsion Laboratory)	123
Reliability and Engineering of Thin-Film Photovoltaic Modules (E. Royal, Jet Propulsion Laboratory)	137
TECHNICAL SESSIONS	147
RELIABILITY PHYSICS (R. Ross, Chairman)	147
Photothermal Degradation Studies (R. Liang, Jet Propulsion Laboratory)	151
Photovoltaic Module Interface: General Purpose Primers (J. Boerio, University of Cincinnati)	157
Encapsulation Materials Research (P. Willis, Springborn Laboratories)	169
Moisture-Temperature Degradation in Module Encapsulants (G. Mon, Jet Propulsion Laboratory)	191
Preliminary Study: Moisture-Polymer Interaction (L.-C. Wen, Jet Propulsion Laboratory)	201
Water Permeation and Dielectric Breakdown (J. Orehotsky, Wilkes College)	217
"(RH + t)" Aging Correlation (E. Cuddihy, Jet Propulsion Laboratory)	235
SILICON MATERIAL AND JPL WEB TEAM (R. Lutwack, Chairman)	247
Silane Process Research and Development (S. Iya, Union Carbide Corp.)	249
JPL In-House Fluidized-Bed Reactor Research (N. Rohatgi, Jet Propulsion Laboratory)	255
Web Team Overview (R. McDonald, Jet Propulsion Laboratory)	261

TECHNICAL SESSIONS (Cont'd)

Silicon Dendritic Web Growth Thermal Analysis Task (R. Richter, Jet Propulsion Laboratory)	263
HIGH-EFFICIENCY DEVICE RESEARCH (D. Burger, Chairman)	299
Heavy Doping Considerations and Measurements in High- Efficiency Cells (F. Lindholm, University of Florida)	301
Advanced Techniques for the Measurement of Multiple Recombination Parameters in Solar Cells (M. Newhouse, M. Wolf, University of Pennsylvania)	313
Measurement of Minority Carrier Transport Parameters in Heavily Doped n-Type Silicon (J. del Alamo, R. Swanson, Stanford University)	329
Studies of Oxygen-Related and Carbon-Related Defects in High-Efficiency Solar Cells (J. Corbett, State University of New York at Albany)	339
Comprehensive Solar Cell Modeling and Correlation Studies (M. Lamorte, Research Triangle Institute)	349
Loss Mechanisms in High-Efficiency Solar Cells (C. Tang Sah, C. T. Sah Associates)	373
High-Efficiency Silicon Solar Cells (L. Olsen, University of Washington)	379
Development of High-Efficiency Solar Cells on Silicon Web (A. Rohatgi, D. Meier, R. Campbell, R. Seidensticker, P. Rai-Choudhury, Westinghouse Electric Corp.)	389
Surface and Bulk-Loss Reduction Research by Low-Energy Hydrogen Doping (S. Fonash, Pennsylvania State University)	401
PROCESS DEVELOPMENT (D. Bickler, Chairman)	409
Pulsed Excimer Laser Processing (D. Wong, Arco Solar, Inc.)	413
Excimer Laser Annealing for Fabrication of Low-Cost Solar Cells (M. Spitzer, A. Greenwald, S. Hogan, Spire Corp.)	429

TECHNICAL SESSIONS (Cont'd)

Amorphous Metallic Films in Silicon Metallization Systems (F. So, E. Kolawa, Marc-A. Nicolet, California Institute of Technology)	435
Mod Silver Metallization: Screen Printing and Ink-Jet Printing (R. Vest, G. Vest, Purdue University)	443
Process Research of Non-Cz Material (R. Campbell, Westinghouse Electric Corp.)	457
Laser-Assisted Solar-Cell Metallization Processing (A. Rohatgi, P. McMullin, P. Rai-Choudhury, Westinghouse Electric Corp.)	467
Microwave-Enhanced Thin-Film Deposition (S. Chitre, Superwave Technology, Inc.)	473
Life-Cycle Costs of High-Performance Cells (R. Daniel, D. Burger, L. Reiter, Jet Propulsion Laboratory)	477
SAMICS on the IBM PC (R. Chamberlain, Jet Propulsion Laboratory)	485
Encapsulation Processing and Manufacturing Yield Analysis (P. Willis, Springborn Laboratories, Inc.)	489
 ADVANCED SILICON SHEET (A. Briglio, Chairman)	 501
Silicon Ribbon Stress/Strain Workshop (M. Leipold, Mobil Solar Energy Corp.)	503
Advanced Dendritic Web Growth Development (R. Hopkins, Westinghouse Electric Corp.)	507
Defect Characterization of Silicon Dendritic Web Ribbons (Li-Jen Cheng, Jet Propulsion Laboratory)	527
Electrical, Structural, and Chemical Characterization of Silicon Sheet Materials (D. Ast, S. Hyland, Cornell University)	537
Analysis of Silicon Stress/Strain Relationships (O. Dillon, University of Kentucky)	543
Stress Studies in Edge-Defined Film-Fed Growth of Silicon Ribbons (J. Kalejs, Mobil Solar Energy Corp.)	565
Analysis of High-Speed Growth of Silicon Sheet in Inclined-Meniscus Configuration (R. Brown, Massachusetts Institute of Technology)	575

TECHNICAL SESSIONS (Cont'd)

High-Purity Silicon Crystal Growth Investigations (T. Ciszek, Solar Energy Research Institute)	587
Silicon Sheet Surface Studies (S. Danyluk, University of Illinois at Chicago)	601
MODULE DEVELOPMENT AND ENGINEERING SCIENCES	
(M. Smokler, Chairman)	621
High-Efficiency Module Design (M. Spitzer, Spire Corp.) . .	623
Module Flammability Research (R. Sugimura, Jet Propulsion Laboratory)	633
Development of Design Criteria and a Qualification Test for Bypass Diodes (D. Otth, Jet Propulsion Laboratory) . . .	637
Development of AM 1.5 Global Measurement Procedures and International Cell Measurement Round Robin (R. Mueller, Jet Propulsion Laboratory)	641
Amorphous-Silicon Cell Reliability Testing (J. Lathrop, Clemson University)	649
Photocurrent Images of Amorphous-Silicon Solar-Cell Modules (Q. Kim, A. Shumka, J. Trask, Jet Propulsion Laboratory)	659
Amorphous-Silicon Module Hot-Spot Testing (C. Gonzalez, Jet Propulsion Laboratory)	673
PVARRAY: A Software Tool for Photovoltaic Array Design (D. Burger, Jet Propulsion Laboratory)	685
Dendritic Web-Type Solar-Cell Mini-Modules (R. Campbell, Westinghouse Electric Corp.)	691

ORIGINAL PAGE IS
OF POOR QUALITY

PROGRESS REPORT

Project Summary

INTRODUCTION

This report describes the activities of the Flat-Plate Solar Array (FSA) Project from September 1984 through May 1985, including the 25th FSA Project Integration Meeting (PIM), held on June 19 and 20, 1985.

The FSA Project at the Jet Propulsion Laboratory (JPL), sponsored by the U.S. Department of Energy (DOE), has the responsibility for advancing solar array technology while encouraging industry to reduce the price of arrays to a level at which photovoltaic (PV) electric power systems will be competitive with more conventional power sources. This responsibility has included developing the technology for producing low-cost, long-life PV modules and arrays. More than 100 organizations have participated in FSA-sponsored research and development (R&D) of low-cost solar module manufacturing and mass-production technology, the transfer of this technology to industry for commercialization, and the development and testing of advanced prototype modules and arrays. Economic analyses were used to select, for sponsorship, those R&D efforts most likely to result in significant cost reductions. The following is an account of the progress that has been made during the reporting period.

SUMMARY OF PROGRESS

Experimental test runs of a fluidized-bed reactor (FBR) at the Union Carbide Corp. (UCC) experimental process system development unit (EPSDU) at Washougal, Washington, continue to demonstrate the practicality of converting silane to silicon. The 6-in.-diameter FBR was equipped with a high-purity quartz liner to prevent metallic impurity contamination of the silicon product from the FBR walls during operation. Three tests, run time totalling over 110 h, at silane concentrations varying from 20 to 30% in hydrogen were made without cracking the liners, although the liners cracked after cooldown. Considerable reduction in the production of fine particles was obtained by the use of a perforated plate in place of the conical porous gas distributor.

Research on silane pyrolysis in an FBR, at JPL, emphasized product purity. Specially prepared and cleaned seed particles were used in the FBR for silicon growth from silane. Preliminary data indicated that the deposited silicon is of high purity and that no contamination occurred in the fluidized-bed processing.

A well-planned, comprehensive, multi-organization research effort on defining growth-induced stresses in silicon ribbons and evaluating the quality of the resultant ribbon, initiated early in 1983, is making good progress. Mathematical models have been created that predict more accurately stress and strain history during the silicon growth process and the residual stresses in the silicon ribbons. These models are an advance over previous ones because they take into account the growth history of the ribbon and the material's

PROJECT SUMMARY

non-linearity and creep behavior. Relevant ribbon-temperature data and boundary conditions are obtained experimentally from various growth equipment and are used to refine and confirm the theoretical analyses. Thus, researchers are evaluating various grower geometric configurations and ribbon temperature distributions, allowing them to identify critical trade-offs in ribbon-growth equipment.

During this reporting period, it was determined that the bulk diffusion length of the stressed float zone (FZ) and Czochralski (Cz) silicon is limited by point-defect recombination to about 15 to 25 μm in dislocation-free regions after high-temperature ($>1200^{\circ}\text{C}$) heat treatment and stress application. One-hour anneals at 575 and 850°C produced, at the most, an increase in diffusion length of a factor of two.

Characterization of edge-defined film-fed growth (EFG) material by Mobil Solar Energy Corp. with varying levels of boron dopant indicate that higher dopant levels reduce the dislocation density and that as-grown diffusion lengths for EFG ribbons doped with gallium are higher than those doped with boron.

Significant progress was made in implementing automated, closed-loop control of dendritic-web growth by Westinghouse. New web growth configurations were designed, built, and tested, and certain of them offer the potential of improved ribbon growth.

Dendritic-web growth records were established by Westinghouse, such as: longest web ribbon to 10.0-m length, 7.1-m length web grown under continuous melt replenishment, widest web grown to 6.7 cm width, highest area growth rate for web ribbons longer than 1 m of about $8\text{ cm}^2/\text{min}$, and a weekly throughput of $27,000\text{ cm}^2$ in 1 week (5 days) from one grower using batch replenishment.

In the silicon surface property modification study by the University of Illinois at Chicago, it was found that a silicon surface scratched in deionized water contained a high density of dislocations, and a surface scratched in ethanol contained isolated regions of dislocations.

The University of Kentucky has developed a new thermal buckling analysis for the plastic range of silicon ribbon. Once in-plane stresses are known, the new-version buckling analysis allows for prediction of buckling modes, if any. The main limitation now is not in the buckling analysis itself, but in understanding the nature of in-plane stresses. A main limiting factor in the determination of in-plane stresses is felt to be a lack of knowledge of high-temperature stress-field silicon dislocation behavior.

Across-the-board progress has been made by the 15 organizations (mainly universities) that are participating in higher-efficiency crystalline silicon solar-cell research. These efforts are directed toward the characterization of various silicon-sheet materials, material-device property interaction investigations, and measurement techniques.

During creep experiments by Cornell University on dendritic web material, the material exhibited a cyclic behavior consisting of a short duration burst of rapid creep followed by a relatively longer duration slow creep. It is thought to be caused by a buildup of mobil dislocations at a

PROJECT SUMMARY

twin plane until a critical density is reached and then the dislocations are dissipated. High oxygen concentrations have been measured, which are believed to be clustered at the twin plane and are assumed to be involved.

A modulated light beam (MLB) instrument designed at the University of Pennsylvania is now operational for deriving the values of minority carrier lifetimes in the various regions of solar cell structure.

At the University of Florida, it was concluded that photoluminescence is the only method likely to succeed in giving meaningful results of Auger lifetimes. In another study, solar cells with polysilicon on the back surface showed better red wavelength response compared to back-surface-field cells. Diffusivity measurements of minority carriers in lightly doped silicon have provided useful data.

C.T. Sah has been working closely with Applied Solar Energy Corp. (ASEC) on designing test devices for studying very high-efficiency solar cell theoretical models.

At the University of Washington, a slow-ramp high-frequency measurement system has been developed for the measurement of surface state densities.

Numerous experimental high-efficiency solar cells using front and back surfaces that are coated with polysilicon have been fabricated and evaluated by Westinghouse.

Westinghouse Electric Corporation's Advanced Energy Systems Division achieved successful sequential front and back diffusion. Additional work in simultaneous diffusion has also shown promise. Both excimer laser and quartz heat lamps have been used with the most successful run obtained with heat lamps.

Metallo-organic deposition (MOD) studies at Purdue were very successful. Addition of a bismuth compound has solved the adhesion problem. Use of ink-jet printing for direct line writing is still being studied.

Westinghouse Electric Corporation's Research and Development Center used the Purdue MOD material and an argon ion laser to produce cells with excellent efficiency, narrow lines, and good adhesion.

Photolytic decomposition was used by ARCO Solar to deposit a tungsten film. The film was adherent, but sharp line definition would be difficult to achieve due to dispersion.

Updated projections of the Cz and dendritic web cell technologies were completed. The Cz projection was for a state-of-the-art late 1980s factory producing 30 MW_p/year. It would produce 4 x 2 ft modules made up of modified square silicon cells cut from 5-in.-diameter ingots. The state-of-the-art web projections were for two production time periods: the late 1980s and the early 1990s. The factory size was 25 MW_p/year for both cases. Energy costs from a PV system using these modules, assumed to have 15% module efficiency, were 17¢, 19¢, and 21.5¢/kWh for the 1990 web, and the 1980 web and Cz, respectively.

PROJECT SUMMARY

The Standard Assembly-Line Manufacturing Industry Simulation (SAMIS) computer program, which is the heart of Solar Array Manufacturing Industry Costing Standards (SAMICS), now runs on a personal computer (PC). In the PC version of SAMIS, the interface between the program and the user has been completely redesigned. The program is written in Turbo-Pascal. SAMICS has been used by the FSA Project at JPL to provide standardized comparisons of prospective manufacturing processes and process sequences in terms of the prices that would have to be received for the final product to recover all costs and make a specified profit.

A methodology and a few preliminary results of a study to estimate the value of a PV system over its useful lifetime have been completed. To estimate the value of a PV system, all costs and revenues associated with the system over its lifetime must be considered as well as the initial purchase cost and installation charges.

Three simulation models developed at JPL were used for the analysis: PVARRAY, which simulates array performance over time; SAMICS, which estimates the process value added and the manufactured module cost; and Lifetime Cost and Performance (LCP), which calculates hourly energy over time, pre-tax revenue from the system, and nominal cost streams over time. All of these programs can be run on an IBM XT or compatible PC.

Analysis has shown that module degradation rates have a significant impact on the economic value of PV modules. A degradation rate of as little as 0.5%/year will reduce the present value of the revenues generated by 7.4%. A degradation rate of 2%/year reduces the economic value of the modules by 25.8%.

A preliminary study evaluating the benefits of extended module lifetime was completed. The measure selected to evaluate the benefits of extended module lifetimes is the additional amount an electric utility can spend on module purchase and installation (initial investment) without lowering their rate of return on investment. The answer is shown to depend heavily on the rate of return earned on investor capital in electric utilities, and allowable depreciation schedules. Under a worst-case scenario, it was found that the utility can spend an additional 14% on modules and their installation if their lives are increased from 20 to 30 years. Under more favorable circumstances, similar to those experienced by utilities in recent years, the utility can increase its investment by 32% without any reduction in the rate of return on investment.

A research forum on "Reliability and Engineering of Thin-Film Photovoltaic Modules" was held in March 1985. A key objective, which was successfully achieved, was the establishment of technical interchange between thin-film module researchers and those knowledgeable of the module technology developments resulting from the 10-year DOE crystalline-silicon module research effort.

Through cooperative relationships with ARCO Solar, Chronar, and Solarex, amorphous-silicon (a-Si) submodules have been obtained and included in the various testing activities at JPL and at Clemson University. At Clemson, a-Si devices are now being subjected to a variety of environmental stress tests similar to those used for reliability attribute evaluation of

PROJECT SUMMARY

crystalline-silicon-type cells over the past several years. At JPL, a series of experiments and efforts have been performed and are continuing on a-Si modules which include: hot-spot performance, electrochemical corrosion mechanisms and corrosion rates, failure analysis techniques and capabilities which have been modified and developed for thin-film modules, and failure analysis of existing commercial a-Si module deficiencies.

Under a JPL contract to develop a high-efficiency module, Spire Corp. has manufactured a module using cells manufactured from FZ-grown silicon ingots. The area of each module cell is 53 cm squared. Module efficiency is 13.7%, and encapsulated cell efficiency is 15.2%. As part of this same effort, the average efficiency of a group of 22 cells was 17.7% with 10 of those cells with efficiencies of 18% or greater.

Based upon a JPL-developed theory, an experimental determination of the direct current (DC) intrinsic dielectric strength of ethylene vinyl acetate (EVA) was made [the alternating current (AC) dielectric strength of EVA was determined previously]. An electrical insulation aging evaluation plan has been developed between JPL and Springborn.

The characterization of aging mechanisms in encapsulants because of photothermal degradation has led to development of an analytical structure for assessing the significance of thermal-ultraviolet (UV)-induced transmission losses in EVA in simulated 30-year field exposure at various U.S. sites.

Module flammability research continued including testing of a module with a back-covering of a relatively expensive glass cloth manufactured by HITCO Materials Division that was impregnated with a proprietary, high-temperature coating material (also from HITCO). The test results were significant because it was the first time that a glass cloth material passed the UL 790, Class A, burning-brand test. Later tests focused on lower-cost glass cloths using the proprietary, high-temperature material.

All testing on the Block-V modules has been terminated with successful completion of the Block-V Qualification Tests by all five manufacturers: ARCO Solar, General Electric Co., MSEC, Solarex Corp., and Spire. The designs and performance of the final modules are described in JPL Publication 85-34, "User Handbook for Block-V Silicon Solar Cell Modules."

A major advance has been made by filtering the large-area pulsed solar simulator (LAPSS) so that its irradiance spectrum closely matches that of the standard American Society for Testing and Materials (ASTM) AM1.5 global spectrum in ASTM E 892-82. The filter is removable, so the prior capability to simulate the standard ASTM AM1.5 direct normal spectrum has been retained. Therefore, whether a direct normal or a global spectrum is specified, it is now possible to make accurate measurements of devices from cell size up to modules or small arrays as large as 6 ft on one side, without the need for specially matched reference cells or the need to perform spectral response measurements and mismatch factor corrections. This capability has been useful for measurement of the large Block-V modules and to assist the Sacramento Municipal Utility District (SMUD) by measuring arrays of modules from three manufacturers destined for use in the second (1 MW) phase of the SMUD PV central power station. Another advantage of the filtered LAPSS capability is

PROJECT SUMMARY

that it enables rapid inexpensive secondary calibration of reference cells, a service that has been performed to assist several manufacturers.

To permit more accurate measurement of a-Si devices, reference cells have been manufactured from wide-band crystalline silicon cells and packaged with filters such that the resultant spectral response is representative of the response of a-Si devices.

In order to help the PV community resolve discrepancies among measurements performed by various organizations, JPL has participated in a round-robin measurement exercise organized by British Petroleum, involving six reference cells and 36 modules, with the measurements being performed by JPL, the Royal Aircraft Establishment, and the Commission of the European Communities (CEC) Joint Research Centre (JRC), at Ispra, Italy. Also, JPL is a participant in a round-robin measurement project initiated by the Summit Working Group and managed by the CEC JRC. This seven-nation effort involves manufacture and calibration of 18 reference cells (including four supplied by JPL) by seven nations. JPL has completed its measurements and has also arranged for the Solar Energy Research Institute (SERI) to make the same measurements.

Area Reports

MATERIALS AND DEVICES RESEARCH AREA

Silicon Materials Research Task and Advanced Silicon Sheet Task

INTRODUCTION

The objectives of the Silicon Materials Task and the Advanced Silicon Sheet Task are to identify the critical technical barriers to low-cost silicon purification and sheet growth that must be overcome to produce a PV cell substrate material at a price consistent with FSA Project objectives, and then to overcome those barriers by performing and supporting appropriate R&D.

Present solar-cell technology is based mainly on the use of silicon wafers obtained by inner-diameter slicing of Cz-grown ingots from Siemens reactor-produced semiconductor-grade silicon. This method of obtaining single-crystal silicon wafers is tailored to the needs of semiconductor-device production (e.g., integrated circuits and discrete power and control devices other than solar cells). The small market offered by present solar-cell users does not justify industry's development of the high-volume silicon production techniques that would result in low-cost PV electrical energy.

It is important to develop alternative low-cost processes for producing refined silicon and sheet material suitable for long-life, high-efficiency solar PV energy conversion. To meet FSA objectives, research must be performed to overcome the barriers to the success of the most promising processes for producing large quantities of pure silicon and large areas of crystallized silicon at a low, competitive cost. The form of the refined silicon must be suitable for use in the sheet-growth processes. The sheet, in turn, must be suitable for direct incorporation into automated solar-array industry schemes.

Silicon purification involving deposition of the material from silane is being pursued because this substance can be purified relatively easily and, because of its high reactivity, can be more readily decomposed or reduced to form silicon than can trichlorosilane (TCS), which is used today in the conventional process. Research on two other processes that offer promise for making less pure, solar-cell grade silicon by refinement of metallurgical-grade silicon (mgSi) is also being conducted because of the potential for further reduction of product cost.

Growth of crystalline silicon material in a geometry that does not require cutting to achieve proper thickness is an obvious way to eliminate costly processing and material waste. Growth techniques such as EFG, dendritic-web growth (web), low-angle silicon sheet (LASS), and edge-supported pulling (ESP) are candidates for such solar cell material. Problems generic to all sheet growth technologies are being addressed in the program. Special

AREA REPORTS

emphasis is placed on the dendritic web process because of its high probability of successfully achieving the program goals for silicon sheet material.

SUMMARY OF PROGRESS Silicon Material Research Task

Semiconductor-Grade Silicon Refinement Process

Silicon Refinement Using Silane (Union Carbide Corp.)

The objective of the UCC program is to solve the critical problem of silane (SiH_4) pyrolysis in FBRs for producing semiconductor-grade silicon for PV applications. The production of ultra-pure SiH_4 by the process developed in this contract has already been demonstrated in a 100-MT/year pilot plant. The SiH_4 -to-silicon conversion reactor in this plant is a modified Siemens reactor (built by Komatsu Electrical Materials, Inc.), which does not have the potential of enabling the achievement of the DOE low-cost goal for polysilicon.

The major problem being dealt with currently in the FBR program is contamination of the polysilicon product. Experiments with quartz liners to shield the reaction zone from the reactor's stainless steel walls have led to better levels of purity, but the liners have frequently failed by cracking on cooldown. Early in the period, the liner system was redesigned to eliminate breakage and then was tested. In the last three tests, the total run time was over 110 h (for silane concentrations varying from 20 to 30% in hydrogen). No liner breakage occurred during the tests, although the liners cracked during cooldown after all three tests. Analysis (by scanning electron microscopy and optical micrographs) of samples from the several kilograms of product showed a layered structure, indicating successive periods of interrupted growth. A 3-in.-diameter single-crystal Cz ingot was grown from the product and wafered. This material will be analyzed for donor/acceptor concentration levels using photoluminescence spectroscopy. Considerable reduction in the production of fine particles was secured by the use of a perforated plate in place of the conical porous gas distributor.

The activities presently underway to improve the reactor operation and to obtain pure product include: (1) the use of a different design for the liner-to-reactor seals; (2) the use of a modified gas distributor plate capable of producing uniform, small bubbles; (3) the use of seed-material cleaning equipment to ensure the preparation of seed particles with the desired level of purity; and (4) the conducting of long-term experimental runs to demonstrate the feasibility of the FBR for producing pure polysilicon.

AREA REPORTS

Solar-Cell-Grade Silicon Refinement Processes

Electrochemical Refining of Metallurgical-Grade Silicon (Energy Materials Corp.)

The objective of this contract was to demonstrate the technical feasibility of producing high-purity silicon from metallurgical-grade silicon in a fused-salt electrochemical process using a $\text{Cu}_3\text{Si}:\text{Si}$ anode. All attempts to operate the reactor were unsuccessful. A draft final report was prepared and reviewed by JPL cognizant personnel. The final report is being published.

Chemical Vapor Transport Process for Purifying Metallurgical-Grade Silicon (Solar Energy Research Institute)

This investigation deals with a chemical vapor transport process in which HCl is reacted with $\text{Cu}_3\text{Si}:\text{Si}$ material (the silicon being metallurgical grade) to generate a mixture of chlorosilanes (mostly trichlorosilane) and silicon is deposited by chemical vapor transport on a filament kept at 1050°C . Production of 99.9999% pure silicon was obtained from the metallurgical-grade silicon (which is about 98% pure). The purification was attributed to four mechanisms: (1) gettering of impurities during casting of the alloy, (2) chemical selectivity of the vapor transport, (3) filtration properties of the $\text{Cu}_3\text{Si}:\text{Si}$ material, and (4) condensation of impurities (as chlorides) on the cold walls and the base plate of the reactor. The optimum deposition rate was at 1160°C for all Cl/H ratios. At a given deposition temperature, the transport rate increased as the Cl/H ratio decreased down to 0.3. For $\text{Cl}/\text{H} < 0.3$, the transport rate was not affected by the initial concentration of the transport agent.

Silicon Particle Growth Research (California Institute of Technology)

The objective of this research is to describe, theoretically, the growth of silicon particles from SiH_4 in a free-space reactor and to develop, experimentally, the conditions for maximum particle growth. The phenomenon of runaway nucleation (during which a 10^4 increase in particle concentration occurs when the SiH_4 concentration is increased from 3% to 3.4%) was studied intensively. The experimental variables of temperature profile along the reactor tube and particle concentration were explored to define the conditions that enable particle growth and prevent excessive new-particle formation. Also, the theory was extended to account for the new observations.

Modeling of Silane Pyrolysis in Fluidized-Bed Reactors (Washington University at St. Louis)

The objective of this effort is to develop a comprehensive model for the preparation of silicon by pyrolysis of SiH_4 in FBRs. The model will be useful for the interpretation of experimental data, for the determination of the ranges of operating parameters for maximum throughput and yield, and for providing a basis for design of scaled-up reactors for pilot plants.

AREA REPORTS

Algorithms suitable for dealing with homogeneous gas-phase nucleation and the population balances for the fine particles formed by nucleation and subsequent reactions were developed. These algorithms were inserted into the FBR model based on the continuous-flow, stirred reactor (CSTR) and the two-phase bubble regime. It was shown that the simulation of the reactor is very sensitive to the interchange coefficient for gases and fines between the jets and the emulsion phase. No general correlation is available for this coefficient; it was assumed that the jet-emulsion exchange coefficient is proportional to the bubble-emulsion coefficient, for which there are correlations. The dominant mode for the growth of the seed particles was shown to be heterogeneous chemical vapor deposition, which is strongly affected by SiH_4 concentration. Most of the fine particles are generated in the bubbles and are elutriated through the bubbles. Experimental results obtained with the JPL FBR were compared with four different models; the bubbling-bed model with homogeneous nucleation gave the closest agreement. The validation of the model will continue using data from long-term experimental runs.

Research on Silane Pyrolysis in Fluidized-Bed Reactors (JPL)

JPL is conducting FBR research with the objective of characterizing the deposition of silicon from SiH_4 and providing information upon which significant improvements in this process can be based.

Emphasis was placed on the product purity investigation. First, seed particles of less than 2-mm diameter, the purest commercially available, were purchased from Dynamit Nobel. Then, a fluid-jet mill was employed to reduce the size of the particles to a range of 200 to 300 μm in diameter. The jet mill grinding characteristics were studied. An acid cleaning procedure was developed to clean the fluid-jet mill product. This procedure (involving a well agitated, fluidized-bed type of liquid mixing column of silicon particles and acid solution) consisted of the following steps: (1) deionized water wash, (2) cleaning with a mixture of two parts of 12N hydrochloric acid and one part of 16N nitric acid for 20 min, (3) deionized water wash, (4) etching with 48% hydrofluoric acid for 20 min, (5) washing with deionized water until the water had a resistivity of 16 $\text{M}\Omega$, and (6) drying in a diffusion furnace at 150°C under a nitrogen blanket. The particles cleaned by the above procedure have impurities below the detection limits of spark-source mass spectroscopy. Using these cleaned seed particles, FBR experiments were carried out with feeds of 30 and 50% of SiH_4 in hydrogen. The FBR was operated for 4.3 h at 650°C and a U/U_{mf} (ratio of superficial gas velocity to the minimum fluidization velocity) of 4, with a feed of 30% SiH_4 in hydrogen. Silicon product in the amount of 6.8 kg was deposited on the bed, which had an initial weight of 11 kg. The product purity analysis by spark-source mass spectroscopy gave results that were close to or below the detection limits: iron ≤ 0.6 ppma, chromium < 0.02 ppma, nickel < 0.5 ppma, copper < 1.02 ppma, manganese < 0.02 ppma, and aluminum = 0.05 ppma. These preliminary data indicated that the deposited silicon is of high purity and that no contamination has occurred in the fluidized-bed processing. Work is underway to identify further to the ppba level some selected metallic impurities by neutron activation analysis.

AREA REPORTS

It is planned to pull a single-crystal Cz ingot from the FBR product and fabricate solar cells from the ingot material. Testing of these cells will conclude the FSA/JPL in-house investigation of the SiH_4 FBR process.

SUMMARY OF PROGRESS Advanced Silicon Sheet Task

Shaped-Sheet Technology

Stress and Efficiency Studies in EFG Silicon (Mobil Solar Energy Corp.)

The goals of this program are to define low-stress configurations for silicon sheet growth that are consistent with producing high-quality material and to investigate causes of deficiency in solar cell performance of low-resistivity silicon. Experimental and theoretical work is in progress aimed at testing a model for predicting sheet residual stress under conditions where plastic deformation is taking place. Dislocations produced in high-temperature creep experiments in FZ and Cz silicon are being studied with electron-beam-induced current (EBIC) microscopy and compared to as-grown EFG material defects in order to relate conditions of formation to behavior in limiting bulk material lifetime. Carbon, oxygen, and dopant impurity (boron and gallium) effects on dislocation behavior are also under investigation.

The following results were obtained in this period. The bulk diffusion length of the stressed FZ and Cz silicon is limited by point-defect recombination to about 15 to 25 μm in dislocation-free regions after high-temperature ($>1200^\circ\text{C}$) heat treatment and stress application. Increases in dislocation density from $1 \times 10^4/\text{cm}^2$ to over $1 \times 10^7/\text{cm}^2$ further decrease the diffusion length to the range of 10 to 15 μm . One-hour anneals at 575 and 850 $^\circ\text{C}$ produce little increase in diffusion length, at most by a factor of two, while preferential gettering at dislocations is weak. Significant differences in silicon with varying oxygen and carbon levels are not observed.

The stress modeling at Harvard University was directed toward implementing a new scheme for calculating residual stress that has important implications for the understanding of creep and strain relationships to residual stress. Stress analysis for an EFG test system is in progress, and growth of ribbon is being carried out for comparison purposes to attempt to reduce dislocation densities and stress. Effects of horizontal temperature gradients are also being investigated. Although dislocation densities have been reduced by an order of magnitude by going to slower-growth (about 1 cm/min) configurations (essentially by decreasing the interface gradient) and stress has been decreased, these configurations do not seem to be compatible with restoration of high-speed growth (>3 to 4 cm/min).

Characterization of EFG material with varying levels of boron dopant indicate that higher dopant levels reduce the dislocation density and that as-grown diffusion lengths for gallium are higher than those for boron.

AREA REPORTS

Dendritic-Web Ribbon Growth (Westinghouse Electric Corp.)

A 3-year program at Westinghouse for development of silicon dendritic-web crystal growth and high-efficiency solar cells made from this material was started early in CY 84. The purpose is to improve this technology and demonstrate capabilities that are consistent with utility requirements. The program is being supported jointly by DOE through both the FSA Project and SERI, and by Westinghouse, the Southern California Edison Co., the Electric Power Research Institute, and the Pacific Gas and Electric Co. The end of CY 84 ribbon-growth contract objectives of this augmented program included demonstration of an area growth rate of at least 10 cm²/min simultaneously with growing 10 m or more of ribbon, under conditions of continuous melt replenishment (constant melt level). The CY 85 contract objectives include demonstration by mid-June of an area growth rate of at least 13 cm²/min simultaneously with growing uninterruptedly, under conditions of constant melt level (CML), 2 m or more of ribbon. A mid-December 1985 objective is to demonstrate an area growth rate of at least 16 cm²/min for the same conditions.

The above end-of-84 and mid-June area growth rate objectives were not achieved. However, during this report period, several increases in record ribbon growth parameters were made. Early in the period, the record length of ribbon grown under CML conditions was increased to 6.8 m, then 7.1 m (the previous longest being 6 m). In June 1985, a ribbon of record length for the case of melt replenishment (7.4 m) was grown, but the replenishment rate was only 50% of that required to maintain CML conditions. For the case of non-replenished growth (no silicon being added during the growth period), the longest ribbon ever grown (10.9 m) was produced in an 18-h period; the longest ribbon previously pulled under these conditions was 9.6 m long.

Records for throughput (defined as ribbon area grown in a single furnace in a week's time, 5 days) were set. For the case of batch replenishment, the throughput was increased to 27,000 cm²/furnace·week, the record at the start of this report period being 9000 cm²/furnace·week. When continuous melt replenishment was employed, a maximum throughput of almost 12,000 cm²/furnace·week was attained. Westinghouse has established throughput goals of 25,000 cm²/furnace·week for the end of June 1985 (this was achieved by the 27,000 cm² results) and 50,000 cm²/furnace·week for the end of December 1985.

A 6.7-cm-wide crystal was produced, the widest silicon dendritic web ribbon ever grown. The web was undeformed and was terminated by interference with the guide system. The maximum area growth rate for this run was 8 cm²/min over a section that averaged about 6.2 cm wide at a pull speed of about 1.3 cm/min. The previous maximum width was 5.8 cm for ribbon grown in 1983.

The highest area growth rate achieved during the augmented program, 13 cm²/min, was attained in April; however, it was for a short length of ribbon, only about 10 cm long. A 5-cm-wide web was grown at 2.65 cm/min for the 10-cm length before stresses caused buckling. For ribbon lengths of over 1 m, the highest area growth rate that was achieved was about 8 cm²/min.

AREA REPORTS

The area rates of 13 cm²/min for short lengths, and 8 cm²/min for lengths in excess of 1 m, do not constitute records because comparable area rates had been achieved by the end of 1982 in tests at Westinghouse.

Significant progress was made in implementing automated, closed-loop control of ribbon growth. In October, discussions were held with vendors of equipment that seemed to offer the potential for non-contact monitoring of dendrite thickness. In December, a purchased system capable of simultaneously monitoring the thickness of both dendrites of a growing crystal, comparing their thicknesses with a reference width, was delivered to Westinghouse. Because a clear furnace sight port is important for use with the dendrite thickness monitor (DTM) system, tests of a sight port with a gas purge for preventing formation of oxide deposits were conducted. The DTM was set up in February on a furnace having gas-purged sight ports, and successful tests were conducted. Also, a motor-driven coil positioner and a control circuit for closed-loop growth control, as part of the DTM system, were bench tested. Signals from the DTM will be used for coil positioning to maintain dendrite thickness.

The laser automatic melt-level control system that Westinghouse is developing will be a part of the closed-loop ribbon growth control system. A melt-level control system having improved electronics for greater melt-level sensitivity was tested. The melt-level sensor is sufficiently sensitive to detect seed insertion and buttoning.

Some new growth configurations were designed, built, and tested, and certain of these offer the potential of improved ribbon growth. Modeling calculations predicted that the addition of a vertical thermal element (VTE) at the top of the shield stack, which is used for thermal control of the ribbon drawn from the melt, could significantly reduce the stress peak that exists where the ribbon emerges above the shields. Tests of a growth configuration (given the designation Z058) having such a VTE (of 0.005-in. thickness) verified the modeling predictions; wide, thin ribbon was produced without buckling. Subsequently, Z058 configurations with 0.010-in.-thick and 0.020-in.-thick VTEs were tested; increased thickness was expected to reduce ribbon stress. The test results confirmed this expectation, with excellent growth being obtained. In the most recent tests of a 0.010-in.-thick element, four ribbons over 5-cm wide were grown, the widest (6.4 cm in width) being grown at an area rate of 7.4 cm²/min; these results surpassed those obtained with a 0.020-in.-thick element.

Modeling of a new furnace lid configuration to reduce ribbon stress near the growth front indicated that this stress diminishes as the temperature of a recessed slot in the lid increases and as recess depth increases. This hot recessed region faces the ribbon as it is pulled from the melt. The first tests of this new lid (designated the N133 lid) were conducted. Although a dipped temperature profile in the melt prevented web widening, growth rates were higher (pull speed of approximately 2 cm/min at the standard 150- μ m ribbon thickness) than the J460 and Z058 configurations, which are earlier high-performance designs.

AREA REPORTS

A data acquisition system (DAS) is being set up that initially will measure and correlate certain parameters such as operation of the pull speed motor and the silicon pellet feed motor. Ultimately, the system will be able to relate ribbon to the conditions under which it is grown. Software was written to monitor, store, and display data acquired from a furnace. Ribbon pull speed, pellet feed rate, output of the light pipe for the crucible temperature control system, and axial thermocouple information were obtained and displayed to test the system. A new computer for the DAS was procured and checked out. Transfer of the software for furnace monitoring is underway. Wiring of the DAS to all furnaces is nearly complete.

Tests were made to obtain information on restarting ribbon at wide widths, to permit saving the long time periods that are required for narrow ribbon to grow wide. The widths at which successful restarts were obtained were increased from 3.5 to 4.9 cm. One crystal was grown for 7 m following restart with no apparent structural degradation.

Using the laser automatic melt-level control, tests were conducted to investigate the effect of varying LIN or ribbon growth. LIN is defined as the vertical distance from the bottom of the furnace lid to the ribbon growth front. LIN ranged from 1.6 to 3.1 mm and was controlled to 0.1 mm. The highest value of pull speed at a ribbon thickness of 150 μm , 1.7 cm/min, for sustained growth was attained at LIN equal to 1.8 mm, but growth was limited by convection-induced pullout.

Simultaneous temperature measurements were made in the melt and at two levels in the gas above the melt. The tests were intended to identify any temporal fluctuations of temperature in the gas and liquid phases during ribbon growth and to identify any correlation between the two. The data are being examined for information on causes of pullouts or thirds, as well as any interaction between gas and liquid temperature changes.

Fluid-flow modeling indicated that baffles 4 to 6 mm high placed in the melt about 1.5 cm from the growing web can reduce melt flow by 30 to 40%. Experimental verification is planned. Fluid flow modeling also confirmed that the introduction of a raised rectangular mesa on the bottom of a crucible can restrict convective flow and possibly reduce temperature fluctuations that promote pullout. A crucible with a 3-mm-high mesa located under the growth slot was fabricated and tested in a furnace, with successful growth being achieved.

Modeling of web buckling behavior for certain configurations was carried out. The aim is to relate the observed behavior to measured thermal parameters, such as lid/shield temperatures, so that further reductions in stress and buckling can be achieved. A buckling analysis for the Z058 and J460 growth configurations was conducted in terms of the variable LIN. The analysis indicates that when the "far" stresses (as differentiated from "near" stresses, which are located near the growth interface) are sufficiently low, the effects of near-stress on buckling start showing up. The Z058 is an example of a configuration with low far-stress.

AREA REPORTS

Model analysis of near-stresses is being undertaken by a working group composed of a WECAN computer program model expert, a plastic flow specialist, and a web growth analyst. The WECAN code will be modified for plastic flow behavior after comparisons of the calculated shear stresses are made against the silicon yield point. The computer code has been modified so that the use of synthetic temperature profiles as input to stress and buckling calculations will be greatly facilitated. Synthetic temperature profiles are a generic modeling approach that facilitates parametric analysis and optimization of lid designs for near-stress reduction. Calculations of factors for the critical resolved shear stress (the stress that is required to make a dislocation move in its preferred direction) for each of the 12 silicon slip systems was completed for the crystal geometry that is being employed for dendritic-web ribbon growth. These will be input to the WECAN stress analysis code as a basis for a first-order estimation of plastic flow during web growth.

The first calculations of resolved shear stress on the 12 slip systems of a silicon web crystal were completed. When the calculated stresses are compared with the critical resolved shear stress from the literature, regions of the crystal are identified in which plastic flow may be expected. The calculations are being evaluated.

Various modifications of equipment were made to improve operation. For example, a new tripod-style susceptor mount was designed, fabricated, and installed in a furnace. This prototype design is intended to improve the mechanical stability and reproducibility of the web growth system. Also, high-frequency transformers were installed on all furnaces having elongated susceptors, to provide load-matching between the power generators and the furnaces, and thereby accommodate the increased thermal load that is required. Improved thermal control was demonstrated after transformer installation.

A new contract to Westinghouse Electric Corp. started on May 15. This contract will provide CY 85 funding for the silicon ribbon growth activities of the augmented program.

Low-Angle Silicon Sheet (Energy Materials Corp.)

The objective of this program is to overcome the critical barriers to the LASS ribbon growth of high-quality material at high linear growth velocities.

Several furnace modifications, including a new heater configuration and a leading-edge heater, were incorporated to improve the quality of horizontally grown ribbon. A cold shoe with elongated gas jets allowed for the use of a video camera to view in real time the solid/liquid interface. The observation of this growth interface led to a better understanding of the growth process and, consequently, substantial improvements in the control and optimization of the technology were made. Ribbon with aligned twin-plane structure across the full width of the material was grown in lengths up to

AREA REPORTS

several meters. In the final growth run of the contract, the power controls were set to the conditions that were known to exhibit the aligned twin-plane growth. Approximately 15% of the 100 m grown in this run demonstrated the aligned structure. This run was the first indication that the growth process of LASS ribbon was controllable. The technical portion of the contract concluded at the end of June.

Silicon Sheet Supporting Studies

Modification of Silicon Surface Properties by Fluid Absorption (University of Illinois at Chicago)

This study is emphasizing the silicon surface property modification by various fluids that may be compatible for high-temperature and high-speed processing, and the measurement of residual stress in silicon sheet by laser interferometry.

Effort continued on evaluating indentation and scratch damage of silicon under various fluid environments. Dislocation propagation from the damage regions was determined by annealing and etching techniques. Transmission electron microscope evaluation of silicon surfaces scratched in deionized water and in ethanol was made. It was found that the scratch made in water contains a high density of dislocations, while the surface scratched in ethanol contains isolated regions of dislocations. The depth of these plastically deformed zones having the dislocations is about 5 μm .

Modeling was performed to describe the indentation damage process. This model describes the damage zone size as functions of indentation force and fluids in terms of surface potential and dislocation dipole shear forces.

A high-temperature (up to 650°C) indentation test jig was fabricated. Preliminary tests on the indentation damage of silicon in fluids at several temperatures were made. It is anticipated that the temperature factor will be added to the model of indentation damage of silicon.

A high-speed wafering facility employing a diamond-impregnated blade was completed. This facility will be used to determine the high-speed and high-temperature sawing damage in silicon in fluid environments.

Residual stresses in silicon dendritic web ribbon and in silicon ribbon grown by the EFG method were measured using shadow moiré interferometry. The fringe patterns show complicated sample-to-sample differences in surface morphology and thickness. The results indicated that the in-plane residual stresses are predominantly tensile in the center and compressive at the edges. The maximum stresses for EFG ribbon were found to be between 5 and 10 MPa. By comparison, the Westinghouse dendritic web ribbon with the dendrites removed had residual stresses of about 1 MPa.

AREA REPORTS

Analysis of Stress/Strain Relationships (University of Kentucky)

This program is aimed at developing stress/strain models for silicon sheet growth processes and evaluating the relationship between silicon growth structure and stress/strain.

The University of Kentucky has developed a new thermal buckling analysis for the plastic range of silicon ribbon. Once in-plane stresses are known, the new-version buckling analysis allows for prediction of buckling modes, if any. The main limitation now is not in the buckling analysis itself, but in understanding the nature of in-plane stresses. A main limiting factor in the determination of in-plane stresses is felt to be a lack of knowledge of high-temperature stress-field silicon dislocation behavior. A Sumino-Haasen stress/strain model is used in the buckling and stress/strain analyses. This model incorporates dislocation multiplication. Through the use of a constant "melt-face dislocation density" and the Westinghouse dendritic web ribbon thermal profile, critical ribbon widths were established. Ribbon widths were varied, and calculations of in-plane stresses resulted in either a convergence (finite dislocation densities) or divergence (infinite or extremely large final dislocation densities). For the specific case analyzed, a 6.24-cm width was the maximum obtainable without a divergent solution.

Several other efforts were undertaken during this reporting period. A code for tracking the motion of any individual dislocation as it forms at the melt interface and moves through stress fields is being developed. Ribbon dislocation density contour maps were developed for various ribbon temperature profiles. Also, sensitivity analyses were performed with respect to critical buckling width and thickness as functions of the temperature profile and starting dislocation density.

A report, titled "Visco Plastic Thermal Buckling of Silicon Sheet," was written. It presents an analysis of the buckling of a visco plastic cantilever plate subjected to typical silicon ribbon thermal profiles that vary along the length of the plate. The main results obtained were critical sheet thicknesses as functions of thermal profile and plate geometry. Also, the report indicated that critical thickness can be accurately determined by elastic analysis without the additional need for plastic analysis. A potential new creep buckling observation was established. Without external load, some buckling modes grew in time while others damped out.

"Numerical instability," sometimes a result in using the Sumino-Haasen stress-strain model, was analyzed. This model's compatibility equations cannot handle instability conditions, for example, twinning or dislocation banding. However, the model was used to discover unstable ribbon locations in growth. For example, one Mobil Solar Energy Corp. EFG ribbon growth temperature profile exhibits an instability at 2-1/4 cm from the growth interface. In this region the temperature is dropping, in-plane stresses are rising, and dislocation densities are rapidly increasing. Depending on the assumed initial dislocation density for this ribbon, growth would either remain stable or go unstable (numerically). For example, 0.5 dislocation/cm²

AREA REPORTS

(starting density) remained stable while $0.56 \text{ dislocation/cm}^2$ produced instability, i.e., an ending dislocation density of $10^{99}/\text{cm}^2$. The instability is felt to be dislocation banding of the type observed by Mobil in their EFG ribbon.

A new high-temperature furnace with mechanical test equipment for conducting tensile tests was fully assembled. The furnace has been "fired up" successfully.

Analysis of High-Speed Growth of Silicon Sheets in Inclined-Meniscus Configurations (Massachusetts Institute of Technology)

This theoretical study is aimed at defining the parameters for high-speed growth of thin silicon sheets. A computer code was completed for the finite-element analysis of inclined sheet growth from a die with moderate inclinations. The program uses the Isotherm-Newton method to solve the free-boundary problem for determining the meniscus shape, melt-solid interface shape, and sheet thickness. The finite-element analysis included heat conduction in the melt and in the solid, as well as radiation and convection from all exposed surfaces. Gravity and surface tension are the two parameters that determine the meniscus shape with the growth angle at the melt/solid/gas tri-junction. The Isotherm-Newton method gives a simultaneous, quadratic convergence for all variables.

Computer runs were made for a horizontal (0-deg inclination) and for an inclined ribbon growth process. The predicted temperature gradients are almost identical for the two conditions of growth. The conclusion drawn from these results was that the growth process could not be improved on by inclining the growing ribbon from the horizontal. The entire heat flux associated with the release of the latent heat of fusion during solidification will still be flowing out of the melt-solid interface parallel to the pull direction.

Optimization of Silicon Crystals for High-Efficiency Solar Cells (Solar Energy Research Institute)

Research continued on obtaining long-lifetime single-crystal silicon grown by the FZ method and on understanding and reducing the mechanisms that limit the achievement of long lifetimes. Several gallium-doped ingots with zero dislocation density were grown in the 0.3 to 0.5- Ω -cm resistivity range for processing into high-efficiency solar cells.

A totally automated photoconductive decay system for measuring the lifetime of low-resistivity material was set up and used to measure the ingots grown in the program. For 0.5- Ω -cm and 0.3- Ω -cm, Ga-doped, 34-mm diameter, dislocation-free (100) materials, the measured lifetimes were greater than 200 s. Also, the effects of carrier lifetime versus crystal cooling rate were investigated. It was found that for dislocated material (0.6- Ω -cm, Ga-doped),

AREA REPORTS

the lifetime decreased from 56 to 23 μs as the cooling rate after solidification increased from 40 to 500°C/min and that for dislocation-free material (2- Ω -cm, Ga-doped), the lifetime decreased from 800 to 200 μs as the cooling rate increased from 40 to 500°C/min. Besides lifetime measurements, both EBIC microscopy and x-ray topography were used to characterize the material.

Crystal Growth Modeling Study (Washington University at St. Louis)

The purpose of this study is to develop a mathematical model to simulate the Cz crystal growth process. The contract started April 26, 1985. The model is intended to serve as a basis for predicting the ingot growth process and the properties of the ingot, and it will also enable the expeditious optimization of the process. In the course of the study, an algorithm/model suitable for predicting the temperature distribution in the crystal and for calculating the melt-surface interface for an assumed melt temperature profile and heat transfer coefficient will be developed; this algorithm/model will be used for parametric calculations. A detailed modeling of the hydrodynamics of the melt will be performed. Experimental data will be used to determine the predictive capabilities of the process model.

Electrical, Structural, and Chemical Characterization of Silicon Sheet Material (Cornell University)

The objective of this effort is to investigate the physical structure and the chemical nature of defects in silicon sheet material.

Work was performed on the high-temperature deformation of dendritic web silicon ribbon. Accurate creep data are required for modeling stress relaxation in silicon ribbon. Because dislocation glide in dendritic web ribbon is restricted by internal twin planes, this material is expected to deform differently at high temperatures from single-crystal silicon. To study these effects, experimental creep tests on web ribbons were performed at Mobil Solar Energy Corp. in four-point bending under constant load conditions. The resulting deflection of the ribbon center was plotted against time. The results indicated that the creep behavior of the ribbon was very different from that seen for single-crystal ingot material. Studies are underway to determine if this behavior of ribbon is perhaps modeled between single-crystal and polycrystalline silicon or is perhaps related to stress in the ribbon.

The mechanical behavior of silicon depends on the oxygen content. The oxygen content of web silicon is unknown because, experimentally, it is difficult to ascertain because the ribbons are very thin and the surfaces cause a great deal of reflection. A program to measure the oxygen content of web ribbons was started. A method was developed to determine the oxygen content through the use of Fourier transform infrared (FTIR) analysis, and the initial measurements were made. The oxygen content was found to be near the

AREA REPORTS

saturation level at the melting point. Interstitial oxygen amounts only to about one-half of the total oxygen. The remainder is in a state close to that of interstitial oxygen, that is affected by its environment.

Materials Properties Modification (JPL)

An effort on determining the interaction of dislocations and crack growth in single-crystal silicon was carried out during the present reporting period.

Crack growth in single-crystal silicon at room temperature in air was evaluated by a double torsion (DT) load-relaxation method and monitored by an acoustic emission (AE) technique.

Both the DT and AE methods indicated lack of subcritical crack growth in silicon. At the critical stress intensity factor, the crack front was found to be jumping several times in a "mirror" region and then followed by fast crack growth in a "hackle" region. Hackle marks were found to be associated with plastic deformation at the tip of the fast-moving crack. No dislocation etch pits were found in the "mirror" region, in which crack growth may result from interatomic bonds broken at the crack tip under stress without any plastic deformation. Acoustic emission seems to be spontaneously generated from both interatomic bonds broken and dislocation generation at the moving crack tip during the crack growth in single-crystal silicon.

Many high-temperature tensile tests were successfully performed on Cz silicon and Westinghouse silicon dendritic web materials. Most tests were performed on Cz material in the 800 to 1300°C temperature range at strain rates varying from $1.5 \times 10^{-3} \text{ s}^{-1}$ to about $7 \times 10^{-7} \text{ s}^{-1}$. Flow stress (or lower yield) values were generally higher, by a factor 2 to 5 than those presented separately by Schroeter, Siethoff, Yonenaga, Sumino, Haasen, or Reppich. Viscous modulus values were obtained from many of the stress-strain test plots. Although there seems to be considerable scatter in modulus (and strength) data, the appropriate "softening" effect was observed. Modulus values ranged from about 0.2×10^6 psi at 1300°C, up to about 4×10^6 psi at 800°C.

The first high-temperature tensile tests on silicon dendritic web ribbon were completed. The initial test temperature was 800°C, and the strain rate was in the mid 10^{-5} s^{-1} range. Two flow stress data points for the 800°C ribbon tests were 8 and 17 MPa. The reasons for this data scatter are to be determined. Other ribbon tests at 1000 and 1200°C were relatively unsuccessful.

The 0.25-in. total travel linear voltage displacement transducer (LVDT) extensometer that has been used for most of the tensile tests was replaced in April 1985 with a more sensitive 0.050-in. total-travel extensometer. The new extensometer was successfully operated on two Cz silicon tensile samples during 600°C pull testing. The new extensometer facilitates recording low-strain sample responses and measuring pseudo moduli.

AREA REPORTS

Device Research Task

INTRODUCTION

The objective of this task is to identify and implement research and development activities in the PV device and measurements area to meet the near-term and long-term objectives of FSA. Task activities encompass research in device physics, device structure, material-device property interaction, and measurement techniques for physical, chemical, and electrical evaluation of devices and materials.

Technical Approach, Organization, and Coordination

To meet FSA objectives, efforts are now directed toward characterization of various silicon-sheet materials, material-device property interaction investigation, and measurement techniques. The program of the Task is structured accordingly.

The program of the Task also includes JPL in-house activities to conduct basic research in material and device characterization to support contractor needs and other Tasks of the Materials and Devices Area.

SUMMARY OF PROGRESS

Cornell University

A technical review of work in progress was conducted by JPL on January 21, 1985.

An investigation of preannealing-induced changes in the defect structure of EFG silicon ribbon was completed in November and two papers were published. There will be no further studies under this subtask.

Preliminary tests to identify any unusual behavior of structural and chemical factors controlling the hydrogen passivation of grain boundaries provided no significant results to warrant a detailed study under this subtask. Therefore, this subtask will be deleted from the work statement of this contract. In its place, a study of the interaction of dislocations and internal twin planes in web silicon using controlled deformation tests and the development of a reliable method measuring oxygen content of web silicon has begun under JPL's direction.

Creep experiments on dendritic web materials were conducted using the test facility at Mobil Solar Energy Corp. For comparison, $\langle 111 \rangle$ FZ material was also tested. The web material with dendrites showed considerably lower creep rates compared to $\langle 111 \rangle$ FZ indicating the stiffening effect of the dendrites. However, without the dendrites, the material exhibited a cyclic behavior consisting of a short duration burst of rapid creep followed by a relatively longer duration slow creep. This is a very interesting result. This type of creep behavior by web silicon material is currently believed to be caused by the interaction between mobile dislocations and a twin plane.

AREA REPORTS

During the period of slow creep, dislocations move toward and pile up at the twin plane region until a critical density is reached. Then the accumulated dislocations punch through the twin plane to reach the surface which is seen as a short burst of very high creep rate.

Studies to confirm the dislocation twin plane interaction model and to understand the role of oxygen in web deformation behavior are being planned carefully.

Surface profile measurements were carried out on web ribbons grown in the J376 configuration. These ribbons were found to be nearly 30 μm thicker in the middle. The shape of the surface varied along the growth direction with no definite trend seen.

Oxygen measurements were carried out at the National Bureau of Standards (NBS) for Cornell. From the NBS data, it appears that high concentrations of oxygen are clustering in the twin planes in the middle of the ribbon. If this is confirmed, laminar structure will be assumed in order to interpret data from tensile and creep tests on these web ribbons.

University of Pennsylvania

A technical review of work in progress of work performed was conducted by JPL on January 18, 1985.

For a solar cell structure with multiple regions, it is very difficult to derive values of minority carrier lifetime (τ) for the individual regions using the model developed by M. Wolf requiring measurement of the light-beam-induced current (LBIC) only. This is presumed to be caused by differences in sensitivities of various regions to the controlled variable, namely, the light intensity. This is the rationale for designing, building, and experimenting with the MLB instrument where the modulation frequency as a variable is expected to provide greater insight into the response of the cell structure to incident light.

The MLB apparatus is operational and, during the following months, emphasis will be placed on obtaining data on the sensitivities of T and S derived from the model to uncertainties in the measured values of light-beam-induced short-circuit current. It is also planned to conduct sensitivity comparisons of all T and S measurement techniques being studied under this contract.

A tunable argon laser, doubler, and modulator for short wavelength high-intensity surface excitation studies using the MLB technique is expected to be acquired soon.

An apparatus resembling the photoconductive decay instrument developed by Stanford and Exxon has been set up and is operational for contactless measurement of carrier decay (following light pulsing) from the impedance change of a VHF coil with a solar cell in its induction path. This technique will be used to independently verify or corroborate other T and S measurements. By etching off various layers in a solar cell and by

AREA REPORTS

suppressing S with hydrogen fluoride, regional and T and S measurements will be obtained for comparison with those obtained using other techniques.

Considerable effort was directed toward locating and remedying the causes of electronic noise (such as radiative coupling between light emitting diode (LED)-driving circuit and the sample test circuit) in the modulated light beam instrument. A high efficiency solar cell made by Spire Corp. was used for the demonstration of operation of the MLB instrument. The transfer function of the solar cell was obtained at 660 nm (red). Practical limitations to the accuracy of MLB measurement were identified and effort will be directed toward eliminating or minimizing some of them.

In order to compare LBIC and MLB techniques, test structures and metallization procedures have been selected with the following criteria: (1) large signal ability, (2) ability to restrict excitation to one side of the junction, and (3) uniform doping on the excited side of the junction. Through theoretical analysis, it was determined that contact impedance will have no effect on the measurement as long as the shunt resistance of the device is large compared to the other resistances (contact and external). Therefore, care was taken to maximize the shunt resistance of the device by preventing nickel plating near the edges of the device.

A shunting junction capacitance in the MLB measurement was suspected for the anomalous frequency response data obtained. Two experiments were performed to confirm the suspicion. A mathematical analysis showed that inclusion of the junction capacitance (0.1 to 0.5 pF) significantly alters the predicted frequency response. Reduction of load resistance with a penalty on signal strength, reduction of device area requiring destructive device processing, and independent measurement of junction capacitance and its inclusion in the model are some of the means available to compensate or account for the effect of junction capacitance. With a low-level LED illumination, reduction of load resistance will lead to unacceptably low signal levels. Therefore, other methods will be pursued. If a tunable argon laser becomes available for this work, adequate signal levels could be obtained even after compensation for junction capacitance.

Because availability of high-intensity illumination is uncertain, a realistic milestone for Subtask 3 (comparison of LBIC and MLB) cannot be proposed or adhered to at this time.

Twenty-three methods of measuring recombination parameters were identified from published literature. The assumptions under which each of these techniques are applied (and results interpreted) were also determined. The methods were classified into single-region and multi-region measurements and each of these were subdivided into further categories.

Studies of measurement techniques for recombination parameter for thin emitters is continuing. The emitter modes are comparable to the higher order modes of the base. The dominant pole approximation traditionally adopted considers only the first mode of the base. The pole coalescence approximation integrates over all the modes of the base in the limit of a long base. These two approximations are useless for studying thin emitters.

AREA REPORTS

University of Florida

After searching through the existing literature, it was concluded that some of the Auger recombination measurement methods (Possin, Weaver, and Swanson) in the past have not taken the effects of doping gradient fields into account. It was further concluded that photoluminescence is, by far, the only method likely to succeed in giving meaningful results of Auger lifetimes.

Evaluation of surface recombination velocity at the front region of a cell are being formed.

Experiments to determine the temperature dependence of I_{SC} at short wavelengths in a uniformly doped emitter solar cell have been performed. Evaluation of the data suggest that the two mobilities (surface recombination and emitter recombination) are not equal. The data are consistent with the model developed at the University of Florida which suggest carrier trapping at localized states about 10 meV above E_v .

The spectral response of solar cells with polysilicon on the back surface shows a better red wavelength response compared to back-surface field (BSF) cells. This confirms an earlier report on enhanced solar cell parameters.

Two papers have been written and sent for publication. One of the papers deals with the evaluation of the luminescence method of Auger recombination lifetime and with the correlations of the results with heavy doping effects.

The second paper relates to the surface passivation of the back surface of a cell using polycrystalline silicon and with the design criteria for the front contact using heavily doped polycrystalline silicon. The mechanism of passivation is explained as due to the amorphized region close to the surface and with dopant atoms which cause pileup of minority carriers.

Further research on heavy doping effects has been instrumental in improving the usefulness of the theoretical model for heavy doping effects and surface recombination velocity.

Back contact and hi-lo interface recombination velocities in polycrystalline silicon back contact and BSF control cells has been measured with the improved admittance bridge method. The results of the measurement are: (1) 2 x 2 cm n-type base cells- $L_p = 190 \mu\text{m}$, thickness = $210 \mu\text{m}$, back surface recombination velocity $s = 100 \text{ cm/s}$, BSF control cells $s(\text{effective})$ (hi-lo interface) = 700 cm/s ; and (2) p-type base, $L_n = 310 \mu\text{m}$, $s = 1000 \text{ cm/s}$, BSF control cells $s(\text{effective}) = 40,000 \text{ cm/s}$.

In general, minority carrier mobility and diffusivity are modeled using a trapping mechanism.

A new model is being developed using scattering mechanisms instead of trapping mechanisms. This new model is being developed because minority carriers that are near the band edge have less kinetic energy than majority carriers so they will be present in the ion force field for a longer

AREA REPORTS

period of time and will be scattered more. This scattering mechanism will not only help explain the difference in transport properties of majority and minority carriers, but will also help solve the transport parameters at the front surface of an n+/p solar cell.

Work on measuring diffusivity of minority carriers in lightly doped silicon (10^{15} to 10^{17} cm^{-3}), using a frequency versus admittance technique, has given useful data which differ from majority carrier data. In heavily doped silicon, the mobility of minority carriers is a factor of 5 to 10 lower than that of majority carriers. These data will be used in the measurement of front-surface recombination velocity.

Work on the measurement of diffusivity of minority carriers in low-doped silicon has given very useful data. The measurement technique is based on measuring transit time of carriers in the heavily doped base of a transistor. It is known that majority carrier hole mobility is higher compared to majority carrier hole mobility for a doping range of 10^{15} to 10^{17} .

University of Washington

Surface characterization capabilities have been improved by the development of a slow ramp capacitance measurement method that covers the low surface state region and can be compared to high frequency capacitance voltage (CV) data to check for charge injection. Double AR MgCl-TiO₂ coatings have been achieved and the process is available for application to high-efficiency cell structures.

Development of the slow-ramp high-frequency measurement system has been completed. This measurement system can measure surface state densities in the 10^9 range on p-type substrates.

A process for photolithographic lift-off of thick (5 μm) aluminum metallization has been developed at the Joint Center for Graduate Studies of the University of Washington.

Tests of the surface state density and recombination velocity on native oxide on n+ silicon substrates are being performed using a modified Rosier method. Photoresponse and CV measurements have been made and ellipsometry and other measurements are underway. Both annealed and unannealed samples are being used in the tests.

C.T. Sah Associates

Work is continuing on a critical evaluation of models of very high-efficiency solar cells. This work includes considerations of the compatibility of the cell structure requirements with cell fabrication processes.

C.T. Sah Associates has been working closely with Applied Solar Energy Corp. on designing test devices to study a theoretical model developed by C.T. Sah Associates.

AREA REPORTS

Reviewing photomasks received from ASEC has been completed. These masks will be used to fabricate proof-of-concept high-efficiency silicon solar cells at ASEC. Presently, C.T. Sah Associates is continuing work on determining the optimum parameters for junction depth, wafer thickness, and other related parameters.

C.T. Sah Associates is working on additional designs for high-efficiency silicon solar cells with different geometry, diffused layer thickness, and dopant concentrations.

C.T. Sah Associates is also working on the design and fabrication of solar cells for testing the floating emitter solar cell transistor concept in collaboration with Applied Solar Energy Corp. A set of four photomasks have been produced that can be used to fabricate all possible configurations of the floating emitter solar cell.

State University of New York at Albany

Work on defect identification concerned with oxygen thermal donors and oxygen precipitation is continuing.

A literature search is being conducted on the behavior of oxygen and carbon in silicon pertinent to high-efficiency solar cell performance.

Plans are being made to perform experiments on the effects of oxygen on silicon material properties.

A contract review meeting was held at the State University of New York at Albany (SUNYA) on January 25, 1985. At the review, it was disclosed that a collaboration with IBM Research Center has been established. The purpose of this collaboration is to improve the understanding of thermal donor and precipitate fraction in silicon which is relevant to impurity carrier lifetime in silicon. IBM will provide a series of silicon samples thermally treated at different temperatures as part of this collaboration.

Work has begun on a survey of techniques to measure minority carrier lifetimes. A summary of the techniques has been prepared and is being sent to JPL.

Work on defect identification concerning the oxygen thermal donors and oxygen precipitation process is underway.

SUNYA has begun to synthesize a broad theory for all defect families that have been established to this point. The theory will give new insight in identifying unknown defects. The literature search on oxygen and carbon in silicon is continuing.

Stanford University

A solatron impedance meter has been ordered for the study of SiO₂/Si interfaces. It is expected by the end of February 1986.

AREA REPORTS

Samples of SiO₂/Si interfaces with 50, 100, and 200 Å thicknesses are being procured from Fairchild Corp. These will be used for chemical analysis of interfaces using the Angular Resolved Auger Parameter Spectroscopy (ARAPS) technique.

Studies using XPS on Si-SiO₂ interfaces with SiO₂ thickness ranging from 15 to 100 Å are being performed. The x-ray photoemission spectroscopy (XPS) study throws light on two aspects of the interface states: the initial state effect, and the final state effect. The final state effect is dependent on the binding energy of the atoms.

Contrary to the normal reports found in the literature, this XPS study has shown no extra-atomic relaxation modes of the binding energy in the final state effect, either for Si-SiO₂ or any of several polymers of SiO₂ studied.

Binding energy of the 2p level in silicon has been measured by embedding Argon in the SiO₂. Results will be reported later.

Results obtained using data from the ARAPS measurement system for 15 to 85 deg angles on oxide films with 13 to 125 Å-thick layers grown on n-type silicon and the crystalline polymorphic forms of SiO₂ (quartz, tridymite, and cristobalite) give the same value of 225.5 ± 0.1 eV. This suggests indigenous dielectric screening by the oxide which is not affected by the silicon substrate at least down to 13 Å oxide thickness. Impedance spectroscopy measurements are planned in the near future.

Analysis of the ARAPS data for silicon dioxide (13 to 200 Å) on silicon and polymorph of silicon dioxide show the same value of 225.3 eV. This is a strong indication of the lack of final state effects. Results of these data are expected to be published soon.

Another technique of inverted Bremsstrahlung Isochromate Spectroscopy (BIS) is being looked into for possible measurement of unoccupied states in the conduction band of silicon dioxide. The technique relies on inverse photoemission.

The Solartron test instruments used to measure interface state density at Si-SiO₂ interfaces has been received.

Work using the BIS to measure unoccupied states at the conduction band near an Si-SiO₂ interface is continuing.

Experiments using BIS to measure unoccupied states at the conduction band near the Si-SiO₂ interface and in the bulk regions of the Si-SiO₂ is underway.

Experimental results using lateral and vertical transistor structures on heavily doped n-type epi-layers are continuing. By reinterpreting data from published literature, it was shown that bandgap narrowing values obtained by various authors are within 10 meV of each other. Data beyond 10²⁰/cm³ doping concentration are being worked on. Similarly, data on diffusion length of holes in n-type samples of 10¹⁸ to 10²⁰/cm³ concentration show remarkable consistency irrespective of the source and measurement technique.

AREA REPORTS

A new contract has been signed with Stanford University to develop theoretical and experimental techniques for the measurement of minority carrier transport and related parameters for heavily doped silicon.

Data in n-type silicon for minority carrier Auger lifetime have begun using the photoluminescence technique.

Transport parameters are being evaluated by measuring the collector current using lateral and vertical transistor structures on heavily doped n-type epilayers acting as the base.

Work using angle resolved Auger spectroscopy on silicon dioxide is continuing. Work on measuring unoccupied states at the conduction band for the silicon-silicon dioxide interface using BIS is also continuing.

Research Triangle Institute

Oxide charge and arbitrary impurity concentration subroutines have been incorporated into the main program and debugged. An additional subroutine to calculate an optimum grid separation has been developed. Several more subroutines will be required to fully support the grid separation subroutine by supplying required device parameters. These parameters include the determination of the diode exponential factor, the equivalent saturation current, and the terminal voltage and current values.

Work to improve the computer modeling program by adding to the documentation and making provisions for up to 30 user inputted parameters or options is underway. Each of the user inputs is prompted by the program and default values are provided for 24 of the inputs.

Fifty-one different output parameters are now available for printing. These parameters cover all of the major device physical phenomena that are important in high-efficiency silicon solar cells. The program has already been used to explore device structures that achieve high efficiency. Affects on the terminal characteristics related to the device parameters such as n and p layer thickness, impurity concentration profiles, energy levels of trap centers, trap concentration, radiation trapping, and Shockley-Reed-Hall (SRH) and Auger recombination values have been determined for some cases.

A problem was uncovered in the mesh point distribution in the base region of the computer model. The problem resulted in a poor simulation accuracy for a small number of mesh points. The problem has been solved so that for as little as 10 test points, the simulation accuracy is good.

The subroutine to determine the equivalent diode relationship for dark current components has been coded and debugged. The optimum grid separation determination has been coded and is giving good results.

Validation of the simulation program has begun. Actual solar cell data supplied by Spire Corp is being used in the validation. The solar cell data include efficiency, fill factor, I_{SC} , V_{OC} , current and voltage of the maximum power point, and the temperature behavior of these parameters.

AREA REPORTS

Initial validation results show that the disagreement between data and simulation is less than 3.5%. However, there was an oversight in the value of the experimental electron diffusion length which, when corrected, may result in better agreement.

Validation studies will continue.

Westinghouse

High-efficiency solar cell production run is underway with a poly emitter design.

An assessment of the effect of twin plane activity on cell performance is continuing.

A matrix of three different cell groups were run to check on the efficiency of gettering for improving web material. All cells had both front and back surfaces coated with polysilicon. One group consisted of cells simulating a standard diffusion run which were heated to 850°C for 1 h. One group was heated in nitrogen for 1 h at 1150°C and one group was heated in POC13 for 1 h at 1200°C. Attempts at high-temperature gettering with polysilicon were not very successful with diffusion length improving from 25 to only 31 μm , and an improvement of 25 to 35 μm for nitrogen. In contrast, the group with standard temperature processing improved from a diffusion length of 25 to a final length of 54 μm .

Some preliminary results were obtained on the third lot of high-efficiency cells from low-resistivity web. Without antireflective (AR) coating, these cells have an efficiency of about 11% and a diffusion length of 110 μm . This compares to a final efficiency on lot 1 in the high 16% range (with AR) and diffusion length of 90 μm . Lot 2 was not as good, with efficiency of 15.8% and 66 μm diffusion length.

A run of cells with polysilicon single-crystal emitters is progressing. It is planned to have polysilicon beneath the metal grids to gain the advantage of a metal-insulator semiconductor (MIS) structure without the processing problems.

Three runs of low resistivity web (0.4 ohm-cm) high-efficiency cells with average conversion efficiencies of 16.9, 15.6, and 16.1% have been made. Diffusion lengths varied from 90 to 56 μm . Quality (as measured by diffusion length) of a pulled web may decline along the length of web. This condition will be explored more fully in the future.

University of California at Los Angeles

A new contract has been signed with the University of California at Los Angeles. A new computer code will be developed for designing the most efficient silicon solar cell. The first step in developing the new computer code will be to install the JPL version of Solar-Cell Analysis Program in One Dimension (SCP1D) simulation program on the IBM computer system at UCLA. The SCP1D is expected to be operational soon.

AREA REPORTS

The SCAP1D program has been compiled and is expected to be on the IBM computer system using a Fortran 77 compiler. A comparison of output data from the Univac at JPL and the IBM at UCLA revealed no discrepancies.

A study of the computer program to become better acquainted with the various calculations that will be performed in an iterative optimization environment is continuing.

University of Southern California

Measurements on high-purity and high-quality silicon crystals currently available in the marketplace gave an absorption coefficient at $1.3 \mu\text{m}$ of about 10^{-3} cm^{-1} , indicating that the best silicon crystals could still have a considerable amount of band tailing into the bandgap. The source of this band tailing might be caused by the residue of structural defects and impurities with concentrations in the order of 10^{13} cm^{-3} . This result could be important for evaluating current silicon technology.

Work on samples prepared from a silicon ingot with 200 ohm-cm resistivity grown by the Cz technique provided by JPL are underway. Experiments are being performed with the objective of determining the origin of the large absorption coefficient at $1.3 \mu\text{m}$ wavelength measured in the FZ samples.

Applied Solar Energy Corp.

An investigation of a high-efficiency solar cell structure proposed by C.T. Sah Associates is underway.

Control wafers of both n- and p-type FZ wafers have been thinned to between 7 and 8 mils thickness preparatory to cell fabrication. The test device mask is expected soon and will permit completion of the critical first round of test devices.

One of the four test device masks was determined to be out of specification and had to be rejected. The rejected mask was the one used at the end of the process sequence, so a lot of cells have already been started and will be completed immediately after receipt of the reworked mask.

North Carolina State University

North Carolina State University is in the first month of its contract with this task. Acquisition of a student research assistant and of silicon wafers from Monsanto have been completed.

An experimental setup to measure lifetimes is being readied.

AREA REPORTS

Pennsylvania State University

Experimental and modeling work is continuing in an effort to determine if any of the regions (emitter, base, or space charge) could be passivated by hydrogen ions. A computer program to determine the spectral response of the different regions and to extract recombination and lifetime parameters has been written. This program takes into account the electric field gradients associated with heavy doping. The program will be used to derive the recombination parameters from spectral response data and vice versa.

Silicon regrowth and residual defects under self-implantation of silicon has been studied. A trap level of 0.3 eV above the valence band was identified following a 1000°C 30 s rapid thermal annealing. This study will be repeated following hydrogen ion implantation to determine the effect of hydrogen ions in regrowth and residual defects.

Work aimed at determining if hydrogen ions could passivate the emitter, space charge, or the base region of solar cells has begun. Arsenic implanted (at 75 keV) n⁺/P diodes were prepared and a selected set of these samples were hydrogen implanted before anneal. No improvement in the base diffusion length of the crystalline solar cells was seen. This is true for both FZ and Cz silicon. From this, it was concluded that H-ions did not significantly improve the base region of the crystalline solar cells. Hydrogen implantation of the web silicon showed that the base region diffusion length can be improved in some cases by as much as a factor of 3.

Upon annealing, the As diodes with no H-implants showed considerable leakage current and their n-factors were about 1.66. H-ion implanted samples showed low leakage current and n-factors very close to 1.0. This clearly points to the passivation of defects in the space charge region. The same conclusion was also drawn from analysis of the H-implanted cells.

Jet Propulsion Laboratory

Solar-Cell Efficiency Estimation Methodology and Analysis (SEEMA) has been used to evaluate the performance of a high-efficiency cell structure. The cell structure is a thin cell with back-surface reflector, passivated on both the front and back surfaces. Preliminary results indicate that this cell design has a limited efficiency of about 70%.

A sensitivity analysis of passivated thin silicon solar cell designs is underway at JPL using the SCAPID program.

A set of thermal diffusion experiments has been performed. These experiments were performed at 850°C with different predeposition and drive-in times. Results indicated no significant difference in open circuit voltages for solar cells. Secondary ion mass spectroscopy (SIMS) data confirmed that no change occurred in surface impurity concentration. This suggests that the oxide formed during predeposition acts as an infinite source of dopant during drive-in. Revised experiments with removal of oxide prior to drive-in are planned.

AREA REPORTS

A sensitivity analysis is being performed using SCAP1D to determine the parameters that limit the efficiency of silicon solar cells. Ignoring some of the heavy doping effects on efficiency, 35 to 36% was obtained for a hypothetical case. Additional runs are being performed to compare with published results.

Work to improve cell efficiency is continuing. Efficiencies of 17.4% have been obtained on 0.2 ohm-cm $\langle 100 \rangle$, 300 μm thick wafers with 0.23 μm junction depths. No BSF was used and $\text{TiO}_2\text{-Al}_2\text{O}_3$ AR coatings of 600 to 1100 \AA thickness were used with no oxide passivating layer. The cells produced $V_{oc} = 640 \text{ mV}$ and $I_{SC} = 270 \text{ mA}$ for 4 x 2 cm areas.

PROJECT ANALYSIS AND INTEGRATION AREA

INTRODUCTION

The objective of the Project Analysis and Integration Area (PA&I) is to support the planning, analysis, integration, and decision making activities of FSA. Accordingly, PA&I supports the Project by developing and documenting Project plans based, in part, on the technical and economic assessments performed by PA&I of the various technical options. Goals for module technical performance and costs, derived from National Photovoltaics Program goals, are established by PA&I for each of the major technical activities in the Project. Assessments of progress toward achievement of goals are made to guide decision making within the Project.

SUMMARY OF PROGRESS

Module Lifetime

A preliminary study evaluating the benefits of extended module lifetime was completed. The measure selected to evaluate the benefits of extended module lifetime is the additional amount an electric utility can spend on module purchase and installation (initial investment) without lowering their rate of return on investment. The answer is shown to depend heavily on the rate of return earned on investor capital in electric utilities, and allowable depreciation schedules. Under a worst-case scenario, it was found that the utility can spend an additional 14% on modules and their installation if module lifetime is increased from 20 to 30 years. Under more favorable circumstances, similar to those experienced by utilities in recent years, the utility can increase its investment by 32% without any reduction in the rate of return on investment.

PVARRAY: A Software Tool for Photovoltaic Array Design

To optimize the performance of a PV array, a number of design factors and resultant system interactions must be considered: series and parallel wiring of a module and the array, module size, cell I-V curve, diode use and placement, failure rate, and replacement policy.

PVARRAY simulates array performance with selected variations of the design factors as well as the power output of the array over its lifetime. There are three major modules in PVARRAY: PVMAIN, for data input; PVPERF, which takes the input data and assigns random cell failures in different time intervals, and then simulates the I-V curves of the modules in the array and the system performance; and PVCD, which simulates module and array performance when each cell has a built-in diode.

At this time, more than 120 simulations have been performed representing a wide variety of cell, module and array specifications, and configurations. Results indicate that higher parallel redundancy is favored as is increasing diode protection. Replacement strategy is less important because a well-protected module rarely must be replaced. High-efficiency cells make a

AREA REPORTS

module more sensitive to failure, where the failure criterion is a back bias of 0.5 V for the module. These results were presented at the 25th PIM; viewgraphs are presented in the Proceedings.

Documentation of Models: CELLOPT and TCMLOSS

Two reports, titled CELOPT: A Grid Optimization Design Program, and TCMLOSS: Optical and Electrical Losses in a TCM, have been written.

CELOPT assists in the design of an optimal (i.e., a minimum power loss) collection grid on round or rectangular grids. The model takes into consideration the sheet resistivity of the photoconductive material, its current-voltage operating point, the resistivity of the grid material contact, and contact resistance. The model calculates the spacing of the grid lines and their width, the width of the busbar (one or two on the round cells and any number on rectangular cells), and grid-material thickness in such a way that the power losses in the cell because of shadowing or resistance are minimized. The model can also consider the effect of having a metallic ribbon as a conductive strap on the busbar.

TCMLOSS helps analyze and calculate the optical and electrical losses associated with using a transparent conducting material (TCM) on a solar cell. One part of the model calculates the short-circuit current density that is to be expected from the solar cell when it is covered with a TCM. It evaluates the transmission, reflection, and absorption losses due to the TCM while taking into account the indices of refraction and extinction of the materials (over wavelength), the solar spectrum, and the conversion efficiency of the solar cell. The model also evaluates the resistive losses of the solar cell when constructed in the typical series-connected configuration used with thin-film cells.

CELOPT can be used to describe the optimal grid pattern (if desired) for a TCM-coated solar cell, after using TCMLOSS to select the TCM with the best characteristics.

SAMIS: A Photovoltaics Factory in a Personal Computer

The SAMIS (Standard Assembly-Line Manufacturing Industry Simulation) computer program, which is the heart of SAMICS (Solar Array Manufacturing Industry Costing Standards), now runs on a personal computer (PC). SAMICS has been used by the FSA Project at JPL to provide standardized comparisons of prospective manufacturing processes and process sequences in terms of the prices that would have to be received for the final product to recover all costs and make a specified profit. The SAMICS Cost Account Catalog includes standardized prices of inputs and standardized formats for describing processes and companies.

In the PC version of SAMIS, the interface between the program and the user has been completely redesigned. The program is written in Turbo-Pascal. Previously, the user had to learn a vocabulary of SAMIS commands. Now, all operational choices are displayed and fully explained. The data

AREA REPORTS

management procedures provide a full-screen editing capability similar in use to that of a spread sheet. A summary of SAMIS PC enhancements was presented at the PIM; viewgraphs are reproduced in the Proceedings.

Module Degradation

Analysis has shown that module degradation rates have a significant impact on the economic value of PV modules. A degradation rate of as little as 0.5%/year will reduce the present value of the revenues generated by 7.4%, a factor of 0.926 (see table). A degradation rate of 2%/year reduces the economic value of the modules by 25.8%. The price escalation rate and the discount rate have only limited effects on economic losses due to degradation of module performance. For example, a price escalation rate of 8.5% and a discount rate of 12.5% reduces the loss due to a 0.5% degradation rate from 7.4 to 6.2%. Conversely, the losses are moderately increased when the price escalation rate exceeds the discount rate.

Price Escalation/Discount Rate, %

Degradation Rate	Equal	8.5/12.5	12.5/8.5
0.5	7.4	6.2	8.6
1.0	14.1	11.8	16.4
2.0	25.8	21.8	29.7

Life-Cycle Cost and Performance Comparisons of Photovoltaic Technologies

A methodology and a few preliminary results of a study to estimate the value of a PV system over its useful lifetime were presented at the PIM; viewgraphs are reproduced in the Proceedings.

To estimate the value of a PV system, all costs and revenues associated with the system over its lifetime must be considered as well as the initial purchase cost and installation charges. A study is in progress that compares the net present values of PV array systems made up of modules from several PV module production technologies. Various array configurations formed by altering the series-parallel circuitry of cells in modules and modules in arrays form the basis of the study. Module production technologies include state-of-the-art cells, and high-efficiency cells packaged in standard size modules (0.3 x 1.2 m) as well as large modules (1.2 x 1.2 m).

Three simulation models developed at JPL were used for the analysis: PVARRAY, which simulates array performance over time; SAMICS, which estimates the process value added and the manufactured module cost; and Lifetime Cost and Performance (LCP), which calculates hourly energy over time, pre-tax revenue from the system, and nominal cost streams over time. All of these programs can be run on an IBM XT or compatible PC.

AREA REPORTS

Use of the three models allows the analyst to identify system and performance trade-offs. The analyst can also determine the value of improvements to the lifetime power output of a system and how much additional expense can be added during cell and module fabrication to acquire that added performance. Results recommend greater parallel redundancy (when there is no replacement strategy specified) and, in the case of large modules, the lifetime economic value of bypass diodes is marginal.

Technology Assessments

Updated projections of the Cz and dendritic web cell technologies were completed. The Cz projection was for a state-of-the-art late 1980s factory producing 30 MW_p per year. It would produce 4 x 2 ft modules made up of modified square silicon cells cut from 5-in.-diameter ingots. The total value added came to \$167/M² (1982 dollars), with the ingot-growing step (including silicon material at \$36/kg) accounting for nearly 47% of the total. The next highest value added was ingot sawing at 24% (a 2-in./min plunge rate was assumed). The state-of-the-art web projections were for two production time periods: the late 1980s and the early 1990s. The factory size was 25 MW_p/year for both cases. The ribbon growth rate was assumed to improve from 20 to 30 cm²/min, and silicon costs were projected to drop from \$36 to \$28/kg (in 1982 dollars) over the period. The total value added for the late 1980s was \$138/M² (with ribbon, growth including silicon material, contributing 57% to the total), and the total value added for the late 1990s was \$112/M² (with ribbon growth, including silicon material, contributing 46%). Energy costs, at an assumed 15% module efficiency, were 17¢/kWh, 19¢/kWh, and 21.5¢/kWh for the 1990 web, and the 1980 web and Cz, respectively.

Sensitivity Study of Photovoltaics Program Goal Parameters

A PV system sensitivity study has been completed. The effect of individual parameters on system energy costs and the allowable trade-offs (consistent with the \$0.15/kWh energy cost goal) between cost and efficiency parameters were explored. Parameters considered in the study were: module cost and efficiency, tracking configuration, balance of system (BOS) efficiency, area-related BOS costs, power-related BOS costs, indirect costs, insolation, the fixed charge rate, and the energy cost goal.

Study results show that: (1) the two most critical components of system energy cost are module cost and efficiency (although a large portion of life-cycle energy cost is related to these items, they also exhibit the greatest potential for improvements through research), (2) one-axis tracking usually offers a lower energy cost than fixed or two-axis tracking systems, and (3) the future of photovoltaics depends on the changing economic status of competing generation technologies as much as it depends on R&D progress in PV technology because of the large influence of the energy cost goal on allowable module costs.

AREA REPORTS

SIMRAND Update

A newly developed random number generator has been incorporated in the FORTRAN ANSI-77 version of SIMRAND. The program is able to duplicate the results of the earlier versions. SIMRAND (SIMulation of Research AND Development Projects) is a general methodology that calculates a measure of performance for any R&D project having a number of systems or tasks that can be quantified in terms of probabilistic variables. The methodology models R&D projects as a network of tasks. SIMRAND I (no network search) has been used to estimate the price of producing silicon solar cell modules. SIMRAND II, which is now in progress, will build upon the methodology of SIMRAND I by incorporating a network search and optimization methodology.

The SIMRAND Computer Program is being put into the form required for JPL publication. The code will be prepared for submission to the Computer Software Management Information Center (COSMIC).

PROCESS DEVELOPMENT AREA

INTRODUCTION

The objective of the Process Development Area is, by conducting research in critical technology areas, to improve high-efficiency cell and module formation. Process research is grouped into three areas for convenience of reporting: junction formation, metallization, and directed-energy technology.

SUMMARY OF PROGRESS

The shift from surface preparation to directed-energy technologies has been fruitful. Results have proven useful in the other two technology areas of interest (junction formation and metallization) and, therefore, have been reported in those areas. A total of four papers and five new technology reports were submitted during this reporting period.

JUNCTION FORMATION

Westinghouse Electric Corporation's Advanced Energy Systems Division achieved successful sequential front and back diffusion. Additional work in simultaneous diffusion has also shown promise. Both excimer laser and quartz heat lamps have been used with the most successful run obtained with heat lamps.

The excimer laser pulse-anneal effort at Spire Corporation was completed. A cost analysis showed negative economic benefits for excimer laser annealing since no significant performance improvement was shown and the process costs were higher.

Arco Solar Corporation also studied excimer laser pulse-annealing as part of a broader laser processing study. Good results were achieved, but the subsequent analysis showed a slight performance penalty and no cost benefit.

METALLIZATION

MOD studies at Purdue were very successful. Addition of a bismuth compound has solved the adhesion problem. Use of ink-jet printing for direct line writing is still being studied.

Westinghouse Electric Corporation's Research and Development Center used the Purdue MOD material and an argon ion laser to produce cells with excellent efficiency, narrow lines, and good adhesion.

Photolytic decomposition was used by Arco Solar to deposit a tungsten film. The film was adherent, but sharp line definition would be difficult to achieve due to dispersion.

PRECEDING PAGE BLANK NOT FILLED

AREA REPORTS

The California Institute of Technology (Caltech) diffusion barrier research has demonstrated stable, non-reactive films on silicon. Both silver and gold metal overlayers were very non-reactive, while aluminum formed a eutectic at 550°C.

DIRECTED-ENERGY

Superwave Technology was successful in demonstrating depositions of silicon and silicon nitride. Use of their microwave plasma enhanced chemical vapor deposition (CVD) process has many potential benefits.

RELIABILITY AND ENGINEERING SCIENCES AREA

Materials Research: Single Junction Thin Film

Thin-Film Testing

A research forum on "Reliability and Engineering of Thin-Film Photovoltaic Modules" was held on March 20, 1985, at the Washington Marriott Hotel, Washington, D.C., immediately prior to the SERI Amorphous Silicon Subcontractors Review Meeting at the same location. The forum was the first technical meeting addressed to the technologies of thin-film modules and was attended by approximately 70 researchers. A key objective, which was successfully achieved, was the establishment of technical interchange between thin-film module researchers and those knowledgeable of the module technology developments resulting from the 10-year DOE crystalline-silicon module research effort. Sixteen technical papers were presented and a luncheon address was given by Charles Gay, Director of Research, ARCO Solar, Inc., on "The Need for Thin-Film Photovoltaic Module Reliability Research." A highlight of the meeting was the first public showing of Sovonics' stainless-steel cells, a Tedlar-EVA-Tedlar encapsulant system, and an injection-molded plastic frame. Amorphous-silicon power modules are also in production in the United States by ARCO Solar, Inc., and Chronar Corp. Among the papers presented were six by JPL personnel:

Cuddihy, E., "Encapsulant Selection and Durability Testing Experience."

Gonzalez, C., "Hot-Spot Heating Susceptibility Due to Reverse-Bias Operating Conditions."

Mon, G., "Module Voltage Isolation and Corrosion Research."

Moore, D., "Glass Breaking Strength: The Role of Surface Flaws and Treatments."

Ross, R., "Crystalline-Silicon Reliability Lessons for Thin-Film Modules."

Sugimura, R., "Electrical Safety Requirements: Implications for the Module Designer."

Through cooperative relationships with ARCO Solar, Chronar, and Solarex, a-Si submodules have been obtained and included in the various testing activities at JPL and at Clemson University. At Clemson, a-Si devices are now being subjected to a variety of environmental stress tests similar to those used for reliability attribute evaluation of crystalline-silicon-type cells over the past several years. Some of this work was reported in the paper, "Accelerated Stress Testing of Amorphous-Silicon Solar Cells," by J. Lathrop et al., presented at the Sixth European Photovoltaic Solar Conference in London, April 15-19, 1985.

AREA REPORTS

A series of experiments has been in progress at JPL to characterize the hot-spot performance of a-Si devices, using test samples supplied by the above manufacturers. These devices have been shown to exhibit hot-spot performance generally similar to that of crystalline silicon cells, but different in detail. Some experimental results are the reduction of cell shunt resistance from about 100Ω to about 10Ω , a back-bias voltage limiting phenomenon at about 8 to 10 V, and erosion of cell material under high currents. An innovation introduced in the testing was the application of back-bias voltage and forward current for microsecond to milisecond periods in order to observe response to electrical stress unobscured by the effects of thermal stress.

Under a JPL contract, Hughes Corp. has designed, manufactured, and delivered six 4 x 1 ft a-Si modules, using Chronar 1 x 1 ft submodules encapsulated in glass and EVA. The modules are undergoing environmental tests at JPL.

Collector Research: Flat-Plate Collectors

Advanced Module Development

Under a JPL contract to develop a high-efficiency module, Spire Corp. has manufactured a module using cells manufactured from FZ-grown silicon ingots. The area of each module cell is 53 cm squared. At 25°C , module efficiency is 13.7%, and encapsulated cell efficiency is 15.2%. A lower than normal nominal operating cell temperature (NOCT), 45°C , was achieved by the inclusion of a back-surface reflector (BSR) in the cell for the purpose of attaining higher efficiency at NOCT and longer module life.

As part of the above contract, Spire has processed batches of cells using the following five different sets of characteristics:

Type	Front Surface	Back Surface	Wafer Resistivity (ohm-cm)
1	Polished	Polished	1.5
2	Textured	Polished	1.5
3	Textured	Textured	0.3
4	Textured	Etched	1.5
5	Polished	Etched	1.5

AREA REPORTS

As required by the contract, quantities ranging from 25 to 50 cells of the first three types have been delivered to JPL. These will be supplied to Clemson University for performance of reliability tests.

In addition, four 12-cell minimodules are being manufactured by Spire using cells of types 1, 2, 4, and 5, respectively. After delivery to JPL, the electrical performance and NOCT of these minimodules will be measured, following which the optimum cell design will be selected as the basis for manufacture of additional minimodules and modules to be delivered on the contract.

Based on Spire measurements of cell efficiency at 25°C, the best results have been achieved with the fourth group of cells. In a 22-cell lot, the average efficiency was 17.7%, the best cell efficiency was 18.2%, and 10 of the cells had efficiencies of 18% or greater. Cells of 18% could be expected to permit manufacture of modules having 15% efficiency.

Systems Research: Module Reliability

Reliability Physics

1. Antisoiling Technology

The work on anti-soiling technology is reported in JPL Publication 84-72, "Antisoiling Technology: Theories of Surface Soiling and Performance of Antisoiling Surface Coatings."

2. Reliability and Durability of Electrical Insulation

Based on a JPL-developed theory, the alternating current (AC) intrinsic dielectric strength of EVA was previously reported as 5404 V/mil, at 60Hz. Recently, the same theory enabled an experimental determination of the direct current (DC) intrinsic dielectric strength of EVA, measured to be near 3450 V/mil. Given the capability to monitor the DC intrinsic dielectric strength of EVA (and other potantants), which by the JPL theory can be considered a true material property, an electrical insulation aging plan was jointly discussed and developed between JPL and Springborn.

In another effort, a set of module-like test specimens was fabricated for the purpose of studying electrochemical corrosion effects resulting from exposure at 500 V to a series of temperature/humidity combinations (see "Electrochemical Corrosion Research"). These samples featured polyvinyl butyrol (PVB) and EVA encapsulants, so it was decided to monitor certain encapsulant electrical parameters as the corrosion testing progressed. These parameters included Corona Inception Voltage (CIV) and a pulse count versus energy profile, taken before the test and after each constant temperature run. These data will be studied to ascertain the effects of exposure on the propensity of insulation to break down electrically.

AREA REPORTS

As of the 25th PIM, testing was in final stages and the data reduction and analyses will follow.

3. Electrochemical Corrosion Research

Two experiments were conducted during this time period: (1) electrochemical corrosion test on a-Si modules, and (2) multiparameter test on crystalline-silicon modules.

The a-Si tests were conducted at 85°C/85% RH/500 V, positive and negative polarity, on a-Si modules encapsulated in PVB and EVA. The purpose of these tests was to determine electrochemical corrosion mechanisms and rates in a-Si modules.

Significant observations and findings were:

- (1) Modules encapsulated in PVB exhibited significantly larger equilibrium leakage current levels, and significantly more severe degradation than modules encapsulated in EVA.
- (2) The only parallel-connected module to be encapsulated in PVB exhibited strange, squiggly, worm-like aluminum metallization loss patterns. This module has been submitted for surface analysis by a scanning electron microscope.
- (3) The most notable difference in degradation between a-Si and crystalline-silicon modules is the pinhole-like loss of silicon in amorphous modules. Quantifying the relationship between cell power output reduction and total charge transferred has revealed that the rate of amorphous-cell degradation is comparable to the rate of degradation of crystalline-silicon cells.

The multiparameter testing of crystalline-silicon module-like coupons was undertaken primarily to establish equilibrium leakage current levels to serve as input to an evolving module life prediction procedure. Also, several parameters were "tweaked" in order to determine module sensitivities to them.

The samples consisted of cell and frame electrodes encapsulated in PVB or EVA. Two electrode separations were tested: 50 mils and 500 mils. Samples included metal/polyester composite back cover films, Tedlar, and no-back cover film. Samples were electrified (cell-to-frame) at 500 V; a limited number were in positive polarity, and in negative polarity.

Samples were exposed at four constant temperatures (40, 55, 70, and 85°C) to a sequence of relative humidity values. Pertinent electrical data were collected before the test and after each constant temperature run. These included I-V curves, CIV partial discharge pulse height spectra, and the usual capacitance and loss factor.

AREA REPORTS

Although this test is still in progress, some of the findings are: (1) there is only a small sensitivity to gap size at very high humidities, and none at all at moderate humidities; (2) leakage currents were lower in negative polarity than in positive polarity; (3) leakage currents were higher in PVB coupons than in EVA coupons; (4) Tedlar reduced leakage currents in PVB coupons, but not in EVA coupons; (5) coupon leakage current data exhibit less sensitivity to temperature variation than bulk conductivity data (for PVB, no difference for EVA), but more sensitivity to relative humidity variations. These observations suggest the important contributions of surfaces and interfaces to the overall module conductance.

4. Water-Module Interaction Research

The purpose of this research is to develop an understanding of the role module moisture content, as a function of temperature and relative humidity, plays in determining overall module conductance. The results will be useful in the development of reliable design and life prediction procedures to be developed.

The primary approach is to use a Cahn Balance to measure water uptake of one sample while measuring surface and volume conductivities of a nearby identical sample while both are at temperature/humidity equilibrium conditions. Data acquisition has been automated. To date, sorption data on PVB at 40 and 55°C have been obtained. As yet, no reliable conductivity data have been obtained.

An alternative approach is to measure surface and volume conductivities as a function of ambient temperature and relative humidity. This was attempted, but the silver electrode material on the samples dissolved and migrated, severely degrading the samples before useful data could be obtained.

Another phase of this research involves injecting a known quantity of water into a module, sealing it, and measuring the surface and volume conductivities at various equilibrium temperatures. This research is still in progress.

Another phase of this research involves development of life prediction procedures and models. Moisture concentration and distribution inside the module encapsulant can be simulated analytically based on the encapsulant characteristics and environmental conditions. Leakage current can be computed based on the applied voltage level and the conduction correlation with respect to temperature and moisture levels. Accumulative charge transfer, which governs electrochemical corrosion of the module, can then be computed according to leakage current rate.

5. Reliability-Durability of Bonded Materials

Part of the chemical bonding structure developed between EVA and glass is a "silicon-oxygen" bond formed on the glass surface as a result of a

AREA REPORTS

chemical reaction between the silane coupling agent and the silanol groups which are natural on the glass surface. There are also "silicon-oxygen" bonds which are part of the normal bulk structure of glass. This examination of the chemically bonded interphase between EVA and glass by infrared (IR) spectroscopy cannot discriminate between the "silicon-oxygen" bonds generated by chemical bonding, and those within the bulk structure of the glass.

The IR frequencies associated with a chemical grouping (such as the "silicon-oxygen" bonded pair) is, in part, dictated by the atomic weights of each of the elements. Normal oxygen has an atomic weight of 16, but there is an isotope of oxygen having an atomic weight of 18, which is available in water forms called isotopic-water. The EVA-glass primer system requires water as a chemical ingredient, and it is being planned to use isotopic-water in place of normal water, such that ultimately "oxygen-18" will be introduced into the "silicon-oxygen" bond on the glass surface, to generate an IR frequency distinct from that of "oxygen 16" in the "silicon oxygen" bonds within the glass bulk.

Springborn Laboratories prepared a glass/EVA primer with isotopic water for the feasibility experimental effort which is being carried out by Dr. Koenig at Case Western. A technical review meeting with Springborn Laboratories was held to discuss and develop, if needed, alternate laboratory techniques relating to the chemical bonding structure between EVA and glass.

They are continuing with the development of advanced pottant formulations in order to maximize the reliability and service life of this critical construction element. Based on previous studies, the following additives have been incorporated into a candidate EVA formulation designated No. 18170. This formulation consists of: ELvax 150, 100 parts; Lupersol TBEC, 1.5 parts; UV-2098, 0.3 parts; and UV-3346, 0.1 parts. This compound has been formed into (tensile) test specimens and has started exposure under RS/4 (50°C), RS/4 (85°C), and RS/4 with water spray. The formulation evacuated every 2,000 h for: tensile strength, ultimate elongation, modulus, gel content, swell index, and yellowing and UV absorption.

A different approach to accelerated aging of candidate encapsulation materials is being evaluated, namely, the use of Outdoor Photothermal Aging Devices (OPTAR). These are devices recently constructed at Springborn Laboratories that constitute a new approach to accelerated weathering.

6. Photothermal Stability Research

Samples of EVA were thermally aged inside a dark oven at 120°C to yellowing chromophores. These yellow samples were then photoirradiated at various intensities (suns) and temperatures to evaluate the rate of photoinduced bleaching. Evaluation of yellowing of EVA with respect to temperature cycling was also studied. These results will be incorporated into an analytical model that can be used to predict yellowing behavior of EVA.

AREA REPORTS

The tabulation below is a summary of yellowing results to date:

T_1 °C	Environmental Conditions	Total Aging Time	Preliminary Results
120	0 sun ^a	10 weeks	Generation of yellowing components steadily rose throughout aging and continues to yellow
	1 sun	16 weeks	Reached a steady-state yellowing ≈ 1.25 absorbance units. Slower rate of yellowing than previous data at 6 suns
	2 suns	10 weeks	Yellowing rate dropped considerably after first 4 weeks. It seems to have reached steady state
135	0 sun ^a	4 weeks	Yellowing at faster rate than at 0.5 suns
	0.5 sun	4 weeks	Steadily yellowing, but at slower rate than at 1 sun and 0 sun
	1 sun	16 weeks	Steadily continues to yellow signifying photothermal yellowing overcame photoinduced bleaching

^aDark oven.

AREA REPORTS

Theoretical modelling of photodegradation of EVA continued at the University of Toronto. Additive effects on degradation rates of EVA were studied. Computer model rate constants were adjusted to match data obtained from outdoor exposure tests. Based on the similarity of results on EVA and pure polyethylene exposed in an UV and pure polyethylene exposed in an UV accelerator and in outdoor sunlight, it seems that the inclusion of processes relating to ester functionalities in this model is unnecessary at this stage.

Polytechnic Institute of New York, Brooklyn, continued its work on synthesis of efficient UV stabilizers that can be incorporated as permanent stabilizers into condensation and addition-type polymers. Their work on the incorporation of UV stabilizers in polyesters and polycarbonates was completed. They also continued their efforts to synthesize monosubstituted compounds in the series of new UV stabilizers of benzotriazole substituted 2,4-dihydroxy-acetophenone BAP, and MBBP. Characterization of these compounds is now in progress.

7. Solar Cell Reliability Testing

Reliability testing has continued at Clemson University on both encapsulated and unencapsulated cells, in accelerated stress tests, and in outdoor real-time environmental durability tests. The Clemson University report for 1984, "Photovoltaic Cell Reliability Research," was issued. Included are the startup activities on reliability-attribute testing of a-Si devices. Some results of the a-Si testing is reported in the paper, "Accelerated Stress Testing of Amorphous-Silicon Solar Cells," by J. Lathrop, et al., presented at the Sixth European Photovoltaic Solar Conference, London, April 15-19, 1985. Related work, including surface analysis and depth-profile investigations of a-Si cells performed by Auger microprobe, is described in a paper by E. Royal of JPL and J. Lathrop of Clemson, titled, "Observed Changes in a-Si H Cell Characteristics Due to Long-Term Temperature Stress," presented at the IEEE Photovoltaic Specialists Conference, October 1985, in Las Vegas, Nevada.

A new and possibly important a-Si cell characteristic response has been observed at Clemson University as a result of reliability stress testing. The following phenomena were observed:

- (1) Amorphous-silicon cells of a specific type, which had moderate to high maximum power output characteristics prior to being stressed, were later observed to have a small (approximately 4%) increase in power.
- (2) Amorphous-silicon cells of the same type as above, with low maximum power output characteristics prior to being stressed, were later observed to have experienced a large increase in power (approximately 150%) following similar stress time periods.

These observations were made during temperature step-stress testing. All cells used in these tests were from the same monolithic submodule. Until more tests are performed, no conclusions can be made on the value of a "burn-in"-type step.

AREA REPORTS

8. Module Temperature-Humidity Reliability Testing

The development of humidity degradation rates and the identification of key electrochemical failure mechanisms continued for generic module designs based upon temperature/humidity testing cycles and data from solar radiation surface meteorological observations (SOLMET) weather tapes. Block V and several commercial designs were combined in the minimodule test set for endurance testing at Wyle Laboratories. This long-term test series included module samples for charge transfer and dual polarity tests under a voltage stress of 250 V, simulating central-station installations. The scheduled environments included: (1) 55°C/40% RH and 55°C/85% RH; (2) 70°C/40% RH and 70°C/85% RH, and (3) 85°C/40% RH and 85°C/85% RH. The test phase was completed for the least-environmental-stress condition of 55°C/40% RH and 55°C/85% RH and is currently under examination. Minimodules featuring dendritic-web cells and thin-film module designs will be added to the existing test set and exposed to 85°C/85% RH and 85°C/0% RH environmental conditions following the data reduction and analyses activity.

9. Reliability Prediction and Management

The characterization of aging mechanisms in encapsulants because of photothermal degradation has led to development of an analytical structure for assessing the significance of thermal-UV-induced transmission losses in ethylene vinyl acetate in simulated 30-year field exposure at various U.S. sites. This work was reported in a paper entitled, "Predicting Field Performance of Photovoltaic Modules from Accelerated Thermal and Ultraviolet Aging Data," by C. Gonzalez, R. Liang, and R. Ross, presented at the Biennial Congress of the International solar Energy Society (ISES), June 23-29, 1985, Montreal, Canada.

Module and Array Engineering Sciences

1. Module Flammability Research

During this reporting period, three separate test series were completed (October 23-24, 1984; March 12-14, 1985; and May 21-22, 1985). The October test series featured Refrasil, a relatively expensive glass cloth manufactured by HITCO Materials Division that was impregnated with a proprietary, high-temperature coating material (also from HITCO). The test results were significant because it was the first time that a glass cloth material passed the UL 790, Class A, burning-brand test.

Because of the high cost of Refrasil, the second test series (March 1985) focused on lower-cost glass cloths using the proprietary, high-temperature material. A key test result was that lower-cost glass cloths, coated with the HITCO proprietary material, were also capable of passing the Class-A burning-brand test. Another finding was that the edges of the module have minimal fire resistance.

AREA REPORTS

The third test series (May 1985) included tests of advanced module edge-seal designs using high-temperature materials. These test results indicated that HITCO M-44 is suitable for the temperatures generated by an A-brand placed over the edge of an aluminum module frame. It remains, however, to implement this candidate material as part of a module-production, edge-seal system. This task does not seem to have an easy solution because the material was subsequently found to be water soluble.

Also, the May test series yielded a surprisingly high number of failures. Subsequent discussions indicated that the coating formulation had been slightly altered, and the coating mixture had been allowed to stand (permitting some of the ingredients to settle) before the coating operation. The consensus was that the coated glass cloth used in this series of tests was not identical to samples tested previously.

During this reporting period, ARCO Solar was joined by Solavolt International and Solarex Corporation who agreed to join the cost-sharing program by providing modules for flammability testing.

Springborn Laboratories plans to investigate two approaches to upgrading the flammability rating of PV modules containing hydrocarbon pottants such as EVA or PVB. The first, which has been discussed in a previous Progress Management Report (PMR), will be to incorporate anti-flammability additives in the pottant layer that is situated on the back side of the solar cells.

Concurrent with the JPL in-house effort described above, Springborn's second approach is to explore back-cover concepts based on flexible and tempered thin-glass materials, and on composites constructed with inorganic polymers and high-temperature reinforcement mats or scrims. Details of these two efforts are covered below in the task entitled, "Reliability-Durability of Bonded Materials."

Also, a paper titled, "Development and Testing of Advanced Fire-Resistant Photovoltaic Modules," by R.S. Sugimura, D.H. Otth, and R.G. Ross, Jr., was presented to the Institute of Environmental Sciences (IES) at its annual meeting in Las Vegas, Nevada, April 29 to May 3, 1985.

Future plans include another test series for October 1-3, 1985. The focus will be on validating the formulation and process coating of candidate materials (such as HITCO glass cloth coated on both sides with the proprietary, high-temperature material), and the testing of candidate, high-temperature, edge-seal/gasket materials suitable for application as part of a module-production system.

2. Bypass and Blocking Diode Research

Research continued on defining heat-sink requirements for diodes to determine if low diode-attributed costs are attainable while maintaining diode reliability. A series of diode tests, including tests on four types of

AREA REPORTS

diode construction, were completed that established magnitudes and limits of application for measuring currents used in a procedure for determining diode junction temperatures under worst-case field environments. Measuring currents selected for the procedure provided a good linear response with temperature (did not heat diode junction significantly), and were then implemented in a series of tests using full-sized Block V and commercial modules. This second series of tests verified the adequacy of the procedure in extrapolating measured junction temperature of diodes with heat sinks to 100 mW/cm² and 40°C field conditions.

The second series also included diode-junction temperature measurements on diode assemblies typically used in central-station arrays, mounted behind large PV panels and bypass high (60 A) source currents. For these externally mounted diodes, a limited amount of heating is received from the PV panel back surface by radiation, which influences the junction temperature.

The results were useful in establishing a cost-effective qualification test procedure to assess diode reliability and specific design criteria for p-n and Schottky diodes used in PV applications. Design criteria were established in terms of allowable diode junction temperatures for two conditions: a maximum operating junction temperature (based on manufacturer limits), and a derated junction temperature (for long life). Test results have shown that of the two diode criteria (derated temperature and maximum operating), the derated temperature is the more stringent design criterion. The derated value is 125°C for p-n diodes, and 75°C for Schottky diodes. The bypass diode effort was summarized in a technical paper entitled, "Development of Design Criteria and a Qualification Test for Bypass Diodes in PV applications," by D.H. Otth, et al., and presented at the 31st Annual Meeting of the IES in Las Vegas, Nevada, on May 1, 1985.

Module Performance and Failure Analysis

1. Module Environmental Testing

All testing on the Block V modules has been terminated with successful completion of the Block V Qualification Tests by all five manufacturers: ARCO Solar, General Electric Co., MSEC, Solarex Corp., and Spire. The designs and performance of the final modules are described in JPL Publication 85-34, "User Handbook for Block V Silicon Solar Cell Modules," May 15, 1985, by M.I. Smokler, and in the paper, "Block V Module Development and Test Results," by the same author, presented at the Sixth European Photovoltaic Solar Energy Conference, April 15-19, 1985, London.

Commercial modules received from several manufacturers in Europe and Japan are mostly in the latter stages of environmental testing. Amorphous silicon modules from ARCO Solar, Chronar, and Hughes are also now under test. The new system developed by L. Wen of JPL for measuring NOCT has proved very effective in reducing the time needed for that measurement.

AREA REPORTS

Results of environmental testing performed during the report period are shown in the following tabulation:

Module Code	Quantity	Test	Results
S5	4	T-50	These were improved modules to resist delamination. Two had no delamination, two had some
	4	HF-10	Delamination was somewhat worse. Isolation to frame dropped during testing
Y5	2	T-200	Power was satisfactory, but there were 10 and 12 cracked cells, respectively
U5	4	T-50 HF-10	Retest of modules with improved J-boxes. J-boxes were satisfactory. There was some darkening of bus bars and interconnects
F2	6	T-50	Extensive delamination and blistering of back surface material, brown stains, and encapsulant splits
	4	HF-10	Some new areas of delamination. Some of the previous delamination disappeared
	4	MI-10K	Not performed because of mounting hole discrepancies
	2	T-200	Much of the T-50 delamination has disappeared
W2	6	T-50	All satisfactory
	4	HF-10	
	4	MI-10K	
	2	T-200	
R3	6	T-50	Satisfactory
	4	HF-10	One module had delamination near the frame
	4	MI-10K	One module had an unacceptable power loss of about 8%

AREA REPORTS

Module Code	Quantity	Test	Results
	2	T-200	Satisfactory
	6	Continuity	One module exceeded the permissible 1V drop at 1.15 V
KP a-Si	4	T-50	Electrical failures at 6, 8, 17, and 47% power losses, respectively. Back-surface material wrinkling and delaminating. Delamination at module glass and cover glass, all modules
	2	HF-10	Electrical failure at 96 and 98% loss, respectively. Continued delamination at glass surfaces. Cell discoloration on one module
KA a-Si	2	T-50	One module had intermittent continuity loss during test and marginal failure at 5.6% power loss after the test
	2	HF-10	100% electrical loss, both modules. One module had two large areas of back surface delamination
UA a-Si	4	T-50	Plastic frame bowed slightly
	4	HF-10	Severe warpage of the frames. Warped frames interfered with power measurements. Removal of frames showed two modules had excessive power losses
J1	6	T-50	Back-surface material wrinkled
	2	T-200	Satisfactory
	4	HF-10	One module had one cracked cell, another had three cracked cells. Isolation from frame dropped to less than 1 M ohm (compared to over 100 M ohm pretest) for the three modules
D3	6	T-50	Satisfactory
	2	T-200	J-box sealant darkened

AREA REPORTS

Module Code	Quantity	Test	Results
	4	HF-10	Satisfactory
	4	MI-10K	Satisfactory
Q5	6	T-50	Electrical failure of five modules at 12-15% power loss
	2	T-200	Open circuit, both modules. Eleven and 26 broken interconnects, respectively
E2	6	T-50	Satisfactory
	4	HF-10	All cell edges discolored. Bus bars and gridlines discolored. J-box adhesive yellowing
O1	6	T-50	Some sealant extruded at most of the frame corners

T-50 = 50 thermal cycles, -40 to +90°C.

T-200 = 200 thermal cycles (150 plus original 50).

HF-10 = 10 humidity/freeze cycles, 85°C/85% RH, then -40°C, 10 cycles (days).

MI-10K = Mechanical cycling, 50 lb/ft² (2400 Pa) alternating, 10,000 cycles.

Continuity = Electric current at twice the I_{sc} across joints in the metal frame for 2 min. Allowable voltage drop, 1 V.

2. Acquisition of Reliability Data from Large Photovoltaic Applications

A meeting on December 19, 1984, between representatives of DOE, Sandia, and JPL confirmed the necessity for a collaborative effort to acquire field data through joint inspection tours of selected large PV field sites to identify, analyze, and quantify module and array failure mechanisms.

An ARCO Tedlar-front-surface module, similar to those used on the John Long House, was submitted for examination by V. Risser of the New Mexico Solar Energy Institute. There is extensive cracking of those portions of the Tedlar surface that have been exposed to UV for about 18 months. Rogers, DuPont Co.,

AREA REPORTS

has determined that the Tedlar formulation is not the most suitable for PV modules from the standpoint of temperature and UV, but does provide 10% better light transmission characteristics than other grades of Tedlar.

Portions of Tedlar from this same ARCO Tedlar-front-surface module, which have not been exposed to UV because of its overlapping shingle installation, are currently undergoing accelerated UV exposure testing. Also, samples of another ARCO Tedlar-front-surface module, which has never been installed in the field, is also being tested.

Related to this same activity, samples of clear Tedlars, used as module front covers, and Tedlar-laminates, used as module rear covers (i.e., T-P-T, T-A-T, and T-Al-P-T) have been received from DuPont and Gila River Products, respectively, for study by JPL. The samples will be used in both accelerated and outdoor UV exposure testing to determine long-term durability characteristics.

3. Electrical Measurements

A major advance has been made by filtering the large-area pulsed solar simulator (LAPSS) so that its irradiance spectrum closely matches that of the standard ASTM AM1.5 global spectrum in ASTM E 892-82. The filter is removable, so the prior capability to simulate the standard ASTM AM1.5 direct normal spectrum has been retained. Therefore, whether a direct normal or a global spectrum is specified, it is now possible to make accurate measurements of devices from cell size up to modules or small arrays as large as 6 ft on one side, without the need for specially matched reference cells or the need to perform spectral response measurements and mismatch factor corrections. This capability has been useful for measurement of the large Block V modules and to assist the Sacramento Municipal Utility District (SMUD) by measuring arrays of modules from three manufacturers destined for use in the second (1 MW) phase of the SMUD PV central power station. Another advantage of the filtered LAPSS capability is that it enables rapid inexpensive secondary calibration of reference cells, a service that has been performed to assist several manufacturers.

To permit more accurate measurement of a-Si devices, reference cells have been manufactured from wide-band crystalline silicon cells and packaged with filters such that the resultant spectral response is representative of the response of a-Si devices.

In order to help the PV community resolve discrepancies among measurements performed by various organizations, JPL has participated in a round-robin measurement exercise organized by British Petroleum, involving six reference cells and 36 modules, with the measurements being performed by JPL, the Royal Aircraft Establishment, and the Commission of the European Communities (CEC) Joint Research Centre (JRC), at Ispra, Italy. Also, JPL is a participant in a round-robin measurement project initiated by the Summit Working Group and managed by the CEC JRC. This seven-nation effort involves manufacture and calibration of 18 reference cells (including four supplied by JPL) by seven nations. JPL has completed its measurements and has also arranged for SERI to make the same measurements.

AREA REPORTS

4. Module Failure Analysis

Failure analysis was performed on five polycrystalline silicon PV modules (L-081151, L-082405, L-0743070, L-0745058, and YL5P-134) from Solarex Corp. Two polycrystalline Solarex Corp. modules (L-081151 and L-082405) were received from Pulstar Corp. for failure analysis. These modules were field-installed approximately 1 year (L-082405) and 6 months (L-0831151), respectively, before experiencing thermal intermittence. Severe power degradation was reported when they were heated to 150°F from 75°F. At the Failure Analysis Laboratory, the thermal intermittence was not observed when the modules were temperature-cycled to 100°C several times in the Sun-u-lator. However, a sharp change in the dark I-V curve was observed when pressure was applied by hand to small areas on the backside of each module. Subsequent temperature cycling to 85°C in an oven showed both modules to exhibit thermal intermittence, as evidenced by a sharp change in the dark I-V curve, although the onset of this intermittent behavior followed no simple pattern. Visual inspection of several interconnect-to-cell solder joints showed poor wetting and dewetting, with open solder joints present in the areas that displayed pressure-sensitive intermittent behavior. Mechanical stress test and LAPSS temperature testing were completed for the two polycrystalline Solarex modules (L-0743070 and L-0745058) from Sandia National Laboratories. The reported failure could not be verified. However, a telephone conversation with E. Daniels of Solarex Corp. revealed that the soldering technique used to attach the interconnect to the cell backside is similar to that used in two other Solarex modules from the Pulstar Corp., recently analyzed here. Solarex PV module YL5P-134 was also received for failure analysis. A report of a possible intermittent, temperature-dependent open-circuit condition was not verified for this module. However, it was noted that the terminal Solarlok connectors did not clamp very snugly to the terminal posts.

Support was also provided to the Module and Array Engineering Science Task by locating bypass diodes with x-rays and by providing external electrical connections to these diodes. Work was performed on three polycrystalline modules (one each from Applied Solar Energy Corp., Solar Power Corp., and Solarex Corp.).

Thin-film a-Si commercial modules were being used to investigate the failures of the design and performance characteristics of existing a-Si technology. To improve the image quality of the microscopic defects of amorphous thin-film silicon solar cells, a Y modulation mode was added to the normal mode of the Solar Cell Laser Scanner.

The short-circuit currents of a-Si modules made by Sanyo, ARCO, and Chronar were measured using three different light sources. One was the Sun-u-lator, which uses an array of tungsten tubular lamps with some IR filtration. The other two were the LAPSS, which uses a high-power xenon lamp, and a portable GE reflector halogen Quartz-line lamp (lamp code ELH). The illumination intensity of the Sun-u-lator and GE light sources were referenced by the JPL Heliotek Cell, Mariner 69/71 type, whereas a pseudo a-Si cell was used to reference the LAPSS light source. With the illumination intensity at one sun as measured by the respective reference cells, it was found that the short-circuit current of each of the modules was four to five times greater under illumination by the GE or LAPSS light sources than by the Sun-u-lator light source.

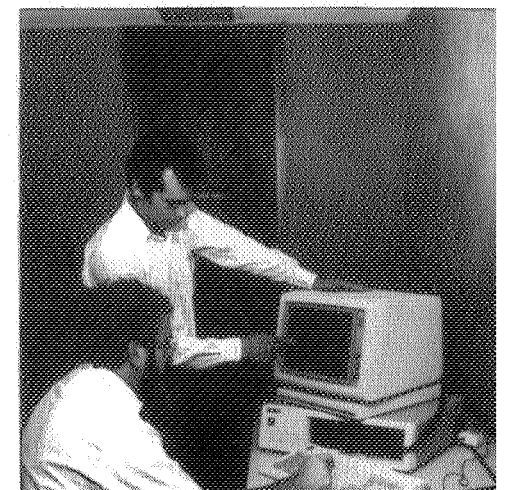
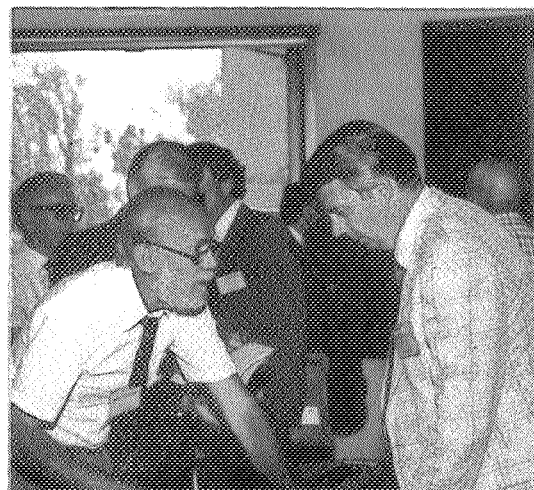
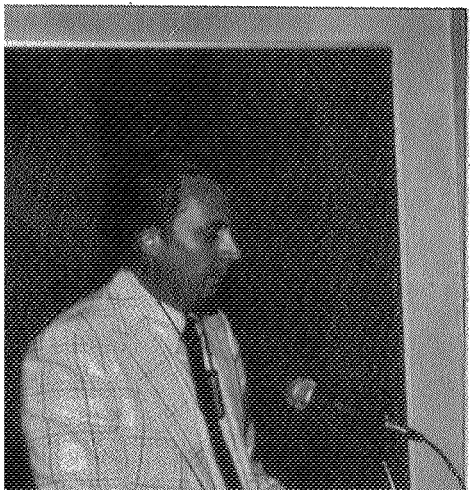
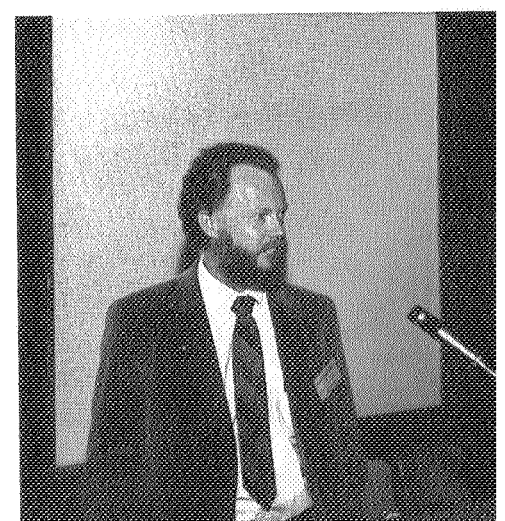
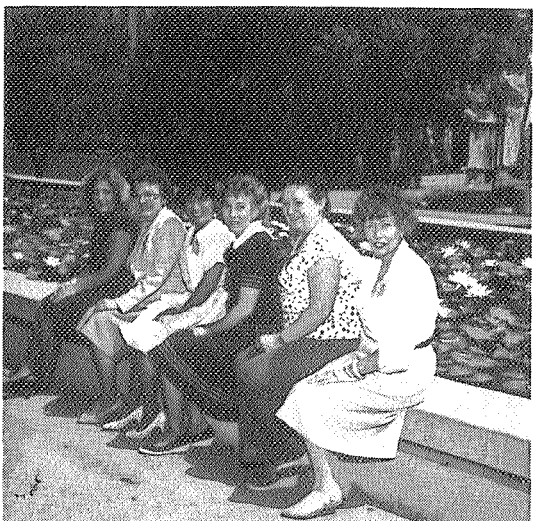
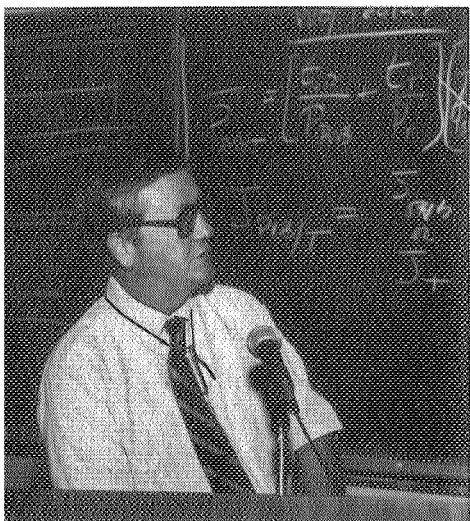
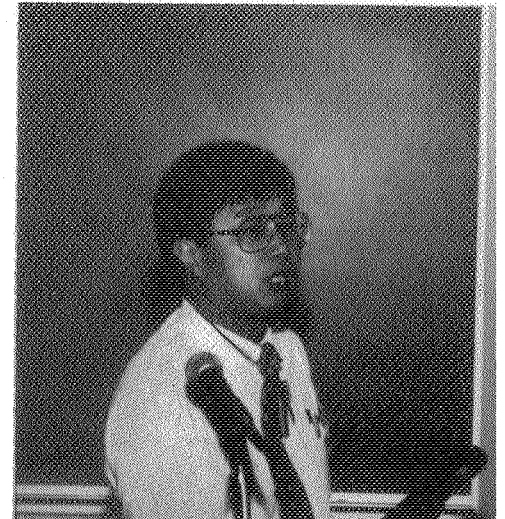
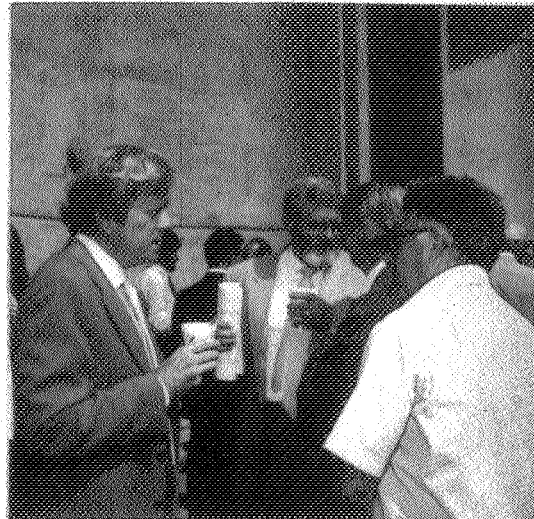
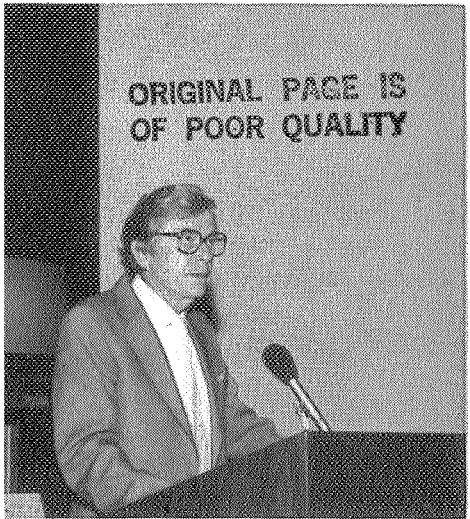
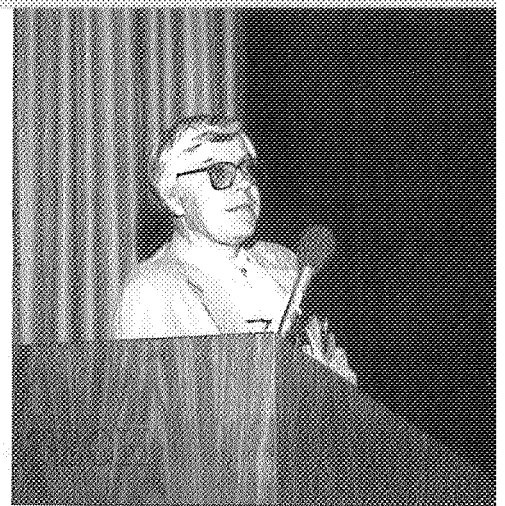
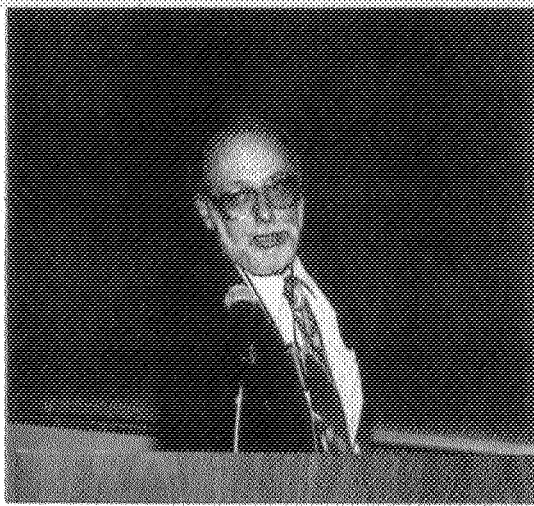
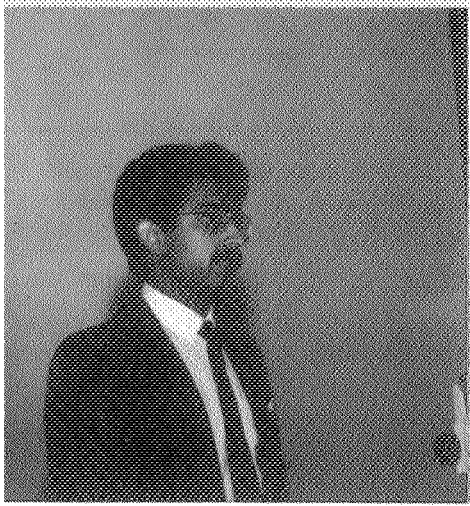
AREA REPORTS

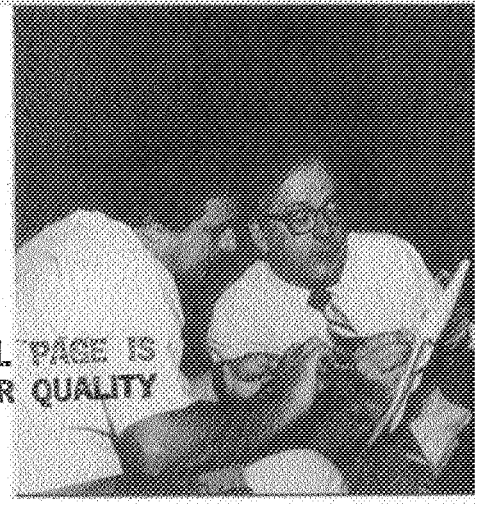
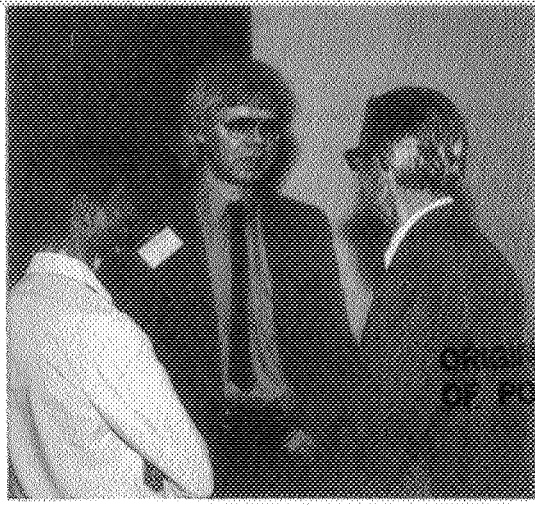
Photocurrent response of the thin-film a-Si solar submodules from Chronar Corp. has been closely analyzed to find the dependence of the photogeneration rate. A higher-efficiency cell generates photocurrent by a 1.05 exponent of the surface generation rate of free carriers within the experimental range (2.1 to 5.6×10^{18} photons/cm²-s). However, for a lower efficiency-cell, there are clearly two different photocurrent generation ranges. Below 5.1×10^{18} photons/cm²-s, the cell generates photocurrent by a 0.90 exponent of the surface generation rate of free carriers; above 5.1×10^{18} photons/cm²-s, the cell generates photocurrent by an exponent of 0.48. This means that the active areas of cells are of different quality, even though each active area is fabricated by the same process. Because the tests were done at room temperature under more than 5 suns, the results could be properly interpreted by the free carrier transport model. The same-quality cells in a module can have different performance characteristics because of the inter-connecting processes. This means that the cell-coupling process is as important as the quality of the multilayers. Photocurrent response of the thin-film a-Si modules was compared with the series resistance of the individual cells of the module, but no close correlation was observed.

Photocurrent responses of the series-coupling edges of the thin-film a-Si solar modules from three different manufacturers (Sanyo 7703-2, Chronar 4, and ARCO G100-108) were compared. The "whisker" signals of the responses were closely compared with the coupling structure of each module, which were processed by laser scribing and/or masking.

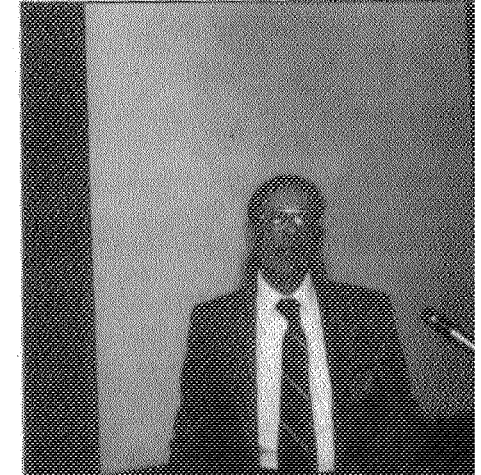
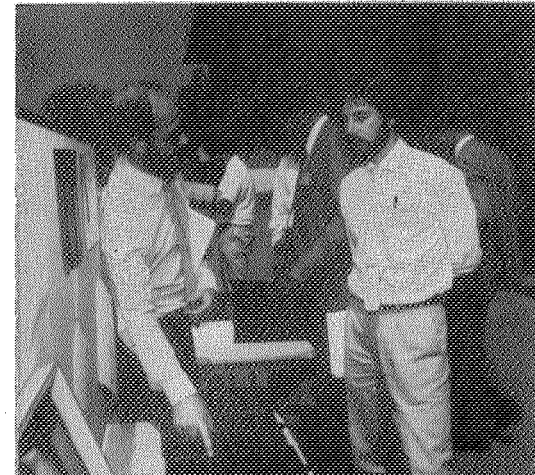
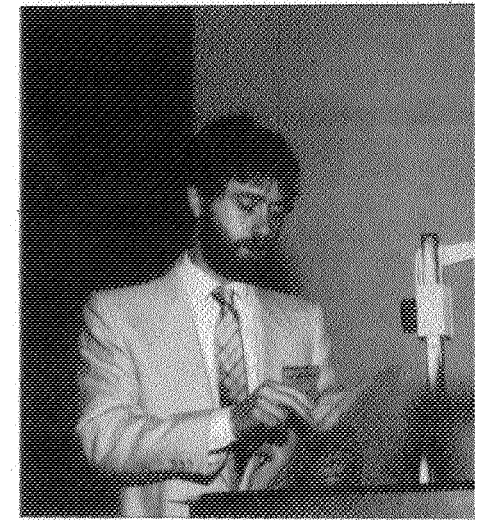
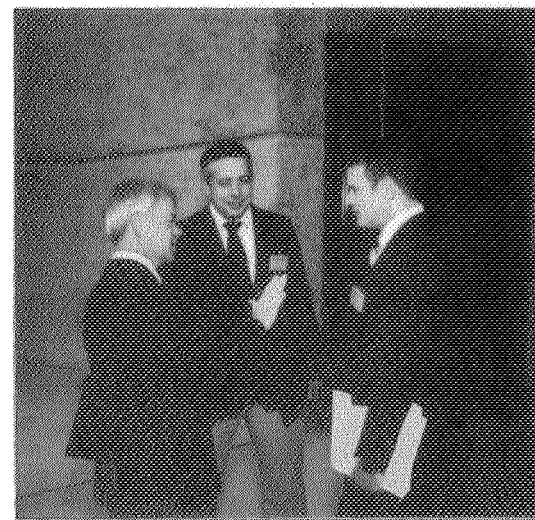
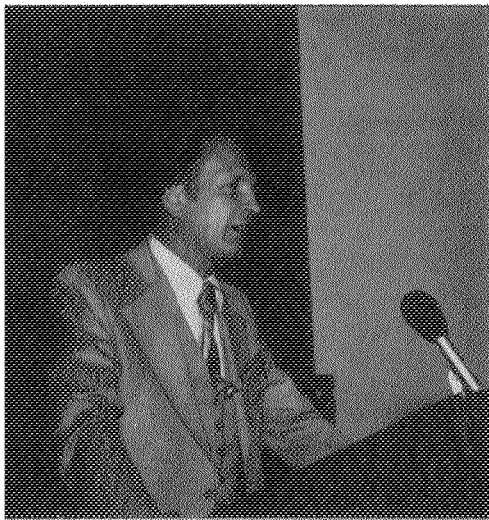
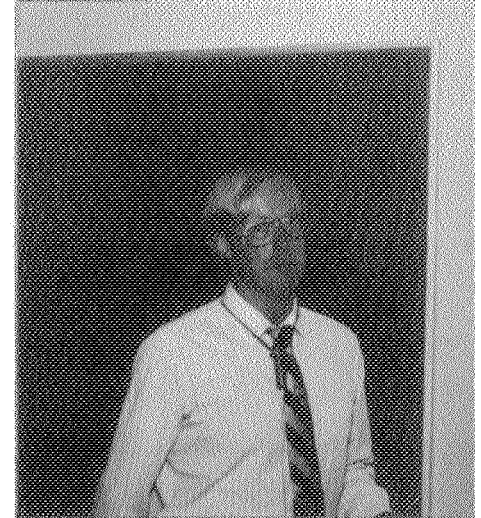
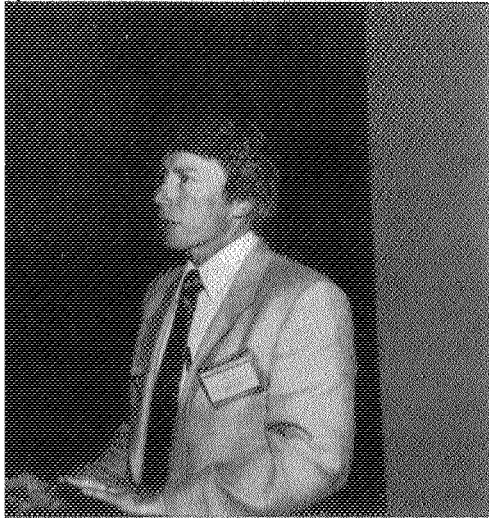
ARCO Genesis a-Si modules were received for failure analysis. All four of these modules exhibited significant power loss (11 to 30%) after humidity-freeze testing of 10 cycles, and also considerable distortion and warpage of the frame. It was noted that the distorted frames covered a large percentage of the cell surface areas for the cells adjacent to the edges of the modules. Power was completely recovered for two of the modules after the frames were removed. Investigation is continuing in order to account for the 8 to 10% power loss remaining with the other two modules.

Two papers were presented. "Effects of Excitation Intensity on the Photocurrent Image of Thin-Film Silicon Solar Modules" was presented by Q. Kim, A. Shumka, and J. Trask at the meeting of the American Physical Society on March 24-29, 1985, in Baltimore, Maryland [Bull. Am. Phys. Soc. 30, 355 (1985)]. "Photocurrent Image of Amorphous Silicon Modules" was given at the 25th PIM by Q. Kim. A paper on "Effects of Excitation Intensity on the Photocurrent Response of Thin-Film Silicon Solar Modules," by Q. Kim, A. Shumka, and J. Trask was also accepted to be published in Solar Cells in 1986.





ORIGINAL PAGE IS
OF POOR QUALITY



PROCEEDINGS OF THE 25th PROJECT INTEGRATION MEETING

**ORIGINAL PAGE IS
OF POOR QUALITY**

PROCEEDINGS

INTRODUCTION

The 25th Project Intergration Meeting (PIM) of the Flat-Plate Solar Array Project of the Jet Propulsion Laboratory was held at the Pasadena Center, Pasadena, California, on June 19 and 20, 1985.

The theme for the 25th PIM was Progress in Processing of Higher-Efficiency, Low-Cost Solar Cells reflecting recent increased emphasis on high efficiency by the National Photovoltaics Program, sponsored by the U.S. Department of Energy.

The results of the FSA Research Forums on crystal growth for High-Efficiency Silicon Solar Cells, held at San Diego, California, December 3-4, 1984, and on reliability and engineering of thin-film photovoltaic modules, held at Washington, D.C., on March 20, 1985, were summarized. Plans and activities within FSA that are directed toward higher efficiency were presented, and specific key issues were discussed. In addition, reports on progress in photovoltaic technologies in other areas were presented.

The FSA Project Integration Meetings continue to enable communication between the Government and the private photovoltaics community about present and future photovoltaics activities. This exchange is essential in assessing recent progress in identifying trends and new developments, in integrating research activities, and in guiding near-term and long-term planning, decision making, and adjustments in Project priorities.

A summary of Plenary Session reports is presented, followed by visual summaries of the reports given in the technical sessions.

PRECEDING PAGE BLANK NOT FILMED

61, 62

AGENDA

25th FLAT-PLATE SOLAR ARRAY
PROJECT INTEGRATION MEETING

WEDNESDAY, June 19, 7:30 a.m.

7:30 a.m. Registration in Lobby of Ramo Auditorium, California Institute of Technology

8:30	Announcements and FSA Overview	Ramo Auditorium	W. Callaghan (JPL)	10 min.
8:40	DOE Comments		M. Prince (DOE)	20 min.
9:00	Summary of Solar Cell High-Efficiency Research Results		R. Kachare (JPL)	25 min.
9:25	Overview of Processing Activities Directed Toward Higher-Efficiency, Large-Area, Crystalline-Silicon Solar Cells and Modules That Would be Economical To Produce		D. Bickler (JPL)	25 min.
9:50	BREAK			30 min.
10:20	Summary of <u>Process Research Analysis</u> Efforts for Higher-Efficiency Crystalline-Silicon Solar Cells; Accomplishments, Potentials and Limitations		D. Burger (JPL)	20 min.
10:40	Summary of <u>Metallo-Organic Process</u> Technology Efforts Leading to Higher-Efficiency Crystalline-Silicon Solar Cells; Accomplishments, Potentials and Limitations		B. Gallagher (JPL)	20 min.
11:00	Summary of <u>Directed Energy Process</u> Technology Efforts Leading to Higher-Efficiency Crystalline-Silicon Solar Cells; Accomplishments, Potentials and Limitations		P. Alexander (JPL)	20 min.

Research Forum Summaries

11:20	Crystal Growth for High-Efficiency Silicon Solar Cells		K. Dumas (JPL)	20 min.
11:40	Reliability and Engineering of Thin-Film Photovoltaic Modules		E. Royal (JPL)	20 min.

12:00 LUNCH

1:15	Parallel Technology Sessions			
	Advanced Silicon Sheet	Ramo Auditorium	A. Briglio (JPL)	4 hrs.
	Module Development & Engineering Sciences	Baxter Lect. Hall	M. Smokler (JPL)	4 hrs.
	Process Development	Beckman Labs.	D. Bickler (JPL)	4 hrs.

5:15 SOCIAL HOUR Alumni House

THURSDAY, June 20

8:00 a.m.	Parallel Technology Sessions			
	High-Efficiency Device Research	Ramo Auditorium	D. Burger (JPL)	4 hrs.
	Reliability Physics	Baxter Lect. Hall	R. Ross (JPL)	4 hrs.
	Silicon Material and JPL Web Team	Beckman Labs.	R. Lutwack (JPL)	4 hrs.

12:00 LUNCH

1:30 p.m.	Future Directions Late News	Ramo Auditorium		
-----------	--------------------------------	-----------------	--	--

3:00 BREAK

3:20 Summaries

4:20 End of Meeting

PRECEDING PAGE BLANK NOT FILMED

Plenary Sessions

SUMMARY

W.T. Callaghan, Manager of the Flate-Plate Solar Array (FSA) Project, opened the meeting by welcoming the participants to the 25th Project Integration Meeting (PIM). He announced that FSA will be phased out by the Jet Propulsion Laboratory (JPL) as of the end of September 1986, as requested by the U.S. Department of Energy (DOE). After that, JPL will support the Solar Energy Research Institute (SERI) in specific DOE photovoltaic (PV) activities in place of FSA. Remaining FSA efforts, through FY86, must be capable of reaching meaningful technical results within that time period and offer significant assistance to the U.S. PV industry through technology transfer.

Morton Prince of the DOE National Photovoltaics Program Office confirmed that the FSA Project is being phased out at the end of FY86. The Project has been successful in developing the fundamental technology for effective terrestrial use of crystalline-silicon PV modules. The technology to bring the manufacturing costs down to the original goals has not been completely achieved, but a viable crystalline-silicon PV industry and user community has been established. He also briefly explained that plans are being devised to continue some of the crystalline-silicon research efforts. DOE has formed a group to evaluate which specific efforts should be continued and how these efforts should be funded.

A.H. Kachare, Manager of the FSA Device Research Task, summarized high-efficiency solar-cell activities supporting efforts to achieve the DOE Five-Year Plan goals. Specific objectives are to identify and resolve key generic problems that limit cell efficiency to below theoretically predicted values and to design and fabricate cells having efficiencies $\geq 20\%$ (AM1.5). Theoretical curves for various p-n junction cells were shown. A chart depicting the effects of practical barriers on cell efficiency along with the modeling parameters and cell design parameters used in the analyses was described. The usefulness and present limitations of the existing modeling capabilities were presented. The historical evolution of crystalline-silicon solar-cell efficiencies, including the most recent results of experimental high-efficiency cells, were explained. The evolution of the efficiencies of cells made from web and edge-defined film-fed growth (EFG) silicon ribbons were also described. The status of contemporary higher-efficiency technical capabilities and future activities to raise efficiencies were stated.

An overview of processing activities aimed at higher efficiencies and economical production was presented by D.B. Bickler, Manager of the FSA Process Development Area. Historically, FSA process development dealt with minimizing the cost to produce solar cells and modules. Present focus is on low-cost process technology for higher-efficiency cells of up to 18% or higher. Today's process development concerns center on the use of less than optimum silicon sheet, the control of production yields, and making uniformly efficient large-area cells. High-efficiency cell factors that require process development are bulk material perfection, very shallow junction formation, front-surface passivation, and finely detailed metallization. Better bulk

PLENARY SESSIONS

properties of the silicon sheet and the keeping of those qualities throughout large areas during cell processing are required so that minority carrier lifetimes are maintained and cell performance is not degraded by high doping levels. When very shallow junctions are formed, the process must be sensitive to metallization punch-through, series resistance in the cell, and control of dopant leaching during surface passivation. There is a need to determine the sensitivity to processing by mathematical modeling and experimental activities.

A summary of solar-cell process research analysis efforts was presented by Dale Burger of JPL. Process design and cell design are interactive efforts where FSA people blend in technology from integrated circuit processes and other processes. The primary factors that control cell efficiency are: (1) the bulk parameters of the available sheet material, (2) the retention and enhancement of these bulk parameters, and (3) the cell design and the cost to produce versus the finished cells performance. The process sequences need to be tailored to be compatible with the sheet form, the cell shape form, and the processing equipment. New process options that require further evaluation and utilization are lasers, robotics, thermal pulse techniques, and new materials. There are numerous process control techniques that can be adapted and used that will improve product uniformity and reduce costs. Two factors that can lead to longer life modules are the use of solar cell diffusion barriers and improved encapsulation.

A summary of metallo-organic deposition (MOD) films for solar cells was presented by Brian Gallagher of JPL. MOD materials are metal ions compounded with organic radicals. MOD technology is evolving quickly for solar cell metallization. Silver compounds, especially silver neodecanoate, have been developed which can be applied by thick-film screening, ink-jet printing, spin-on, spray, or dip methods. Some of the advantages of MOD are: high uniform metal content, lower firing temperatures, decomposition without leaving a carbon deposit or toxic materials, and a film that is stable under ambient conditions. Molecular design criteria were explained along with compounds formulated to date, and the accompanying reactions for these compounds. Phase stability and the other experimental and analytical results of MOD films were presented.

A summary of directed-energy process technology for solar cells was presented by Paul Alexander of JPL. This technology is defined as directing energy or mass to specific areas on solar cells to produce a desired effect in contrast to exposing a cell to a thermal or mass flow environment. Some examples of these second generation processing techniques are: (1) ion implantation; (2) microwave-enhanced chemical vapor deposition; (3) rapid thermal processing; and (4) the use of lasers for cutting, assisting in metallization, assisting in deposition, and drive-in of liquid dopants. Advantages of directed energy techniques are: (1) surface heating resulting in the bulk of the cell material being cooler and unchanged; (2) better process control yields; (3) better junction profiles, junction depths, metal sintering, etc; (4) lower energy consumption during processing; and (5) smaller factory space requirements. These advantages should result in higher-efficiency cells at lower costs. The results of the numerous contracted efforts were presented as well as the application potentials of these new technologies.

PLENARY SESSIONS

The 2-day research forum on Crystal Growth for High-Efficiency Silicon Solar Cells, which was held in December 1984, was summarized by Katherine Dumas of JPL. The forum objectives were to review the state of the art in the growth of silicon crystals for high-efficiency solar cells, define sheet requirements, and to identify future areas of research. Silicon sheet material characteristics that limit cell efficiencies and yields were described as well as the criteria for the ideal sheet-growth method. The device engineers "wish list" to the material engineer included: silicon sheet with long minority-carrier lifetime that is uniform throughout the sheet, and which doesn't change during processing; and sheet material that stays flat throughout device processing, has uniform good mechanical strength, and is low cost. Impurities in silicon solar cells depreciate cell performance by reducing diffusion length and degrading junctions. The impurity behavior, degradation mechanisms, and variations in degradation threshold with diffusion length for silicon solar cells were described. The forum conclusions and future areas of research were explained.

The 1-day research forum on Reliability and Engineering of Thin-Film Photovoltaic Modules, held in March 1985, was summarized by Ed Royal of JPL. The forum objectives were to: (1) examine thin-film cell attributes that influence module performance and reliability, (2) explore the lessons and applicability of crystalline-silicon module technology to thin-film modules, (3) review the current status of thin-film module technologies, and (4) identify problem areas and needed research. A major need is to separate the effects and reasons for reversible degradation from non-reversible degradation. Amorphous-silicon (a-Si) reliability investigations at Clemson University are focusing on exploratory research investigations, accelerated Arrhenius-type testing of a-Si cells, real-time outdoor exposure testing of a-Si cells, cell failure analysis, and failure mechanism research. Studies at JPL included the reduction in strength of glass by high temperature depositions on glass and laser scribing, encapsulation materials development needs, and the testing of modules. The new materials and processes in thin-film modules will require a delinquent reliability effort, including;

- (1) Establishment of mechanism-specific reliability goals.
- (2) Quantification of mechanism parameter dependencies.
- (3) Prediction of expected long-term degradation.
- (4) Identification of cost-effective solutions.
- (5) Testing and failure analysis of trial solutions.

Two presentations were made covering the future direction and activities of the FSA Project through FY86. Martin Leipold explained the silicon material, advanced silicon sheet, device research, and process research activities. Ron Ross explained the reliability and engineering sciences research activities.

Martin Leipold stated that there will be no new initiatives, that many specific activities are targeted for completion, and that emphasis will be on technology transfer. Industry is continuing development of at least some of the technologies initiated by the Project. The major silicon material objectives have been achieved, technology transfer has been essentially

PLENARY SESSIONS

completed, and industry development of fluidized-bed reactor (FBR) deposition technology is proceeding. In the advanced silicon sheet efforts, many activities will be at various levels completion, such as: dendritic web development, generic sheet stress/strain analyses, and an understanding of the influence of growth-related defects on solar-cell efficiency. Technology transfer and industry funding of sheet development are continuing. Further research is required to improve sheet linear growth rate and area throughout, and to improve sheet quality under high-speed growth conditions. In the device research activities, solar-cell model development will be completed, but the proof-of-concept demonstration will be phased out. The high-efficiency technology has not been implemented by industry. Further research is strongly recommended to gain a better understanding of surface/interface losses and losses in the bulk material versus sheet quality, and to develop better measurement techniques. In process research, the ongoing activities that are planned to be completed are: excimer laser processing, MOD metallization techniques, liquid dopant techniques, and the development of lower-cost processing approaches. Industry has adopted the many low-cost processes that have been developed over the life of the Project. Generic research for processes appropriate for the new higher-efficiency solar cells is needed as new cell designs are established.

The four topics covered by Ron Ross were: engineering science, reliability physics, module development, and module performance and failure analysis:

- (1) The objectives of the engineering science efforts are to develop module design requirements for large-scale PV applications and to develop generic module and array design and construction technology to meet the needed performance, safety, reliability, and system interfaces. Most module requirements for large-scale use are established and the basic technology for modules and arrays is nearly complete for modules with crystalline-silicon solar cells, but needs to be developed for modules with thin-film cells. The activities in 1986 will focus on updated module specifications and identification/development of module rear-surface material, and new encapsulants for thin-film modules.
- (2) The objective of the reliability physics effort is develop the technology for 30-year life modules. This has been established for a number of times, but there are still significant unknowns. The 1986 efforts are focused on thin-film module studies, but there are also long-term studies that are needed for all modules.
- (3) The objectives of the module development efforts are to transfer new technology to PV manufacturers and their products, and to evaluate these advanced modules. This has been accomplished by five successive crystalline-silicon module development (block) programs that have established international module designs and technology. Incomplete technologies that are being worked on in 1986 are: dendritic-web modules, high-efficiency modules, module rear-surface material, and initial studies and evaluations of thin-film modules.

PLENARY SESSIONS

- (4) The objectives of the module performance and failure analysis efforts are to determine PV module performance, to identify needed development, and to assess suitability for large-scale use. Block-V modules have been qualified and many other contemporary modules have been evaluated. There are still deficiencies in electrical performance measurements, especially accuracy. Efforts are continuing in 1986, but at much lower funding levels.

FSA FUTURE DIRECTIONS

INTRODUCTION

JET PROPULSION LABORATORY

W.T. Callaghan

- In February of this year, Dr. Robert San Martin, DAS for Renewable Energy, requested JPL to phase out FSA by the end of FY86
 - JPL responded to this request by developing a plan to carry out an orderly, professional phase-out of FSA
 - FSA will remain a major DOE project until 30 September 1986 (through FY86)
 - After FY86 JPL will support SERI in DOE PV program activities—not as FSA
 - Scope and level of effort is currently under discussion
 - Dr. Prince, DOE, will discuss post-FY86 activities
 - Remaining FSA activities through FY86 will meet several criteria:
 - Ongoing contractual work that can reach meaningful technical achievement by end of FY86 will be continued within budgetary constraints
 - Ongoing contractual work that cannot reasonably be expected to reach significant achievement levels by end of FY86 will not be renewed
 - All work must offer promise of significant assistance to U.S. PV industry through technology transfer by end of FY86
- OR
- Be of interest to SERI for continuance beyond FY86 for longer-term-goal achievement

PRECEDING PAGE BLANK NOT FILMED

PLENARY SESSIONS

- **The following two presentations will detail the remaining FY85/FY86 Project activities**
 - 1. Silicon materials, sheet, and high-efficiency device work**
 - 2. Module-level reliability physics, testing, development and failure analysis**

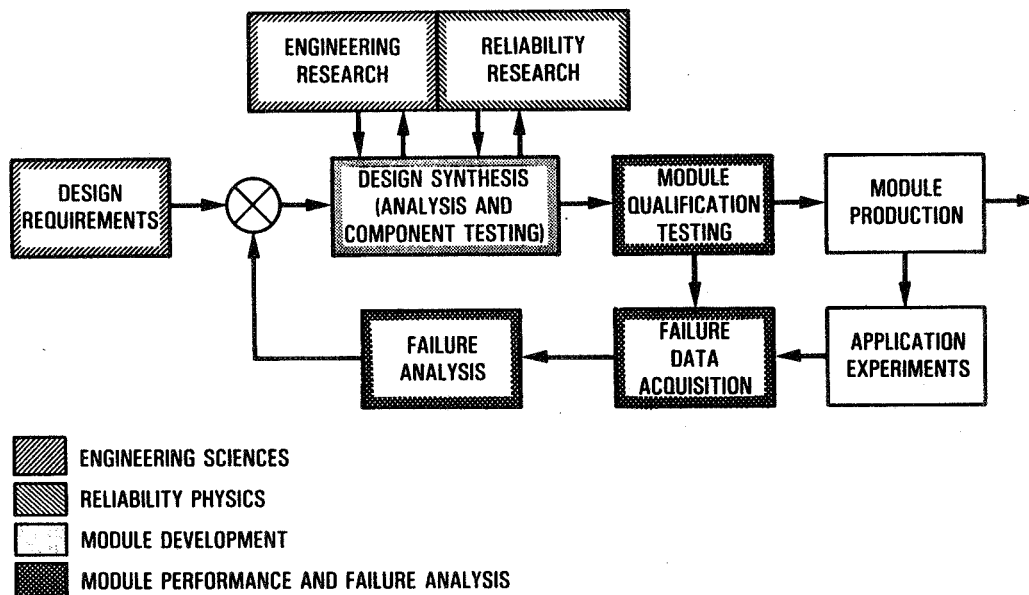
FSA FUTURE DIRECTIONS

RELIABILITY AND ENGINEERING SCIENCES FY85-FY86 ACTIVITIES AND PLANS

JET PROPULSION LABORATORY

R.G. Ross, Jr.

Reliability and Engineering Sciences Functional Organization



PLENARY SESSIONS

Engineering Sciences Objective and Approach

- **Develop module design requirements associated with future large-scale PV applications**
 - **Performance**
 - **Safety**
 - **Reliability**
 - **System interface**
- **Develop generic design and construction technology base required to achieve the above-defined safety and performance requirements**
 - **Module encapsulant materials**
 - **Thermal design methods**
 - **Electrical connection means**
 - **Module safety design practices**
 - **Array electrical circuit analysis methods**
 - **Module flammability considerations**

Engineering Sciences Current Status and Problems

- **Status**
 - **Most module requirements for large-scale applications are in place for both c-Si and thin-film modules**
 - **Module-engineering technology base nearly complete for crystalline-Si but needs updating for thin films**
- **Problems**
 - **Possible problem with reliability of present rear-surface materials (Tedlar)**
 - **Unknown reliability of fire-resistant rear-surface materials**
 - **Need to update 1981 Block V Module Specification for c-Si to incorporate learning of past four years**
 - **Need to develop generic (thin-film) module specifications to focus thin-film module development and assist industry**
 - **Need for thin-film encapsulant development**

PLENARY SESSIONS

Engineering Sciences FY85-FY86 Research Activities

- **Drafting of Block VI Module Design Specification for c-Si:**
 - **New NOCT test method**
 - **New reference spectrum**
 - **Bypass diode qual test**
 - **Expanded hot-spot test**
 - **Revised hipot test procedure**
 - **UV exposure test**
- **Initial development of generic (including thin-film) module design specification**
- **Identification/development of environmentally durable and safe rear-surface materials for c-Si and thin-films**
 - **Conventional constructions (films)**
 - **Flame-resistant constructions**
 - **Special materials for thin films**
- **Identification/development of new encapsulants suitable for thin-film modules**
 - **Lower-processing-temperature pottants**
 - **Transparent front covers**

Reliability Physics Objective and Approach

- **Develop the technology base required for 30-year-life modules**
 - **Establish mechanism-specific reliability goals**
 - **Identify key degradation mechanisms**
 - **Determine system energy-cost impacts**
 - **Allocate system-level reliability**
 - **Quantify mechanism parameter dependencies**
 - **Understand mechanism physics**
 - **Governing materials parameters**
 - **Governing environmental-stress parameters**
 - **Develop degradation prediction methods**
 - **Quantitative accelerated tests**
 - **Life-prediction analysis methods**
 - **Identify cost-effective solutions**
 - **Component design features**
 - **Circuit redundancy and reliability features**

PLENARY SESSIONS

Reliability Physics Current Status and Problems

- **30-year module design technology available for**
 - Glass fracture (c-Si)
 - Cell fracture (c-Si)
 - Hail impact (c-Si)
 - Hot-spot heating (c-Si)
 - Interconnect fatigue (c-Si)
 - Bypass diodes (c-Si and T-F)
 - Soiling (c-Si and T-F)
- **30-year technology available except for some important unknowns**
 - Electrochemical corrosion w/EVA (unknown encapsulant water concentration)
 - Photothermal degradation of EVA (unknown synergism with moisture)
- **Significant technology gap for 30-year life**
 - Voltage breakdown (basic mechanism unknown)
 - Delamination (time-stress dependence unknown)
 - Integrity of rear surface materials
 - Unknown reliability of new high-efficiency c-Si cells
 - Unknown reliability of thin-film solar cells and modules

Reliability Physics FY85-FY86 Research Activities

- Water-module interaction studies
- Electrochemical corrosion studies
- Photothermal degradation of polymers (EVA, Tedlar and T-F encapsulants)
- Delamination of bonded interfaces
- Voltage breakdown of polymers
- Hot-spot testing of thin-film modules
- Glass strength and impact resistance of thin-film modules
- Development of mechanism-specific reliability allocations for thin-film modules
- Cell and module life testing (Clemson, Wyle)
- Bypass diode qual test development

Module Development Objective and Approach

- **Objective**
 - **Facilitate the transfer of DOE-sponsored technology developments into PV manufacturers and their products**
 - **Facilitate the evaluation of recent technology developments in the context of the manufacturing and operating performance of complete modules**
- **Approach**
 - **Prepare module specifications reflecting the most advanced PV technology and requirements for future large-scale applications**
 - **Contract for module design and fabrication by industry**
 - **Conduct design reviews and technical discussions**
 - **Evaluate electrical and reliability performance in laboratory and field tests**
 - **Employ failure analysis to analyze module deficiencies**
 - **Iterate design, design reviews, manufacture and tests until successful module qualification**

Module Development Current Status and Problems

- **Status**
 - **Maintained continual advance in module performance over 10-year period by implementation of five successive development programs (Blocks I through V) and transferred majority of crystalline-silicon module technology to manufacturers**
 - **Resultant design features have been adopted internationally**
- **Problems**
 - **Dendritic-web module development and technology transfer incomplete**
 - **High-efficiency module development and technology transfer incomplete**
 - **Rear-surface material development and technology transfer incomplete**
 - **Significant need for development of thin-film modules**

PLENARY SESSIONS

Module Development FY85-FY86 Activities

- **Technology evaluations**
 - **Dendritic web (Westinghouse)**
 - **High-efficiency cells (Spire)**
- **Fire-resistant encapsulants (Solavolt, ARCO)**
- **Thin-film modules**
 - **ARCO**
 - **Hughes**
 - **Chronar**
 - **Others(?)**

Module Performance and Failure Analysis Objective and Approach

- **Objective**
 - **Accurately quantify PV module performance**
 - **Identify areas of needed development**
 - **Assess suitability for large-scale application**
- **Approach**
 - **Perform qualification testing on state-of-the-art modules incorporating latest technologies (Block Program modules and commercial modules)**
 - **Develop equipment, procedures and techniques for accurate measurement of the electrical performance of PV modules**
 - **Perform failure analysis to determine exact cause of observed anomalies**

PLENARY SESSIONS

Module Performance and Failure Analysis Current Status and Problems

- **Status**
 - **Most current U.S. and foreign production-module designs have been evaluated (SMUD PV2 modules in work)**
 - **Block V qualification testing, performance evaluation and failure analysis completed February 1985**
- **Problems**
 - **National and international electrical performance measurements capability in poor shape**
 - **Limited facilities for module measurements**
 - **Recent change of AM1.5 Global spectrum**
 - **Poor international agreement on measurements**
 - **Limited international qualification test capability**
 - **Major problem is electrical performance measurement accuracy**

Module Performance and Failure Analysis FY85-FY86 Activities

- **Module qualification testing (increasing international demand for JPL qualification)**
- **Performance measurement of SMUD PV2 modules (ARCO, Solarex and Mobil)**
- **Establishment of AM1.5 Global module measurement standards**
 - **Reference cell calibration procedures**
 - **Simulator spectrum modifications**
 - **International round robins**
- **Continuing failure analysis**
- **Possible contract for continuation of qual testing by private testing laboratory**

FSA FUTURE DIRECTIONS

FSA TECHNOLOGY ACTIVITIES IN FY86 JET PROPULSION LABORATORY

M. H. Leipold

Introduction

- NO NEW INITIATIVES
- MANY SPECIFIC ACTIVITIES TARGETED FOR COMPLETION
- CONTINUED DEVELOPMENT IN INDUSTRY
- EMPHASIS ON TECHNOLOGY TRANSFER
- FURTHER GENERIC RESEARCH IN HIGH RISK ELEMENTS RECOMMENDED

Silicon Material Task

- NO NEW INITIATIVES
- MAJOR PROGRAM OBJECTIVES ACHIEVED
- INDUSTRY DEVELOPMENT OF FBR DEPOSITION TECHNOLOGY UNDERWAY
- TECHNOLOGY TRANSFER COMPLETED
- FURTHER GENERIC RESEARCH IN THE PROGRAM NOT REQUIRED

PRECEDING PAGE BLANK NOT FILMED

PLENARY SESSIONS

Silicon Material Task: Technical Accomplishments

- COMPLETED DEVELOPMENT OF SiH_4 PRODUCTION SECTION OF SILICON PROCESS (UNION CARBIDE-CONTRACTOR)
- COMPLETED PILOT PLANT (120 MT/YEAR) DEMONSTRATION OF SILANE PROCESS WHICH INCORPORATES CVD REACTORS (UNION CARBIDE-CONTRACTOR)
- DEMONSTRATED LABORATORY OPERATION OF SiH_4 -FBR DEPOSITION
 - OPERATION AT VERY HIGH CONCENTRATIONS (INCLUDING 100% SiH_4) FOR SHORT-TIME RUNS (JPL IN-HOUSE)
 - OPERATIONS WITH 20% SiH_4 FOR EXTENDED-TIME RUNS (UP TO 66 HRS) (UNION CARBIDE-CONTRACTOR)
- DEMONSTRATED TECHNICAL FEASIBILITY OF DICHLOROSILANE CVD PROCESS (HEMLOCK SEMICONDUCTOR)
- SHOWED QUANTITATIVELY THE INFLUENCE OF IMPURITIES ON LIFETIME IN SILICON (WESTINGHOUSE)

Advanced Silicon Sheet Task

- NO NEW INITIATIVES
- MANY ACTIVITIES WILL BE AT VARIOUS LEVELS OF COMPLETION
 - WEB RIBBON DEVELOPMENT AT WESTINGHOUSE AND JPL
 - GENERIC STRESS/STRAIN ANALYSIS
 - GROWTH RELATED DEFECTS/DEVICE EFFICIENCY
- INDUSTRY FUNDING OF SHEET DEVELOPMENT HEALTHY
- STRONG TECHNOLOGY TRANSFER WILL CONTINUE
- FURTHER RESEARCH IN GENERIC RIBBON GROWTH REQUIRED

PLENARY SESSIONS

Advanced Silicon Sheet Task: Remaining Technical Problems

LINEAR GROWTH RATE/AREAL THROUGHPUT

- UNDERSTANDING AND CONTROL OF STRESS AND STRAIN PHENOMENA
 - MEASUREMENT AND UNDERSTANDING OF HIGH TEMPERATURE MECHANICAL PROPERTIES OF SILICON
 - MEASUREMENT AND CONTROL OF TEMPERATURES AND HEAT FLOW IN THE HOT ZONE
 - CHARACTERIZATION OF STRESS AND STRAIN RELATED DEFECTS IN THE SILICON
 - DEVELOPMENT OF A COMPREHENSIVE INTEGRATED ELASTIC/PLASTIC MODEL TO GUIDE HOT ZONE ENGINEERING

SILICON SHEET QUALITY

- UNDERSTANDING THE RELATIONSHIP BETWEEN GROWTH-RELATED DEFECTS AND FABRICATED DEVICE PROPERTIES (IN CONJUNCTION WITH THE DEVICE AND MEASUREMENTS TASK)
- UNDERSTANDING THE IMPORTANCE OF THE STRUCTURE (ESPECIALLY THE TWIN PLANES IN WEB) ON THE GROWTH PROCESS AND, ULTIMATELY, DEVICE PERFORMANCE
- INTERFACE STABILITY/IMPURITY REDISTRIBUTION

Device Research Task

- NO NEW INITIATIVES
- SPECIFIC ACTIVITIES TARGETTED FOR COMPLETION
 - MODEL DEVELOPMENT TO BE COMPLETED
 - PROOF-OF-CONCEPT DEMONSTRATION PHASED OUT
- HIGH EFFICIENCY DEVICE TECHNOLOGY NOT IMPLEMENTED IN INDUSTRY
- TECHNOLOGY EXCHANGE THROUGH RESEARCH FORUMS
- FURTHER RESEARCH STRONGLY RECOMMENDED
 - SURFACE/INTERFACE LOSSES
 - BULK LOSSES/SHEET QUALITY
 - MEASUREMENT TECHNIQUES

C-2

PLENARY SESSIONS

Device Research Task: Remaining Problems

BULK LOSS

- BULK RECOMBINATION/PASSIVATION
 - MECHANISMS
- QUALITY OF SILICON SHEET
 - GROWTH/PROPERTIES RELATIONSHIPS

SURFACE LOSS

- SURFACE RECOMBINATION/PASSIVATION
 - FUNDAMENTAL UNDERSTANDING
 - MEASUREMENTS
 - PROCESS DEVELOPMENT

MODELING

- VERIFICATION OF HIGH-EFFICIENCY DEVICE DESIGNS AND SENSITIVITY ANALYSIS

MEASUREMENTS

- MATERIALS AND DEVICE PARAMETERS FOR HEAVILY DOPED FRONT SURFACE LAYER

Process Research Area

- NO NEW INITIATIVES
- ACTIVITIES TARGETED FOR COMPLETION
 - EXCIMER LASER PROCESSING
 - MOD METALLIZATION
 - LIQUID DOPANT
 - DEVELOPMENT OF LOW-COST APPROACHES
- INDUSTRY HAS ADOPTED LOW-COST PROCESSES
- TECHNOLOGY EXCHANGE OF HIGH EFFICIENCY PROCESSES EMPHASIZED
- GENERIC RESEARCH FOR HIGH EFFICIENCY DEVICE PROCESSES RECOMMENDED

SUMMARY OF HIGH-EFFICIENCY SOLAR-CELL RESEARCH

JET PROPULSION LABORATORY

Ram Kachare

Outline

- TASK OBJECTIVES
- THEORETICAL PREDICTION OF CELL EFFICIENCY
- MODELING OF CELL EFFICIENCY
- HIGH-EFFICIENCY CELL RESULTS
- STATUS AND FUTURE ACTIVITIES

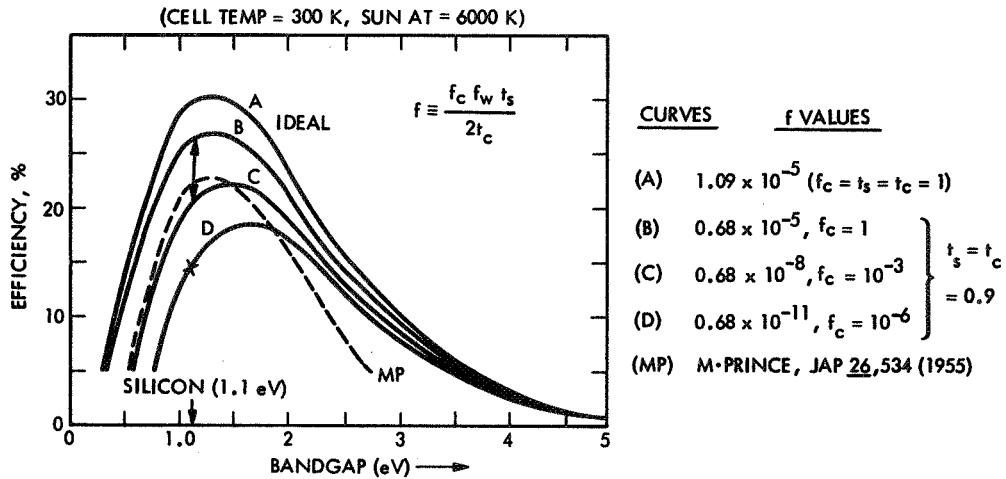
Task Objectives

1. IDENTIFY AND RESOLVE KEY GENERIC PROBLEMS THAT LIMIT CELL EFFICIENCY TO BELOW THEORETICALLY PREDICTED VALUE

AND

2. DESIGN AND FABRICATE CELLS HAVING EFFICIENCY $\geq 20\%$ (AM1.5)

Theoretical Curves for p-n Junction Solar Cell



f_c = RADIATIVE RECOMBINATION, A FRACTION OF ALL RECOMBINATION PROCESSES REPRESENTED BY f
 f_w = RELATED TO ILLUMINATION INTENSITY
 t_s and t_c = PROBABILITIES OF PRODUCING ELECTRON-HOLE PAIRS BY PHOTON HAVING ENERGY GREATER THAN BANDGAP INCIDENT ON THE SURFACE (t_s) AND ENTERING THE BODY OF THE CELL (t_c) RESPECTIVELY.

[SHOCKLEY AND QUIESSER, JAP 32,510 (1961)]

Parameters for Modeling Cell Efficiency

- BASE MATERIAL
 - THICKNESS
 - RESISTIVITY
 - MINORITY CARRIER LIFETIME (τ)
- EMITTER AND BACK-SURFACE (BSF) DOPING
 - SURFACE CONCENTRATION
 - DOPING PROFILE
- HEAVY DOPING EFFECTS
 - BANDGAP NARROWING (B)
 - AUGER RECOMBINATION (A)
- SHOCKLEY-REED-HALL RECOMBINATION
- FRONT (S_F) AND BACK (S_B) SURFACE RECOMBINATION VELOCITIES
- FRONT (AR) AND BACK SURFACE (BSR) OPTICAL PROPERTIES
- FRONT-SURFACE METAL SHADOWING
- SERIES AND SHUNT RESISTANCES

Cell Design Parameters

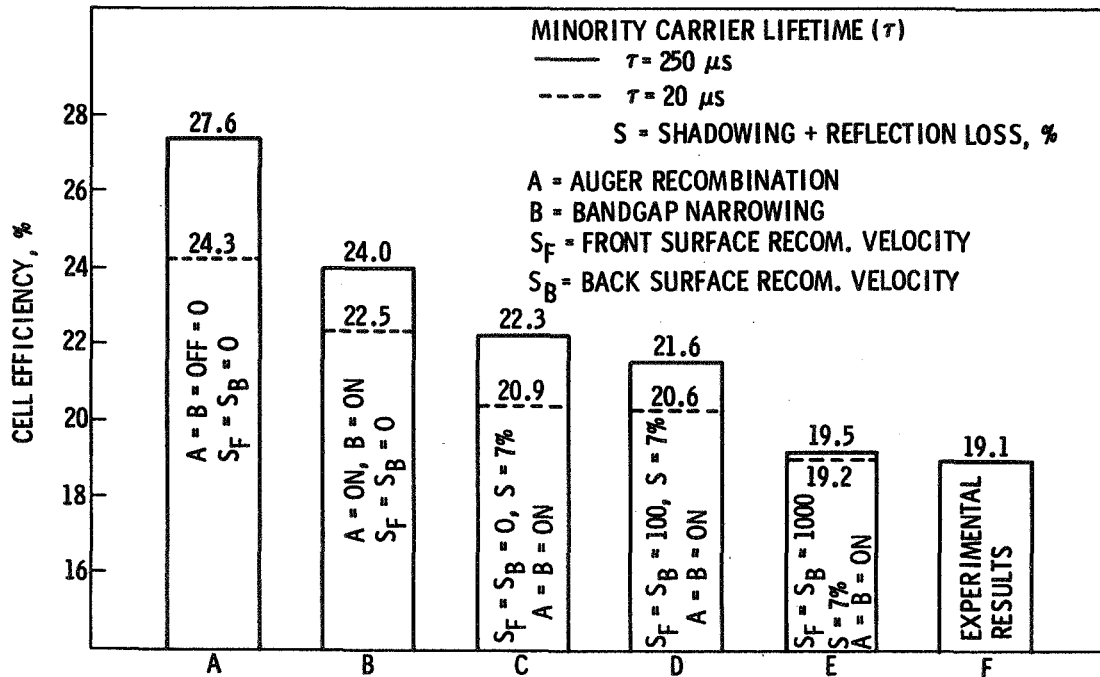
FIXED:

- EMITTER DOPING:
 - PROFILE: COMPLEMENTARY ERROR FUNCTION
 - SURFACE CONCENTRATION = 1×10^{18} P ATOMS/cm³
- JUNCTION DEPTH = 0.2 μ m
- BULK DOPING = 5×10^{17} B ATOMS/cm³
- CELL THICKNESS = 100 μ m; BACK-SURFACE REFLECTOR PROVIDED
(\therefore EFFECTIVE THICKNESS \cong 200 μ m)
- ILLUMINATION = 100 mW/cm²

VARIED:

- MINORITY CARRIER LIFETIME (τ)
- HEAVY DOPING EFFECTS: CONSIDERED
 - AUGER RECOMBINATION (A) } ON OR
 - BANDGAP NARROWING (B) } OFF = 0
- FRONT (S_F) AND BACK (S_B) SURFACE RECOMBINATION VELOCITIES
- FRONT-SURFACE REFLECTION AND METAL SHADOWING LOSSES (S)

Effect of Practical Barriers on Cell Efficiency



High-Efficiency Cell Modeling

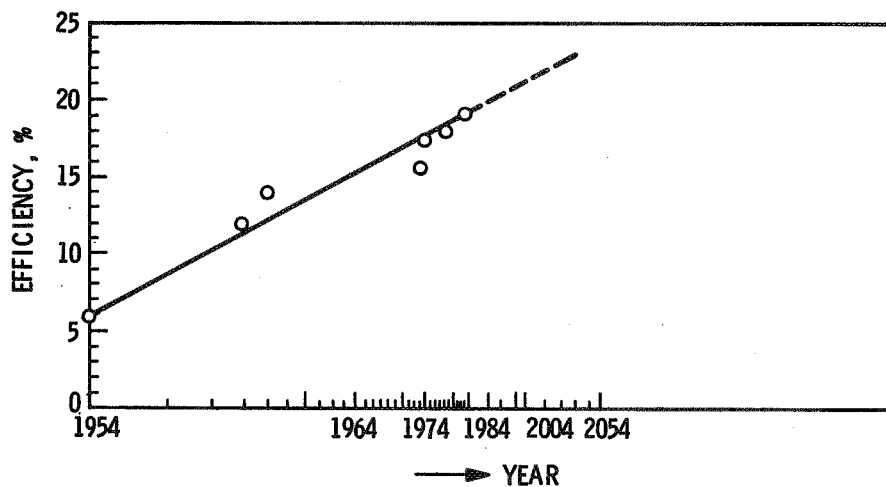
USEFUL FOR

- SENSITIVITY ANALYSIS
 - MATERIALS
 - DEVICE DESIGN
 - DEVICE PROCESSING
- COMPARISON OF VARIOUS DESIGNS
- ANALYSIS OF EXPERIMENTAL RESULTS
- PREDICTION OF EFFICIENCIES AS
 - VARIOUS TECHNOLOGY BARRIERS ARE OVERCOME
 - DESIGNS AND MATERIAL PROPERTIES CHANGE

CURRENT LIMITATIONS

- MAINLY DUE TO LACK OF RELIABLE DATA ON:
 - HEAVY DOPING EFFECTS
 - AUGER RECOMBINATION COEFFICIENT
 - BANDGAP NARROWING
 - FRONT- AND BACK-SURFACE RECOMBINATION VELOCITIES
 - MINORITY CARRIER LIFETIME (THIN EMITTER)
 - MINORITY CARRIER MOBILITY

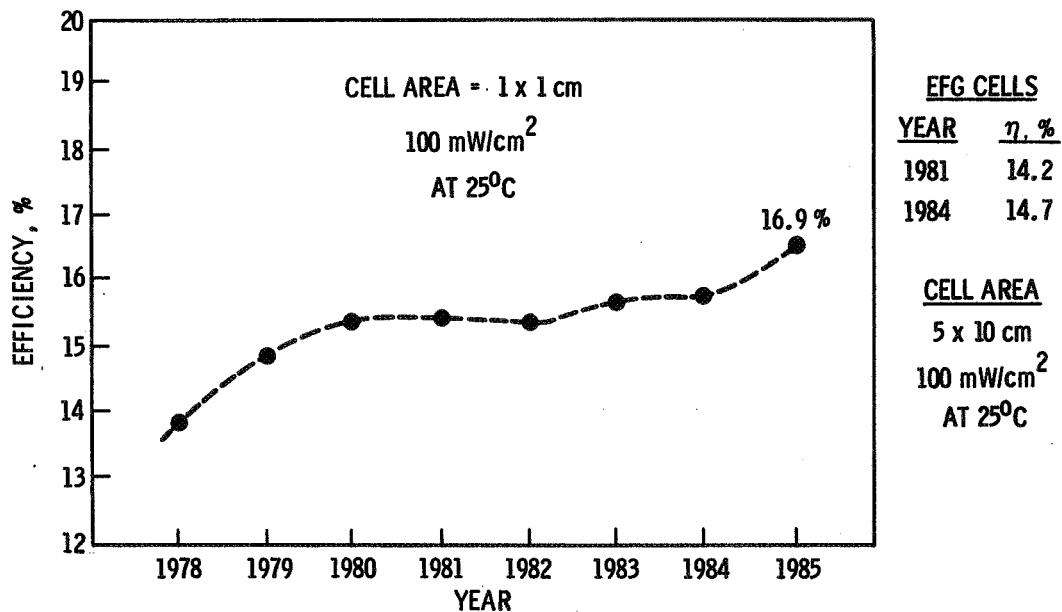
Historical Development of Silicon Solar Cells



Recent High-Efficiency Results

SUBSTRATE RESISTIVITY, Ω -cm	CELL EFFICIENCY, %	SOURCE	CELL AREA, cm^2
0.25	18.4	WESTINGHOUSE	4.0
0.30	18.1	SPIRE CORP.	4.0
0.15	18.1	ASEC	4.0
0.25	19.1	UNIVERSITY OF SOUTH WALES, AUSTRALIA	4.0
0.30	17.1	CATHOLIC UNIVERSITY OF LEUVEN, BELGIUM	1.0?
0.30	17.5	SANDIA LAB CONC.	4.0
0.20	17.4	JPL	8.0

History of Highest-Efficiency (η) Web and EFG Cells



PLENARY SESSIONS

Current Technical Status

- THEORETICAL KNOWLEDGE OF HIGH-EFFICIENCY DEVICE CONCEPT EXISTS
- EXPERIMENTAL UNDERSTANDING OF THE CONCEPT IS NOT MATURE
- QUALITY OF SILICON SHEET CONTINUES TO BE A MAJOR TECHNICAL BARRIER

Future Activities

- DEVELOPMENT OF SURFACE PASSIVANT(S)
- SURFACE / INTERFACE CHARACTERIZATION
- FRONT-SURFACE RECOMBINATION VELOCITY AND LIFETIME
(IN THIN EMITTER) MEASUREMENT TECHNIQUE
- UNDERSTANDING AND CONTROL OF BULK LOSS
- HIGH-EFFICIENCY DEVICE DESIGN MODELING OPTIMIZATION

**OVERVIEW OF PROCESSING ACTIVITIES AIMED AT
HIGHER EFFICIENCIES AND ECONOMICAL PRODUCTION**

JET PROPULSION LABORATORY

D.B. Bickler

Outline

- **Background**
- **Process development concerns**
- **High efficiency elements**
- **Sensitivities**
- **A proposed design**
- **Process development for proposed design**

Background

- **Historically, JPL process development dealt with minimizing \$/watt**
- **Current focus on achieving cell efficiencies greater than 18%**

Process Development Concerns

- **Less than optimum Si sheet**
- **Control of yield**
- **Large area cells**

PLENARY SESSIONS

High-Efficiency Elements Requiring Process Development

- **Bulk material perfection**
- **Very shallow junction**
- **Front surface passivation**
- **Finely detailed metallization**

Bulk Material Perfection

- **Maintain minority carrier lifetime**
- **High doping levels add concern**
- **Large area**

Very Shallow Junction

- **Sensitive to metallization punch-through**
- **Series resistance problems**
- **Control dopant leaching during passivation**

Front-Surface Passivation

- **Mechanical integrity**
- **Optical characteristics**
- **Electrical requirements**
- **Process selection**
 - **Thermal oxidation**
 - **Thermal CVD**
 - **Plasma CVD**
 - **Sputtering**
 - **Evaporation**

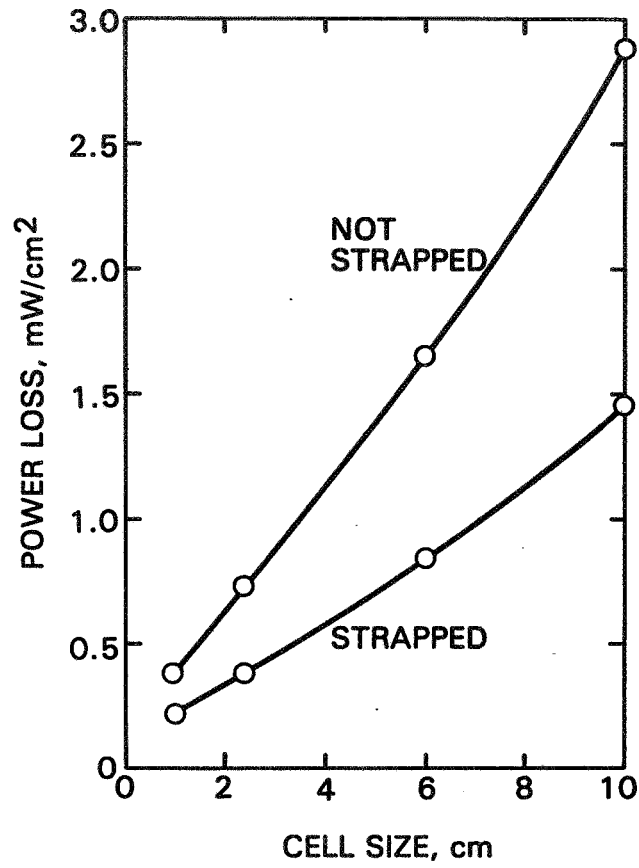
Finely Detailed Metallization

- **Aspect ratio (thickness/width)**
- **Laser processing**
- **Electrochemical deposition**

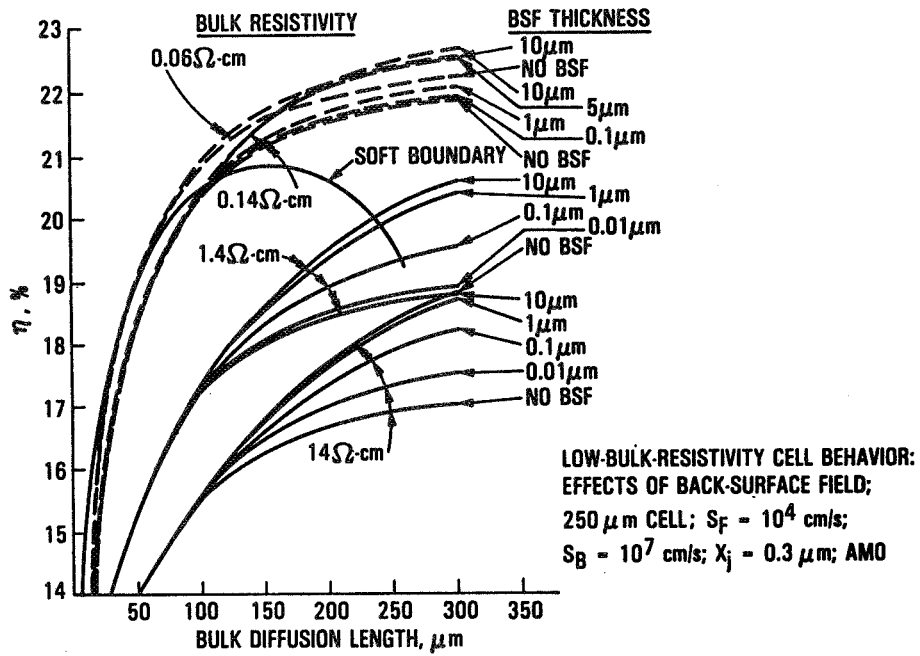
Determining Sensitivity to Processing

- **Use of mathematical modeling**
 - **Cell model SPCOLAY from University of Pennsylvania**
 - **Metal pattern optimization CELCAL from JPL**
 - **Processing models in SUPREM from Stanford University**
- **Experimental lab work**
 - **Individual process steps**
 - **Combine into process sequences**

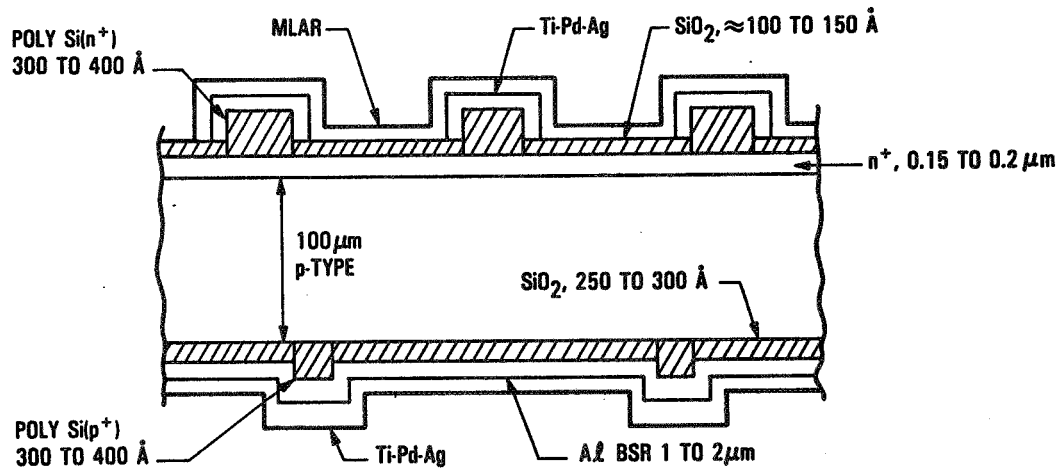
Power Loss vs Cell Size



Low-Resistivity Cell Behavior



A Proposed High-Efficiency Design



PLENARY SESSIONS

Process Development Required for Proposed Design

- **Thinning process**
- **BSR optics**
- **Patterned doped silicon**
- **Metal grid alignment**

SUMMARY OF PROCESS RESEARCH ANALYSIS EFFORTS

JET PROPULSION LABORATORY

Dale R. Burger

Introduction

- **Process design/cell design**
- **Cell efficiency drivers:**
 - **Bulk parameters and cell parameters**
 - **Tailored process sequences**
 - **New process options**
 - **Process control**
- **Lifetime improvement drivers:**
 - **Diffusion barriers**
 - **Encapsulation**

Process Design and Cell Design

- **Interactive effort**
- **Physics determines efficiency and sensitivity**
- **Research interest areas**
 - **Previous PV research (MIS)**
 - **IC processes (poly Si, light pulse)**
 - **Miscellaneous industries**
 - **Thick Film (MOD)**
 - **Ink-jet printing (MOD)**
 - **Magnetic memory (high-rate metallization)**

Cell Efficiency Drivers

- **Bulk parameters and cell parameters**
 - **Available bulk parameters**
 - **Cost and availability**
 - **Size**
 - **Retention and enhancement of parameters**
 - **Thermal history: precipitates, dislocation clusters, gettering**
 - **Contamination: environmental, handling, materials**
- **Cell design**
 - **Design goal, not specification: -e.g., poly vs thin oxide**
- **Cost vs performance**
 - **Life-cycle cost**
 - **Learning curve**
 - **Metallization system**

Tailored Process Sequences

- **Bulk material dependency**
 - **Cz**
 - **FZ**
 - **Web**
- **Shape-dependent**
- **Equipment-dependent**

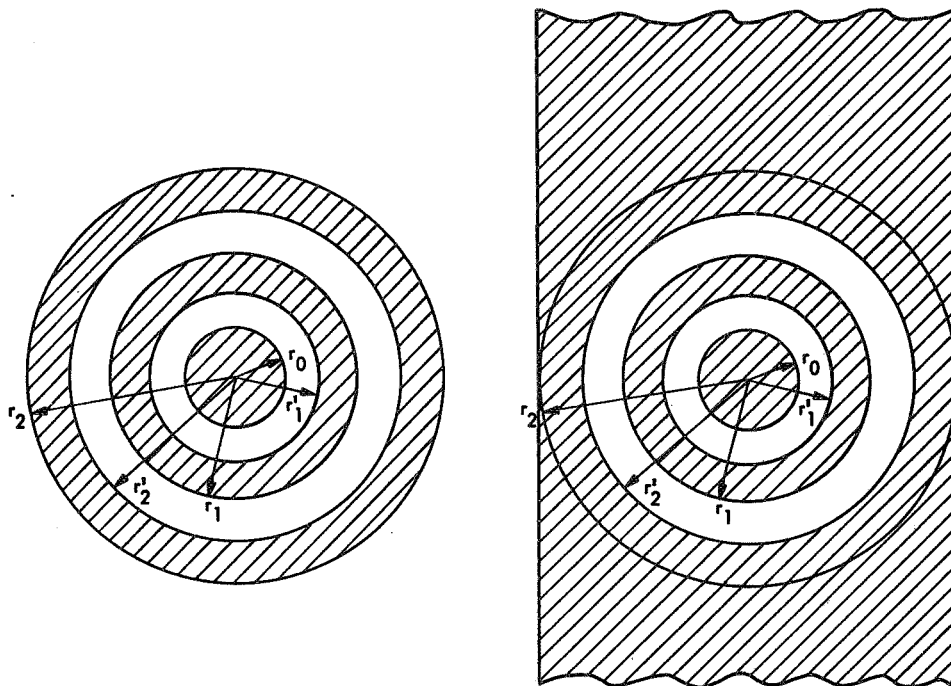
New Process Options

- **Lasers**
- **Robotics**
- **Thermal pulse**
- **New materials**
 - **Polysilicon**
 - **MOD**

Process Control

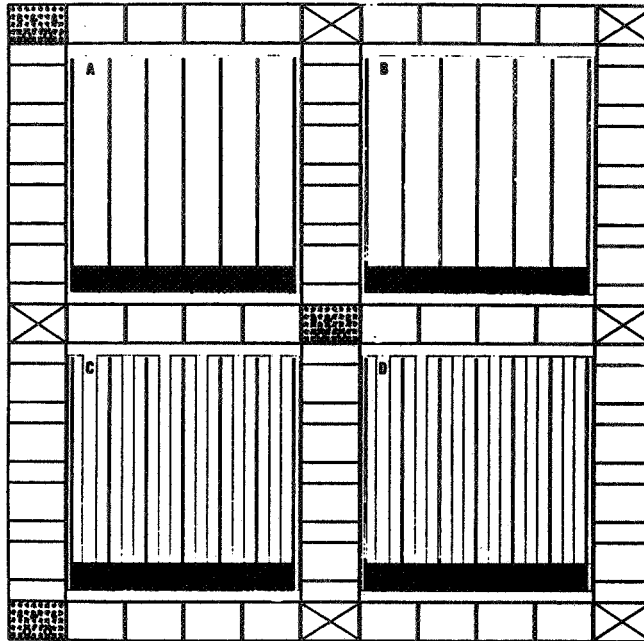
- **Yield Management = profits**
- **Low-cost data acquisition and analysis**
- **IEEE-488 compatibility**
- **Test patterns**
 - **Circular TLM**
 - **NBS-22 pattern (NBS 81-2260)**
- **Non-contacting testing**
 - **Therma probe**
 - **X-ray photoemission spectrometry**
 - **FTIR**
- **Contact testing**
 - **1/f noise**

CTLM Test Patterns

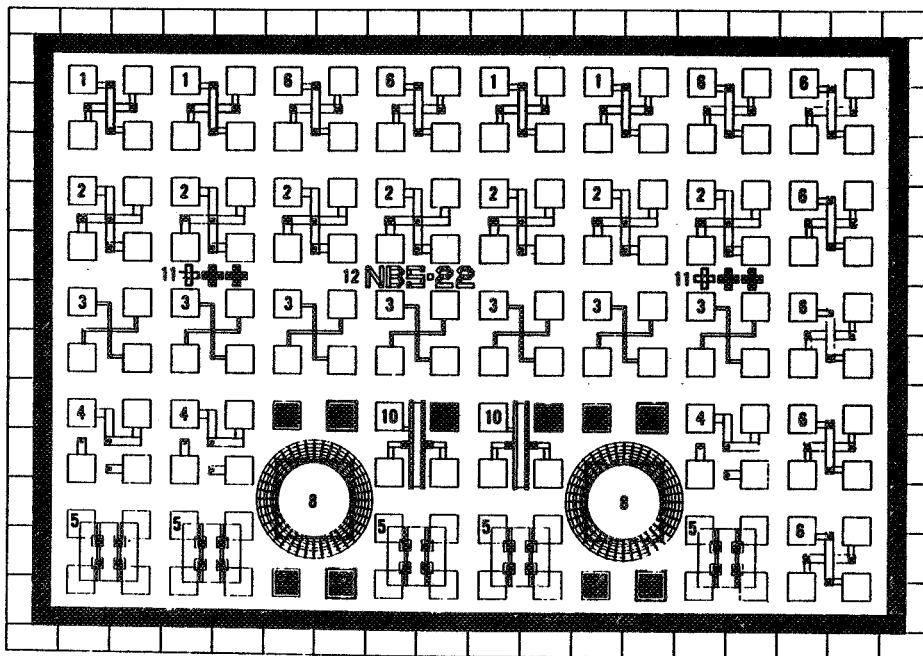


PLENARY SESSIONS

NBS-22 Solar-Cell Test Pattern



Reference Test Structures



Lifetime Improvement Drivers

- **Diffusion barriers**
 - **Reduce rate of ambient thermal diffusion**
 - **Reduce rate of chemical activity**
- **Encapsulation**
 - **Provide environmental barrier**
 - **Provide circuit insulation**
 - **Low degradation rate**
 - **Should not enhance chemical activity**

METALLO-ORGANIC DECOMPOSITION FILMS

JET PROPULSION LABORATORY

B.D. Gallagher

Metallo-Organic Decomposition (MOD) Films

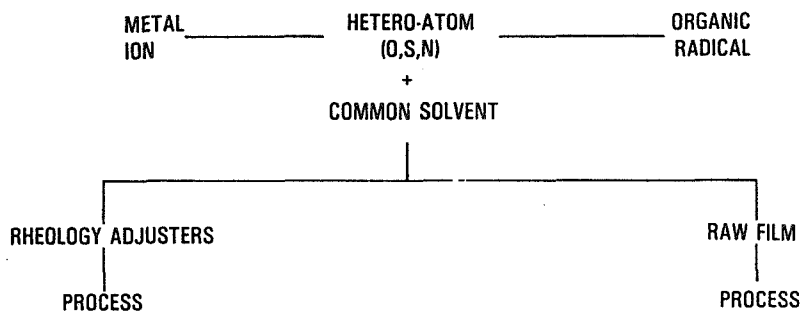
Introduction

Materials

Process

Status

What are Metallo-Organic Compounds?



PRECEDING PAGE BLANK NOT FILMED

Advantages of MOD Compounds

- Generic synthesis procedures
- High solubility in organic solvents
- High uniform metal content
- Lower firing temperatures
- Decompose without melting or leaving a carbon deposit
- Stable under ambient conditions
- Non-toxic — do not produce toxic decomposition products

Disadvantages of MOD Compounds

- Low inorganic content
- Limited information available on pure compounds
- Large volume of volatiles

Molecular Design Criteria

- As the chain length of the organic radical increases:
 - (1) The solubility of the compound in organic solvent increases
 - (2) The metal content of the compound decreases
- The solubility of the compound increases if the organic radical is branched

Compounds Formulated

2-ETHYLHEXANOATES

Bi, Cd, Co, Cr, Cu, Ga, In, Ir, Ni, Pb, Rh, Ru, Si, Sn, Y, Zn, Zr

AMINE 2-ETHYLHEXANOATES

Au, Pt

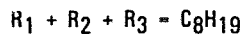
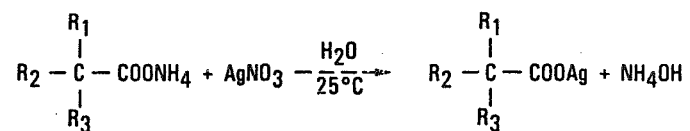
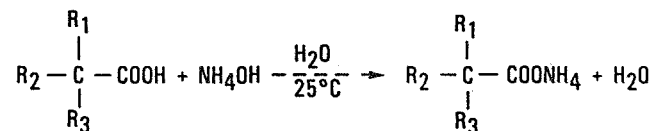
NEODECA-NOATES

Ag, Ba

OTHER

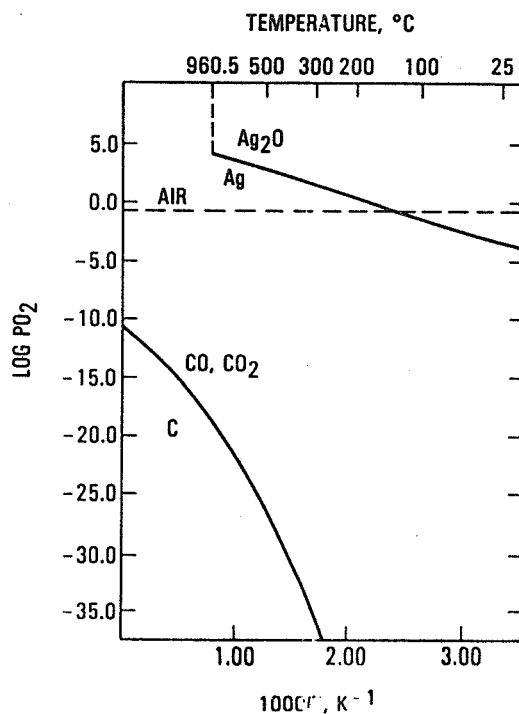
B pyridine
 Pd acetate
 Sb autoxide
 Ti 2-ethylhexoxide

Reactions

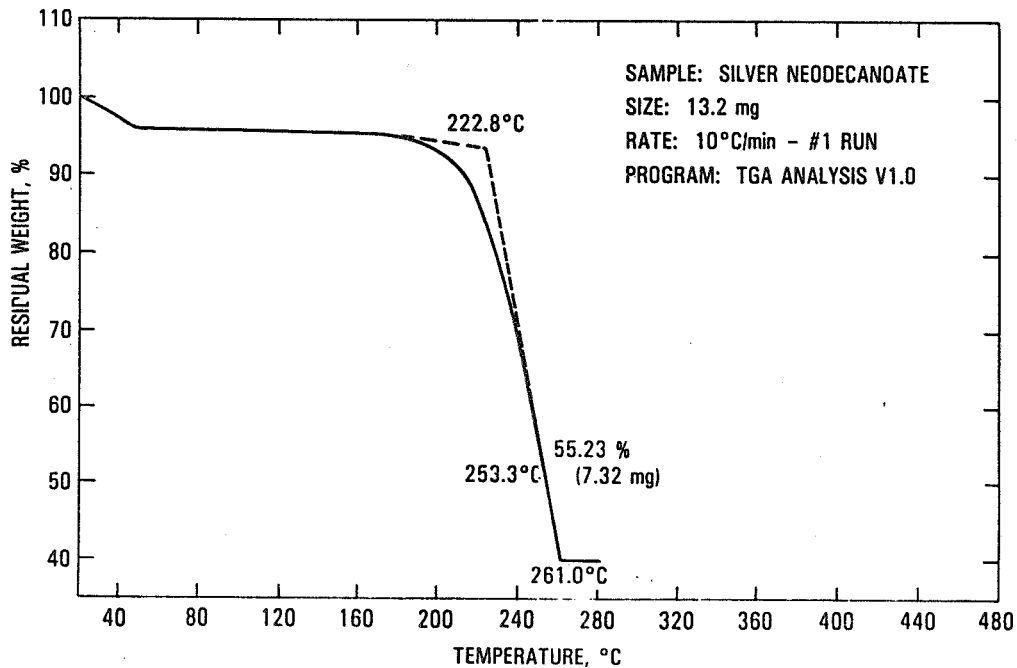


Wt % SILVER: 38.7
 FORM: WHITE SOLID
 SOLUBILITY: AROMATIC SOLVENTS

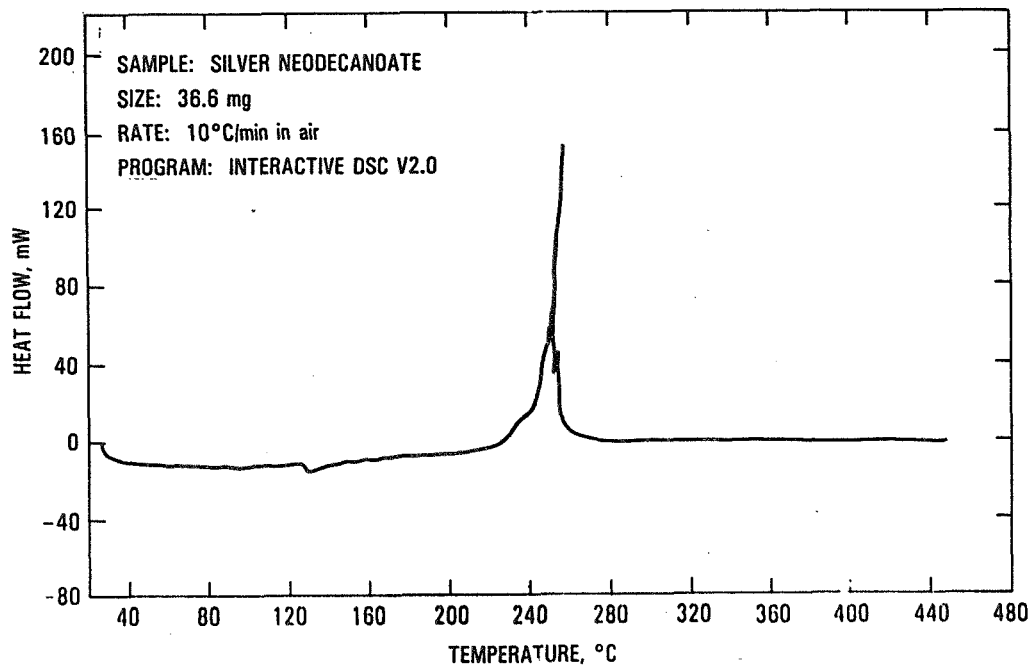
Phase Stability Diagram for the Ag-C-O System



TGA



DSC



Status

- **Materials**

Ag	AgNi
AgPt	AgCo
AgBiPt	AgCr
AgBi	

- **Processes**

- **Application methods**

- Thick-film screening
- Ink-jet printing
- Spin-on
- Spray
- Dip

- **Pyrolytic decomposition**

- Resistance furnace
- Coherent light
- Incoherent light

PLENARY SESSIONS

- **Applications**
 - Photovoltaic devices
 - VLSI devices
 - Hybrid microelectronics
 - Hermetic sealing
- **Technology transfer:**
 - New technology disclosures
 - Papers
 - ISHM
 - SPIE
 - ECS
 - MRS
 - Industry availability

DIRECTED-ENERGY PROCESS TECHNOLOGY EFFORTS

JET PROPULSION LABORATORY

Paul Alexander

Directed Energy

Definition: Directing energy or mass to specific areas on solar cells to produce an effect

This compares with exposing solar cells to a thermal or mass flow environment to produce an effect

Examples of environmental exposures for cell processing include:

- Thermal diffusion, furnace anneal
- Metal sintering, cleaning, etching
- CVD, belt furnace operations

The above might be considered as first-generation processing

Examples of directed-energy processing include:

- Ion implantation: Pulsed electron beam anneal (PEBA)
Pulsed excimer laser anneal (PELA)
- Laser cutting
- Laser assisted metallization
- Laser-assisted deposition
- Laser drive-in of liquid dopants
- Microwave-enhanced chemical vapor deposition (MECVD)
- Rapid thermal processing (RTP)

The above might be considered as second generation processing

PLENARY SESSIONS

Advantages of Directed Energy and Mass Processing

- **Surface heating**
 - Allows bulk temperature of cell to remain near ambient
 - Thereby preserving bulk lifetime; (laser processing, heat lamps)
- **Better process control:**
 - Tighter control of process parameters should yield better control of junction profiles, junction depths, metal sintering, etc.
- **Lower process energy costs:**
 - Energy is used directly on the cell instead of into the total cell environment
- **Less working space:**
 - e.g., laser space versus furnace space
- **Should produce higher-efficiency cells at lower costs**

Disadvantages of directed energy and mass processing

- **High throughput not yet demonstrated**
- **High equipment costs and maintenance costs. Reliability not yet demonstrated**

Directed-Energy Contracts

DOE/FSA has funded the following directed-energy/mass contracts in FY/84/85; Earlier contracts included ion implantation, pulsed electron beam annealing

- **Pulsed excimer laser anneal: special DOE funding, competitively awarded to Spire Corporation, No. 956797 and ARCO Solar, Inc., No. 956831; ARCO also investigating laser-assisted metal and film deposition on No. 956831.**
- **Laser-assisted metallization: Westinghouse, No. 956615**
- **Laser drive-in of liquid dopants: Westinghouse, No. 956616 (rapid thermal processing also investigated)**
- **Microwave-enhanced chemical vapor deposition (MECVD), Superwave Technology, Inc., No. 956828**

PLENARY SESSIONS

Results of Excimer Laser Annealing Studies

- Textured surfaces not ideal for laser annealing; difficult to control surface melting conditions. Stress buildup after annealing decreased V_{OC} substantially
- Surface cleanliness affects cell performance after laser anneal much more than it affects cell performance after thermal anneal. Particulates left on surface may form nucleation sites during laser anneal. Preferential etching confirmed this
- Optimum laser density determined to be between 1.4 J/cm^2 and 1.6 J/cm^2 . Energy densities outside these limits were characterized by poor fill factors and low V_{OC}
- Laser parameters that produced the best cells were: 1.4 to 1.6 J/cm^2 , 50% overlap, 25 nanoseconds pulse duration, 1 mm^2 spot size
- Ion implantation parameters that produced the best cells were: 5 keV implant energy, 1 to 2×10^{15} atoms/cm² fluence

Excimer Laser Annealing

- Economic analysis
 Assumptions:
 1985 dollars
 80% up time
 0.886 yield
 600 wafers/hour throughput
 1850 hours/shift/year
 3 shifts
 100 mm diameter, as-cut, silicon wafers

<u>Module Efficiency, %</u>	<u>PELA, \$/watt</u>	<u>Diffusion, \$/watt</u>	<u>Output, MW/yr</u>
12	6.85	6.79	2.22
13	6.32	6.27	2.41
14	5.87	5.87	2.59
15	5.48	5.44	2.78
16	5.14	5.10	2.96

- Cell fabrication
 Best $2 \times 2 \text{ cm}$ cell: 15.5%

PLENARY SESSIONS

Excimer Laser-Assisted Metal Deposition

Surface passivation

Goal: To deactivate the silicon dangling bonds at the surface

$$V_{oc} \propto LN \frac{1}{U}$$

where U = rate of recombination

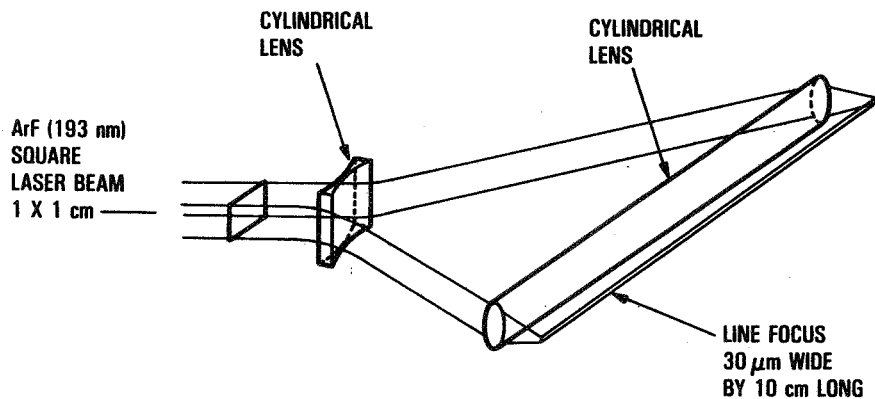
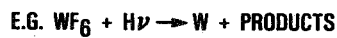
Conventional method: thermal oxide

Propose: Laser-assisted photochemical dissociation of oxide



Fine grid-line metallization

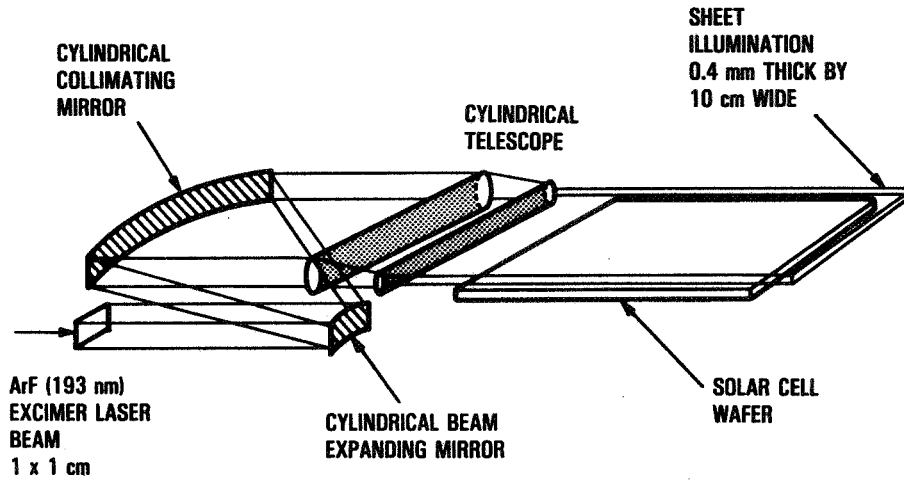
Goal: Laser-assisted metal deposition; eliminate "wet" steps in photolithography process. Process could also be applicable to thin-film solar cells



Excimer Laser-Assisted Film Deposition

Surface passivation (Continued)

Rate of deposition = 600-800 Å/min



Excimer Laser-Assisted Metal and Film Deposition

- Experiments have just started
- No data on metal and film deposition

PLENARY SESSIONS

Microwave-Enhanced Chemical Vapor Deposition System

Objective:

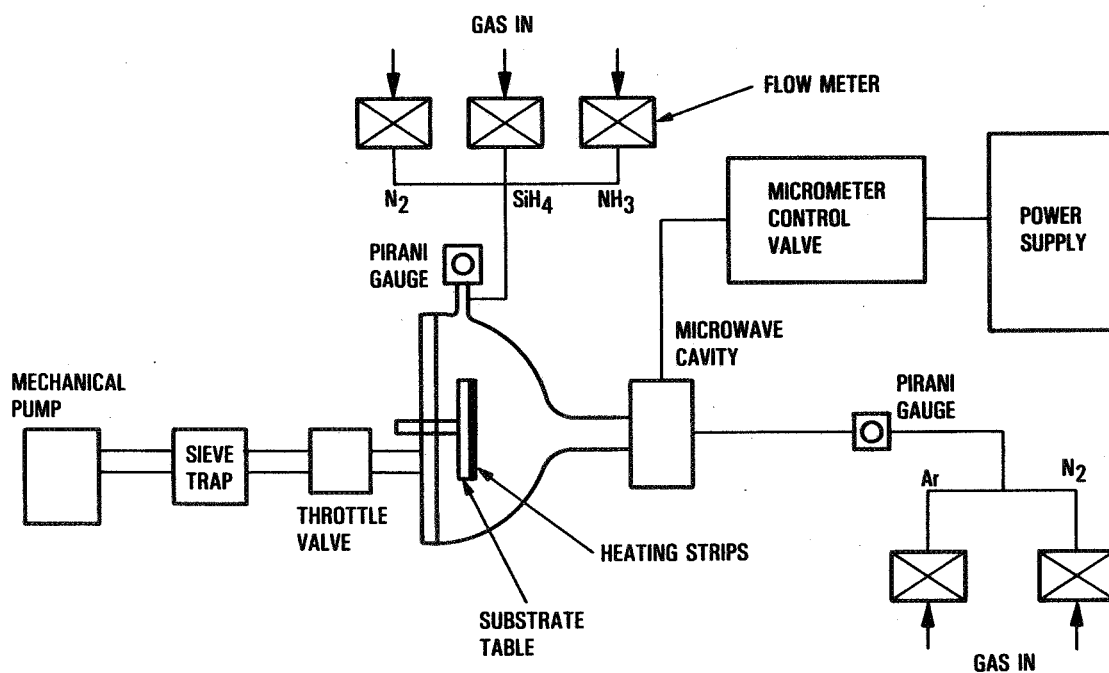
Design, fabricate and demonstrate a microwave-enhanced CVD system to show feasibility of depositing silicon nitride

Rationale:

Microwave-enhanced chemical vapor deposition of passivation coatings has the potential advantages of:

- Higher electron plasma density ($10^{13}/\text{cm}^2$ vs $10^9/\text{cm}^2$ for RF) where W_p is 2.45 GHz instead of 13.56 MHz
- Long lifetime in species, which allows reaction chamber and plasma generation chamber to be separated
- More control of deposition kinetics with less damage to substrate
- Controlling film gradients or doping profiles
- Lower power requirements
- Lower reactive gas consumption

Schematic of Microwave-Enhanced Chemical Vapor Deposition System



Results of Microwave-Enhanced Chemical Vapor Deposition

- Contractor effort completed
- Feasibility has been demonstrated; silicon nitride deposited using MECVD technique
- Adhesion problems noted and problem solved by substrate heating
- Film non-uniformity noted; possible solution involves hardware redesign for a more even reactant gas distribution
- Follow-on development effort desirable: funding problems

Laser-Assisted Metallization

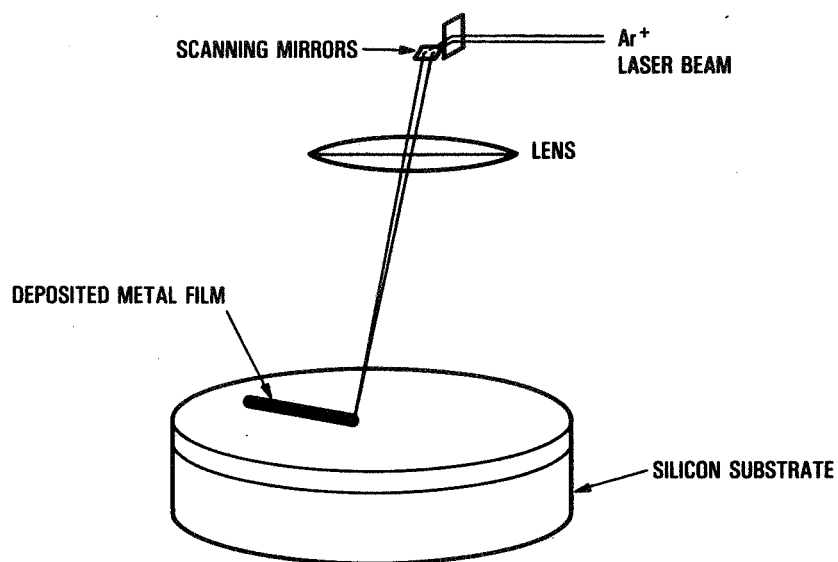
A photolithographic system for fine line metallization employs sequential multistep process

- Spin-on photoresist
- Bake
- Expose pattern
- Develop (remove polymerized layer)
- Rinse
- Vacuum evaporate metal
- Lift-off (remove excess metal and photoresist)
- Clean

Laser-assisted metallization steps are significantly reduced

- Cover cell with metal film (spin-on, vacuum evap., etc.)
- Laser-write on metal film
- Plate-up on "written" surfaces
- Remove excess metal film

Laser Pyrolysis of Spun-on Metallo-Organic Film



**SAMPLE BASE TEMPERATURE 75°C
FOCUSED LASER SPOT DECOMPOSES SPUN-ON FILM
METALLIZATION PATTERNS ARE FORMED BY DIRECTWRITING**

Lighted I-V Data

Photolithography Baseline	Short-Circuit Current, mA	Open-Circuit Voltage, V	Fill Factor	Efficiency, %
Best Cell	36.5	0.579	0.738	15.6
Average Cell	33.8	0.569	0.703	13.6
Worst Cell	30.1	0.566	0.570	9.7
Laser- Metallized				
Best Cell	36.1	0.589	0.776	16.5
Average Cell	33.9	0.576	0.766	15.0
Worst Cell	32.0	0.571	0.751	13.7

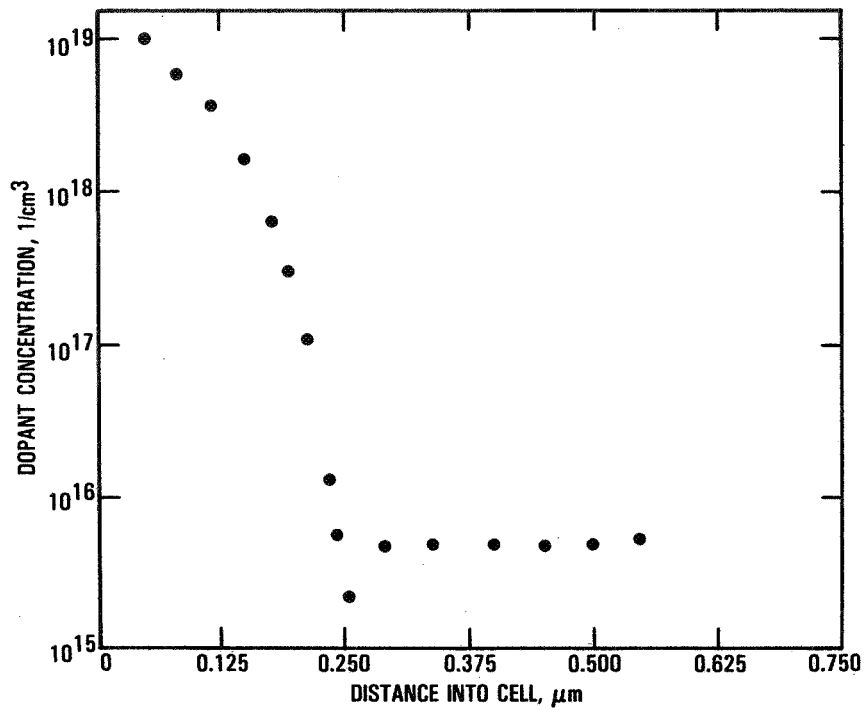
- High-quality solar cells obtained by laser metallization technique: AR-coated cell efficiency = 16.7%
- IN-SITU sintering occurs during laser writing process: low series resistance obtained with no further heat treatment
- Laser processing does not degrade solar cell characteristics: high shunt resistance and low leakage currents are achieved
- Higher efficiency possible by writing finer lines and optimizing grid pattern
- Program continuing to add high efficiency processes

Excimer Laser Drive-in of Liquid Dopants
(Westinghouse)

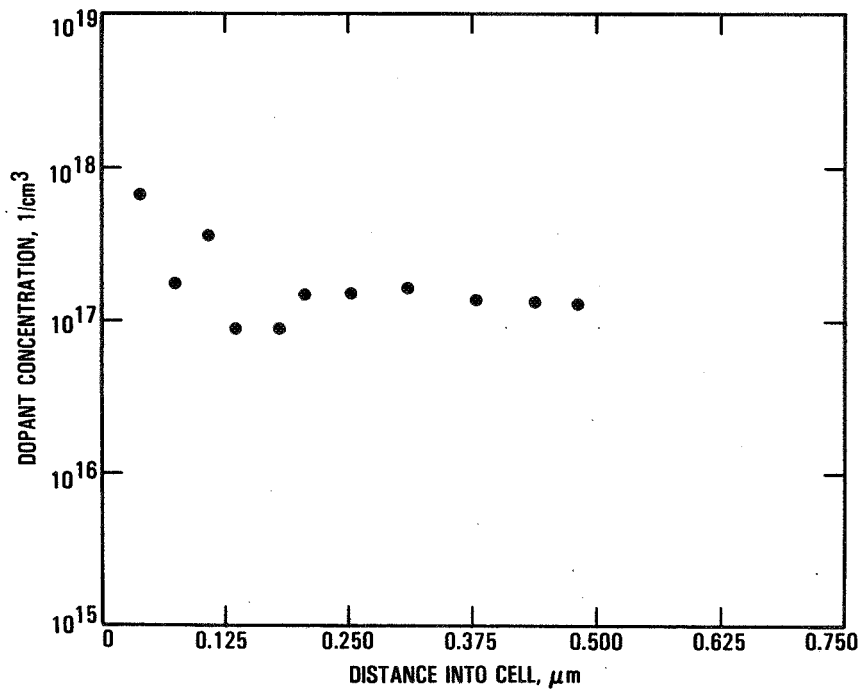
- Simultaneous drive-in of front and back junctions by thermal diffusion was unsuccessful. Cross-contamination of dopants occurred under all diffusion conditions using different diffusion masks. Cell efficiencies varied between <1% to 7 %
- Investigation of laser-drive-in of liquid dopants was started
- Three sets of web strips subjected to laser drive-in tests performed by Spectra Technology, Bellevue, Washington
- No cross-contamination of dopants occurred on any laser drive-in tests
- Front-junction profile looks good. See profile figure
- Back-junction profile is not good. See profile figure
- Laser parameters for front junction: 1.5 j/cm², 25 nanoseconds pulse duration, 1 mm² spot size, 50% overlap
- Laser parameter for back junction not yet established

PLENARY SESSIONS

n^+p Front Junction by Excimer Laser Drive-in



p^+p Back Junction by Excimer Laser Drive-in



**Results and Status of Excimer Laser
Drive-in of Liquid Dopants**

- **Best cells produced to date: 8% to 10% efficiency; inadequate back ohmic contact identified as cause of poor cell performance**
- **One final set of low-resistivity (0.4 ohm-cm) web strips to be subjected to laser drive-in tests. Back ohmic contact should be improved**
- **Successful demonstration of laser drive-in of liquid dopants will achieve the simultaneous junction drive-in goals**
- **Exploratory tests using rapid thermal processing (RTP) to simultaneously drive-in liquid dopants**
- **Initial results are very encouraging; 15% efficient cells produced**
- **Will conduct more tests to obtain statistical data**

Application Potential

- **Excimer laser anneal (after ion implantation)**
 - **Near term (<3 yr):** Not good. Only marginally equal to thermal anneal; probably will not supplant it
 - **Far term (3-15 yr):** Fair. Has best chance if lasers are used in other parts of the process sequence
- **Laser-assisted metallization (laser writing) (pyrolytic)**
 - **Near term (<3 yr):** Good potential for near-term use. Eliminates photolithography; immediate cost savings
 - **Far term (3-15 yr):** Same good potential. May dominate metallization processes
- **Excimer laser drive-in of liquid dopants**
 - **Near term (<3 yr):** Not good. Back-junction problems, needs more test evaluation
 - **Far term (3-15 yr):** Not good. Must compete with rapid thermal processing (RTP)
- **Microwave-assisted deposition (MECVD)**
 - **Near term (<3 yr):** Fair. Needs more evaluation
 - **Far term (3-15 yr):** Good. Microwave-assisted techniques have good potential in other processes -i.e., baking, sintering
- **Laser-assisted deposition (photolytic)**
 - **Near term (<3 yr):** (metal and surface passivation)
Cannot assess. No data available yet; may require extensive research
 - **Far term (3-15 yr):** Cannot assess. May have good potential for amorphous silicon
- **Rapid Thermal Processing (RTP)**
 - **Near term (<3 yr):** Good. Limited data very encouraging. Has good potential for junction formation and annealing
 - **Far term (3-15 yr):** Good. May dominate ion implantation anneal

**CRYSTAL GROWTH FOR HIGH-EFFICIENCY
SILICON SOLAR CELLS WORKSHOP:
SUMMARY**

JET PROPULSION LABORATORY

Katherine A. Dumas

Workshop Objectives

- **Review the state of the art in the growth of silicon crystals for high-efficiency solar cells**
- **Define sheet requirements for high-efficiency solar cells**
- **Identify future areas of research**

Presentation Outline

- **Session contents**
- **Technical highlights**
- **Conclusions**
- **Future areas of research**

Session Contents

Session I:

Material Requirements for High-Efficiency Silicon Solar Cells

Martin Wolf (University of Pennsylvania)

The Status of Silicon Ribbon Growth Technology for High-Efficiency Solar Cells

Ted Ciszek (Solar Energy Research Institute)

Future Application of Czochralski Pulling for Silicon

John Matlock (SEH America)

Potential Productivity Benefits of Float-Zone vs Czochralski Crystal Growth

Takao Abe (SEH)

PLENARY SESSIONS

Session II:

A New Outlook on Control of Crystalline and Chemical Perfection During Growth of Silicon

August Witt (Massachusetts Institute of Technology)

MCz: Striations in Cz Silicon Crystals Grown Under Various Axial Magnetic Field Strengths

George Kim (IBM)

High-Purity, Low-Defect FZ Silicon

Hiroshi Kimura and Glen Robertson (Hughes Research Laboratories)

Defects in Silicon Effect on Device Performance and Relationship to Crystal Growth Conditions

Lubek Jastrzebski (RCA Laboratories)

Session III:

Simulation of the Temperature Distribution in Crystals Grown by Czochralski Method

Milorad Dudukovic (Washington University)

Convective Effects in Float-Zone and Czochralski Melts

Paul Neitzel (Arizona State University)

Session IV:

Thermal-Capillary Models of Meniscus-Defined Crystal Growth: Interactions of Melt/Solid and Melt/Gas Interfaces with Crystal Size

Robert Brown (Massachusetts Institute of Technology)

Impurities in Silicon Solar Cells

Richard Hopkins (Westinghouse)

Oxygen and Carbon in Silicon

James Corbett (Suny-Albany)

Solar Cell and I.C. Aspects of Ingot-to-Slice Mechanical Processing

Lawrence Dyer (Texas Instruments)

Defects and Device Performance

George Storti

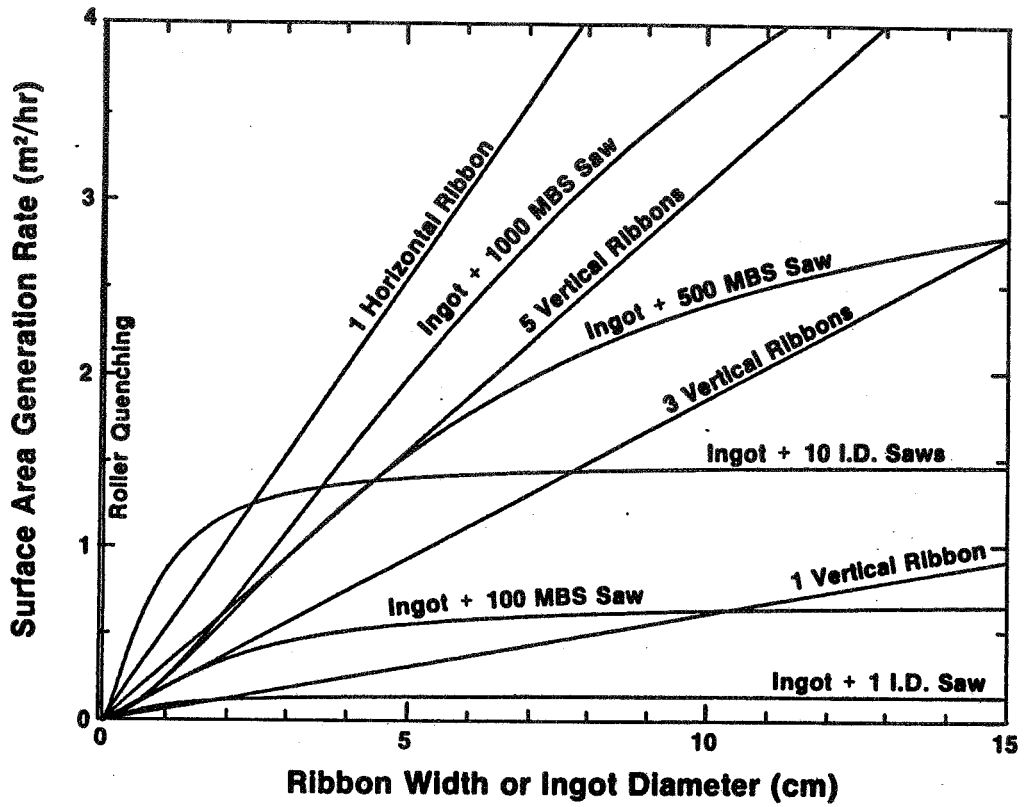
PLENARY SESSIONS

The Device Engineer's Wish List to the Materials Engineer

1. SILICON OF LONG MINORITY CARRIER LIFETIME
(e.g., 0.2 Ω cm p-type with $\tau > 500 \mu\text{s}$)
2. SILICON OF REPEATEDLY UNIFORM LIFETIME
(not 50-1000 μs)
3. SILICON WHOSE LIFETIME DOES NOT DECREASE DURING NORMAL
DEVICE PROCESSING
(a repeatable, uniform increase is o.k.)
4. SILICON SHEET (WAFER) WHICH IS FLAT, AND STAYS FLAT
THROUGHOUT NORMAL DEVICE PROCESSING
5. SILICON WHICH UNIFORMLY HAS REASONABLE MECHANICAL STRENGTH
6. SILICON SHEET OF LOW COST
($< \$50/\text{m}^2$)

Efficiency/Yield-Limiting Materials Characteristics

- Dislocations in grain boundaries
- Dislocations in subgrain boundaries
- Intragrain isolated dislocations
- Gross impurities: inclusions, precipitates
- Isolated impurities
- Dimensional evenness, processibility

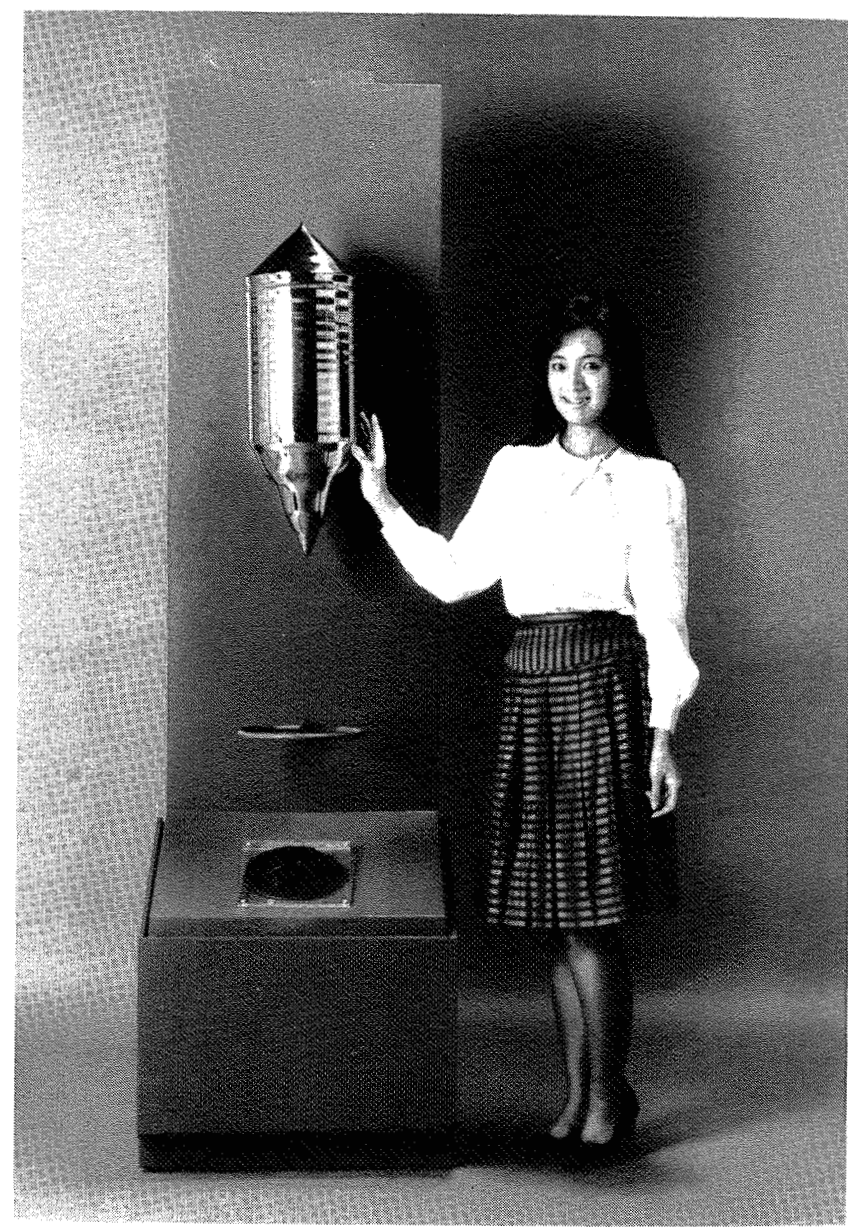


Criteria for the Ideal Sheet-Growth Method

- Good Crystal Perfection
- Flat Smooth Surface
- High Purity
- Easy Control
- High Throughput



FZ Single Crystal, 100 mm in Diameter
1.6 m in Length



Cz Single Crystal, 250 mm in Diameter
45 kg in Weight

PLENARY SESSIONS

Growth Conditions in 5-in. FZ and Cz Methods

	FZ* (1st + 2nd)	CZ
DIAMETER (mm)	128	130**
DIRECTION	<100>	<100>
POLY DIA LENGTH (mm)	128 1800	—
POLY WEIGHT (kg)	<u>50</u>	<u>30</u> ***
GROWTH RATE (mm/min)	1st 4 } 2nd 3 }	⊥

* 2pass FZ shows higher single crystal yield than that of single pass FZ.

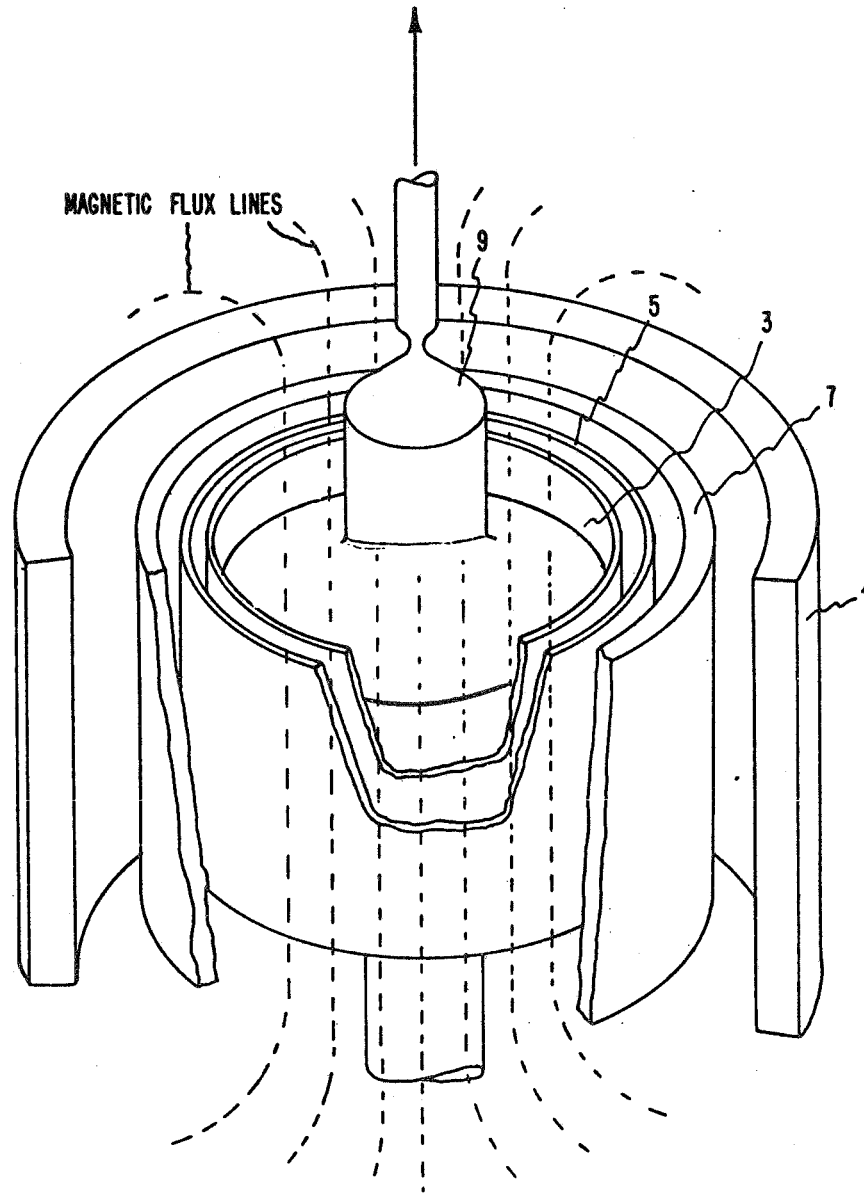
** FZ diameter control is easier than that of CZ.

*** 30 kg charge in 5" shows the most effective productivity (productivity x yield).

MCz Crystal Growth

APPARATUS FOR CZOCHRALSKI SILICON CRYSTAL GROWTH THROUGH AXIAL MAGNETIC FIELD FLUID FLOW DAMPING

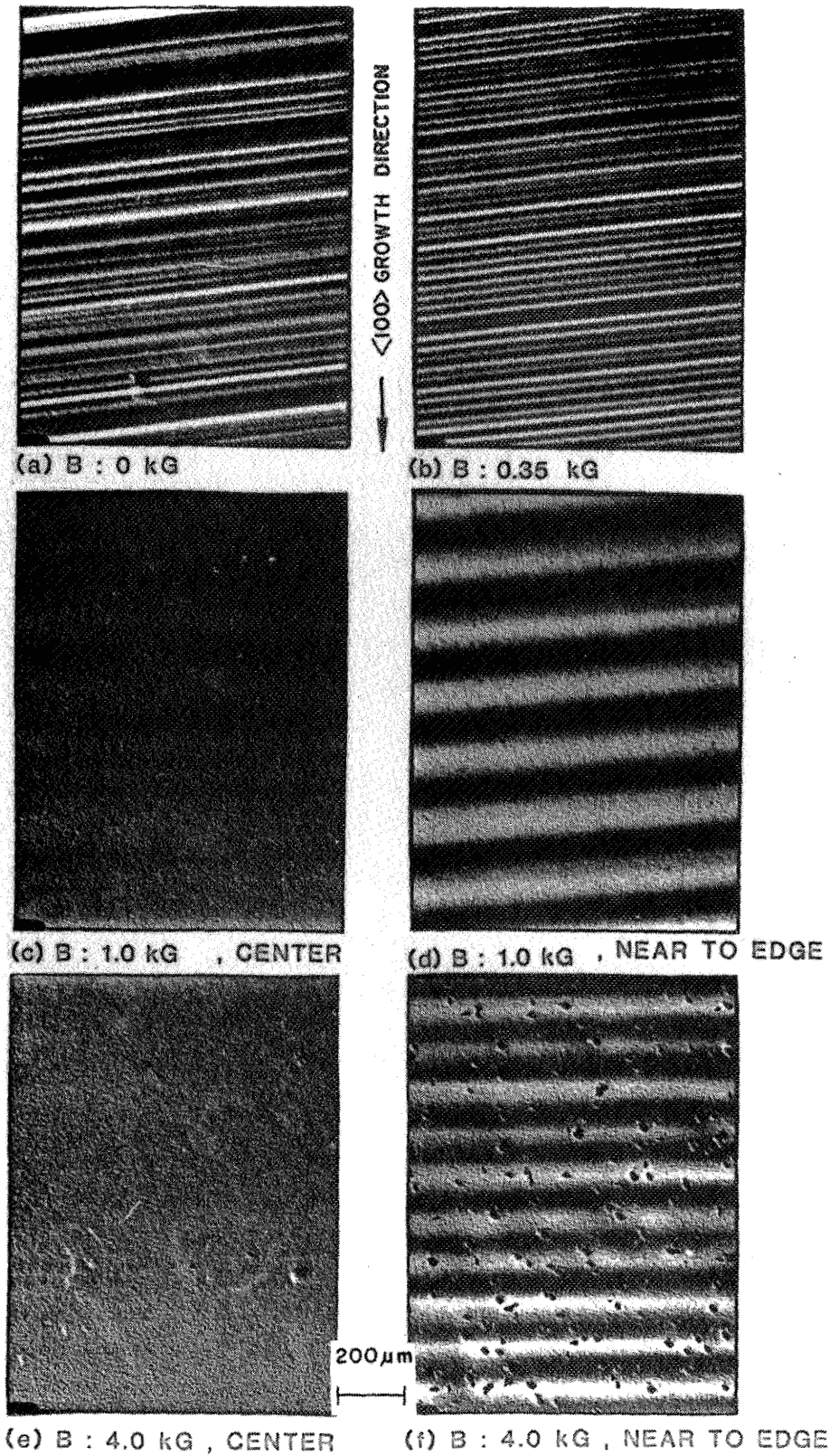
K. M. Kim, G. H. Schwuttke and P. Smetana



An arrangement is provided for utilizing axial magnetic fields to suppress the fluid flow in the melt of Czochralski-type silicon crystal growth systems.

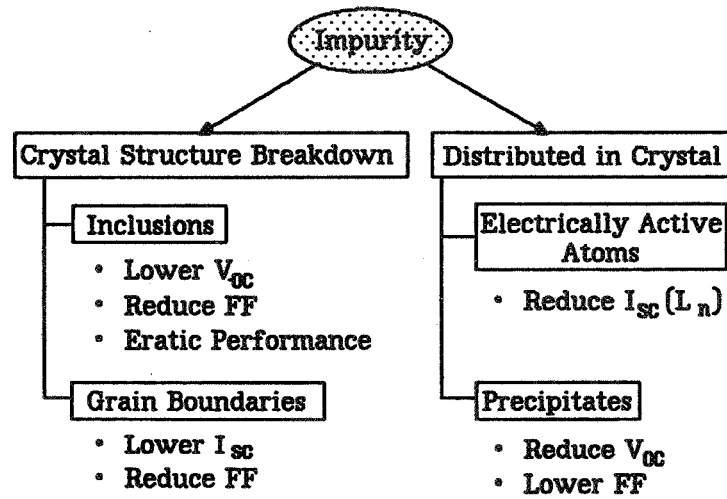
PLENARY SESSIONS

ORIGINAL PAGE IS
OF POOR QUALITY



Photomicrographs of Representative AMCz Crystal Sections. Note That Central Region of 4 kg crystal is free of striations; dislocation etch pits in (f)

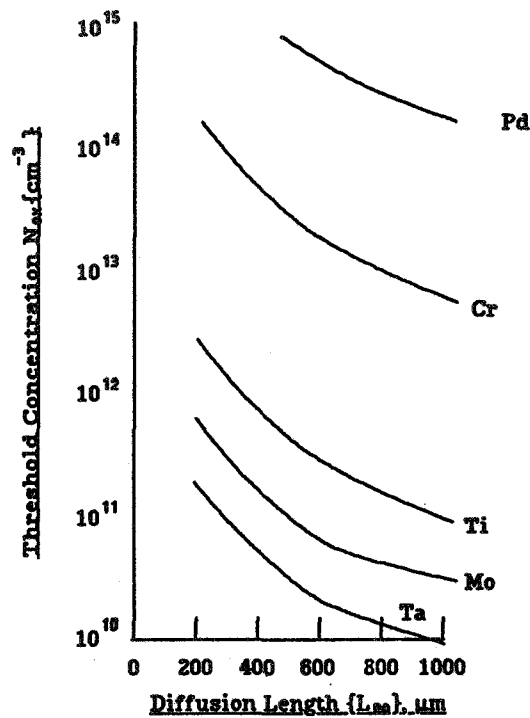
Impurity Degradation Mechanisms in Silicon Solar Cells



Impurity Behavior

- Degrade Junction
Cu, Ni
- Reduce Diffusion Length
Nb, Ti, V, Ta, W, Mo, Pd, Au, Zr, Mn, Al, Sn
- Both
Fe, Co, Ag

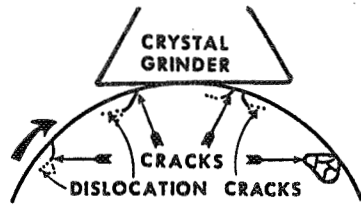
Variation in Degradation Threshold With Diffusion Length of Baseline SE Cell



Summary

1. Impurities Depreciate Cell Performance
 - Reduce Diffusion Length by Trap Formation
 - Degrade Junctions via Precipitates/Inclusions
2. Impurity Model Describes Well the Behavior of Conventional Cells (SE) with Single and Multiple Contaminants
3. Models Can be Used to Understand Impurity Effects in:
 - High Efficiency Designs
 - Polycrystalline Material
 - Sheet or Ribbon Crystals
4. High Efficiency Devices More Sensitive to Impurities than Conventional Devices
5. Improved Data on Impurity Effects Required to Quantify Model Predictions for High Efficiency

Schematic of Slip Generation From Excessively Deep Crystal Grind Cracks



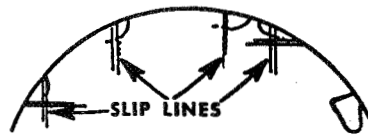
A. GRINDING OF SILICON INGOT CAUSES CRACKS AND DISLOCATION CRACKS.



B. SLICING PUTS IN SAW DAMAGE AND CHIPS OUT SOME GRINDING CAVITIES.



C. LAPPING, ETCHING AND POLISHING REMOVES SAW DAMAGE BUT NOT ALL OF THE GRINDING DAMAGE.



D. PROCESSING IN FURNACE OR EPI REACTOR GENERATES SLIPLINES.

ORIGINAL PAGE IS
OF POOR QUALITY

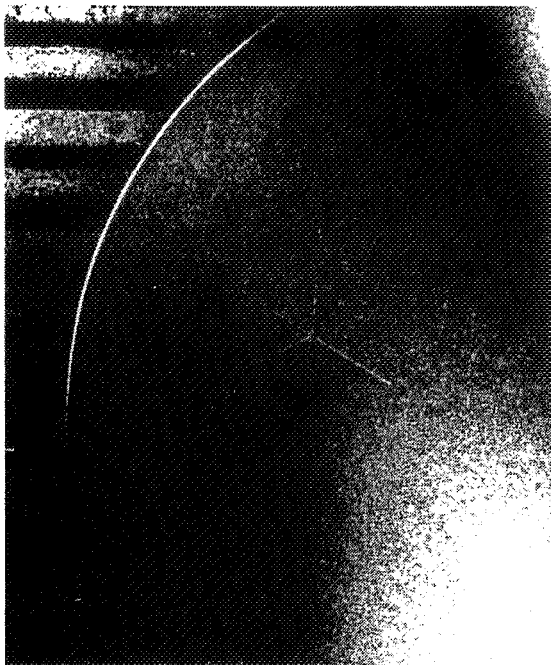


Fig. 10. Crow's-foot fracture from burr on vacuum chuck.

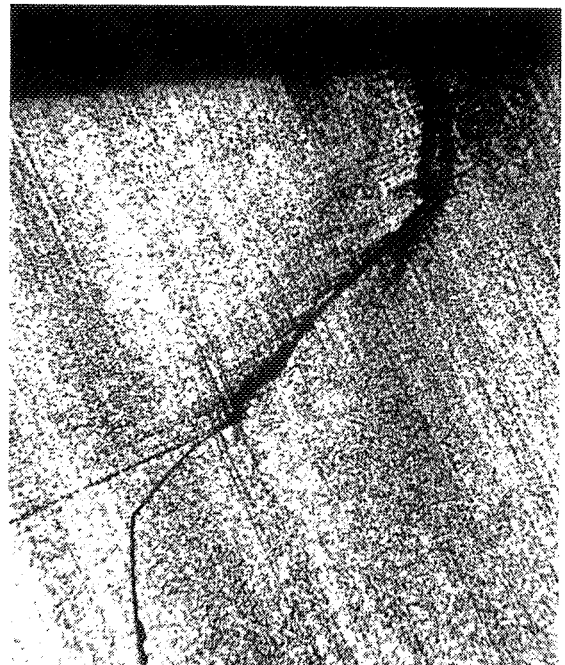


Fig. 12. Edge crack from heat-treating silicon slice in quartz boat.

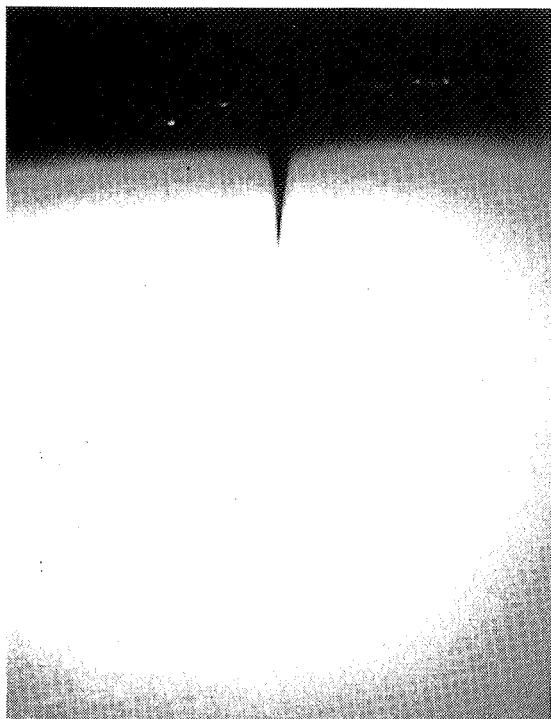


Fig. 13. Edge crack at polish.

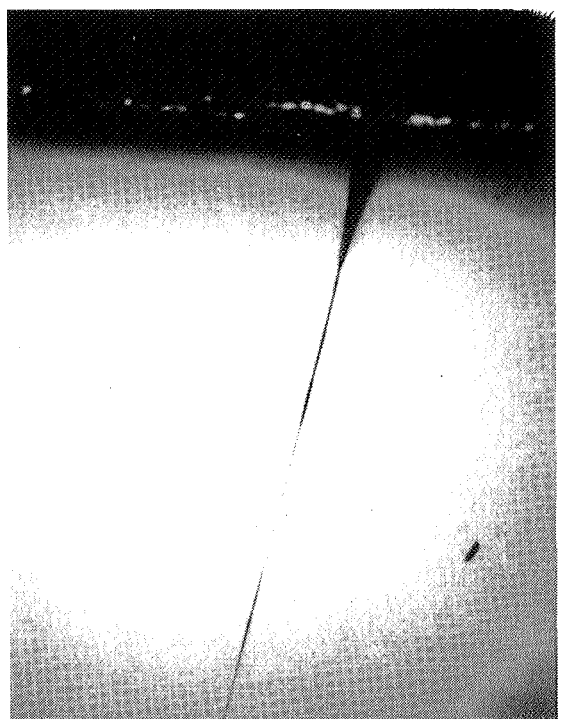


Fig. 14. Edge crack at polish.

Conclusions

1. **Present-day FZ and Cz are of sufficient quality to obtain efficiencies in excess of 20%. FZ is the preferred material because higher diffusion lengths can be obtained for a given base doping**
2. **FZ and Cz silicon are very useful to the device researcher for determining the importance of the various loss mechanisms and for devising the processing technologies to reduce the losses**
3. **Economic cell-processing technologies that take advantage of the experience gained in the laboratory will also have to be devised**
4. **Ultimately, it is unlikely that either Cz or FZ silicon is economic for photovoltaics; this is true for any technology**
5. **The important issue for the alternate in silicon technologies is whether sufficiently high diffusion lengths for a given base doping and wafer thickness are achievable, and, if achievable, whether it can be done quickly and economically**
6. **Five-Year Plan does not include technology development effort on ingot growth and there are not sufficient funds to do all the research that needs to be done**

PLENARY SESSIONS

Future Areas of Research

- **Technology development for float-zone-grown silicon is needed**
- **Implement innovative concepts to improve material perfection of Czochralski-grown silicon**
- **If ingot technology is supported, need for wafering research is unquestionable**
- **Continue research in ribbon technology to develop "ideal" ribbon growth process**

RELIABILITY AND ENGINEERING OF THIN-FILM PHOTOVOLATAIC MODULES

JET PROPULSION LABORATORY

E. L. Royal

Research Forum

Title: Reliability and Engineering of Thin-Film Photovoltaic Modules
Date: March 20, 1985
Washington, D.C.

- Technical Sessions: 3
- Session I Cell and System Characteristics Affecting
 Module Design
 Chairman L. Herwig, DOE HQ
- Session II Thin-Film Module Developments Within
 U.S. Companies
 Chairman E. Royal, JPL
- Session III Reliability Research and Performance
 Investigations
 Chairman R. Ross, JPL
- Attendees: 68
- Papers: 17

Research Forum Overview

The purpose of the Research Forum was to: (1) examine critically the attributes of thin-film cells that influence module performance and reliability, (2) explore the lessons and applicability of crystalline-Si module technology to thin-film modules, (3) review the current status of thin-film module technologies, and (4) identify problem areas and needed research. Another important objective was to accelerate the sharing of technical experience between solid-state device researchers and engineering reliability researchers. Forum arrangements were designed to encourage interaction and exchange of information among the wide range of researchers who attended.

The keynote address, presented by Dr. Charles Gay, Vice President, Research and Development, ARCO Solar, Inc., was titled "The Need for Thin-Film Reliability Research." In this address, Dr. Gay praised the work of JPL for its reliability research support as a key factor in the success of crystalline-silicon technology. He urged that a similar type and level of support be committed for thin-film cell and module reliability research.

PLENARY SESSIONS

Dr. Gay gave equal praise to SERI as a developing center of excellence in basic research studies and measurements. In addition to papers presented, two domestic private-industry photovoltaic companies used the Research Forum to announce new a-Si module designs. Both modules were shown and each was described in considerable technical detail.

Reversible Degradation Versus Non-Reversible Degradation

- **Concern**
 - **How to separate Staebler-Wronski-effect-related degradation from degradation incurred during Arrhenius-type reliability research investigations**
 - **Pros and cons on use of annealing**

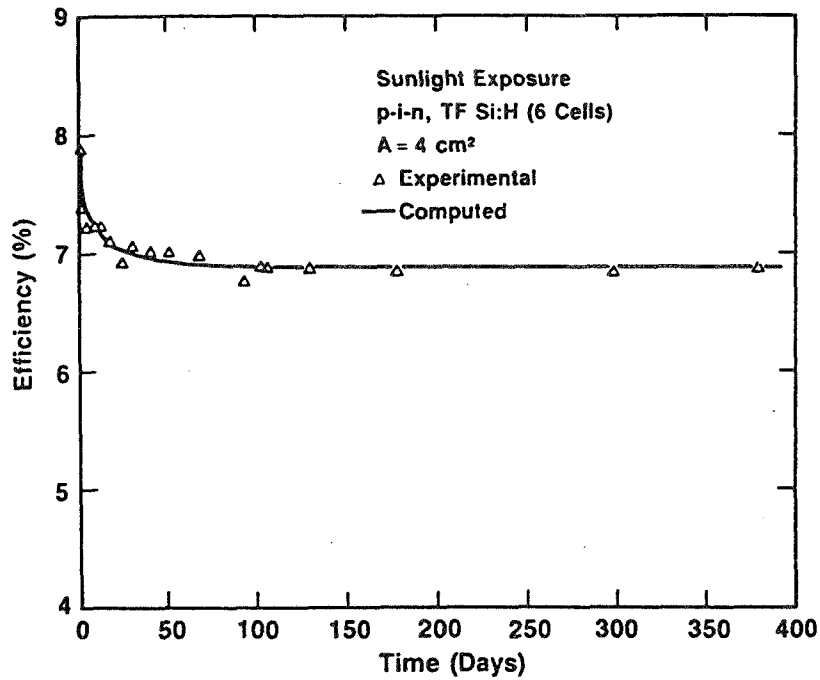
Staebler-Wronski Effect

LIGHT-INDUCED CHANGES:
GENERATION OF METASTABLE
DEFECT STATES THAT CAUSE DECREASES
IN BOTH DARK CONDUCTIVITY AND
PHOTOCONDUCTIVITY

Degradation

- **10% to 15% (from as-made, initial measurement)**
- **Major contributor: bulk**
- **Reversible**

Staebler-Wronski Effect



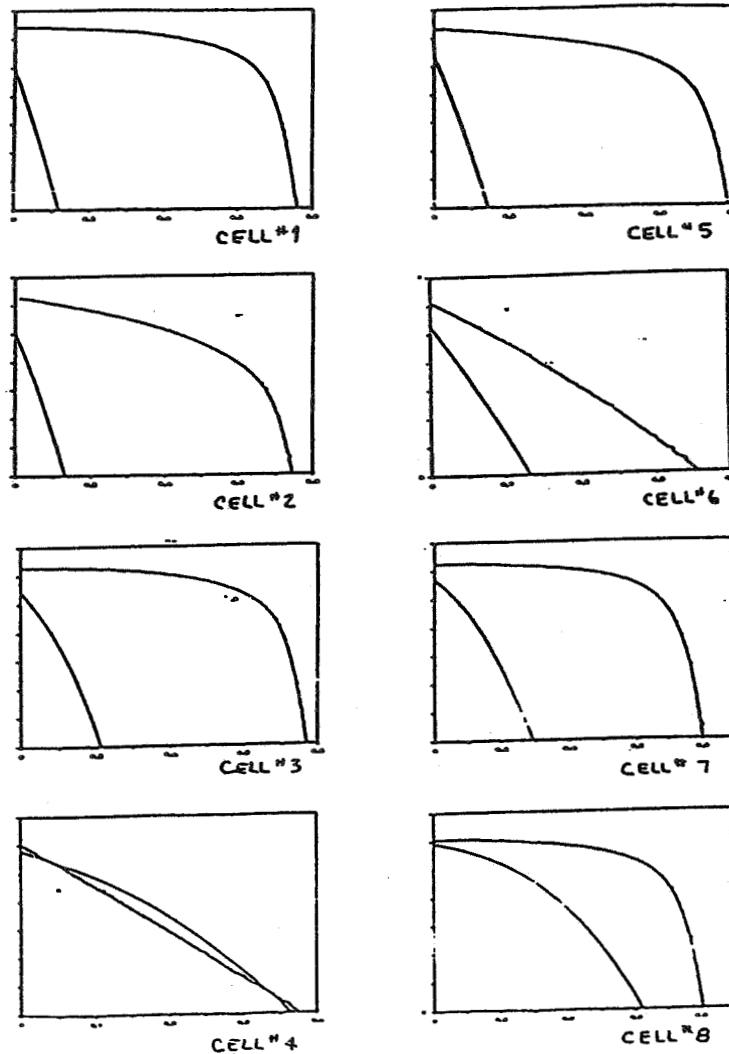
Ullal, Morel, Wilett, Kanani

Amorphous-Silicon Reliability Investigations (Clemson University)

- Research areas: major focus
 - Exploratory research investigations
 - α -Si cell accelerated Arrhenius-type testing underway
 - α -Si cell real-time outdoor exposure testing
 - Cell failure analysis and failure mechanism research (includes new state-of-the-art Auger microprobe)
- Support activity
 - Device measurement research (major new development to be announced!)

PLENARY SESSIONS

Eight Amorphous-Silicon Cells in Same Submodule
Pre- and Post-Stress IV Curves (140°C Step)



Range of Amorphous-Silicon Reliability Data

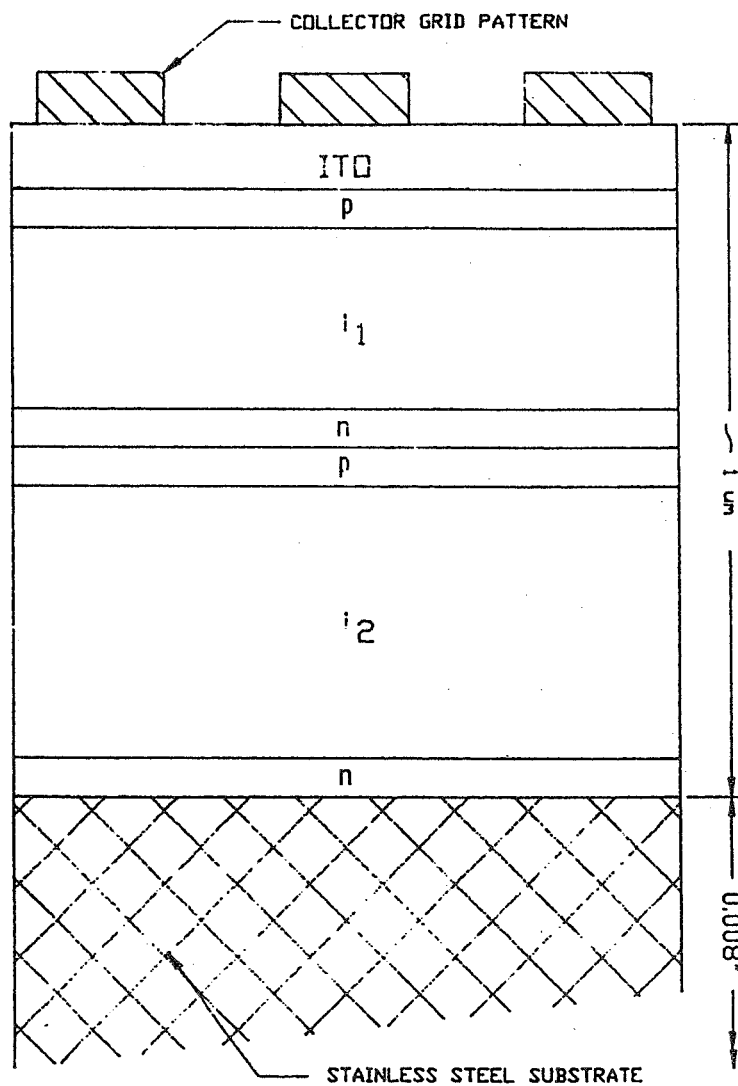
- o BIAS VS-OPEN CIRCUIT CONDITIONS
- o DARK-VS-ILLUMINATED DURING STRESS
- o MEASUREMENTS UNDER VARIABLE LIGHT INTENSITIES
- o ENCAPSULATED VS-UNENCAPSULATED
- o ELECTRICAL CHANGES CORRELATED WITH PHYSICAL CHANGES

PLENARY SESSIONS

NEW DEVELOPMENTS REVEALED:

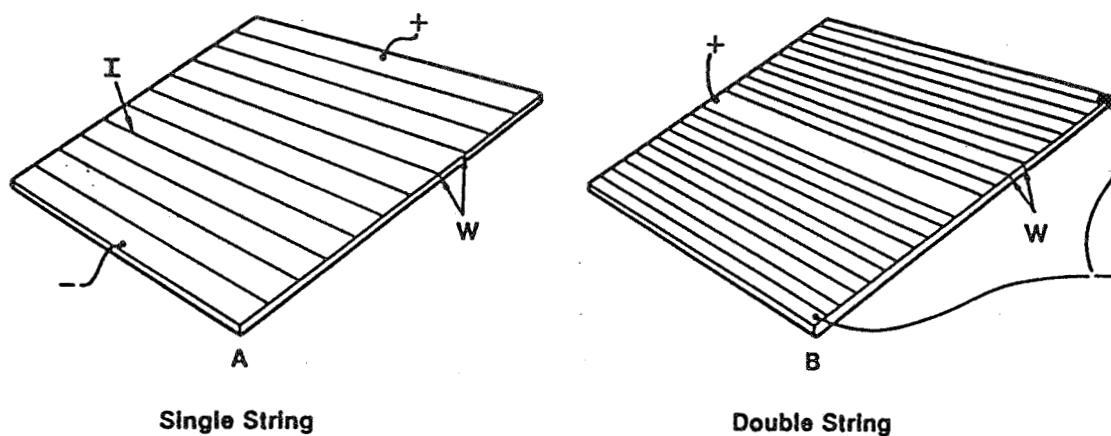
- Two unique a-Si module encapsulation approaches
 - All glass
 - Glass substrate, front cover
 - Glass backsheet (tempered), back cover
 - All polymer
 - Tedlar, front cover
 - PET/Tedlar, back cover
- New tandem (multijunction) a-Si cell

Amorphous-Silicon Tandem Cell Profile



PLENARY SESSIONS

Module Options



Glass Strength Research

- o STRENGTH REDUCTION STUDIED
 - o DURING HIGH TEMPERATURE DEPOSITION OF ITO
 - o DURING LASER SCRIBING
- o SAMPLES FROM A-SI CELL/SUBMODULE MANUFACTURERS
- o BURST PRESSURE TEST DEVELOPED
- o DATA ANALYSIS CONSIDERATIONS

Encapsulation Materials Developments

- o CONSIDERATION FOR FLEXIBLE THIN-FILM MODULES
- o UV STABILIZATION ADDITIVE RESEARCH
- o NOVEL OUTDOOR CONTROLLED TESTING

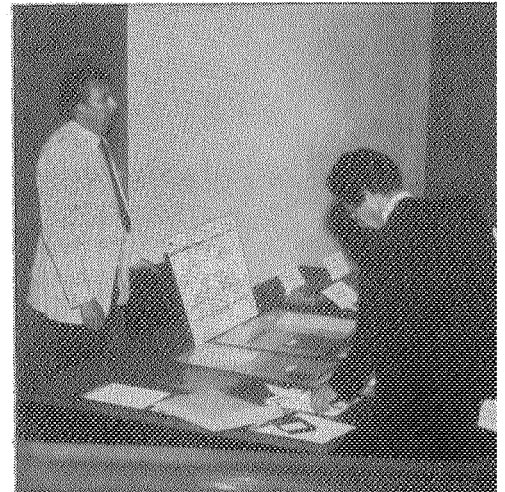
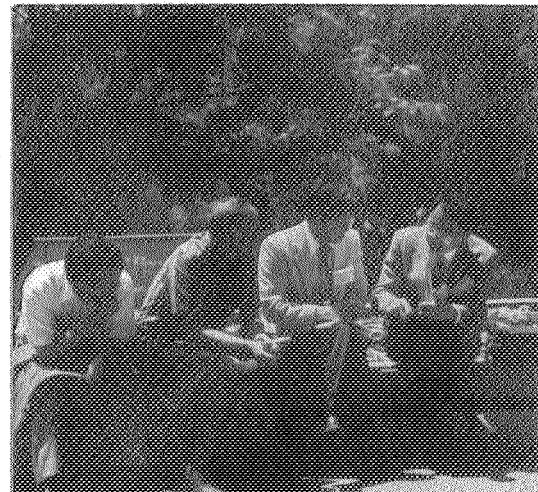
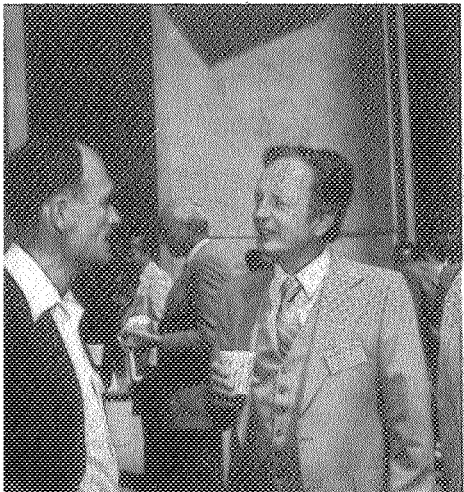
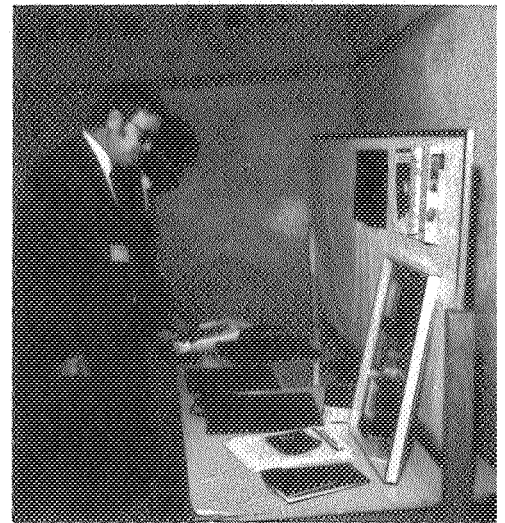
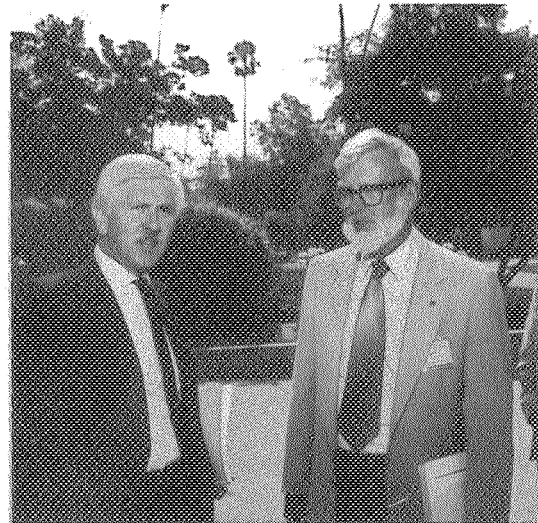
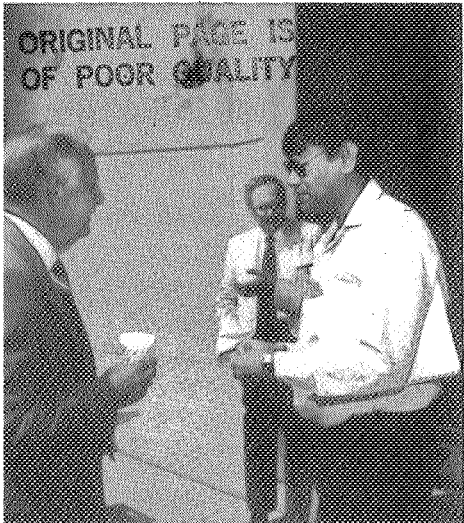
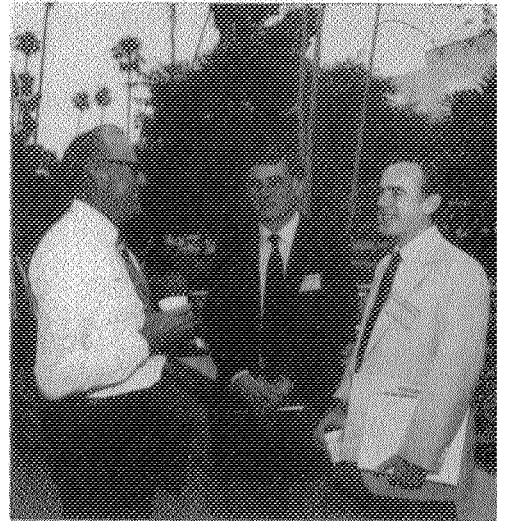
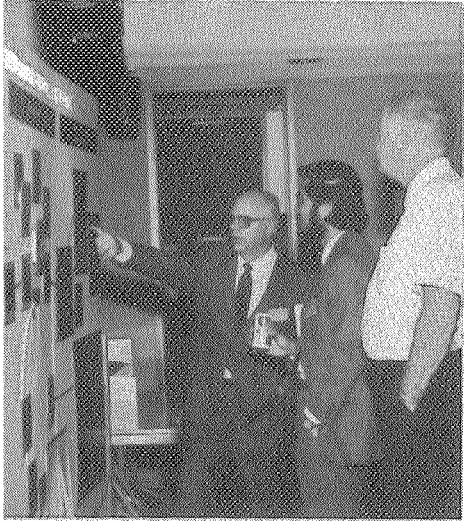
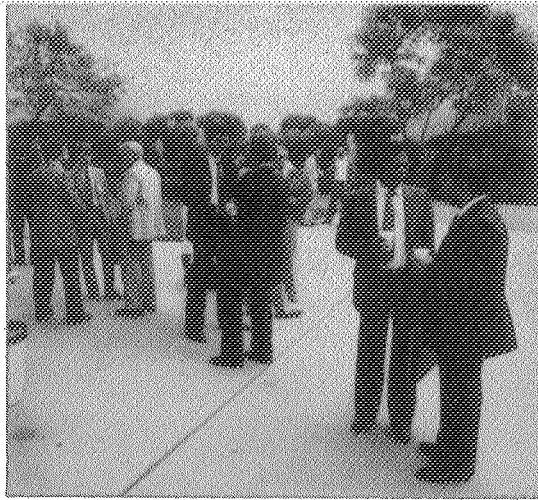
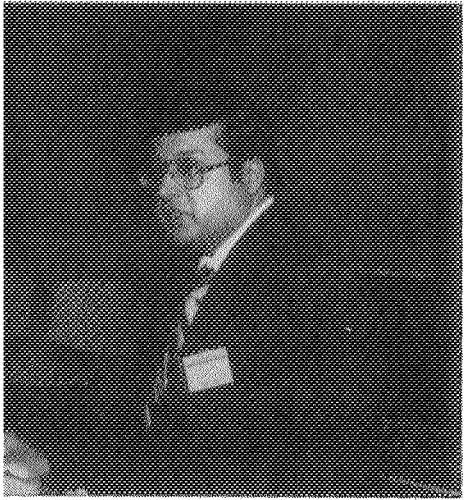
PLENARY SESSIONS

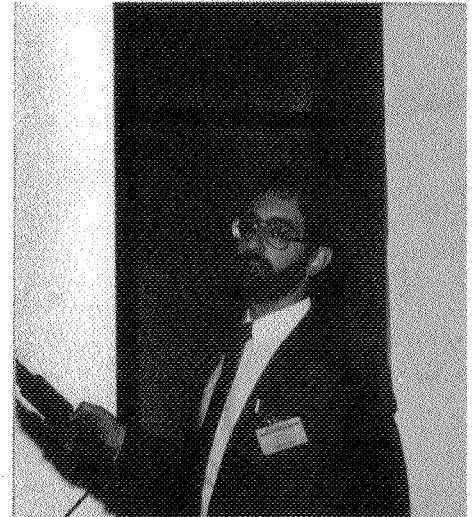
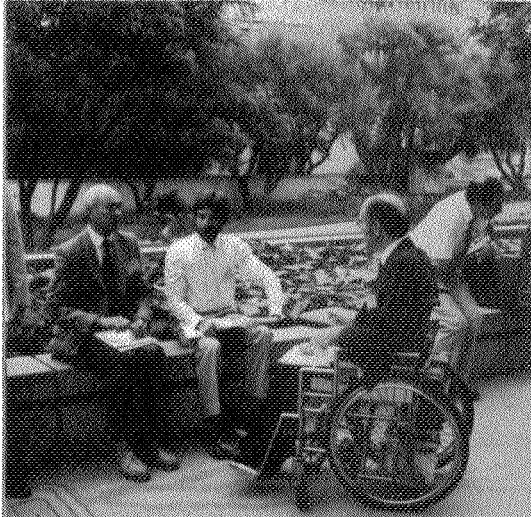
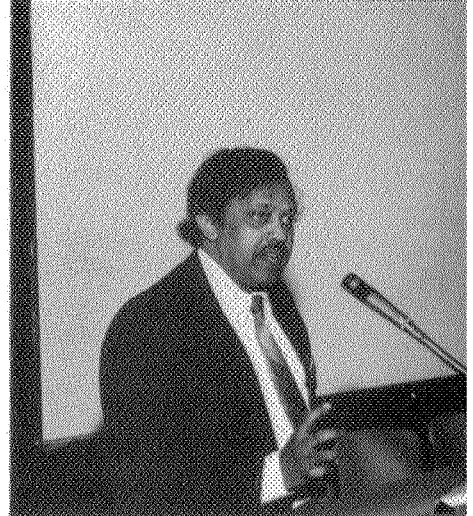
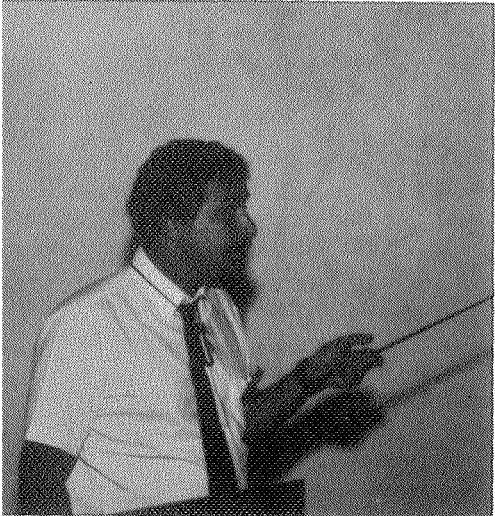
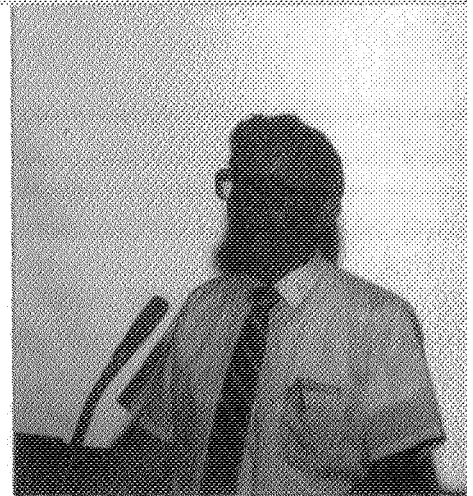
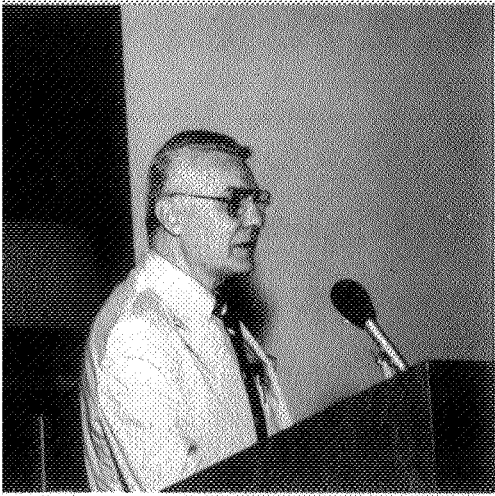
Expanded Needs for Reliability Research Data (Cells/Submodules/Modules)

- o EFFECTS OF ANNEALING PROCESS
- o ACTIVATION ENERGY OF REVERSIBLE PROCESS

Conclusions

- Crystalline-Si and thin-film modules are expected to have much in common with respect to reliability problems, methods and solutions
- New materials and processes in thin-film modules will require a diligent reliability program
 - Establishment of mechanism-specific reliability goals
 - Quantification of mechanism parameter dependencies
 - Prediction of expected long-term degradation
 - Identification of cost-effective solutions
 - Testing and failure analysis of trial solutions





Technical Sessions

RELIABILITY PHYSICS

Ronald G. Ross, Jr., Chairman

R. Liang, of JPL, discussed key reaction intermediates of photooxidation identified and characterized by laser flash Electron Spin Resonance (ESR) spectroscopy. Effects of temperature and ultraviolet (UV) intensity were studied in order to develop meaningful accelerated testing procedures for encapsulant evaluation. In a program to study the failure of Tedlar/ethylene vinyl acetate (EVA)/stainless steel modules, failure modes similar to those observed outdoors in real-time conditions were simulated in accelerated testing. An experimental technique was developed to quantitatively assess the extent of degradation.

S. Mattai, of the University of Toronto, described the continuation of efforts on their computer model of the photooxidation of polymers. They have completed preliminary modeling of EVA degradation. Their results showed that photooxidation degradation rates of EVA are similar to those of the model compound polyethylene.

P. Gomez, of Polytechnic Institute of New York, explained that head-to-head polyvinyl naphthalene was synthesized in order to test and evaluate electronic energy dissipation pathways in polymers following absorption of photons.

Dr. Boerio has demonstrated that he can experimentally observe the interfacial chemistry established between EVA and the aluminized back surface of commercial solar cells. The technique employed is called "Fourier Transform Infrared (FTIR) spectroscopy, with the infrared signal being reflected back from the aluminum surface through the EVA film. Reflection infrared (IR) spectra are given and attention is drawn to the specific IR peak at 1080 cm^{-1} which forms on hydrolytic aging of the EVA/aluminum system. With this fundamental finding, and the workable experimental techniques, Dr. Boerio can progress to employ candidate silane coupling agents at the interface, and monitor for their effects on eliminating or slowing hydrolytic aging of the EVA/aluminum interface.

Three topics dominated the presentation by P. Willis of Springborn Laboratories: (1) the successful use of outdoor mounting racks as an accelerated aging technique (these devices are called optal reactors); (2) a beginning list of candidate pottant materials for thin-film encapsulation, which process at temperatures well below 100°C ; and (3) description of a preliminary flame-retardant formulation for EVA which could function to increase module flammability ratings.

Outdoor Photothermal Aging Device (OPTAR) reactors provide a new and different approach to outdoor accelerated aging. The predominant cause of outdoor deterioration is photothermal aging, and the combination of heat and UV light. In all the laboratory techniques devised to date, it is mainly the light that is increased (photoacceleration) through the use of arcs and

RELIABILITY PHYSICS

discharge lamps. In the OPTAR reactors, natural sunlight is used as the light source and only the specimen temperature is increased. The OPTAR reactors consist of heated aluminum blocks surfaced with stainless steel and mounting hardware to hold the test specimens flush with the surface. The reactors are tilted at 45° south, and the device turns on at sunrise and off at sunset. Three temperatures have initially been selected: 70, 90, and 105°C. This approach eliminates the difficulties associated with the irregular spectrum of artificial light sources, exposes the specimens to other environmental conditions such as rain and pollution, and also incorporates a dark cycle. The only acceleration, therefore, is in the temperature, all other environmental conditions being present in their natural occurrence and intensity.

Polypropylene was selected as a model polymer for an initial test because of the fact that its induction period (t_i) is sharp and easily measured. This is shown as a sudden drop in the elongation at break. Tensile bars of unstabilized compression molded polypropylene were placed on the OPTAR devices at the three temperatures and the log of the induction period measured as a function of reciprocal temperature. The graph presented shows that the relationship is linear and that a close approximation to the Arrhenius function exists.

Extrapolation of the data line to lower air temperatures impressively predicts the actual outdoor aging time of this polypropylene at ambient conditions. Future work will emphasize encapsulation materials and fabricated modules.

G. R. Mon, of JPL, outlined a general research approach toward understanding water-module interactions and the influence of temperature involving the need to: (1) quantify module performance loss versus level of accumulated degradation, (2) establish the dependence of the degradation reaction rate on module moisture and temperature levels, and (3) determine module moisture and temperature levels in field environments. These elements were illustrated with examples drawn from studies of the now relatively well-understood module electrochemical degradation processes.

New research data presented include temperature and humidity-dependent equilibrium leakage current values for multiparameter module material and design configurations. The contributions of surface, volume, and interfacial conductivities was demonstrated. New research directions were suggested to more fully understand the contributions to overall module conductivity of surface, volume, and interfacial conductivities over ranges of temperature and relative humidity characteristic of field environments.

L. Wen discussed the problems associated with mathematically modeling water-module interaction phenomena, including sorption and desorption, diffusion, and permeation, i.e., transient behavior. With reliable analytical models, an extensive materials database, and solar radiation surface meteorological observations (SOLMET) weather data, predicting module lifetimes in realistic environments can become a practical reality.

Dr. Wen gave a status report on the present techniques of simulating the various transport mechanisms. The "Dent" model [a modified B-E-T (Brunauer-Emmett-Teller) approach] represented PVB sorption data. A 100-layer

RELIABILITY PHYSICS

material model and Fick's diffusion model gave diffusivity values exhibiting adequate agreement with those measured for polyvinyl butyral (PVB). Diffusivity of PVB is concentration dependent, decreasing as the water content in PVB increases. The temperature dependence of diffusion in PVB is well modeled by the Arrhenius rate equation. Equilibrium conductivity and leakage current data are well represented by Hearle's model for bulk ionic conductivity. A nodal network analysis using the Systems Improved Numerical Differencing Analyzer (SINDA) Thermal Analyser gave reasonable correlation with measured data. It is concluded that realistic lifetime predictions seem to be feasible.

Professor Orehtsky, of Wilkes College, addressed two topics: moisture transport and dielectric breakdown of PVB, Tedlar, and PVB/Tedlar composites. Professor Orehtsky presented data between 20 and 80°C showing : (1) that the moisture flux through the composite is governed by the "slower" material; and (2) that the composite permeability is intermediate to those of the component materials, as predicted by theory. Data for Tedlar at 71°C, showing the dependence of moisture flux on relative humidity, was also presented. Dielectric breakdown data were less precise and less conclusive. The generally applied theoretical model does not match the experimental data. The PVB/Tedlar composite exhibited greater voltage breakdown resistance than either component. Testing of EVA and EVA/Tedlar composites is underway.

E. Cuddihy, of JPL, pointed out that electrical products having organic materials functioning as pottants, encapsulants, and insulation coatings are commonly exposed to elevated conditions of temperature and humidity. In order to assess service life potential from this method of accelerated aging, it has been empirically observed that service life seems proportional to an aging correlation which is the sum of temperature in degrees Celsius (t), and the relative humidity (RH) expressed in percent. Specifically, the correlation involves a plot of "time-to-failure" on a log scale versus the variable " $\text{RH} + t$ " plotted on a linear scale (overall, a semo-log plot).

The presentation provides a theoretical foundation for this empirically observed correlation by pointing out that the correlation actually involves a relationship between the electrical resistivity (or conductivity) of the organic material, and the variable " $\text{RH} + t$." If "time-to-failure" is a result of total number of coulombs conducted through the organic material, then the correlation of resistivity versus " $\text{RH} + t$ " is synonymous with the empirical correlation of "time-to-failure" versus " $\text{RH} + t$."

PHOTOTHERMAL DEGRADATION STUDIES

JET PROPULSION LABORATORY

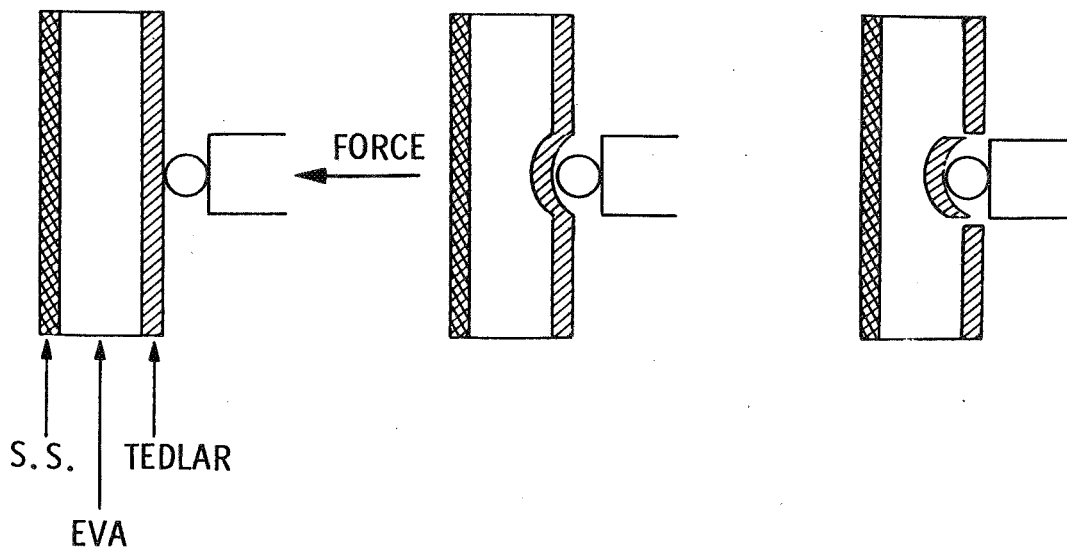
Ranty H. Liang

Accelerated Testing Development

- OBJECTIVE
 - DEVELOP VALID ACCELERATED TESTING METHODOLOGY IN ORDER TO EVALUATE MATERIALS FOR 30 YEARS LIFE

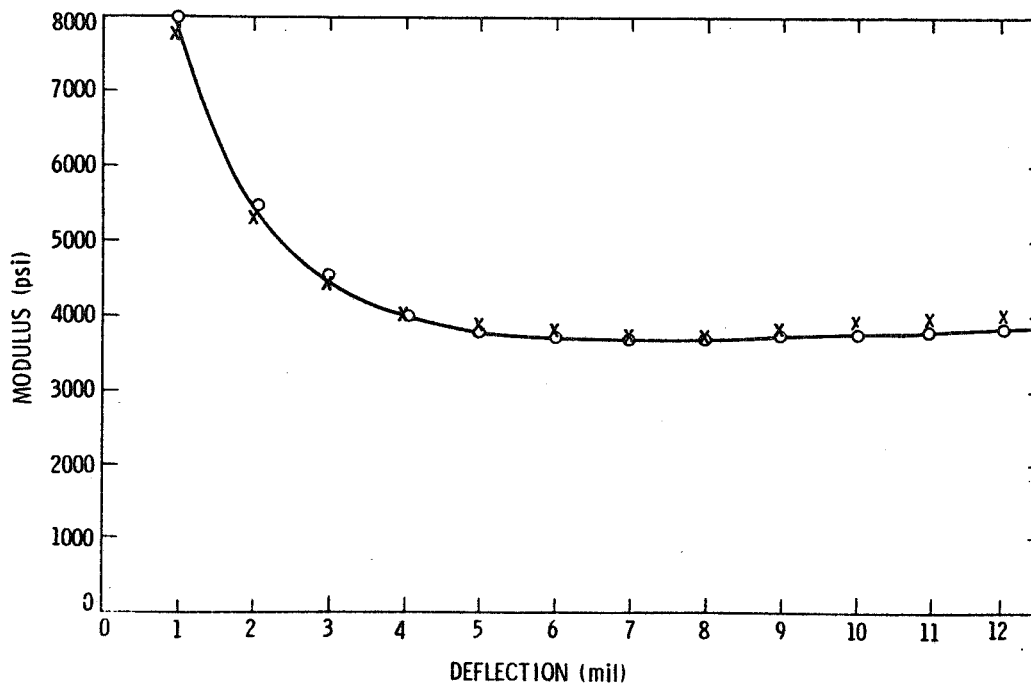
- APPROACH
 - IDENTIFY FAILURE MODES
 - DETERMINE ACCELERATED TEST CRITERIA
 - DEVELOP ACCELERATED TESTING METHODOLOGY

Compression Testing of Tedlar/EVA/S.S. Module

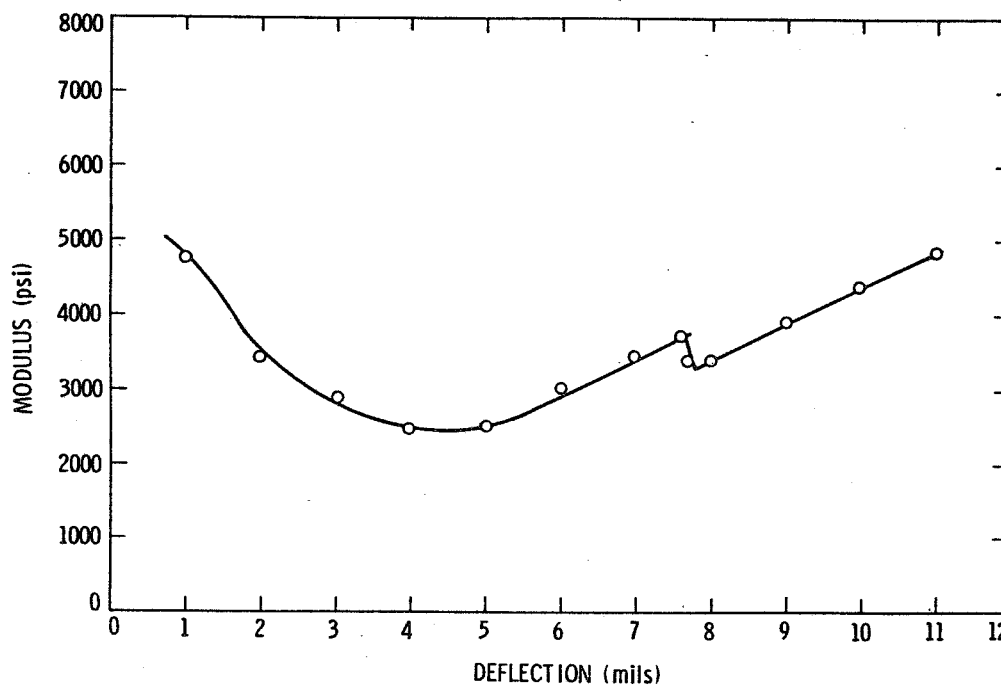


PRECEDING PAGE BLANK NOT FILMED

Control Sample (Between Cell)



Sample B (Between Cell)



Compression Testing of Tedlar/EVA/S.S. Module

	SAMPLE	DEFLECTION POINT (mil)	MODULUS (psi)
OVER CELL	A	4.4	9,000
	B	3.8	8,000
	C	9.7	5,200
BETWEEN CELL	A	9.0	4,700
	B	7.7	3,800
	C	> 12	2,900

A = OUTDOOR, REAL TIME, 500 DAYS, 75⁰C

B = ACCELERATED, 6.5 DAYS, 85⁰C, 8 SUNS

C = ACCELERATED, 6.5 DAYS, 98⁰C, 5.5 SUNS

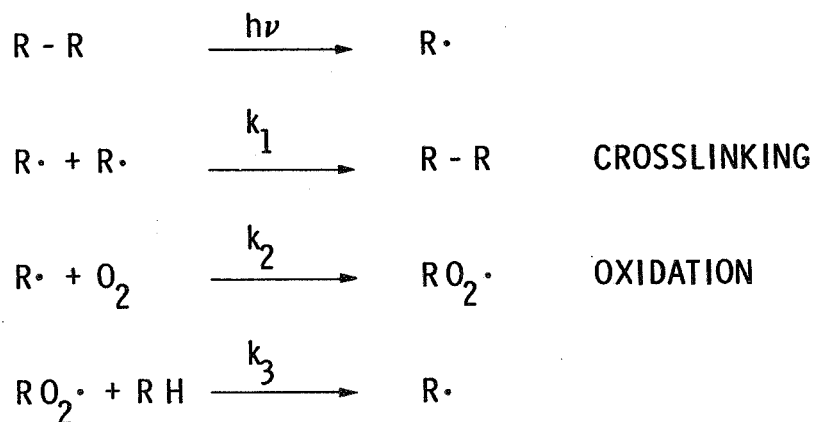
Simulation and Modeling of Photothermal Degradation of Tedlar (Conclusion)

- TWO OR MORE DEGRADATION PATHWAYS EXIST
- THEY HAVE SUBSTANTIALLY DIFFERENT E_{act} , SO THAT
 - RATE k_1 PREDOMINATES AT TEMP $\leq 85^0C$
 - RATE k_2 PREDOMINATES AT TEMP $> 90^0C$
- DAMAGE IS CHIEFLY UV DRIVEN
- TEDLAR IS THE MATERIAL UNDERGOING DEGRADATION
- QUAL TEST TEMPERATURE SHOULD BE $\leq 85^0C$

Mechanistic Studies of Photothermal Degradation

- OBJECTIVES
 - TO STUDY MECHANISTIC PATHWAYS OF PHOTOTHERMAL DEGRADATION
 - TO DETERMINE PHOTOTHERMAL REACTION RATES FOR MOLECULAR KINETIC MODELING
- APPROACH
 - LASER-FLASH ESR SPECTROSCOPY TO DETERMINE KEY REACTION INTERMEDIATES AND THEIR KINETICS

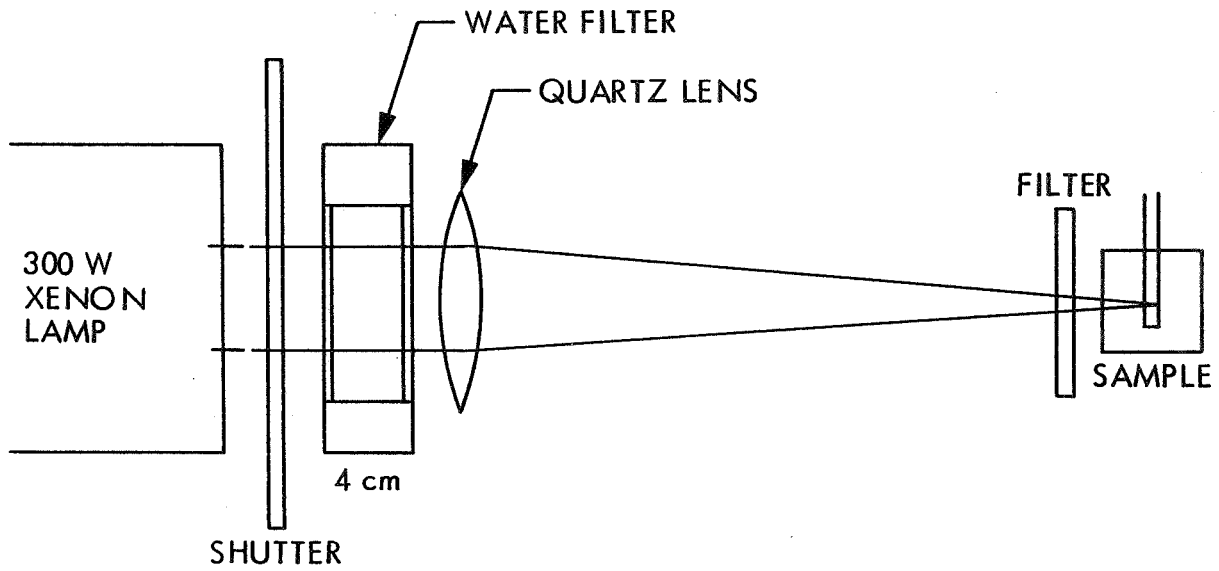
Mechanism of Photooxidation



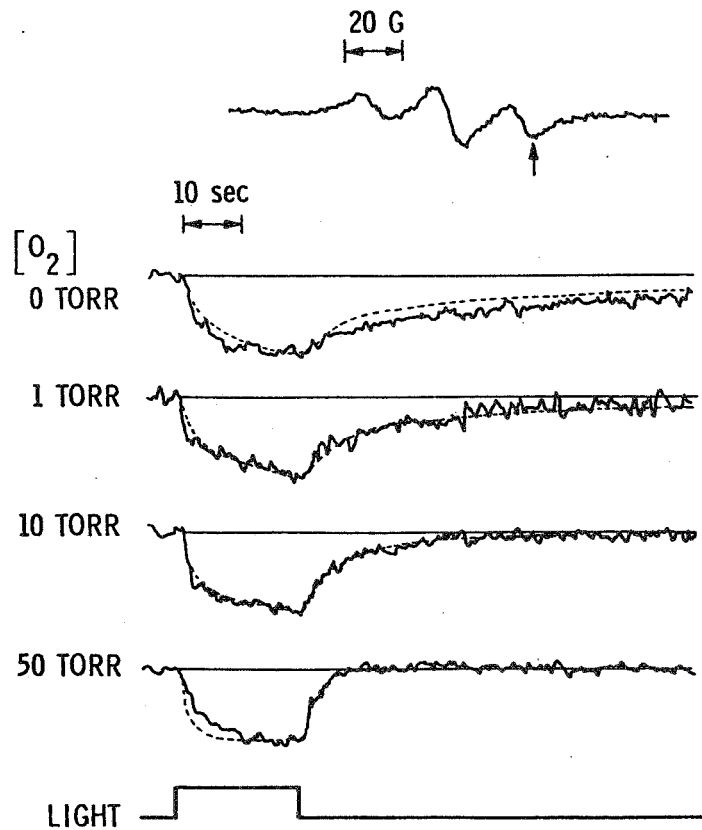
PRELIMINARY RESULTS

$$\begin{array}{l}
 k_1 = 10^{-2} \text{ liter/mole sec} \\
 k_2 = 1.3 \times 10^{-2} / \text{sec} \\
 k_3 = 10^{-1} / \text{sec}
 \end{array}$$

Flash ESR Apparatus



Time Resolved ESR Spectra of Photogenerated Polymeric Radicals



RELIABILITY PHYSICS

Photothermal Mechanistic Studies (Conclusion)

- KEY TRANSIENT RADICALS RESPONSIBLE FOR PHOTOTHERMAL DEGRADATION IDENTIFIED AND CHARACTERIZED
- ALL IMPORTANT RATE CONSTANTS FOR TEMPERATURE AND O_2 LEVEL
- PHOTO-OXIDATION DEGRADATION MODEL DEVELOPED

PHOTOVOLTAICS MODULE INTERFACE:
GENERAL PURPOSE PRIMERS

UNIVERSITY OF CINCINNATI

J. Boerio

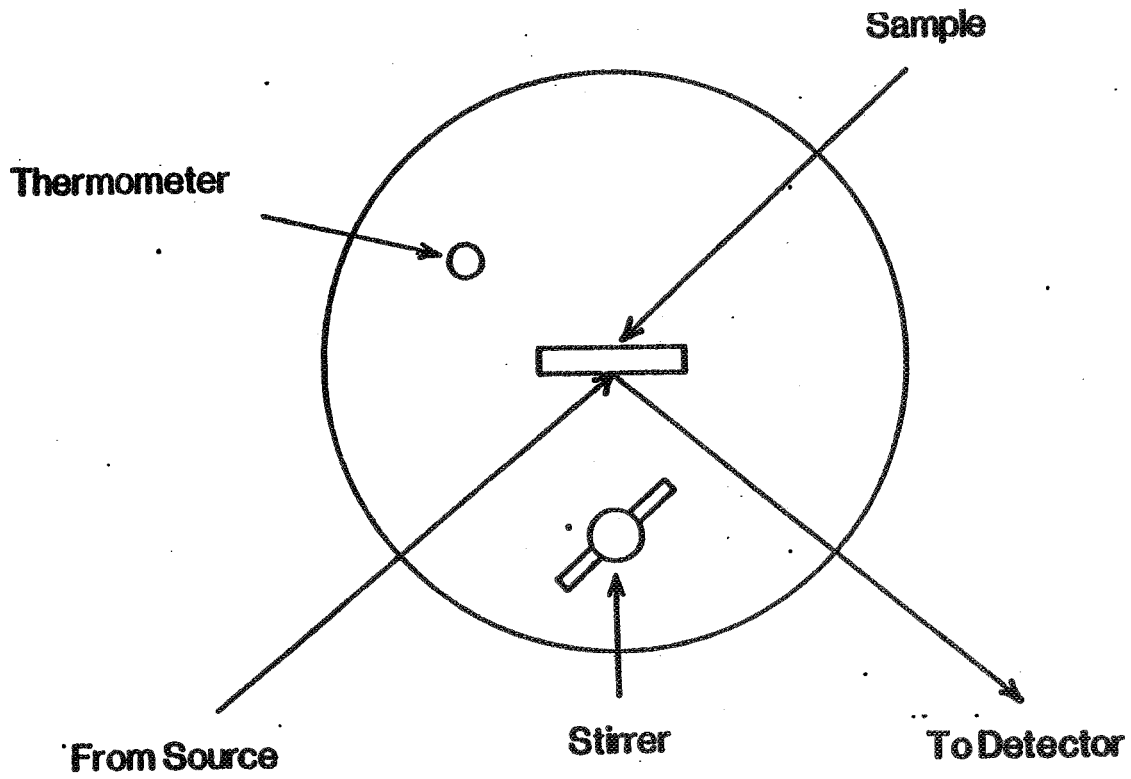


Figure 2. Sample cell for in-situ ellipsometry of metals exposed to water.

RELIABILITY PHYSICS

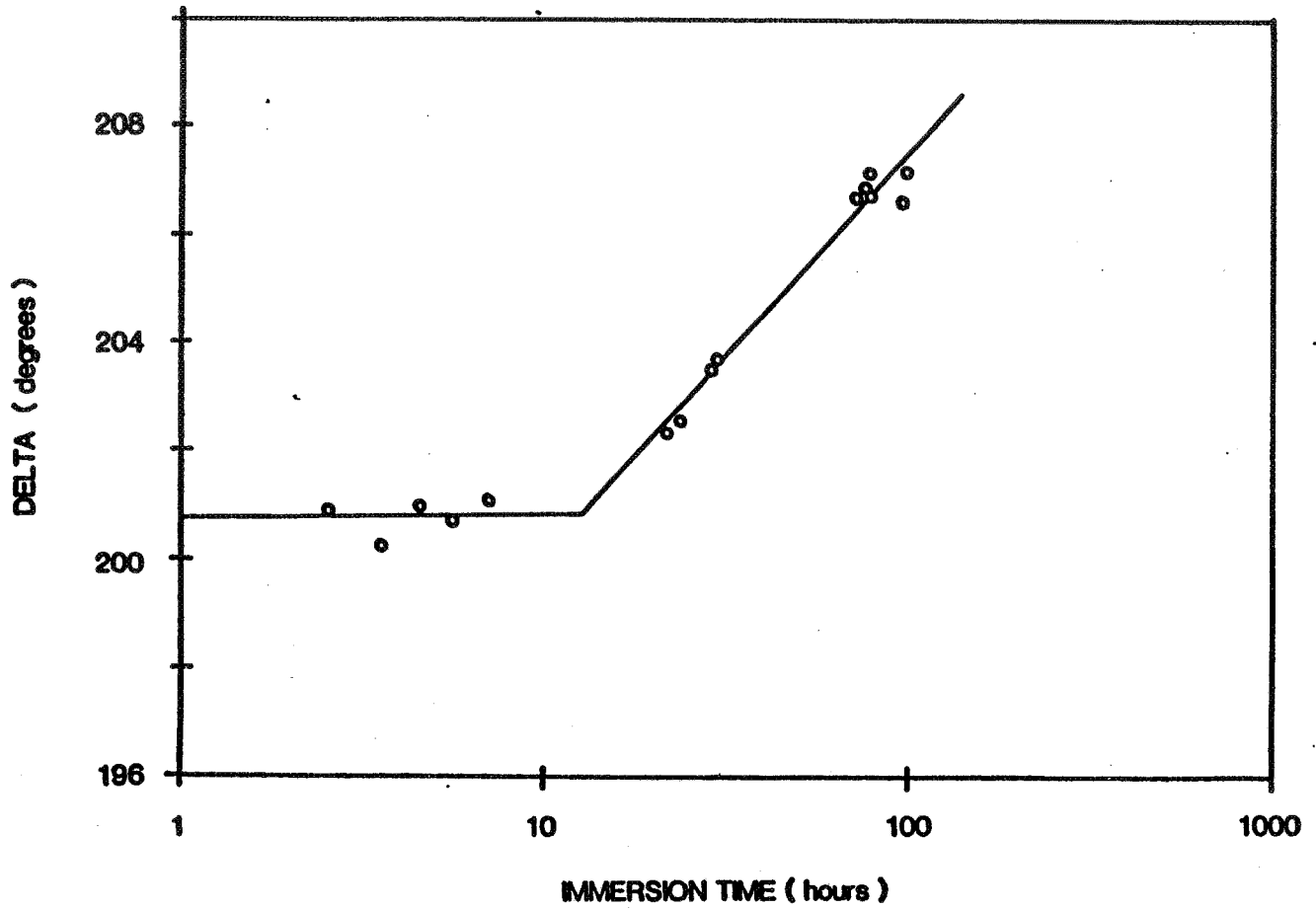


Figure 4. In-situ ellipsometry for EVA/Al in water at 40°C; no primer.

RELIABILITY PHYSICS

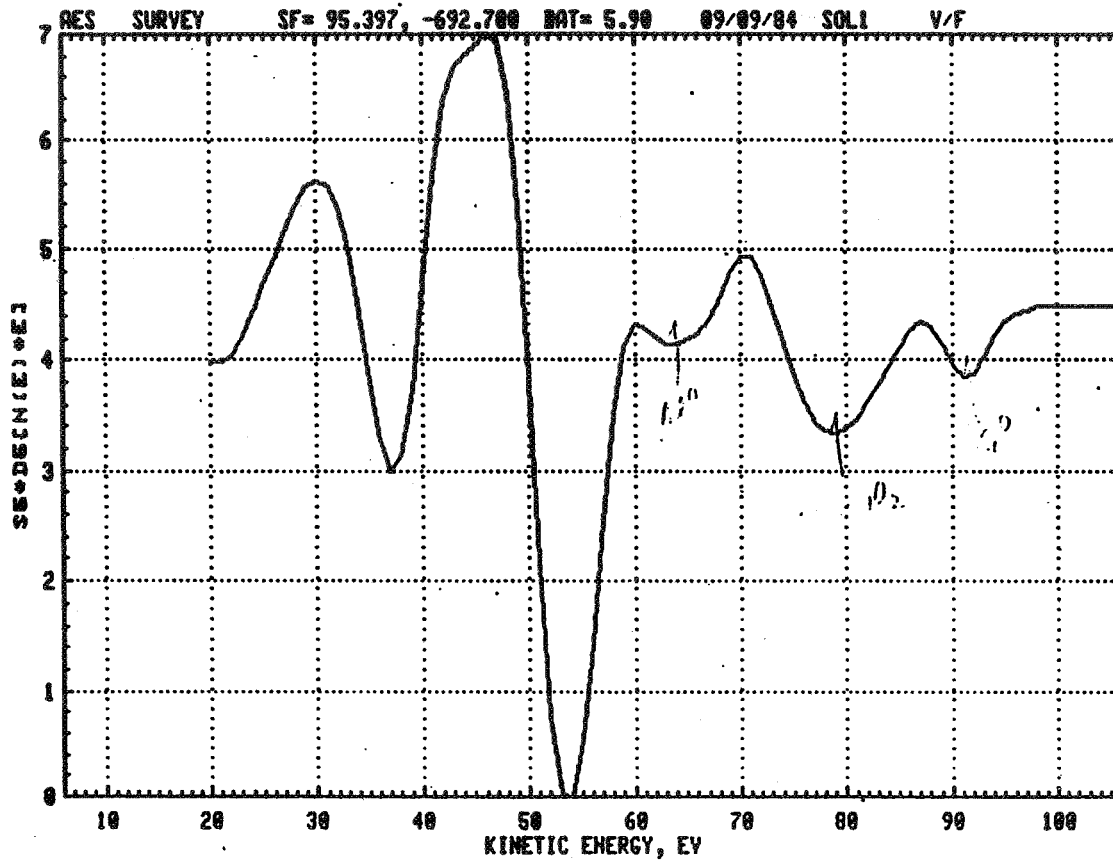


Figure 2. Aluminum and silicon Auger electron spectra from back surface of silicon wafer.



Figure 3. Scanning electron micrograph of "rough" aluminized backside of silicon wafer at 2000X.

ORIGINAL PAGE IS
OF POOR QUALITY

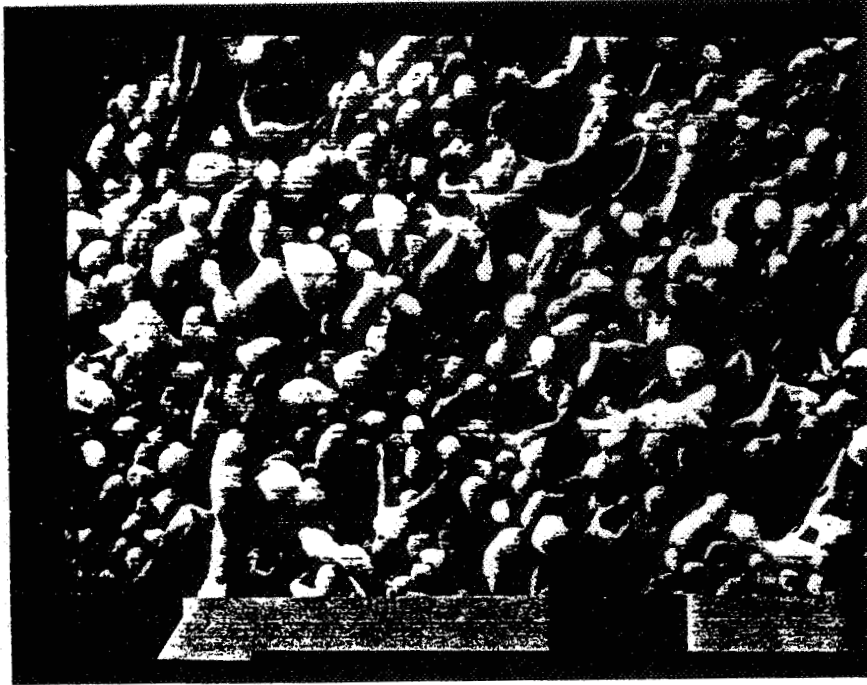


Figure 5. Scanning electron micrograph of "rough" aluminized backside of silicon wafer at 2000X.

RELIABILITY PHYSICS

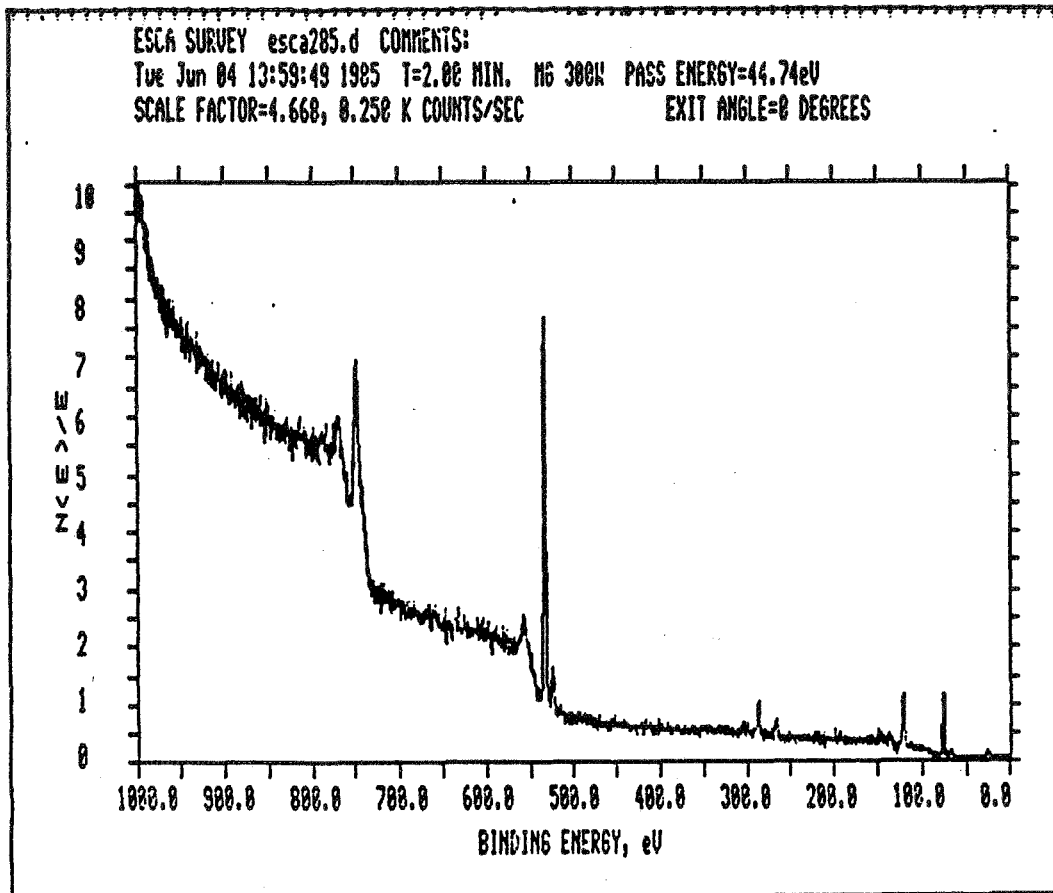


Figure 1. XPS spectrum of "rough" aluminized backside of silicon wafer.

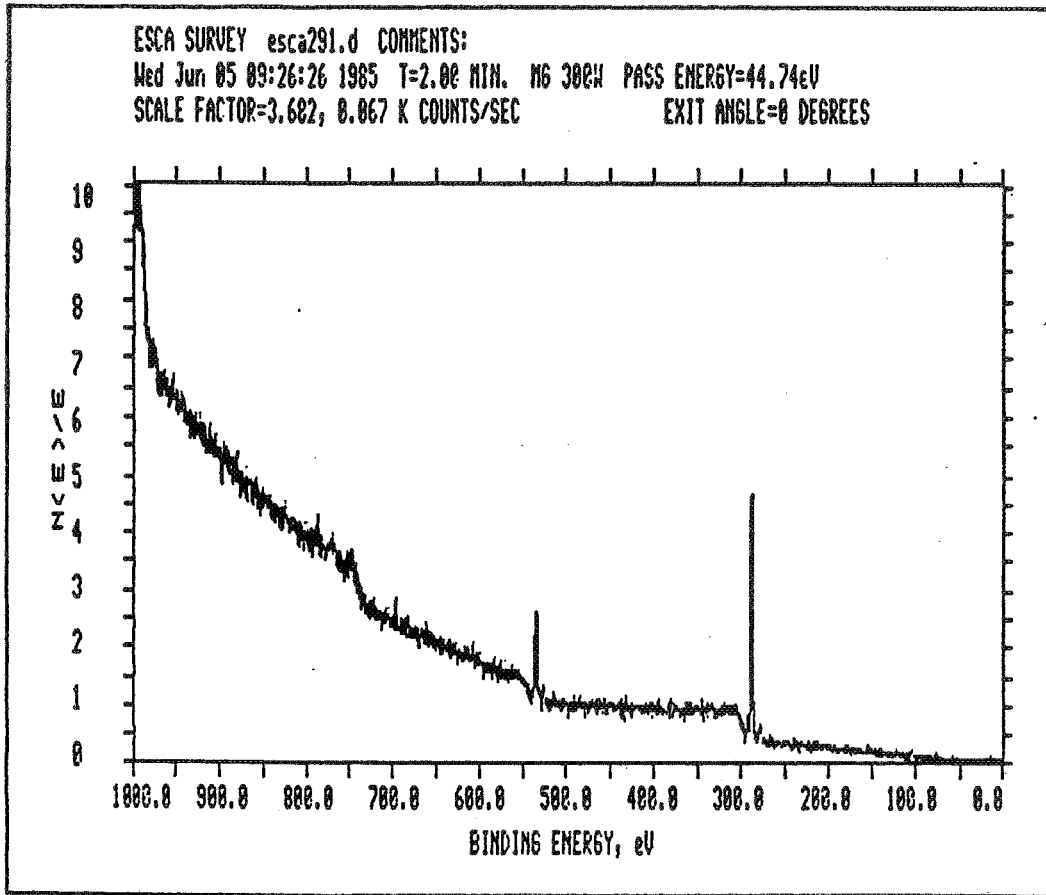


Figure 2. XPS spectrum of laminated silicon wafer after peeling EVA film.

RELIABILITY PHYSICS

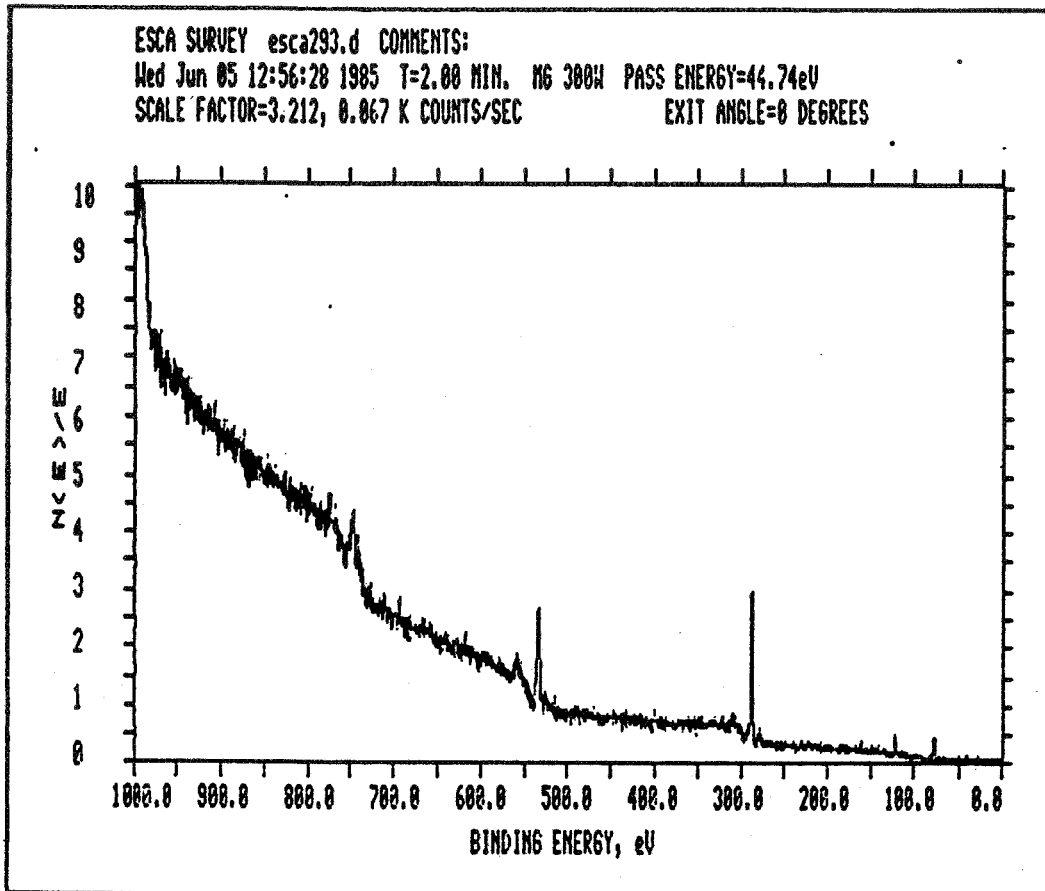


Figure 3. XPS spectrum of laminated silicon wafer after boiling for one hour and peeling EVA film.

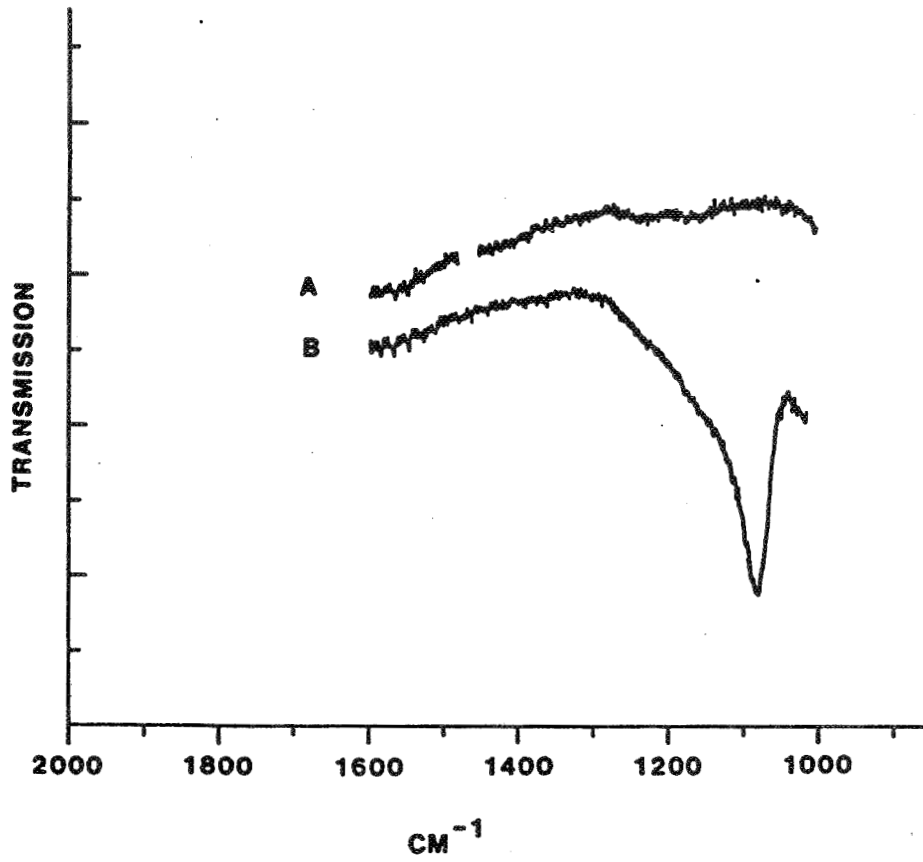


Figure 9. Reflection infrared spectra obtained from "rough" aluminized backsides of silicon wafers (A) - before and (B) - after immersion in boiling water for 30 minutes.

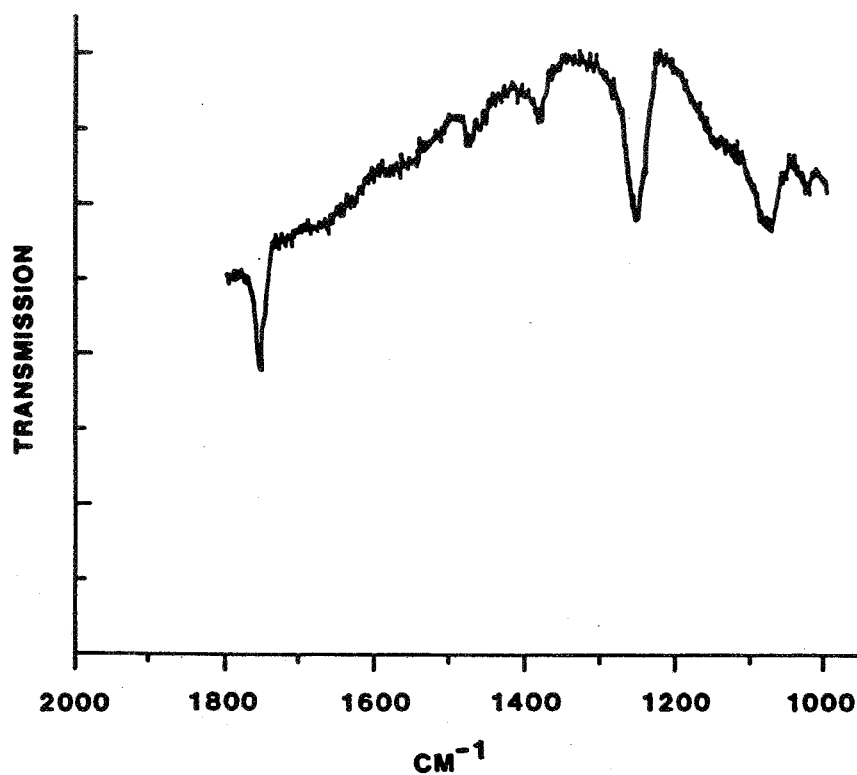


Figure 8. Reflection infrared spectrum obtained from "rough" aluminized backside of silicon wafer that was boiled in water for 30 minutes and then coated with a thin film of EVA.

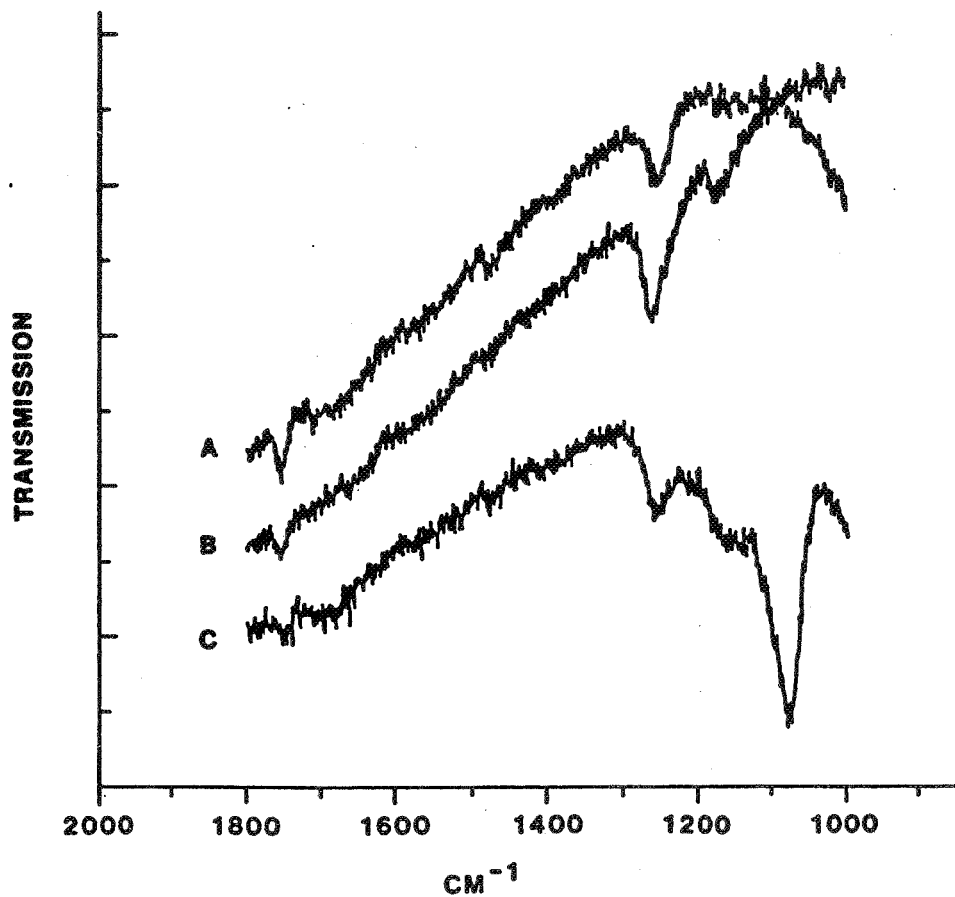


Figure 10. Reflection infrared spectra obtained from "rough" aluminized backsides of silicon wafers coated with thin films of EVA (A) - before immersion in boiling water and after immersion for (B) - 20 minutes (C) - 50 minutes.

Conclusions

1. A hydrated oxide known as pseudoboehmite is formed on the aluminized backside of silicon wafers during exposure to warm, moist environments.
2. Formation of pseudoboehmite leads to the failure of adhesive bonds between EVA and the aluminized backside of silicon wafers.
3. A-11861 is an effective primer for obtaining durable bonds between EVA and "rough" aluminized backsides of silicon wafers.
4. A-11861 may not be adequate for obtaining durable bonds between EVA and "smooth" aluminized backsides of silicon wafers.
5. Infrared spectroscopy is an effective, non-destructive technique for characterizing the interface between EVA and the aluminized backsides of wafers that are "rough" or "smooth."
6. Ellipsometry is an effective, non-destructive technique for characterizing the interface between EVA and the aluminized backsides of wafers that are "smooth."

ENCAPSULATION MATERIALS RESEARCH

SPRINGBORN LABORATORIES

P. Willis

Phase I

IDENTIFY AND DEVELOP LOW COST
MODULE ENCAPSULATION MATERIALS

- POTTANTS
- COVER FILMS
- SUBSTRATES
- ADHESIVES/PRIMERS
- ANTI-SOILING TREATMENTS

Phase II

MATERIALS RELIABILITY

- AGING AND LIFE ASSESSMENT
- ADVANCED STABILIZERS
- ADHESIVE BOND DURABILITY
- FLAMMABILITY
- ELECTRICAL ISOLATION

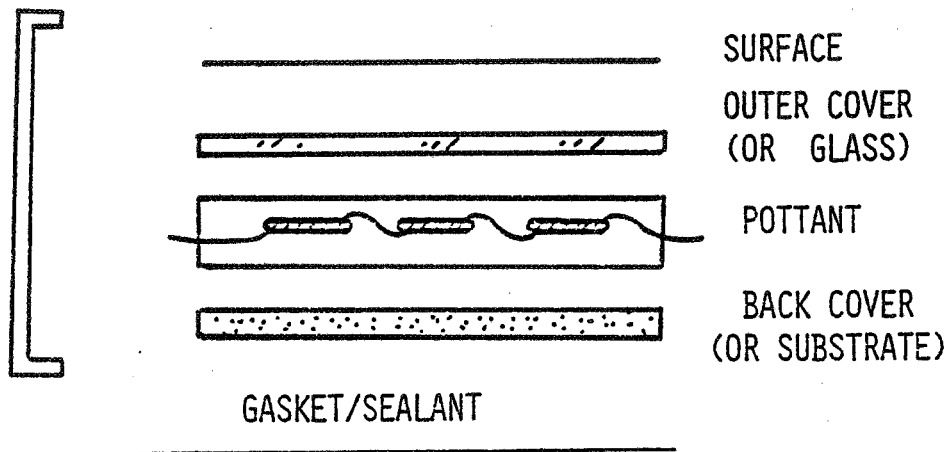
Phase III

PROCESS SENSITIVITY

- INTERRELATIONSHIPS OF
 - FORMULATION VARIABLES
 - PROCESS VARIABLES
- MANUFACTURING YIELD ANALYSIS

(PROCESS DEVELOPMENT SECTION)

Module Components



CURRENT EMPHASIS ON MATERIALS AND MODULE
PERFORMANCE CHARACTERISTICS

- DETERMINE CURRENT LEVEL OF PERFORMANCE
- ENHANCE PERFORMANCE (E.G. REFORMULATION)
- SERVICE LIFE PROGNOSIS

PERFORMANCE CRITERIA

- FLAMMABILITY
- ADHESIVE BOND DURABILITY
- ELECTRICAL INTEGRITY
- ENVIRONMENTAL DEGRADATION
- WHAT ARE DOMINANT FAILURE MODES ?
- WHERE IS STABILIZATION NEEDED ?

RELIABILITY PHYSICS

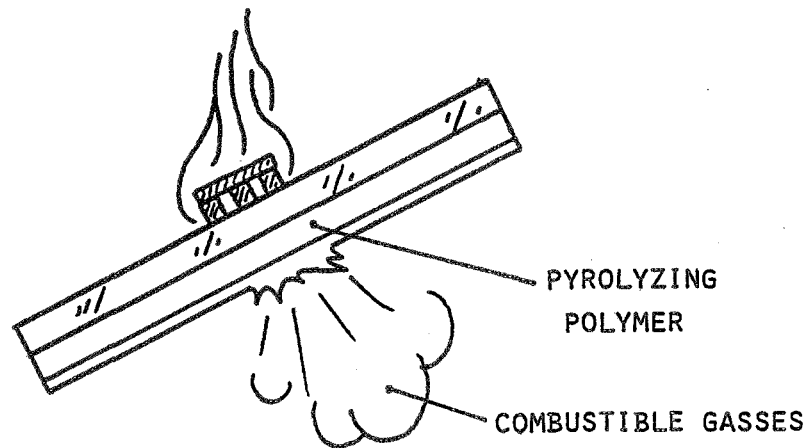
Module Flammability

PROBLEM:

- BURNING MODULES CAN SERVE AS IGNITION SOURCE FOR OTHER STRUCTURES
- MOST MODULES CONSTRUCTIONS NOT PASSING UL-790 BURNING BRAND TEST

MECHANISM(?)

- APPEARS TO BE RUPTURE OF THE BACK COVER WITH THE EVOLUTION OF BURNING GASSES



- MODULES WITH KAPTON BACK COVERS (HIGH STRENGTH) PASS TEST DUE TO ABILITY TO RETAIN COMBUSTIBLE GASSES ("B" BRAND)
- KAPTON IS VERY EXPENSIVE
- INEXPENSIVE HIGH STRENGTH HIGH TEMPERATURE BACK COVER NEEDED
- SOME SUCCESS WITH COATED FIBERGLASS CLOTH (PROPRIETARY COATINGS) ("A" BRAND)

RELIABILITY PHYSICS

GOAL:

- PREVENT SPREAD OF FLAME
- PASS UL-790

APPROACHES:

- (1) HIGH STRENGTH HEAT RESISTANT BACK COVERS
 - CERAMIC PAPER
 - POLYMER FILM LAMINATES WITH GLASS CLOTH INTERLAYER
 - METAL FOILS
 - RESIN IMPREGNATED GLASS CLOTH
- (2) REDUCTION OF COMBUSTIBLE MATERIALS
 - THINNING OF POTANT LAYER
- (3) FIRE RETARDANT ADDITIVES
 - INERT DILUENTS (TALC, CALCIUM CARBONATE)
 - RELEASE OF WATER WITH HEAT ALUMINA TRIHYDRATE (35% WATER)
 - FIRE RETARDANTS (FREE RADICAL TRAPS)
ANTIMONY OXIDE, ZINC BORATE
BROMINATED ORGANICS
ORGANIC PHOSPHATES
- (4) COMBINATION OF ALL THREE
(MOST LIKELY)

RELIABILITY PHYSICS

EVALUATION OF CANDIDATE MATERIALS

CONVENTIONAL TESTS:

- UL-94 VERTICAL BURN TEST
- ASTM E-262 FLAME SPREAD INDEX
- ASTM D-2863 LIMITING OXYGEN INDEX

SPECIAL TEST METHOD:

- HIGH TEMPERATURE BURST CELL
- DETERMINE BURST STRENGTH AS FUNCTION OF TEMPERATURE AND PRESSURE
- CORRELATE TO ACTUAL EFFECTIVENESS UNDER FIRE CONDITIONS
- DETERMINE ADD-ON COST FOR IMPROVEMENT IN FIRE RATING
- RECOMMEND CANDIDATES FOR UL-790 TESTING

DATA:

	BURST STRENGTH, PSI				
	<u>300</u>	<u>400</u>	<u>500</u>	<u>600</u>	°F
TEDLAR 200BS30WH	~ 5	<< 5	0	0	
KAPTON (4 MIL)	>50	40	30	20	
GLASS CLOTH (PROPRIETARY COATING)	- - - -	- - - -	POROUS	- - - -	

- MOST EFFECTIVE BACK COVER IS POROUS ?
- RELEASED GASSES DILUTED BELOW LOWER EXPLOSION LIMIT ? ?

RELIABILITY PHYSICS

FIRE RETARDANT ADDITIVES:

- GOAL: FIRE RETARDANT EVA

<u>FORMULATION:</u>	<u>PARTS</u>	<u>PERCENT</u>
ELVAX 150	100	49
TBEC PEROXIDE	1.5	0.7
ANTIMONY OXIDE	7.0	3.4
DECARBROMODIPHENYL OXIDE	20.0	9.8
ALUMINUM TRIHYDRATE	75.0	36.8

EVALUATION:

- UL-94 VERTICAL BURN V-0 (SELF EXTINGUISHING)
— COMPRESSION MOLDED WITH "CRANGLAS " CLOTH:
- ASTM D-23863 LIMITING OXYGEN INDEX 30% (GOOD)

FOR COMPARISON:

<u>MATERIAL</u>	<u>OXYGEN INDEX</u>
PARAFFIN	16
EVA (ELVAX 150)	18
SILICONE RUBBER	30
PVC	~ 50
TEFLON (FEP)	~ 93

CONCLUSIONS:

- FIRE RETARDANCY INCREASES WITH AMOUNT OF ALUMINUM TRIHYDRATE
- 4:1 BROMINE: ANTIMONY RATIO APPEARS TO BE OPTIMUM
- NON-WOVEN GLASS CLOTH PREVENTS DRIPPING - REINFORCES THE COMPOSITION
- EVA CAN BE FORMULATED TO HAVE FLAMMABILITY EQUIVALENT TO SILICONE RUBBER
- HIGHER OXYGEN INDEX VALUES POSSIBLE

Adhesion Experiments

STATUS:

- PRIMER FORMULATIONS IDENTIFIED FOR ALMOST ALL INTERFACES IN MODULES
- SELF-PRIMING FORMULATIONS OF EVA (TO GLASS, CELLS) DEVELOPED; AVAILABLE

CONTINUED PRIMER STUDIES:

- GOAL: REDUCE LIST OF PRIMERS TO "UNIVERSAL" FORMULATION(S)
- EVALUATE THE THREE "BASIC" PRIMERS -
DR. PLUEDDEMANN - DOW CORNING
 - POLYMER/METAL
 - POLYMER/INORGANIC
 - POLYMER/ORGANIC
- METAL PRIMER (ALUMINUM) RECOMMENDATIONS
DR. JIM BOERIO - UNIVERSITY OF CINCINNATI

DURABILITY

ADHESIVE BONDS ARE RESPONSIBLE FOR MECHANICAL INTEGRITY OF ENTIRE MODULE - WHAT IS THEIR LIFETIME ?

- HOW DURABLE ARE ADHESIVE BONDS ?
- UNDER WHAT CONDITIONS ?
- REVERSIBILITY AND RECOVERY ?
- MODELLING AND PREDICTION ?
- TEST METHODS ?

ADHESION DIAGNOSTICS:

- PROGRAM STARTED WITH CASE WESTERN RESERVE UNIVERSITY - JACK KOENIG

C-3

Adhesion Diagnostics

TEST SPECIMENS:

- EVA COMPOUNDED WITH HIGH LOADINGS OF SILANE TREATED GLASS BEADS - RESEMBLES GLASS REINFORCED POLYMER
- GLASS: SPHERICAL "A" - GLASS BEADS, MEAN DIAMETER $20\ \mu$, 2% BY WEIGHT SILANE PRIMER
- SPECIMENS AT CASE WESTERN FOR "DRIFT" ANALYSIS (SPECTROSCOPY)
- SPECIMENS AT SPRINGBORN FOR MECHANICAL ANALYSIS

GOALS:

- CORRELATE SPECTROSCOPIC OBSERVATIONS WITH MECHANICAL PERFORMANCE
- DETERMINE DEGRADATION RATES (KINETICS)
- ASSESS SERVICE LIFE

AGING CONDITIONS:

- HYDROLYSIS CONSIDERED TO BE DOMINANT FAILURE MECHANISM
- WATER IMMERSION:
TEMPERATURES: 40° , 60° , 80°
TIMES: 100, 250, 500, 1000, 2000 HRS.
- TESTING: MECHANICAL, SPECTROSCOPIC

RELIABILITY PHYSICS

- LARGEST MEASURABLE CHANGE: WEIGHT GAIN
(WATER ABSORPTION)

TEMPERATURE	<u>PERCENT WEIGHT GAIN</u>		
	<u>40° C</u>	<u>60° C</u>	<u>80° C</u>
EVA/GLASS <u>NO</u> PRIMER	51 % 2,000 HR	2015 % 2,000 HR	500 % 500 HR
EVA/GLASS <u>WITH</u> PRIMER	3.5 % 2,000 HR	35 % 2,000 HR	62 % 1,000 HR
EVA, CONTROL	0.3 % 2,000 HR	0.4 % 2,000 HR	1.0 % 2,000 HR

* NO SPECIMENS SURVIVING THIS POINT

- WEIGHT GAIN ASSUMED TO BE WATER ABSORPTION AT
POLYMER/GLASS INTERFACE
(ALSO OBSERVED BY SPECTROSCOPY)
- PRIMER HAS SIGNIFICANT EFFECT ON ABSORPTION
- MECHANICAL PROPERTIES: LITTLE CHANGE UP TO 50 %
WEIGHT GAIN-ELONGATION BEGINS TO DECREASE
- ALMOST NO CHANGE IN POLYETHYLENE/GLASS BEAD SPECIMENS

REVERSIBILITY:

- DRIED AT 105° C / 72 HRS - LIMIT OF REVERSIBILITY

	40°	60°	80°
<u>NO</u> PRIMER	ALL	500 HRS	250 HRS
<u>WITH</u> PRIMER	ALL	ALL	1,000 HRS

RELIABILITY PHYSICS

- WATER ABSORPTION - LARGEST PROPERTY CHANGE
- PRIMER STABILIZERS GLASS/POLYMER INTERFACE
- HYDROTHERMAL " DAMAGE " TO BONDS AT THE INTERFACE IS REVERSIBLE UP TO A LIMIT
- EQUILIBRIUM WATER ABSORPTION VALUES MAY PROVIDE NEW METHOD OF EVALUATING ADHESIVE BONDS - RECOVERY PROPERTIES

LIFETIME:

- DOES POLYMER GAIN WATER TO POINT OF NON-REVERSIBILITY, OR IS IT " INDUCTION PERIOD " TYPE ?
- NEED MORE DATA POINTS FOR MODELING

Electrical Isolation

- POTTANTS AND COVER FILMS SERVE AS ELECTRICAL INSULATION
- NEED TO KNOW THICKNESS REQUIRED FOR VOLTAGE STANDOFF
- VARIATION WITH TEMPERATURE, ABSORBED WATER ?
- NEED TO KNOW VARIATION DIELECTRIC STRENGTH WITH AGING:
LIGHT, HEAT, HUMIDITY, FIELD STRESS

METHOD:

- HV-DC POWER SUPPLY, SYMMETRIC ELECTRODES
- SPECIFIED RATE OF RISE (500 V/SEC)
- PLOT AVERAGE BREAKDOWN VOLTAGE, V_A VS THICKNESS
- STRAIGHT LINE RELATIONSHIP: SLOPE EQUALS
"INTRINSIC DIELECTRIC STRENGTH" (DC)
- MEASUREMENTS TO DATE:
EVA 9918, $dV/dT = 3.65$ kv/MIL

GOALS:

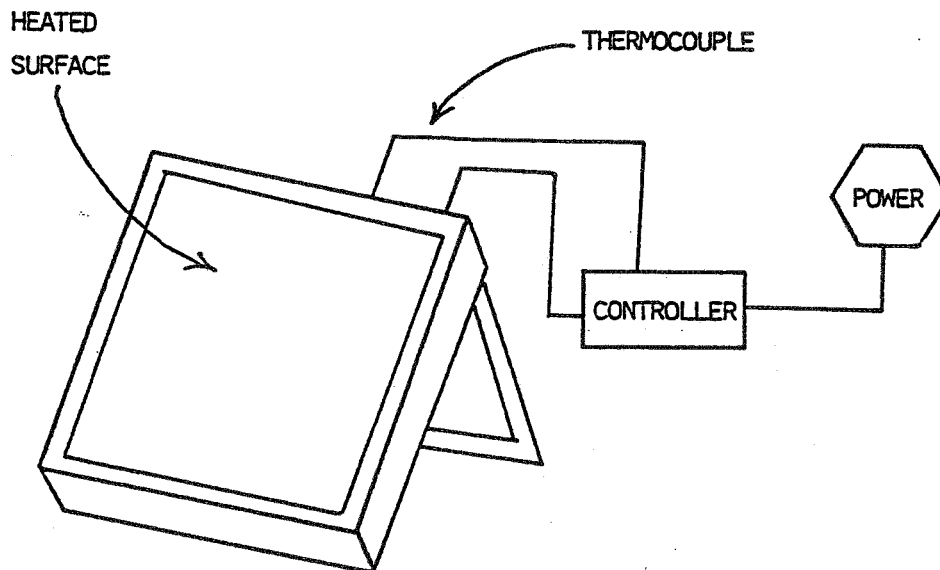
- REMEASURE dV/dT :
 - THERMAL AGING
 - WATER ABSORPTION
 - ENVIRONMENTAL EXPOSURE
 - FIELD STRESS AGING
- RECALCULATE THE REQUIRED INSULATION THICKNESS FOR SERVICE LIFE OF THE MODULE

RELIABILITY PHYSICS

Accelerated Aging Test Program

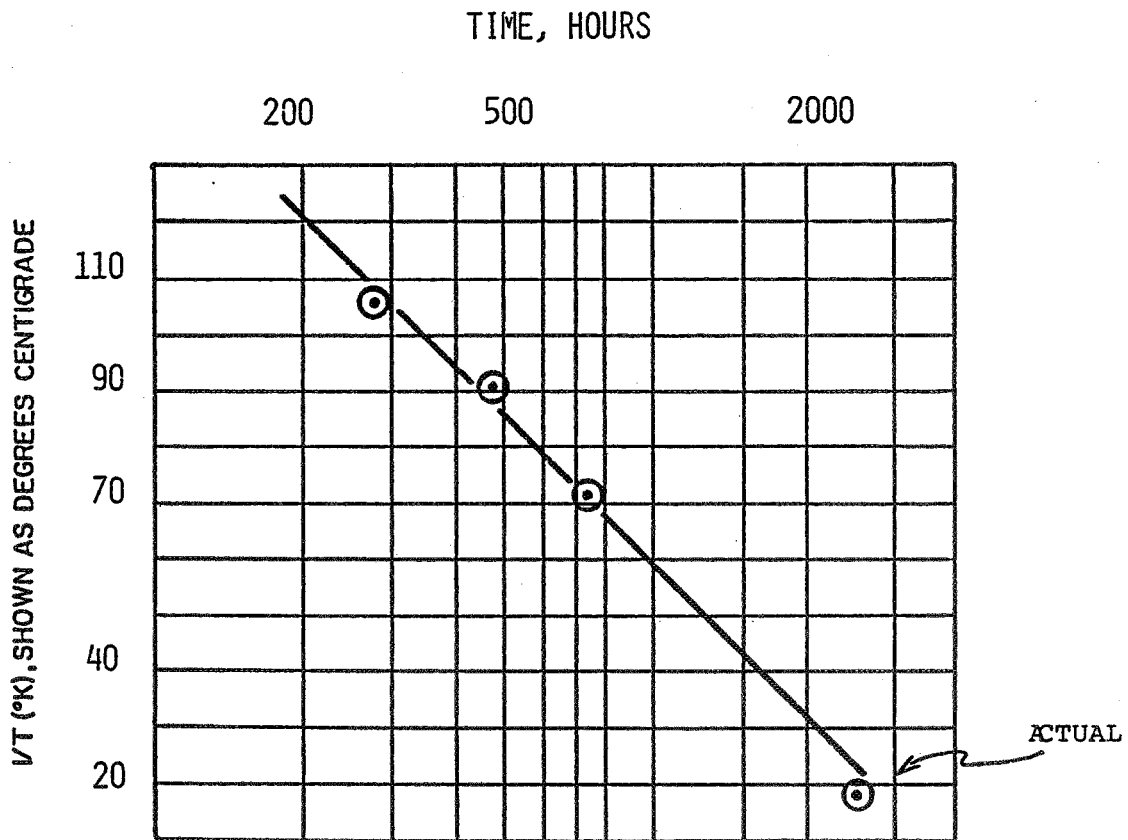
OUTDOOR PHOTOTHERMAL AGING REACTORS (OPTAR)

- USE NATURAL SUNLIGHT, AVOIDS SPECTRAL DISTRIBUTION PROBLEMS WITH ARTIFICIAL LIGHT SOURCES
- USE TEMPERATURE TO ACCELERATE THE PHOTOTHERMAL REACTION
- INCLUDES DARK CYCLE REACTIONS
- INCLUDES DEW/RAIN EXTRACTION
- INTENDED PRIMARILY FOR MODULE EXPOSURE
- EXTRAPOLATE EFFECTS TO LOWER TEMPERATURES



Accelerated Aging

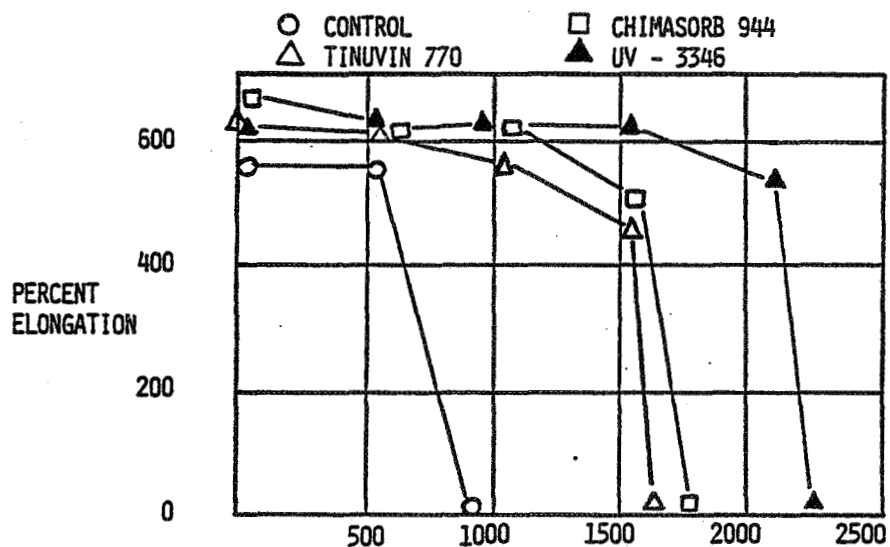
- USEFUL FOR EVALUATING CANDIDATE FORMULATIONS - COMPARISON
- EVALUATED WHOLE MODULES
- DETERMINE UPPER LEVEL SERVICE TEMPERATURES
- MODELLING:
 - TIME TO ONSET OF DEGRADATION (INDUCTION PERIOD, t_i)
EXAMPLE: POLYPROYLENE
 - ARRHENIUS: LOG, t_i ; vs. $1/K^0$
 - PREDICT SERICE LIFE BY EXTRAPOLATION TO LOWER TEMPERATURES



RELIABILITY PHYSICS

Accelerated Aging (OPTAR)

- INDUCTION PERIOD MEASUREMENT - USEFUL FOR STABILIZER SELECTION
- EXAMPLE: HALS TYPE STABILIZERS



- ADVANCE EVA FORMULATION (NO. 18170) LUPERSOL TBEC, UV-2098 (CYANAMIDE, UV-SCREEN) UV-3346 (CYANAMIDE, HALS)
- MASSIVE TEST PROGRAM STARTED: MODULES, OUTER COVERS, ADHESION TEST SPECIMENS, POTTANT FORMULATIONS, ETC.
- RADIOMETER INSTALLED ON OPTAR DEVICES - POSSIBILITY FOR MODELING BASED ON HEAT PLUS LIGHT ???

Anti-Soiling Treatments

SURFACE CHEMISTRY:

- HARD
- SMOOTH
- HYDROPHOBIC
- OLEOPHOBIC
- ION FREE
- LOW SURFACE ENERGY

SURFACE INVESTIGATED:

- SUNADEX GLASS
- TEDLAR (100 BG 30 UT)
- ACRYLAR (ACRYLIC FILM)

TREATMENTS REMAINING:

- L-1668 FLUROSILANE (3M)
- E-3820 PERFLUORODECANOIC ACID/
SILANE (DOW CORNING)
- STILL EFFECTIVE AT 46 MONTHS
OUTDOOR EXPOSURE
- RESULTS IN IMPROVED POWER OUTPUT
- FLUOROALKYL SILANE CHEMISTRY
APPEARS TO BE MOST EFFECTIVE

NEW TREATMENTS :

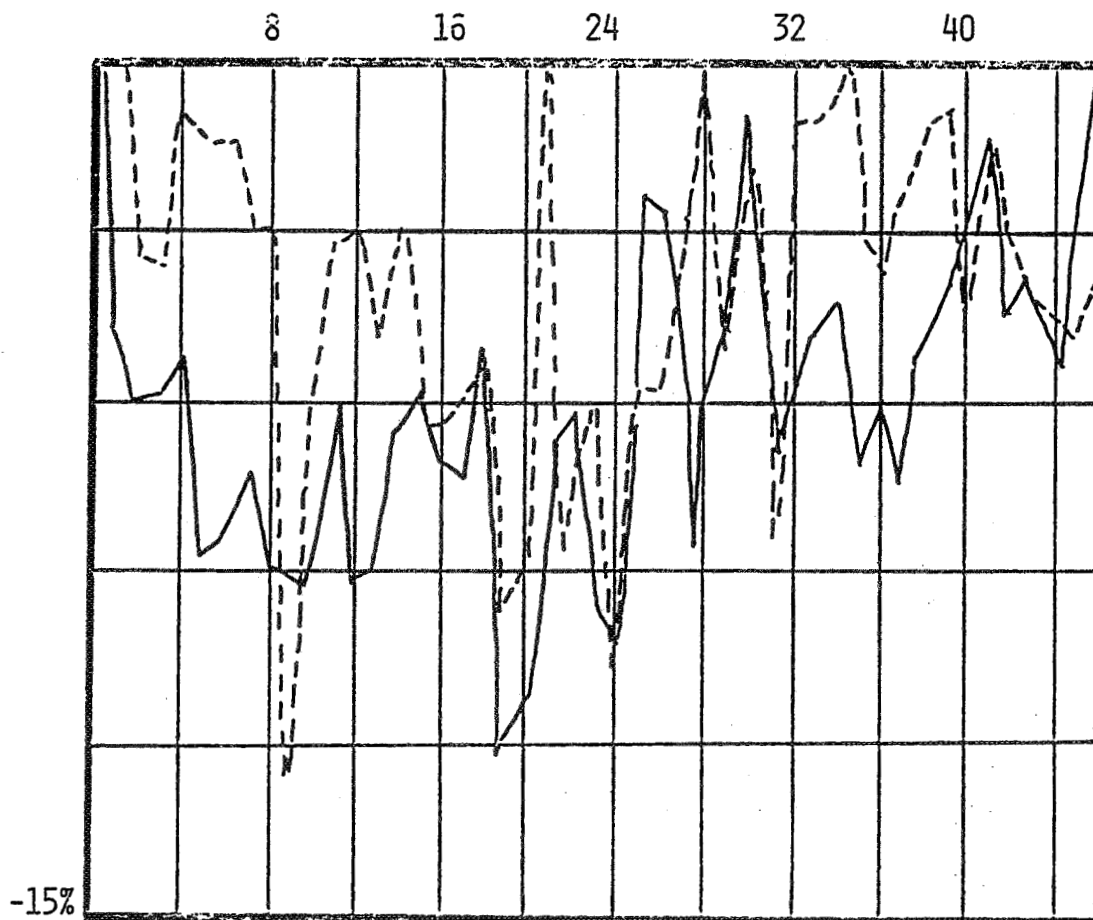
- TWO NEW CANDIDATES FROM DOW CORNING -
JUST STARTED

Soiling Experiments

FORTY SIX MONTHS EXPOSURE
ENFIELD, CONNECTICUT

% LOSS IN I_{sc} WITH STANDARD CELL TREATED
SUNDEX GLASS

46 MONTHS EXPOSURE



———— CONTROL, NO TREATMENT

- - - - - L1668 (3M)

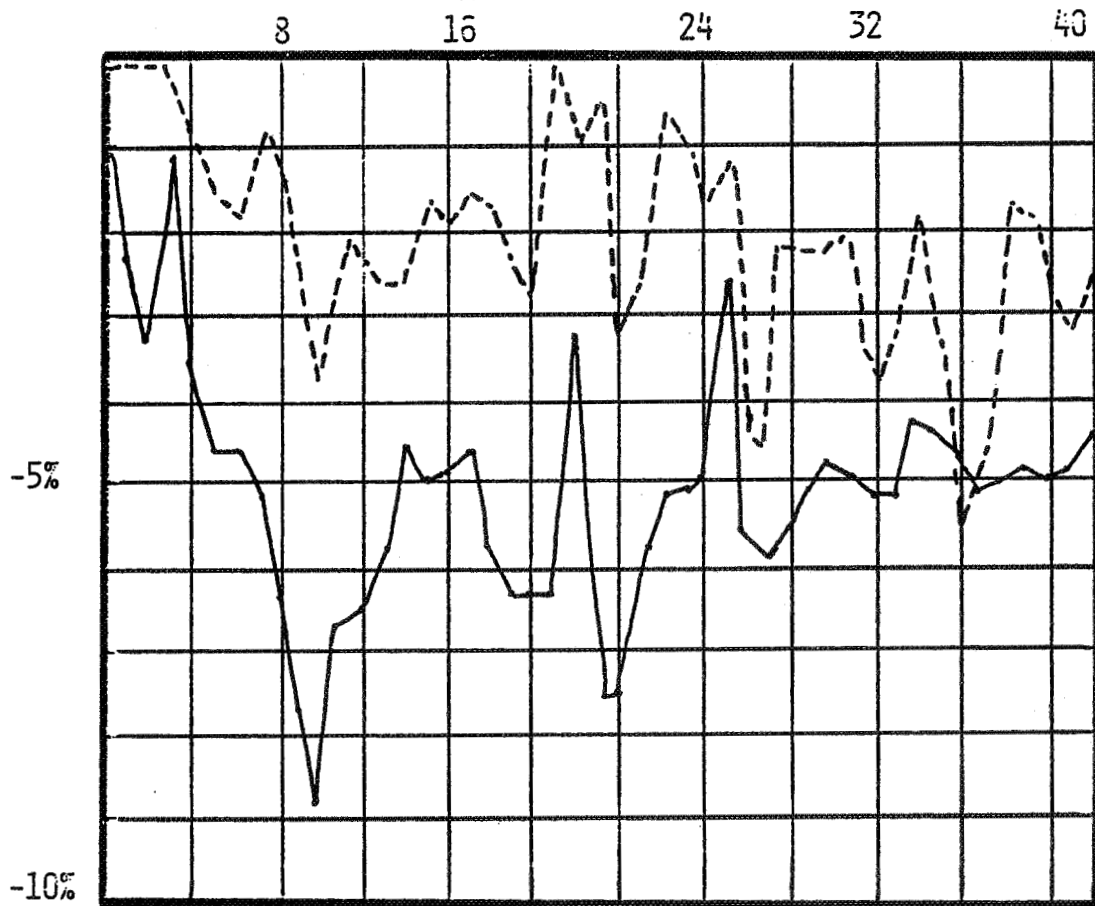
● ESTIMATED AVERAGE POWER IMPROVEMENT, 1%

RELIABILITY PHYSICS

FORTY SIX MONTHS EXPOSURE
ENFIELD, CONNECTICUT

% LOSS IN I_{sc} WITH STANDARD CELL TREATED
TEDLAR 100B6300UT

(SUPPORT ON GLASS)
MONTHS EXPOSURE



———— CONTROL, NO TREATMENT

----- E3820

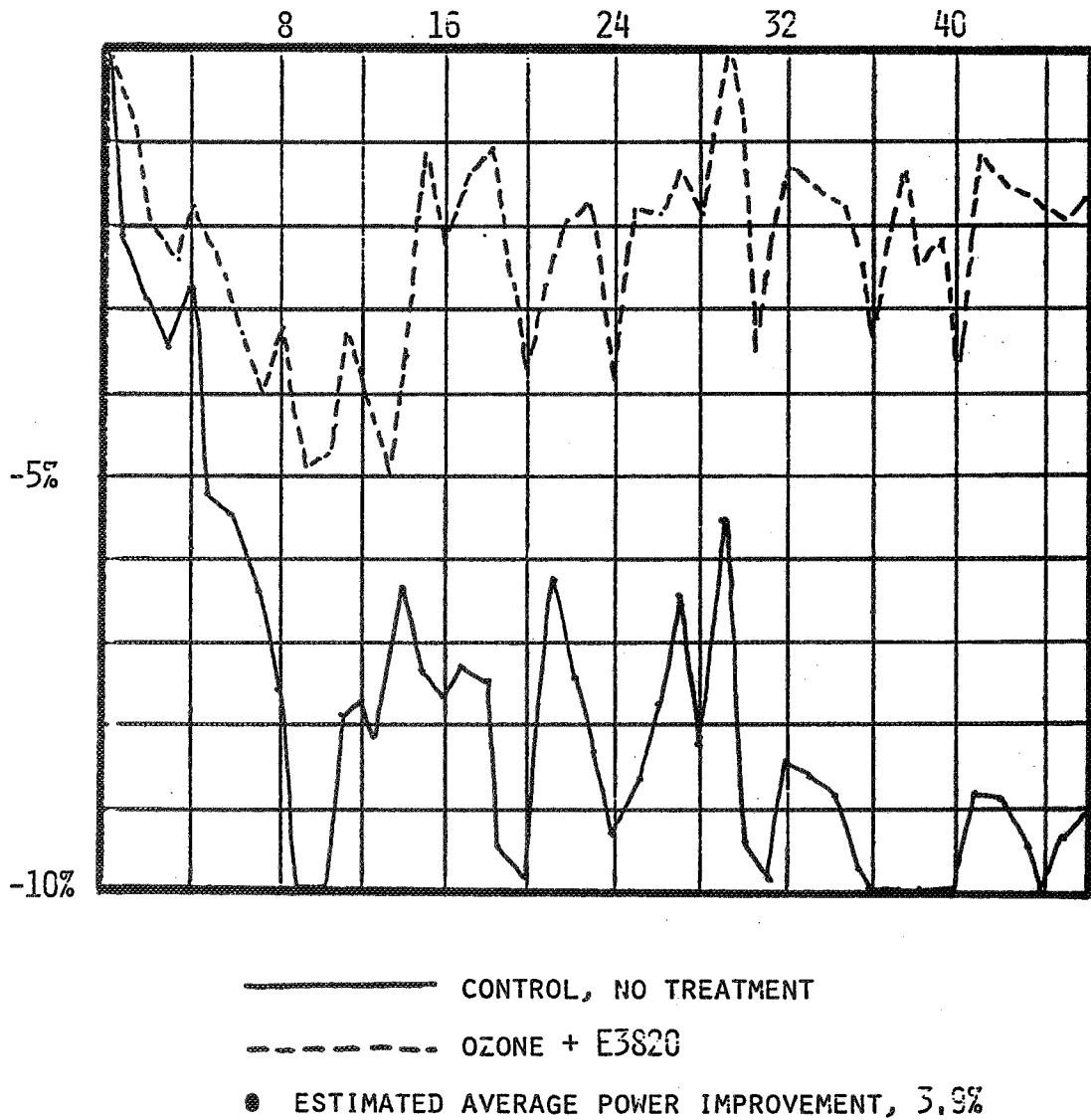
● ESTIMATED AVERAGE POWER IMPROVEMENT, 3.8%

RELIABILITY PHYSICS

FORTY SIX MONTHS EXPOSURE
ENFIELD, CONNECTICUT

% LOSS IN I_{SC} WITH STANDARD CELL TREATED ACRYLAR
(SUPPORTED ON GLASS)

45 MONTHS EXPOSURE



Outer Covers

(SUBSTRATE DESIGN)

- RECENT INDUSTRIAL INTEREST - BOTH CRYSTAL AND THIN FILM AMORPHOUS APPLICATIONS
- NEW CONCEPT: POTTANTS ARE VERY STABLE - NO FURTHER NEED FOR UV SCREENING IN OUTER COVER (?)
- NON-SCREENING FILM REQUIREMENTS:
TRANSPARENT, LOW SHRINKAGE, WEATHERABLE, BONDABLE
- BEST CANDIDATES: FLUOROPOLYMERS

<u>FILM</u>	<u>REF. INDEX</u>	<u>% T</u>	<u>COST \$/FT²/MIL</u>
TEFZEL	1.403	85.6	0.128
KAYNAR	1.420	88.8	0.055
HALAR	1.40	85.3	0.096
PFA	1.30	88.4	0.123
FEP	1.34	93.6	0.109
FLUOREX	1.46	90.0	0.17

- FEP MAY BE GOOD CHOICE:
 - HIGH TRANSPARENCY
 - OUTSTANDING WEATHERABILITY
 - MAY IMPROVE OPTICAL THROUGHPUT BY 2% DUE TO OPTICAL COUPLING
 - REQUIRES BONDING TECHNOLOGY:
SURFACE TREATMENT NOT UV STABLE (DU PONT)
 - UNDER EVALUATION IN MODULE FABRICATION AND OUTDOOR EXPOSURE EXPERIMENTS

RELIABILITY PHYSICS

Thin-Film/Amorphous Photovoltaics

CANDIDATE POLYMERS:

- PROCESSABLE $< 100^{\circ}$ C
- OPTICALLY TRANSPARENT
(BEFORE OR AFTER CURING)
- CURABLE: NO THERMAL CREEP
- EXTRUSION: THIN FILMS DESIRABLE
- WEATHERABLE OR UNGRADABLE
- FLEXIBLE

<u>MATERIAL CLASS</u>	<u>MANUFACTURER</u>	<u>\$/LB</u>
POLYETHYLENE (LDPE)	MANY	.50 - .60
ETHYLENE/VINYL ACETATE	DU PONT, USI	.60 - .80
ETHYLENE/ACRYLIC IONOMER	DOW, GULF DU PONT	.80 - 1.00 1.08 - 1.60
ALIPHATIC URETHANE	UPJOHN	1.70 - 2.50
HOT MELT ADHESIVES (HYDROCARBON, POLYAMIDE POLYETHER, ACRYLIC)	MANY	.80 - 2.50

ENCAPSULATION METHOD:

- EXTRUSION COATING
- FILM LAMINATION; EXTRUDE THE POTTANT ON AN OUTER
COVER FILM AS A CARRIER, USE COMBINATION FOR LAMINATION.

CURE METHOD:

- MOISTURE CURE (MODIFIED CHEMISTRY)
- PEROXIDE DECOMPOSITION (HEAT)
- UV CURE (PHOTOINITIATION)
- ELECTRON BEAM (?)
MAY BE POSSIBLE WITH AMORPHOUS SILICON

Conclusions

FLAMMABILITY:

- BACK COVERS - - FUNCTION ?
- SELF EXTINGUISHING FIRE RETARDANT EVA DEVELOPED

ADHESION:

- NEW TEST METHOD FOR PRIMER EVALUATION AND BOND DURABILITY
- CAN DEMONSTRATE BOND RECOVERY & LIMIT OF REVERSIBILITY

ELECTRICAL ISOLATION:

- INTRINSIC DIELECTRIC TEST METHOD DEVELOPED

ACCELERATED AGING:

- " OPTAR " METHOD BEST AGING TECHNIQUE DISCOVERED SO ARE
- MODELING/LIFE PREDICTION ENCOURAGING
 - 70⁰ & 90⁰ C VERY GOOD CONDITION
 - COPPER REACTIONS NOT AS SEVERE AS ANTICIPATED - EXCEPT AT 105⁰ C
 - LUPERSOL - TBEC CURED FORMULATIONS APPEAR MORE STABLE
- BEST STABILIZERS: UV-2098 SCREENER, UV-3346 HALS TYPE (BOTH CYANAMIDE)

SOILING:

- TREATMENTS STILL EFFECTIVE AFTER 46 MONTHS
- MOST EFFECTIVE ON ORGANIC FILMS

THIN-FILM PV:

- ENCAPSULANT INVESTIGATIONS BEGUN

Future Work

- FLAMMABILITY:
 - ENHANCED FIRE RETARDANT FORMULATIONS
 - SMALL SCALE MODULE "BURNS "

- ADHESION:
 - MORE WORK ON " UNIVERSAL " PRIMERS
 - MORE DEVELOPMENT OF DIAGNOSTIC TEST METHOD
 - AGING OF ADHESION TEST SPECIMENS

- ELECTRICAL INTEGRITY: DIELECTRIC STRENGTH VERSUS AGING OF ENCAPSULATION MATERIALS:
 - ACCELERATED AGING
MASSIVE NUMBER OF TEST SPECIMENS BEING DEVELOPED - MODULES, OUTER COVERS
ADVANCED STABILIZER SYSTEMS
 - NON-SCREENING WEATHERABLE OUTER COVERS
EMPHASIS ON BONDING
 - THIN-FILM PV: DEVELOPMENT WORK AND MATERIALS RECOMMENDATIONS

MOISTURE-TEMPERATURE DEGRADATION IN MODULE ENCAPSULANTS

JET PROPULSION LABORATORY

G.R. Mon

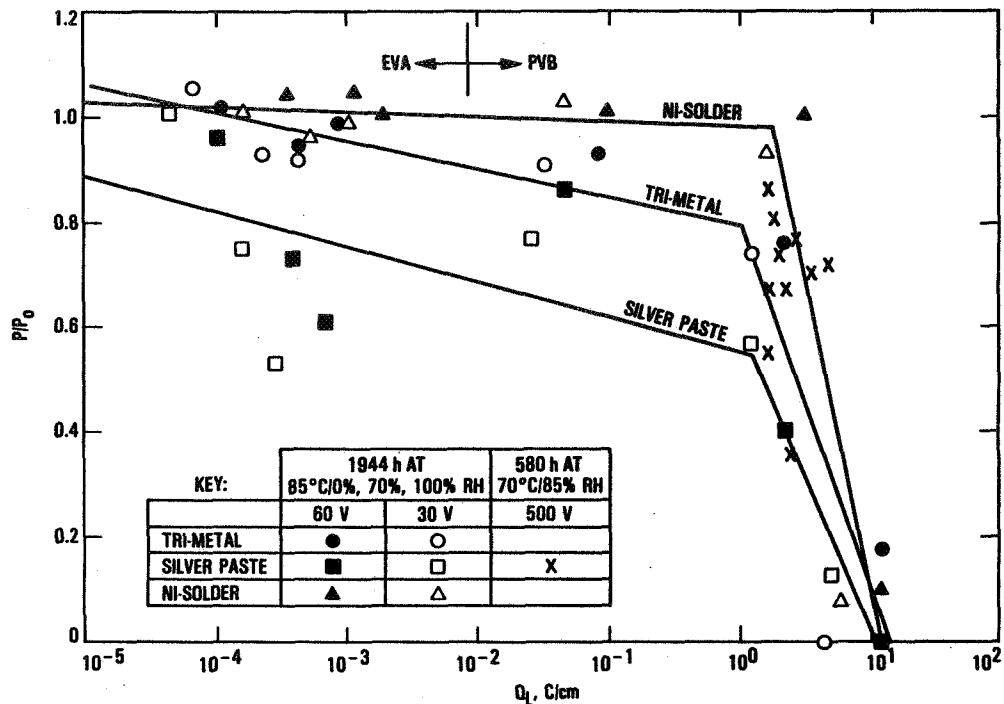
The General Problem of Moisture in Photovoltaic Encapsulants

- **Water transport**
 - **Rain, snow**
 - **Condensation, dew**
 - **Changes in water vapor pressure**
- **Effects of water in photovoltaic modules**
 - **Swelling of polymers and gaskets**
 - **Delamination of encapsulant**
 - **Galvanic (contact) corrosion**
 - **Electrochemical (leakage current) corrosion**
 - **Plays an active role in**
 - **Photo degradation**
 - **Voltage breakdown**

General Research Approach

- **For a given degradation mechanism, establish module performance loss versus level of accumulated degradation**
- **Establish dependence of rate of degradation reaction on moisture and temperature level in module**
- **Establish moisture and temperature level in module versus time in field environment and module construction**
 - **Sealed module**
 - **Partially sealed module**
 - **Unsealed module**

Power Output Reduction vs Accumulated Unit Charge Transfer

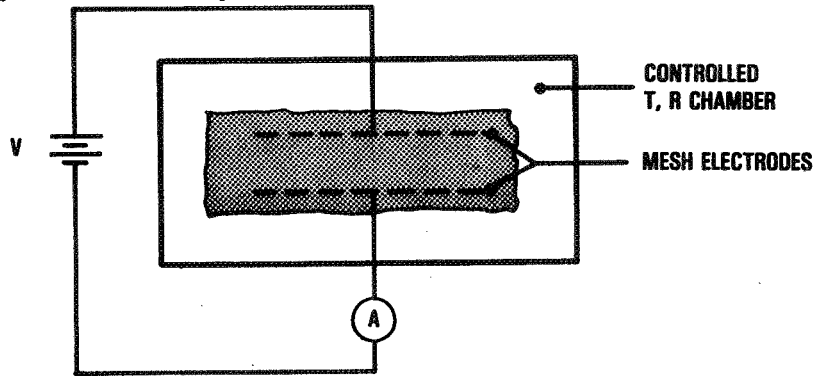


Electrochemical Corrosion: Analysis of Leakage Current

- Leakage Current
 - Leakage current (rate of transfer of charge) is responsible for electrochemical corrosion
 - Leakage current magnitude is determined by
 - Applied (or generated) voltage V
 - Insulation (encapsulant) surface and volume conductivities
- Encapsulant conductivity
 - Insulation conductivity increases with increasing
 - Temperature
 - Moisture content

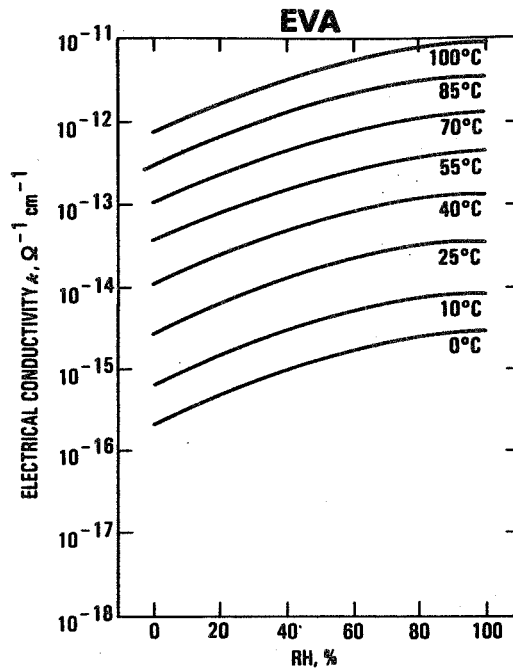
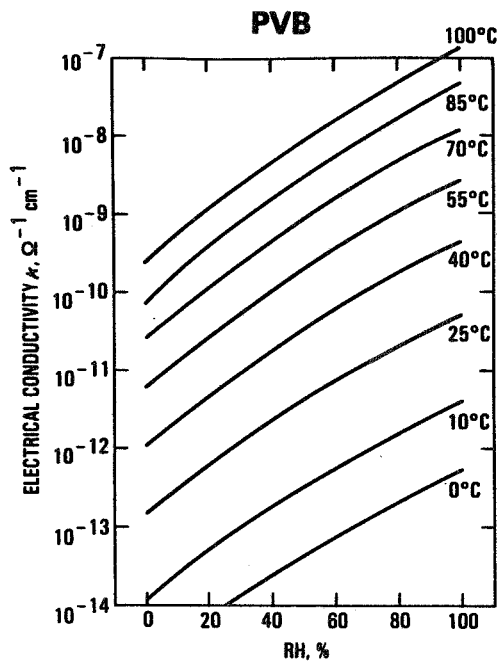
Experimental Determination of the Electrical Conductivity of PVB and EVA

- **Experimental setup:**

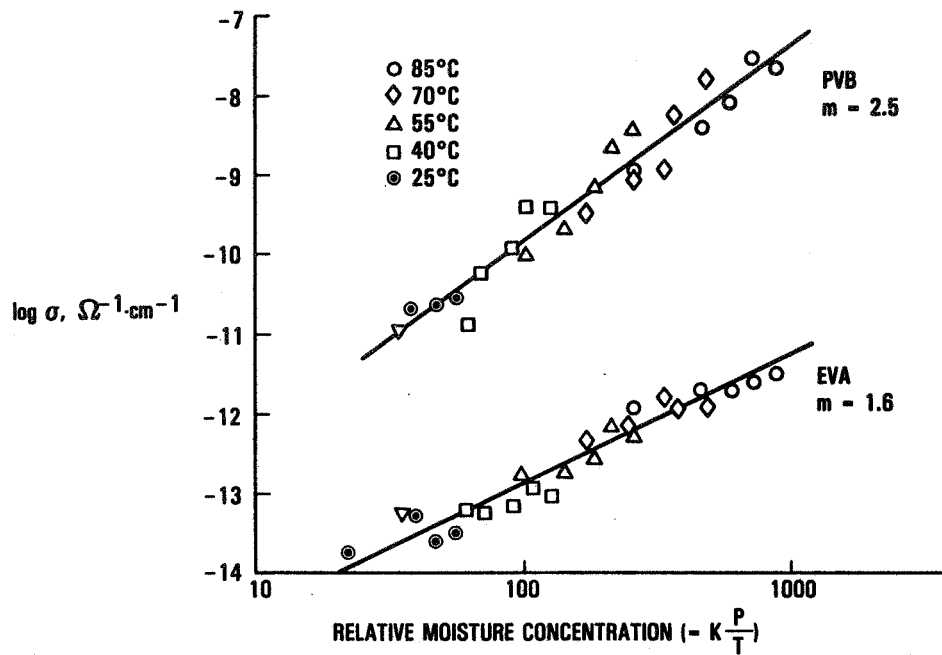


- **Equilibrium values measured by Professor J. Orehotsky**
- **Experimental equilibrium values were processed, yielding sets of "best-fit" data curves**

Electrical Conductivity of PVB and EVA

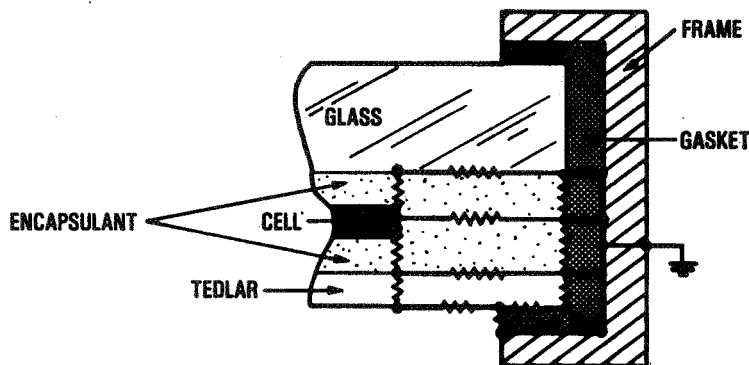


Bulk Conductivity vs Moisture Concentration
(From Orehotsky Data and Ideal Gas Law)



Module Performance Analysis

- Life prediction requires calculation of charge transfer in a real module
 - Through the bulk pottant
 - Along material interfaces
 - On free surfaces
- Leakage current path modelling

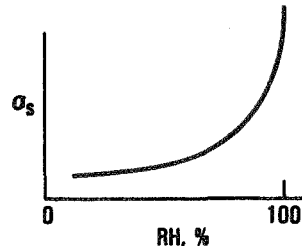


Research Questions About Module Conductivity

- **Over what ranges of temperature and relative humidity do the various conductivities dominate overall module conductivity?**
- **In what ways do the various forms of water in polymers contribute to overall module conductivity?**
 - **Bound water**
 - **Free water**
 - **Clustered water**
- **Does exposure to liquid water result in same measured conductivity values as exposure to saturated water vapor?**

General Dependencies Involving Insulation Electrical Conductivities

- **Surface conductivity values are strongly affected by contaminants**
- **Surface conductivity responds rapidly to changes in relative humidity and surface-water films**

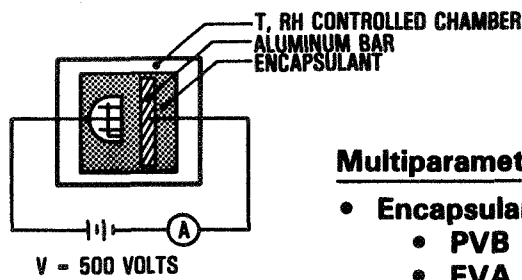


- **Volume conductivity responds rapidly to changes in temperature, less rapidly to changes in relative humidity**
- $\sigma_v = A e^{-E/T}$ (ASTM D257-78)
- **Generally, $\sigma_s > \sigma_v$**

RELIABILITY PHYSICS

Experiments to Determine Module Equilibrium Leakage Current Levels and Response to Parameter Variation

Test setup



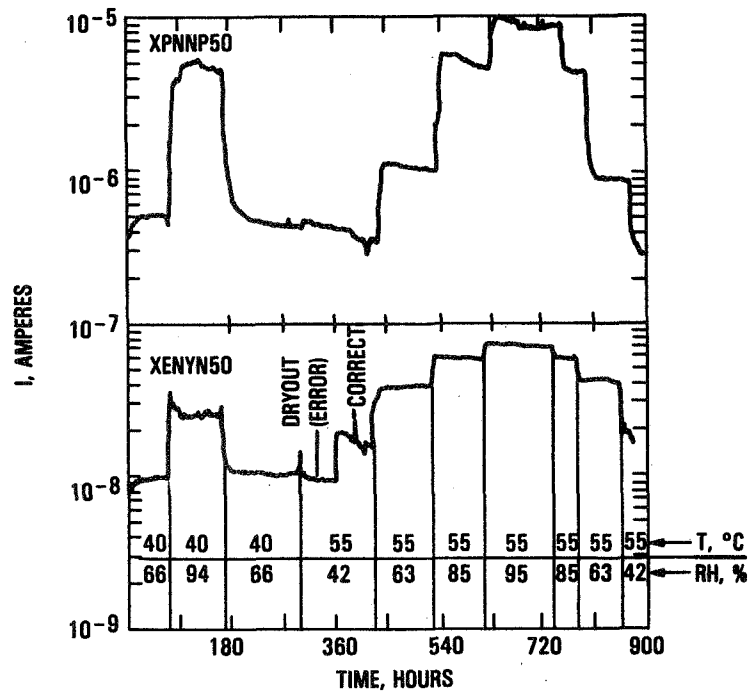
Test sequence

		RH, %				
T, °C	40	66	94			
	55	42	63	85	95	
	70	<10	50	71	85	95
	85	<10	30	50	70	85

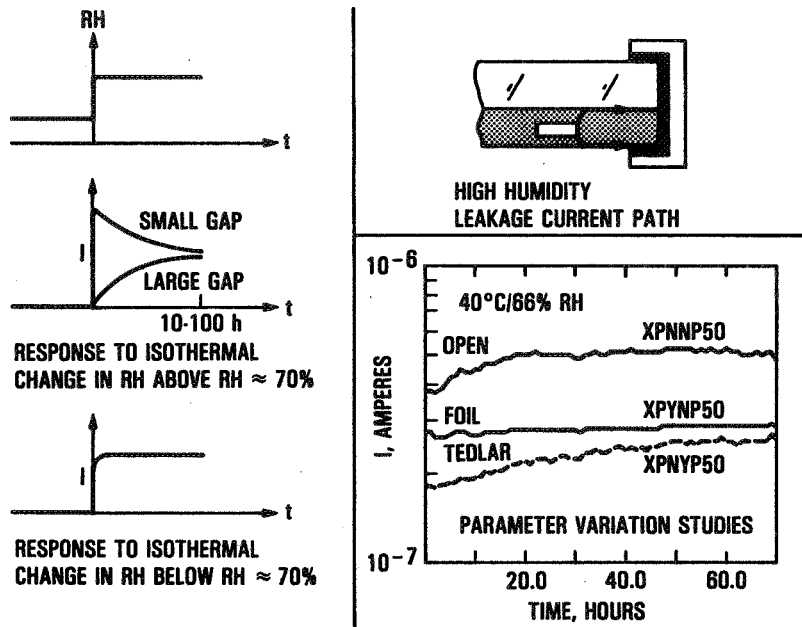
Multiparameter testing

- Encapsulants
 - PVB
 - EVA
- Polarity
 - Positive
 - Negative
- Electrode spacing
- Rear-surface barriers
 - Polymers
 - Metal foils
 - None
- Cell metallizations

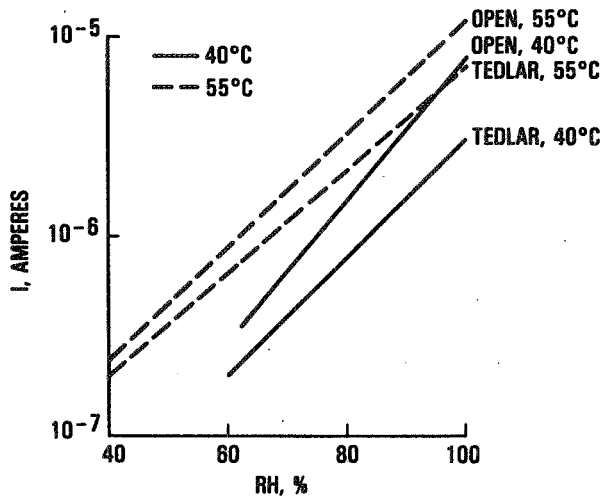
Current vs Time



Some General Observations

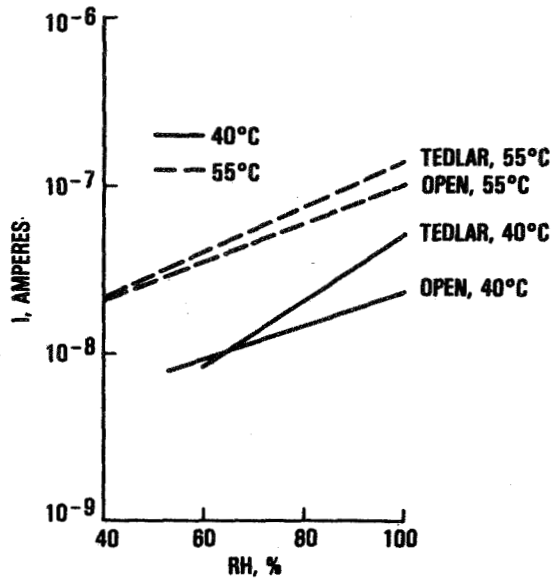


Leakage Current Sensitivity to Relative Humidity at 40°C and 55°C: PVB, Positive Polarity, 50-Mil Gap



RELIABILITY PHYSICS

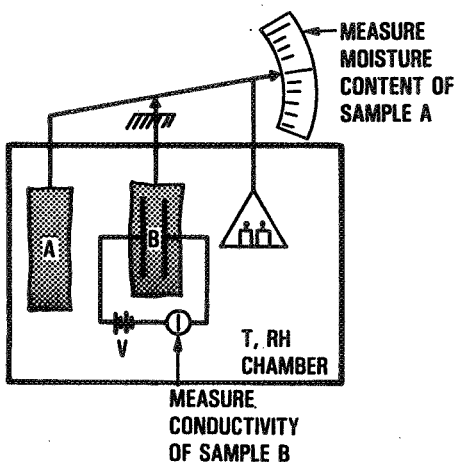
Leakage Current Sensitivity to Relative Humidity at 40°C and 55°C: EVA, Positive Polarity, 50-Mil Gap



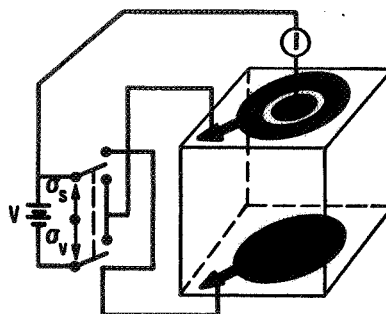
Conclusion

- Because of the importance of bulk, interfacial, and free-surface conductivities, additional experiments are necessary to separate the relative contributions of these to overall module conductivity

Direct Conductivity Measurements



- Cahn balance sorption test
 - $c = S(T) RH$
 - $\sigma = \sigma(V; T, c(T, RH))$
 $= \sigma(V; T, RH)$



- Guarded electrode measurements
 - Surface and volume conductivities
 - PVB
 - EVA
 - Interfacial conductivity
 - Glass/polymer
 - Polymer/Tedlar

PRELIMINARY STUDY: MOISTURE-POLYMER INTERACTION
 JET PROPULSION LABORATORY

L.-C. Wen

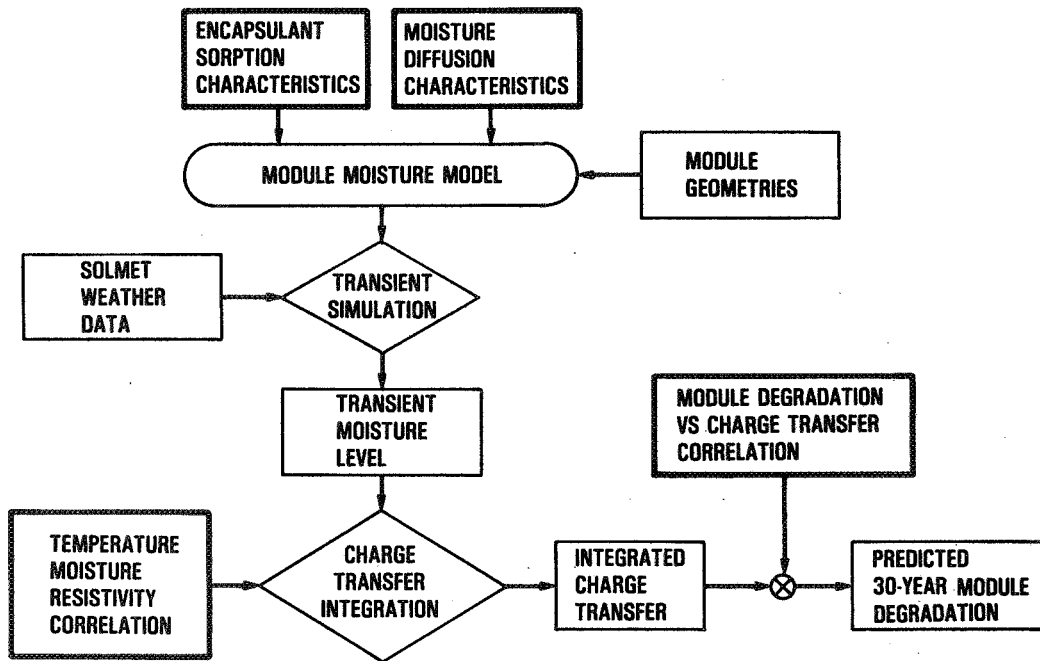
Study Objectives

To develop methodology for predicting module temperature, humidity and surface moisture level versus time in field environment

- Water sorption
- Moisture diffusion
- Simulation using SOLMET weather tape

To apply the above temperature-moisture prediction methodology together with electrochemical corrosion temperature-moisture dependence to predict module corrosion lifetime in the field

Simulation Flow Diagram

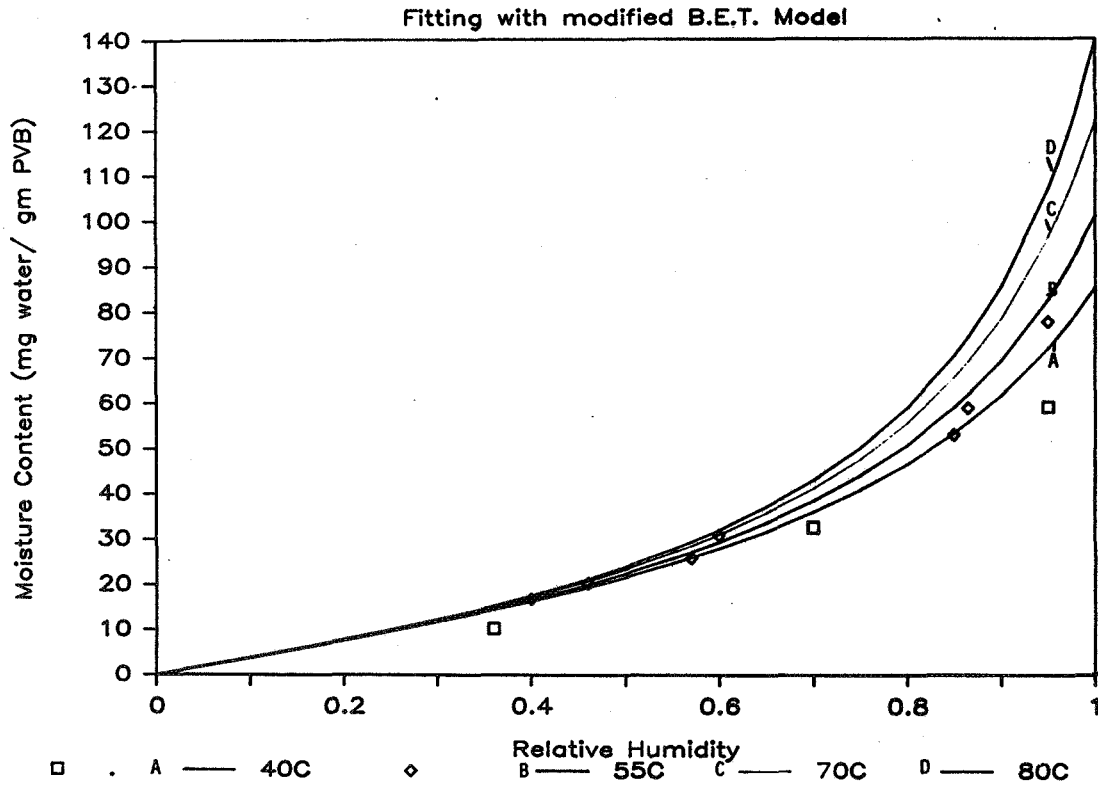


PRECEDING PAGE BLANK NOT FILMED

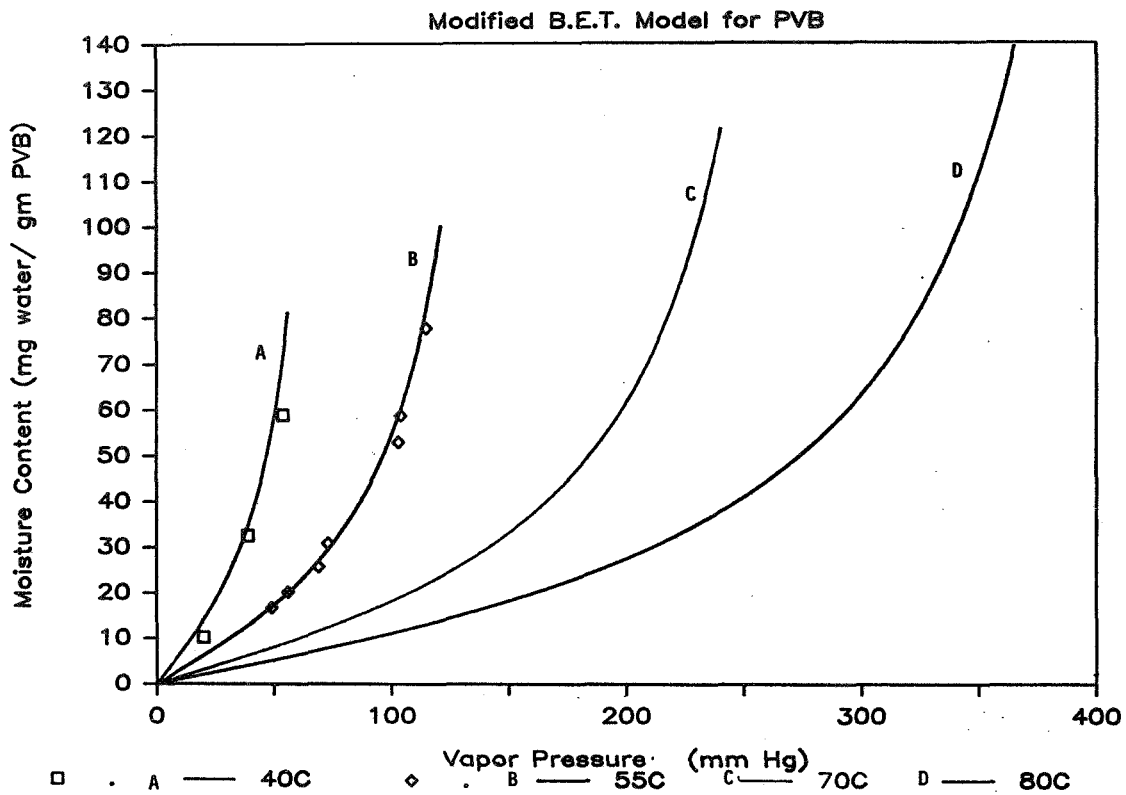
Sorption Study

- **Objective**
 - **To establish an analytical model for predicting moisture sorption isotherms for relevant polymers**
- **Approach**
 - **Gravimetric measurements using a Cahn balance**
 - **Isothermal system: humidity chamber**
 - **Relative humidity from 40% to 95%, no liquid water**
 - **Data fitting with an analytical model (modified B.E.T. equation)**

Water Sorption for PVB



Water Sorption Isotherms



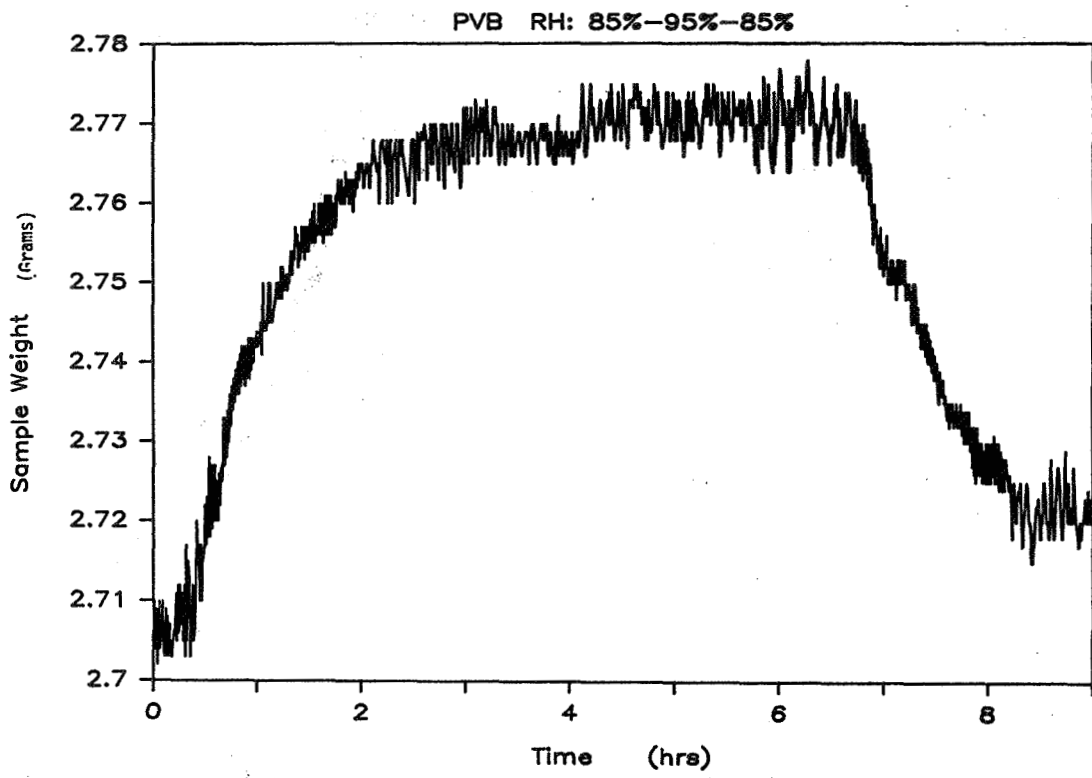
Moisture Sorption

- **Status**
 - Limited samples were used (PVB)
 - Reasonable data fitting with a modified B.E.T. equation
- **Required R&D**
 - Expanded sorption data base for different materials, composite layers and conformal coatings
 - Sorption-desorption in non-isothermal conditions
 - Kinetics and thermodynamics of adsorption/absorption (both liquid and vapor water)
 - Factors influence moisture sorption in polymer; plasticizer, cross-linking agent
 - Free-to-bound water transformation

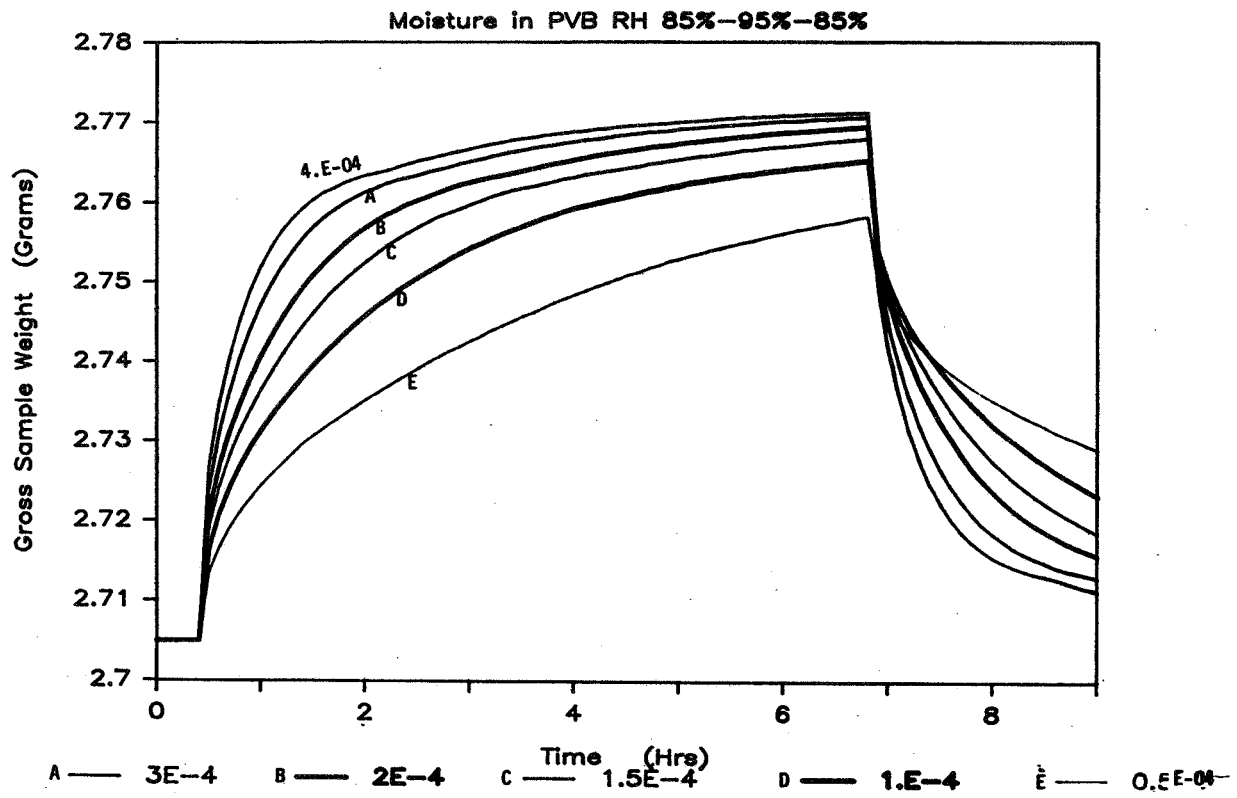
Moisture Diffusion

- **Objective**
 - **To develop a moisture transport model and diffusion/permeation parameters**
- **Approach**
 - **Transient experimental data based on sorption measurements**
 - **Nodal network representation of Fick's diffusion model**
 - **100-layer model**
 - **Isothermal system**
 - **Parametric iteration of constant diffusivity levels**
 - **Determination of diffusivity based on transient data**
 - **To establish equations to correlate diffusivity/permeability as a function of temperature and moisture content**
- **Status**
 - **Diffusivity increases with moisture content in PVB**
 - **Arrhenius-type variation with temperature**
 - **Good correlations between data and model**
- **Required R&D**
 - **Moisture diffusion in composite encapsulants**
 - **Diffusion of unbound water**
 - **Bulk water movement**
 - **Transition of bound and unbound water**
 - **Apparent diffusivity**
 - **Non-isothermal system**
 - **Models for simultaneous heat and mass transfer**
 - **Thermal diffusion**
 - **Factors affecting moisture diffusion and permeation**

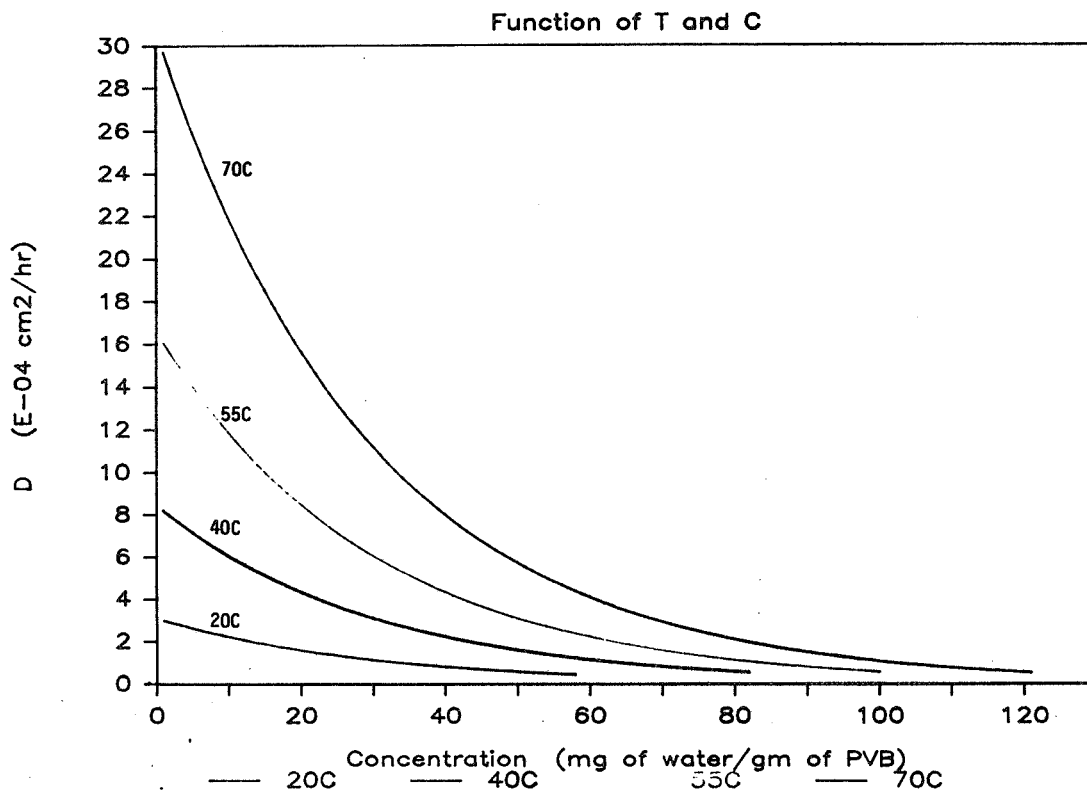
Moisture Sorption-Desorption



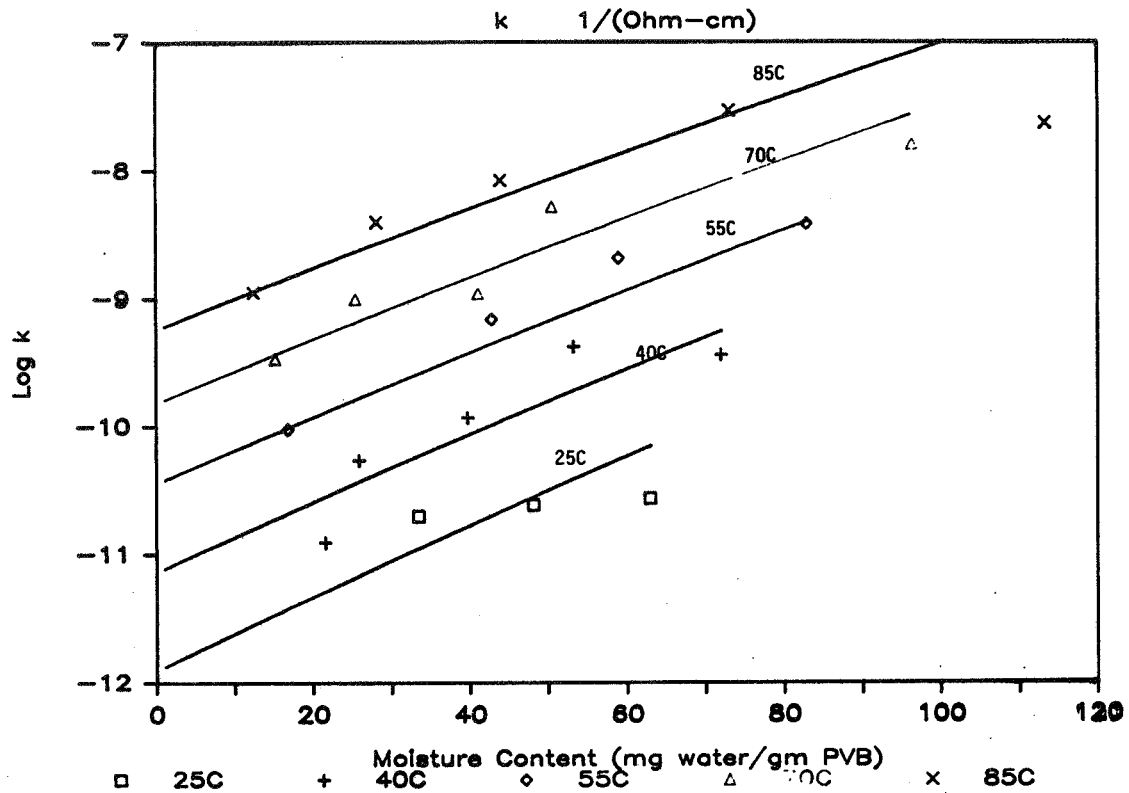
Diffusivity Simulation at 55°C



Diffusivity of Moisture in PVB



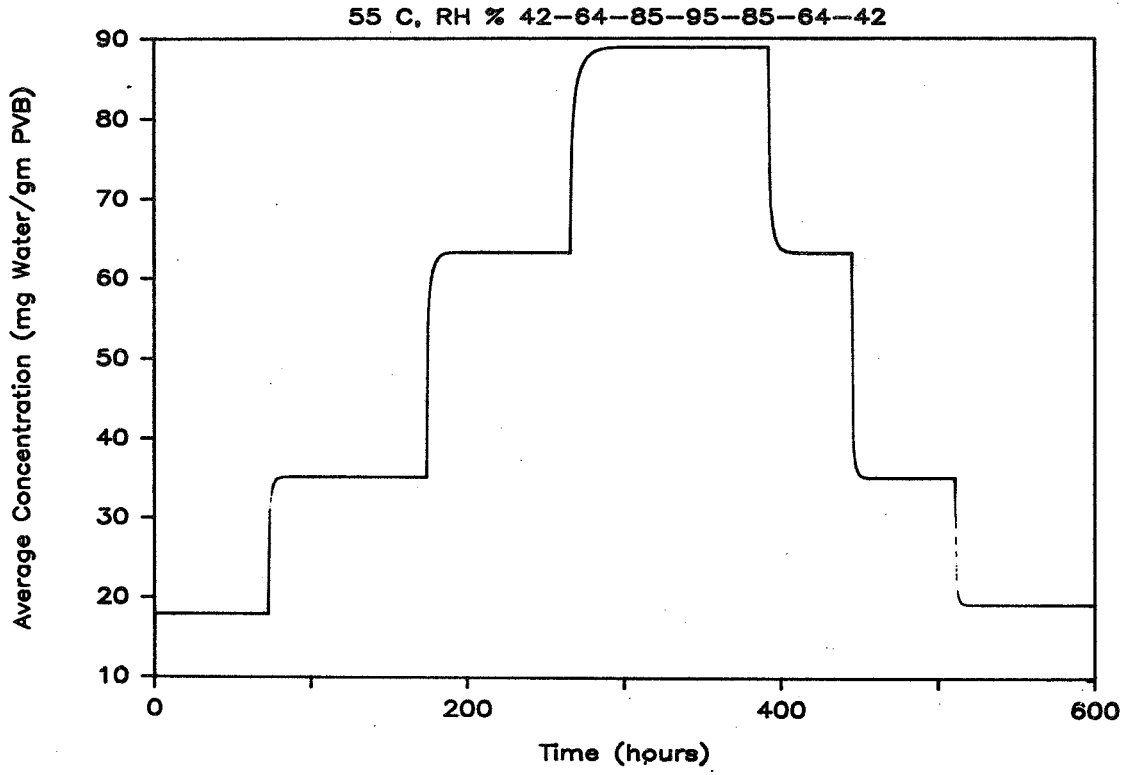
Bulk Conductivity of PVB



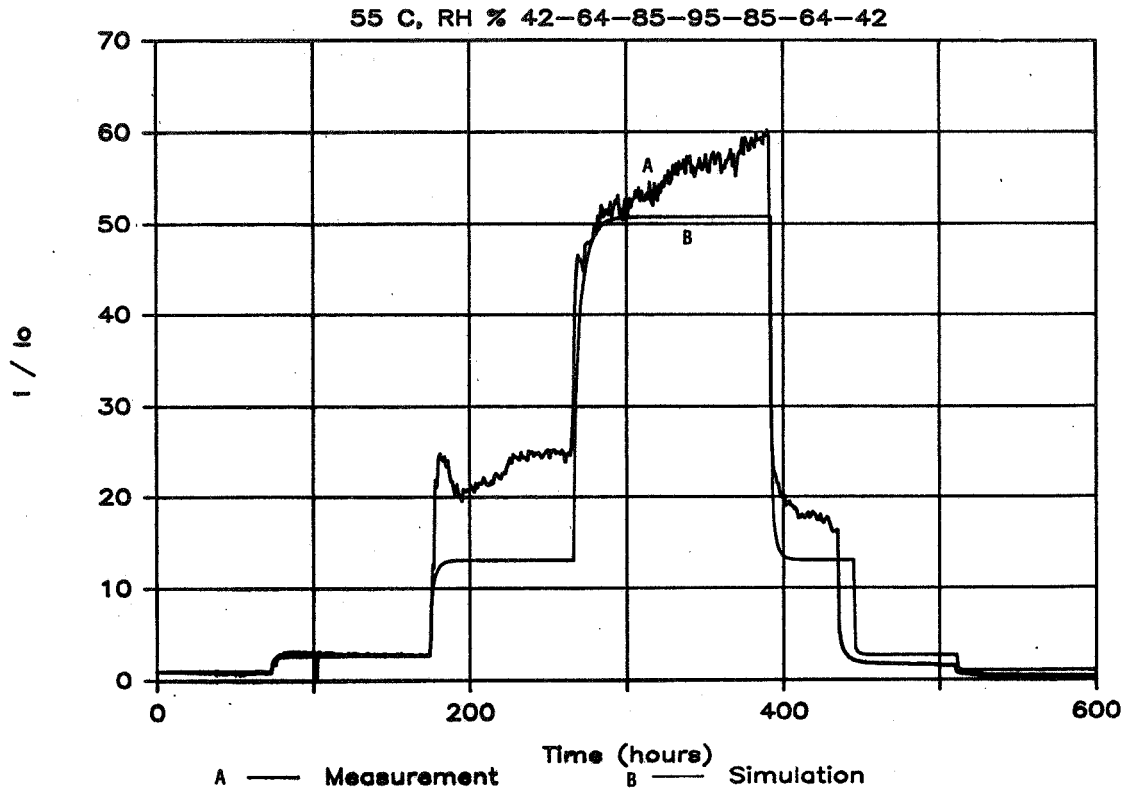
Electrochemical Corrosion

- Objective
 - To simulate module leakage current vs time in operating environment
- Approach
 - Construct preliminary analytical model
 - Conduction across encapsulant
 - No surface resistance, no lateral volumetric conduction
 - Include equations for sorption and diffusivity
 - Nodal network analysis using thermal analyzer SINDA
 - Equation to represent bulk ionic conductivity as a function of temperature and moisture content
 - Exercise model with transient chamber boundary conditions
 - Exercise model with SOLMET field data

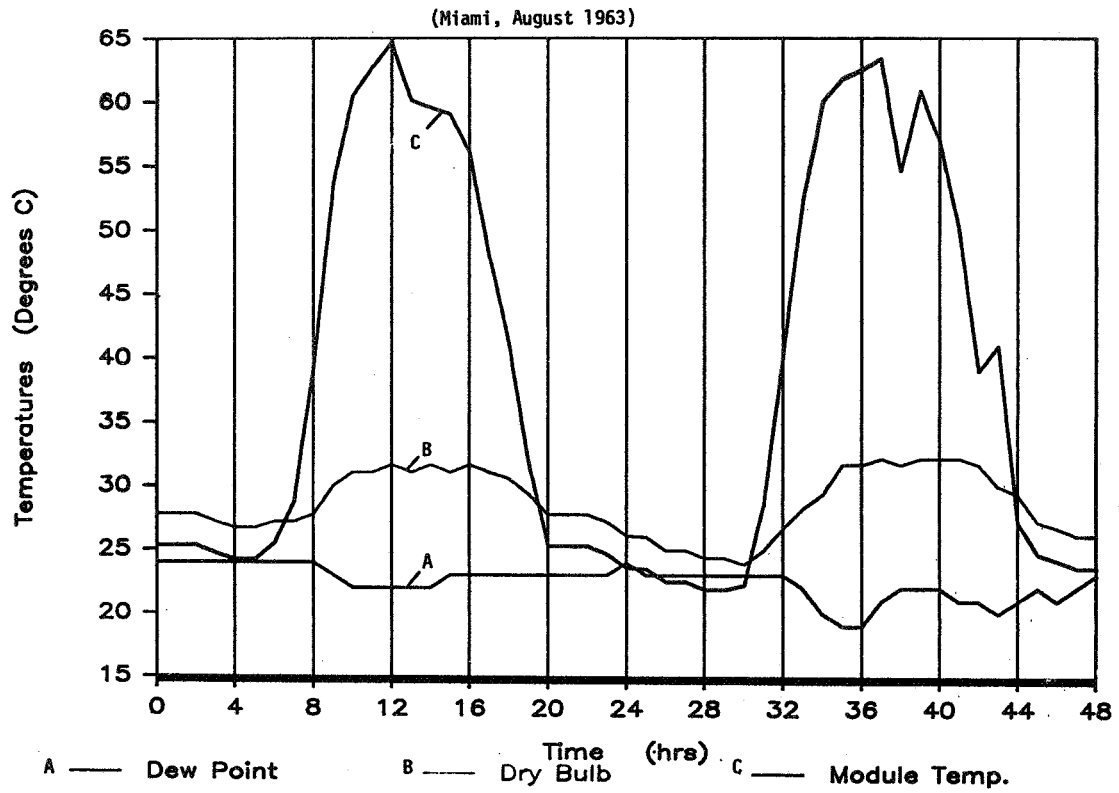
Moisture Content, PVB



Normalized Leakage Current

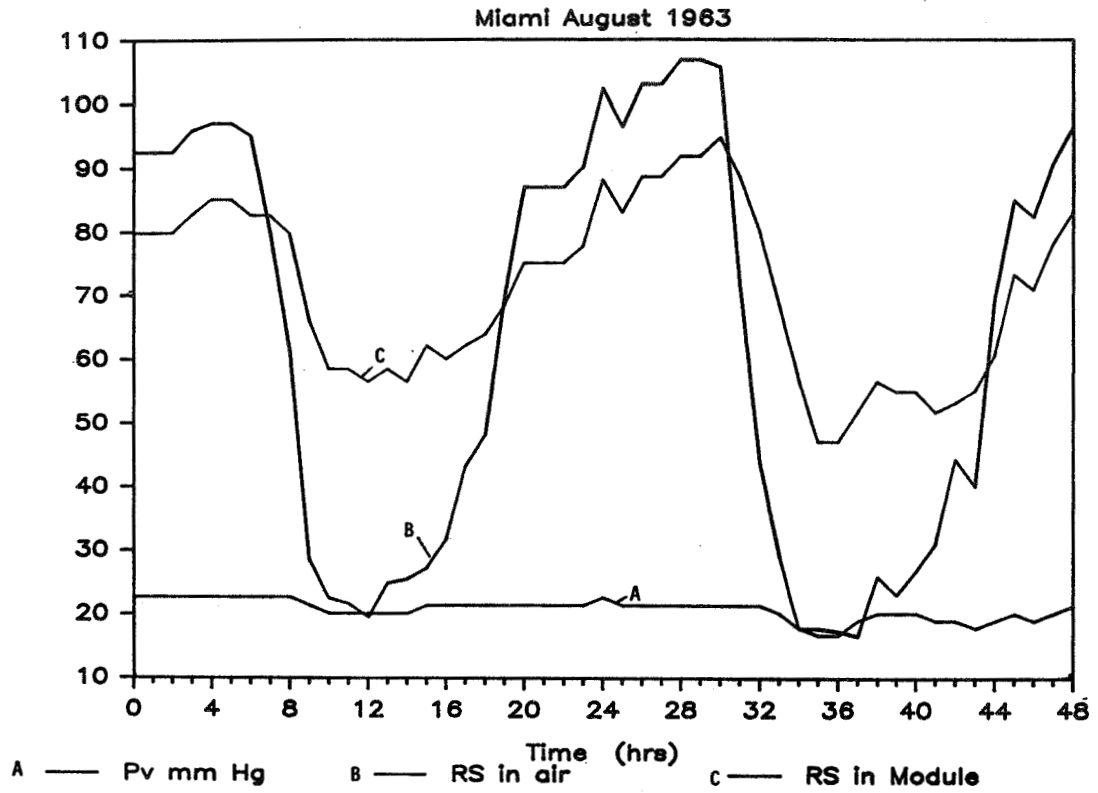


Temperature Profiles

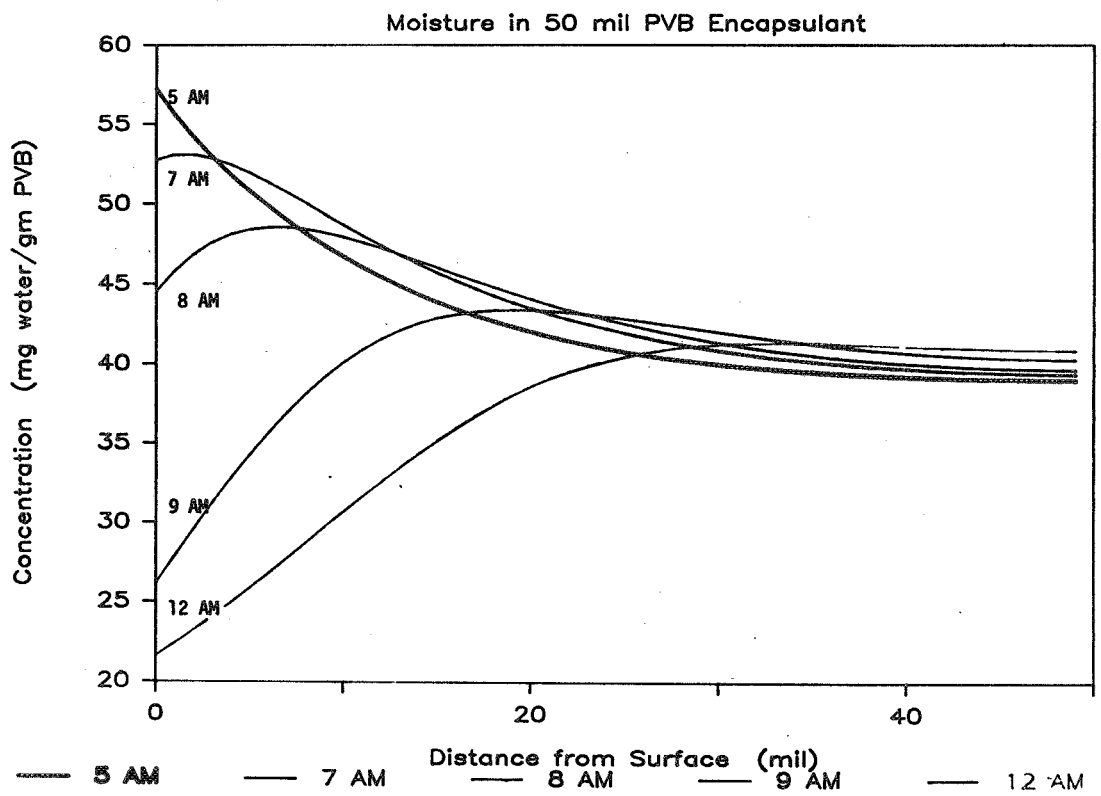
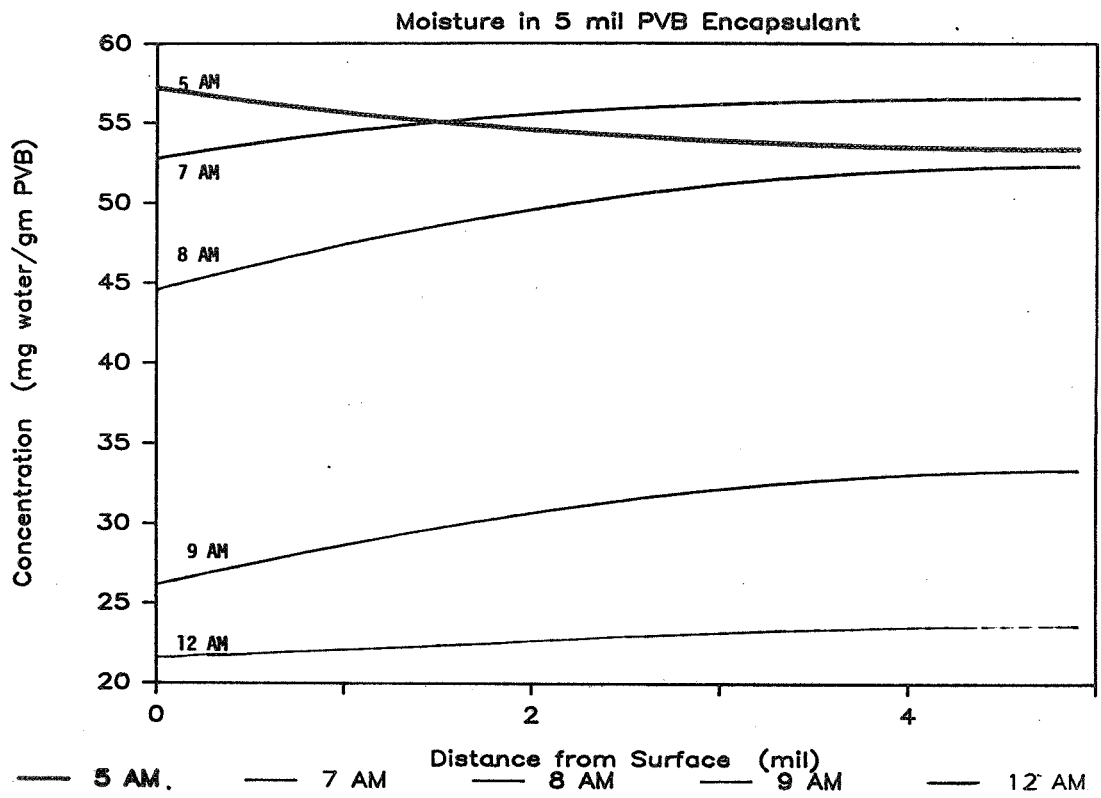


RELIABILITY PHYSICS

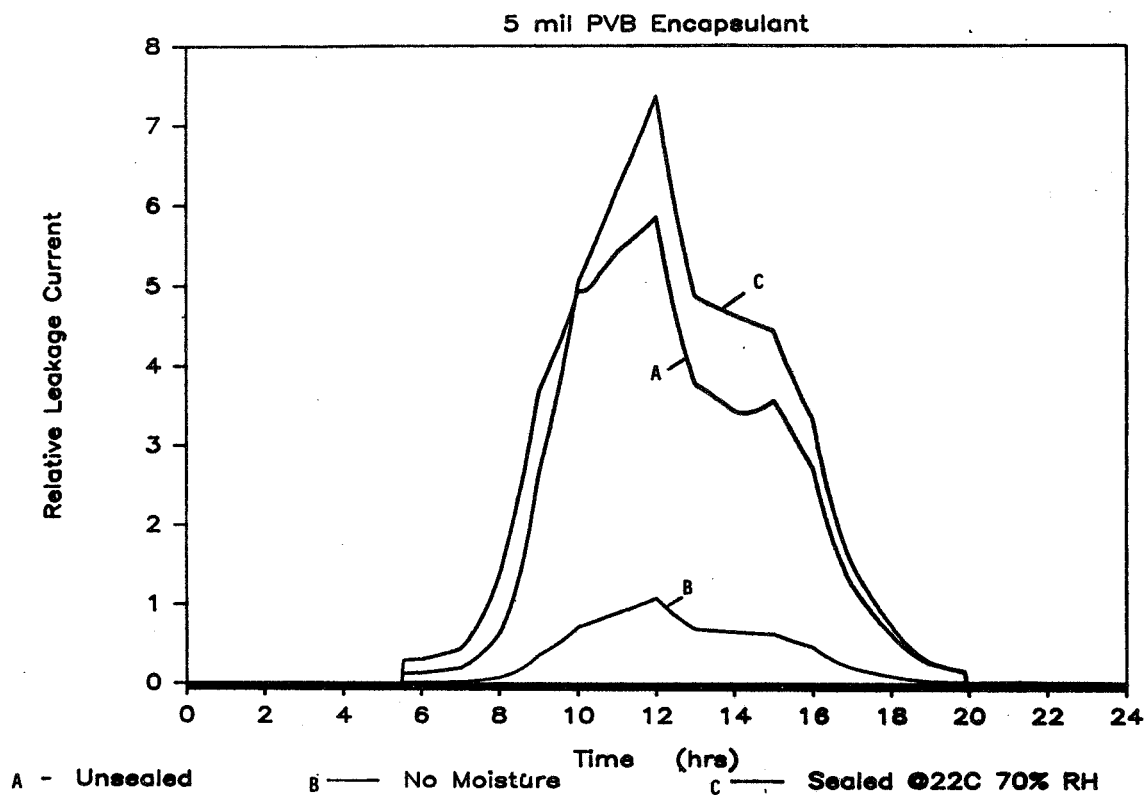
Vapor Pressure and Relative Saturation



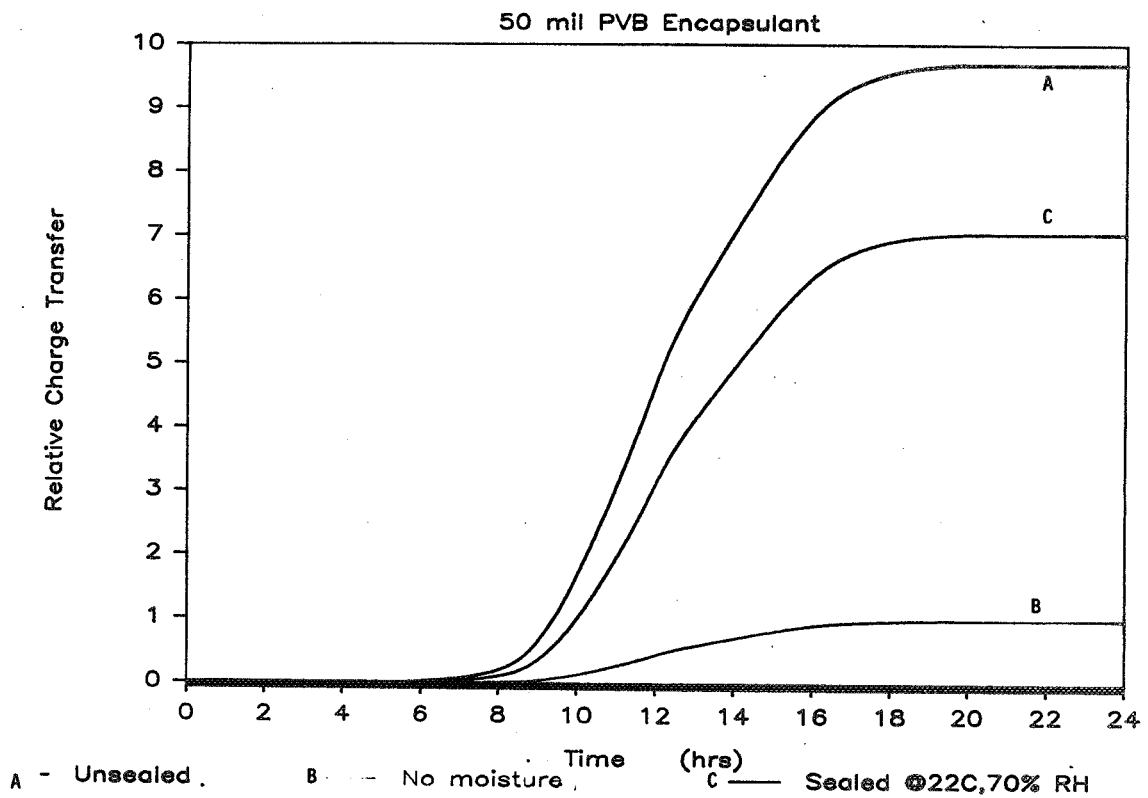
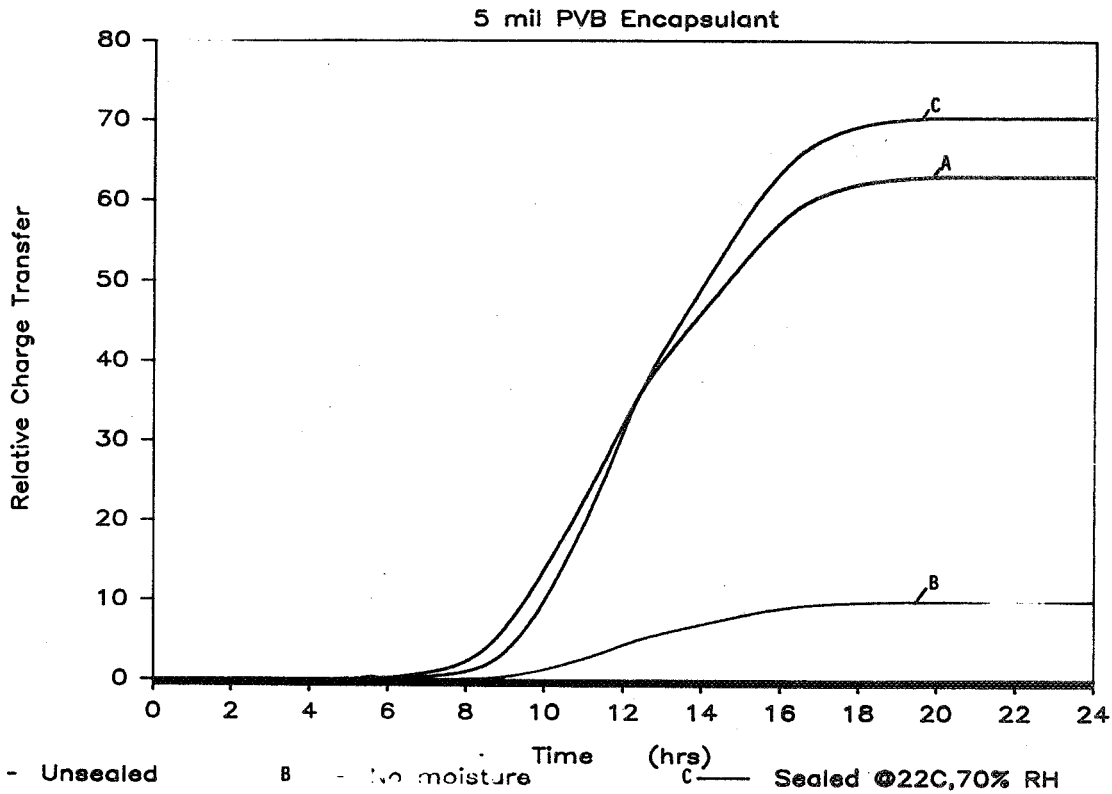
Concentration Distribution



Leakage Current in Field



Charge Transfer in Field



Summary

- **Realistic lifetime prediction appears to be feasible**
- **Refinements in prediction techniques are required**
- **Research areas:**
 - **2-dimensional ionic conduction model**
 - **Composite layers**
 - **Non-isothermal system**
 - **Effects of liquid water**
 - **Interfacial adsorption/absorption**

WATER PERMEATION AND DIELECTRIC BREAKDOWN

WILKES COLLEGE

John Orehotsky

WATER PERMEABILITY

in

PVB

TEDLAR

PVB / TEDLAR

AS

A

FUNCTION

OF

TEMPERATURE

AND

HUMIDITY

THEORY

ASSUMPTIONS:

(1) FICK'S LAW

$$J = P dp/dx$$

(2) IDEAL GAS BEHAVIOR

(3) IMMISCIBILITY

(4) SPONGE STRUCTURED

(5) DIFFUSION THROUGH
WATER FILLED VOID
SPACE

(6) CLAUSIUS-CLAPEYRON

PVB AND TEDLAR

TEMPERATURE DEPENDENCE

$$P = \frac{P_0 \exp(-Q_u / RT)}{T}$$

Q_u IS ACTIVATION ENERGY FOR
WATER SELF DIFFUSION

$$J = \frac{J_0 \exp(-[Q_u + \Delta H_v] / RT)}{T^{6.57}}$$

ΔH_v IS ENTHALPY OF WATER EVAPORATION

HUMIDITY DEPENDENCE

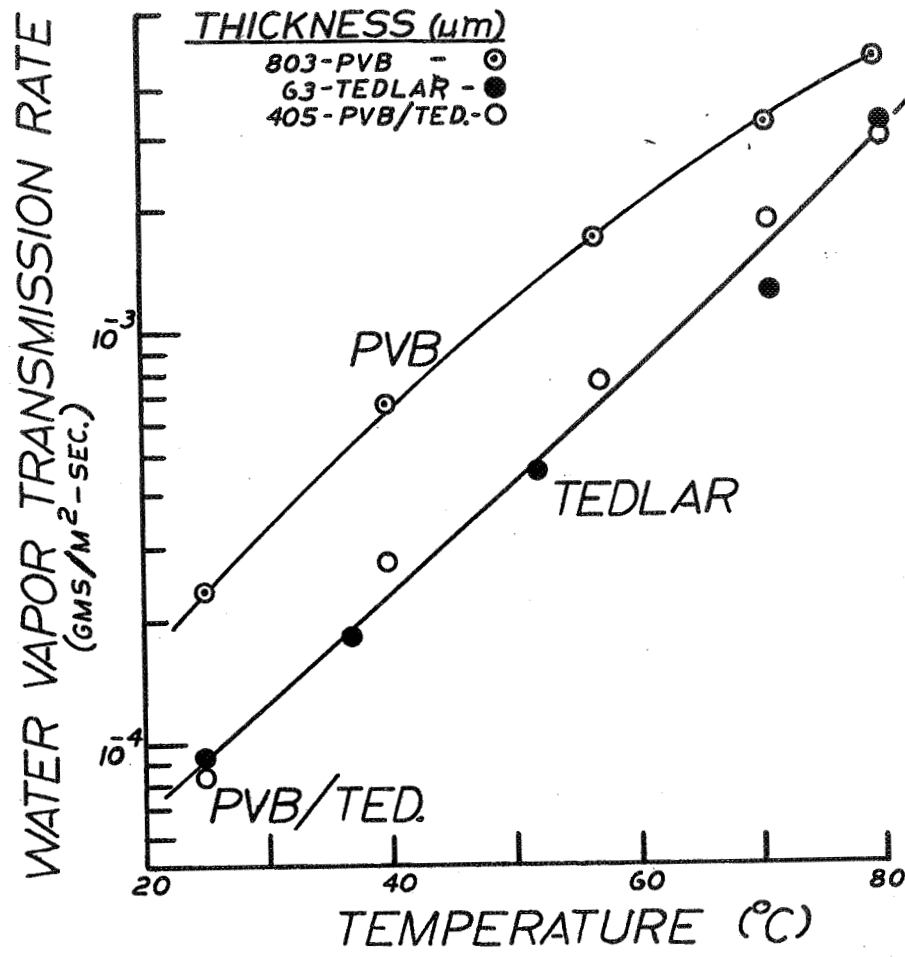
$$J = K [A.H.]$$

PUB/TEDLAR COMPOSITE

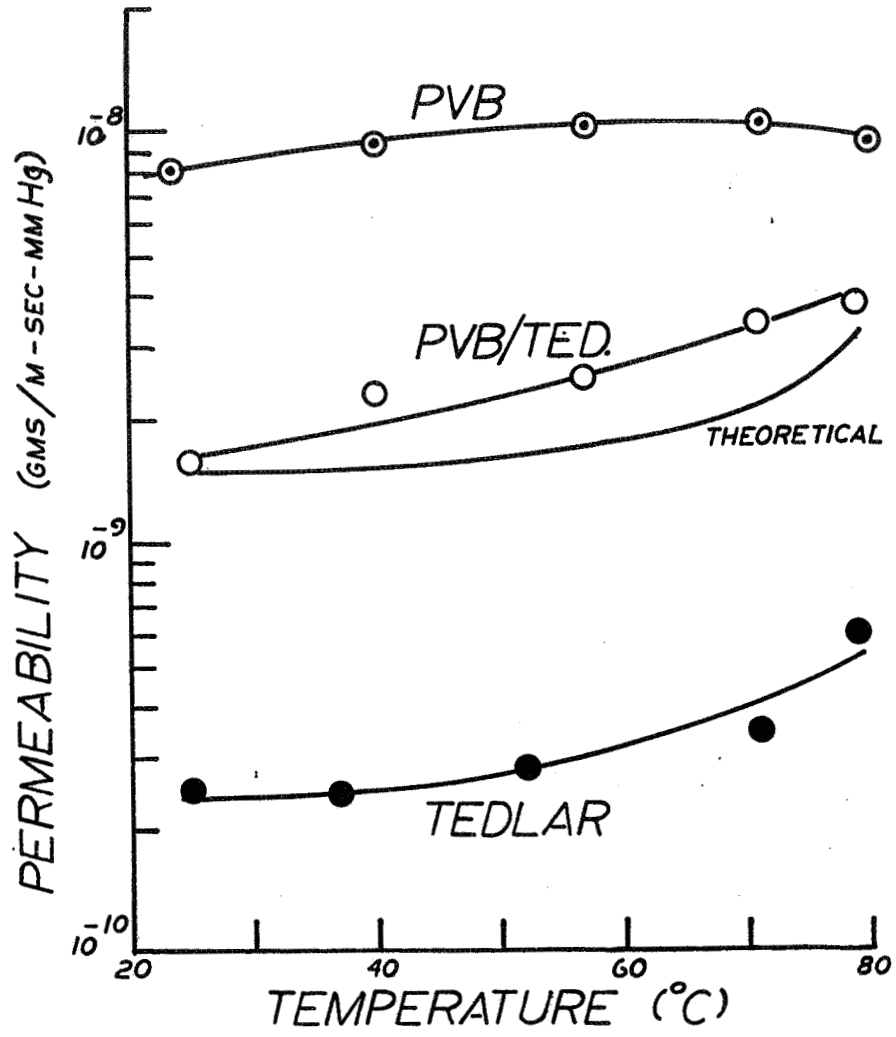
$$\frac{1}{P_{\text{PUB/T}}} = \left[\frac{t_{\text{PUB}}}{P_{\text{PUB}}} + \frac{t_{\text{T}}}{P_{\text{T}}} \right] \left[\frac{1}{t_{\text{PUB}} + t_{\text{T}}} \right]$$

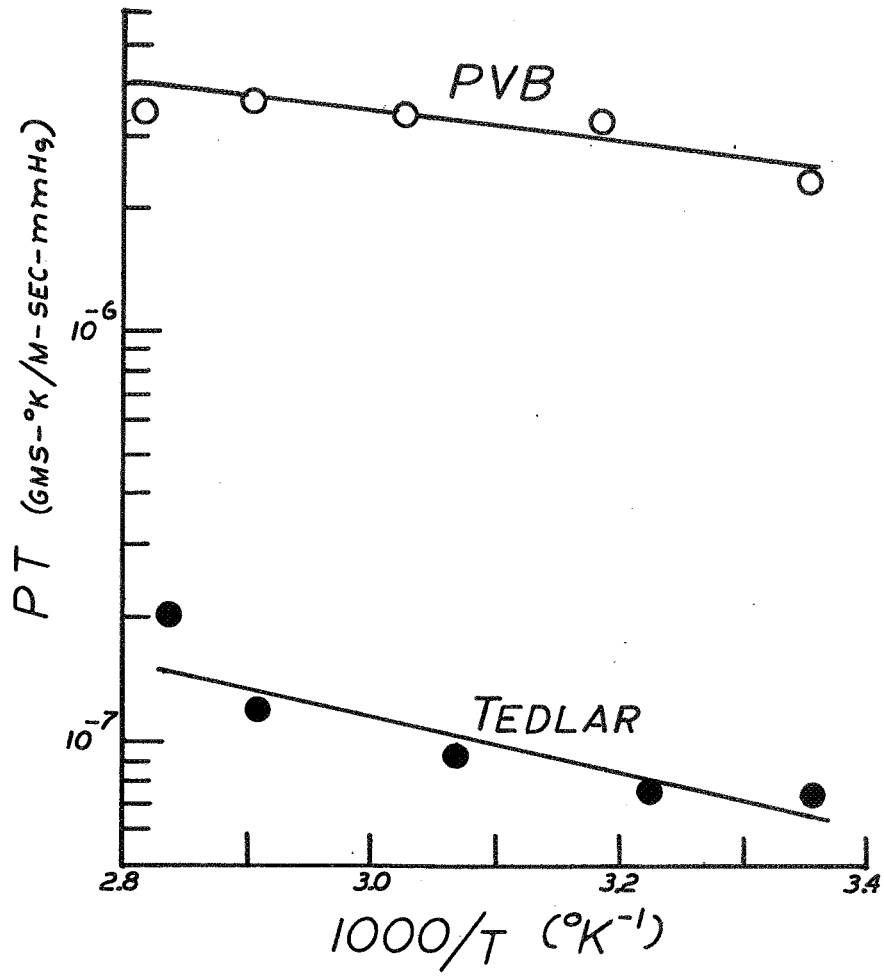
$$J_{\text{PUB/T}} \begin{cases} = J_{\text{PUB}} \text{ (if } J_{\text{PUB}} < J_{\text{T}}) \\ \text{or} \\ = J_{\text{T}} \text{ (if } J_{\text{T}} < J_{\text{PUB}}) \end{cases}$$

RELIABILITY PHYSICS

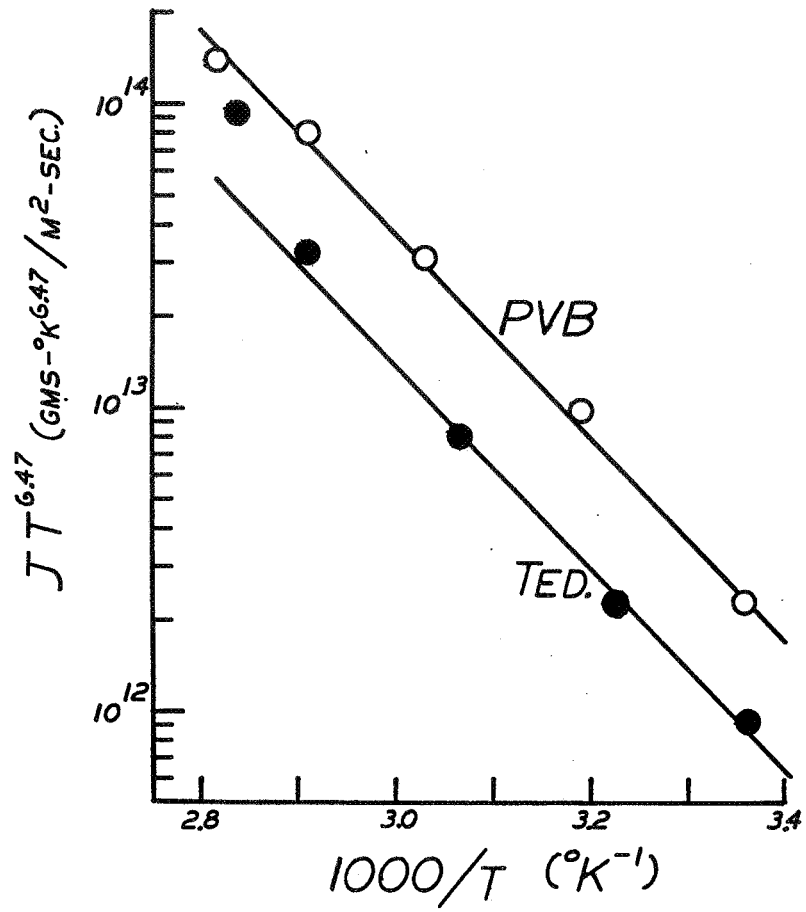


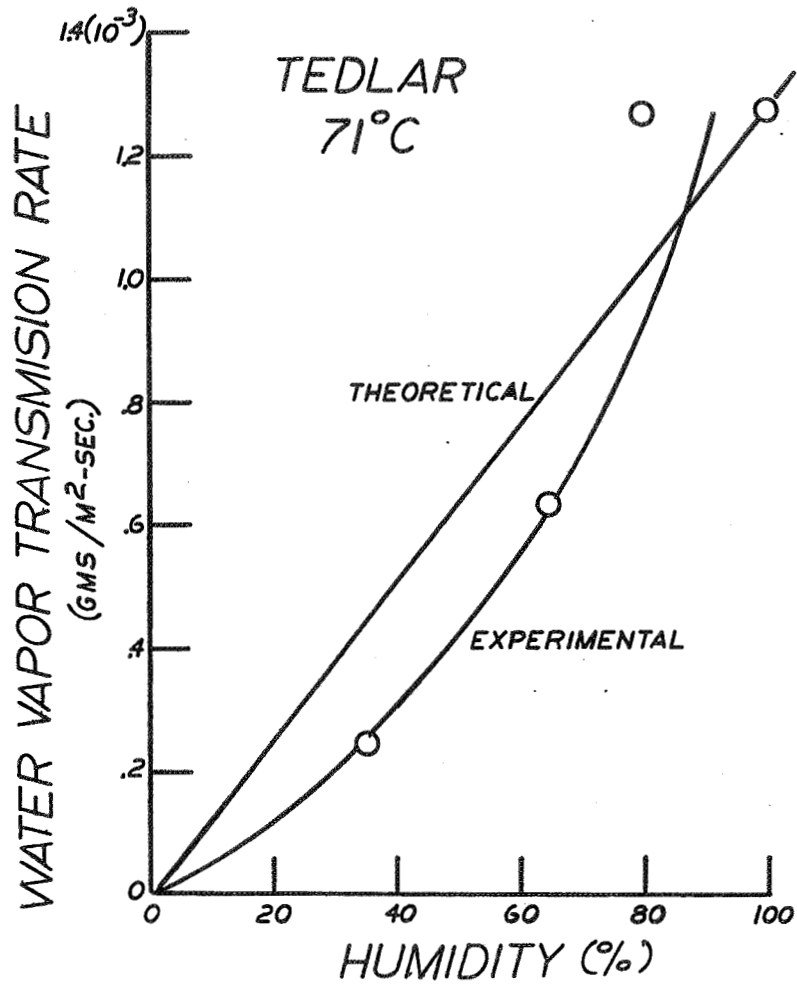
RELIABILITY PHYSICS





RELIABILITY PHYSICS





RESULTS & CONCLUSIONS

$$(1) \frac{P_{PUB}}{P_T} \equiv 100$$

$$(2) \frac{J_{PUB}}{J_T} \equiv 3 \left(\begin{array}{l} t_{PUB} = 803 \mu m \\ t_T = 63 \mu m \end{array} \right)$$

(3) **THEORY=EXPT** for J(T) & P(T)
EXPT

$$Q_u + \Delta H_u = 15 \text{ Kcal/mole}$$

LITERATURE:

$$Q_w = 4.6 \text{ Kcal / mole}$$

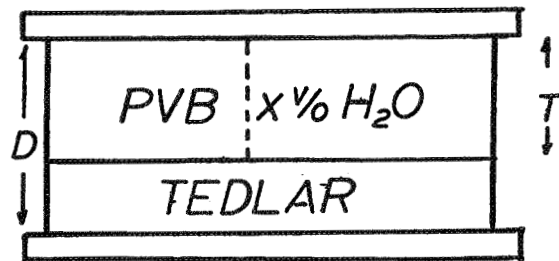
$$\Delta H_p = 9.8 \text{ Kcal / mole}$$

$$Q_w + \Delta H_p = 14.4 \text{ Kcal / mole}$$

(4) **NEED THERMODYNAMIC INFORM**

RELIABILITY PHYSICS

- RESISTANCE
- CAPACITANCE
- BREAKDOWN VOLTAGE



DIELECTRIC CONSTANT:

$$K = \left[\frac{K_T [X][K_W - K_P] + K_P}{TK_T + [D - T][X][K_W - K_P] + K_P} \right] \left[\frac{l}{D} \right]$$

RESISTIVITY:

$$\rho = \rho_T \left[\frac{D - T}{D} \right] + \left[\frac{T}{D} \right] \left[\frac{\rho_W \rho_P}{\rho_W + [\rho_P - \rho_W][X]} \right]$$

DIELECTRIC BREAKDOWN

AT

25° C

IN

PVB

TEDLAR

PVB/TEDLAR

} 0%
R.H.

AND

PVB

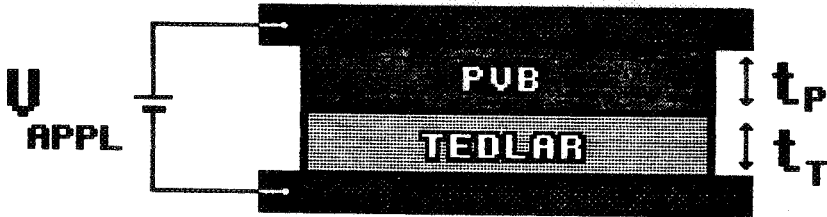
TEDLAR

PVB/TEDLAR

} 100%
R.H.

THEORY

GAUSSES' LAW:



VOLTAGE DIVISION

$$U_P = \left[\frac{t_P / K_P}{t_P / K_P + t_T / K_T} \right] U_{APPL}$$

$$U_T = \left[\frac{t_T / K_T}{t_P / K_P + t_T / K_T} \right] U_{APPL}$$

BREAKDOWN VOLTAGE (0% R.H.)

LARGER OF:

$$U_{BR} = E_{BR_T} K_T \left[\frac{t_P}{k_P} + \frac{t_T}{k_T} \right]$$

OR

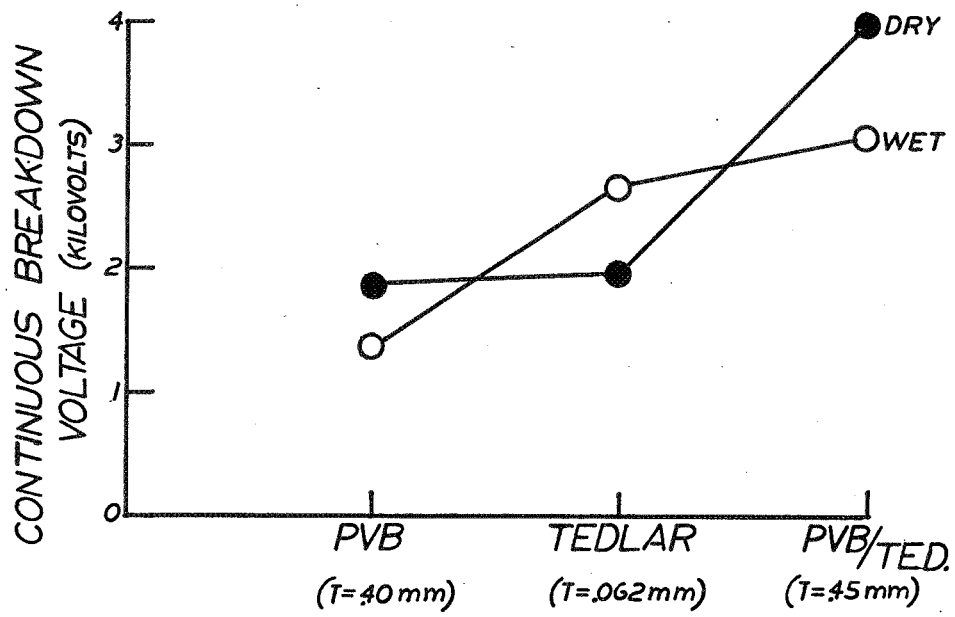
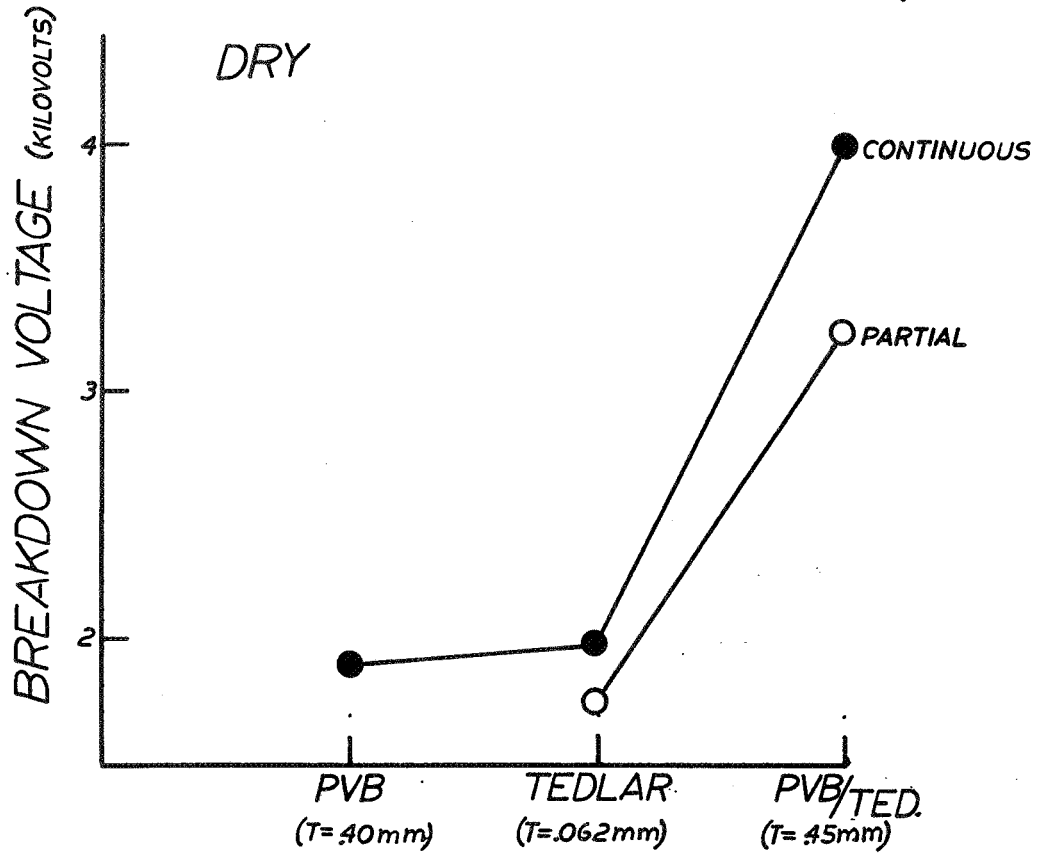
$$U_{BR} = E_{BR_P} K_P \left[\frac{t_P}{k_P} + \frac{t_T}{k_T} \right]$$

WHERE

$$E_{BR_P} = U_{BR_P} / t_P$$

$$E_{BR_T} = U_{BR_T} / t_T$$

RELIABILITY PHYSICS



ELECTRIC FIELDS AT BREAKDOWN

	<u>E_{BR} (KV/cm.)</u>
PVB	25
TEDLAR	280
AIR	30

PVB/TEDLAR
BREAKDOWN VOLTAGE

	<u>V_{BR} (KV)</u>	<u>K_{PVB}</u>	
EXPT.	3.2	-	
THEORY	{	10.1	4.2
		6.1	6.1
		5.3	10.0

CONCLUSIONS

BREAKDOWN VOLTAGES

THEORY \neq EXPT. (PVB/T)

DRY > WET (PVB \dagger PVB/T)

WET > DRY (TEDLAR)

PARTIAL \approx .8 CONTINUOUS

DESTRUCTIVE (TEDLAR)

NON-DESTRUCTIVE (PVB \dagger PVB/T)

CRITICAL ELECTRIC FIELD

TEDLAR > PVB \approx AIR.

“(RH + t)” AGING CORRELATION

JET PROPULSION LABORATORY

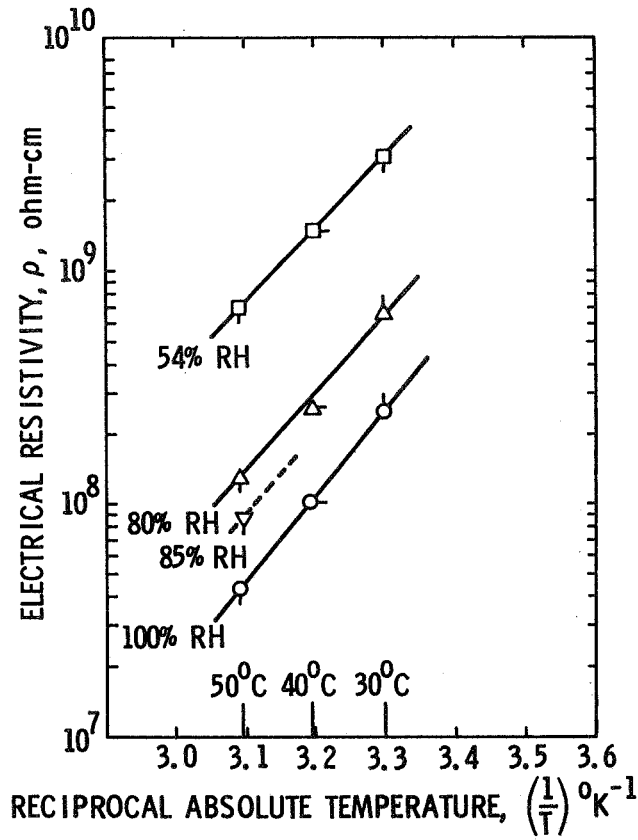
E. F. Cuddihy

Electrical Resistivity of PVB at Various
Temperatures and Relative Humidities
(Experimental Data Measured by Prof. John Orehotsky)

<u>RH, RELATIVE HUMIDITY, %</u>	<u>t, TEMP °C</u>	<u>ρ, RESISTIVITY, OHM-CM</u>	<u>DATA SYMBOL</u>
100	30	$2.53 \cdot 10^8$	o
	40	$9.86 \cdot 10^7$	o-
	50	$4.44 \cdot 10^7$	o
85	50	$8.86 \cdot 10^7$	∇
80	30	$6.24 \cdot 10^8$	△
	40	$2.60 \cdot 10^8$	△-
	50	$1.35 \cdot 10^8$	△
54	30	$3.02 \cdot 10^9$	□
	40	$1.51 \cdot 10^9$	□-
	50	$7.07 \cdot 10^8$	□

PRECEDING PAGE BLANK NOT FILMED

Electrical Resistivity of PVB



EQUATION

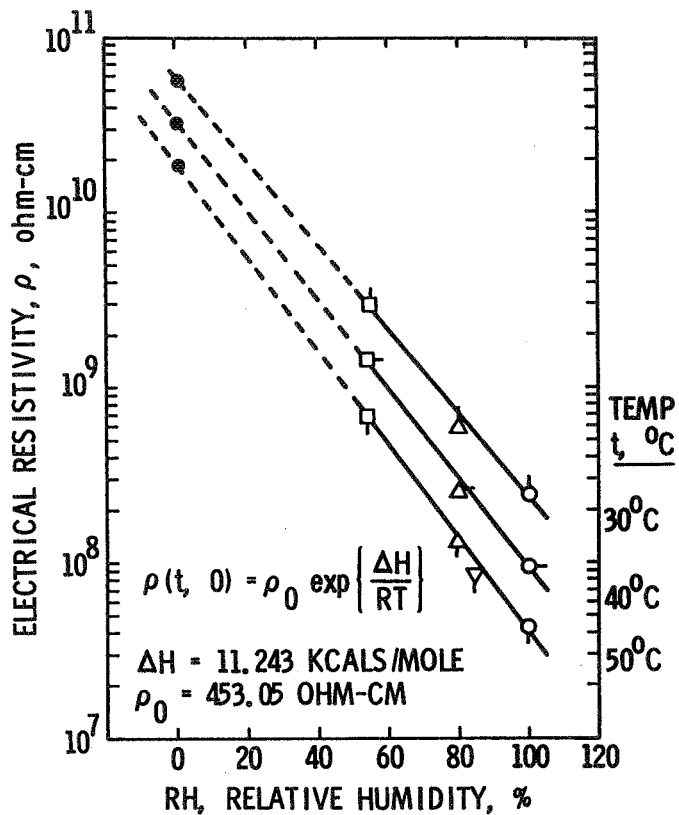
$$\rho(t, RH) = \rho_0(RH) \exp\left\{\frac{\Delta H}{RT}\right\}$$

$$\left\{T (^{\circ}K) = t (^{\circ}C) + 273\right\}$$

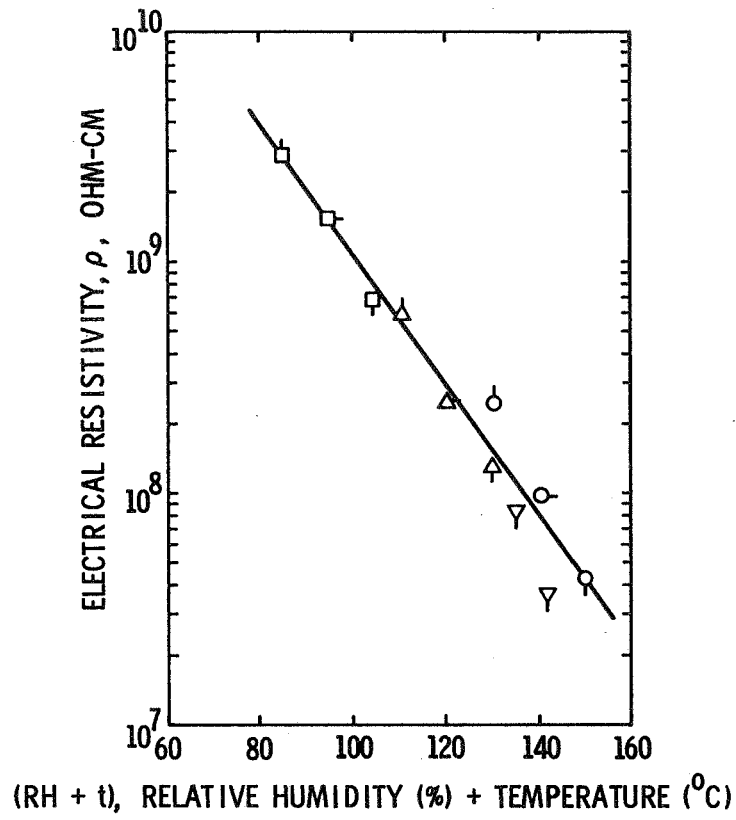
Electrical Resistivity of PVB as a Function of Relative Humidity

ρ AT 0% RH
(FROM LINEAR EXTRAPOLATION)

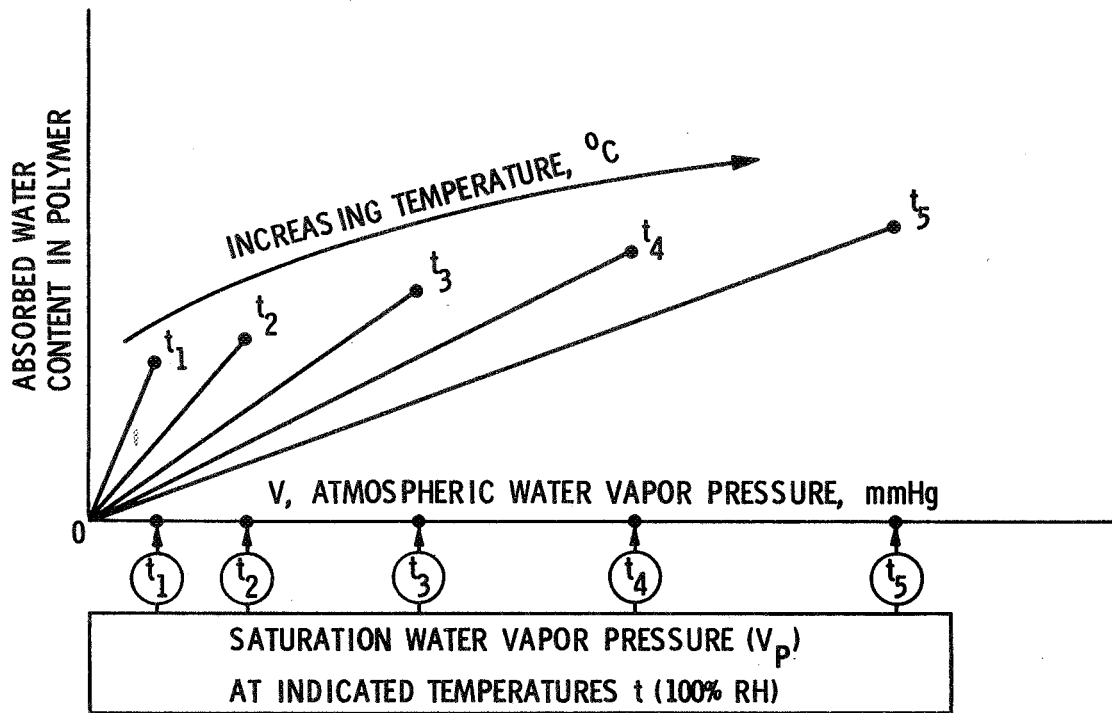
TEMP. °C	ρ , ohms-cm
30	5.8×10^{10}
40	3.3×10^{10}
50	1.8×10^{10}



Electrical Resistivity of PVB as a Function of the Variable (RH + t)

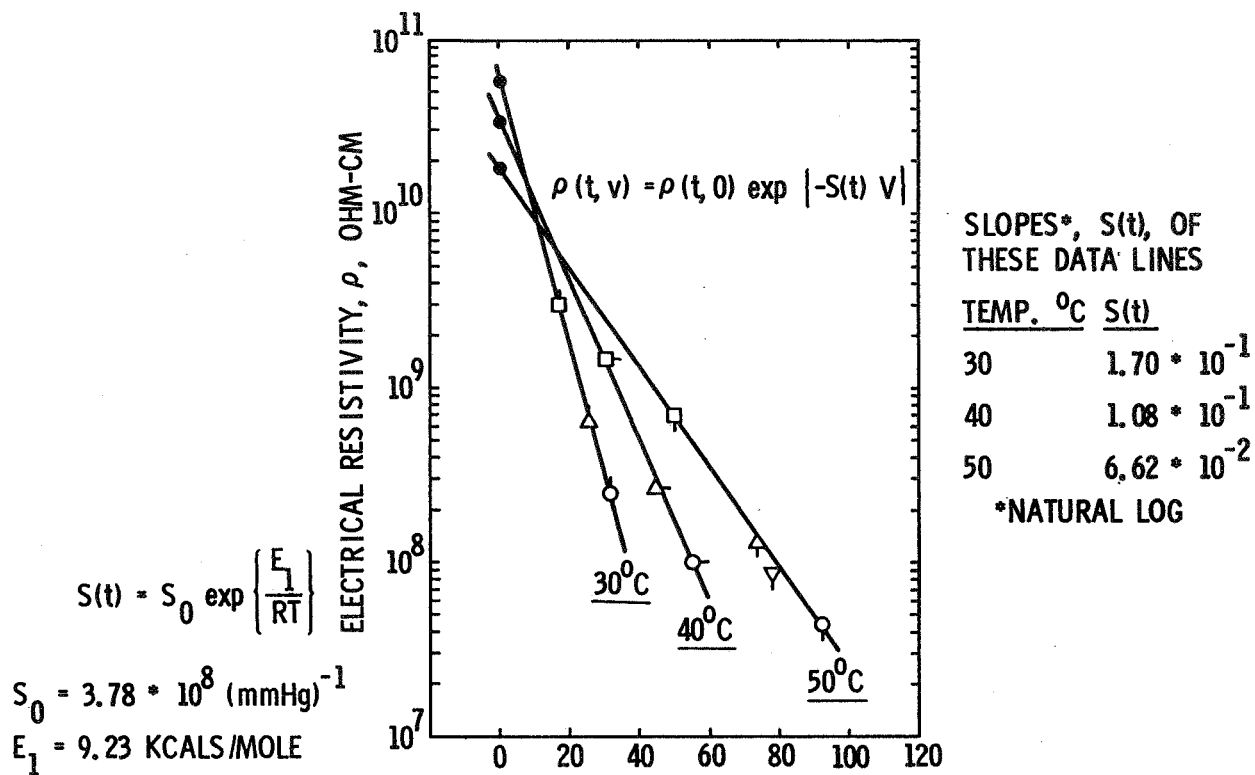


Generalized Hygroscopic Behavior of Polymeric Materials



RELATIVE HUMIDITY AT TEMP. $t = V/V_p(t)$

Electrical Resistivity of PVB Versus Atmospheric Water Vapor Pressure (Absolute Humidity)



The Basic Equations

SLOPES OF ρ VERSUS V

$$S(t) = S_0 \exp\left\{\frac{E_1}{RT}\right\}$$

$$S_0 = 3.78 \cdot 10^{-8} \text{ (mmHg)}^{-1}$$

$$E_1 = 9.23 \text{ KCALS/MOLE}$$

SATURATION VAPOR PRESSURE

$$V_p(t) = V_0 \exp\left\{\frac{-E_2}{RT}\right\}$$

$$V_0 = 1.031 \cdot 10^9 \text{ mmHg}$$

$$E_2 = 10.41 \text{ kcals/mole}$$

RELATIVE HUMIDITY

$$RH(t) = 100 \cdot V/V_p(t) : V = \left(\frac{V_0}{100}\right) (RH) \exp\left\{\frac{-E_2}{RT}\right\}$$

RESISTIVITY AT 0% RH

$$\rho(t, 0) = \rho_0 \exp\left\{\frac{\Delta H}{RT}\right\}$$

$$\rho_0 = 453.05 \text{ OHM-CM}$$

$$\Delta H = 11.243 \text{ kcals/mole}$$

(R = 1.987 CAL/DEG-MOLE)

Derivation of the "(RH + t)" Variable

$$1) \quad \rho(t, V) = \rho(t, 0) \exp \{-S(t) V\}$$

$$2) \quad \rho(t, V) = \rho_0 \exp \left\{ \frac{\Delta H}{RT} \right\} \exp \{-S(t) V\}$$

$$3) \quad \ln \rho(t, V) = \ln \rho_0 + \frac{\Delta H}{RT} - S(t) V$$

$$\longrightarrow V = \left(\frac{V_0}{100} \right) (RH) \exp \left\{ \frac{-E_2}{RT} \right\}$$

$$\longrightarrow S(t) = S_0 \exp \left\{ \frac{E_1}{RT} \right\}$$

$$4) \quad \ln \rho(t, RH) = \ln \rho_0 + \frac{\Delta H}{RT} - \frac{S_0 V_0}{100} \exp \left\{ \frac{E_1 - E_2}{RT} \right\} (RH)$$

$$\longrightarrow \frac{\Delta H}{RT} = \frac{\Delta H}{R} \left\{ \frac{1}{T_0} + \frac{t}{T_0^2} + \frac{t^2}{T_0^3} - \dots \right\}$$

a) TAYLOR'S EXPANSION

$$b) \quad T_0 = 273 : T (^{\circ}K) = 273 + t (^{\circ}C)$$

Derivation of the "(RH + t)" Variable (Cont'd)

$$5) \quad \ln \rho(t, RH) = \ln \rho_0 + \frac{\Delta H}{RT_0} - \frac{\Delta H}{RT_0^2} (t) - \frac{S_0 V_0}{100} \exp \left\{ \frac{E_1 - E_2}{RT} \right\} (RH)$$

DEFINE

$$A = \ln \rho_0 + \Delta H/RT_0$$

$$k_1 = \Delta H/RT_0^2$$

$$k_2 = \frac{S_0 V_0}{100} \exp \left\{ \frac{E_1 - E_2}{RT} \right\}$$

$$6) \quad \ln \rho(t, RH) = A - k_1 t - k_2 (RH)$$

$$\rightarrow k_1 = (11, 243) / (1.987) (273)^2 = 0.0759$$

$$\rightarrow \underline{k_2} \quad \underline{\text{TEMP. } ^\circ\text{C}}$$

0.0548	30
--------	----

0.0584	40
--------	----

0.0619	50
--------	----

$$7) \quad \ln \rho(t, RH) = A - k (t + RH)$$

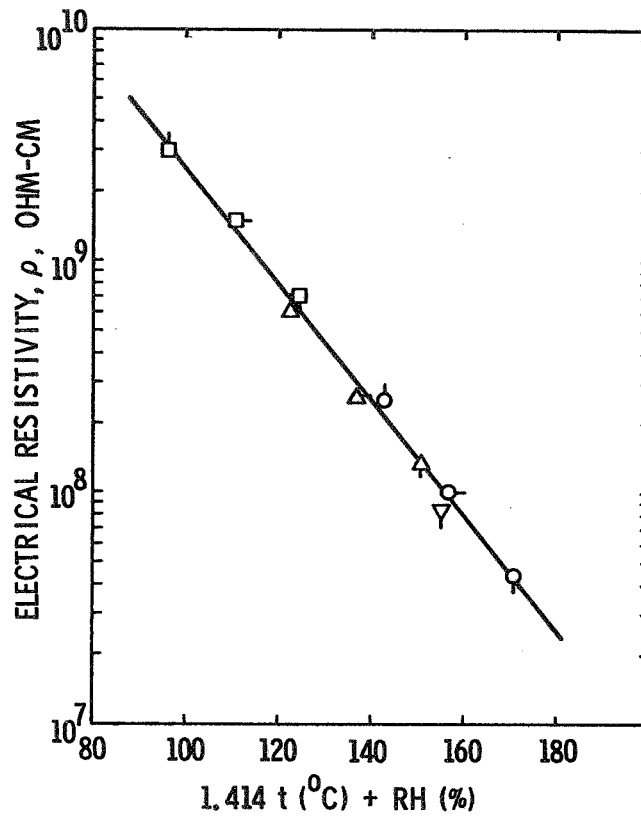
Least Squares Analysis

- $\ln \rho(t, RH) = A - k_1 t - k_2 (RH)$
 - $A = 25.9468$
 - $k_1 = 0.08033$
 - $k_2 = 0.0568$

- $k_1 = \frac{\Delta H}{RT_0^2}$
 - $\Delta H = 11.89 \text{ kcal/mole (FROM LEAST SQUARES)}$
 - $\Delta H = 11.24 \text{ kcal/mole (FROM DATA CURVES)}$

- $\ln \rho(t, RH) = A - k_2 \left\{ \frac{k_1}{k_2} t + RH \right\}$
 - $k_1/k_2 = 1.414$

Electrical Resistivity of PVB Versus
the Variable $(1.414 t + RH)$



SILICON MATERIAL AND JPL WEB TEAM

Ralph Lutwack, Chairman

This session consisted of four presentations on silicon material activities and two presentations describing the efforts of the JPL Web Team.

Union Carbide Corp. described progress in the program to develop fluidized-bed technology for the silane system. Quartz liners used in experimental runs continue to fail on cool-down. A modified reactor has been designed to permit the use of commercially available quartz tubes and to improve the liner seals. Experiments with the new reactor will be done during the contract extension (ending December 31, 1985). Improvements in the cleaning procedure for the seed material were indicated by the purity measurements. In a 110-h run at a silane concentration in the range of 20 to 30% in H₂, several kilograms of product were obtained. A layered structure of the particles was found using scanning electron microscope (SEM) analyses.

Washington University at St. Louis reported on the development of a model of the silane fluidized-bed system. The sensitivity of the model predictions to the reaction kinetics and to the grid design parameters were examined. Both factors have significant influence on the model predictions. It is evident that the reaction kinetics and the distributor plate must be subjects of experimental studies to supply the information needed for refining the model.

JPL reported progress in the in-house program for the study of the silane fluidized-bed system. A seed-particle cleaning procedure was developed to obtain material purity near the level required to produce a semiconductor-grade product. The liner-seal design has been consistently proven to withstand heating-cooling cycles in all of the JPL experimental runs. A summary of the JPL silane fluidized-bed program is being written.

The California Institute of Technology (Caltech) presented a more complete analysis of the phenomenon of runaway nucleation in a silane-free space reactor system which occurred in its program to describe, theoretically, the growth of silicon particles and to develop, experimentally, the conditions for particle growth. The experimental conditions with a silane concentration increment leading to the condition and the theoretical treatment of the phenomenon were described.

JPL presented a thermal analysis model to describe the dendritic ribbon process. The model uses a melt-dendrite interface which projects out of the bulk melt as the basic interpretation of the ribbon production process. This is a marked departure from the interpretations of the interface phenomena which have been used previously. The model was extensively illustrated with diagrams and pictures of ribbon samples. This model would have great impact on the analyses of experimental data as well as on future design modifications of ribbon-pulling equipment.

JPL also presented simplified models of the residual stress in dendritic ribbons and of the associated ribbon properties.

SILANE PROCESS RESEARCH AND DEVELOPMENT

UNION CARBIDE CORP.

S. Iya

FSA Project

<u>TECHNOLOGY</u> POLYCRYSTALLINE SILICON R&D	<u>REPORT DATE</u> JUNE 20, 1985
<u>APPROACH</u> SILANE DECOMPOSITION IN A FLUIDIZED BED REACTOR <u>CONTRACTOR</u> UNION CARBIDE CORPORATION	<u>STATUS</u> <ul style="list-style-type: none"> • LONG DURATION TEST RUNS WERE CONDUCTED USING A QUARTZ LINER • GAS DISTRIBUTOR WAS MODIFIED AND TESTED • FBR PRODUCT WAS MELTED AND SINGLE CRYSTALLIZED • PRODUCT PURITY IMPROVEMENTS WERE NOTED
<u>GOALS</u> <ul style="list-style-type: none"> • DEMONSTRATE PROCESS FEASIBILITY • DETERMINE OPERATING WINDOW • CONDUCT LONG-DURATION TESTS • DEMONSTRATE SILICON PURITY 	

Summary of Activities

- PDU LINER SUPPORT SYSTEM DESIGN WAS MODIFIED
- SEED BED WAS PREPARED BY GRINDING, SCREENING AND ACID WASHING UCC POLYSILICON NUGGETS
- SEVERAL LONG DURATION TEST RUNS WERE CONDUCTED
- PERFORATED PLATE TYPE GAS DISTRIBUTOR WAS INSTALLED AND TESTED
- FBR SEED AND PRODUCT SAMPLES WERE ANALYZED BY SPARK SOURCE MASS SPECTROMETRY
- FBR PRODUCT SAMPLE WAS SINGLE CRYSTALLIZED AND EVALUATED FOR PURITY

Overview of Recent FBR Test Runs

RUN NO.	DURATION, HOURS	SILANE CONCENTRATION RANGE	GAS DISTRIBUTOR	COMMENTS
H-01	31	20-30%	CONICAL POROUS METAL	
H-02	45	25-30%	"	12 KG. PRODUCT FOR CRYSTAL GROWTH
H-04	34	25-30%	"	25 KG. PRODUCT TO JPL
H-05	39	40-60%	PERFORATED PLATE	REDUCED POWDER FORMATION

FBR Test Run H-02 Run Summary

- QUARTZ LINER
- 45 HOURS RUN DURATION
- 280 μ M SEED GROWN TO 500 μ M PRODUCT
- SILANE FEED CONCENTRATION 25-30%
- AVERAGE DEPOSITION RATE 1.2 KG/HR
- BED TEMPERATURE 600-750°C
- U/U_{MF} 3.5-4.0
- COMPLETE SILANE CONVERSION WITHIN THE BED
- POWDER COLLECTED IN FILTERS 3.6%
- 12 KG. PRODUCT FOR CRYSTAL GROWTH
- POWER CONSUMPTION 25 KWH/KG.

SILICON MATERIAL AND JPL WEB TEAM

FBR Test Run H-02 Mass Balance

INITIAL BED WEIGHT	=	20.2 KG.
SILICON IN	=	53.5 KG.
		<hr/>
TOTAL	=	73.7 KG.

PRODUCT WITHDRAWN	=	69.2 KG.
POWDER IN FILTERS	=	1.9 KG.
		<hr/>
TOTAL	=	71.1 KG.

ERROR IN MASS BALANCE = 3.5%

Spark Source Mass Spec Data for Heavy Metals

ELEMENT	RUN H-02		RUN H-04	
	SEED PPMA	PRODUCT PPMA	SEED PPMA	PRODUCT PPMA
FE	3	1	≤ 0.5	< 0.5
AL	10	2	1	0.5
CR	0.05	0.03	0.03	0.03
MN	0.3	0.1	0.03	≤ 0.02
NI	< 0.5	< 0.5	< 0.5	< 0.5
CU	≤ 0.02	≤ 0.02	≤ 0.02	≤ 0.02

SILICON MATERIAL AND JPL WEB TEAM

Czochralski Crystal Growth Runs

- HAMCO CG-3000 CRYSTAL GROWER
- 12 KG. SILICON CHARGE
- INTRINSIC SILICON CRYSTAL GROWTH

RUN 1

MARCH 26-27, 1985
 FBR RUN H-02 SEED
 CONTINUOUS OXIDE SLAG
 3" DIA. 30" LONG-POLY INGOT

RUN 2

MARCH 28-29, 1985
 FBR RUN H-02 PRODUCT
 INITIAL OXIDE SLAG
 3" DIA. 21" LONG-DISLOCATION-FREE CRYSTAL
 7" LONG-SINGLE
 4" LONG-POLY

FTIR Analysis of Single Crystal Wafers
 from FBR Run H-02

	<u>TOP END</u>	<u>BOTTOM END</u>
PHOSPHORUS, PPBA	4.2	8.5
BORON, PPBA	8.5	10.0
ARSENIC, PPBA	0.1	0.28
ALUMINIUM, PPBA	1.2	4.6
ANTIMONY, PPBA	< 0.02	0.07
CARBON, PPMA	4.99	22.0
OXYGEN, PPMA	14.0	18.0
CALCULATED RESISTIVITY, OHM-CM	50	40
	P TYPE	P TYPE
MEASURED RESISTIVITY, OHM-CM (AVERAGE OF 10 POINTS)	87	87.6
	P TYPE	P TYPE

SILICON MATERIAL AND JPL WEB TEAM

Future Plans

- IMPROVED SEED MATERIAL PREPARATION
- LONG DURATION TEST RUNS TO ESTABLISH PRODUCT PURITY
- TECHNICAL AND ECONOMIC ASSESSMENT

SILICON MATERIAL AND JPL WEB TEAM

Polysilicon Plant No. 1: Washougal R&D Center

- POLYSILICON & SILANE RESEARCH & DEVELOPMENT
- POLYSILICON & SILANE QUALITY CONTROL & QUALITY ASSURANCE
- POLYSILICON CUSTOMER SERVICE

Polysilicon Plant No. 2: Moses Lake Production Status

- POLYSILICON SHIPMENTS BEGAN APRIL, 1985
- 90% OF PLANT REACTOR CAPACITY IS CURRENTLY ON STREAM
- 1000 MT/YEAR PRODUCTION RATE BY END OF 1985
- 1200 MT/YEAR EXPECTED IN 1986

Polysilicon Plant No. 2-E: Future Moses Lake Polysilicon Capacity

- ADDITIONAL 1200 T POLYSILICON CAPACITY IS UNDER CONSTRUCTION
- PLANT EXPANSION IS SCHEDULED FOR COMPLETION IN 1987
- MOSES LAKE OVERALL CAPACITY WILL BE 3000 MT/YEAR SILANE OR 2400 MT/YEAR POLYSILICON

Polysilicon Plant No. 3: Future Polysilicon Capacity

- 1985 - PLANT DESIGN & ENGINEERING
- 1986 - START OF CONSTRUCTION
- LATE 1988 - 4000 MT/YEAR SILANE OR 3000 MT/YEAR POLYSILICON PLANT OPERATIONAL

JPL IN-HOUSE FLUIDIZED-BED REACTOR RESEARCH

JET PROPULSION LABORATORY

N. K. Rohatgi

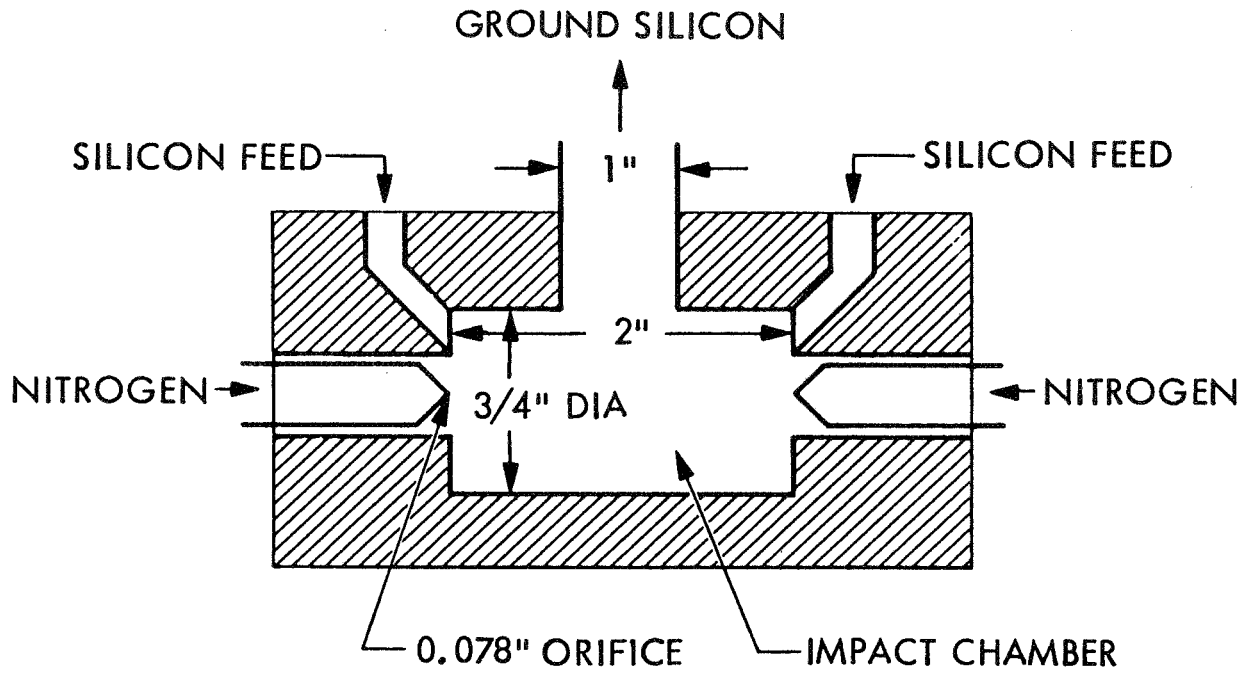
Objectives

- ESTABLISH ANALYTICAL TECHNIQUES TO VERIFY METALLIC IMPURITIES IN SILICON
- OBTAIN CLEAN SILICON SEED PARTICLES
- CONDUCT PURITY EXPERIMENTS
- DRAW SINGLE CRYSTAL Cz INGOT USING SILICON PARTICLES GROWN IN THE FLUIDIZED BED REACTOR.

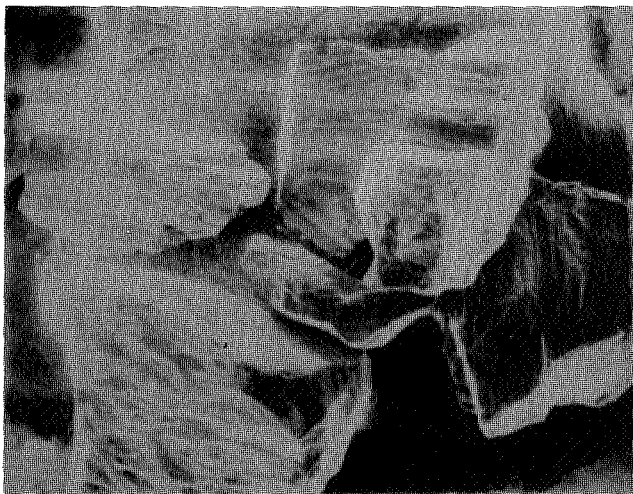
Silicon Seed Particles

- SILICON PARTICLES OF LESS THAN 2 MM SIZE WERE PURCHASED FROM DYNAMIT NOBEL. THESE PARTICLES WERE PREPARED BY MECHANICAL BREAKING OF SILICON ROD PRODUCED BY THE SIEMENS PROCESS.
- THE SIZE OF THESE PARTICLES WAS FURTHER REDUCED TO 200 TO 300 μm DIAMETER BY THE FLUID JET MILL.
- PARTICLES WERE ACID CLEANED AND DRIED UNDER NITROGEN BLANKET BEFORE FED INTO THE FLUIDIZED BED REACTOR.

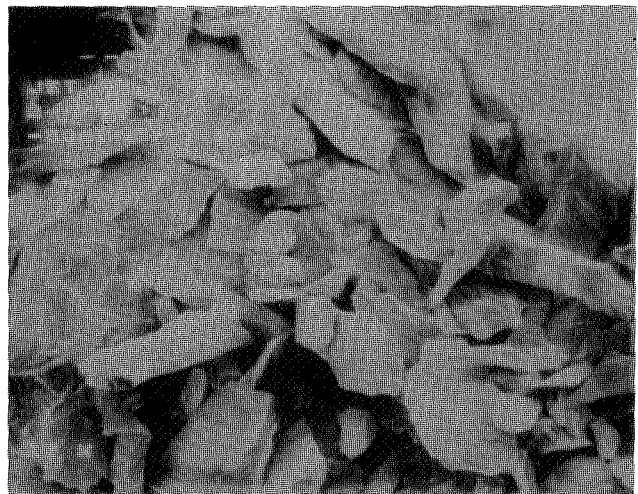
Jet Milling Device for Seed Particle Generation



Silicon Seed Particles from Jet Mill



FEED, 20x



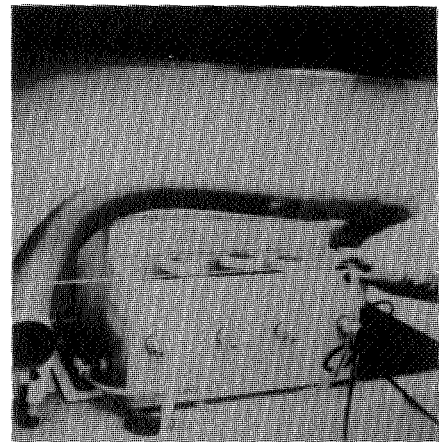
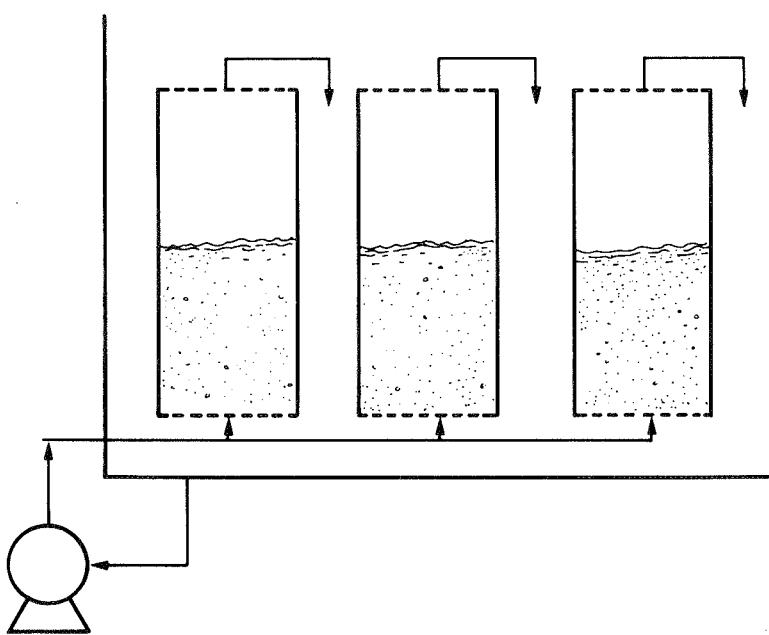
PRODUCT, 20x

NITROGEN FLOW RATE : 20 SCFM
SILICON FEED RATE : 40 gram/min

Silicon Cleaning Procedure

- DEIONIZED WATER WASH TO REMOVE FINE SILICON PARTICLES
- CLEANING IN THE MIXTURE OF TWO PARTS OF 12N HCl AND ONE PART OF 16N HNO₃ FOR 20 MINUTES.
- WASHING WITH DEIONIZED WATER UNTIL EFFLUENT WATER IS NEUTRAL.
- ETCHING WITH 48% HF FOR 20 MINUTES
- WASHING WITH DEIONIZED WATER UNTIL EFFLUENT WATER IS NEUTRAL AND HAS A RESISTIVITY OF 16 MEGAOHMS.
- DRYING IN DIFFUSION FURNACE AT 150°C UNDER NITROGEN BLANKET

Fluidized Bed Cleaning of Silicon Seed Particles



SILICON MATERIAL AND JPL WEB TEAM

Purity Experiment

- SEED PARTICLES WERE PREPARED VIA JET MILL GRINDING OF LESS THAN 2 MM SIZE SILICON PARTICLES PURCHASED FROM THE DYNAMITE NOBEL.
- PARTICLES WERE WASHED AND CLEANED VIA FLUIDIZED BED CLEANING SYSTEM.
- EXPERIMENTAL CONDITIONS
 - AVG. INITIAL SEED PARTICLE SIZE: 250 μM
 - INITIAL BED WEIGHT: 11 Kg (= 24" BED HEIGHT)
 - $U/U_{MF} = 4$
 - SILANE CONCENTRATION: 30% (IN H_2)
 - BED TEMPERATURE: 650°C
 - DURATION OF RUN: 4.30 HRS.

Results

- MASS BALANCE
 - TOTAL SILICON FED: 7.3 Kg
 - SILICON DEPOSITED ON PARTICLES: 6.8 Kg (93.1%)
 - SILICON RECOVERED AS FINES: 0.4 Kg (5.5%)
- PRODUCTION RATE: 1.5 Kg/HR.
- PARTICLE GROWTH: $\approx 10 \mu\text{M}$ (RADIUS).

Purity of Silicon (PPma)*

ELEMENTS	RAW PARTICLES "AS PURCHASED"	JET MILLED AND ACID CLEANED "SEED FOR FBR"	FBR PRODUCT
P	0.2	0.2	0.1
FE	20	≤0.6	≤0.6
CR	0.05	0.03	<0.02
NI	10	<0.5	<0.5
CU	0.06	≤0.02	<0.02
ZN	<0.02	≤0.04	<0.04
CO	≤0.1	≤0.1	≤0.1
MN	0.5	≤0.02	<0.02
NA	≤0.1	≤0.1	≤0.1
MG	≤1	<1	<1
AL	2	0.05	0.05
S	<1	<1	<1
K	≤0.07	<0.1	<0.1
CA	0.6	0.1	0.1

* SPARK SOURCE MASS SPECTROSCOPY

Work in Progress

- DRAW SINGLE CRYSTAL Cz INGOT USING SILICON PARTICLES GROWN IN THE FLUIDIZED BED REACTOR.
- DETERMINE METALLIC IMPURITIES IN INGOT AND SILICON LEFT IN THE CRUCIBLE.
- FABRICATION OF SOLAR CELLS
- CHARACTERIZATION OF SOLAR CELLS

WEB TEAM OVERVIEW

JET PROPULSION LABORATORY

R. R. McDonald

Background

- Major factor in DOE'S PV Plan is low cost Si sheet
- Leading contender is dendritic web
- Requirement for DOE goals is sustained growth of 20 to 30 cm²/m
- Major problems are thermal stresses and instability at the growth interface
- Progress in solving these problems has been slow
- FSA Project suggested in-house development effort to help solve technical problems
- DOE approved suggestion
- Accordingly, Web Team was formed within the FSA Project

Objective

- To conduct an in-house development activity which will increase the likelihood that web technology will help achieve the DOE goals

PRECEDING PAGE BLANK NOT FILMED

Approach

- **Team effort consists of combination of analytical and experimental work**
- **Operate a Westinghouse web growth system**
- **Measure high temperature properties of silicon**
- **Use stress model to determine a temperature profile which will yield satisfactory web**
- **Use thermal model of web to determine a thermal configuration which will yield the desired temperature profile**
- **Use thermal analysis of growth interface and the susceptor—crucible—melt to determine a thermal configuration which will improve stability of growth process**
- **Design, fabricate and test the thermal configurations and feed results back into the models**

SILICON DENDRITIC WEB GROWTH THERMAL ANALYSIS TASK

JET PROPULSION LABORATORY

R. Richter
P. Bhandari

Objectives

- o ESTABLISH THE PERTINENT THERMAL ASPECTS OF SILICON DENDRITIC WEB GROWTH
- o EVALUATE THE PRESENT SILICON DENDRITIC WEB GROWTH SYSTEM
- o PROVIDE THERMAL DESIGN INPUTS FOR THE SILICON WEB GROWTH STRESS MINIMIZATION TASK
- o GENERATE THERMAL DESIGN GUIDES FOR AN ADVANCED SILICON WEB GROWTH SYSTEM

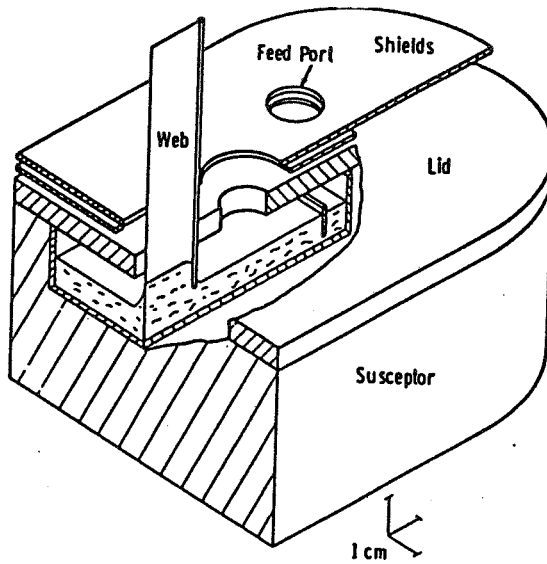
Silicon Dendritic Web Growth

- o BASIC CONCEPTS : DESIGN AND OPERATING PARAMETERS
- o THERMAL MODELING OF SUSCEPTOR - CRUCIBLE - SILICON SYSTEM
- o SOURCE OF THERMAL CONVECTION CURRENTS AND THEIR SUPPRESSION
- o THERMAL ANALYSIS OF SILICON DENDRITIC WEB GROWTH SYSTEM
- o THERMAL STACK : ANALYSIS AND DESIGN
- o COLD SHOE : ANALYSIS AND DESIGN

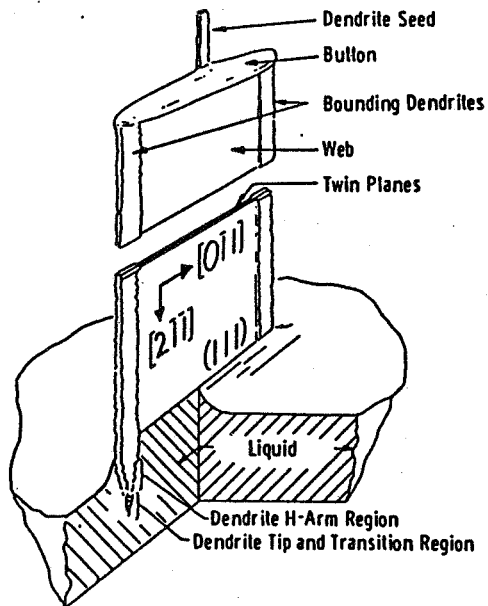
Basic Concepts:

Design and Operating Parameters

Growth Procedure (Westinghouse Concepts)

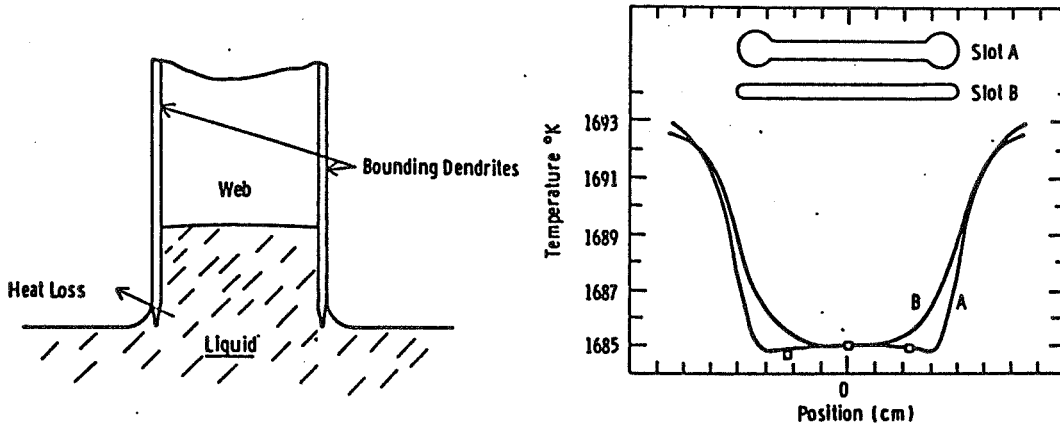


HOT ZONE - SECTIONAL VIEW (REFERENCE 1)



SILICON WEB GROWTH (REFERENCE 1)

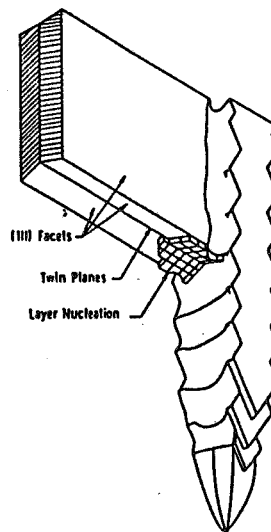
Thermal Factors
(Westinghouse Concepts)



TEMPERATURE PROFILE AS A FUNCTION OF SLOT GEOMETRY (REFERENCE 1)

- CONDITION FOR GROWTH: FLAT TEMPERATURE PROFILE UNDER THE GROWTH INTERFACE AND POSITIVE TEMPERATURE GRADIENT IN REGIONS AWAY FROM THE GROWTH INTERFACE.

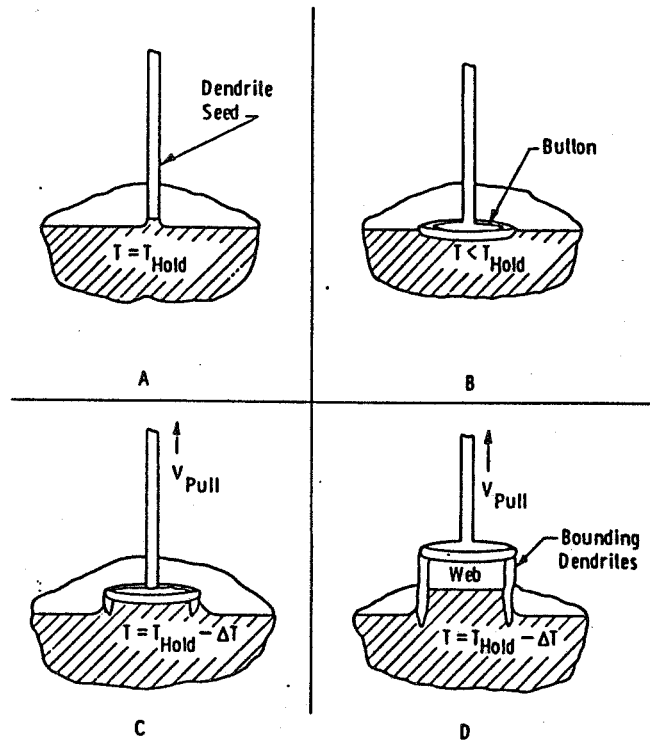
Growth Procedure



GROWTH FRONT (INTERFACE)

- STABILITY OF LIQUID-SOLID INTERFACE IS KEY TO STABLE GROWTH (REFERENCE 1)

Web Growth Initiation (Westinghouse Concepts)

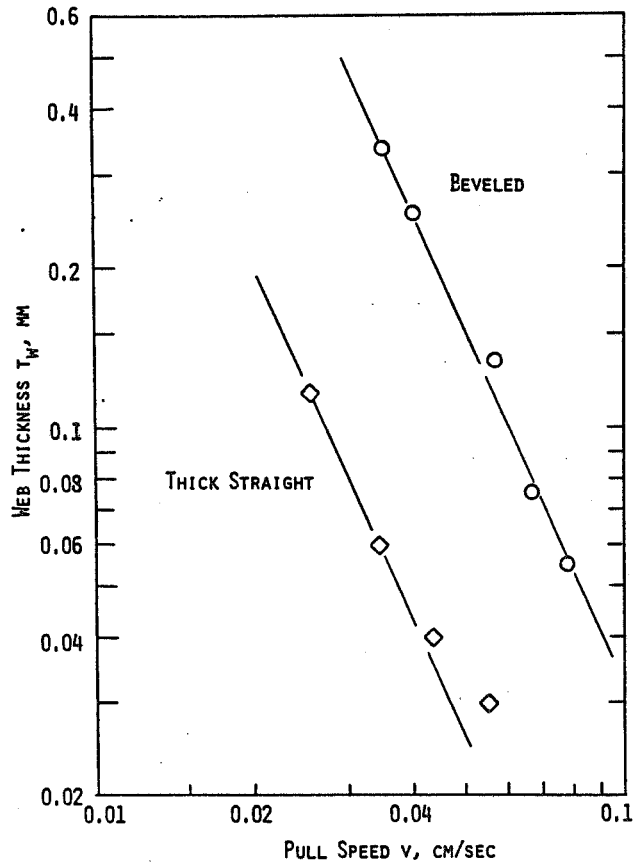
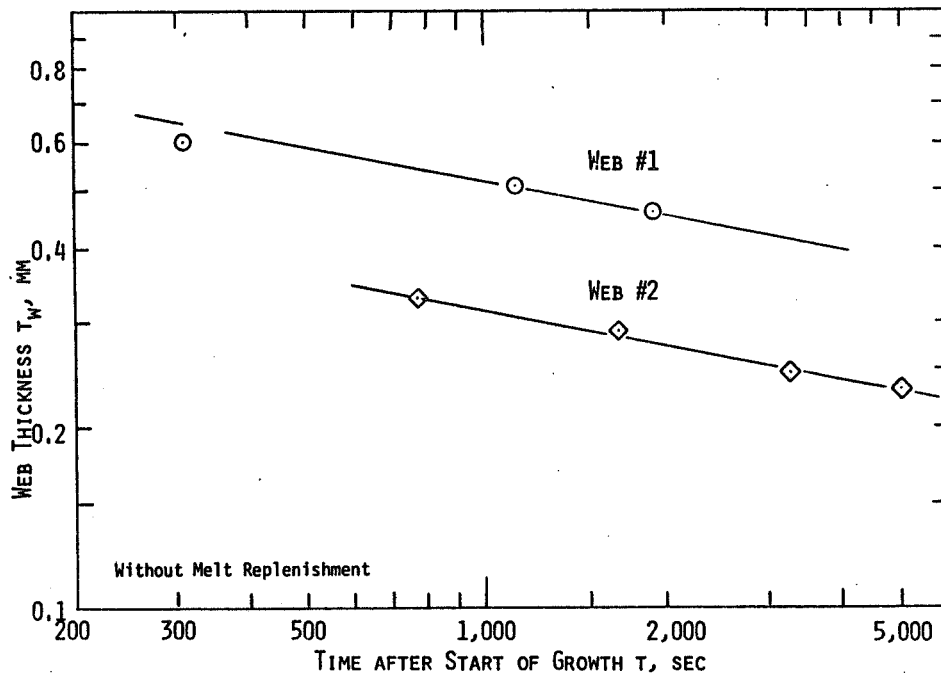


SEEDING AND WEB PULLING (REFERENCE 1)

System Configured for:

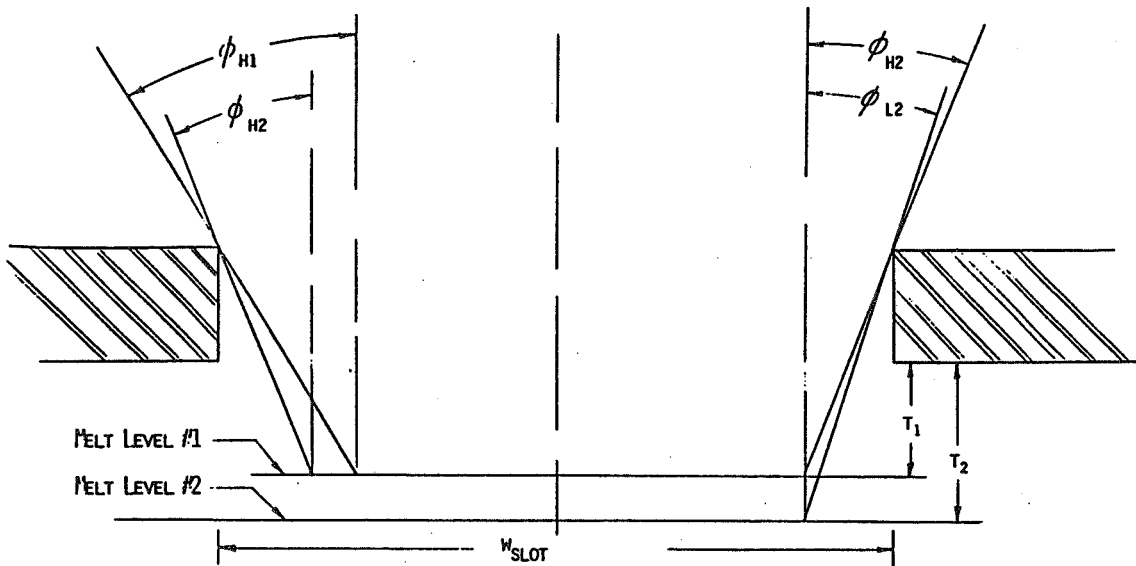
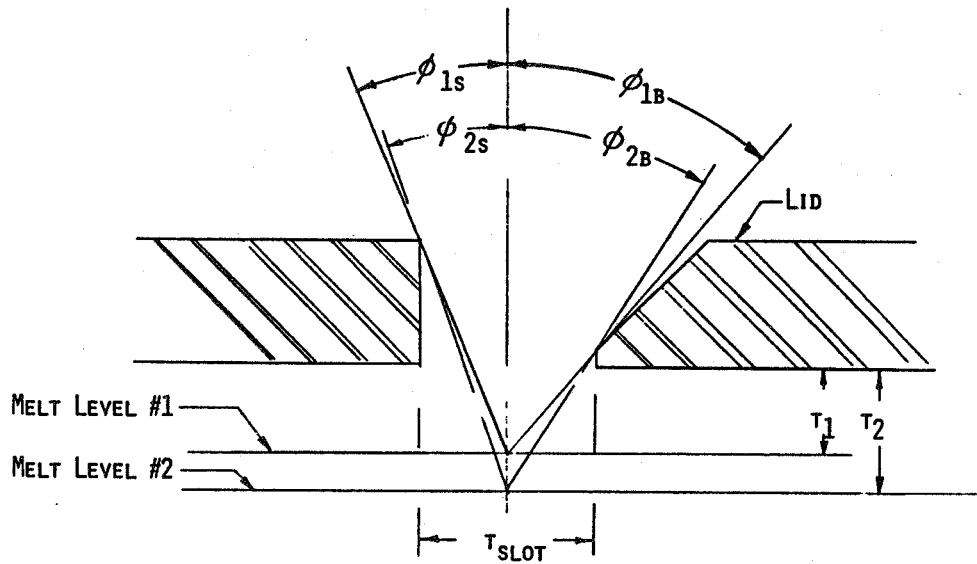
- o GROWTH OF A BUTTON
- o GROWTH OF DENDRITIC WEB
- o CONTROLLED COOLING OF DENDRITIC WEB

Web Growth Correlations
(Derived from Data of Reference 2)

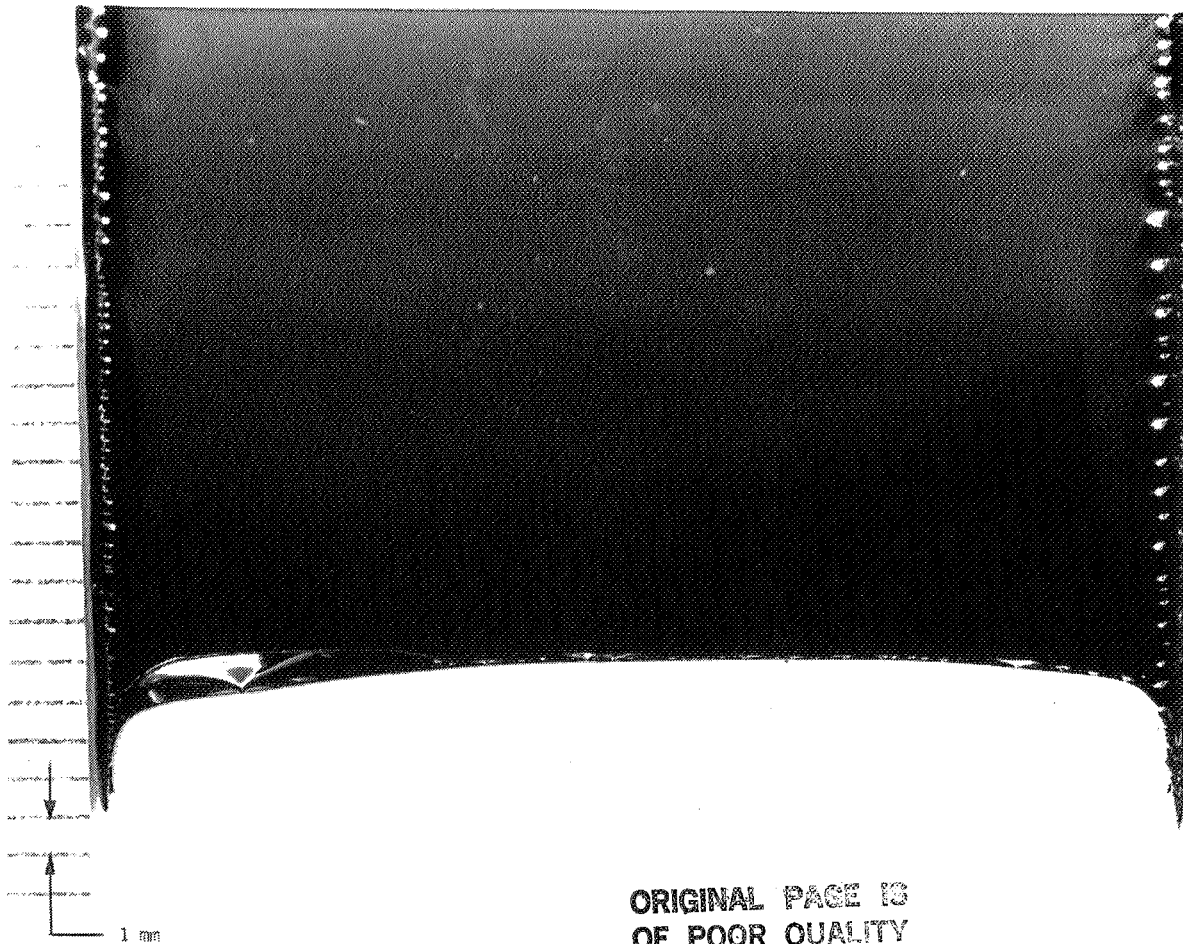


Parameters Affecting Web Growth Rate

- o MELT TEMPERATURE
- o VIEW FACTOR (COOLING RATE)
 1. MELT-LID GAP
 2. SLOT WIDTH
 3. SLOT CONFIGURATION
- o PULL SPEED

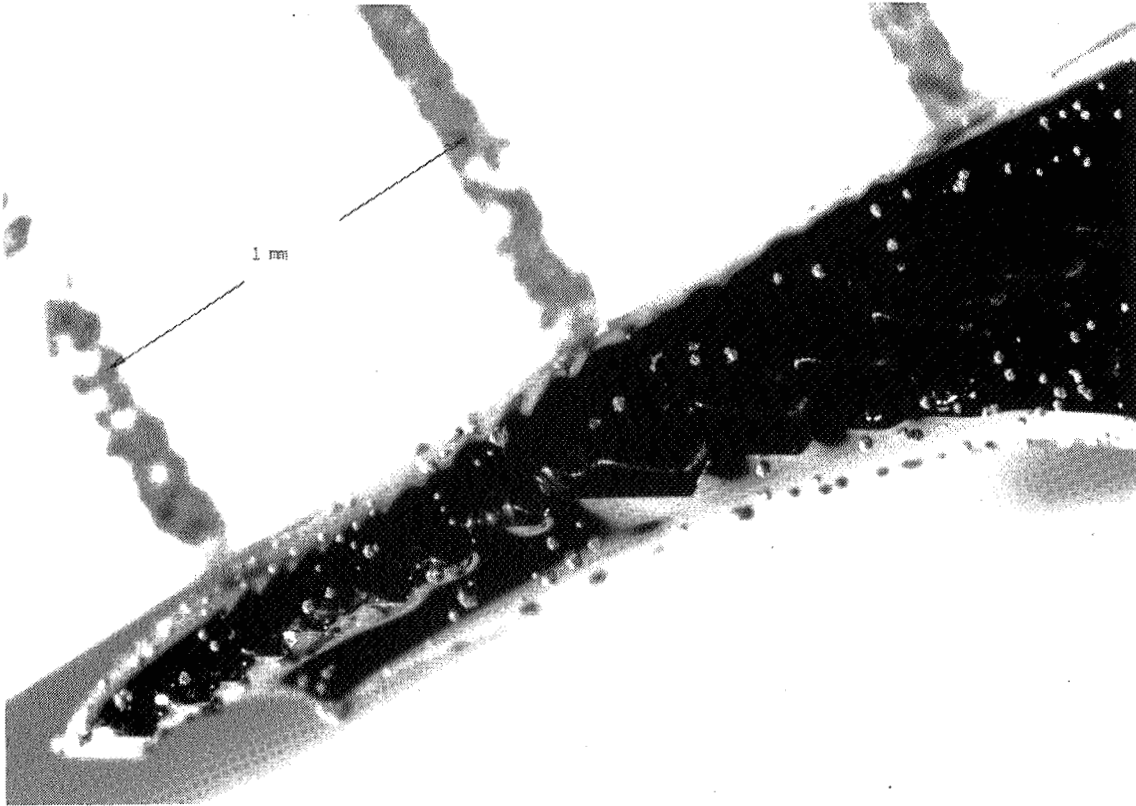


Tail of Silicon Web After Hot Pullout

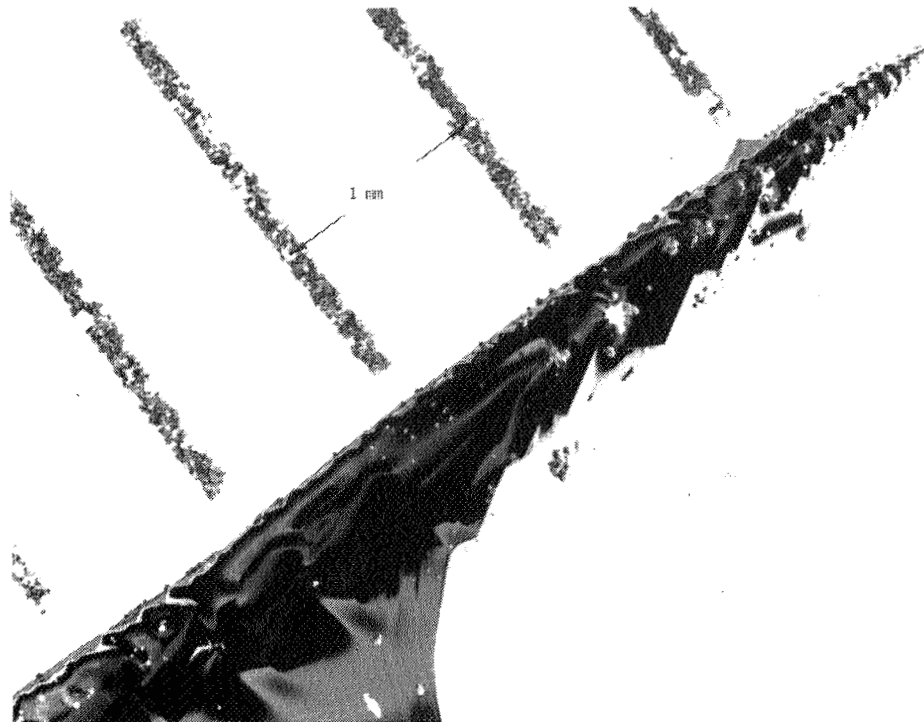


Left Side of Silicon Web

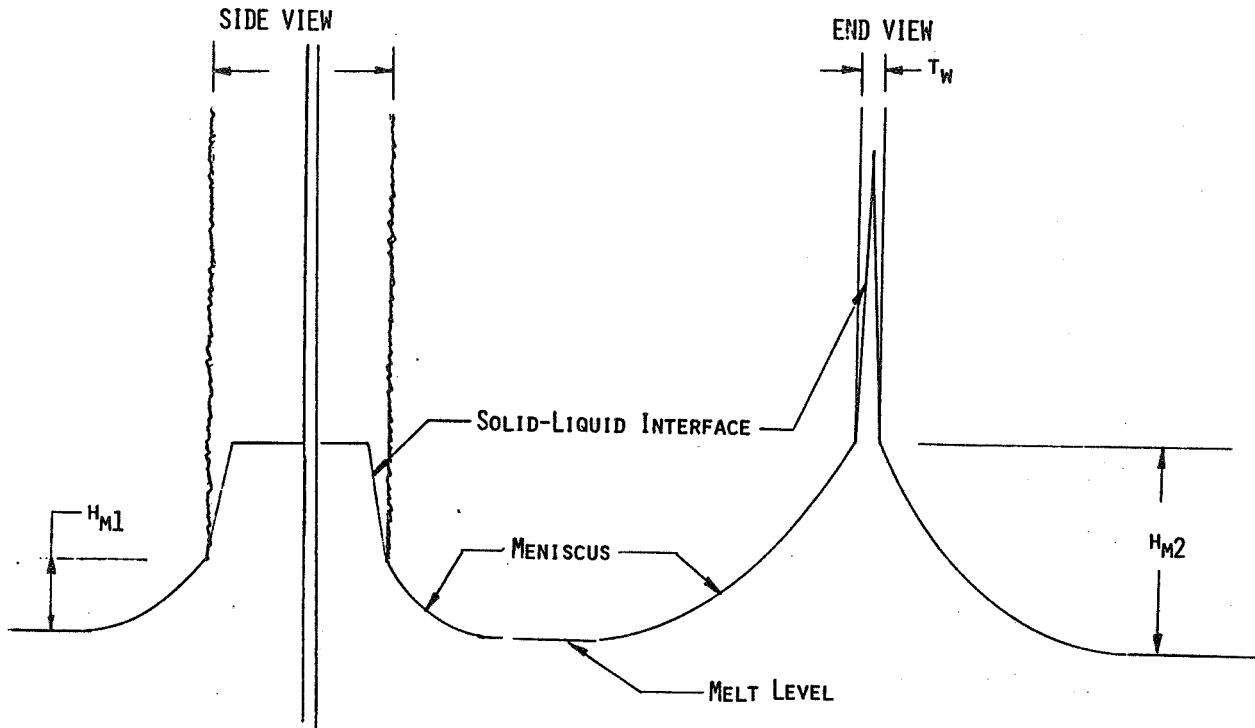
ORIGINAL PAGE IS
OF POOR QUALITY



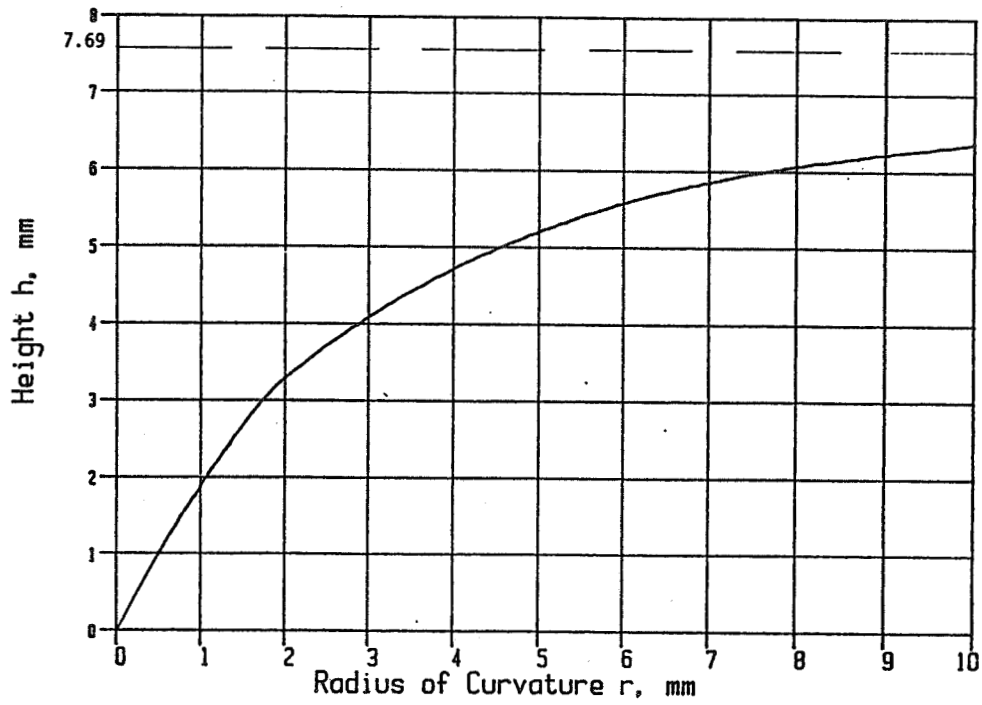
Right Side of Web



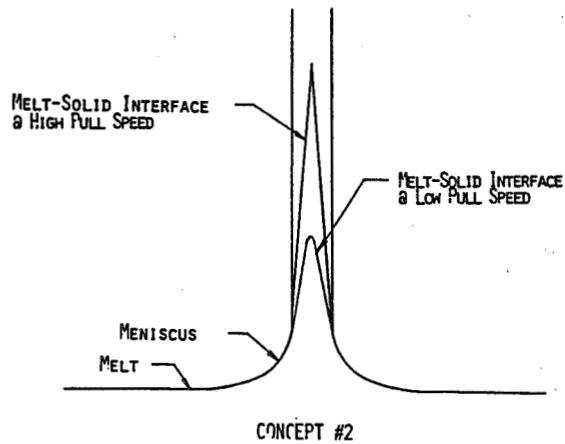
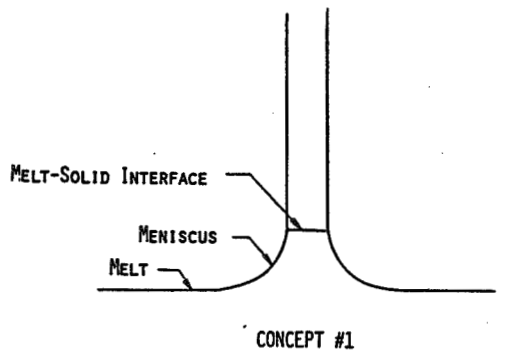
Apparent Configuration During Growth



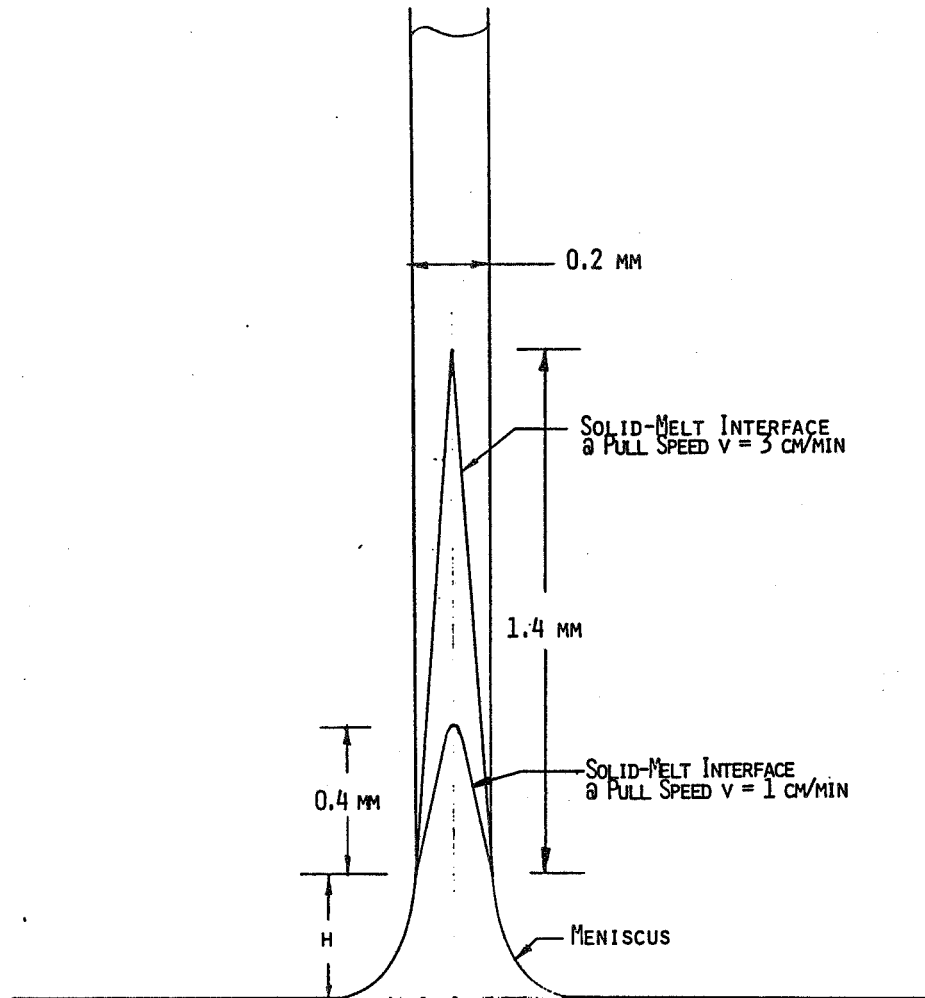
Meniscus Height at Zero Degree



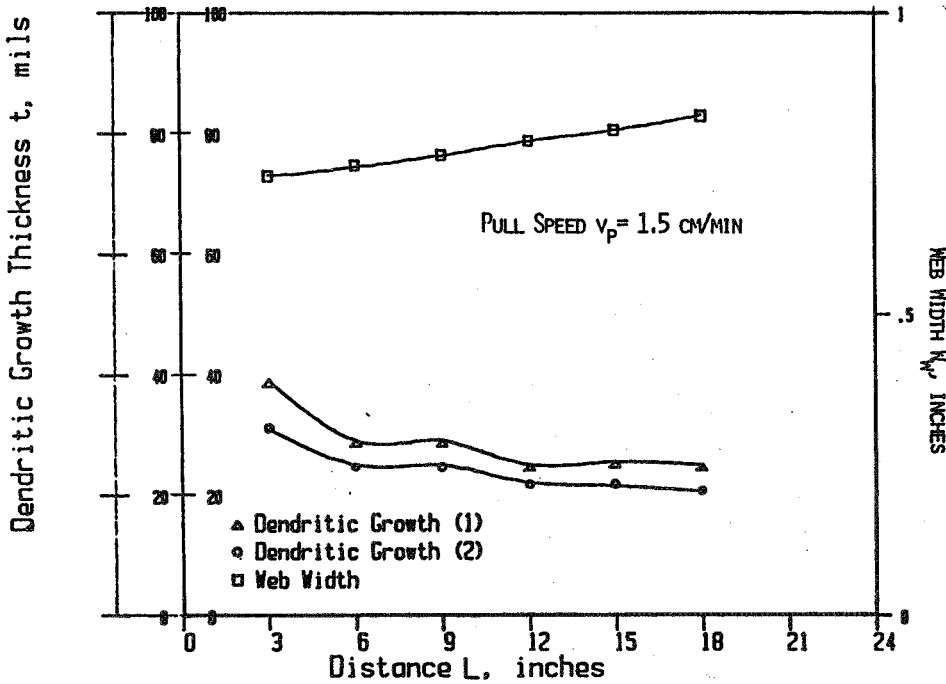
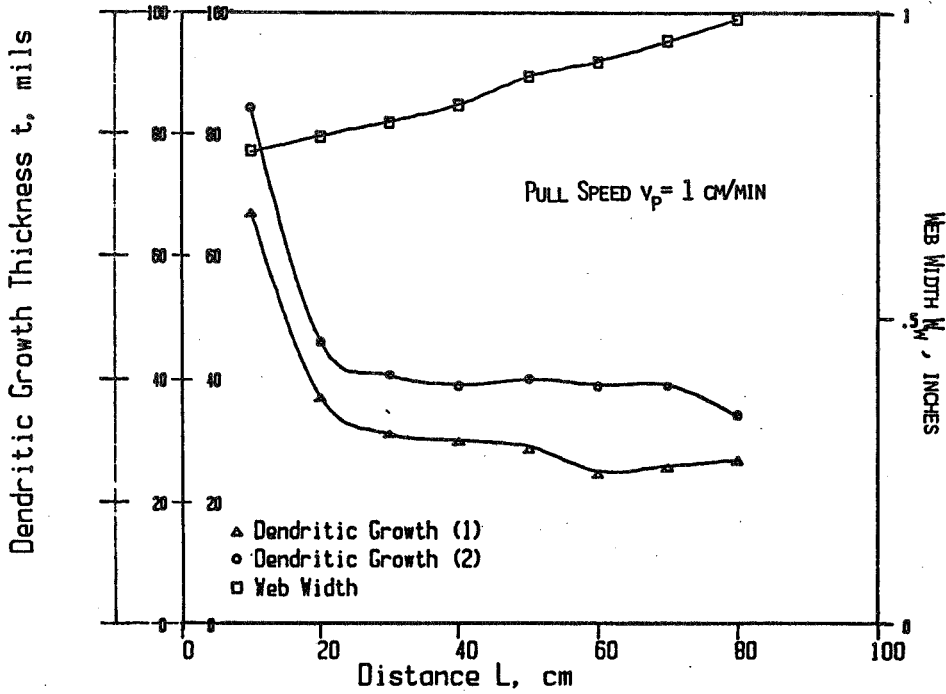
Melt-Solid Interface



Melt-Solid Interface

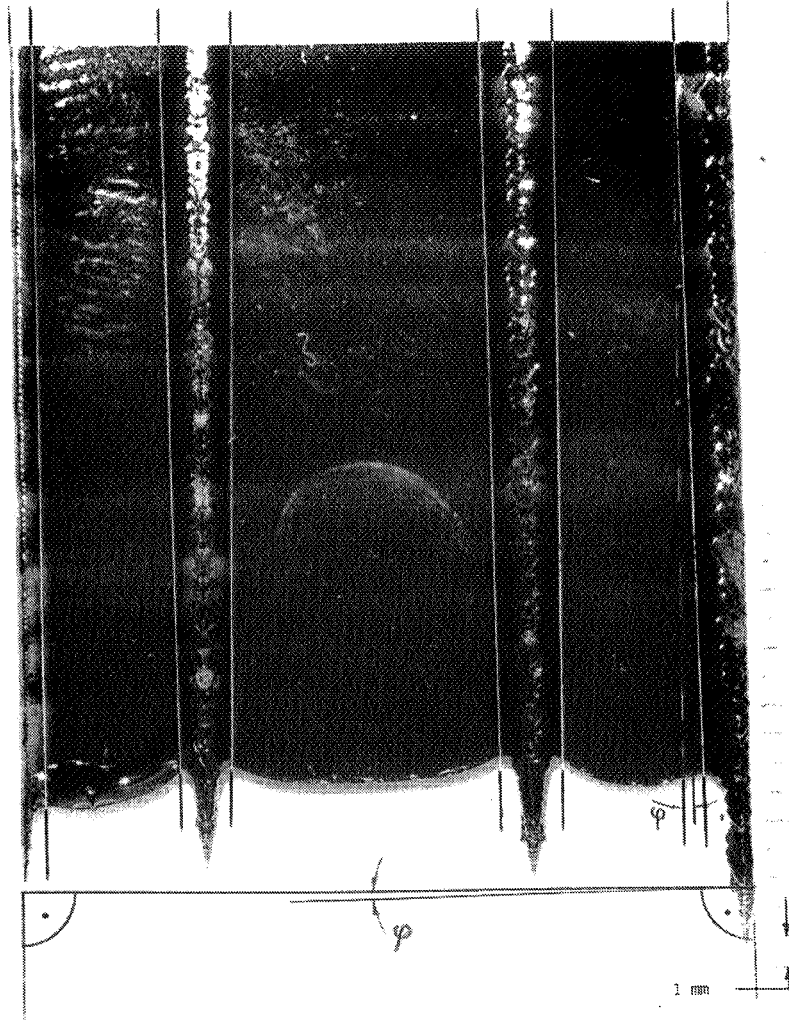


Web Width and Dendritic Growth (Westinghouse Lid)



Web Growth Phenomena

ORIGINAL PAGE IS
OF POOR QUALITY



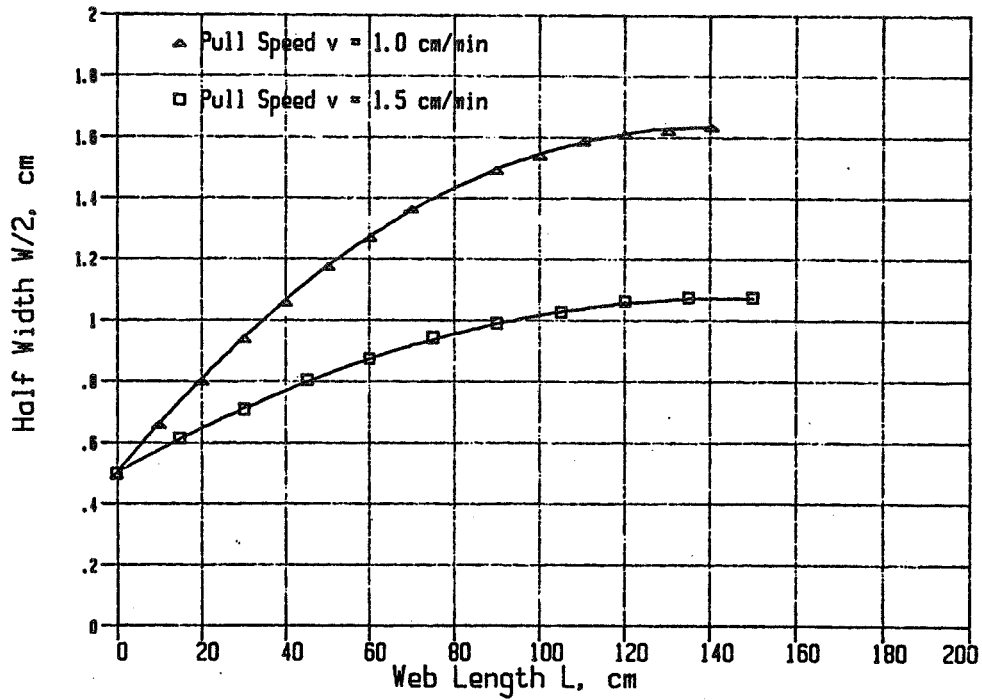
Web Growth Relationship

$$\left\{ \left(\frac{DX}{DL} \right)^2 + R^2 \right\}^{1/2} v = \left[z F(x) \epsilon \sigma T_m^4 - k \gamma \Delta T / H_m \right] / \left[\rho (\Delta H + c_p \Delta T) \right]$$

$$\left\{ \left(\frac{DX}{DT} \right)^2 + (vR)^2 \right\}^{1/2} =$$

$$\Delta T = T - T_m$$

Predicted Silicon Web Growth (Westinghouse Lid Configuration)

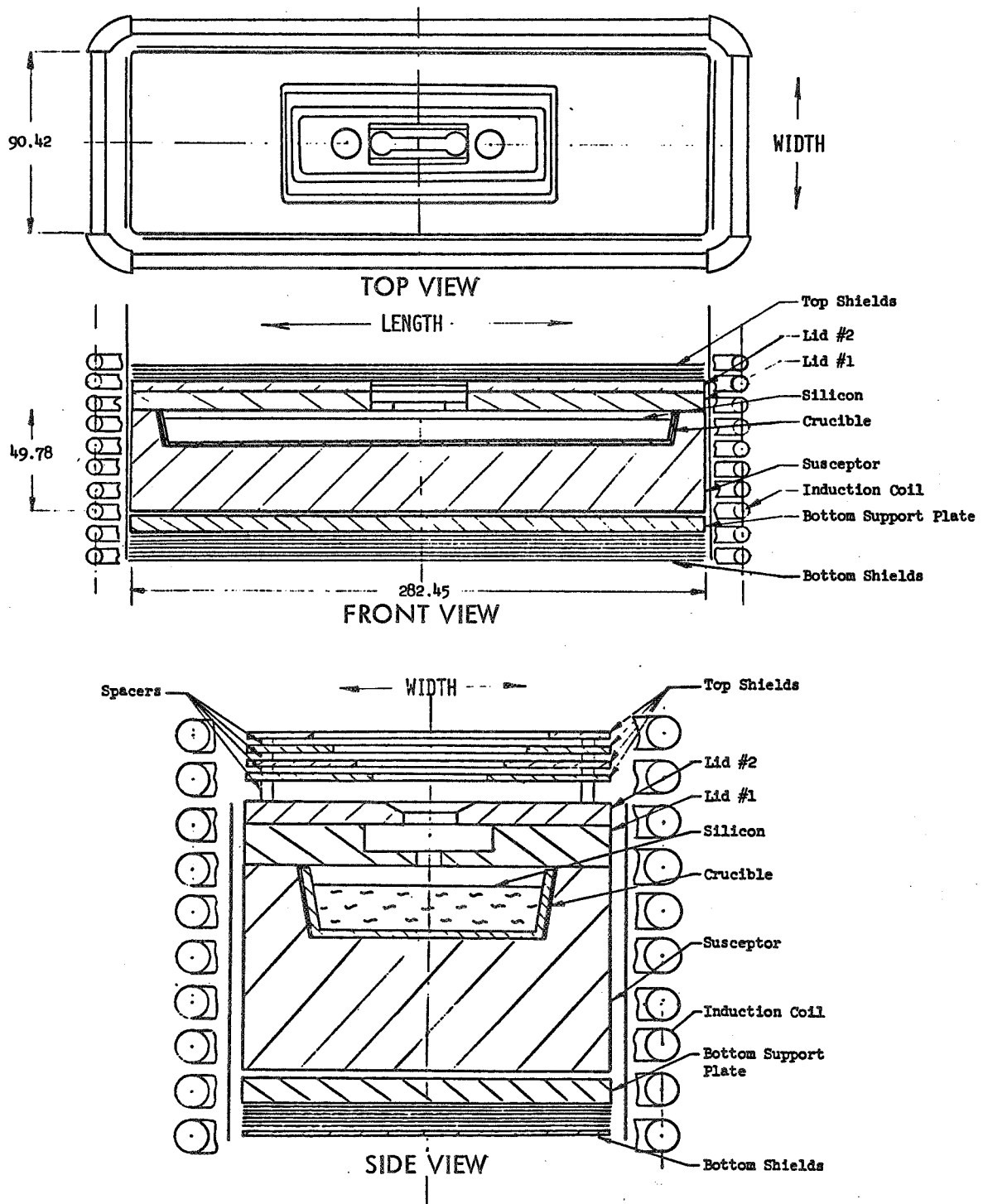


Growth Parameters

- o PULL SPEED
- o VIEW FACTOR
 - A. MELT LEVEL
 - B. WEB POSITION
- o MELT TEMPERATURE
 - A. MELT STABILITY
 - B. TEMPERATURE CONTROL

Thermal Modeling
of
Susceptor/Crucible/Silicon System

Silicon Web Growth System
(As Delivered by Westinghouse)



SILICON MATERIAL AND JPL WEB TEAM

Material Properties

SILICON
@ Melting Temperature

Heat of Fusion 1.80x10⁶ J/kg (11)
Melting Temperature 1685 +2K (1)

	<u>Solid</u>	<u>Liquid</u>
Density	2288 kg/m ³ (1)	2540 Kg/m ³ (1)
Specific Heat	1036 J/kg-K (1)	1008 J/kg-K (1)
Thermal Conductivity	23.0 W/m-K (1)	67 W/m-K (1) 14 W/m-K (estimated)
Kinematic Viscosity		36.36X10 ⁻⁸ m ² /s (1)
Surface Tension		0.736 N/m (1)
Volume Expansivity		1.49X10 ⁻⁴ 1/K (1)
Emissivity	0.46 (2,12)	0.64 (3)

MOLYBDENUM
@ 1700K

Density (@ 20°C) 10300 kg/m³ (13)
Specific Heat 335 J/kg-K (8)
Thermal Conductivity 97 W/m-K (5)
Coefficient of Expansion (linear) 5.4X10⁻⁶ 1/K (13)
(@ 20°C)
Emissivity (polished surfaces, non-oxidized) 0.2 (9)
Emissivity(machined surfaces, oxidized) 0.8 (9)

ARGON

Thermal Conductivity 1700K 0.0615 W/m-K (7)
1200K 0.0481 W/m-K
700K 0.0336 W/m-K

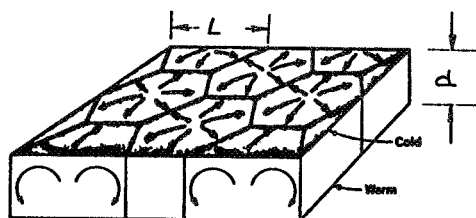
$$k = 3.87259 \times 10^{-4} T^{0.68129} \text{ W/m-K}$$

FUSED QUARTZ
@ 1700K

Density 2.2 grams/cm³ (4)
Specific Heat 0.7535 J/gram-K (4)
Thermal Conductivity 2.0 W/m-K (6)
Coefficient of Expansion (linear) 5.6X10⁻⁷ 1/K (4)
Total Transmission (2 mm thickness) 0.68 (10)
Softening Point (approximately) 1938 K (4)

**Source of Thermal Convection Currents and
Suppression of Thermal Instabilities**

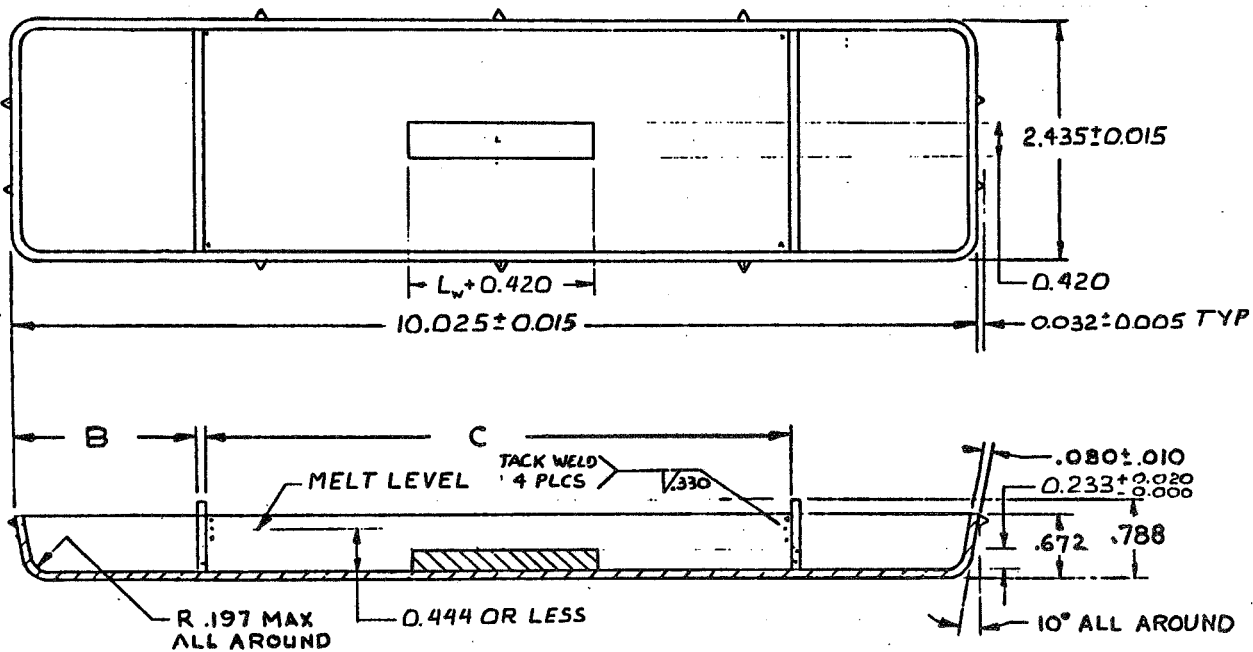
Thermal Convection in Silicon Melt



BENARD CELL STRUCTURE

$$d_{cr} = [C_{cr} / (\rho g \beta / R \alpha \nu)]^{1/4}$$

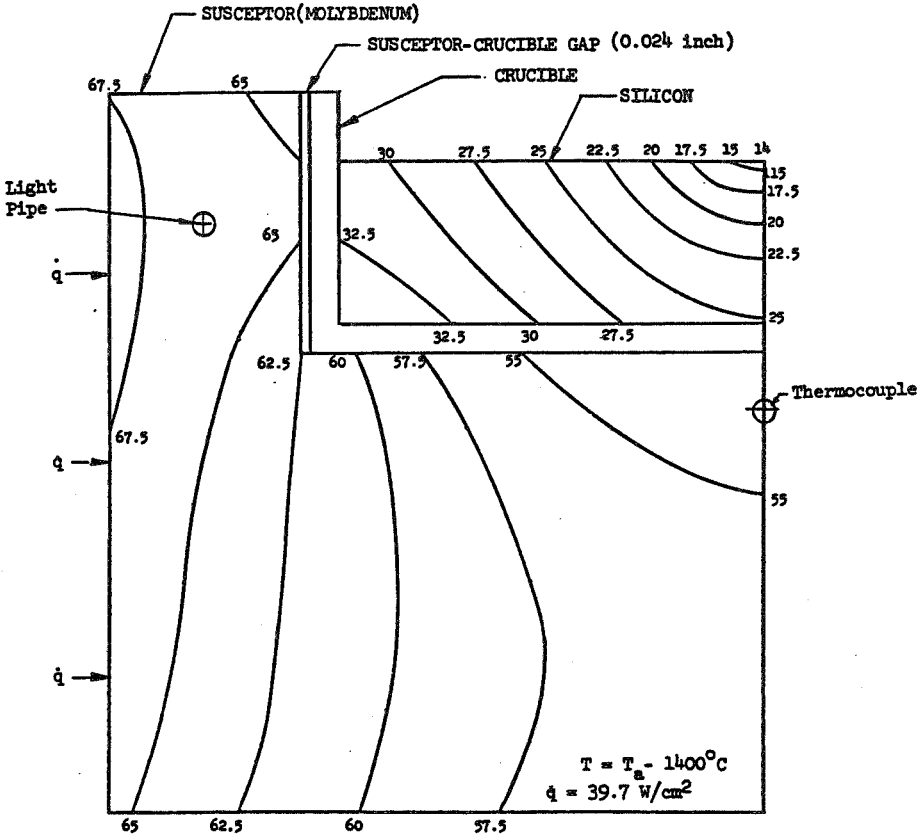
Suggested Crucible Design



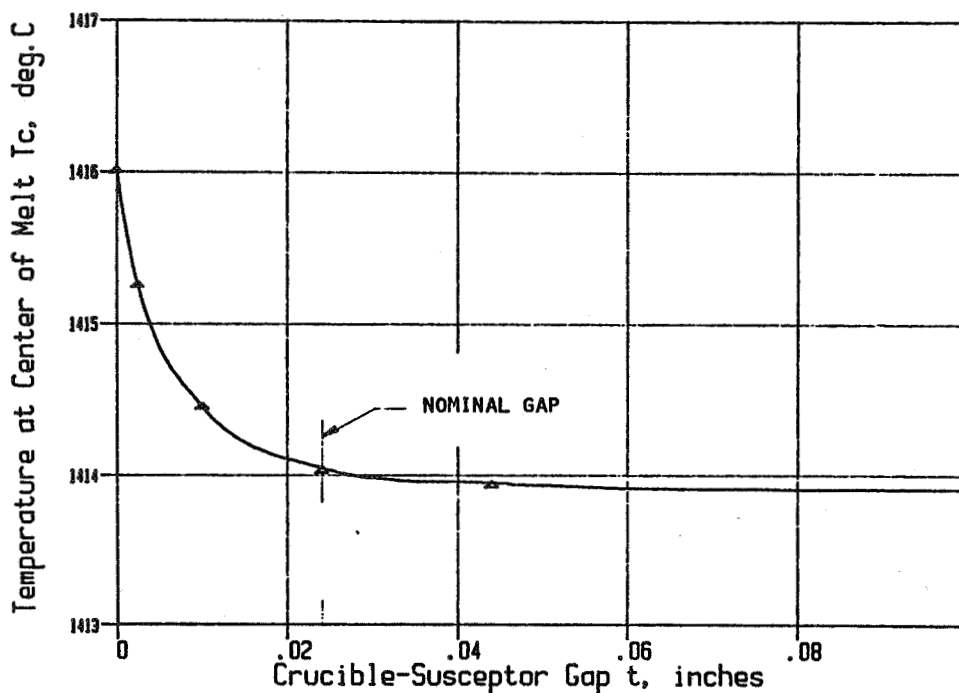
REFERENCE: DRAWING 390 DR08

**Thermal Analysis of Silicon Dendritic Web
Growth System: Present and Future**

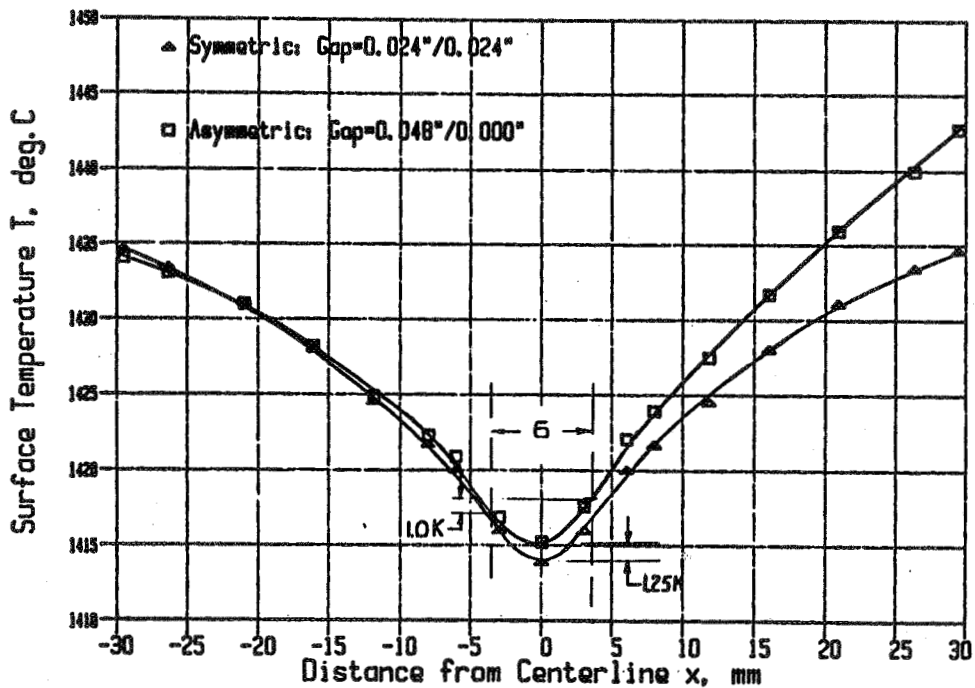
Temperature Distribution in Silicon Web Growth System (Hold Condition)



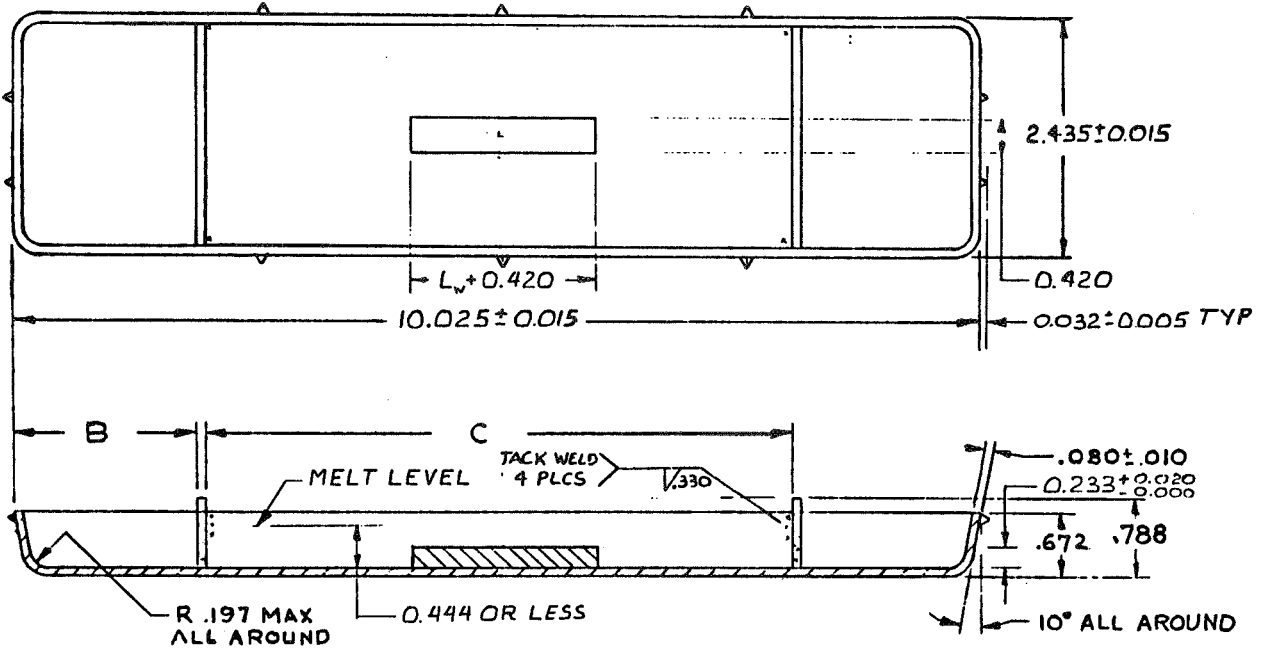
Melt Center Temperature Versus Crucible-Susceptor Gap



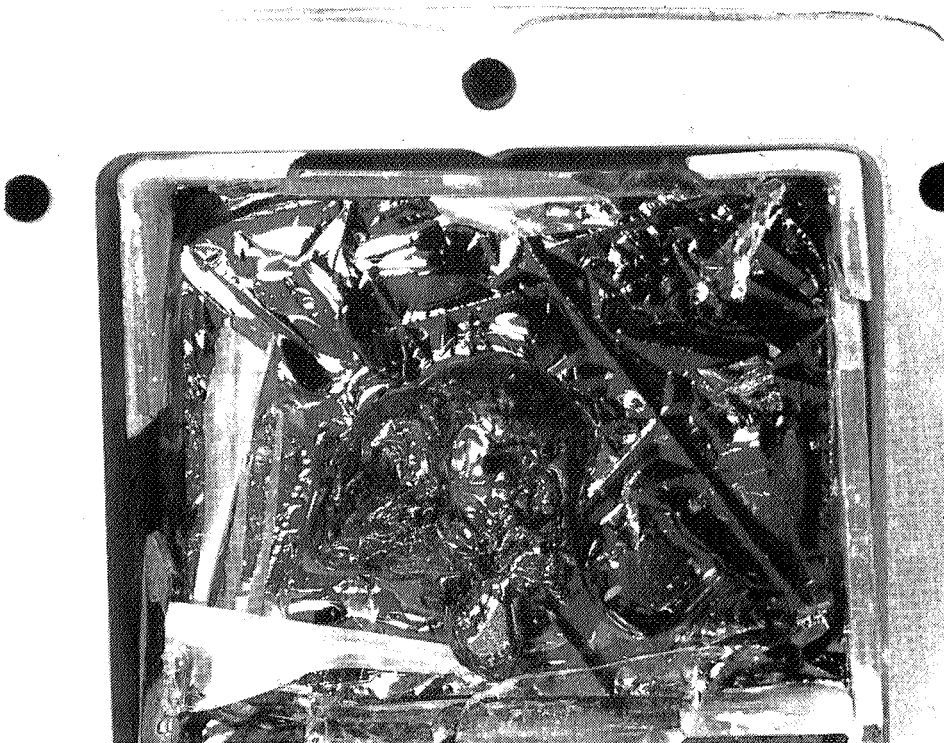
Effect of Gaps on Surface Temperature



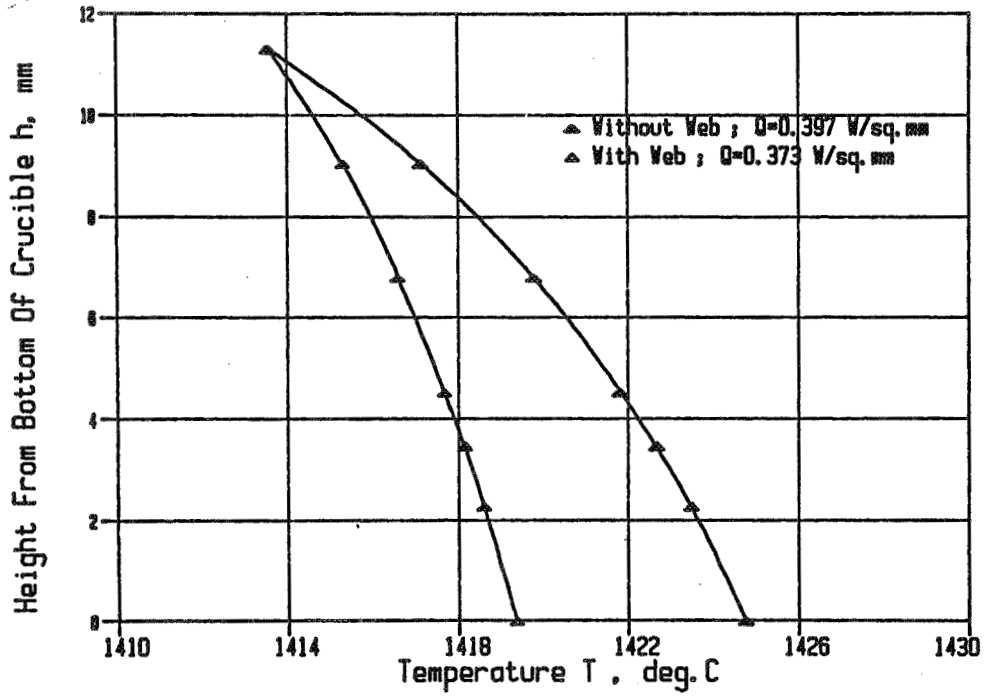
Proposed Crucible Modification
(Spacer Protrusions Added to Crucible)



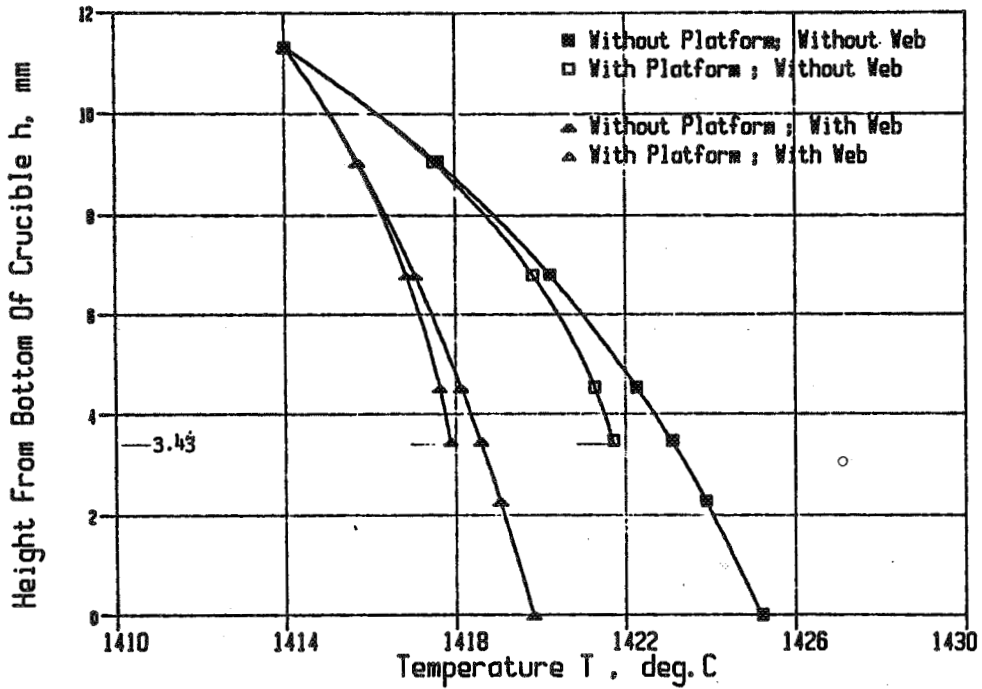
Crucible After 5 Days of Operation
(Spacer Protrusions Machined Into Susceptor)



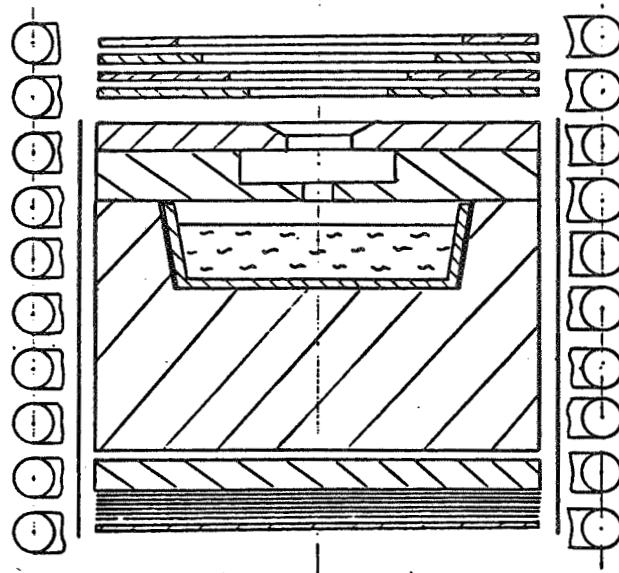
Centerline Temperature Distribution



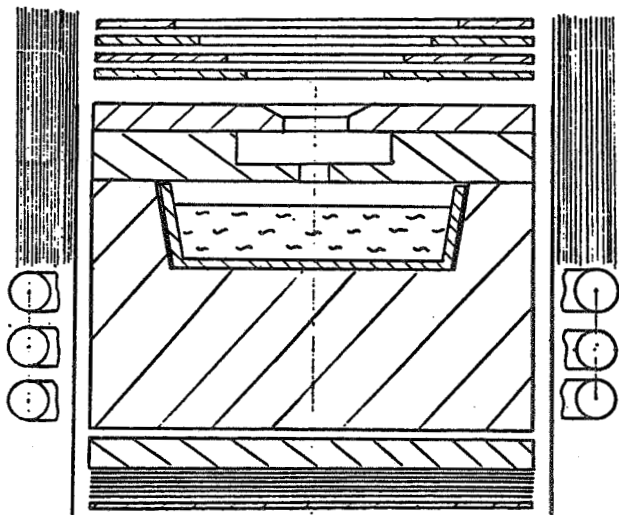
Effect of Platform on Temperature Distribution



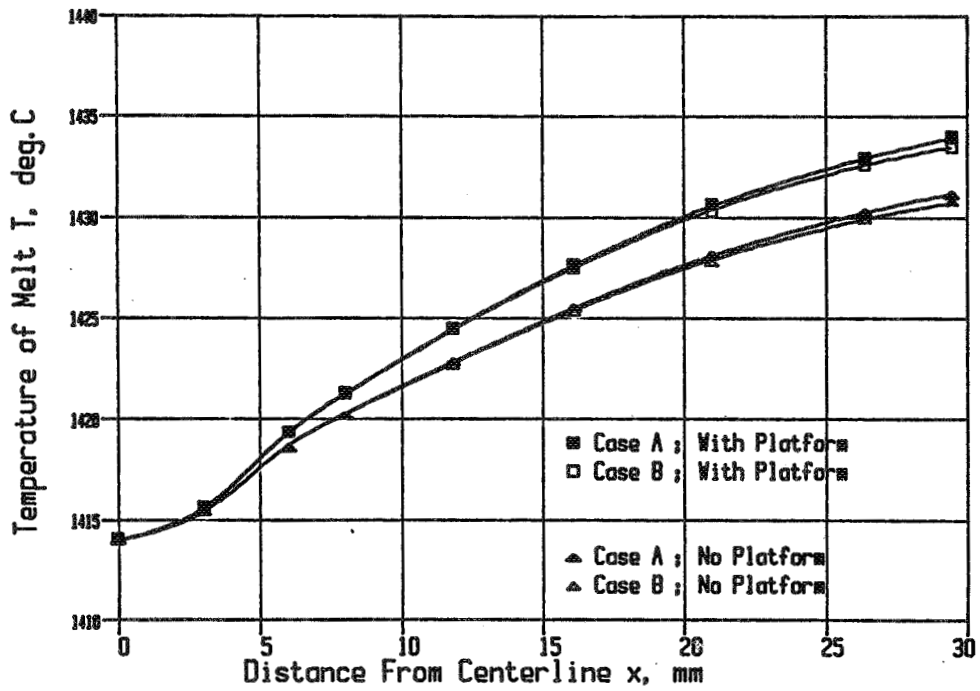
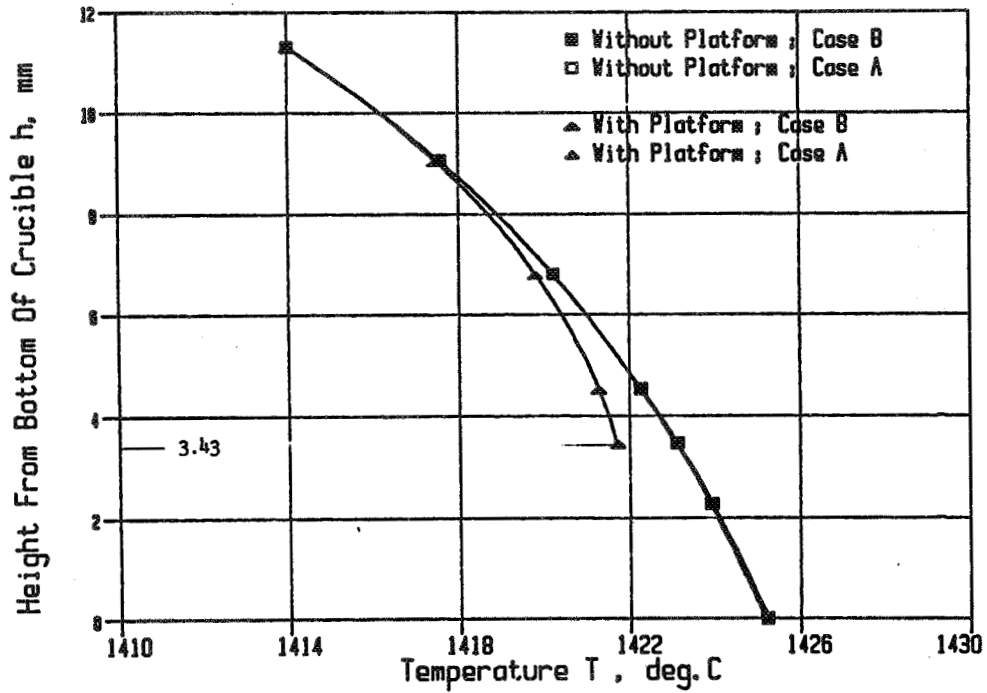
Present Westinghouse Configuration (Case A)



Configuration for Minimum Power Consumption (Case B)

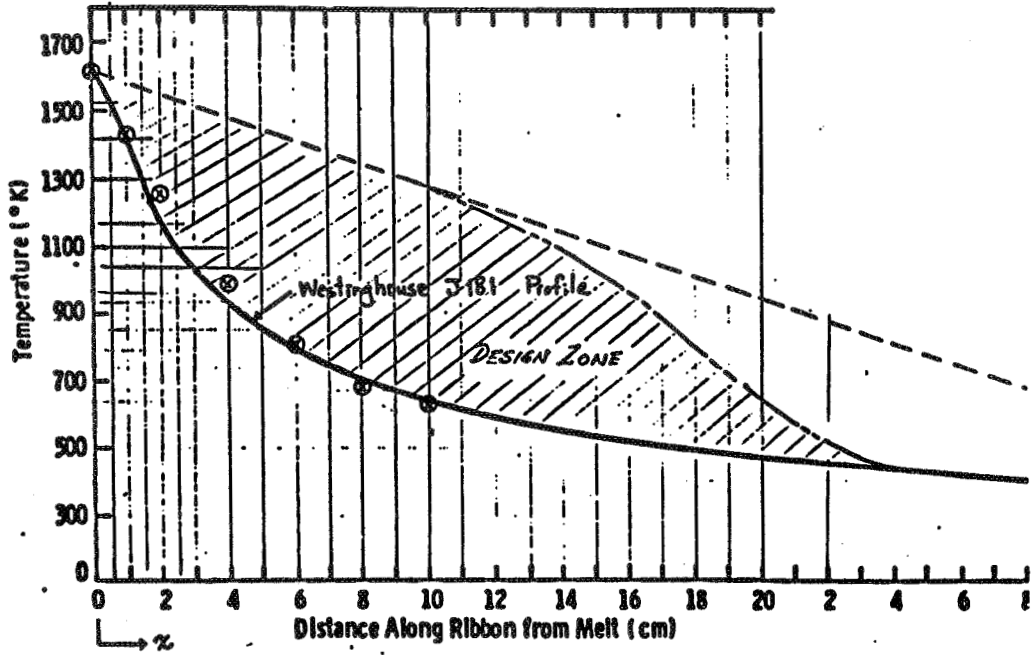


Effect of Power Distribution on Temperature in Melt

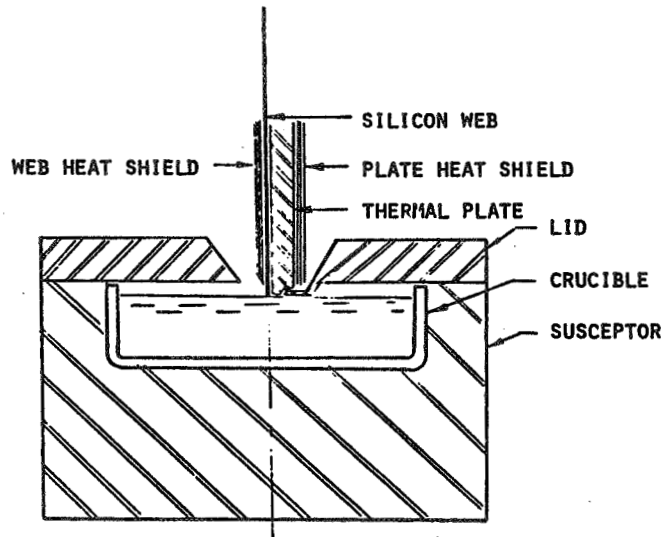


Thermal Stack: Analysis and Design

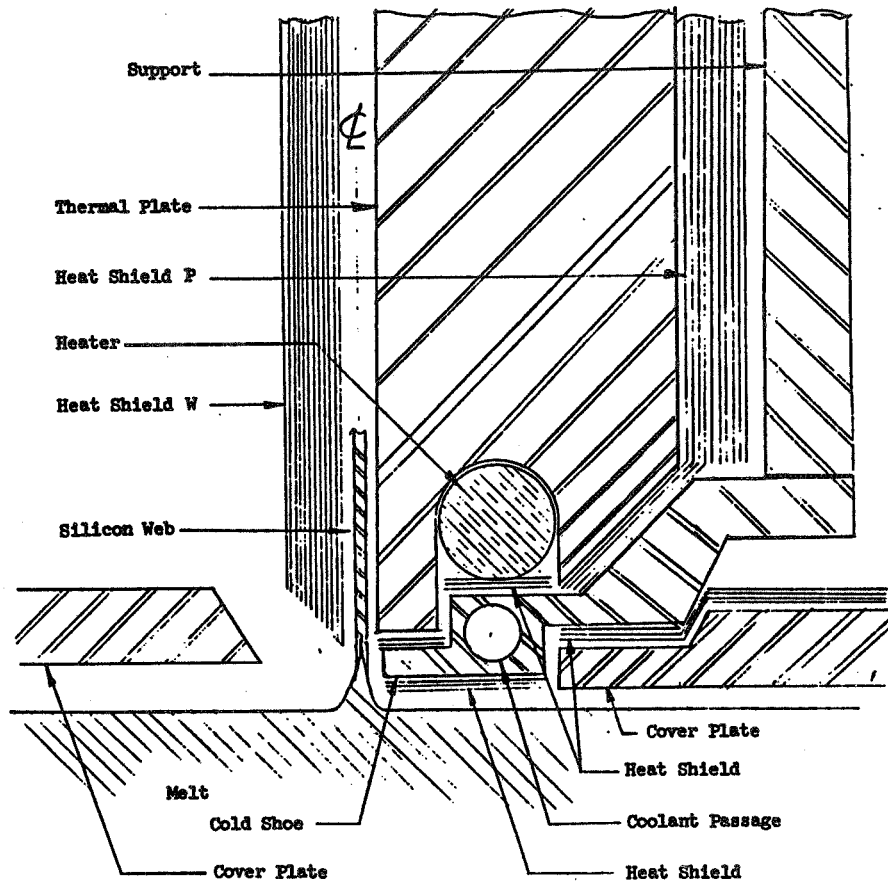
Thermal Web Profile



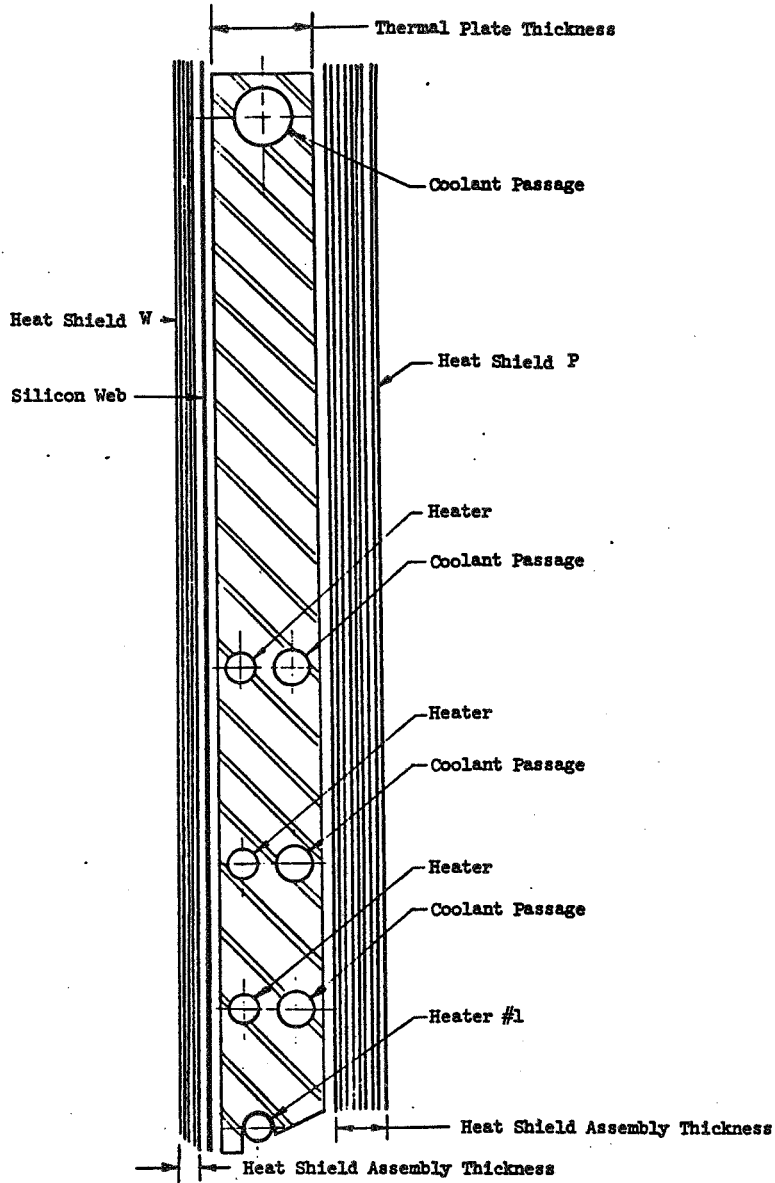
Proposed Silicon Dendritic Web Growth System
(Single Cold Shoe Design)



Proposed Single Cold Shoe Design

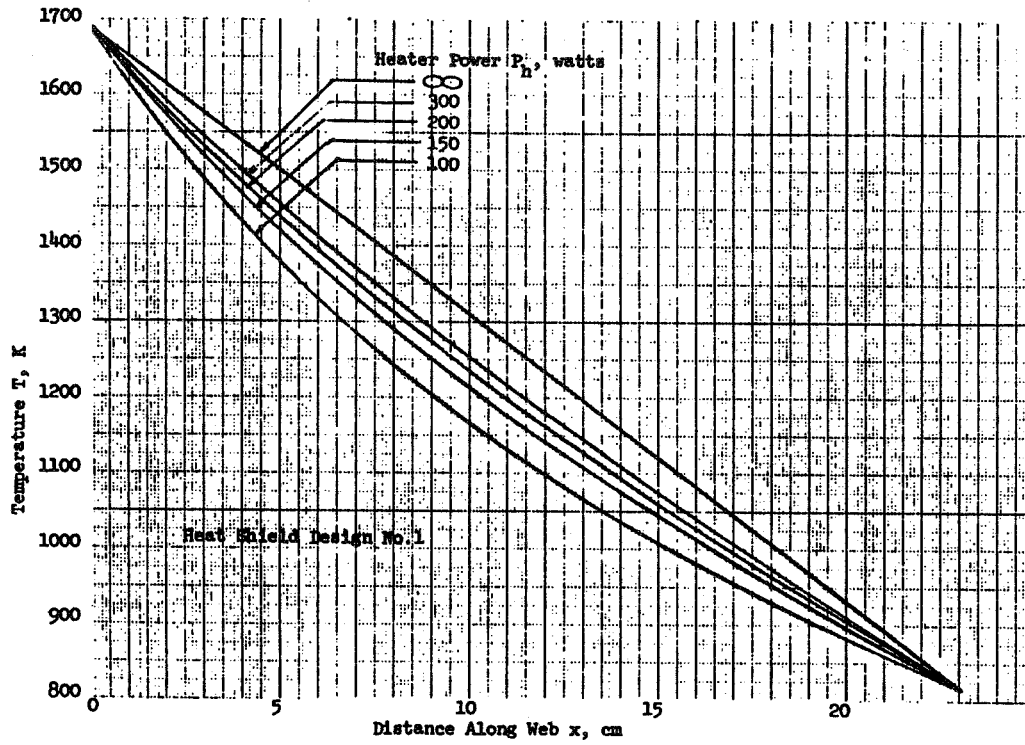


Thermal Stack Design (General Layout)

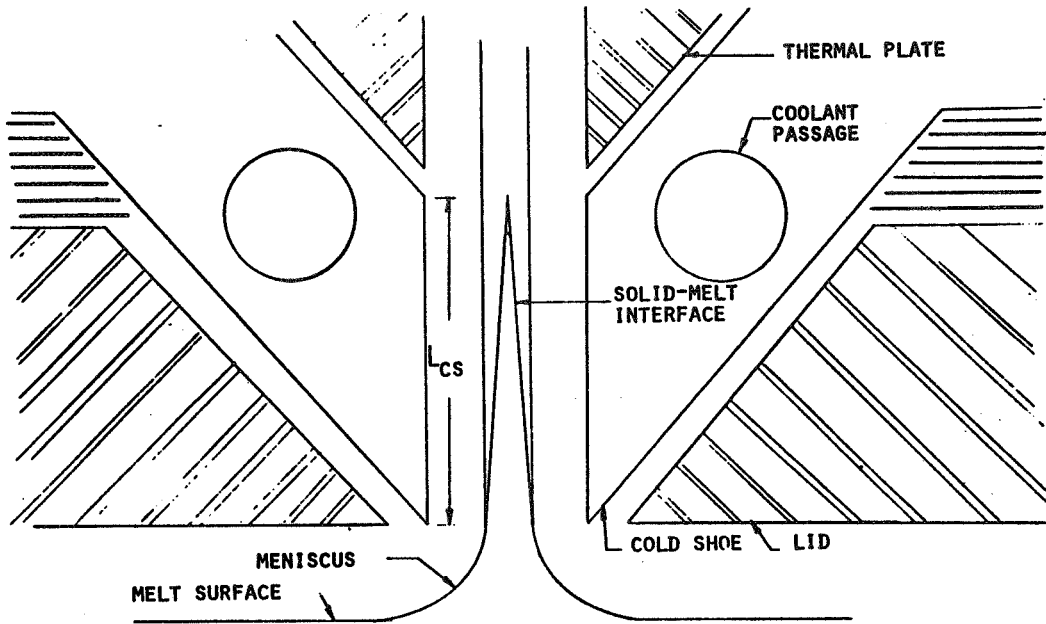


Cold Shoe: Analysis and Design

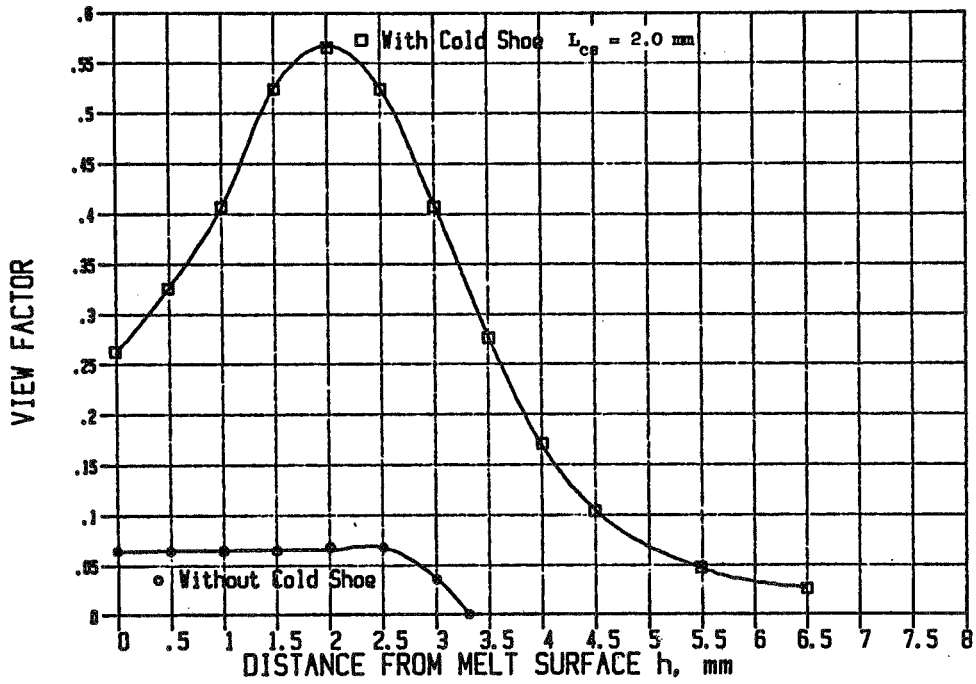
Temperature Distribution Along the Silicon Web for Various Thermal Plate Designs



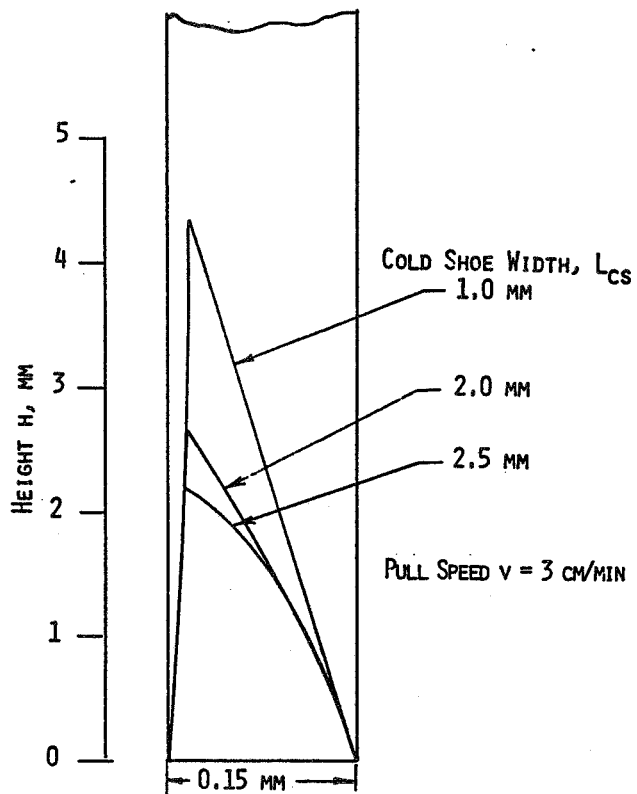
Ideal Cold Shoe Design



View Factor Distribution Along Web Surface



Melt-Solid Interface (Single Cold Shoe Design)



SILICON MATERIAL AND JPL WEB TEAM

REFERENCES

1. Raymond G. Seidensticker, "Dendritic Web Growth of Silicon," Crystals 8, Springer Verlag, Berlin Heidelberg, 1982 (HC)
2. R. G. Seidensticker and R. H. Hopkins, "Silicon Ribbon Growth by the Dendritic Web Process," Journal of Crystal Growth 50 (1980) 221-235, North-Holland Publishing Company (HC)

HIGH-EFFICIENCY DEVICE RESEARCH

N 86 - 29369

Dale R. Burger, Chairman

Progress reports on research in high-efficiency silicon solar cells were presented by 11 contractors. The presentations covered the issues of: heavy doping, bulk and surface recombination, and cell modelling.

The University of Florida's theoretical work on heavily doped silicon was described. Heavily doped polysilicon was used as a back-surface passivant replacing the usual back-surface field (BSF). Very good first results were achieved and there is the promise of a simple, low temperature deposition process. Short-circuit current-decay measurement methods were also covered.

A survey of bulk recombination measurement techniques was presented by the University of Pennsylvania. Classical methods were reviewed along with their limiting assumptions and simplifications. A modulated light measurement system was built and showed the large effects of junction capacitance. Techniques for extension of classical methods for measurement of multiparameter multiregression measurements were identified and analyzed.

Measurement of minority carrier transport parameters in heavily doped silicon was covered by Stanford University. The basic transport equations were used to define two independent parameters. Use of special vertical and lateral transistor test devices permitted the measurement of both parameters. Prior studies were normalized to show excellent agreement over the heavy doping region.

The State University of New York at Albany presentation featured oxygen and carbon related defects, both native and process-induced. A summary of oxygen processes in silicon versus process temperature was shown along with experimental results. The anomalous diffusion of oxygen was explained by the dissociation of the (V.O) center allowing O_i to move through the lattice.

Modelling and correlation studies of solar cells was discussed by the Research Triangle Institute. Recursive relationships were used to generate solutions at a number of mesh points within the emitter region. Photoexcited hole concentration and built-in electric field were calculated as a function of position. Simulated and experimentally determined I-V curves were shown to have good fit.

C. T. Sah Associates discussed loss mechanisms in high-efficiency solar cells. Fundamental limitations and practical solutions were stressed. Present cell efficiency is limited by many recombination sites: emitter, base, contacts, and oxide/silicon interface. Use of polysilicon passivation was suggested. After reduction of these losses, a 25% efficient cell could be built. A floating emitter cell design was shown that had the potential of low recombination losses.

Fabrication and characterization of high-efficiency metal insulator, n-p (MINP) cells was described by the University of Washington Joint Center for Graduate Studies. Particular attention was paid to development of

HIGH-EFFICIENCY DEVICE RESEARCH

measurement methods for surface recombination and density of surface states. A modified Rosier test structure has been used successfully for density of surface states. Silicon oxide and silicon nitride passivants were studied. Heat treatment after plasma enhanced chemical vapor deposition (CVD) of silicon nitride was shown to be beneficial. A more optimum emitter concentration profile was modelled.

Westinghouse Electric Corporation's Research and Development Center showed their work on high-efficiency dendritic web cells. The influence of twin planes and heat treatment on the location and effect of trace impurities was of particular interest. Proper heat treatment often increases efficiency by causing impurities to pile up at twin planes. Oxide passivation had a beneficial effect on efficiency. A very efficient antireflective (AR) coating of zinc selenide and magnesium fluoride was designed and fabricated. An aluminum back-surface reflector was also effective.

Pennsylvania State University examined surface and bulk loss reduction by low-energy hydrogen doping. Hydrogen ions provided a suppression of space charge recombination currents. Implantation of hydrogen followed by the Spire anneal cycle caused more redistribution of boron than the Spire anneal which could complicate processing.

HEAVY DOPING CONSIDERATIONS AND MEASUREMENTS IN HIGH-EFFICIENCY CELLS

UNIVERSITY OF FLORIDA

ORIGINAL PAGE IS
OF POOR QUALITY

F. Lindholm

HEAVY DOPING CONSIDERATIONS AND
MEASUREMENTS IN HIGH-EFFICIENCY
CELLS (UNIVERSITY OF FLORIDA)

FACULTY: F. LINDHOLM, A.
NEUGRUSCHEL

STUDENTS: T. JUNG, J. LIU, J.
PARK, K. MISIAKOS

PRESENTATION ORDER

- HD POLYSILICON-CONTACTED CELLS
measurement method (S, τ)
- HD POLYSILICON (MECHANISMS)

- ASSESSMENT OF AUGER LIFETIME
- MINORITY-CARRIER MOBILITY
expt. trapping model
- IMPROVED ACCURACY FOR ΔE_G
implications for μ and D
- LOW-DOPED MINORITY-CARRIER μ
implications for HD μ and S

HIGH-EFFICIENCY DEVICE RESEARCH

description: FIRST USE OF HD ($\sim 10^{20}/\text{cm}^3$) POLY AS PASSIVANT FOR BACK SURFACE, REPLACING BSF REGION.

rationale:

- LOWER TEMP. PROCESSING (675°C)
- NON-CRITICAL DEPOSITION PROCESS
- POST-DEPOSIT HEATING UNIMPORTANT
- DROPS S EVEN IF DOPING $> 10^{17}/\text{cm}^3$

samples:

- N- AND P-BASES (2 $\Omega\text{-cm}$): CZ Si
- 2x2 cm; $210 \pm 10 \mu\text{m}$ except ONE
- RESULTS AVERAGED, 10 TO 20 CELLS
- BSF AND BOC CONTROLS

results:

- S AND RED RESPONSE ($\lambda > 0.6 \mu\text{m}$)
- S = 100 cm/s FOR n-BASE.
- S and RSR BETTER THAN BOC AND BSF
- FIRST PROOF THAT Si:B POLY WORKS
- SUMMARIZED ON TABLE (VG)
- ESCCD METHOD MEASURES S (VG)

publication: LINDHOLM, NEUGROSCHER, ARIENZO, ILES, IEEE ELECTRON DEV. LETT, 6/85

TABLE 1

Summary of measured parameters at 28° C, (no AR coating). The cells have area $A = 4 \text{ cm}^2$ and thickness of about $210 \pm 10 \mu\text{m}$ except for cell 2N which was 330 μm thick. The results are the average values from 10-20 cells.

Cell	Base type	Back contact	V_{oc} (mV)	$I_{SCR}(\lambda > 0.6 \mu\text{m})$ (mA)	L (μm)	S (cm/s)
1P	p	ohmic	573	63	310-350	
2P	p	BSF	574	64	310-350	$4.2 \times 10^4 - 5 \times 10^4$
5P	p	poly-Si BSF	583	67.7	310-350	1100-1500

1N	n	ohmic	566	62.7	190-250	
2N	n	BSF	565	65.2	190-250	700-1000
5N	n	poly-Si BSF	591	65.5	190-250	100-160

HIGH-EFFICIENCY DEVICE RESEARCH

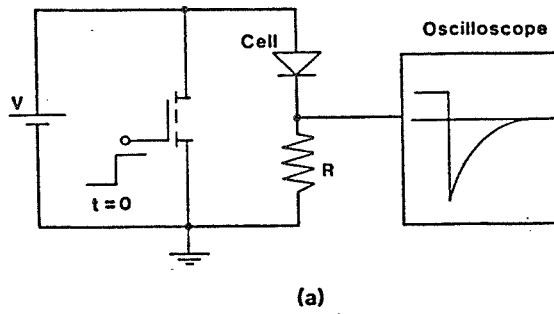


Fig. 4(a) Electronic circuit used in the SCCD method. The switching time of the power MOSFET is less than 100 nsec.

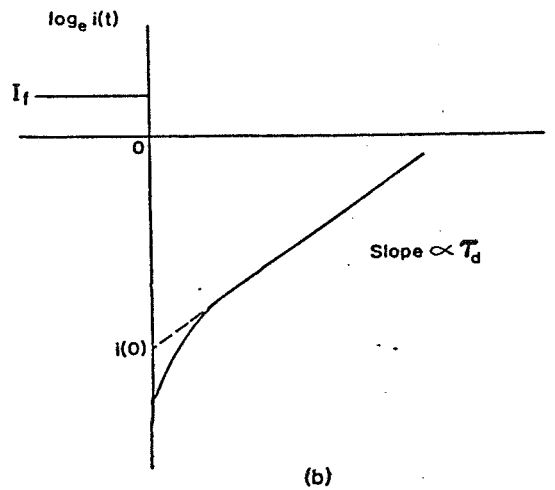


Fig. 4(b) Schematic illustration of the current decay displayed on a log scale.

HIGH-EFFICIENCY DEVICE RESEARCH

FUTURE & ONGOING: HD POLY CONTACT

1. ONE ADDITIONAL RUN COMPLETED.
• P-BASE, $\rho=0.15\Omega\text{cm}$, FZ Si, 8 mil.
• $L(\text{expected}) > 300\mu\text{m}$, $L(\text{got}) = 125\mu\text{m}$
PROCESS NOT UNDER CONTROL
• SLIGHT IMPROVEMENTS (I, V, RSR)
rationale: SHOW BSF ACTION FOR
 $\rho=0.15\Omega\text{cm}$

2. PRESENT RUN
• P-BASE, $\rho=0.3\Omega\text{cm}$, FZ, 14 mils.
• POLY UNDER GRID LINES
rationale: REPLACES TUNNEL OXIDE
IDEA. AREAL INHOMOGENEITY \downarrow \therefore
 $V_{OC}\uparrow$

3. NEAR FUTURE RUNS
USE THIN ($< 150\mu\text{m}$) BASES OF
 $\rho \sim 0.1\Omega\text{cm}$... CONTACT BACK BY HD
POLY... INTERLEAVE FRONT WITH
OXIDE AND POLY/METAL CONTACT.

4. PREDICTIONS OF MAX η
IF USE ABOVE SCHEME, AND ASSUME
RADIATIVE AND AUGER PROCESSES
CONTROL τ , $\eta \approx 23\%$... SAH, TR
JPL-056289-84-1... RESULTS BASED
ON NUMBERS FOR S IN VU GRAPHS TO
FOLLOW.

HD POLY (MECHANISMS)

description:

SPECIAL TEST STRUCTURES
CHEM. & STRUCT ↔ ELECTRICAL
DETERMINE S AT INTERFACE
HD POLY IS Si:As
NO INTERFACIAL OXIDE
CVD POLY AT 670°C

results: 2 MECHANISMS

- 1) LOW μ INTERFACE REGION ~ 100Å
 - D_p (interface) ~ 0.005 cm²/s
 - L_p (interface ~ 100Å
 - $C(As)_{max}$ (interf) ~ 10²¹/cc
 - Grain size < 40Å or amorph.
- 2) LOW-HI JCT IF $N(\text{low}) < 10^{19}/\text{cc}$

IF $N \sim 10^{19}/\text{cc}$, $S \leq 15$ cm/s

IF $N > 10^{19}/\text{cc} \approx N(\text{EFF})$, $S \leq 1000$ cm/s

implications: HD POLY CAN CUT
RECOMBINATION LOSS AT BOTH FRONT
AND BACK SURFACES

publication: A. Neugroschel, et.
al, IEEE Trans. Electron
Devices, 807-815, 4/85

HIGH-EFFICIENCY DEVICE RESEARCH

4D) POLY MECHANISMS: KEY IDEAS

PREVIOUS WORK ON POLY/N+.
HARD TO SEPARATE S AND τ .

HERE USE THIN ($0.8\mu\text{m}$) N-EPI.
LOW DOPING ($10^{18}/\text{cc}$) ON $0.06\ \Omega\text{cm}$
P-TYPE SUBSTRATE.

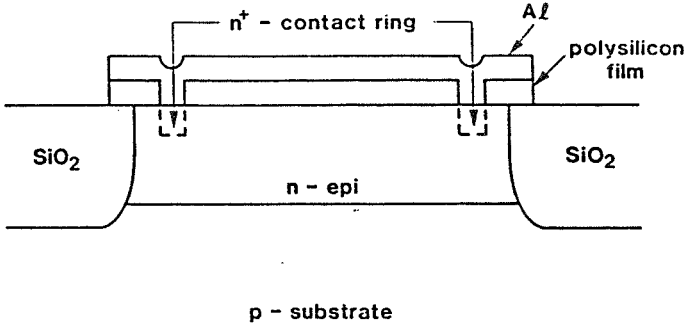
SAMPLES: METAL/POLY/N-EPI/P+
CONTROLS: METAL/N-EPI/P+

THICKNESS OF N-EPI VARIED.

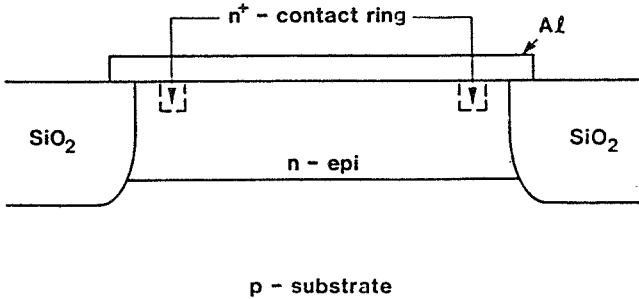
VARIOUS TYPES OF 1500\AA POLY
AND HEAT TREATMENTS STUDIED WITH
TEM AND SIMS TO REVEAL STRUCTURE
AND CHEMISTRY

ELECTRICAL MEASUREMENTS VS. T
AND V TO SEPARATE THE CURRENT
COMPONENTS.

HIGH-EFFICIENCY DEVICE RESEARCH

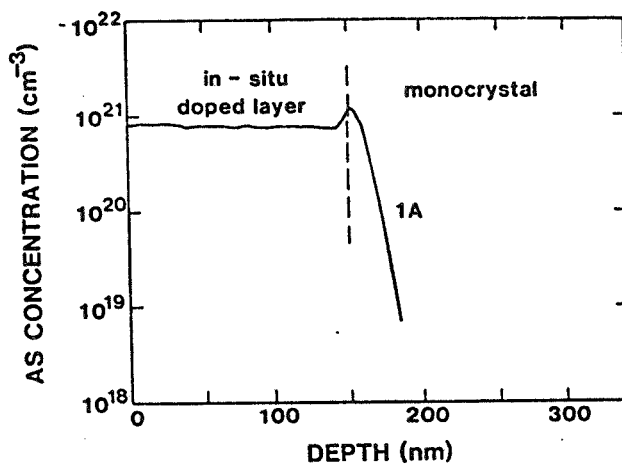


(a)

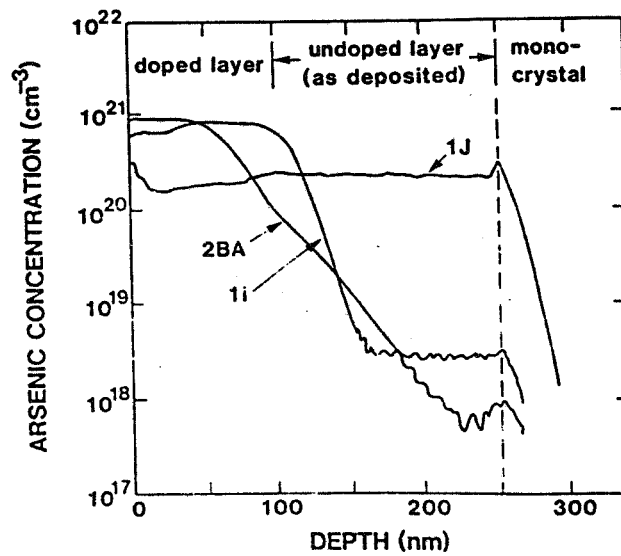


(b)

HIGH-EFFICIENCY DEVICE RESEARCH

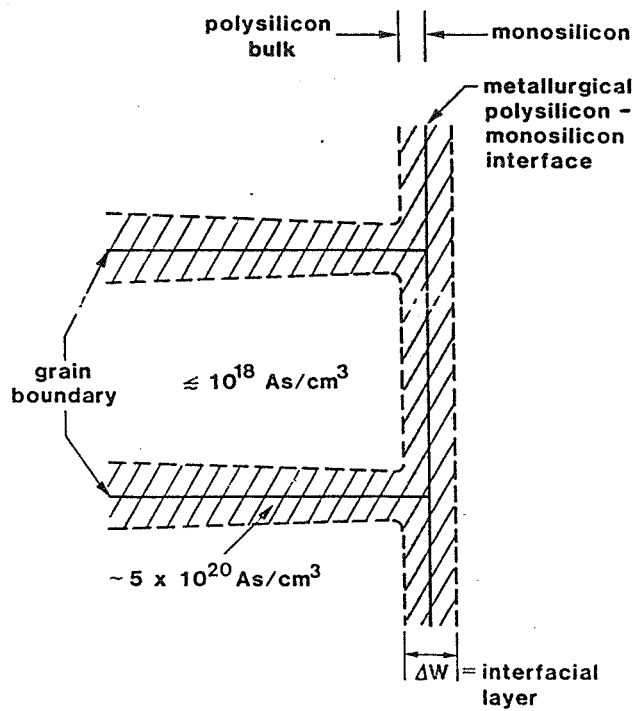


(a)



(b)

HIGH-EFFICIENCY DEVICE RESEARCH

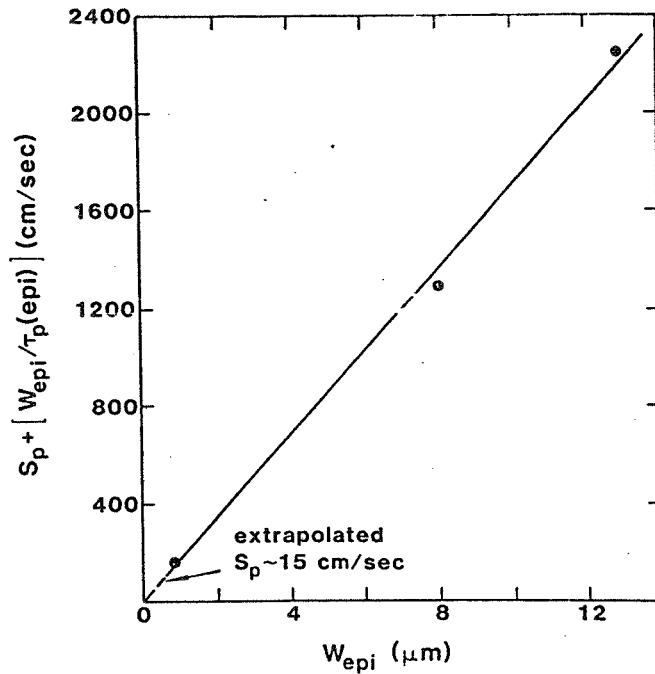


HIGH-EFFICIENCY DEVICE RESEARCH

TABLE I

Summary of heat treatments and electrical measurements. Heat treatments for polysilicon contacts were performed in argon. Electrical measurements were done at 25°C.

CONTACT	DEVICE	HEAT TREATMENT	J_{po} ($10^{-13}A/cm^2$)	S_{pmax} (cm/sec)
Undoped	1E	none	$(5.8 \pm 0.4) \times 10^3$	$\sim 10^6$
Polysilicon (1500 Å)	1F	800°C, 64 hrs	$(5.5 \pm 0.5) \times 10^3$	$\sim 10^6$
	1G	900°C, 5 min	$(5.5 \pm 0.5) \times 10^3$	$\sim 10^6$
In-situ Doped Polysilicon (1500 Å)	1A	none	7 ± 0.3	175
	1B	800°C, 64 hrs	10 ± 1.5	250
	1C	900°C, 5 min	6.6 ± 0.5	175
	1D	900°C, 15 min	6.5 ± 0.3	165
	2BE	1000°C, 15 min	6 ± 0.5	165
Bilayer: 1500 Å undoped + 1000 Å in-situ doped	1I	none	$(4.2 \pm 0.2) \times 10^3$	$\sim 10^6$
	1J	800°C, 64 hrs	4.9 ± 0.6	175
	1K	900°C, 15 min	$(4.2 \pm 0.2) \times 10^3$	$\sim 10^6$
	1L	850°C, 14 hrs	5.2 ± 0.6	180
	2BA	750°C, 8 hrs	$(4.0 \pm 0.3) \times 10^3$	$\sim 10^6$
Metal Reference		450°C, 20 min	$(5 \pm 1) \times 10^3$	$\sim 10^6$



• HD POLYSILICON-CONTACTED CELLS

• measurement method (S, τ)

• HD POLYSILICON (MECHANISMS)

• ASSESS AUGER τ (J. Appl. Phys)

• MINORITY-CARRIER MOBILITY

expt: trap model (SOLAR CELLS)

• IMPROVED ACCURACY FOR ΔE_G

if $10^{20}/\text{cc}$, $188 \rightarrow 169 \text{meV}$

minority hole $\mu = 12, D = 0.3$

• LOW DOPED MINORITY-CARRIER μ

based on transit time

doping $\sim 10^{18}/\text{cc}$

electron minority $\mu \approx \text{maj } \mu$

hole minority $\mu = 1.3 \mu(\text{maj})$

implications for HD μ and S

IEEE Electron Dev Lett.

• FC DECAY FOR τ DETERMINATION

If large defect density,

$\tau(\text{inferred}) > \tau$. Explained via

multiple time constants for

transient decay via bound

states. (SOLAR CELLS).

ADVANCED TECHNIQUES FOR THE MEASUREMENT OF MULTIPLE RECOMBINATION PARAMETERS IN SOLAR CELLS

UNIVERSITY OF PENNSYLVANIA

M. Newhouse
M. Wolf

Model Equations

$$n(x, t) = \sum_m A_m \phi_m(x) e^{-\lambda_m t}$$

$$n(x, \omega) = \int \sum \frac{\phi_m(x) \phi_m^*(x)}{i\omega + \lambda_m} h(x) dx$$

$$A_m = \int_0^d n(x, 0) \phi_m(x) dx$$

$h(x) \equiv$ steady state excitation

$$\sqrt{\frac{\beta_m}{D}} d \tan \sqrt{\frac{\beta_m}{D}} d = \frac{sd}{D}$$

$d \equiv$ device length

$$\lambda_m = 1/\tau + \beta_m$$

s AND μ DEPENDENCE IN BOTH EIGENVALUE AND EIGENMODE

τ DEPENDENCE ONLY IN EIGENVALUE

PRECEDING PAGE BLANK NOT FILMED

Model

EIGENVECTORS Φ_M

DETERMINED BY μ AND BOUNDARY CONDITIONS

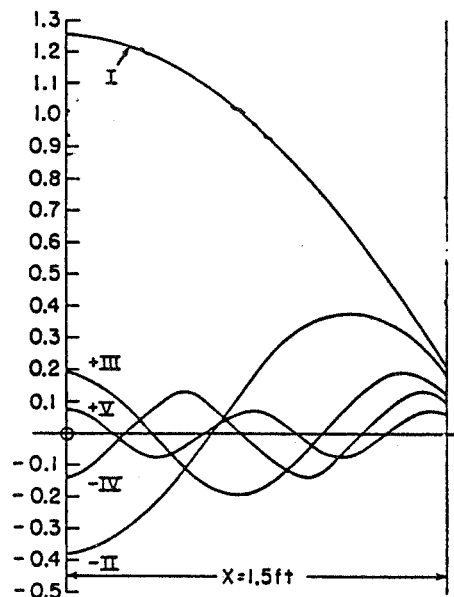


FIG. 3.1. Representation of the initial temperature distribution for $\theta = 1$ F by means of a Fourier series.

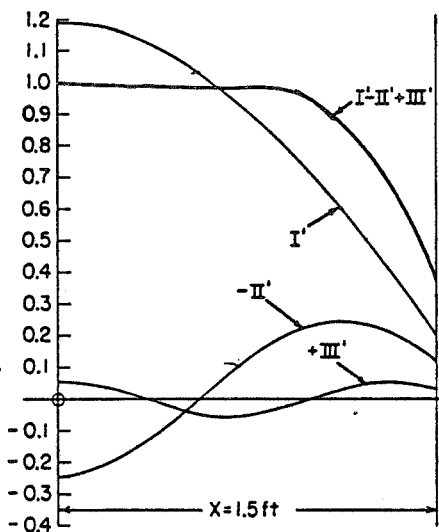
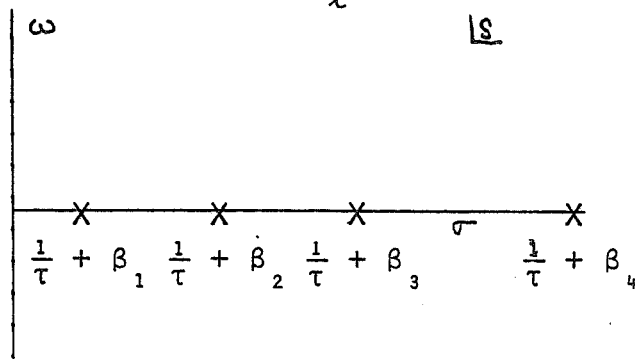


FIG. 3.2. Representation of the temperature distribution after 5 hr by means of a Fourier series.

EIGENVALUES (POLES) $\lambda_M = \beta_M + 1/\tau$

OVERALL DISPLACEMENT DETERMINED BY $1/\tau$

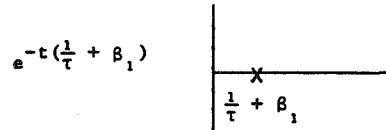
RELATIVE POSITION β_i DETERMINED BY μ BOUNDARY CONDITIONS



Assumptions and Approximations

1. POLE POSITION

A. DOMINANT POLE



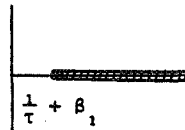
1. BEST IN THIN DEVICES WHERE POLES ARE WELL SEPARATED
2. LARGE TIME (DECAY) OR LOW FREQUENCY (MODULATIONS METHODS) FIRST POLE DOMINATES
3. UNIFORM EXCITATION PREFERENTIALLY EXCITES FIRST MODE

B. FIRST POLE AT $1/\tau$

1. ONLY TRUE FOR $u = 0$ AT BOUNDARIES.

C. POLE COALESCENCE

DISTANCE BETWEEN POLES BECOMES SMALL.
POLES BECOME BRANCH-CUT.



1. BEST IN LONG DEVICES
2. NOTE: STEP AND IMPULSE RESPONSES DIFFER AND ARE NO LONGER EXPONENTIAL
 - A. STEP ERFC $(\sqrt{\epsilon/\tau})$
 - B. PULSE $\frac{\exp(-t/\tau)}{\sqrt{\epsilon}}$

HIGH-EFFICIENCY DEVICE RESEARCH

2. IGNORE "NONDOMINANT REGIONS"
 - A. SENSITIVE TO EXCITATION
 1. EXTERIOR EXCITATION BETTER THAN INJECTION
 - B. HELPS IF IT IS DOMINANT POLE
3. DEPLETION LAYER APPROXIMATIONS
 - A. PROBLEMS
 1. UNKNOWN BOUNDARY CONDITIONS
 2. CAPACITANCE
 - A. YIELDS EXTRA POLE (DECAY TERM)
UNRELATED TO RECOMBINATION
 - B. AREA DEPENDENT, LOAD DEPENDENT
 - C. CAN BE SHUNTED WITH FORWARD CONDUCTANCE
 3. CONDUCTANCE
 4. GENERATION RECOMBINATION
 - B. ROUGH ORDERING OF SENSITIVITY TO EFFECTS
 - LEAST
 1. DC SHORT CIRCUIT
 2. AC SHORT CIRCUIT
 3. DC OPEN CIRCUIT
 4. AC OPEN CIRCUIT
 - MOST
4. KNOWN STRUCTURE
5. LIGHT MEASUREMENTS REQUIRE ABSORPTION COEFFICIENTS
EXCEPTION: PENETRATING RADIATION
6. SIMPLE RECOMBINATION
 - A. LOW INJECTION
 - B. SINGLE RECOMBINATION LEVEL
 - C. LOW PROBABILITY OF OCCUPATION
 - D. LEVEL NEAR MIDGAP
7. SIMPLE STRUCTURE & CONSTANT KNOWN PHYSICAL PARAMETERS
 - A. CONSTANT τ μ
 - B. KNOWN μ
 - C. NO DRIFT FIELDS
 - D. NO BAND GAP NARROWING
 - E. ZERO OR INFINITE RECOMBINATION VELOCITIES

Recombination Parameter Gradients and
Nonclassical Mobility References

MEASUREMENT OF DIFFUSION LENGTH GRADIENTS IN
HYDROGEN PASSIVATED SILICON R.H. MICHAELS 1984
APPL. PHYS. LETT., 46 415 (1985).

MEASUREMENT OF CARRIER LIFETIME PROFILES IN DIFFUSED
LAYERS OF SEMICONDUCTORS B.J. BALIGA AND MICHAEL S.
ADLER IEEE ED-25, 472 (1978).

THE USE OF SPATIALLY-DEPENDENT CARRIER CAPTURE RATES
FOR DEEP-LEVEL DEFECT TRANSIENT STUDIES G.P LI AND
K.L. WANG SSE 26, 825 (1983).

PHOTOGENERATED CARRIER COLLECTION IN SEMICONDUCTORS
WITH LOW MOBILITY-LIFETIME PRODUCTS F. GALLUZZI
J PHYS D. APPL PHYS, 18 685 (1985).

MEASUREMENT OF MINORITY CARRIER DRIFT MOBILITY IN
SOLAR CELLS USING A MODULATED ELECTRON BEAM,
S. OTHMER AND M.A. HOPKINS NASA CP-2169
PP 61-66, 1980.

EFFECTIVE LIFETIMES IN HIGH QUALITY SILICON DEVICES,
D.K. SCHRODER SSE 27, 247 (1984).

HIGH-EFFICIENCY DEVICE RESEARCH

Second Generation

REQUIREMENTS

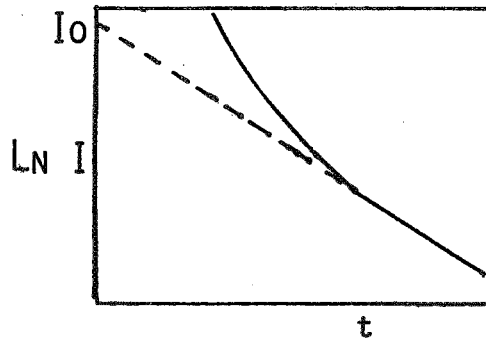
1. MEASURE MULTIPLE PARAMETERS
2. ACCOUNT FOR COMPLEX DEVICE BEHAVIOR, MULTIREGION NONUNIFORMITY, DRIFT FIELDS, BGN, JUNCTION

MULTIPLE UNKNOWN: DETERMINATION REQUIRES MULTIPLE DATA TWO SOURCES

1. TWO PIECES OF DATA FROM SINGLE RESPONSE
 - A. EIGENVALUE, EIGENVECTOR
 - I. SCCD
 - B. REAL PART, IMAGINARY PART
 - I. MLM
 - II. IMPEDANCE
2. VARY EXTERNAL PARAMETERS
 - A. HIGHER ORDER POLES CONTAIN INFORMATION ABOUT NONDOMINANT REGIONS AND s & μ
 - B. RESOLVE POSITION/SHAPE OF HIGHER ORDER POLES/EIGENMODES BY THE VARIATION OF EXTERNAL PARAMETERS

RESOLUTION SENSITIVITY AND UNIQUENESS MUST BE CONSIDERED
IN GENERAL: THE MORE VARIABLE PARAMETERS, THE
MORE RESOLUTION AND SENSITIVITY

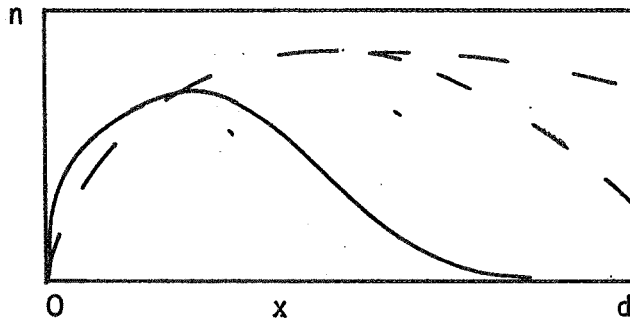
SCCD



- o SLOPE AT $t = \text{LARGE}$ IS FIRST POLE OR EIGENVALUE

$$I_0 = -qD \frac{d}{dx} \int_0^d n(x) \phi_1(x) dx$$

\uparrow
 FIRST EIGENMODE



HIGH-EFFICIENCY DEVICE RESEARCH

Three Variable Parameters Identified as Useful

1. SPATIALLY VARYING EXCITATION
 - A. DIFFERENT MINORITY CARRIER DISTRIBUTIONS
 - B. VARIES DEGREE OF EXCITATION OF PARTICULAR EIGENMODE. REGION AND DEPTH RESOLUTION
 - C. ASLBIC, MLM

2. TIME VARYING EXCITATION
 - A. MODULATION FREQUENCY OR FREQUENCY CONTENT (PULSE EXCITATION) VARIED
 - B. CONTRIBUTION OF POLE TO RESPONSE IS INCREASED AS ASSOCIATED KNEE FREQUENCY IS PASSED
 - C. MLM, CAPACITANCE CONDUCTANCE

3. VARYING BOUNDARY CONDITION
 - A. BIAS AT JUNCTION OR SURFACE
 - B. SHAPE OF EIGENMODE AND POSITION OF EIGENVALUE CHANGES
 - C. B.H. ROSE I_{sc} & V_{oc} DECAY; POSSIBLY MLM

HIGH-EFFICIENCY DEVICE RESEARCH

Multiparameter Multiregion Measurements

METHOD	EXCITATION	MEASURED QUANTITY	VARIED PARAMETERS	NUMBER OF MEAS QUANT. PLUS 2 TIMES NUMB OF VAR. PAR.	REFERENCE
Isc-Voc PHOTO-DECAY	PENETRATING LIGHT	TIME DEPENDENT CURRENT OR JUNCTION VOLTAGE	BOUNDARY CONDITIONS	2	B.H. ROSE H.T. WEAVER J. APPL PHYS 238 54 (1983)
PHOTO-COND. DECAY	PENETRATING LIGHT	INTEGRATED CONDUCTIVITY AT TWO TIMES DURING SQUARE PULSE RESPONSE	NONE	2	S. ERÄNEN M. BLOMBERG J APPL. PHYS. 2372 (1984)
CAPACITANCE CONDUCTANCE	INJECTION	DYNAMIC DIFFUSION CAPACITANCE & CONDUCTANCE	FREQUENCY (BOUNDARY CONDITIONS)	4 (6)	A. NEUGROSHEL ET. AL. IEEE TRANSACTIONS ED-24 485 (1978)
SCCD	INJECTION	STEADY STATE & TIME DEPENDENT CURRENT	NONE	2	TOE-WON JUNG ET. AL. IEEE TRANSACTIONS ED-31 588 (1984)
ASLBIC	LIGHT	STEADY STATE CURRENT	WAVELENGTH	2	M. WOLF ET. AL. 17 PHOTOVOLTAIC SPECIALISTS CONF. 1984
EBIC	ELECTRON BEAM	STEADY STATE CURRENT	ENERGY	2	L.D. PARTAIN ET. AL. 17 PHOTOVOLTAIC SPECIALISTS CONF. 1984
SMLM	MODULATED LIGHT	MODULATED CURRENT (VOLTAGE) MAGNITUDE & PHASE	FREQUENCY WAVELENGTH (BOUNDARY CONDITIONS)	6 (8)	M. NEWHOUSE JPL CONTRACT 956290 REPORTS

HIGH-EFFICIENCY DEVICE RESEARCH

Range of Poles

short circuit $1/\tau + \frac{D}{d^2} \frac{\Pi}{2}$ minimum

$$1/\tau + \frac{D}{d^2} \Pi \text{ maximum}$$

open circuit $1/\tau$ minimum

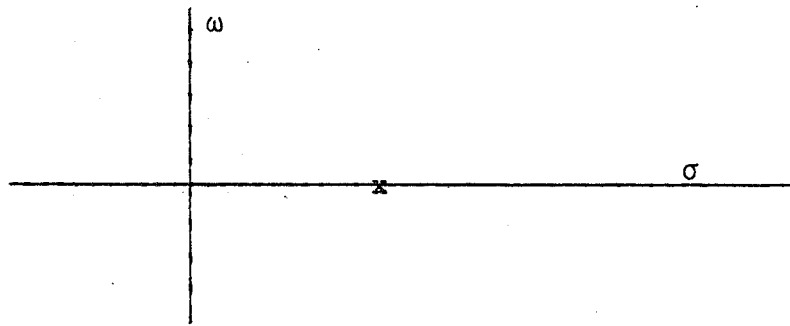
$$1/\tau + \frac{D}{d^2} \frac{\Pi}{2} \text{ maximum}$$

exact value determined by $\frac{sd}{D}$

\therefore problems when $\frac{D}{d^2} \gg 1/\tau$

or

$$\frac{1}{d^2} \gg 1/L^2$$



then pole position determined by s , d , D and not by τ

Not solved with AC $\frac{L}{\sqrt{1 + i\omega\tau}}$

Proof

d.c

$$n(x, t) = \int_0^d \sum_m \frac{\phi_m^2(x)}{D \left(\frac{c}{d^2} + \frac{1}{\tau} \right)} h(x) dx$$

$$= \int_0^d \sum_m \frac{\phi_m^2(x) h(x)/D}{\frac{c}{d^2} + 1/L^2} dx$$

∴ if $L \gg \frac{d}{c}$ than

$$\approx \int_0^d \sum_m \frac{\phi_m^2(x) h(x)/D}{\frac{c}{d^2}} dx$$

No L dependence

for a.c. $L^* = L/\sqrt{1 + i\omega\tau}$

$$n(x, t) = \int_0^d \sum_m \frac{\phi_m^2(x) h(x)/D}{\frac{c}{d^2} + \frac{1 + i\omega\tau}{L^2}} dx$$

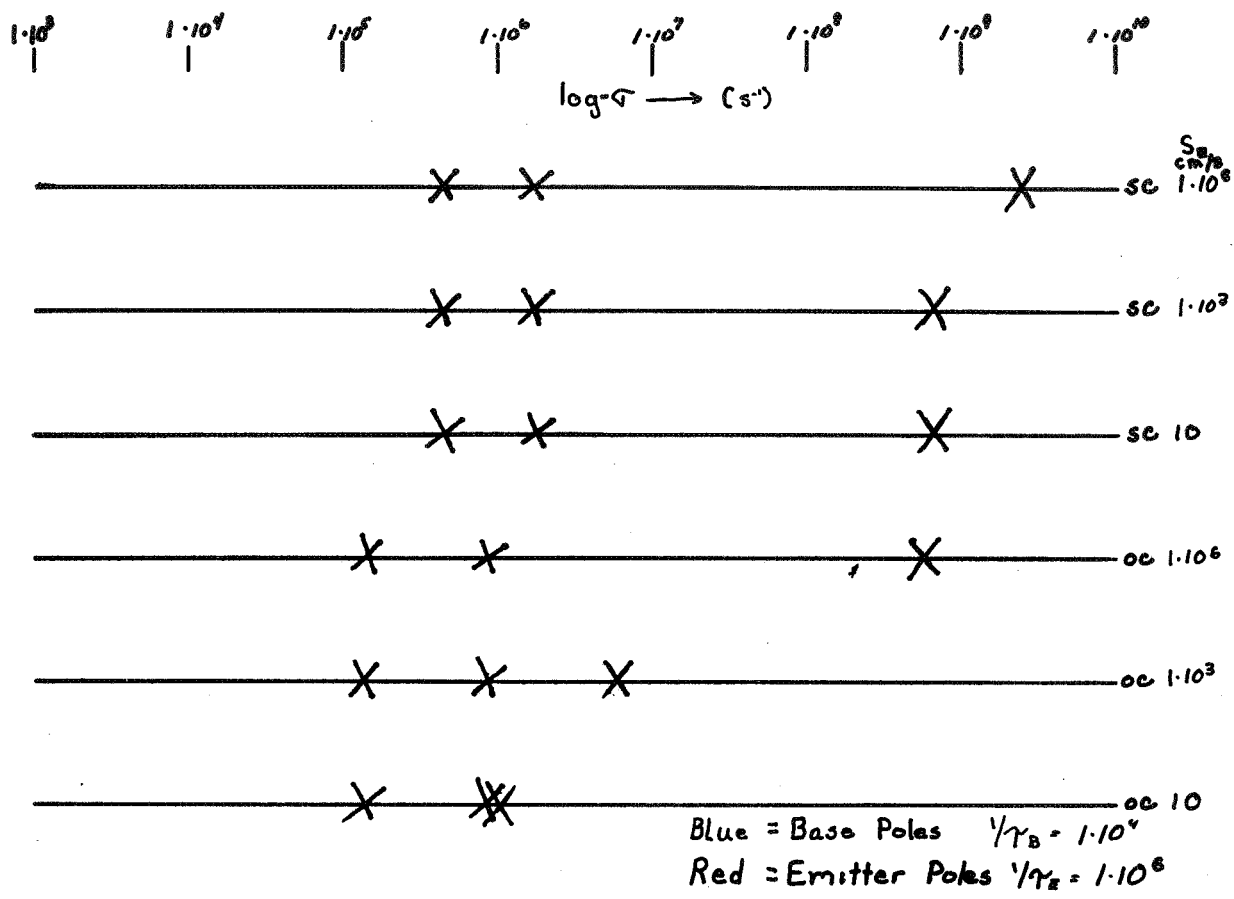
$$= \int_0^d \sum_m \frac{\phi_m^2(x) h(x)/D}{\frac{c}{d^2} + \frac{1}{L^2} + \frac{i\omega}{D}} dx$$

if $L \gg \frac{d}{c}$ than

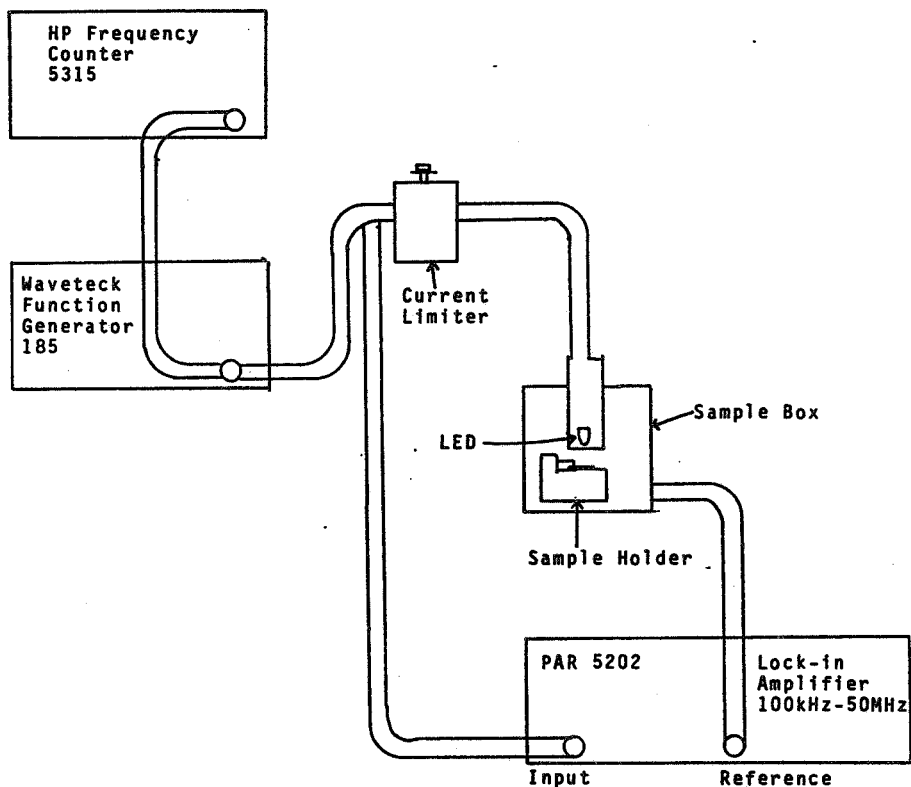
$$\approx \int_0^d \sum_m \frac{\phi_m^2(x) h(x)/D}{\frac{c}{d^2} + \frac{i\omega}{D}} dx$$

Still no L dependence

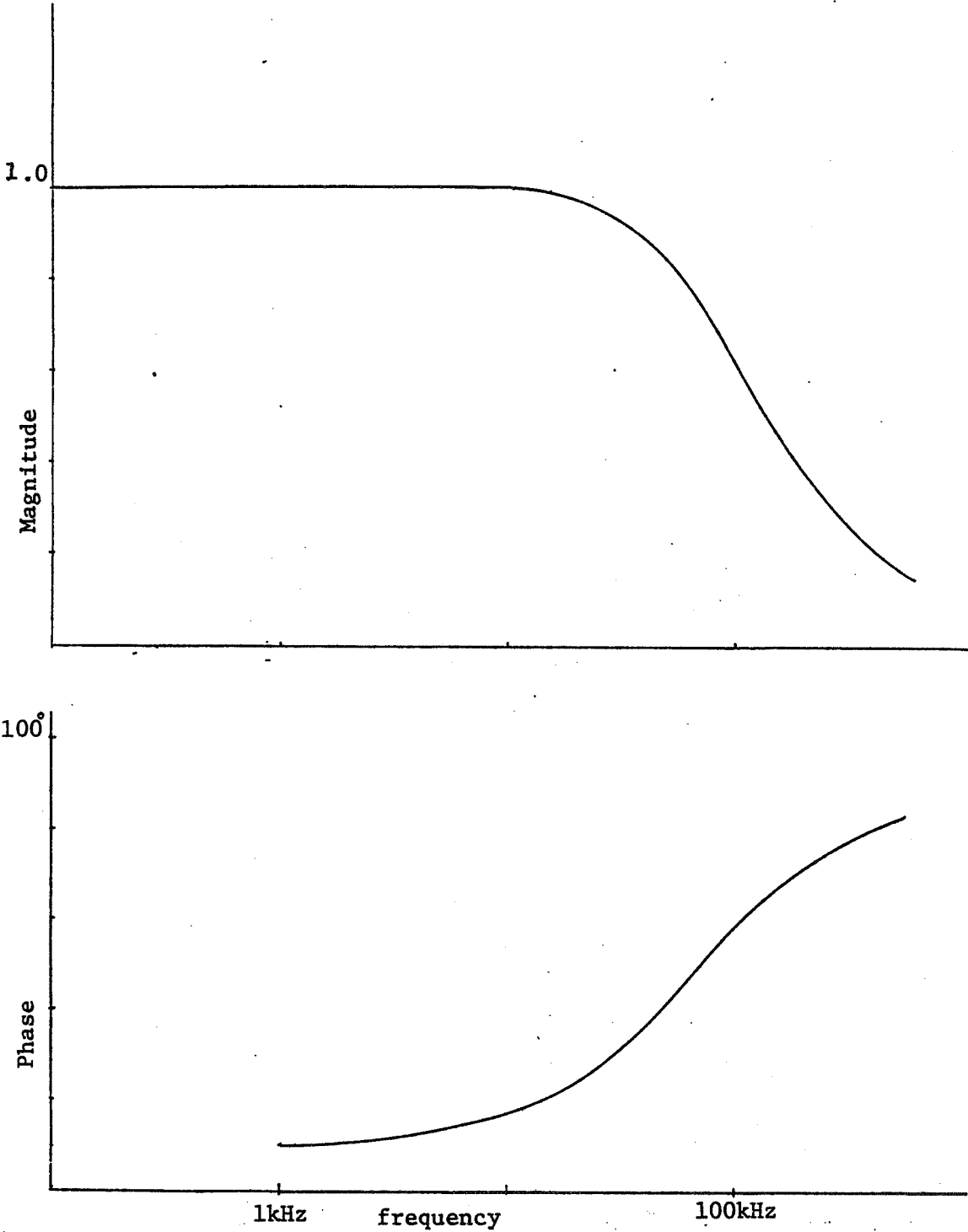
HIGH-EFFICIENCY DEVICE RESEARCH



Ortec 9505 Lock-in Amplifier, 10-200 kHz



MLM Data



HIGH-EFFICIENCY DEVICE RESEARCH

MLM Junction Capacitance

- o FULL SIZED DEVICES HAVE .1 TO .5 μ F JUNCTION CAPACITANCE
- o WITH 10 Ω LOAD RC \sim 30 TO 160 KHz
- o INFLUENCE IDENTIFIED WITH REVERSE BIAS EFFECT ON 3DB POINT
- o SOLUTION: REDUCE AREA AND LOAD RESISTANCE, MEASURE AND ACCOUNT FOR EFFECT, WORK AT OPEN CIRCUIT WITH BIAS LIGHT

Summary

- o UTILIZED MODEL TO FORMULATE PROBLEM
- o REVIEWED CLASSICAL METHOD CLASSIFYING AND IDENTIFYING LIMITING ASSUMPTIONS AND SIMPLIFICATIONS
- o IDENTIFIED AND ANALYZED TECHNIQUES REQUIRED FOR EXTENSION OF CLASSICAL METHODS FOR MULTIPARAMETER MULTIREGION MEASUREMENT
- o CONSIDERED IMPLICATIONS FOR THIN REGIONS
- o BUILT MODULATED LIGHT MEASUREMENT FACILITY AND MADE MEASUREMENTS SHOWING THE LARGE EFFECTS OF JUNCTION CAPACITANCE

Future

- o A MORE COMPLETE EXPERIMENTAL EVALUATION OF SMLM
- o AN ANALYTICAL TREATMENT TO HELP RIGOROUSLY DECONVOLVE MULTIPOLE, MULTIPARAMETER AND MULTIREGION DATA
- o COMPUTER SIMULATIONS TO EMPIRICALLY EVALUATE ANALYTICAL TECHNIQUES AND MODEL MULTIPARAMETER, MULTIREGION, DRIFT FIELD AND BAND GAP NARROWING EFFECTS
- o USE ANALYSIS AND SIMULATIONS TO ADDRESS QUESTIONS OF RESOLUTION, SENSITIVITY AND UNIQUENESS

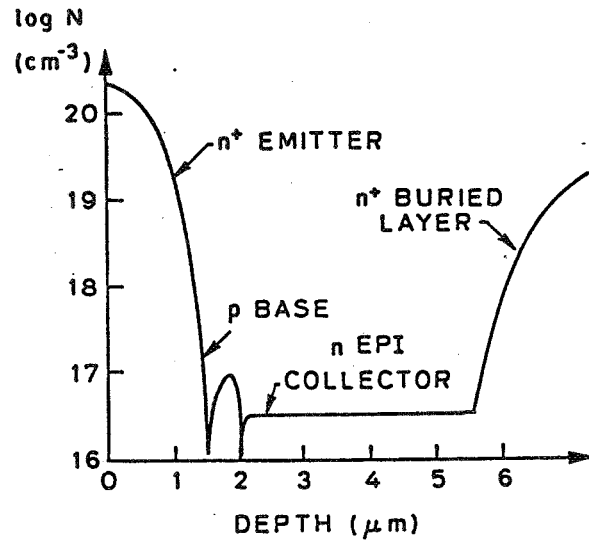
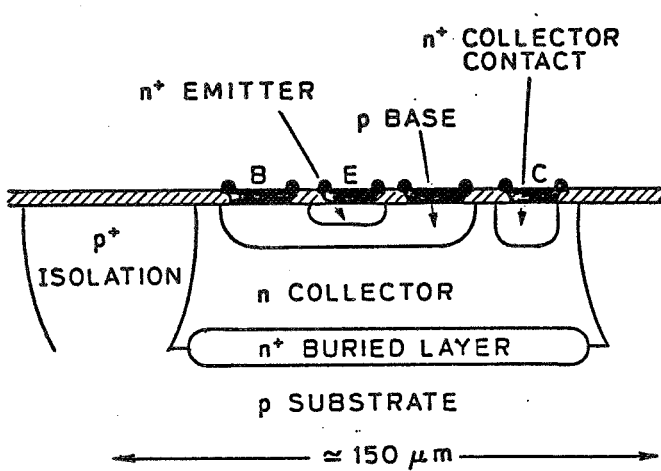
MEASUREMENT OF MINORITY CARRIER TRANSPORT PARAMETERS IN HEAVILY DOPED n-TYPE SILICON

STANFORD UNIVERSITY

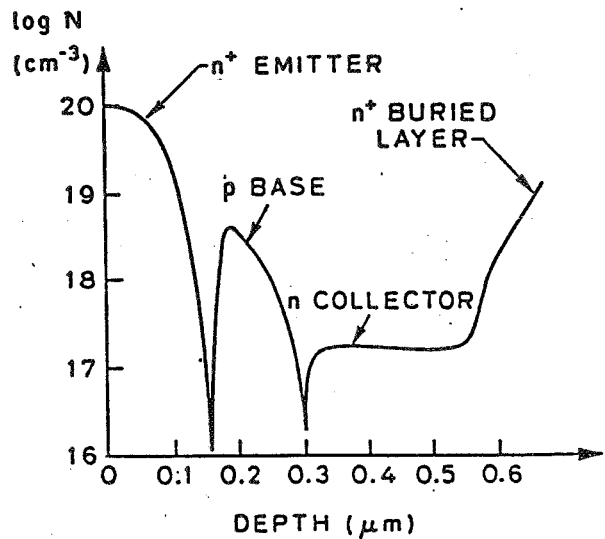
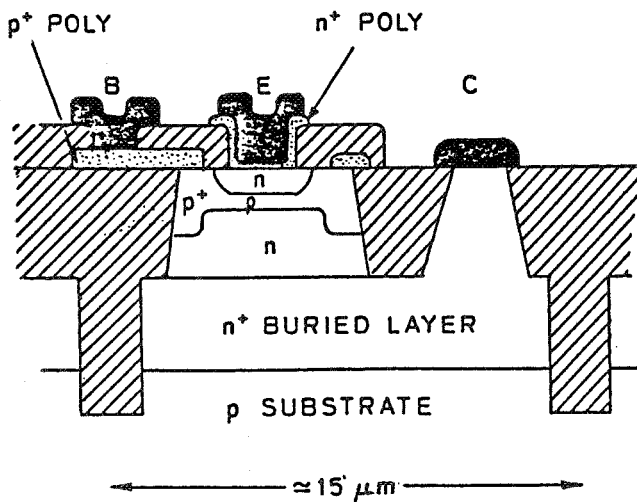
J. del Alamo
R.M. Swanson

Scaled Bipolar Devices

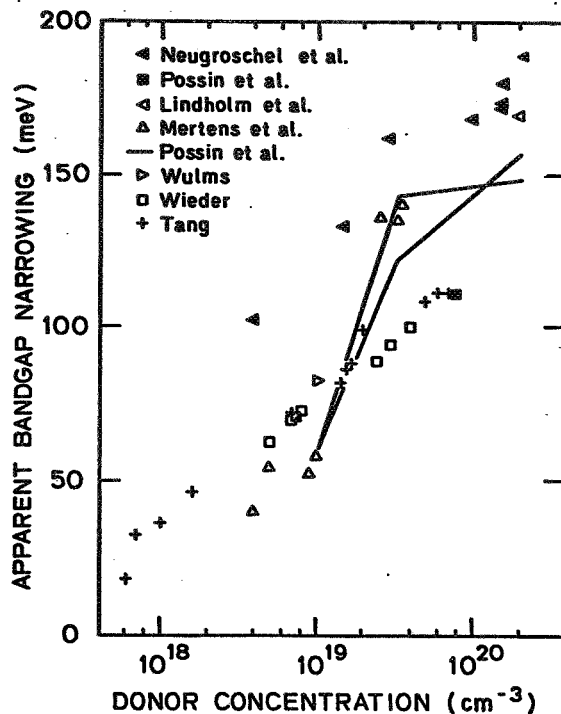
1970's



1980's



PRECEDING PAGE BLANK NOT FILLED



Basic Transport Equations

Assumptions:

- n-type silicon
- steady state
- quasi-neutrality
- low injection
- 1-D

1. Hole current equation:

$$J_p = p\mu_p \frac{dE_{fp}}{dx}$$

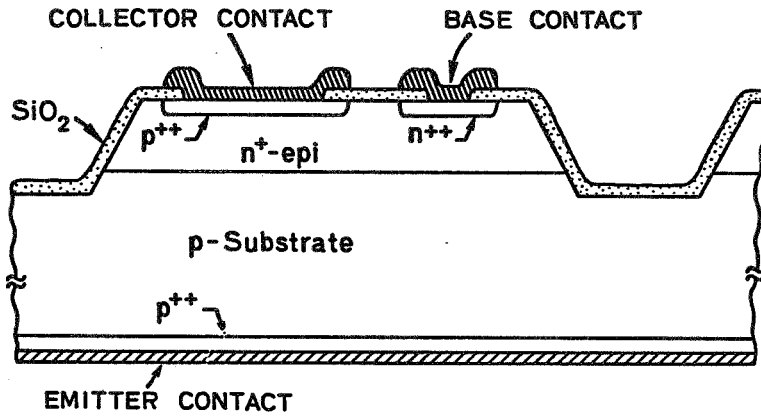
2. Hole continuity equation:

$$\frac{1}{q} \frac{dJ_p}{dx} = -R = -\frac{p - p_0}{\tau_p}$$

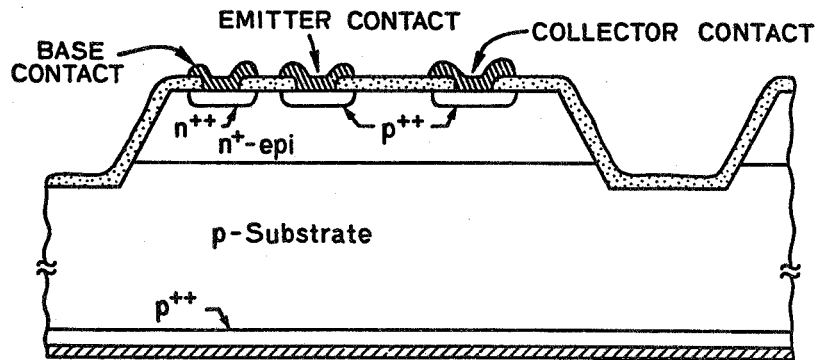
3. Hole density equation:

$$p = \int_{-\infty}^{\infty} \rho_v(E)[1 - f(E)]dE = p_0 \exp \frac{E_F - E_{fp}}{kT}$$

Vertical Transistor



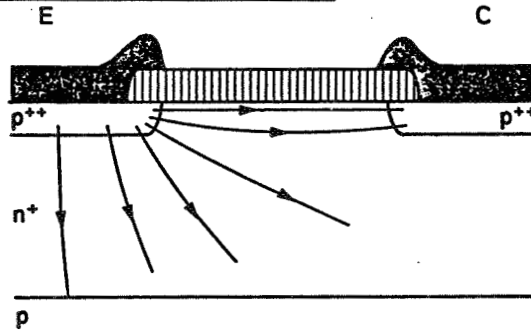
Lateral Transistor



PRECEDING PAGE BLANK NOT FILMED

Lateral Transistors

Extraction of diffusion length



Collector current:

$$I_{oci} = qAF_L(p_o D_p) \left(\frac{1}{L_p} \right) \frac{1}{\sinh\left(\frac{W_{Bi}}{L_p}\right)}$$

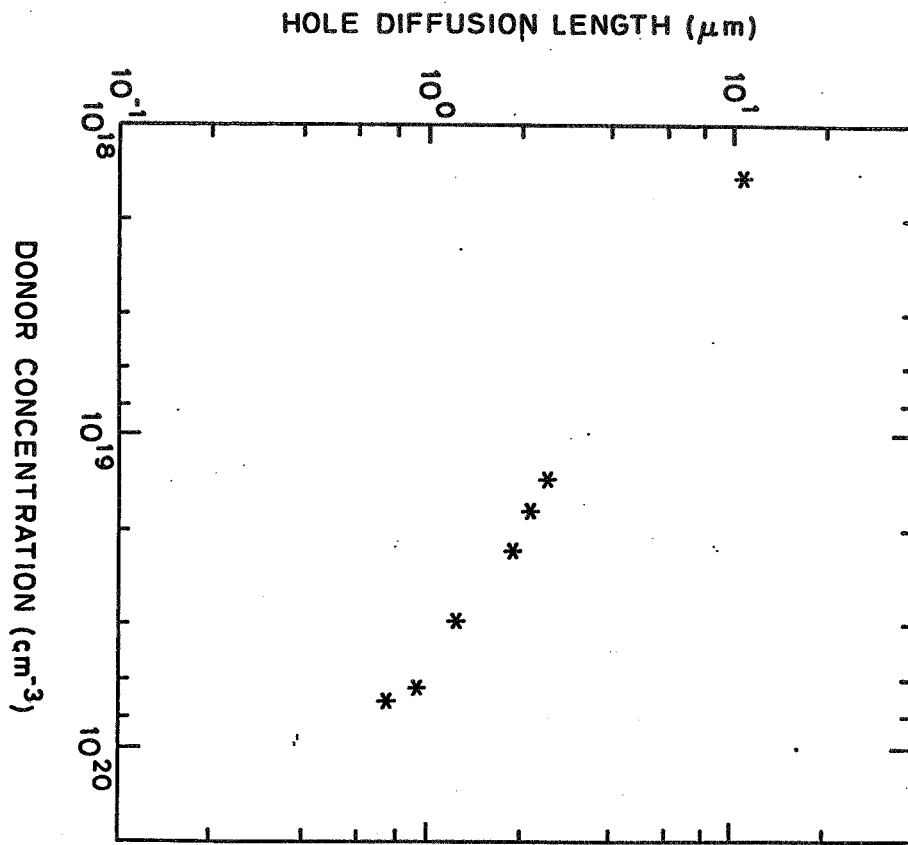
If $W_{Bi} \gg L_p$

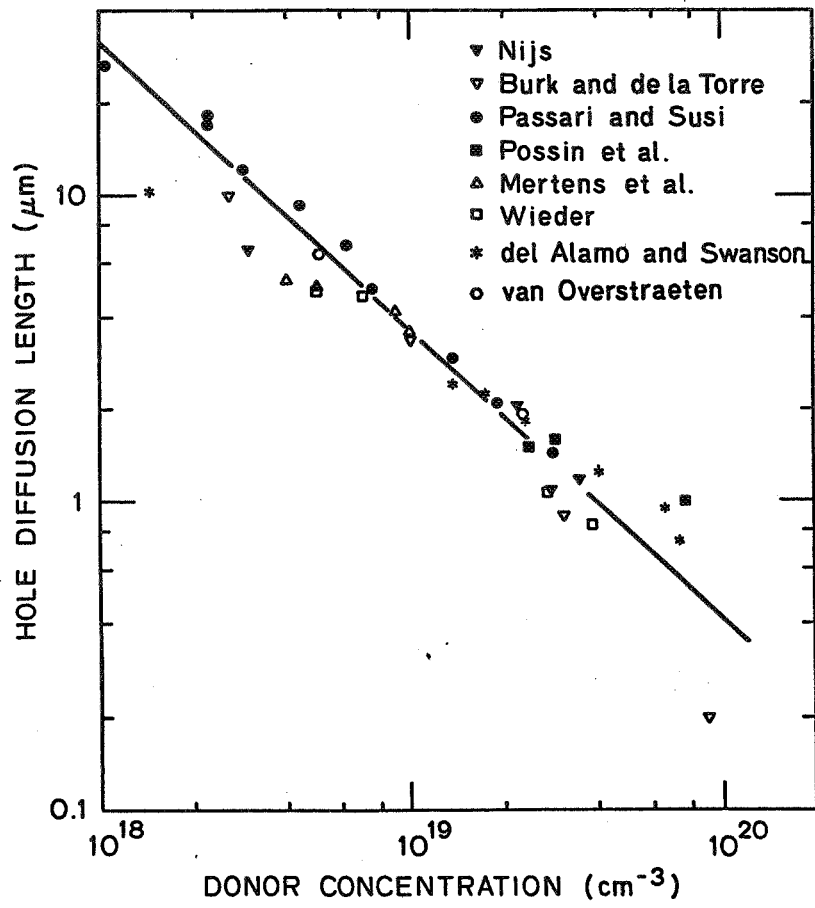
$$I_{oci} = qAF_L(p_o D_p) \left(\frac{2}{L_p} \right) \exp - \left(\frac{W_{Bi}}{L_p} \right)$$

Then

$$\frac{I_{oci}}{I_{oc1}} = \exp - \left(\frac{W_{Bi} - W_{B1}}{L_p} \right)$$

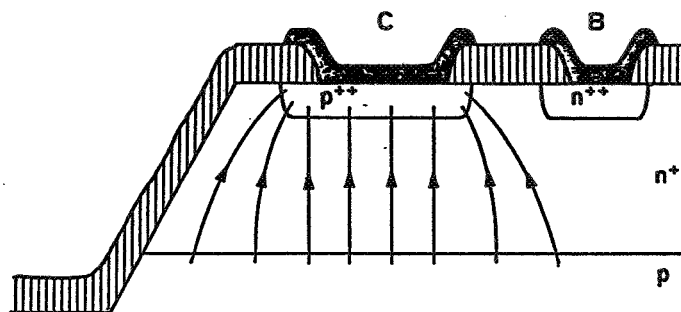
HIGH-EFFICIENCY DEVICE RESEARCH





Vertical Transistors

Measurement of $p_0 D_p$



Collector current:

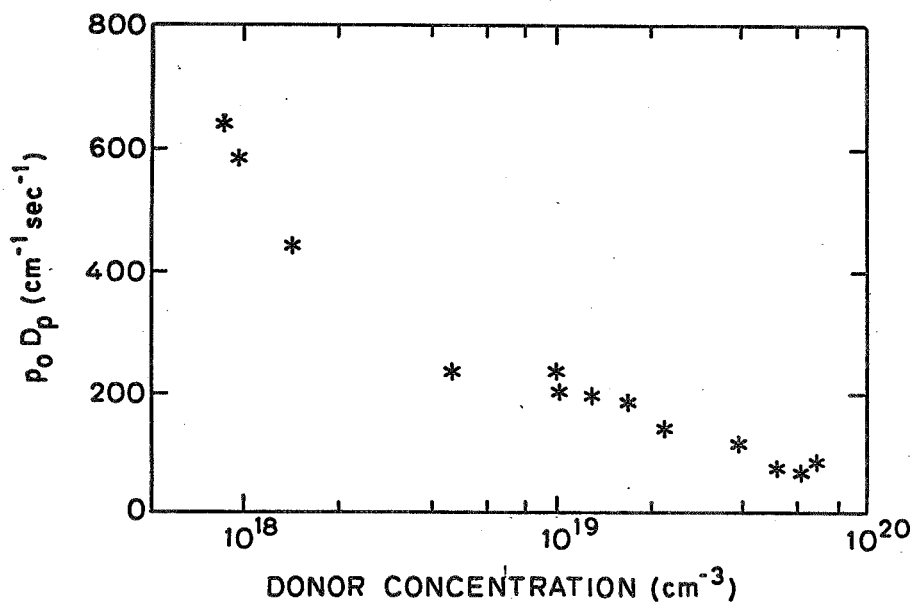
$$J_{oc} = p_0 D_p \left(\frac{1}{L_p} \right) \frac{1}{\sinh\left(\frac{W_B}{L_p}\right)}$$

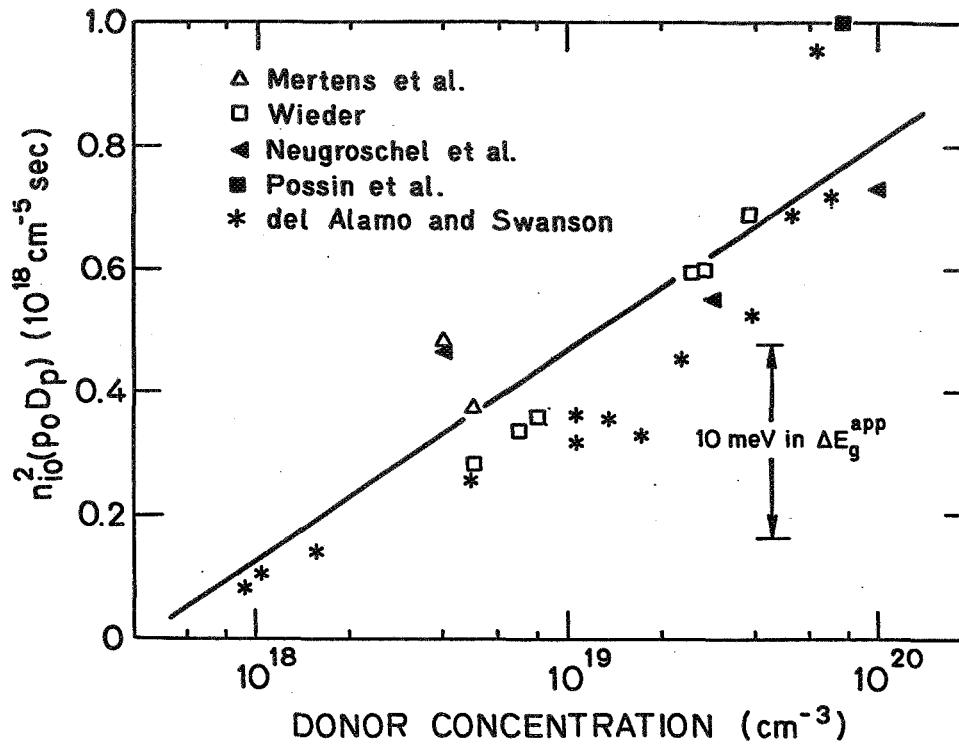
If $W_B \ll L_p$

$$J_{oc} \approx p_0 D_p \frac{1}{W_B}$$

If $W_B \gg L_p$

$$J_{oc} \approx p_0 D_p \frac{2}{L_p} \exp\left(-\frac{W_B}{L_p}\right)$$





Authors	$N_s (cm^{-3})$	$x_j (\mu m)$	$J_o (A/cm^2)$	
			measured	calculated
Kwark and Swanson	3.3×10^{19}	1.0	8.3×10^{-13}	1.1×10^{-12}
Kwark and Swanson	4.6×10^{19}	0.66	1.1×10^{-12}	1.5×10^{-12}
Ning and Isaac	1.2×10^{20}	0.20	2.8×10^{-12}	2.8×10^{-12}
Patton and Plummer	2.1×10^{19}	0.20	3.2×10^{-12}	3.6×10^{-12}
Patton and Plummer	4.4×10^{19}	0.23	2.6×10^{-12}	2.6×10^{-12}

Conclusions

1. There are only two independent parameters that control minority carrier transport and recombination in heavily doped silicon: $p_0 D_p$ and L_p .
2. These parameters have been measured in heavily phosphorus doped silicon.
3. With the use of these measured parameters, accurate prediction of the emitter saturation current of bipolar transistors has been demonstrated.

**STUDIES OF OXYGEN-RELATED AND CARBON-RELATED
DEFECTS IN HIGH-EFFICIENCY SOLAR CELLS**

STATE UNIVERSITY OF NEW YORK AT ALBANY

James W. Corbett

We are studying oxygen- and carbon-related defects in silicon, particularly as related to high-efficiency silicon solar cells. We are carrying out a survey of these process-induced defects, of life-time measurement techniques, and of defect aggregates in general. We are carrying out coordinated experimental and theoretical studies of process-induced defects, and have initiated a new series of annealing experiments, including flash-lamp heating of "as-received," pre-heat-treated and homogenized samples, using DLTS, IR, TEM, positron annihilation, and, as needed, EPR and x-ray scattering studies.

PRECEDING PAGE BLANK NOT FILMED

HIGH-EFFICIENCY DEVICE RESEARCH

Isolated oxygen is an interstitial (O_i) in a puckered bond-centered position as shown in Fig. 1. This defect is NOT electrical active. It has several infra-red bands, the one

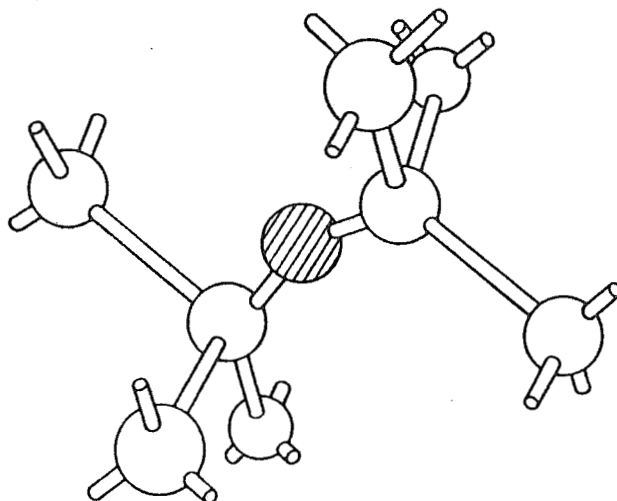


Figure 1. Configuration of interstitial oxygen in the silicon lattice.

that will concern us being at ca. 1100 cm^{-1} . But oxygen in Czochralski-grown silicon is supersaturated with oxygen at all practical temperatures for processing and use, and oxygen does a number of strange and wonderful things. These are outlined in Fig. 2. There appear now to be (at least) two lines of precipitation for oxygen. One line progresses through the original thermal donors (found first by Fuller et al. in 1955, before it was known that oxygen is in the lattice), to the $\langle 110 \rangle$ rods (shown by Bourret to be coesite, a high pressure phase of silica - SiO_2) with their associated extrinsic/interstitial dislocation dipoles. It is presumed that interstitials are emitted in this precipitation process; we have shown that the emission of $\text{Si}=\text{O}$ is energetically favorable vs a silicon interstitial, and that this option may be operative at high temperatures and in oxidation processes. Note that this line of precipitation does not persist to high

HIGH-EFFICIENCY DEVICE RESEARCH

temperatures, i.e., the rods (and dislocations dipoles) dissolve in favor of the second line of precipitation.

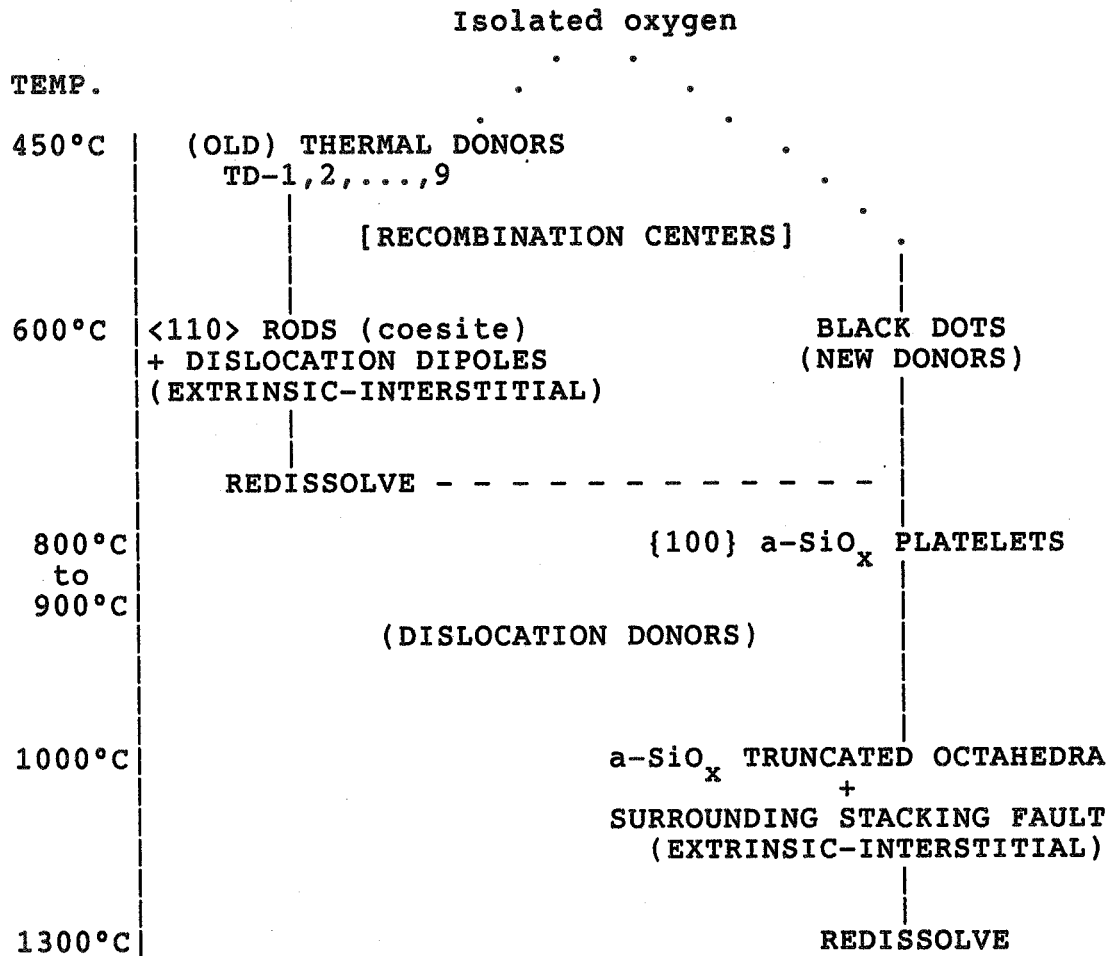


Figure 2. Summary of oxygen processes in silicon.

HIGH-EFFICIENCY DEVICE RESEARCH

The second line of precipitation is first evident with "black dots" in transmission electron microscopy experiments. These grow into amorphous SiO_x defects, {100} platelets at higher temperatures and into truncated octahedra at even higher temperatures. Then at temperatures approaching the melting point of silicon (e.g., 1300°C) the precipitated oxygen dissolves into the isolated interstitials that we started with. Depending on the thermal cycling that the samples experience, the precipitates can give rise to prismatic dislocation loops, and other dislocation networks.

At 450°C recombinations centers appear along with the thermal donors. It is not clear which of the lines of precipitation they belongs to, or if either, but these centers are oxygen dependent.

Thus oxygen introduces shallow donors and centers deep in the forbidden gap. But the defects produced by oxygen precipitation also provide gettering centers for recombination centers, e.g., the iron-group transitions elements, which tend to be fast diffusers. It is not exactly clear how this gettering works, but it is known that iron and copper precipitate at different sites.

And the means by which oxygen precipitates is still not certain. Kaiser, Frisch and Reiss argued that the main features of the formation of the (old) thermal donors could be explained as the sequential agglomeration of oxygen atoms. The difficulty was that the mobility of the oxygen is not sufficient to account for the rate of thermal donor formation. In verifying our earlier measurements of the diffusion coefficient of oxygen with an activation energy of 2.54 eV, Stavola et al. found that in "as-received" samples the oxygen motion occurs with an activation energy of 1.9 eV. This anomalous diffusion has been presumed to be defect-assisted.

HIGH-EFFICIENCY DEVICE RESEARCH

In irradiated silicon we had earlier established the (vacancy+oxygen) center, $(V \cdot O)$, as shown in Fig. 3. [We also

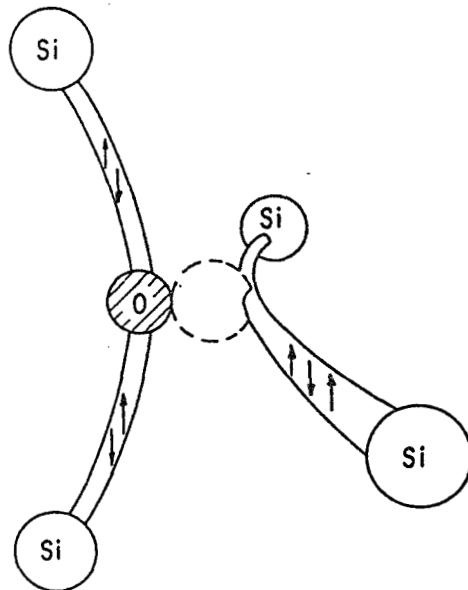


Fig. 3. The (vacancy + oxygen) center in silicon.

found $(V_2 \cdot O)$, $(V_2 \cdot O_2)$, $(V_3 \cdot O)$, $(V_3 \cdot O_2)$, and $(V_3 \cdot O_3)$ centers but they will not concern us here.] When the $(V \cdot O)$ center disappears on annealing, the $(V \cdot O_2)$ center is created (see

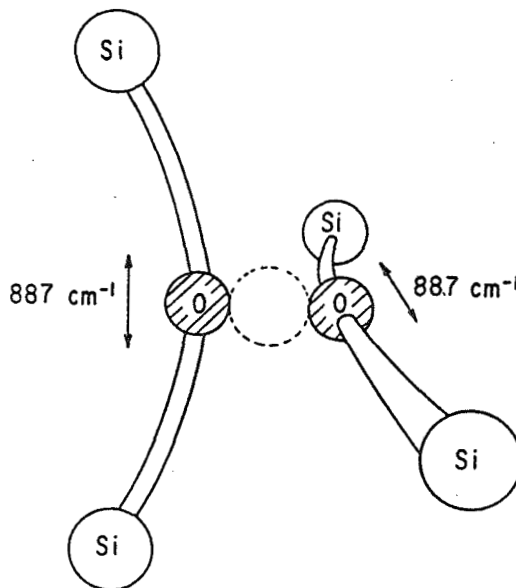


Fig. 4. The (vacancy + two-oxygen) center in silicon.

HIGH-EFFICIENCY DEVICE RESEARCH

Fig. 4), as we have recently verified by studying the dependence of the formation of this defect on the oxygen concentration. Subsequent annealing of this center leads to a $(V \cdot O_3)$ center, or what might be called a $(V \cdot O_2) + O_i$ center, as shown in Fig. 5.

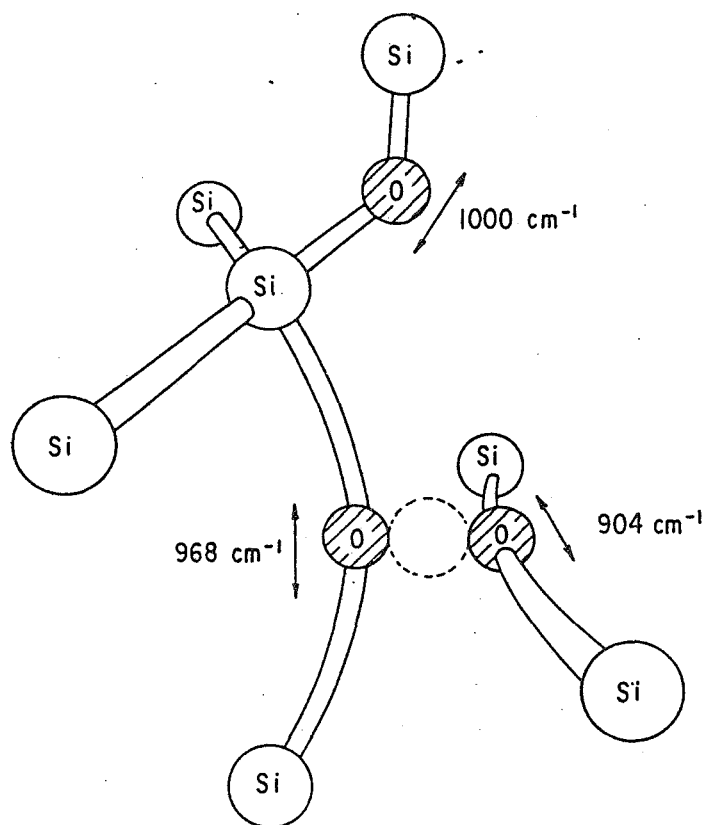


Fig. 5. $(V \cdot O_2) + O_i$ center in silicon.

In recent studies we have found that the growth of the $(V \cdot O_2)$ band is characterized by a ~ 1.9 eV activation energy, i.e., essentially the same as the anomalous diffusion of Stavola *et al.* (See Fig. 6) This argues that the anomalous diffusion occurs by the dissociation of the $(V \cdot O)$ center,

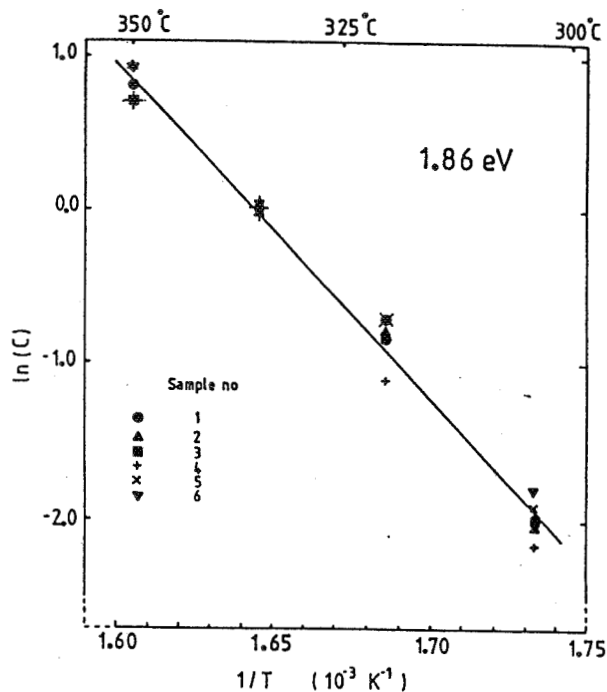
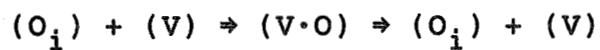
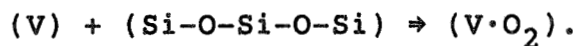


Fig. 6. Arrhenius plot for the growth of the $(V \cdot O_2)$ defect.

with that process causing the O_i to move through the lattice, e.g.,



and the growth of the $(V \cdot O_2)$ by the free vacancy encountering two adjacent oxygens, e.g.,



This important advance needs further experiments to test its several implications, and these experiments are being done.

HIGH-EFFICIENCY DEVICE RESEARCH

In related studies we have found that infra-red bands associated with thermal donors can be found in floating-zone silicon (i.e., low-oxygen) silicon that has been neutron-irradiated in transmutation doping. Thus the vacancies created in that process can substantially accelerate defects agglomeration, a point that also is important in ion-implantation.

As is seen in Fig. 2, there are nine different thermal donors which have been resolved by infra-red studies, where they have Rydberg transitions characteristic of double donors. What then are these thermal donors? The consensus is that they consist of a core (or perhaps there are several such cores) which has a double plus charge state, that the Rydberg states arise from the attraction of electrons to this double plus center, and that successive donors occur as additional oxygens are added to, or adjacent to, this core. We have developed a theory that describes the electrical behavior of this hierarchy of thermally-induced double donors, including a core and an electronically repulsive oxygen-rich region, which repulsive region grows in size as oxygens are added to the defect. We have succeeded in fitting the perturbation to the ground state energies all nine double donors as shown in Fig. 7.

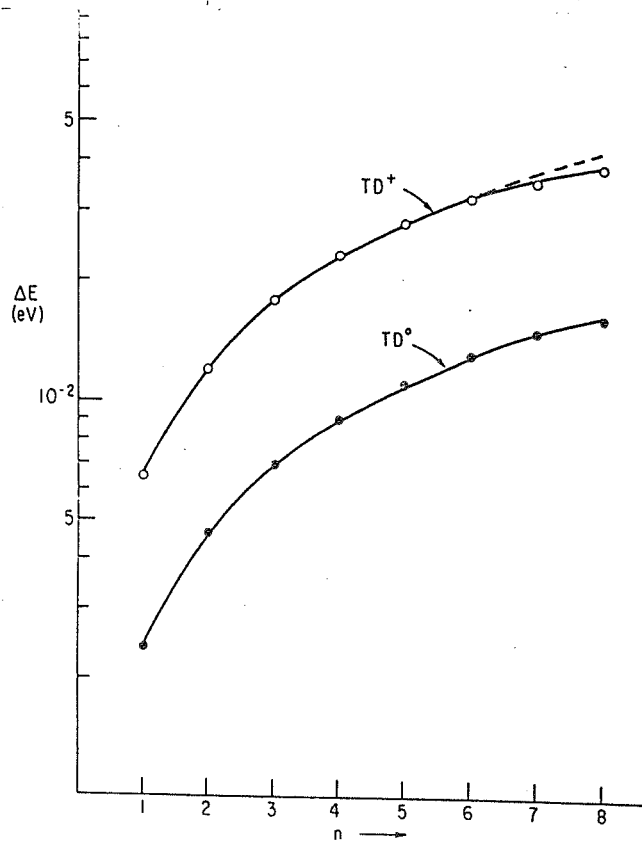


Fig. 7. Perturbation energy for the thermal donor ground states versus added oxygens.

What then is the core (or are the cores)? We have identified the most likely core for the homogeneously-nucleated oxygen precipitate as the "ylid," the saddle-point for oxygen diffusion, stabilized by the presence of two or more additional oxygens. We conclude as well that the precipitation strain-energy can also cause the emission of an interstitial leaving the core as the $(V \cdot O_2)$ center. These processes are consistent with precipitation processes which yield coesite plus interstitial dislocation dipoles. They also provide a mechanism for the loss of thermal donor activity, as is observed, and for the creation of recombination centers. But a number of lines of investigation need to be pursued to be certain of these models.

HIGH-EFFICIENCY DEVICE RESEARCH

Why then the two line of precipitation? Our working hypothesis is that the "black dot" line involves carbon. Since carbon contracts the lattice, it will relieve the strain associated with oxygen agglomeration, delaying the formation of the strain-induced formation of the thermal donors which we employed for the "old" thermal donors. This permits the "new" thermal donors to be associated with carbon, as is observed, and to be more stable. But these matters must be pursued further to achieve certainty.

What about the recombination centers? As we indicated the processes that we have discussed can create recombination centers, e.g. the $(V_2 \cdot O)$, $(V_2 \cdot O_2)$, etc. centers, which we passed over. But the experimental results are becoming quite incisive. Suezawa and Sumino have argued persuasively that one of the thermal donors involves eight oxygens. But just as persuasively Glinchuk et al. have observed a recombination center that contains eight oxygens!

Clearly the agglomeration can follow several paths, and much needs to be done to sort out these matters. Still we have made great progress.

COMPREHENSIVE SOLAR CELL MODELING AND CORRELATION STUDIES

RESEARCH TRIANGLE INSTITUTE

M. L. Lamorte

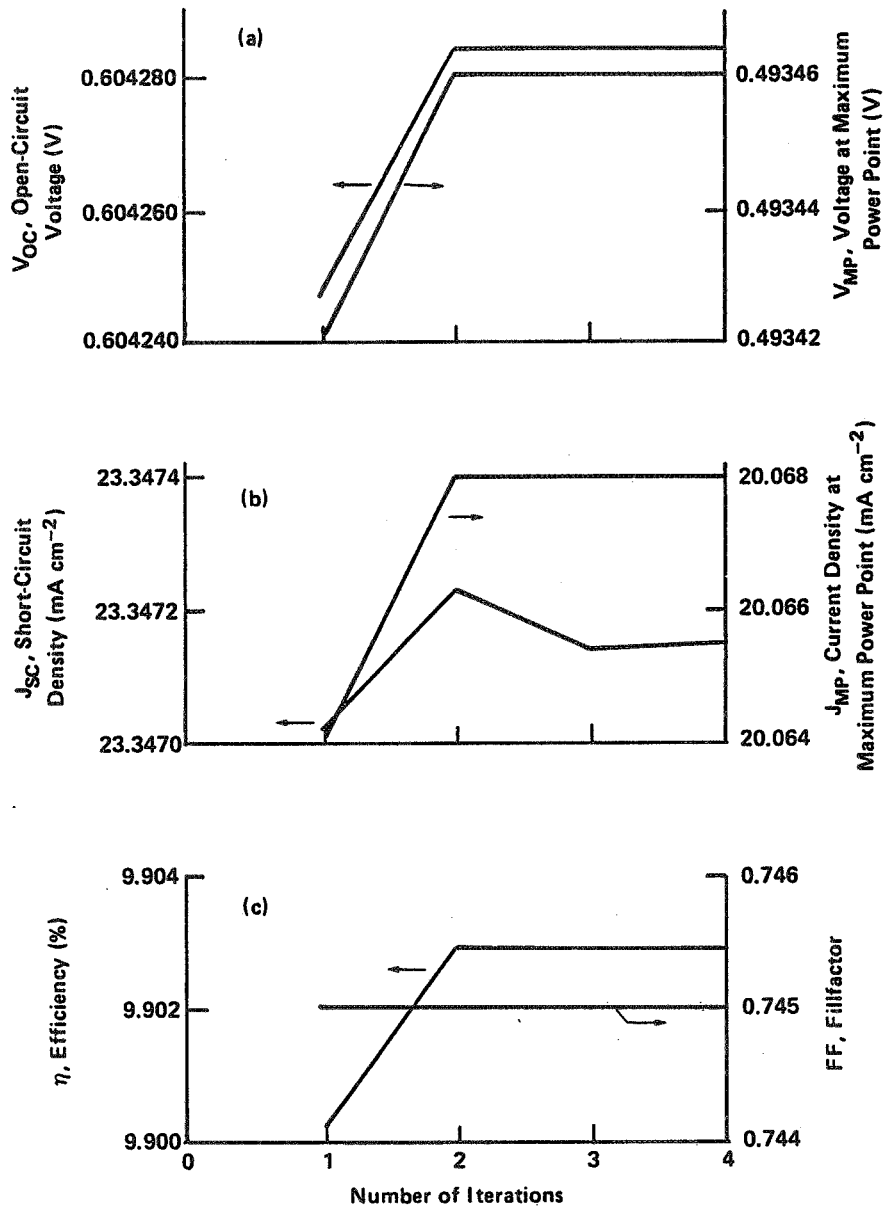


Figure 1. Solar cell terminal characteristics vs. number of iterations: (a) open-circuit and maximum power point voltages; (b) short-circuit and maximum power point current densities; and (c) efficiency and fillfactor. Twenty mesh points, twelve junction photovoltage simulations, and twenty V-I points were used.

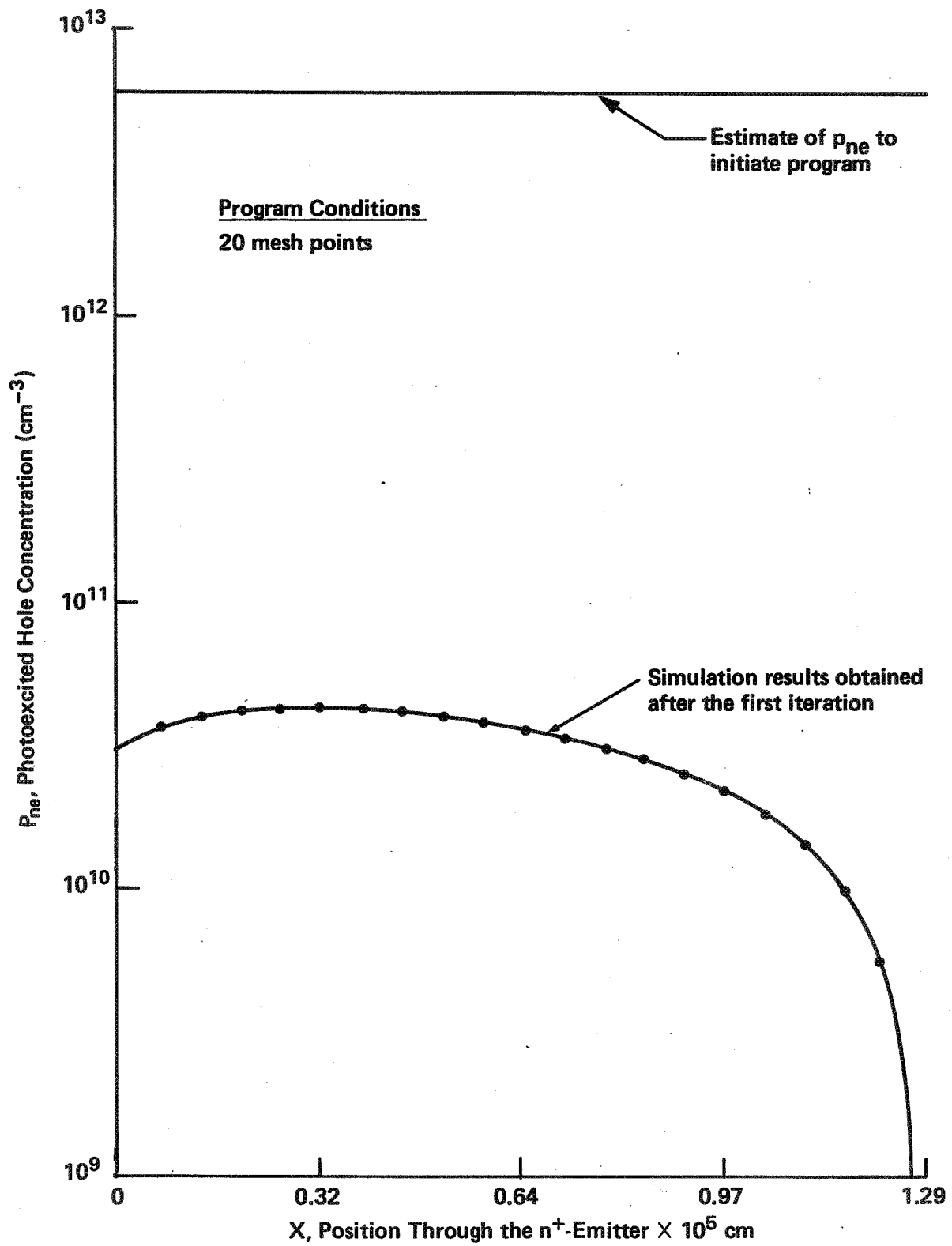


Figure 2. Photoexcited hole concentration vs. position in the n^+ -emitter.

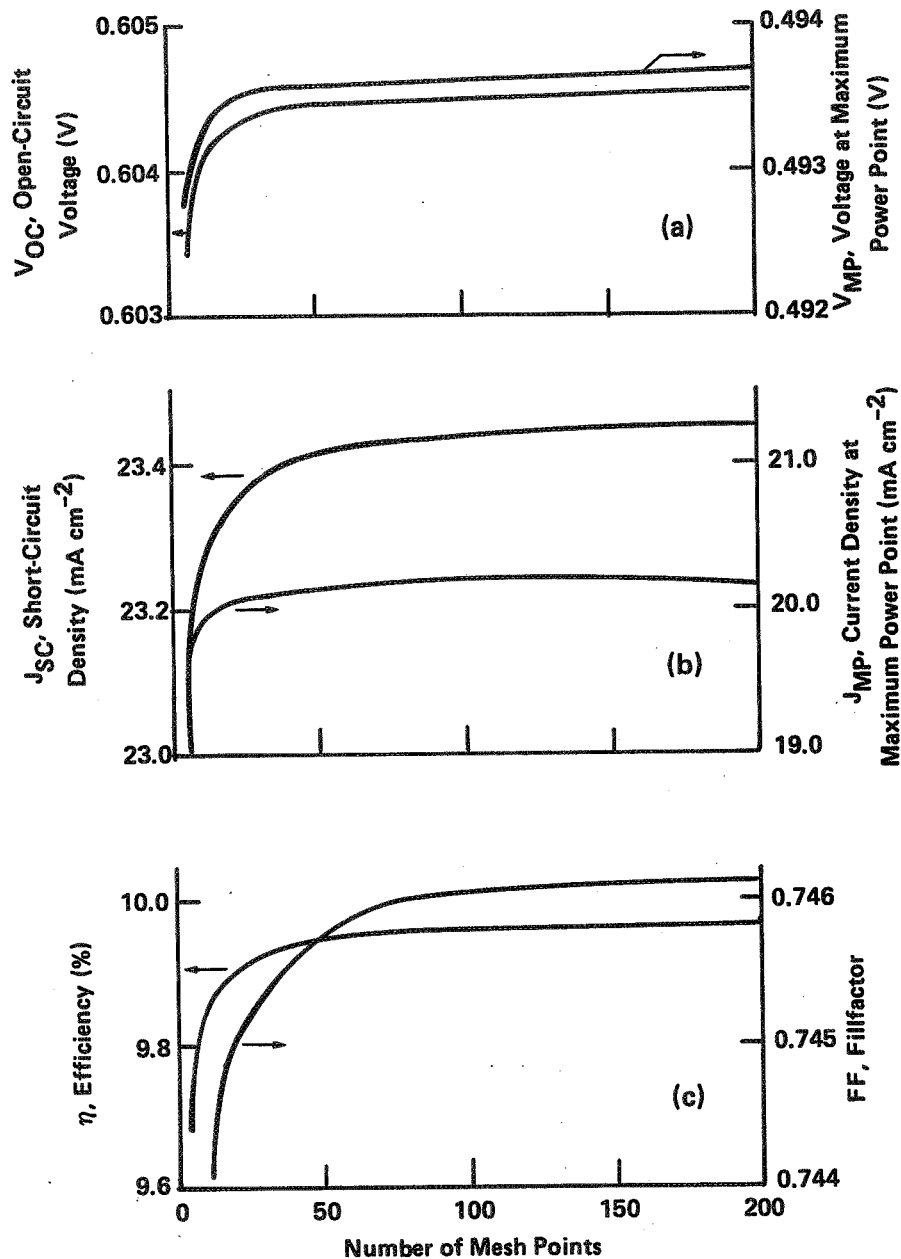


Figure 3. Solar cell terminal characteristics vs. number of mesh points: (a) open-circuit and maximum power point voltages; (b) short-circuit and maximum power point current densities; and (c) efficiency and fillfactor. Three iterations per mesh point, twelve junction photovoltage simulations, and twenty V-I points were used.

HIGH-EFFICIENCY DEVICE RESEARCH

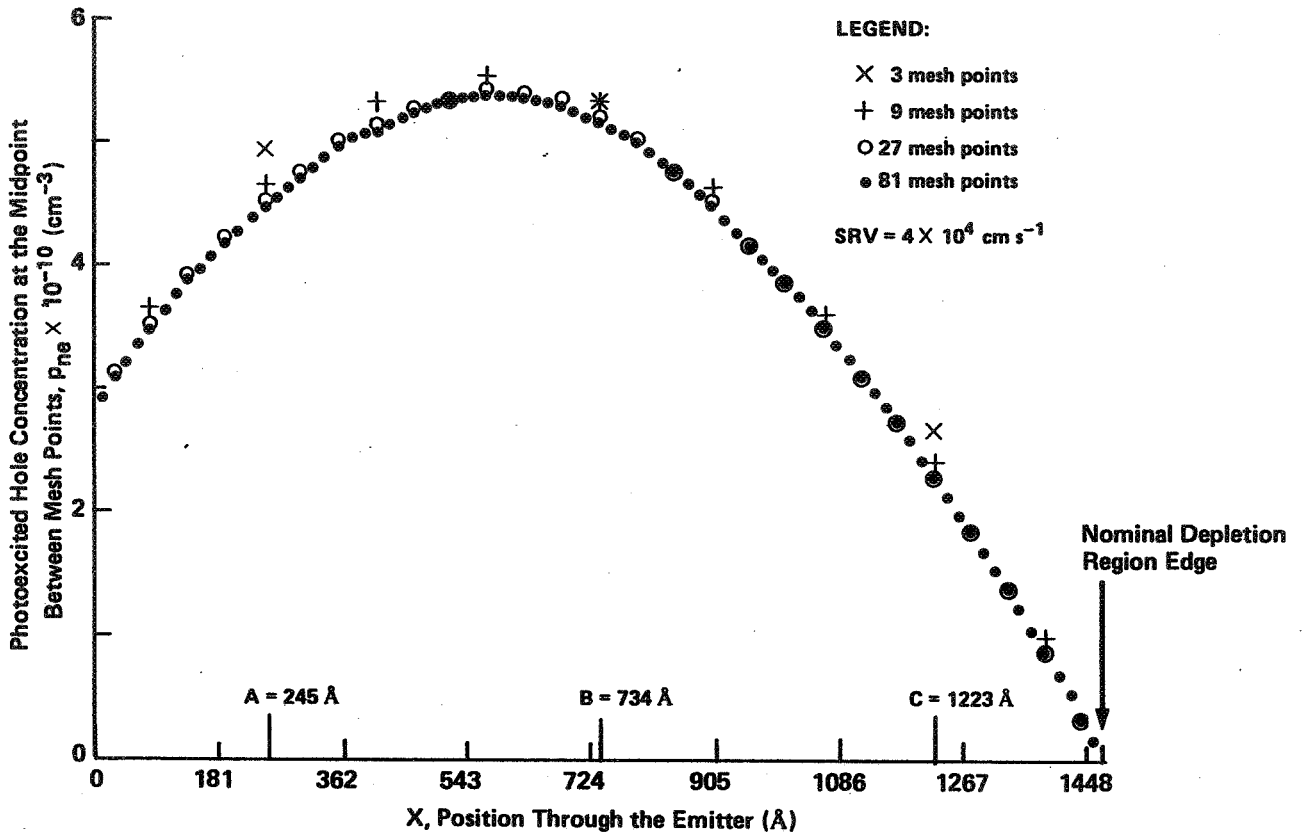


Figure 4. Photoexcited hole concentration calculated midway between mesh points in the n^+ -emitter for 3, 9, 27, and 81 mesh points under short-circuit conditions and for three iterations per mesh point.

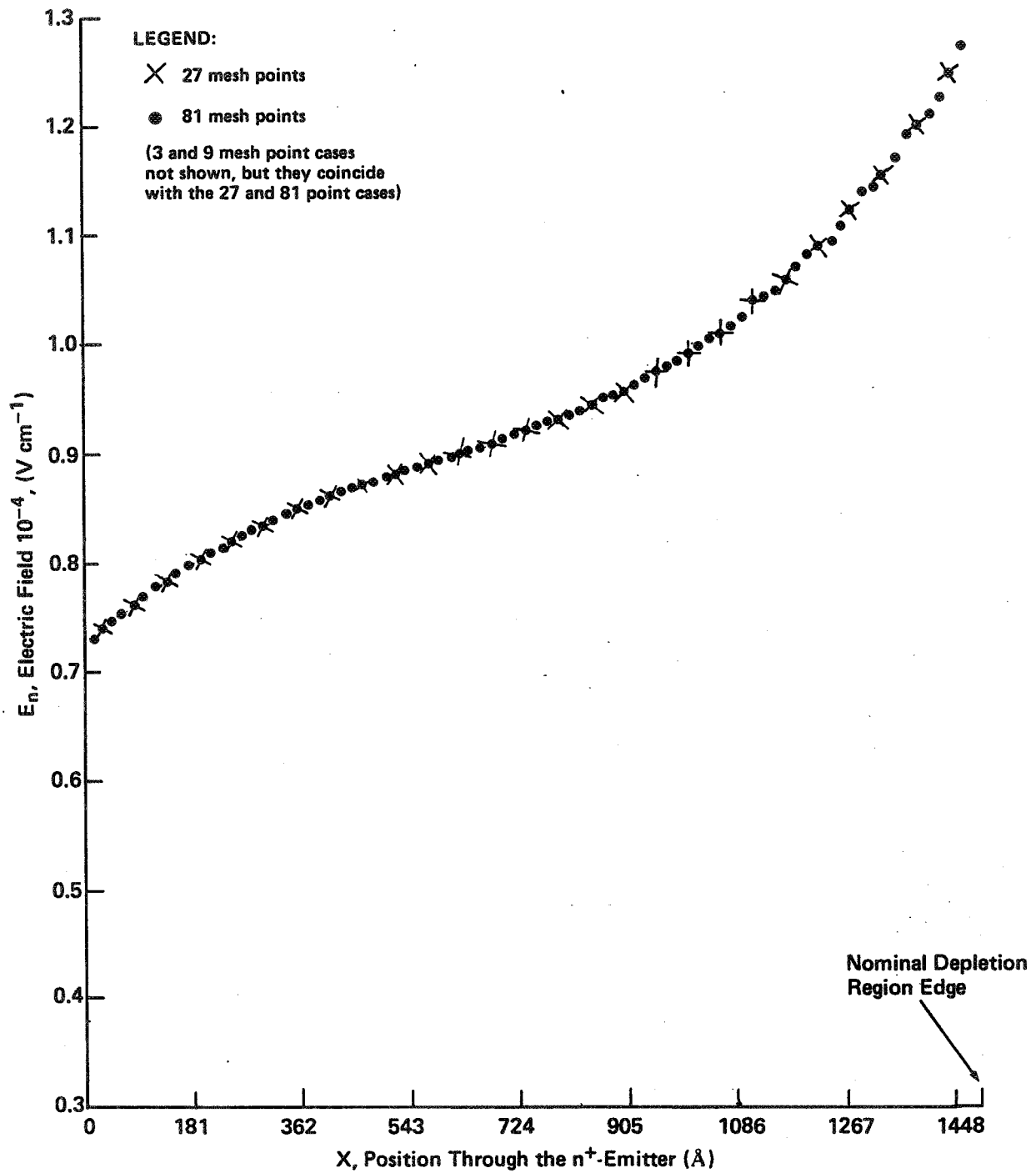


Figure 5. Built-in electric field vs. position in the n^+ -emitter of a solar cell using 27 and 81 mesh points under short-circuit current conditions and for three iterations per mesh point.

HIGH-EFFICIENCY DEVICE RESEARCH

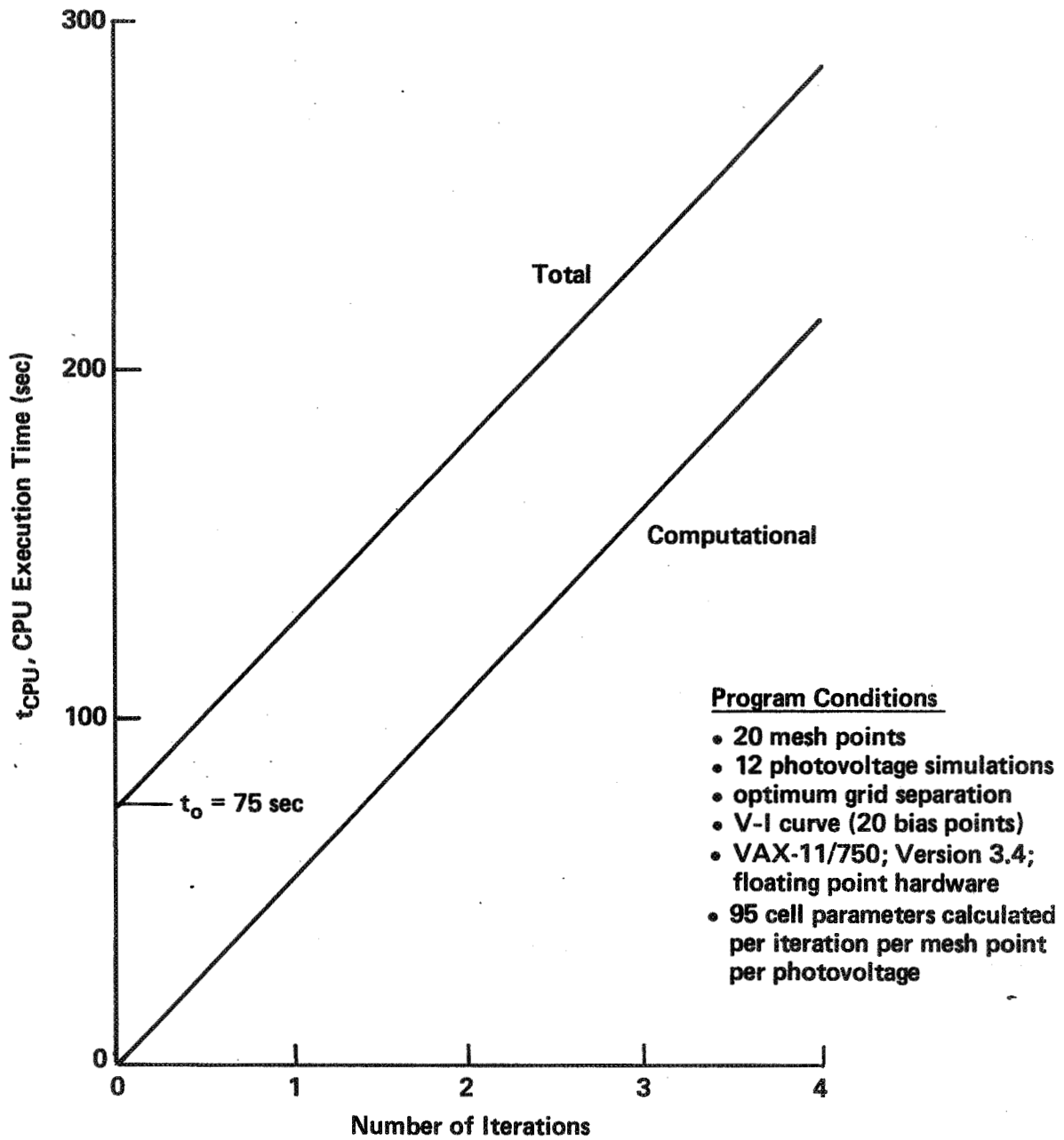


Figure 6. CPU execution time vs. number of iterations using 20 mesh points and 12 photovoltage simulations.

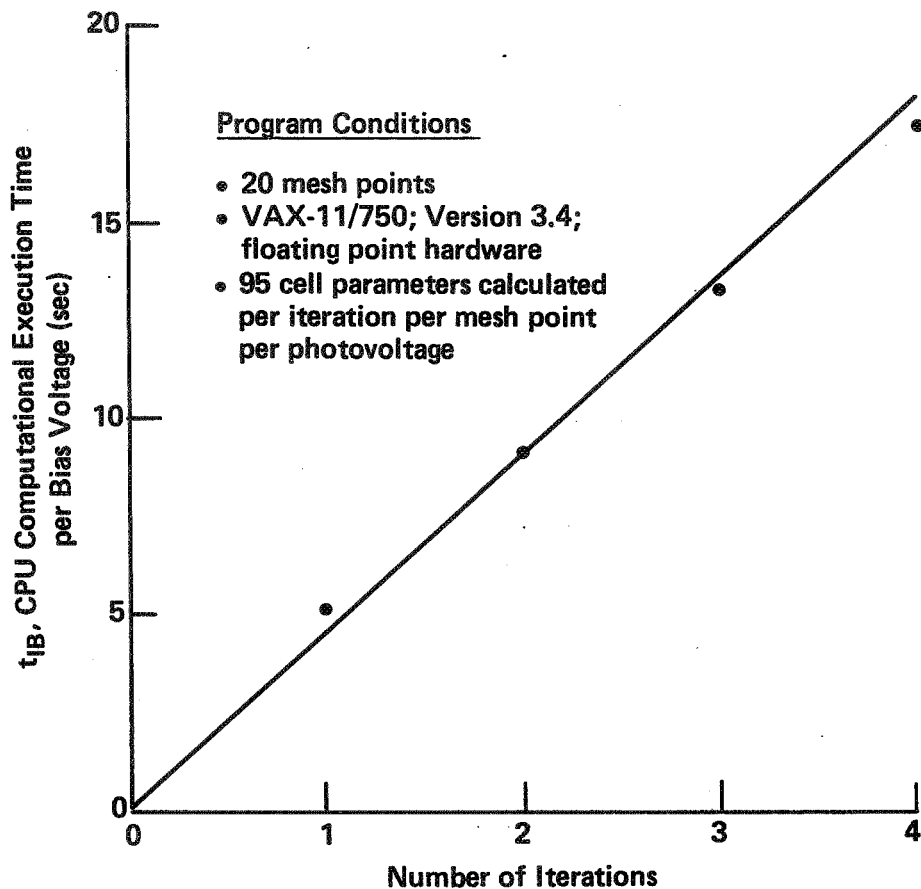


Figure 7. CPU computational time per photovoltage vs. number of iterations per mesh point using 20 mesh points.

HIGH-EFFICIENCY DEVICE RESEARCH

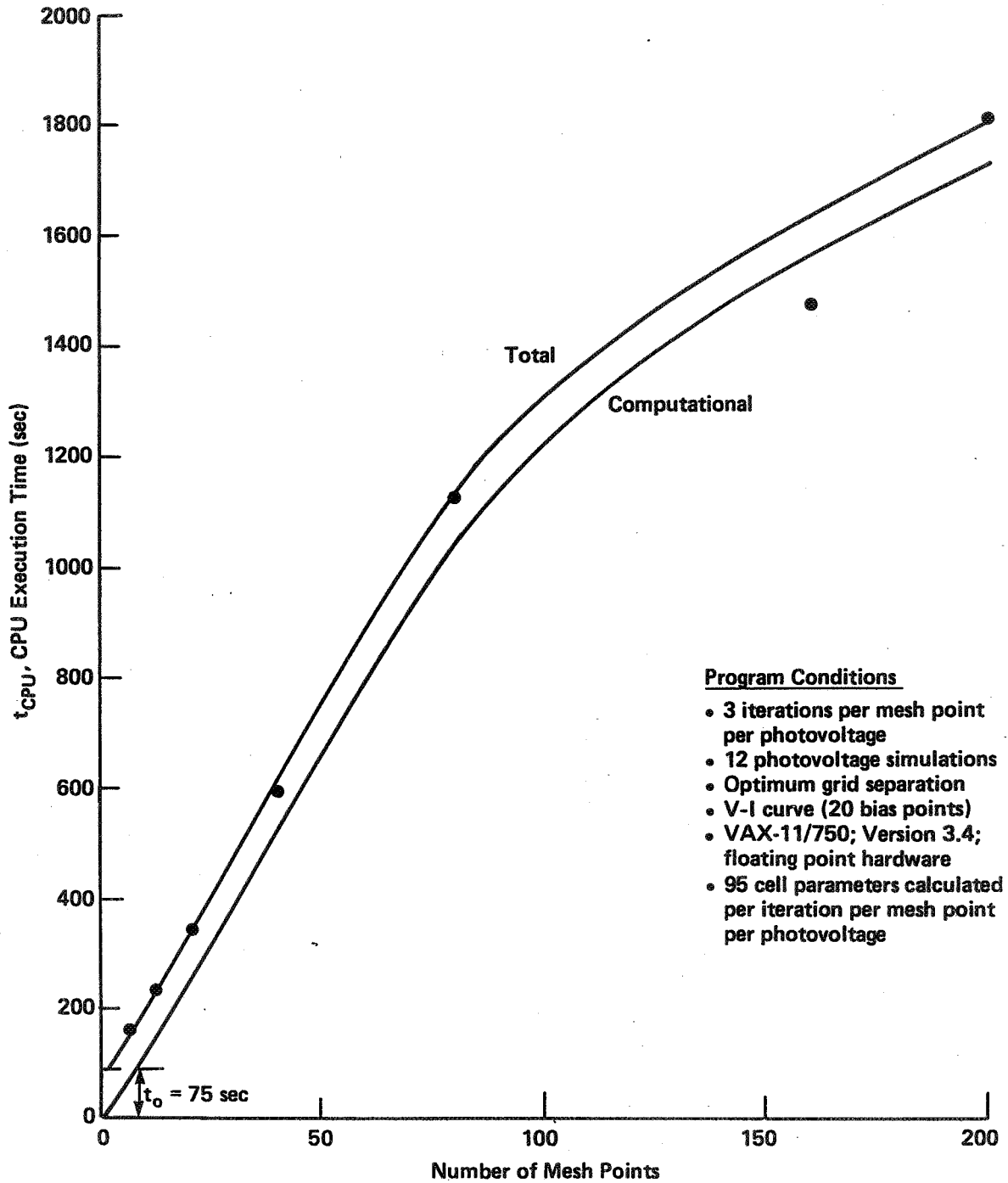


Figure 8. CPU execution time vs. number of mesh points using three iterations per mesh point and 12 photovoltage simulations.

HIGH-EFFICIENCY DEVICE RESEARCH

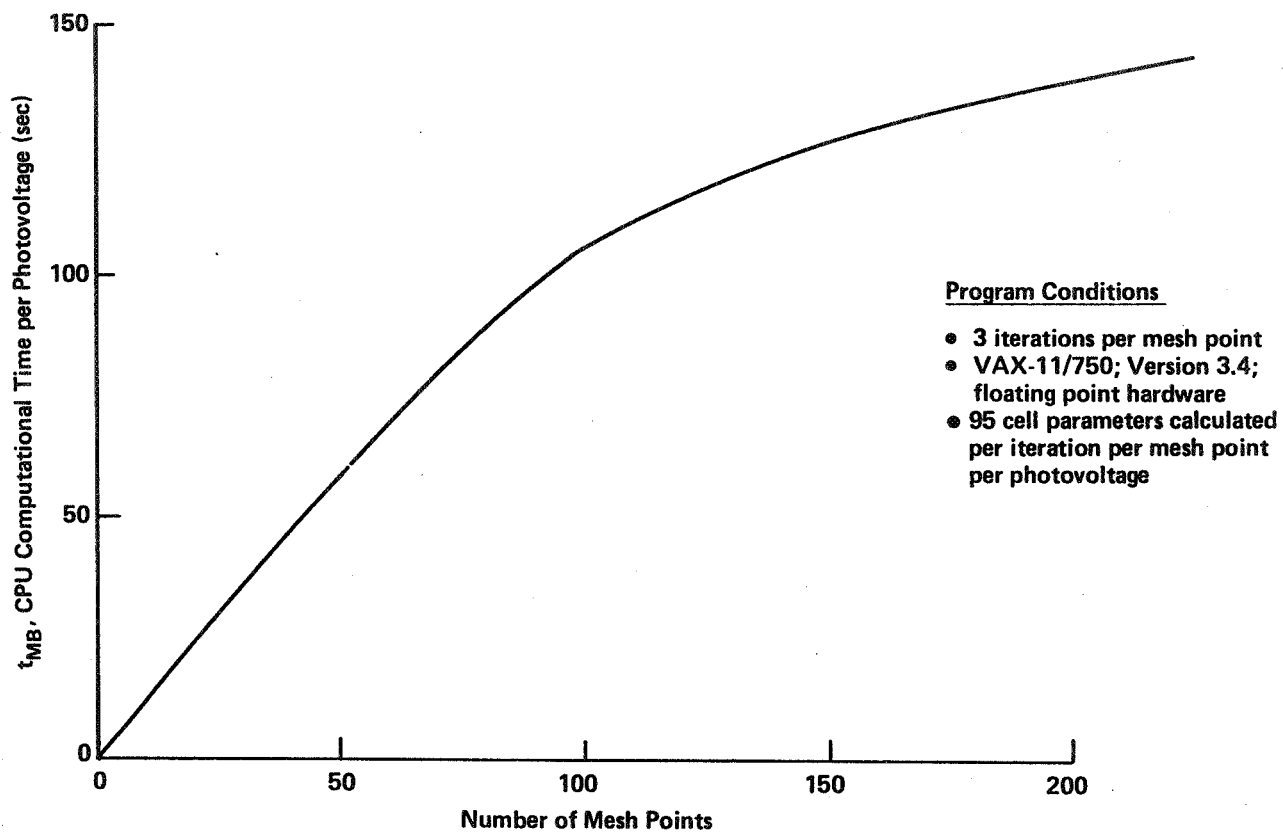


Figure 9. CPU computational time per photovoltage vs. number of mesh points using three iterations per mesh point.

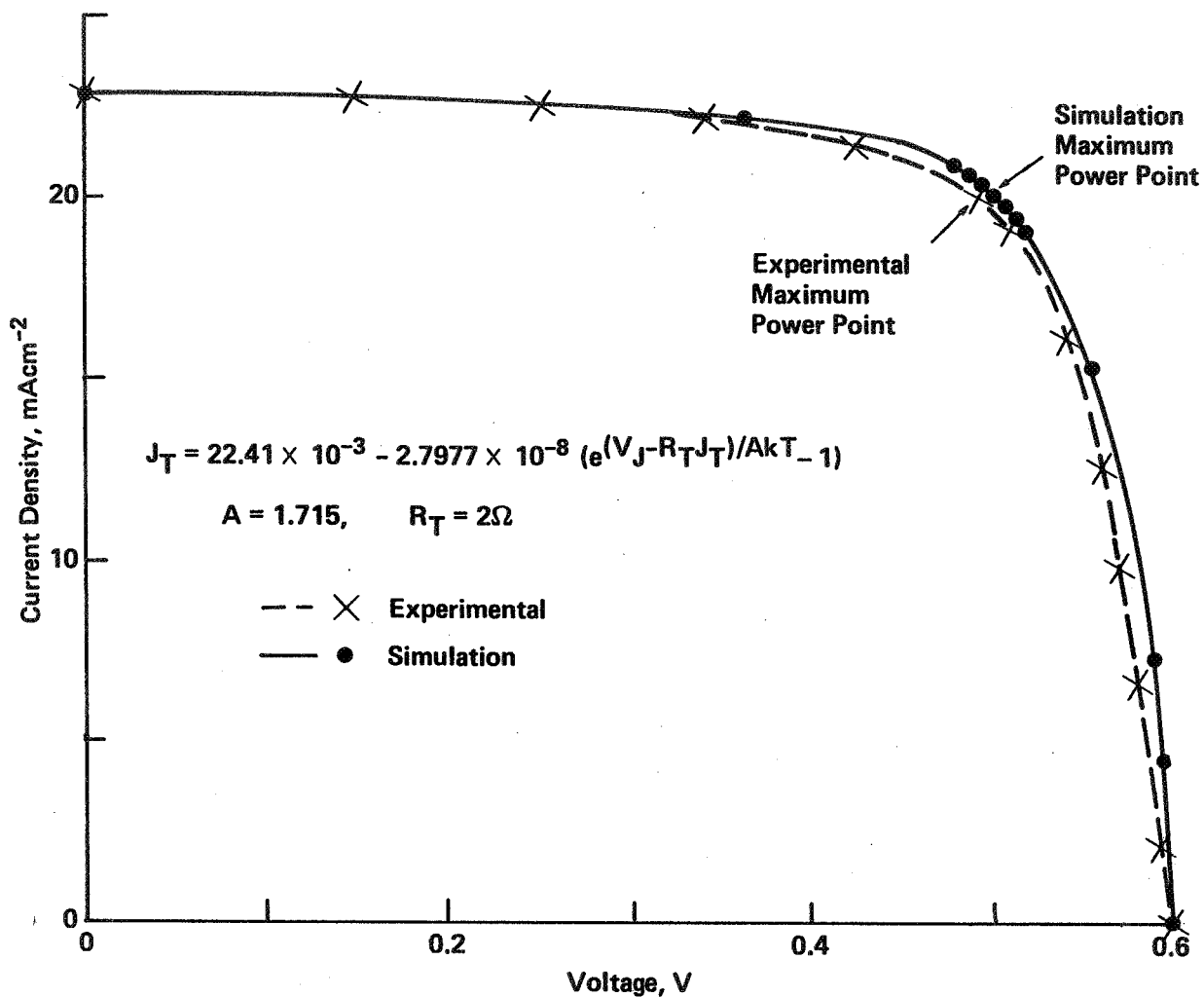


Figure 10. Simulated and experimentally determined V-I curve for cell No. 24C at 300 K, and the simulated diode equation.

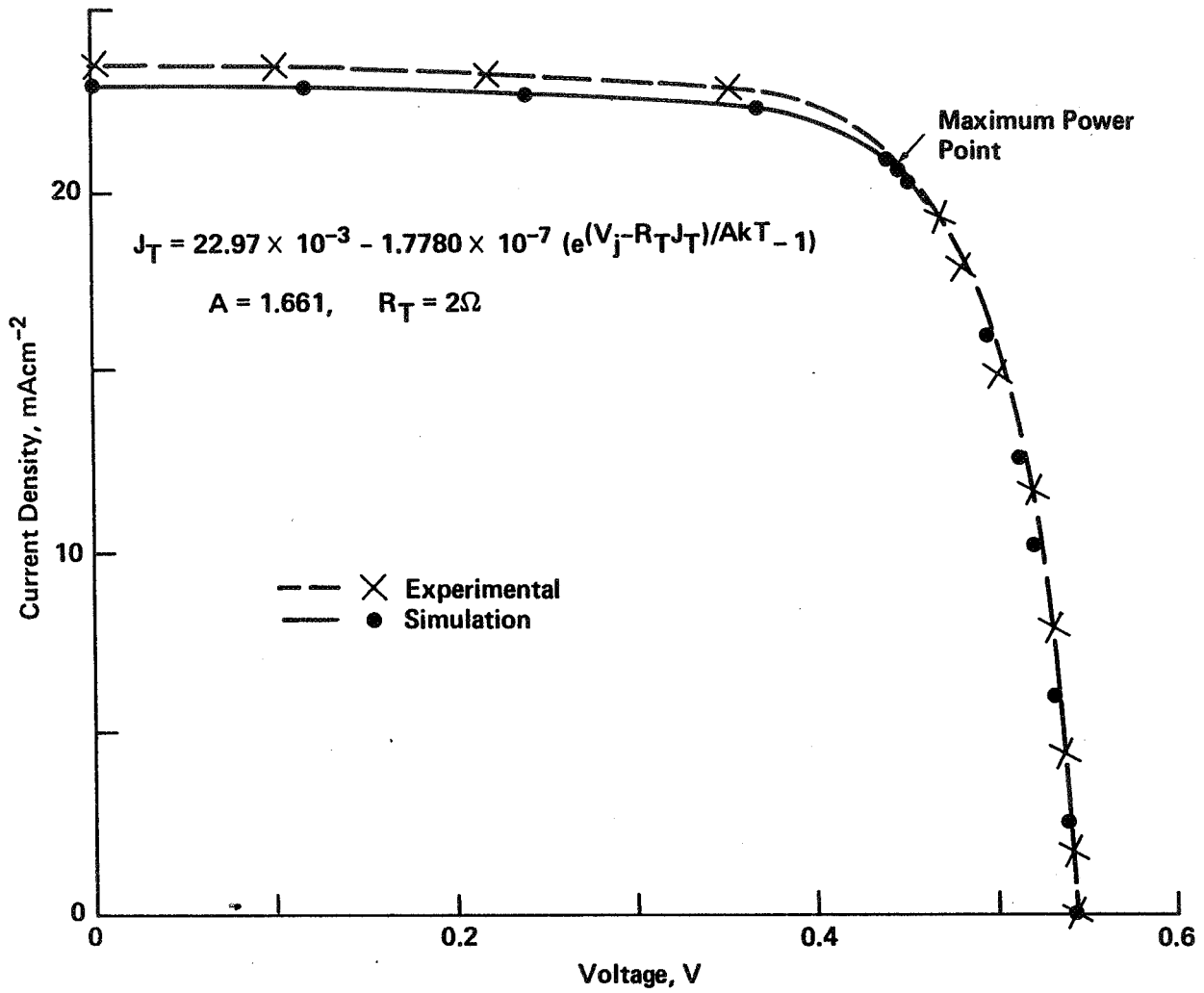


Figure 11. Simulated and experimentally determined V-I curve for cell No. 24C at 326 K and the diode equation obtained from the simulation program.

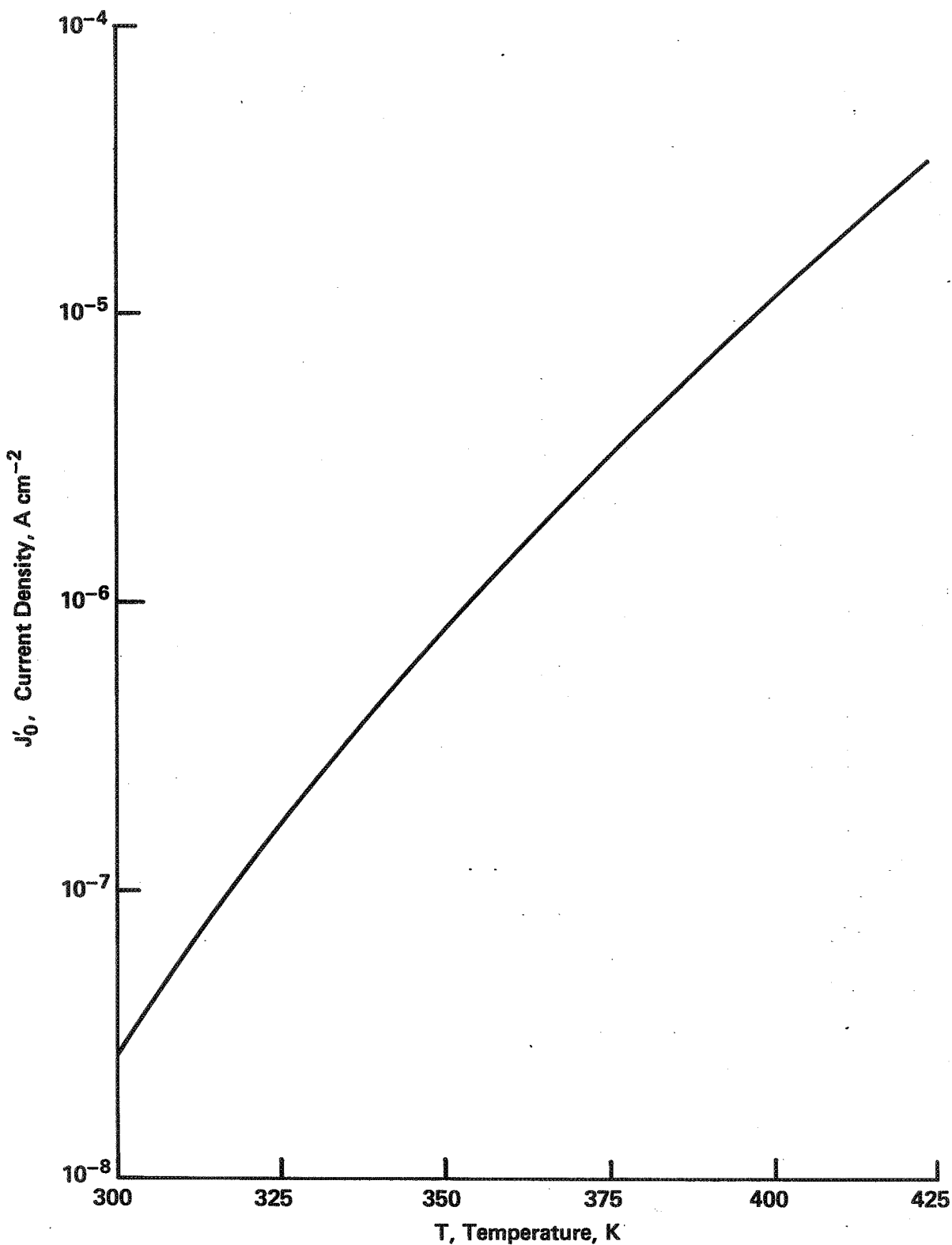


Figure 12. Equivalent saturation current density vs. temperature for cell No. 24C, obtained from simulation results.

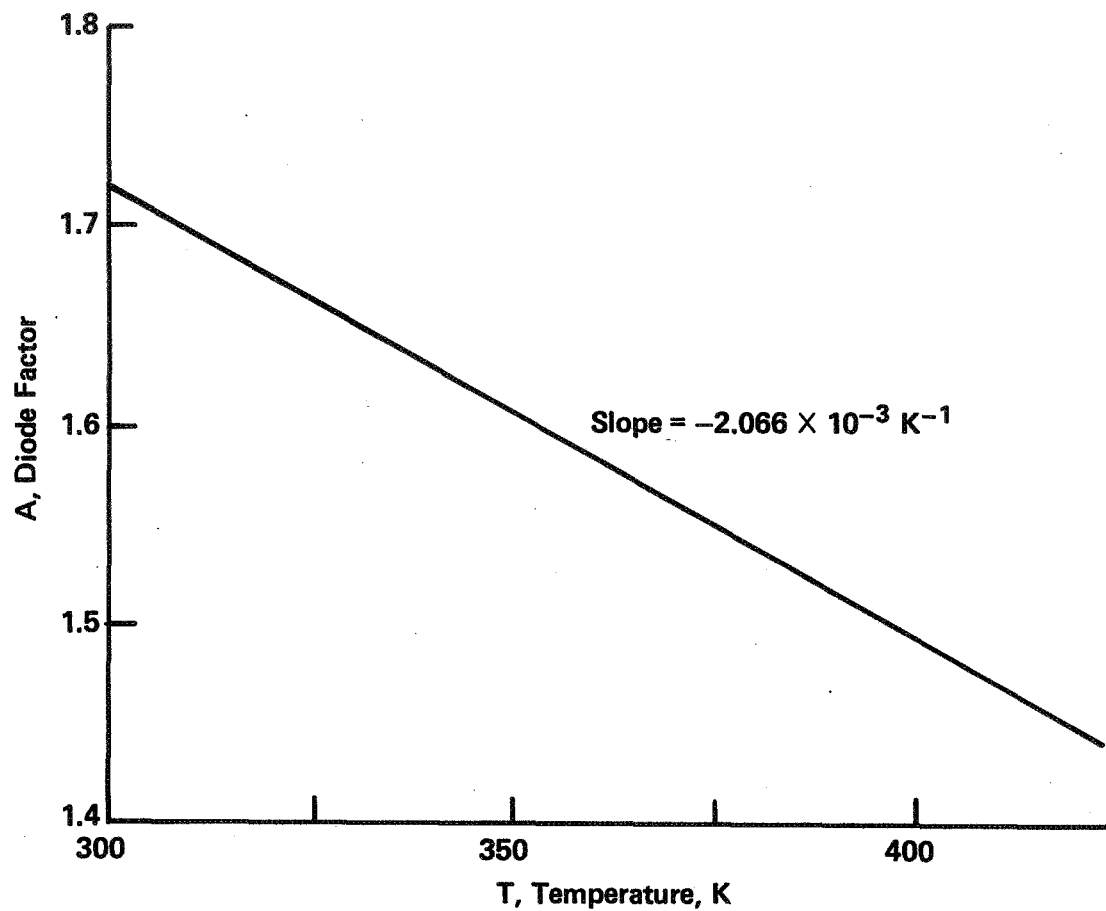


Figure 13. Diode factor vs. temperature for cell No. 24C, obtained from simulation results.

HIGH-EFFICIENCY DEVICE RESEARCH

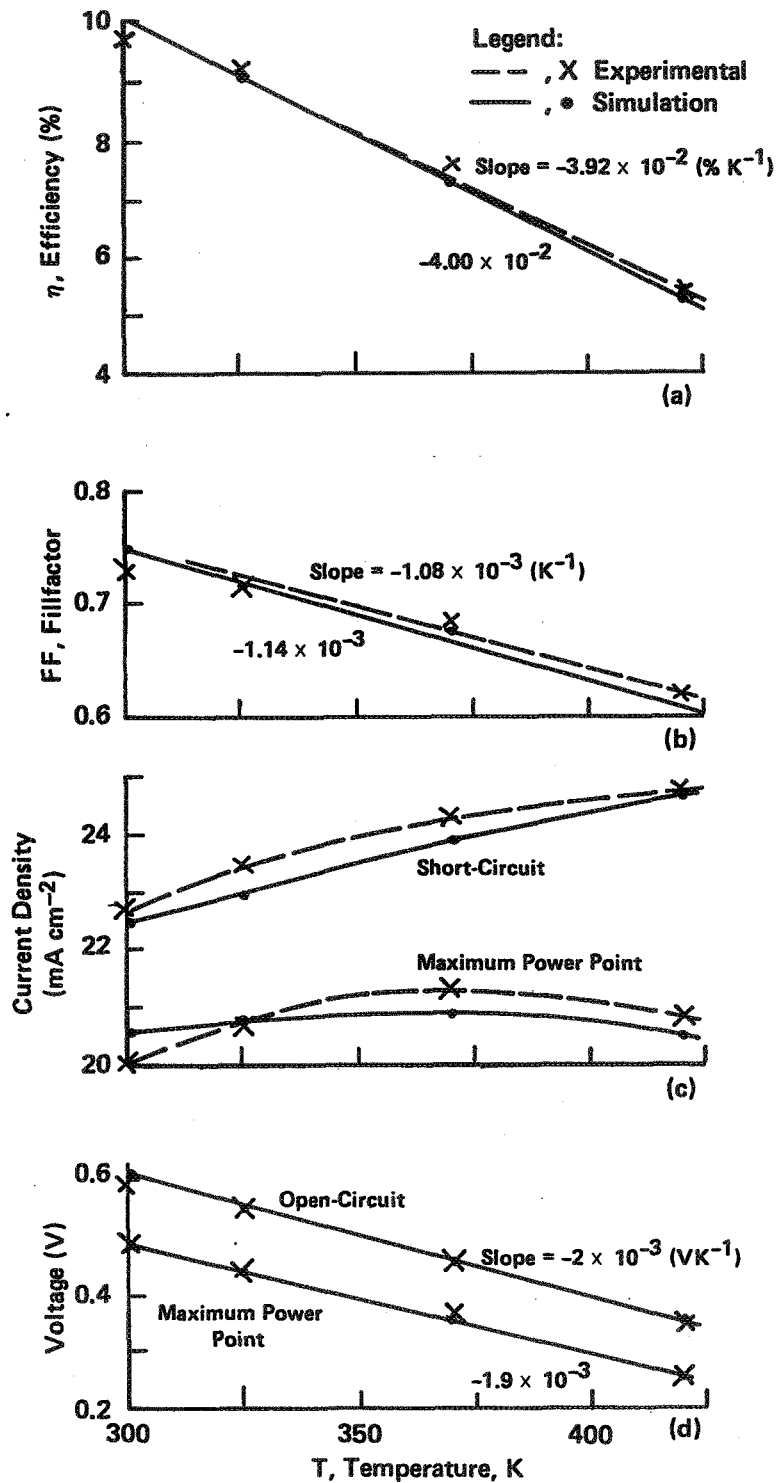


Figure 14. Simulation and experimental behavior of device terminal characteristics are presented over the temperature range of 300 to 421 K for solar cell No. 24C. Temperature coefficients represented by corresponding slopes are also shown where the slope is uniquely defined.

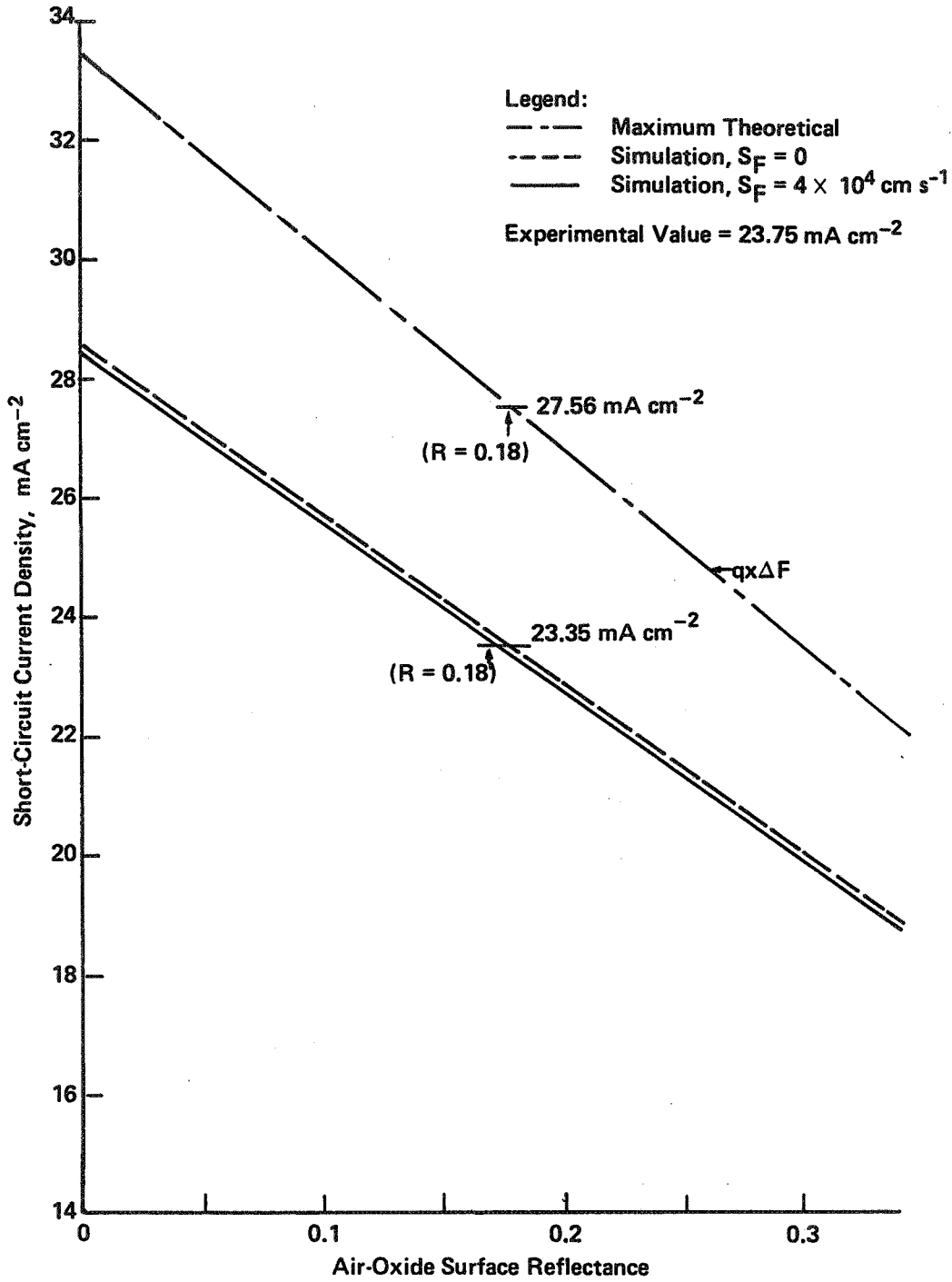


Figure 15. Maximum theoretical and simulation values of short-circuit current density vs. air-oxide reflectivity for cell No. 24C where shadowing correction is not made. Maximum theoretical current is calculated independently of the model and is based only on the absorbed photon flux and assuming 100-percent collection efficiency.

C-5

HIGH-EFFICIENCY DEVICE RESEARCH

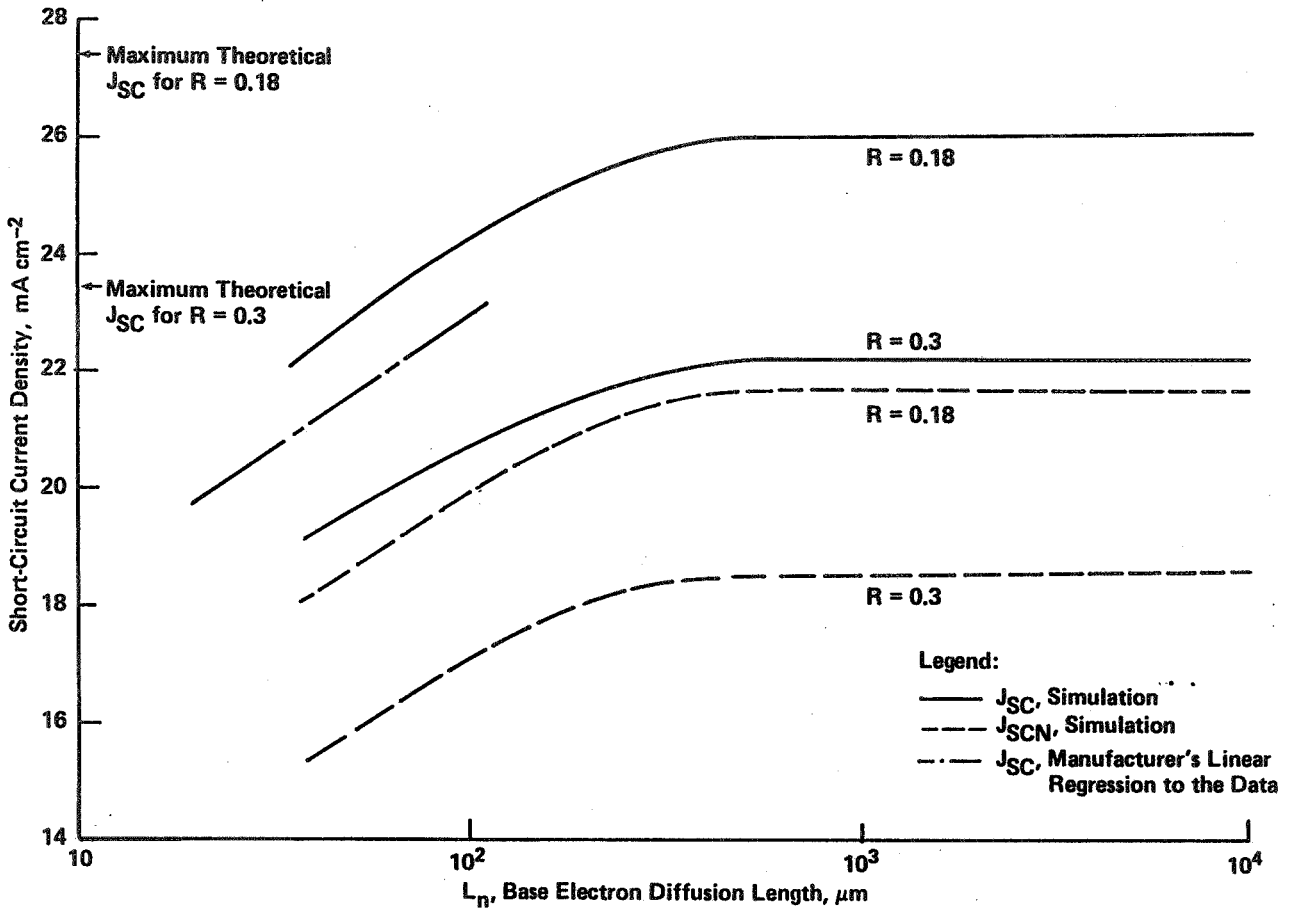


Figure 16. Simulation of total and base region electron contribution to short-circuit current density and linear regression to experimental data at 300 K. Maximum theoretical current is calculated independently of the model and is based only on the absorbed photon flux and assuming 100 percent collection efficiency.

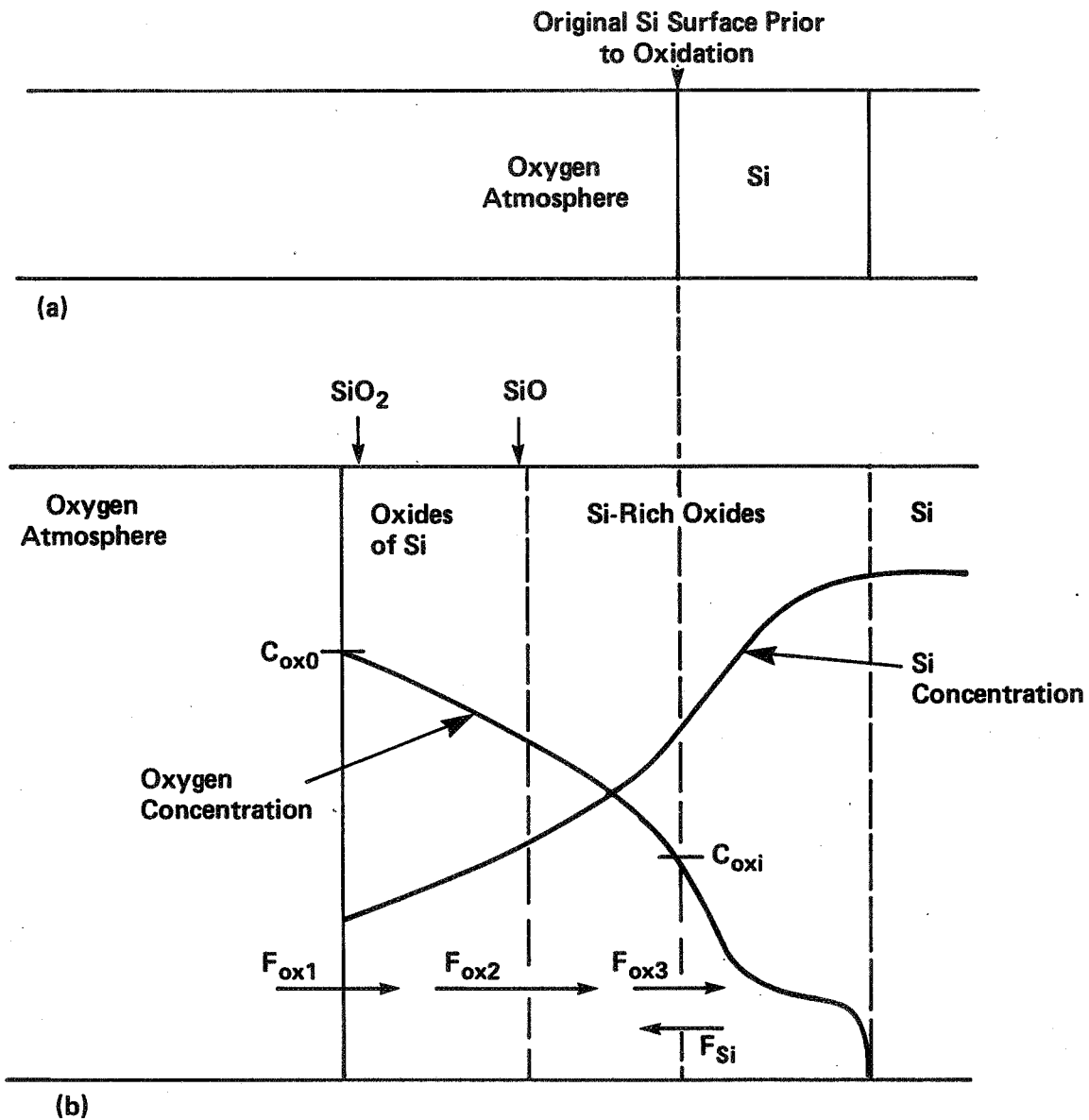


Figure 17. One-dimensional model representing the thermally grown Si-rich oxides: (a) prior to oxidation; and (b) during oxidation.

HIGH-EFFICIENCY DEVICE RESEARCH

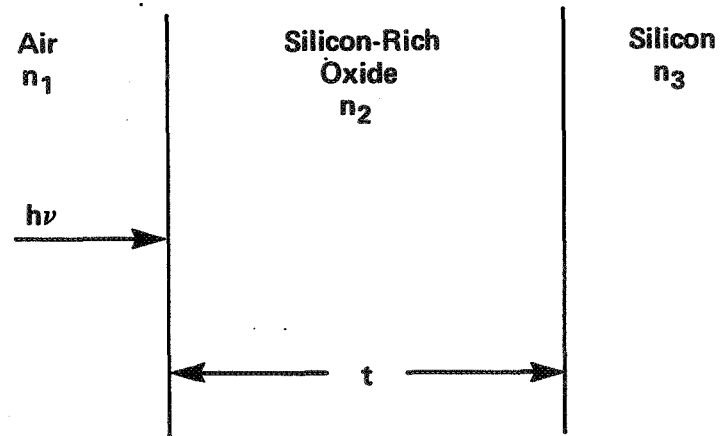


Figure 18. Model of thin film oxide on silicon under normal incidence.

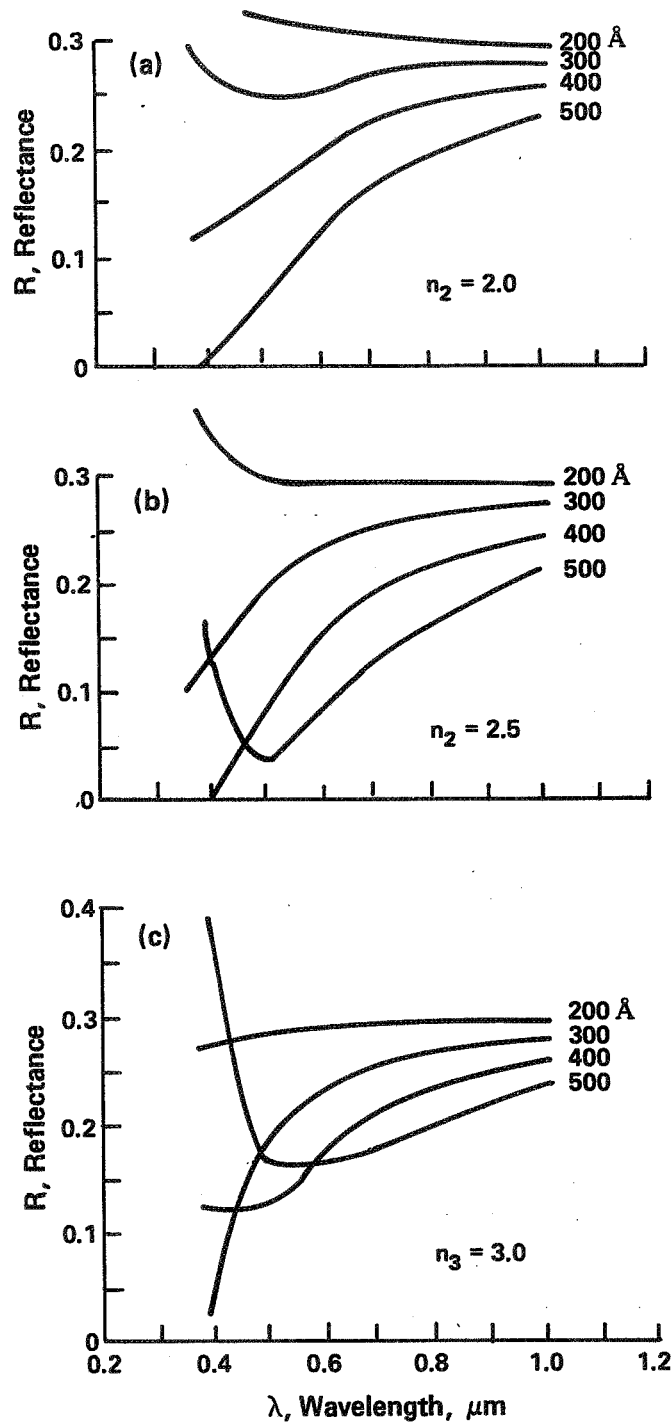


Figure 19. Reflectance under normal incidence at the air-oxide interface vs. wavelength for refractive indices representing silicon-rich oxides: (a) 2.0; (b) 2.5; and (c) 3.0. Oxide thickness is a parameter.

HIGH-EFFICIENCY DEVICE RESEARCH

Table 2. Photoexcited hole concentrations, their derivatives, and the percent differences in an n^+ -emitter region at three points (A, B, and C), for four mesh point distributions (3, 9, 27, 81) using three iterations at each mesh point.

Location	I, Emitter Mesh Points	P_{ne1} cm^{-3}	$\frac{dp_{ne1}}{dx}$ cm^{-4}	$\frac{P_{ne1} - P_{ne(81)}}{P_{ne(81)}} \times 10^2$ %	$\frac{\frac{dp_{ne1}}{dx} - \frac{dp_{ne(81)}}{dx}}{\frac{dp_{ne(81)}}{dx}} \times 10^2$ %
A = 245 Å	3	$P_{ne1} = 4.9185 \times 10^{10}$	7.4080×10^{15}	+10.1	+47.3
	9	$P_{ne2} = 4.6128 \times 10^{10}$	5.3105×10^{15}	+3.3	+5.6
	27	$P_{ne5} = 4.5050 \times 10^{10}$	5.0746×10^{15}	+0.9	+0.9
	81	$P_{ne(14)} = 4.4670 \times 10^{10}$	5.0286×10^{15}	—	—
A = 734 Å	3	$P_{ne2} = 5.2937 \times 10^{10}$	-3.8439×10^{15}	+2.8	-36.4
	9	$P_{ne5} = 5.2697 \times 10^{10}$	-3.0244×10^{15}	+2.3	-7.3
	27	$P_{ne(14)} = 5.1820 \times 10^{10}$	-2.8725×10^{15}	+0.6	-1.9
	81	$P_{ne(41)} = 5.1504 \times 10^{10}$	-2.8181×10^{15}	—	—
A = 1223 Å	3	$P_{ne3} = 2.6625 \times 10^{10}$	-6.9382×10^{15}	+16.9	+11.7
	9	$P_{ne8} = 2.3454 \times 10^{10}$	-7.8405×10^{15}	+3.0	+0.3
	27	$P_{ne(23)} = 2.2880 \times 10^{10}$	-7.8819×10^{15}	+0.5	-0.3
	81	$P_{ne(68)} = 2.2772 \times 10^{10}$	-7.8618×10^{15}	—	—

HIGH-EFFICIENCY DEVICE RESEARCH

Table 3. Parameters used in the simulation were provided by or deduced from manufacturers' specifications for cell No. 24C.

Cell Type	n+p
Total cell thickness	3.8×10^{-2} cm
Junction depth	1.8×10^{-5} cm
Contact shadowing	4 percent
Front surface concentration	4×10^{19} cm ⁻³
Front surface profile	erfc
Back surface concentration	0
Front SRV	4×10^4 cm S ⁻¹
Back SRV	3×10^3
Base region acceptor concentration	1.2×10^{17} cm ⁻³
Base electron diffusion length (at 300 K)	59×10^{-4} cm
n-Type dopant	Arsenic
Recombination trap level in n-region (As)	0.049 eV
p-Type dopant	Boron
Recombination trap level in p-region (B)	0.045 eV
Recombination concentration constant in p-region	1×10^{14} cm ⁻³
Recombination concentration constant in p-region	9.195×10^{12} cm ⁻³
Thickness of SiO ₂ passivation layer	50 to 200 Å
Air-oxide reflectivity (not provided by manufacturer)	0 to 0.34
Diode Resistance*	2 Ω
Temperature*	300 K 326 K 371 K 421 K

*Measured by RTI.

HIGH-EFFICIENCY DEVICE RESEARCH

Table 4(a).

Parameter	Simulation	Manufacturer		RTI/NC A&T	
		Data	% Diff	Data	% Diff
η , %	10.12	10.1	-0.2	9.8	-3.3
FF	0.749	0.74	-1.2	0.73	-2.6
J_{sc} , mA cm ⁻²	22.41	22.80	1.7	22.70	1.3
V_{oc} , V	0.6029	0.595	-1.3	0.5956	-1.2
J_{mp} , mA cm ⁻²	20.58	—		20.00	-2.9
V_{mp} , V	0.4918	—		0.4922	0.08

Table 4(b).

Parameter	Simulation	RTI/NC A&T	% Difference
η , %	9.1	9.3	2.2
FF	0.724	0.723	-0.1
J_{sc} , mA cm ⁻²	22.97	23.45	2.1
V_{oc} , V	0.5493	0.5458	-0.6
J_{mp} , mA cm ⁻²	20.79	20.71	-0.4
V_{mp} , V	0.4394	0.4462	1.5

Table 4(c).

Parameter	Simulation	RTI/NC A&T	% Difference
η , %	7.33	7.6	3.6
FF	0.674	0.687	1.9
J_{sc} , mA cm ⁻²	23.83	24.28	1.8
V_{oc} , V	0.4564	0.4556	-0.2
J_{mp} , mA cm ⁻²	20.85	21.37	2.5
V_{mp} , V	0.3518	0.3561	1.2

Table 4(d).

Parameter	Simulation	RTI/NC A&T	% Difference
η , %	5.29	5.4	2.04
FF	0.609	0.62	1.77
J_{sc} , mA cm ⁻²	24.63	24.78	0.67
V_{oc} , V	0.3525	0.3522	-0.10
J_{mp} , mA cm ⁻²	20.41	20.85	2.10
V_{mp} , V	0.2592	0.258	-0.70

Table 4. Results of validation study using cell No. 24C, with corresponding parameters listed in Table 3, and where 0.18 is used for the air-oxide reflectivity: a) 300 K; b) 326 K; c) 371 K; and d) 421 K. Simulation results are obtained using three iterations and 20 mesh points equally separated in the n- and p-regions.

Table 5. Simulation and experimental temperature coefficients and the percent difference for cell No. 24C.

Temperature Coefficient	Simulation	Experimental	Percent Difference
$d\eta/dT, (\% K^{-1})$	-4.00×10^{-2}	-3.92×10^{-2}	-2.04
$d(FF)/dT, (K^{-1})$	-1.14×10^{-3}	-1.08×10^{-3}	-5.90
$dV_{oc}/dT, (VK^{-1})$	-2.10×10^{-3}	-2.04×10^{-3}	-2.90
$dV_{mp}/dT, (VK^{-1})$	-1.93×10^{-3}	-1.94×10^{-3}	0.52

Table 6. Summary of experimental, calculated, and simulated short-circuit current density for cell No. 24C at 300 K.

Method	Short-circuit current density*	Reflectivity	Comments
Experimental	$23.75 \times 10^{-3} \text{ mA cm}^{-2}$	unknown	agreement with RTI data
Calculated (simulation program was not used)	$18.50 \times 10^{-3} \text{ mA cm}^{-2}$	unknown	using manufacturer's spectral response curve and the revised AM1.5 spectral data
Calculated (simulated program was not used)	$22.90 \times 10^{-3} \text{ mA cm}^{-2}$	0.32	maximum theoretical value by calculating absorbed flux and assuming 100% collection efficiency
	$27.56 \times 10^{-3} \text{ mA cm}^{-2}$	0.18	
Simulation Results	$23.35 \times 10^{-3} \text{ mA cm}^{-2}$	0.18	RTI simulation program used (resultant collection efficiency is approximately 85%)

*Uncorrected for contact shadowing.

LOSS MECHANISMS IN HIGH-EFFICIENCY SOLAR CELLS

C.T. SAH ASSOCIATES

C. Tang Sah

Study of Material Properties and High-Efficiency Solar-Cell Performance on Material Composition: Project Tasks

- (1) EFFICIENCY-LIMITING IMPURITY AND DEFECT LEVEL CHARACTERIZATION.
- (2) COMPUTER MODELING OF CELL PERFORMANCE.
- (3) FUNDAMENTAL LIMITATIONS.
- (4) PRACTICAL SOLUTIONS.
 - To be discussed here.

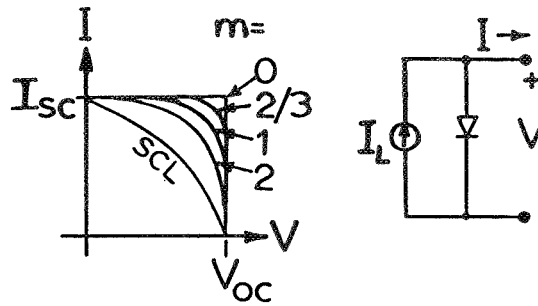
Outline

- (3) FUNDAMENTAL LIMITATIONS
 - * Best Cell I-V Curve.
 - * State-of-the-Art and Fundamental Limit.
 - * Summary of Limiting Recombination Losses.
- (4) PRACTICAL SOLUTIONS
 - * Design Alternatives
 - * Test Structure No.1.

PRECEDING PAGE BLANK NOT FILMED

HIGH-EFFICIENCY DEVICE RESEARCH

ORIGINAL PAPER IS
OF POOR QUALITY



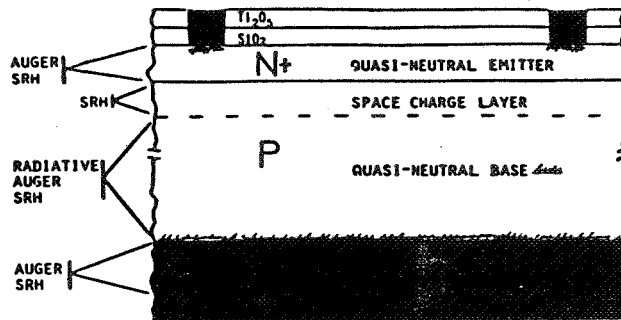
$$I = I_L - I_m e^{\frac{qV}{mKT}}$$

or

$$= I_L - I_{scl}$$

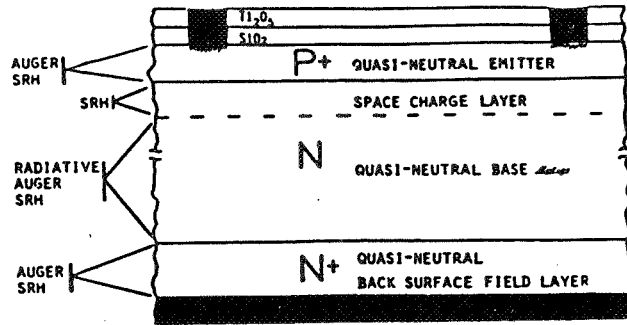
BEST: $m=1$ or less
for $IV = \max.$ $J_{sc} = \text{High}$
 $V_{oc} = \text{High}$

1984
1985 Production 16%



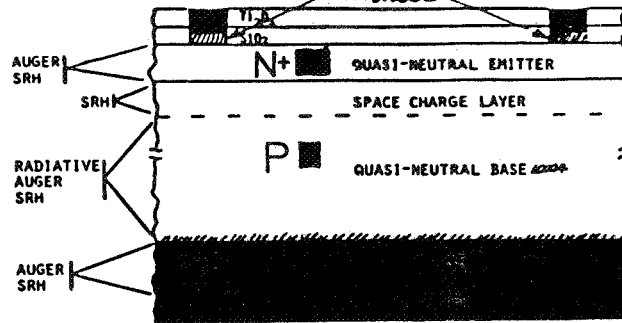
Major Recombination Loss sites:
Interfaces: FRONT CONTACT, BACK
Base

1984 SPIRE (Spitzer) 18% N^+PP^+
1978 SANDIA 18% P^+NN^+



Major Recombination Loss Sites:
Interfaces: FRONT CONTACT
Base

Green 19%
tunnel oxide
contacts



Major Recombination Loss Sites:
Interfaces: FRONT CONTACT eliminated
BACK CONTACT
Base:

State of the Art and Fundamental Limited
Silicon Solar Cells

SOURCE	J _m (A)	J _{SC} (mA)	V _{OC} (mV)	FF	EFF (%)	LOSS MECHANISM	SEFF m (cm/s)	CELL TYPE	
FUNDAMENTAL LIMITED	THEORY	5E-16	36	840	0.864	25.4	RadRec Base 1	3.1 DC	
	THEORY	3E-22	36	786	0.897	25.4	AugerH Base 2/3	0.3 DC	
	THEORY	2E-15	36	776	0.858	24.0	AugerL Base 1	14 N+/P/P+	
ESTIMATE	4E-15	36	769	0.861	23.8	SRH PolyEmi 1	112/100	P+/N/N+	
STATE-OF-THE-ART	Green	3E-13	36	653	0.811	19.1		M/I/N/P	
	Theory	3E-13	36	660	0.840	20.0	SRH Base 1	850	
	Spitzer		36	622	0.801	18.0			
	Theory	1E-12	36	627	0.834	18.9	SRH Base 1	1100	N+/P/P+
	Rohatgi	2E-12	36	605	0.786	17.2			
	Theory	2E-12	36	605	0.830	18.2	SRH Base 1	650	N+/P/P+
	ASEC		35	620	0.793	17.1			
	Theory	1E-12	35	620	0.833	17.9	SRH Base 1	880	N+/P

Upper four theory: T=24C, n_i=1E10, Area=1cm², XB=50um, NB=1E17, DB=20, LB=100ua, Cⁿn²=6E5, Cⁿ₁=Cⁿ₂=2.8E-31, Cⁿ₁=Cⁿ₂+C^p=3.8E-31cm²/s.

Summary of Efficiency-Limiting Mechanisms

EFFICIENCY RANGE (%)	CURRENT STATUS	LIMITING MECHANISMS AND RECOMBINATION SITES	MAXIMUM DARK CURRENT J ₁ (A/cm ²)
25+	Must eliminate all emitter recomb. losses.	Interband Auger and radiative in base.	5.0E-16
20-24	Must reduce all base recomb. losses.	SRH at traps at the contact and oxide/silicon interface. Use polySi barrier for contacts.	2.0E-15 to 2.0E-13
18-20	Current best cell.	SRC at traps in the base layer.	2.0E-13 to 2.0E-12
<18	Current production.	SRC at traps in both the base and emitter.	>2.0E-12

Floating Emitter Solar-Cell Transistor

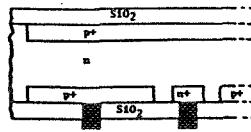


Fig. 1.1 BSC-VFE-SCT

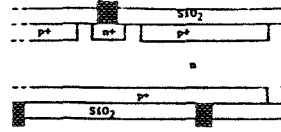


Fig. 1.2 FSC-VFE-SCT

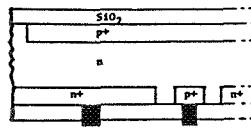


Fig. 1.3 BSC-LVF-SCT

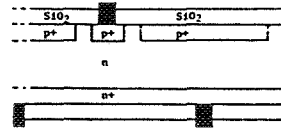


Fig. 1.4 FSC-LFE-SCT

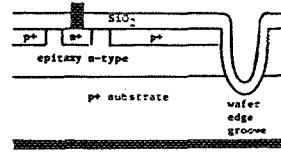


Fig. 1.5 EP: FSC VFE SCT

From
"Floating Emitter Solar Cell
transistor," Docket No. 16467,
JPL Office of Patents and
Technology Utilization,
March 20, 1984.

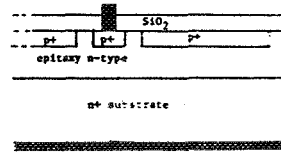


Fig. 1.6 EP: FSC LFE SCT

JPL1403

HIGH-EFFICIENCY SILICON SOLAR CELLS

UNIVERSITY OF WASHINGTON

Larry C. Olsen

**ORGANIZATION: JOINT CENTER FOR GRADUATE STUDY
(UNIVERSITY OF WASHINGTON)**

PRINCIPAL INVESTIGATOR: DR. LARRY C. OLSEN

CONTRACT NO.: 956614

CONTRACT PERIOD: SEPTEMBER, 1984 — AUGUST, 1985

**OTHER CONTRIBUTORS: DR. BILL ADDIS
DR. WES MILLER
GLEN DUNHAM
ERIC EICHELBERGER
DAN DOYLE**

Objectives and Approach

OBJECTIVES

- ACHIEVE AN AMI EFFICIENCY $> 19\%$.
- IDENTIFY LIMITING CURRENT MECHANISMS FOR HIGH EFFICIENCY CELLS.
- INVESTIGATE APPROACHES FOR PASSIVATING SURFACES OF SILICON SOLAR CELLS.

APPROACH

SILICON MINP SOLAR CELLS

- INCREASE J_{PH} TO 36 mA/cm^2 WITH $\text{TiO}_2/\text{MgF}_2$ DBLAR AND BY USING COLLECTOR GRID WITH 4% SHADOWING.
- OPTIMIZE EMITTER DONOR CONCENTRATION PROFILE TO MINIMIZE CURRENT LOSSES.

CURRENT LOSS MECHANISMS

- CONDUCT TEMPERATURE-DEPENDENT I-V ANALYSES TO IDENTIFY CURRENT LOSS MECHANISMS.
- MODELING CALCULATIONS FOR INTERPRETING EXPERIMENTAL RESULTS.

SURFACE PASSIVATION

- INVESTIGATE PECVD SiN_x FOR PASSIVATION OF SILICON.
- DETERMINE SURFACE RECOMBINATION VELOCITY FROM PHOTO RESPONSE.
- DETERMINE D_{SS} FROM CAPACITANCE MEASUREMENTS ON HIGHLY DOPED N-TYPE WAFERS AND ON N^+ SURFACES OF N^+/P CELLS.

PRECEDING PAGE BLANK NOT FILMED

Surface Passivation Studies

SURFACE STATE DENSITY

DETERMINE D_{SS} FROM HIGH FREQUENCY AND SLOW RAMP MEASUREMENTS WITH Al GATES.

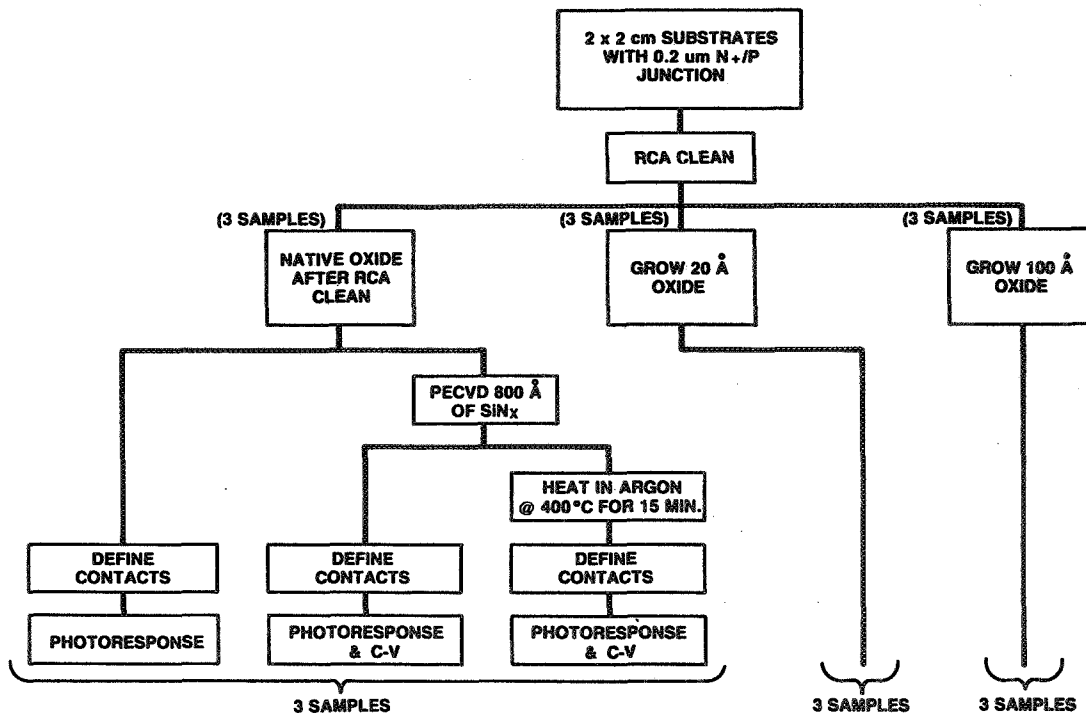
- 2 ohm-cm ($N_A = 7 \times 10^{15} \text{ cm}^{-3}$) P-TYPE
- 0.2 ohm-cm ($N_A = 2 \times 10^{17} \text{ cm}^{-3}$) P-TYPE
- .08 ohm-cm ($N_D = 7 \times 10^{17} \text{ cm}^{-3}$) N-TYPE
- .01 ohm-cm ($N_D = 5 \times 10^{18} \text{ cm}^{-3}$) N-TYPE

MODIFIED ROSIER MEASUREMENT

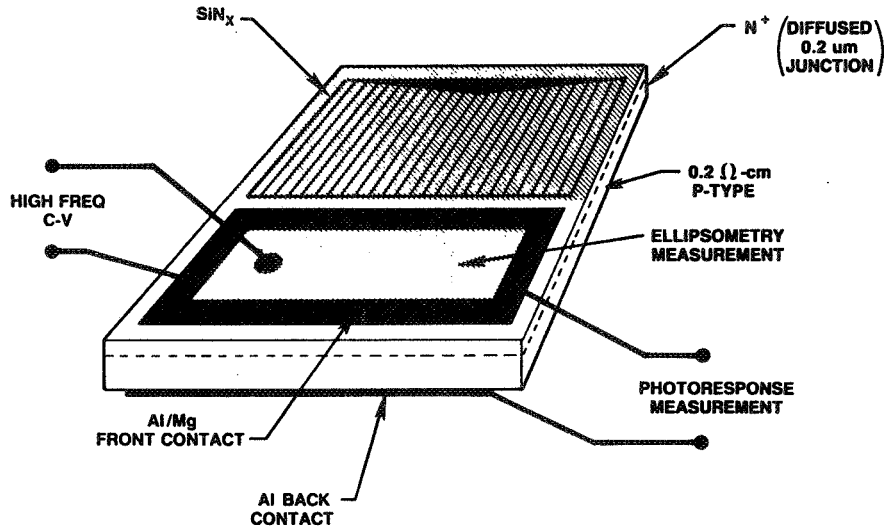
FABRICATE DEVICE STRUCTURE WITH SiN_x DEPOSITED ONTO DIFFUSED N^+ /P JUNCTIONS WHICH ALLOWS MEASUREMENTS OF:

- D_{SS} FROM HIGH FREQUENCY C-V APPLIED TO N^+ SURFACE.
- SURFACE RECOMBINATION VELOCITY FROM PHOTORESPONSE.

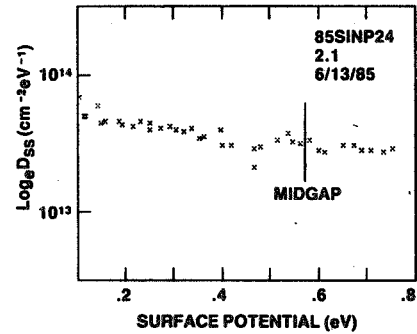
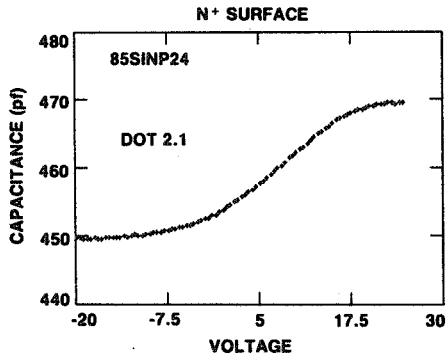
Processing Outline for Recombination Study



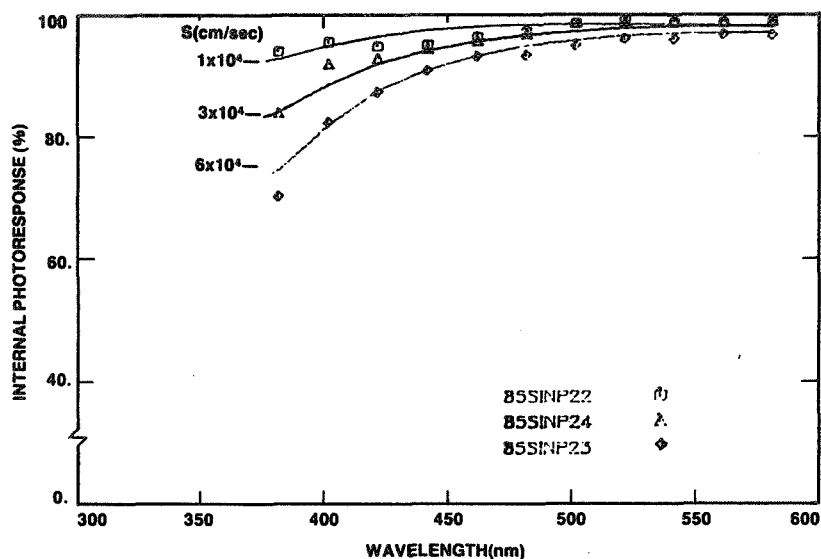
Device Structure for Surface Recombination Study



Modified Rosier Measurements: Density of States on Surface of n^+/p Cell



Internal Photoresponse vs Wavelength



Surface Recombination Studies

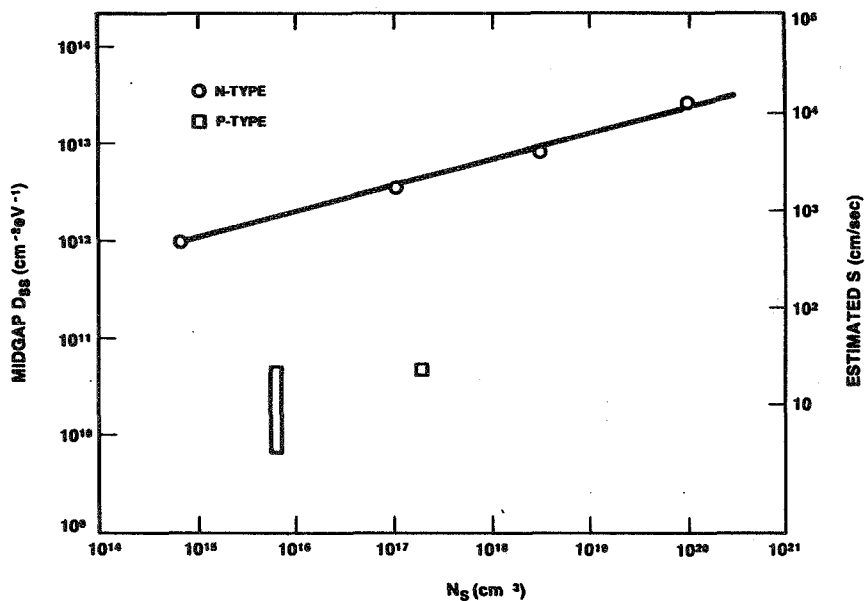
SAMPLE	OXIDE THICKNESS (Å)	SIN _x THICKNESS (Å)	ANNEAL OF SIN _x	S (cm/sec)	D _{SS} (cm ² eV ⁻¹)
85-15	NATIVE	---	---	1.0x10 ⁵	---
85-17	NATIVE	890	---	5.5x10 ⁴	2.5x10 ¹³
85-16	NATIVE	820	H.T.	2.0x10 ⁴	2.5x10 ¹³
85-24	20 Å	---	---	3.0x10 ⁴	---
83-23	20 Å	1020	---	6.0x10 ⁴	2.5x10 ¹³
85-22	20 Å	1030	H.T.	1.0x10 ⁵	2.4x10 ¹³
85-20	100 Å	---	---	8.0x10 ³	---
85-19	100 Å	950	---	4.0x10 ⁴	2.5x10 ¹³
85-18	100 Å	1020	H.T.	9.0x10 ³	2.4x10 ¹³

NOTES: H.T. REFERS TO HEAT TREATMENT AT 400°C FOR 15 MINUTES.

Variation of Surface State Density With Dopant Concentration

SAMPLE RESISTIVITY (ohm-cm)	DOPANT CONCENTRATION (cm ⁻³)	D _{SS} (cm ⁻² eV ⁻¹) DEPOSITED	D _{SS} (cm ⁻² eV ⁻¹) AFTER H.T	ESTIMATED SURFACE RECOMB VELOCITY (cm/sec)
2.0 P-TYPE	7x10 ¹⁵	5x10 ¹¹	<5x10 ¹⁰	25
0.2 P-TYPE	2x10 ¹⁷	5x10 ¹¹	5x10 ¹⁰	25
7.0 N-TYPE (P-DOPED)	7x10 ¹⁴	1.7x10 ¹²	1.0x10 ¹²	500
.08 N-TYPE (Sb-DOPED)	1.3x10 ¹⁷	3x10 ¹²	3x10 ¹²	1.5x10 ³
.01 N-TYPE (Sb-DOPED)	3.0x10 ¹⁸	8x10 ¹²	8x10 ¹²	4.1x10 ³

NOTES: (1) MEASUREMENTS ON 'MOS' STRUCTURES BASED ON PECVD SiN_x ON HOMOGENEOUSLY DOPED WAFERS.
 (2) H.T. REFERS TO 40 MINUTES AT 450°C IN ARGON.
 (3) ESTIMATED SURFACE RECOMBINATION VELOCITY BASED ON $\sigma = 10^{-16}$ cm².



NOTE: ESTIMATED S BASED ON $\sigma = 10^{-16}$ cm².

Effect of Illumination on I-V Parameters

DARK CHARACTERISTICS

$n = 1.00$

$J_0 = 2.1 \times 10^{-12} \text{ A/cm}^2$

$\phi = 1.04 \text{ eV}$

**DOMINANT LOSS MECHANISM:
EMITTER RECOMBINATION**

ILLUMINATED CHARACTERISTICS

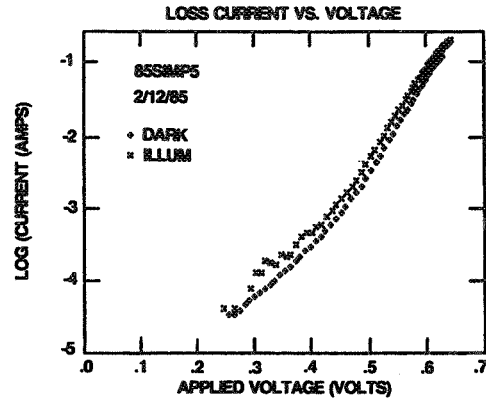
$n = 1.10$

$J_0 = 4.0 \times 10^{-11} \text{ A/cm}^2$

$\phi = 1.01 \text{ eV}$

**DOMINANT LOSS MECHANISM:
DEPLETION LAYER RECOMBINATION**

POSSIBLE TRAP CHARACTERISTICS:
 $E_C - E_T \approx 0.2 \text{ eV}$ $N_T = 10^{17} \text{ cm}^{-3}$



Depletion Layer Recombination Revisited

THEORY

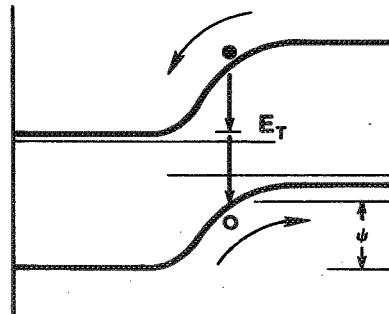
$$J_R = \int_0^W R(x) dx = \int_0^W \frac{R(\psi) d\psi}{\frac{d\psi}{dx}}$$

$R \equiv$ Shockley - Read - Hall
Expression For
Recombination Rate

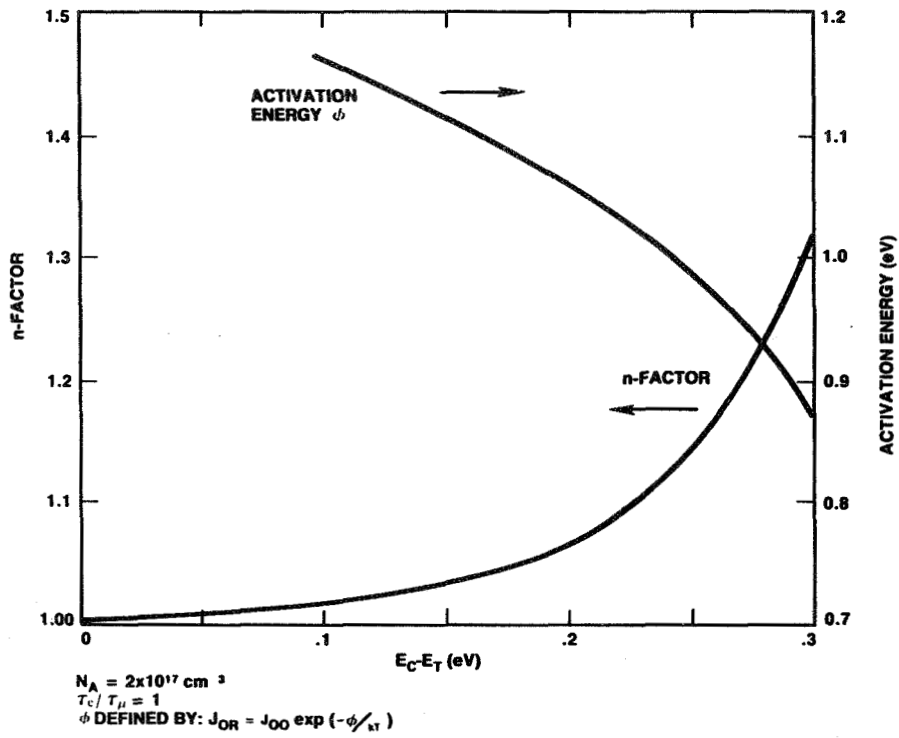
MODELING CALCULATIONS

$J_R = J_{OR} \exp\left(\frac{V}{nKT}\right) \quad V \gg KT$

$J_{OR} = J_{00} \exp\left(-\frac{\phi}{KT}\right)$



Modeling Calculations for Depletion Layer Recombination



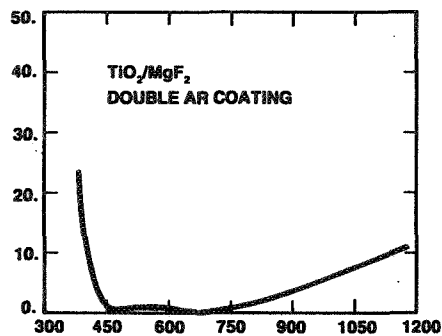
Short-Circuit Current Improvement

OBJECTIVE

- POLISHED, 0.2 Ω -cm P-TYPE SUBSTRATE
L = 150 μ m, DBLAR of TiO_2 and MgF_2 } $J_{PH} = 37.5 \frac{\text{mA}}{\text{cm}^2}$
- ASSUMING 4% SHADOWING DUE TO CURRENT COLLECTOR GRID. } $J_{SC} = 36.0 \frac{\text{mA}}{\text{cm}^2}$

STATUS

- POLISHED CELL
WITH SiO_x AR:
 $J_{SC} = 32.3 \frac{\text{mA}}{\text{cm}^2}$
- TEXTURED CELL
WITH SiO_x AR:
 $J_{SC} = 35.5 \frac{\text{mA}}{\text{cm}^2}$



CALCULATED REFLECTANCE VS WAVELENGTH

PROGRESS

- DEVELOPED PROCEDURES FOR DEPOSITING TiO_2 AND MgF_2 . ELLIPSOMETRIC MEASUREMENTS WERE USED TO OBTAIN OPTICAL CONSTANTS. CALCULATED OPTIMUM FILM THICKNESSES FOR $\text{TiO}_2/\text{MgF}_2$ DBLAR COATING.
- DEVELOPED PROCEDURES FOR DEFINING FRONT COLLECTOR GRID BY LIFTOFF OF FULL METALLIZATION THICKNESS.
- DESIGNED AND ACQUIRED SHADOW MASK WHICH WILL YIELD COLLECTOR GRIDS WITH 4% SHADOWING.

Voltage Improvement

OBJECTIVE

- $FF = 0.81$ and $V_{OC} = 650 \text{ mV}$

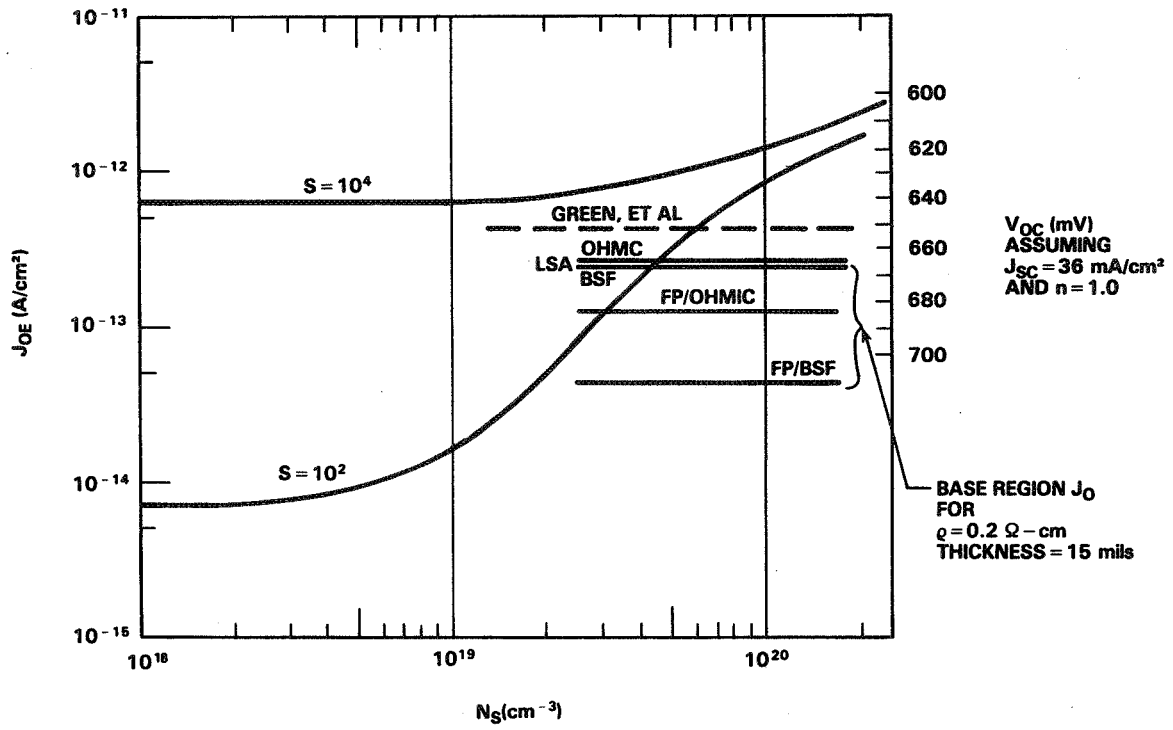
STATUS

- $FF = 0.81$ and $V_{OC} = 636 \text{ mV}$

APPROACH

- EMITTER OPTIMIZATION USING ION IMPLANTATION:
 $N_s \approx 3 \text{ to } 4 \times 10^{19} \text{ cm}^{-3}$
 $R_s \approx 200 \Omega/\square$
- REDUCTION OF SURFACE RECOMBINATION:
 $S = 10^3 \text{ cm/sec.}$
- $V_{OC} = 650 \text{ mV.}$
- ASSUMING $J_{SC} = 36 \text{ mA/cm}^2$, AMI EFFICIENCY = 19.0%.

Emitter j_0 vs Surface Donor Concentration



Key Results

MINP SOLAR CELLS

- DOUBLE AR COATING CONSISTING OF $\text{TiO}_2/\text{MgF}_2$ AVAILABLE.
- APPROACH TO MORE OPTIMUM EMITTER CONCENTRATION PROFILE
- EFFICIENCIES: 16.3%(POLISHED), 17.0%(TEXTURED)
- VOLTAGE: $V_{OC} = 636$ mV.

CURRENT LOSS MECHANISMS

- HAVE IDENTIFIED LIGHT ENHANCED CURRENT LOSS MECHANISM IN HIGH EFFICIENCY CELLS. CAN BE EXPLAINED BY DEPLETION LAYER RECOMBINATION.
- HAVE EXTENDED Sah-Noyce-Shockley MODELING CALCULATIONS TO INCLUDE TEMPERATURE DEPENDENT I-V CHARACTERISTICS AND ENERGY ACTIVATION ANALYSIS.

SURFACE PASSIVATION

- STUDIES OF 'MOS' STRUCTURES WITH SiN_x INSULATING LAYERS ON N-TYPE WAFERS INDICATE SURFACE STATE DENSITY CORRELATES WITH DONOR DENSITY.
- MODIFIED ROSIER MEASUREMENT DEVELOPED. INVOLVES PHOTO-RESPONSE ANALYSIS TO OBTAIN SURFACE RECOMBINATION VELOCITY AND HIGH FREQUENCY C-V TO OBTAIN SURFACE STATE DENSITY.
- DETERMINED THAT PECVD SiN_x ANNEALED AT 400°C RESULTS IN $S = 10^4$ cm/sec ON N^+ SURFACE WITH $N_S = 10^{20}$ cm⁻³, SIMILAR RESULT OBTAINED WITH 100 Å SiO_2 PASSIVATION.

**DEVELOPMENT OF HIGH-EFFICIENCY
SOLAR CELLS ON SILICON WEB**

WESTINGHOUSE ELECTRIC CORP.

A. Rohatgi
D.L. Meier
R.B. Campbell
R.G. Seidensticker
P. Rai-Choudhury

Tasks

- **Perform Model Calculations to Design High Efficiency Web Cells**
- **Investigate the Influence of Twin Planes, Trace Impurities and Heat Treatment to improve Minority Carrier Lifetime in Web**
- **Develop and Optimize Advanced Design Features, Like Passivation, AR Coating and Back Surface Reflector**
- **Fabricate High Efficiency Web Cells With Efficiency Approaching 18%**

Calculated AM1 Performance of Standard and Low-Resistivity Web Cells With Base Diffusion Length as a Parameter

A. 4 Ohm-cm ($3.5e15/cm^3$) P-Type, 150 Microns Thick

Ln (Microns)	J_{oe} (A/cm ³)	J_{ob} (A/cm ³)	J_{sc} (mA/cm ²)	V_{oc} (V)	FF	Eff (%)	Eff' (%)
10	1.6e-12	32.1e-11	24.6	.471	.793	9.2	8.3
30	1.6e-12	9.5e-11	30.6	.508	.802	12.5	11.2
60	1.6e-12	5.3e-11	33.2	.525	.809	14.1	12.7
150	1.6e-12	2.0e-11	36.5	.551	.815	16.4	14.8
300	1.6e-12	1.1e-11	37.6	.566	.819	17.4	15.7

B. 0.2 Ohm-cm ($1.0e17/cm^3$) P-Type, 150 Microns Thick

Ln (Microns)	J_{oe} (A/cm ³)	J_{ob} (A/cm ³)	J_{sc} (mA/cm ²)	V_{oc} (V)	FF	Eff (%)	Eff' (%)
10	1.6e-12	7.5e-12	24.2	.563	.817	11.1	10.0
30	1.6e-12	2.5e-12	30.0	.589	.824	14.6	13.1
60	1.6e-12	1.2e-12	33.0	.601	.826	16.4	14.8
150	1.6e-12	0.6e-12	35.1	.609	.831	17.8	16.0
300	1.6e-12	0.5e-12	35.7	.611	.832	18.1	16.3

Note:

1. Calculations Were Made Using Martin Wolf's Program SPCOLAY.BAS
2. Calculated Values Do Not Account For Grid Shadowing, Light Reflection, Or Resistive Losses. In Order To Estimate These Effect, The Calculated Efficiency (Eff) Was Multiplied By 90% To Give A More Realistic Efficiency (Eff').
3. The Model Accounts For Variation In Doping Density In The Emitter And In The Back Region. For Both The n+p And p+p Regions The Junction Depth Was Taken To Be 0.3 Microns With A Surface Concentration Of $8.0e19/cm^3$.
4. $S_{front} = 10^4$ cm/sec (AR On Bare Si); $S_{back} = 10^6$ cm/sec (Metal on Si)

Resistivity and Diffusion Length Requirements
for 17.5%-Efficient Web Solar Cells

$$W = 150 \mu\text{m}$$

$$S_{op^+} = 500 \text{ cm/sec}$$

$$N_{xj} = 3 \times 10^{17} \text{ cm}^{-3}$$

$$S_{on^+} = 500 \text{ cm/sec}$$

$$N_s = 2 \times 10^{20} \text{ cm}^{-3}$$

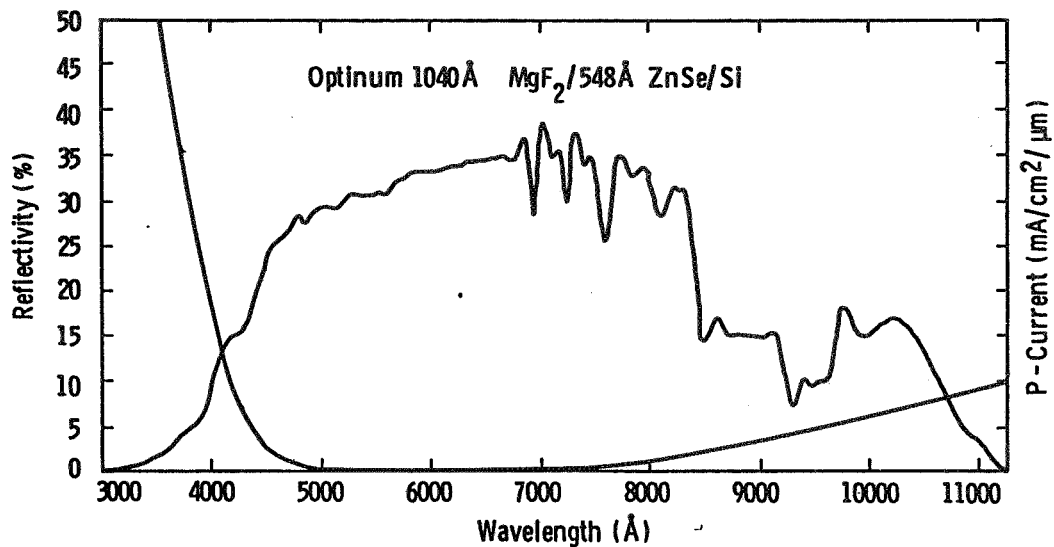
$$S_{p-p^+} = 100 \text{ cm/sec}$$

ρ $\Omega\text{-cm}$	L μm	J_{sc} ma/cm^2	V_{oc} Volts	η %
4.0	360	35	.589	17.0
4.0	467	35.2	.597	17.5
0.2	360	35.0	.643	18.8
0.2	125	33.2	.634	17.5

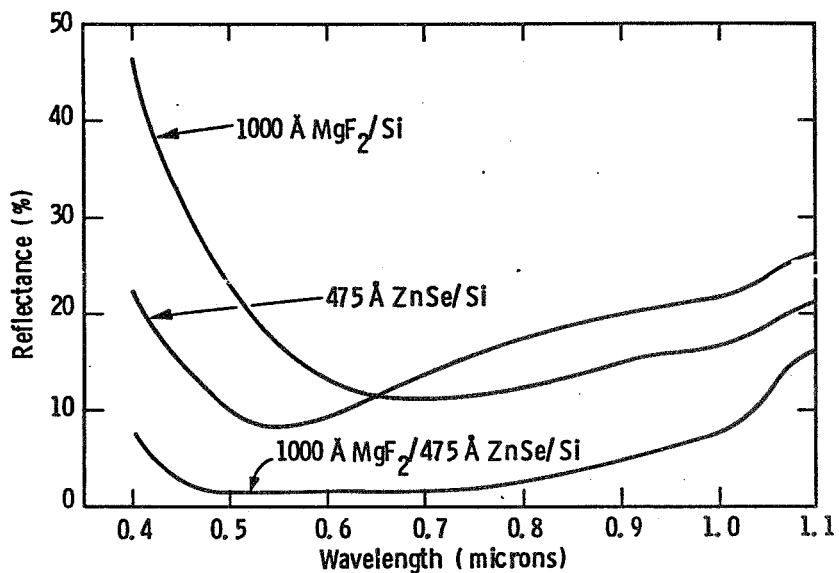
Solar-Cell Data on 4 Ohm-cm Web With
and Without Oxide Passivation

Cell ID	Short-Circuit Current J_{sc} (mA/cm ²)	Open-Circuit Voltage V_{oc} Volts	Fill Factor	Cell Efficiency (%)
<u>Without Passivation</u>				
W6	32.7	0.575	0.782	14.7
W7	33.1	0.577	0.784	15.0
<u>With Oxide Passivation</u>				
W1	34.6	0.584	0.784	15.9
W2	34.5	0.586	0.794	15.8

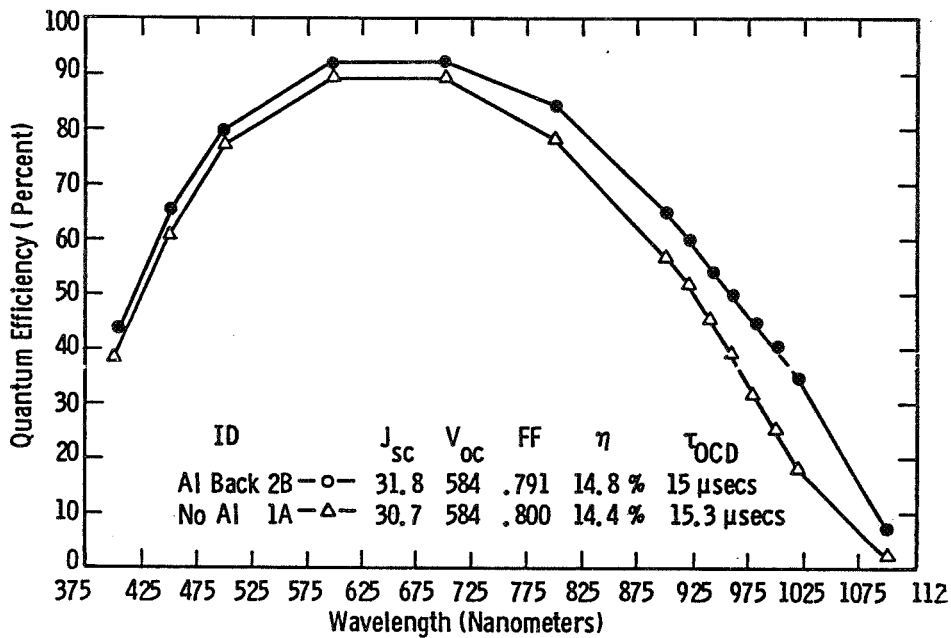
HIGH-EFFICIENCY DEVICE RESEARCH



Experimentally Determined Reflectance Curves for
 (a) 1000 Å MgF₂/Si; (b) 475 Å ZnSe/Si, and
 (c) 1000 Å MgF₂/475 Å ZnSe/Si



Effect of Aluminum Back-Surface Reflector on Web Cell Performance



Baseline Web Solar Cells on 0.37 Ohm-cm Web
(Crystal No. 4-275) Without AR Coating,
Back-Surface Reflector, and Oxide Passivation

Cell ID	J_{sc} mA/cm ²	V_{oc} mV	FF	Efficiency %
6-1-2	21.3	579	.790	9.7
6-2-6	21.6	575	.803	10.0
6-3-6	22.1	574	.778	9.9

Hiefy 20, Qual.

Crystal #6

AM1, 100 mW/cm² Illumination

HIGH-EFFICIENCY DEVICE RESEARCH

Low-Resistivity (0.37 Ohm-cm) High-Efficiency Web Solar Cells With Surface Passivation, BSR and Evaporated Double-Layer AR Coating

<u>Cell ID</u>	<u>Area cm²</u>	<u>J_{sc} mA/cm²</u>	<u>V_{oc} mV</u>	<u>FF</u>	<u>η %</u>
1-1	1.0	35.2	600	0.800	16.9
1-2	1.0	35.2	600	0.800	16.9
1-3	1.0	35.0	598	0.802	16.8
1-4	1.0	34.9	598	0.800	16.7
1-5	1.0	35.2	596	0.793	16.7
1-6	1.0	35.1	596	0.792	16.6

*Run # Hiefy 20, Web #1

*AM1, 100 mW/cm² Illumination

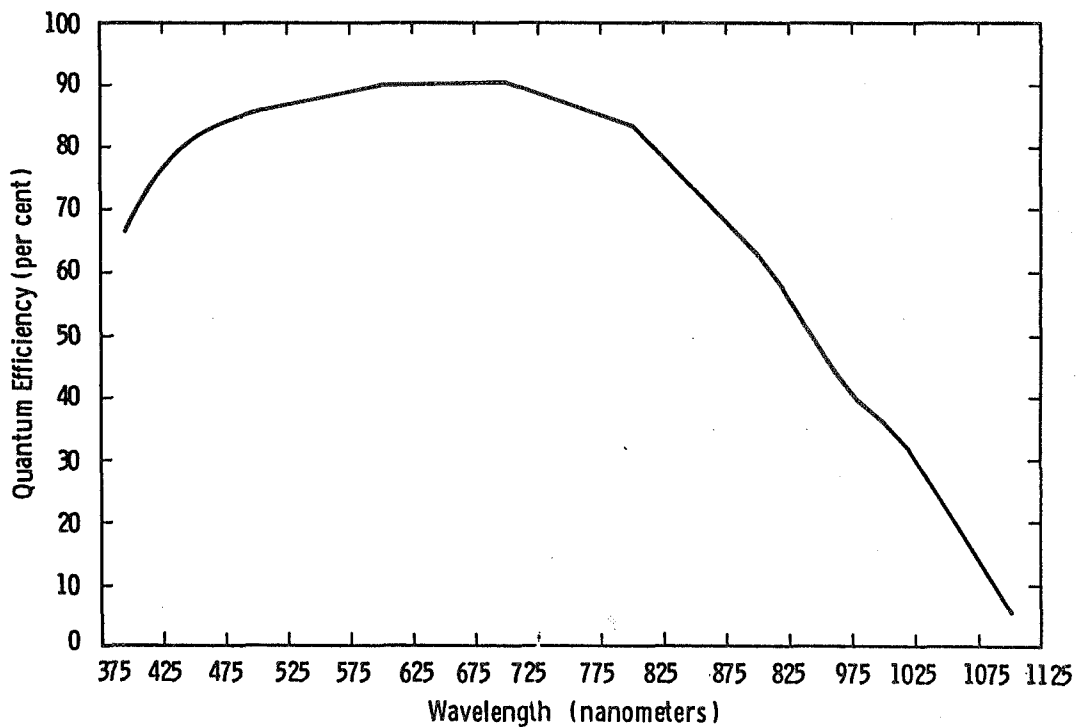


Fig. 6 – Internal quantum efficiency versus wavelength plot for 16.9% efficient web solar cell with oxide passivation, evaporated double-layer AR coating and aluminum back-surface reflector (hiefy 20, web 1-4)

HIGH-EFFICIENCY DEVICE RESEARCH

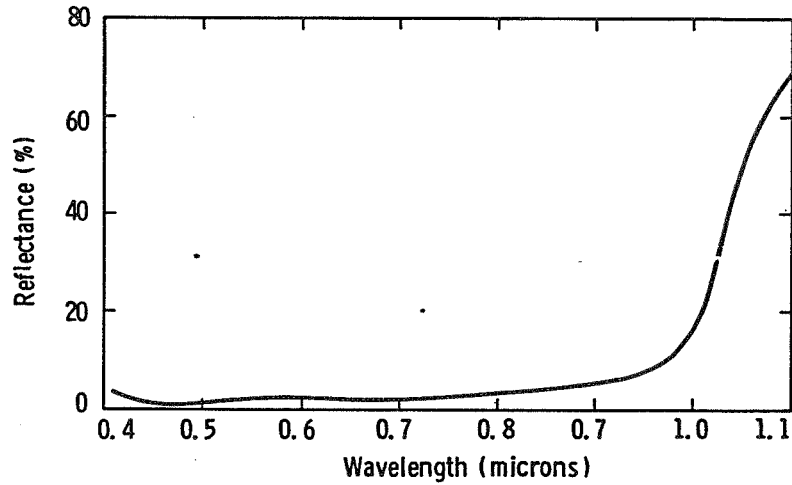


Fig. 8 - Reflectance as a function of wavelength for 16.9% efficient wet cell with oxide passivation, evaporated Zn Se + MgF₂ double-layer antireflective coating, and aluminum back-surface reflector

Diffusion Length in Low-Resistivity Web Crystal
No. 4-275, Which Gave 16.9%-Efficient Web Cells

As Grown Crystal - 30 μm - SPV

Processed Cell - 90 μm - SPV

150 μm - OCVD

HIGH-EFFICIENCY DEVICE RESEARCH

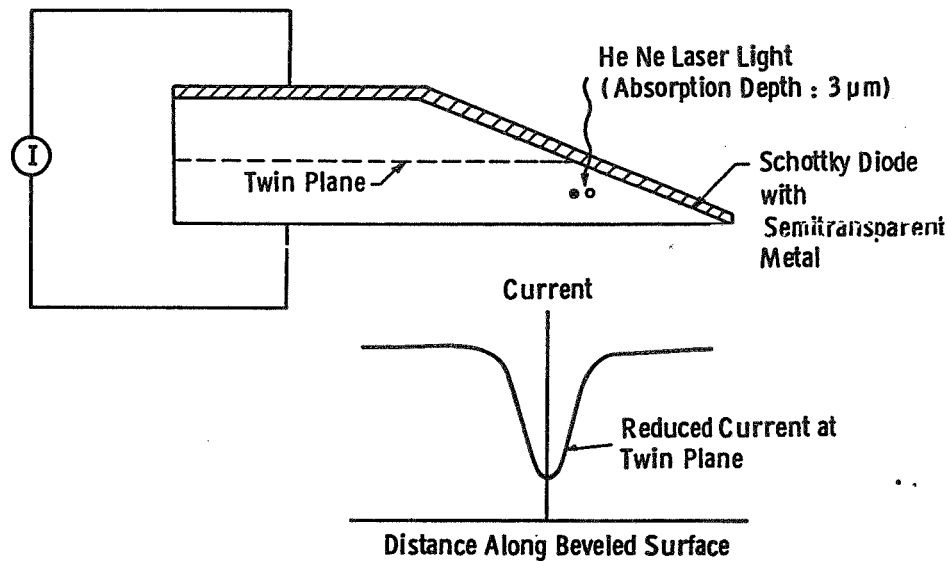


Fig. 6—Sensing the electrical activity of the twin plane with light-beam-induced current (LBIC)

Examples of Large-Area Web Cells With Ratio of Twin Plane Depth to Minority Carrier Diffusion Length as a Parameter

Twin Plane Depth Diffusion Length	Diffusion Length μm	Twin Plane Depth μm	Cell Thickness μm	J _{sc} mA/cm ²	V _{oc} V	FF	Eff %
0.33	78	26	153	31.4	0.591	0.81	15.1
0.50	116	58	164	31.6	0.591	0.81	15.3
0.72	86	62	133	30.8	0.591	0.81	14.9
0.84	61	51	130	30.9	0.590	0.80	14.6
1.14	50	57	132	30.8	0.589	0.80	14.5
1.52	65	99	165	31.1	0.589	0.81	14.9

- Notes:**
1. Cell Size is 9.8 × 2.5 cm, and Base is Boron-Doped to 4 Ohm-cm.
 2. Cell Data Acquired Using AM1 Spectrum, 100 mW/cm² Intensity at Room Temperature.
 3. Diffusion Length Measured by Surface Photovoltage Technique.

Observations: For Cells Where Twin Plan Depth << Diffusion Length, the Carrier Recombination at the Twin Planes is Not Significant Compared to Recombination in the Bulk.

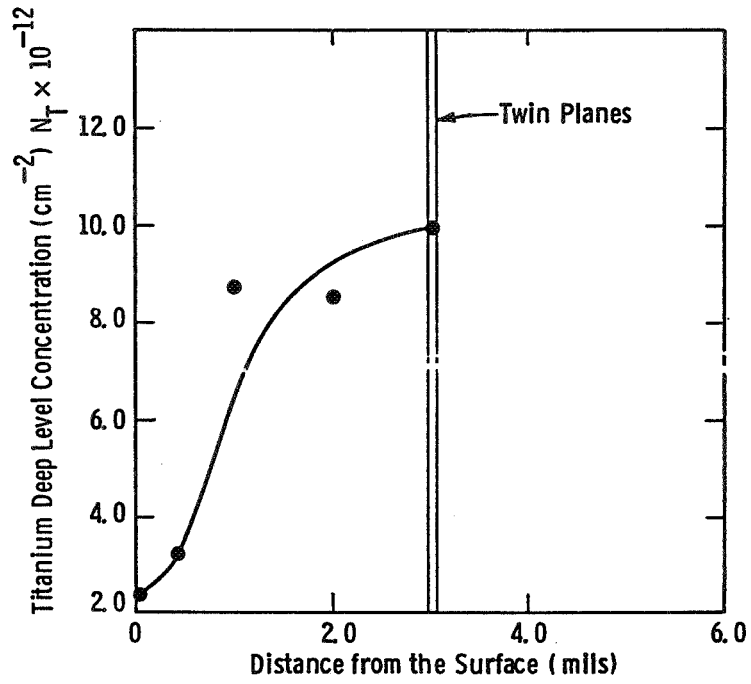
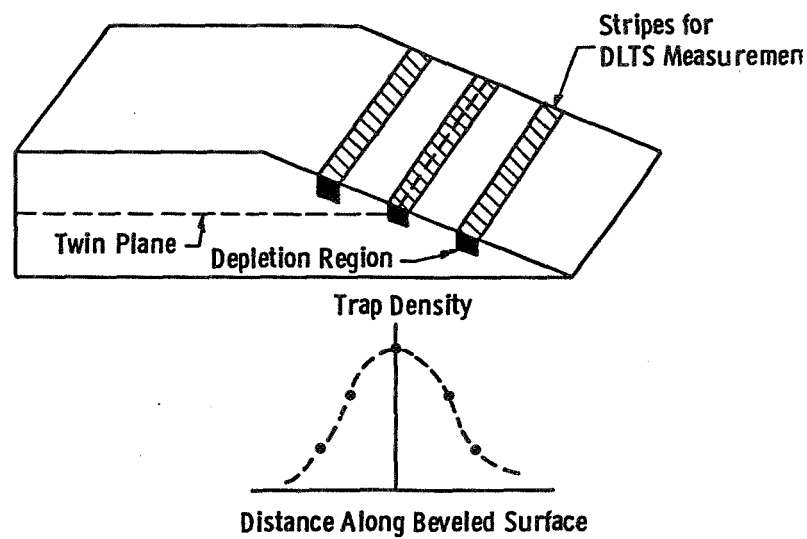


Fig. 5—DLTS study of the interaction between grown-in Titanium impurity and the twin planes in dendritic web silicon

HIGH-EFFICIENCY DEVICE RESEARCH



- Use a Grown-In Impurity (Ti, V) as an Internal Tracer
- Observe Trap Density as a Function of Distance from Twin Plane, Both As-Grown and After Processing (Including Gettering)
- Compare Web Having High Diffusion Length with Web Having Low Diffusion Length (As Determined by SPV) Using this Technique

Fig. 1—Detecting and identifying impurities piled up at the twin plane by DLTS

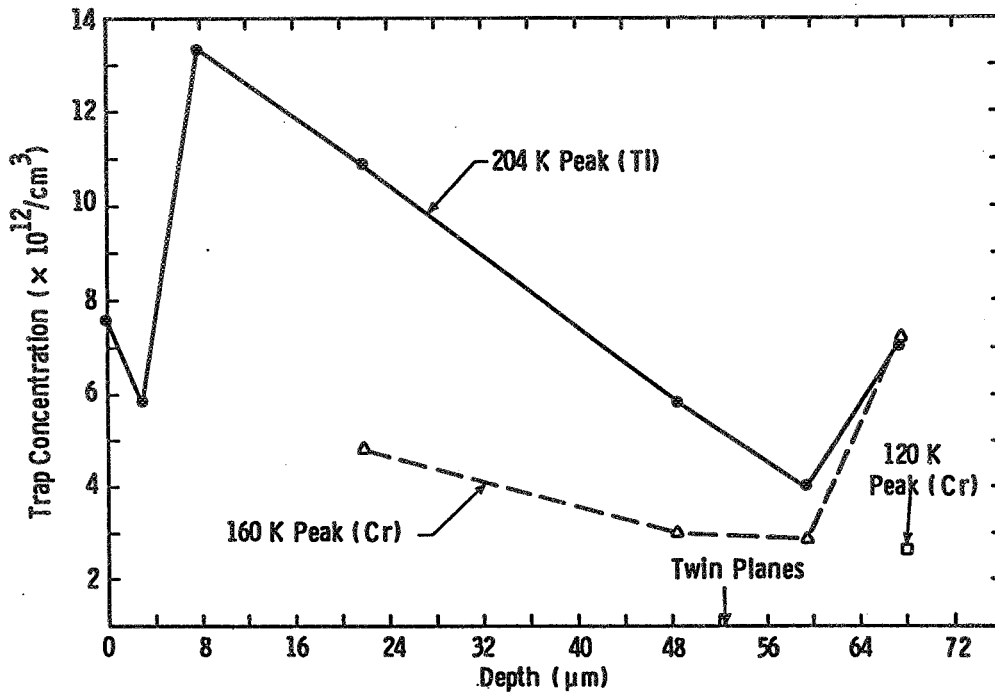


Fig. 3—Depth profile of traps detected by DLTS for Ti-doped dendritic web silicon crystal J167-1.1, as-grown. (Sample #T4 from Run TP-4). Web crystal is 4 ohm-cm, p-type

SURFACE AND BULK-LOSS REDUCTION RESEARCH
BY LOW-ENERGY HYDROGEN DOPING

PENNSYLVANIA STATE UNIVERSITY

S. Fonash

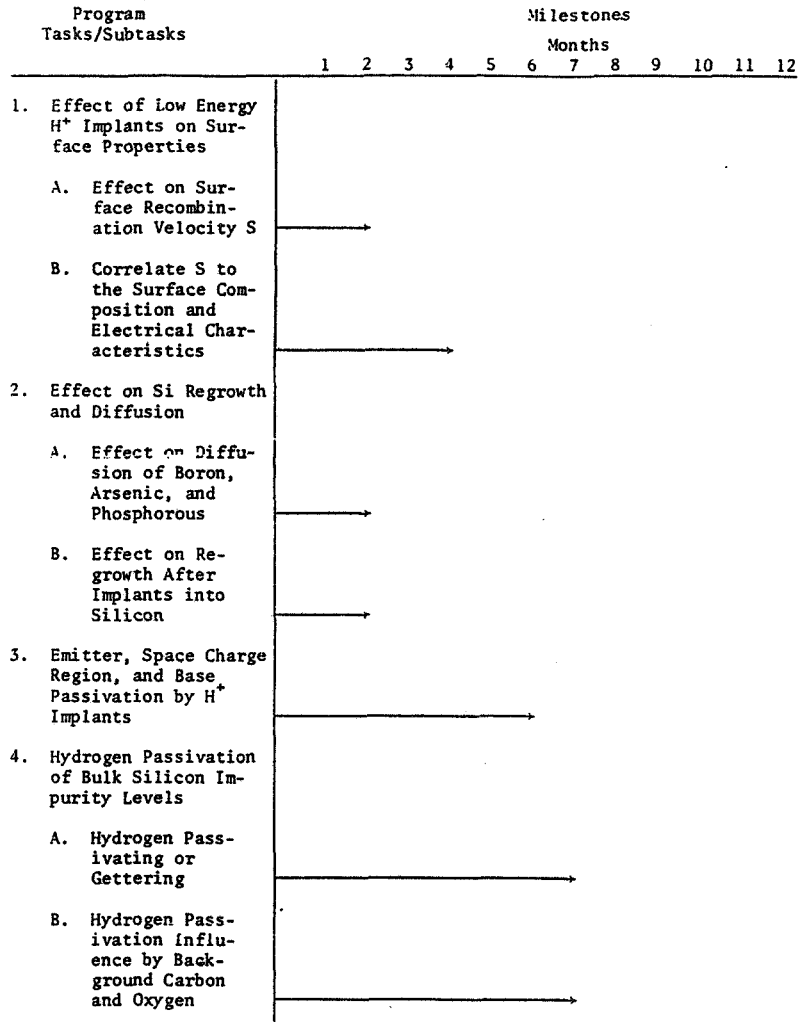
Junction Properties Determined by:

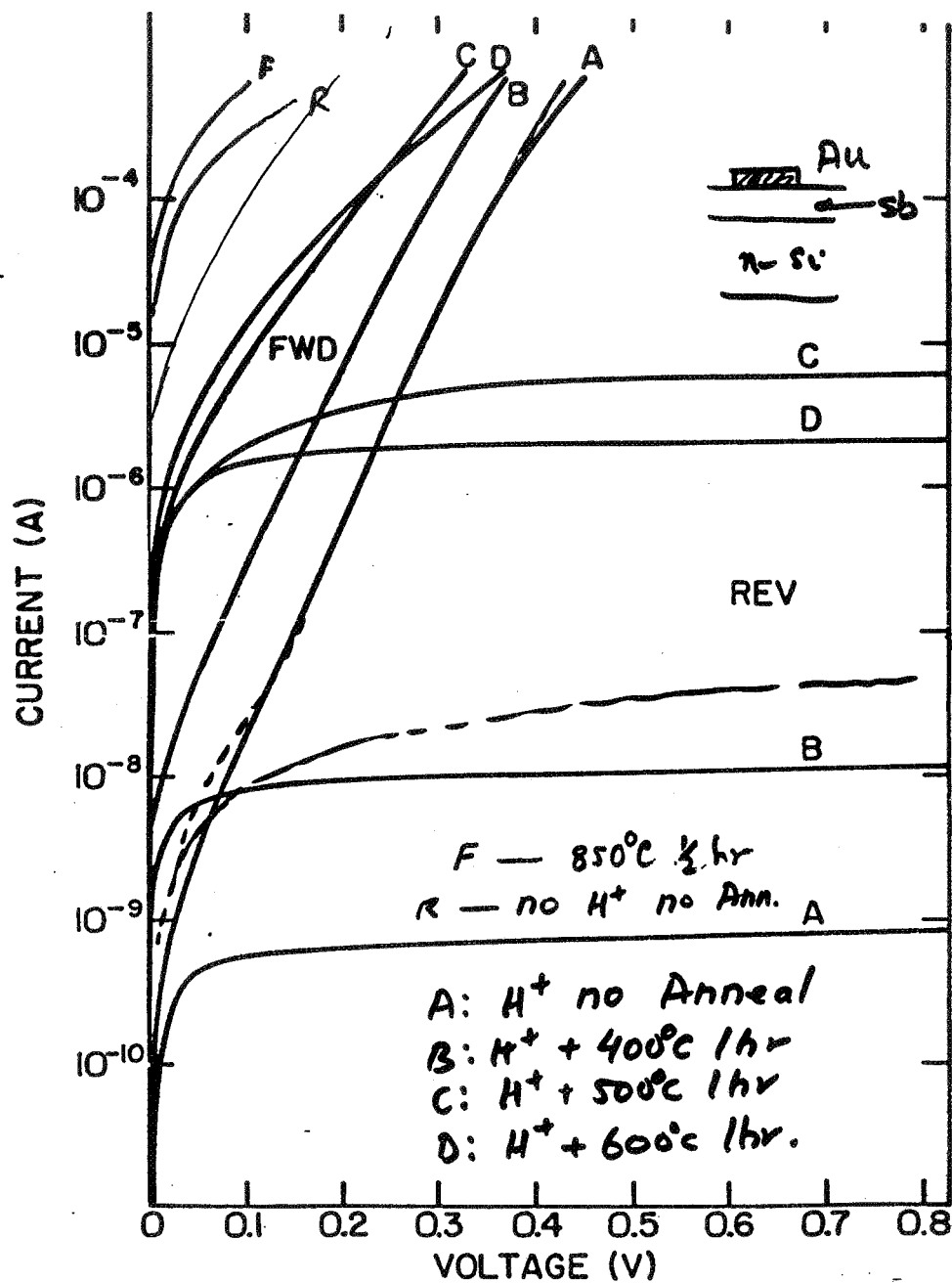
- * 1. **EMITTER** S_p
- 2. **EMITTER : DIFFUSION LENGTH AND WIDTH**
- * 3. **Heavy doping effects in the emitter.**
- 4. **EFFECTIVE FIELDS IN THE EMITTER**
- * 5. **Space - charge recombination**
- * 6. **BASE : DIFFUSION LENGTH AND WIDTH.**
- 7. **BACK SURFACE S.**

PRECEDING PAGE BLANK NOT FILMED

HIGH-EFFICIENCY DEVICE RESEARCH

Program Plan





HIGH-EFFICIENCY DEVICE RESEARCH

H^+ showed a suppression of space charge recombination currents.

CAN H^+ IONS MODIFY S_p ?

- DIODES WHERE EMITTER INJECTION EFFICIENCY < 1
- SHALLOW EMITTERS
- SPIRE SOLAR CELLS.
- J_{0b} from spectral response.
- J_{rec} subtraction.
- J_{0e} determined.
- USE A MODEL FOR HEAVY DOPING and EXTRACT S_p .

ORIGINAL PAGE IS
OF POOR QUALITY

Processing	J_o (pA/cm ²)	J_{oe} (pA/cm ²)
4412-5C as is	3.78	1.71
4412-5C no oxide	7.13	5.06
4412-5C no oxide after H ⁺	3.90	1.83

$$J_{ob} = 2.07 \times 10^{-12} \text{ A/cm}^2$$

$$J_{oe} = \frac{q n_i^2}{\int_0^{W_E} \frac{N_D(x)}{D_p(x)} \cdot \frac{n_i^2}{n_{ie}(x)} dx} + \frac{N_D(0)}{S_p} \cdot \frac{n_i^2}{n_{ie}(0)}$$

Model	S_p with oxide	S_p no oxide	S_p no oxide with H ⁺
Roulston	1.53×10^4	5.66×10^4	1.65×10^4

$$J_{oe} \text{ (with oxide)} = 3.786 \times 10^{-12} \text{ A/cm}^2.$$

$$J_{oe} \text{ (without oxide)} = 7.13 \times 10^{-12} \text{ A/cm}^2.$$

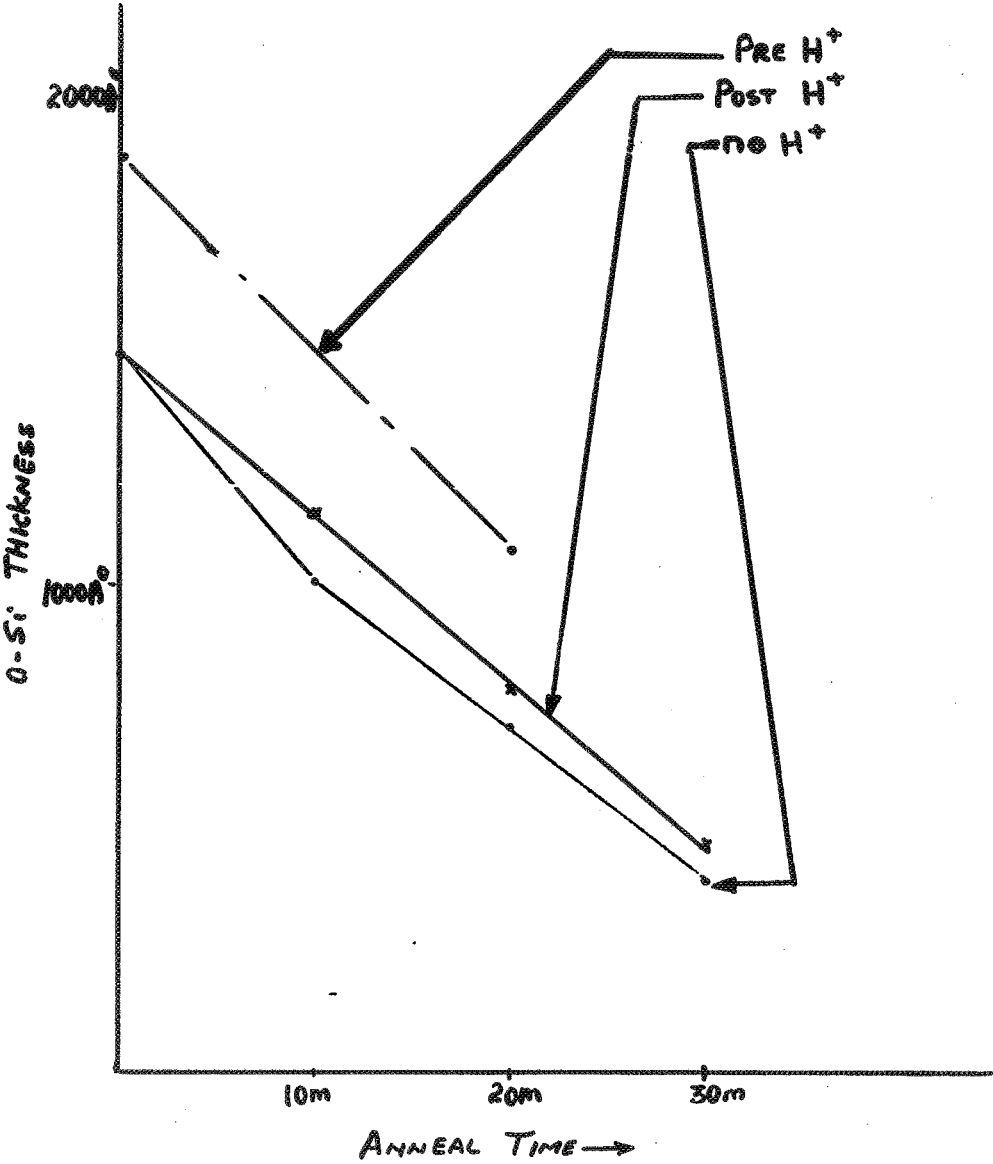
$$J_{oe} \text{ (no oxide + 0.4 keV H}^+) = 3.90 \times 10^{-12} \text{ A/cm}^2.$$

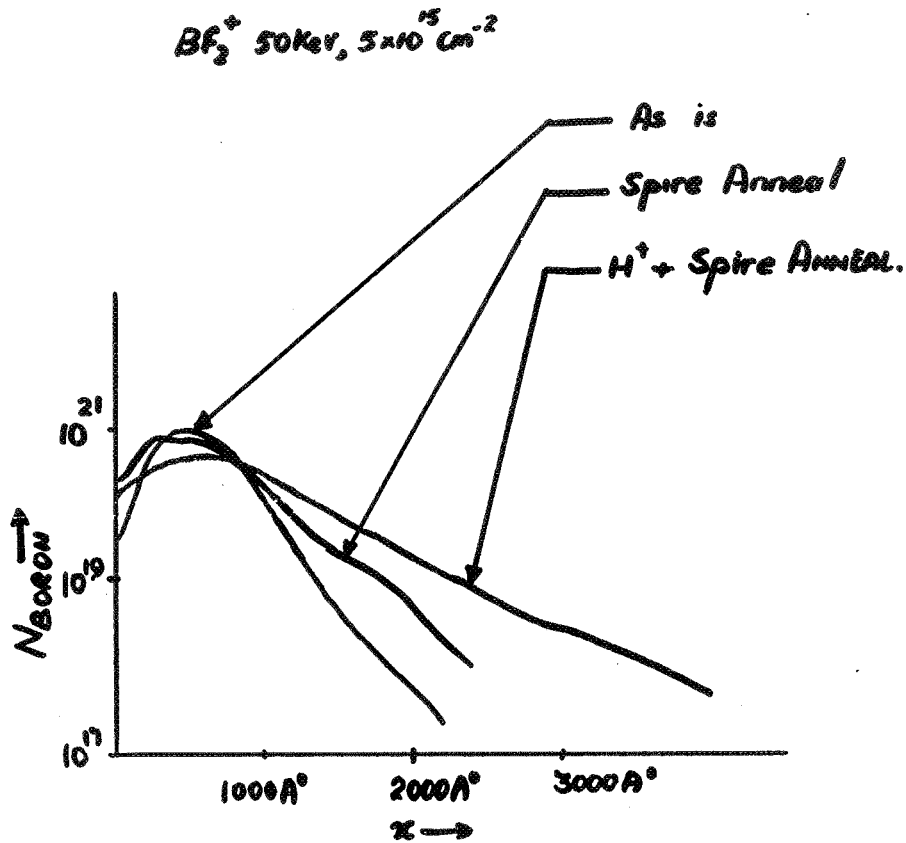
Emitres

- **ARBITRARY Doping PROFILE**
- **1-d FINITE DIFFERENCE FORMULATION**
- **EFFECTIVE FIELDS AS $N_D = f(x)$**
- **HEAVY Doping EFFECT AS $n_{ie}(x)$**
- $\frac{1}{\epsilon} = \frac{1}{\epsilon_0} + \frac{1}{\epsilon_0} \frac{n}{N_{ref}} + C_n n^2$
- **SOLVE FOR MIN. CARRIER CONC. WITH NEUMANN b.c. at front surface and DIRICHLET b.c. at the EMITTER EDGE.**
- **PARAMETER EXTRACTION by MINIMIZATION OF SQUARE OF DEVIATION OF CALCULATED AND MEASURED SR.**

HIGH-EFFICIENCY DEVICE RESEARCH

180 KeV As⁺ 5x10¹⁵ cm⁻².





Conclusions

- DEMONSTRATED PASSIVATION LEADING TO SPACE CHARGE CURRENT REDUCTION
- DEMONSTRATED H^+ CAN REDUCE Sp. NEEDS MORE WORK FOR OPTIMIZATION
- DEVELOPMENT OF A NUMERICAL CODE FOR CALCULATING SR AND EXTRACT PARAMETERS.
- INVESTIGATION OF REGROWTH AND DOPANT REDISTRIBUTION IN (H^+ PROCESSED) IMPLANT AMORPHIZED LAYERS.

PROCESS DEVELOPMENT

Donald B. Bickler, Chairman

Presentations on seven process development activities were made during this technology session. Also included in the session were three presentations on analytical subjects, and one on encapsulation as this material had relevance to PV-cell or module processing. A 30-min coffee break was included to allow time to attend a poster session on in-house research efforts.

Arco Solar, Inc., presented the status of pulsed excimer laser processing of PV cells. Laser annealing results were promising with the best AR coated cell having an efficiency of 16.1%. Better results would be expected with larger laser spot size because there was some degradation in open-circuit voltage (V_{oc}) caused by laser spot overlap and edge effects. Surface heating and photolytic decomposition by the laser was used to deposit tungsten from the reaction of tungsten hexafluoride and hydrogen. The line widths were 5 to 10 mils, and the depositions passed the tape adhesion test. Thinner lines are practical using an optimised optical system.

Another excimer laser processing presentation was given by Spire Corporation. Pulsed excimer laser annealing was successfully performed using a 50 W laser. Both polished and texturized cells were tried, however, there are serious problems with nonuniformity on texturized cells. A number of cells were produced and compared to diffusion furnace annealed cells. There was no clear economic advantage in using an excimer laser and there was a small penalty on average efficiency. The conclusion was that the excimer laser anneal process must be able to produce superior cells to be considered as a viable process option.

Diffusion barrier research at Caltech has been focussed on lowering the chemical reactivity of amorphous thin films on silicon. An additional area of concern is the reaction with metal overlays such as aluminum, silver, and gold. Gold was included to allow for technology transfer to gallium arsenide PV cells. Amorphous tungsten nitride films have shown much promise. Stability to annealing temperatures of 700, 800, and 550°C were achieved for overlays of silver, gold, and aluminum, respectively. The lower results for aluminum were not surprising because there is an eutectic that can form at a lower temperature. It seems that titanium and zirconium will remove the nitrogen from a tungsten nitride amorphous film and render it unstable. Other variables of research interest were substrate bias and base pressure during sputtering.

The MOD work at Purdue is nearly complete. Basic material efforts have proven to be very successful. Adherent and conductive films have been achieved by the investigator as well as other laboratories. A silver neodecanoate/bismuth 2-ethylhexanoate mixture has given the best results in both single and double layer applications. Another effort is continuing to examine the feasibility of applying MOD films by use of an ink-jet printer. Direct line writing would result in a saving of process time and materials. So far, some well defined lines have been printed. Future emphasis will be on reducing line width and improving ink characteristics.

PROCESS DEVELOPMENT

Efforts by the Westinghouse Electric Corporation Research and Development Center were aimed at achieving a simultaneous front and back junction. Lasers and other heat sources were tried. Successful results were gained by two different methods: laser and flash lamp. Polymer dopants were applied to both sides of dendritic web cells. Rapid heating and cooling avoided any cross contamination between the two junctions after removal of the dendrites. Both methods required subsequent thermal annealing in an oven to produce maximum efficiency cells.

Another Westinghouse effort has been directed toward metal patterning by use of an argon laser and Purdue's silver/bismuth MOD material. Excellent cell efficiencies were seen along with good ohmic contact and adhesion. Line widths down to .002 in. were achieved. The only remaining process drawback is line thickness. At present, a secondary electroplating process step is required to obtain sufficient conductivity.

Superwave Technology reported on their microwave-enhanced plasma deposition experiments. Advantages foreseen for use of microwaves are: higher electron plasma density by about 4 orders of magnitude, long species lifetime to allow separation of reactor and plasma generation, more control of deposition kinetics with less substrate damage, controlled film gradients or doping, lower power requirements, and lower reactive gas consumption. The feasibility of this process was demonstrated by the formation of silicon and silicon nitride films.

An updated version of the Solar Array Manufacturing Industry Costing Standards (SAMICS) was presented by the FSA Project Analysis and Integration Area (PA&I) Group. This version will run on the IBM PC-XT or compatibles, and embodies user friendly input screens and numerous "help" options. Use of this microcomputer version will still produce the "old" main frame direct cost driven analysis, although at some cost in turnaround time. A typical simulation will take about 4 h. The program allows for unattended report printout. Also available is the IBM PC (or compatibles) version of the Improved Price Estimation Guidelines (IPEG). This program allows rapid analysis of process variables using SAMICS-generated coefficients.

Another PA&I Group presentation was a life-cycle cost analysis of high-efficiency cells. Although high-efficiency cells produce more power, they also cost more to make and are more susceptible to array "hot-spot" heating. Three different computer analysis programs were used: SAMICS, PVARRAY (an array failure mode/degradation simulator), and Lifetime Cost and Performance (LCP). The high-efficiency cell modules were found to be more economical in this study, but parallel redundancy is recommended.

Springborn Laboratories, Inc., has continued their evaluation of the EVA encapsulation system. This work is part of the materials baseline needed to demonstrate a 30-year module lifetime capability. Process and compound variables are both being studied along with various module materials. Results have shown that EVA should be stored rolled up, and enclosed in a plastic bag to retard loss of peroxide curing agents. The TBEC curing agent has superior shelf life and processing than the earlier Lupersol-101 curing agent. Analytical methods were developed to test for peroxide content, and experimental methodologies were formalized.

PROCESS DEVELOPMENT

The poster session covered two areas of in-house research: amorphous-silicon deposition and process-variable sensitivity analysis. Amorphous-silicon deposition efforts have focussed on the basics of large chamber radio frequency (RF) plasma deposition. Significant findings include means to inhibit formation of silane polymers and the calculation of a monosilane diffusivity value one order of magnitude higher than most published values (better agreement with textbook values).

Process variable sensitivity analysis was used to define useful regions of substrate material characteristics. A region of practical material and processing specifications was defined to show areas where process research activities would have the maximum effect.

PULSED EXCIMER LASER PROCESSING

ARCO SOLAR, INC.

David Wong

Goal

TO DEMONSTRATE THE COST EFFECTIVE FEASIBILITY OF FABRICATING HIGH EFFICIENCY SOLAR CELLS ON CZ WAFERS USING A PULSED EXCIMER LASER FOR JUNCTION FORMATION, SURFACE PASSIVATION, AND FRONT METALLIZATION.

Objectives

I. JUNCTION FORMATION

- A. ION IMPLANT PARAMETERS
- B. SURFACE CONDITIONS
- C. LASER ANNEALING
 - LASER BEAM UNIFORMITY & OVERLAP FACTOR
 - LASER ENERGY DENSITY

II. METALLIZATION

LASER-ASSISTED CHEMICAL VAPOR DEPOSITION

- A. DEPOSITION RATE
- B. ADHESION
- C. PLATE UP

III. SURFACE PASSIVATION (SiO₂)

- A. DEPOSITION RATE
- B. ADHESION
- C. EFFECTIVENESS IN PASSIVATION

PRECEDING PAGE BLANK NOT FILLED

PROCESS DEVELOPMENT

I. JUNCTION FORMATION

A. IMPLANT PARAMETERS

1. IMPLANT ENERGY: SHALLOW JUNCTION REQUIRES LOW KEV
LOWEST AVAILABLE -5 KEV
OPTIMIZED JUNCTION DEPTH ≥ 0.25 MICRON

EXTENSIVE SEARCH FOR LOWER ENERGY IMPLANT SERVICES
UNSUCCESSFUL.

ALTERNATE APPROACHES INCLUDED:

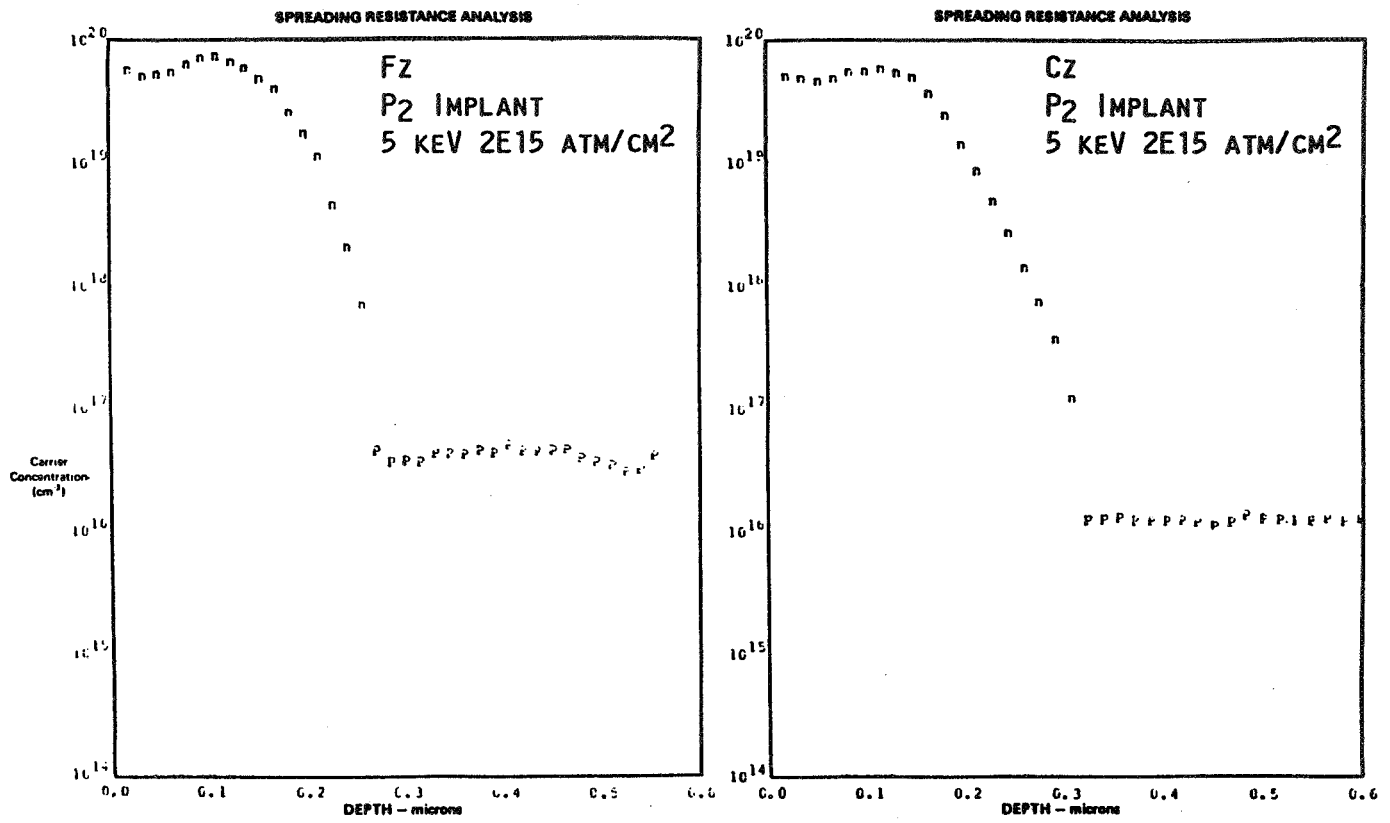
- PH_3 , BF_2 MOLECULAR IMPLANT AT CALCULATED ENERGY -3 KEV
(EFF 9.1%)
- $^{62}\text{P}_2$ ION IMPLANT AT 5 KEV
GOOD RESULT ON FZ MATERIAL (EFF $\geq 10.8\%$)
COULD NOT REPEAT ON Cz
DEPTH PROFILE SUGGESTED SLOWER GRADIENT THAN $^{31}\text{P}_1$

EMPIRICALLY CHOSEN - 1.8 TO 2.5×10^{15} ATOMS/ CM^2 ,
SHEET RHO -40-60 OHMS/SQ

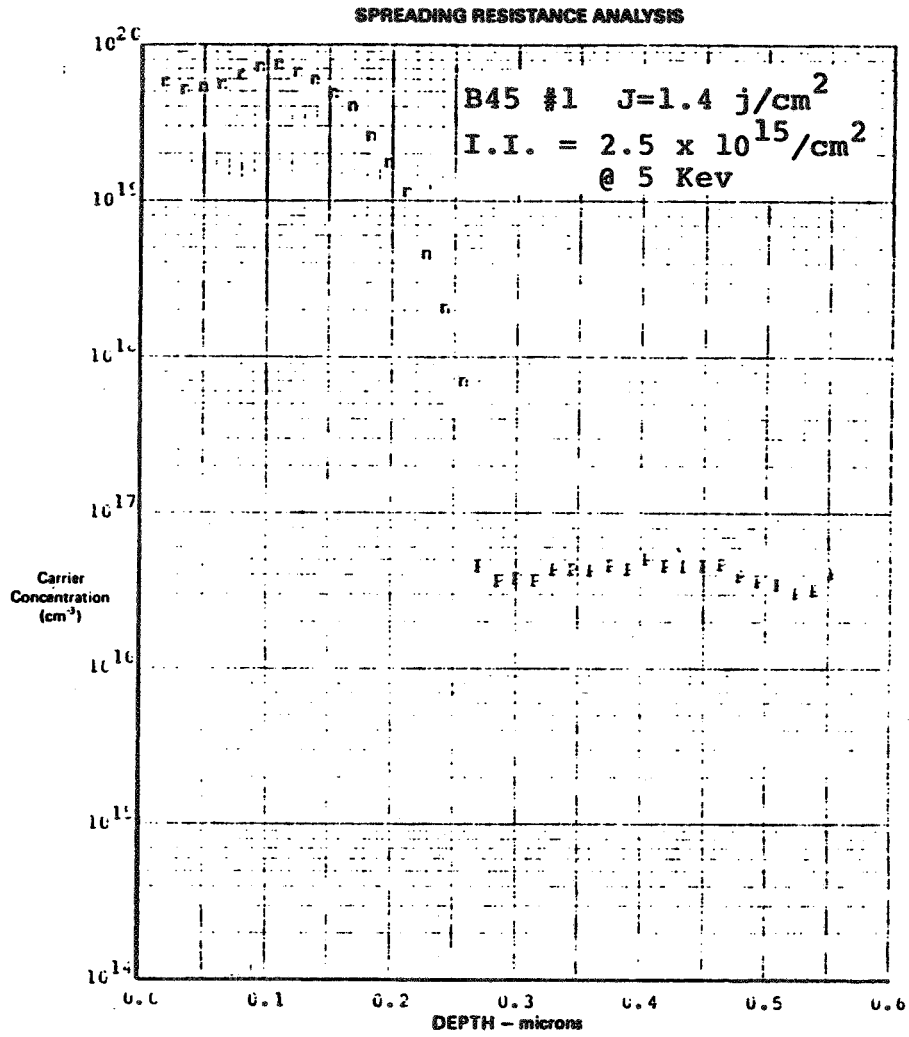
AGREEABLE TO THE SUGGESTED SURFACE CONCENTRATION PER UNIT AREA
FOR CRITICAL MISFIT DISLOCATION GENERATION.

HOWEVER, JUNCTIONS ALWAYS HAVE A DEGENERATE LAYER DEEPER THAN
0.1 MICRON, LIMITING BLUE RESPONSE.

PROCESS DEVELOPMENT



PROCESS DEVELOPMENT



ORIGINAL PAGE IS
OF POOR QUALITY

1.B. SURFACE CONDITIONS

SURFACE CONDITION SERIOUSLY AFFECTED CELL V_{OC} AND FILL FACTOR; MUCH MORE CRITICAL THAN IN CONVENTIONAL THERMALLY DIFFUSED CELL. (LIQUID PHASE DIFFUSION VS SOLID PHASE DIFFUSION.)

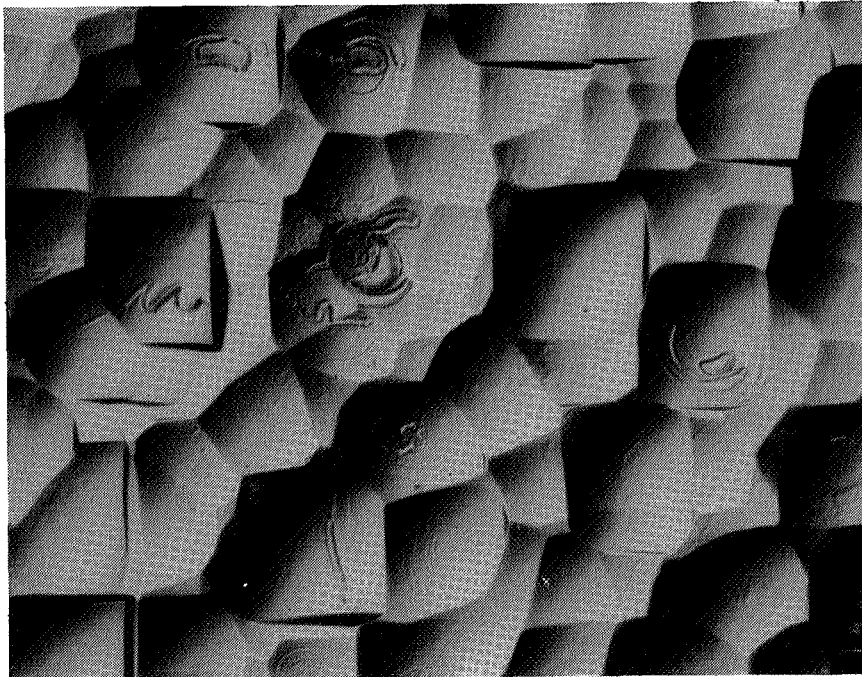
SURFACE FINISHING:

- TEXTURED SURFACE NOT RECOMMENDED FOR LASER ANNEALING; NONUNIFORM MELTING INTRODUCED STRESS ON SURFACE.
- CHEMICALLY POLISHED SURFACE ALSO LOWERED FILL FACTOR, ALTHOUGH TO LESSER EXTENT.
- ONLY HIGH QUALITY CHEM-MECH POLISHED WAFER FOUND SUITABLE FOR THE PROCESS.

SURFACE CLEANING: (BEFORE AND AFTER IMPLANT)

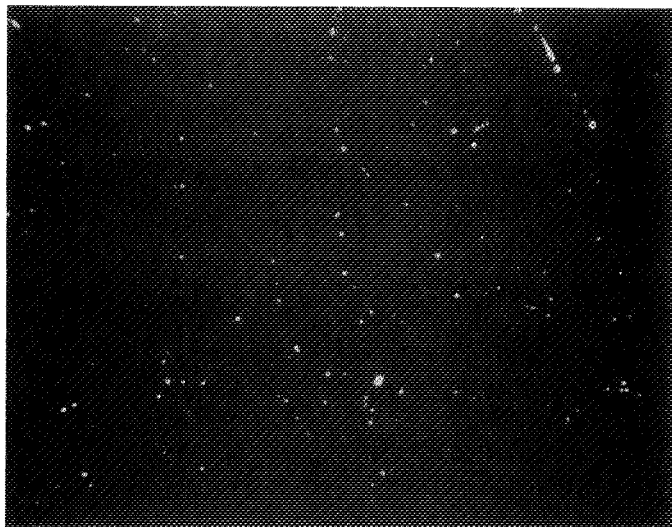
BESIDES STANDARD DEGREASING AND ACID RINSING, ION IMPLANTED WAFER MUST BE SPRAY ETCHED WITH 1% HF FOLLOWED BY SPRAY RINSE WITH 18 MEG-OHM DOUBLE-FILTERED @ 0.2 MICRON ABSOLUTE DI WATER.

Laser-Annealed, Chemically Polished Silicon Wafer

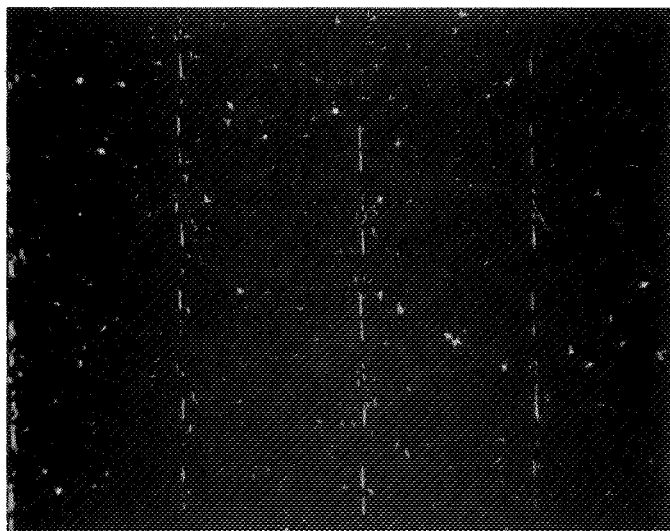


PROCESS DEVELOPMENT

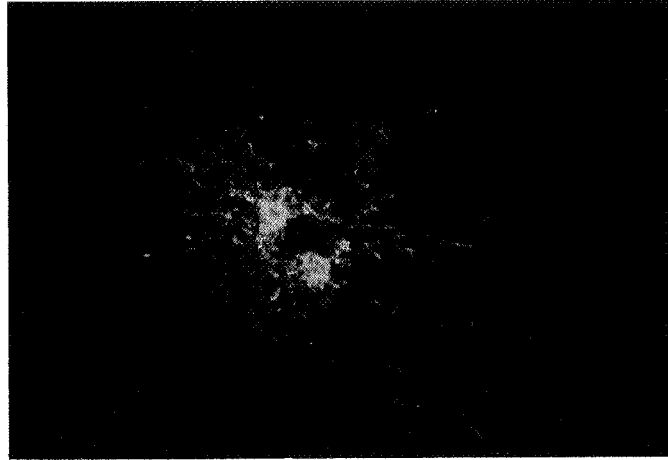
Surface Contamination After Cleaning



Laser Annealed



Laser Annealed



I.C. LASER ANNEALING

- BECAUSE OF NONUNIFORM LASER (EXCILITE 1) BEAM, OVERLAP FACTOR WAS FOUND BEST AT 50%; 4X ANNEALING ON EACH SPOT.

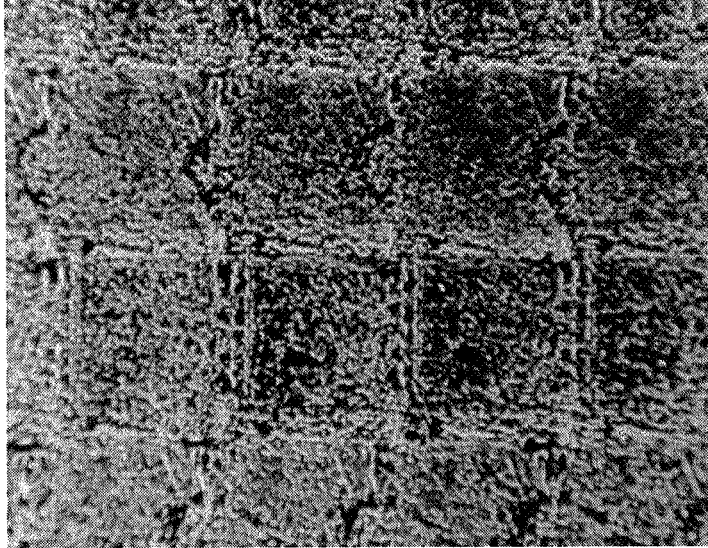
HOWEVER, 50% OVERLAP ALSO DRIVES JUNCTION DEEPER THAN DESIRED WITH THE PRESENCE OF A FLAT DEGENERATE LAYER LIMITING BLUE RESPONSE.

JUNCTION MUST BE ETCHED BACK IN HF:HNO₃ SOLUTION IN ORDER TO RECOVER SHORT WAVELENGTH RESPONSE.

- ENERGY DENSITY
EMPIRICALLY FOUND $\sim 1.5 \text{ J/cm}^2$

LOWER THAN 1.4 J/cm^2 -- INCOMPLETE ANNEALING
HIGHER THAN 1.6 J/cm^2 -- SURFACE DAMAGE

Surface Damage at 1.6 j/cm², 50% Overlap



II. METALLIZATION

CONDITIONS: ARF AT 198 NM, OUTPUT ENERGY -15 MJ
ENERGY DENSITY -1.2 J/cm².

REACTION CHAMBER PRESSURE -5 TORR, BEAM PERPENDICULAR
TO SURFACE.

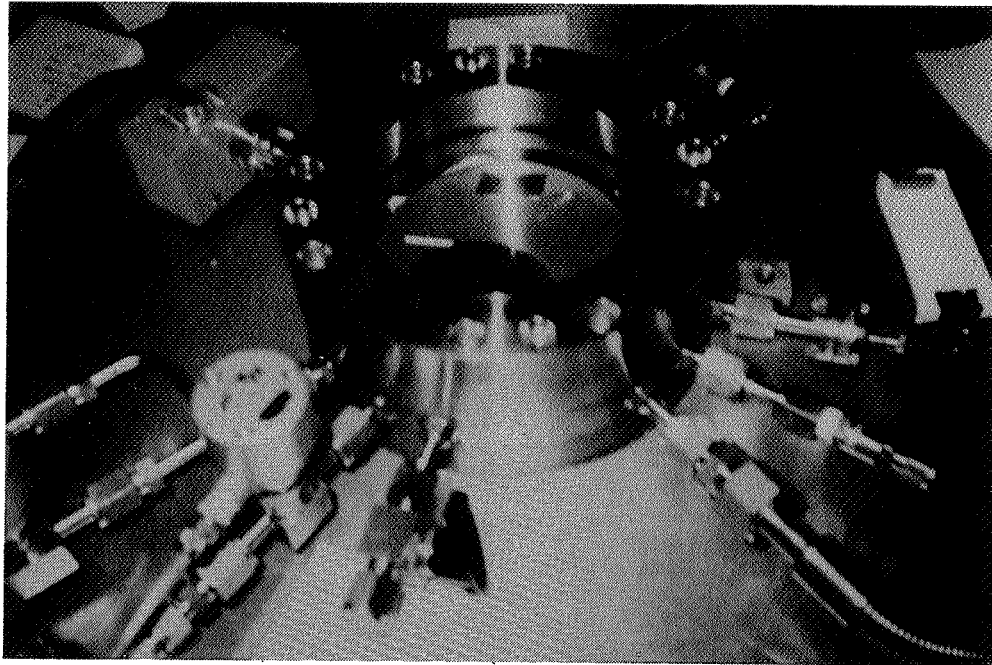
CHEMICAL REACTION: $WF_6 + 3H_2 \xrightarrow{h\nu} W + 6HF$

RESULTS (PRELIMINARY):

- TUNGSTEN LINE OBTAINED -5-10 MILS WIDE
- PASSED TAPE TEST
- THICKNESS -500-1000Å (250 SHOTS);
HOWEVER, DOUBLE HUMP STRUCTURE: FLAT AT THE CENTER.
- EXACT METAL COMPOSITION IS BEING DETERMINED BY AUGER
ANALYSIS.

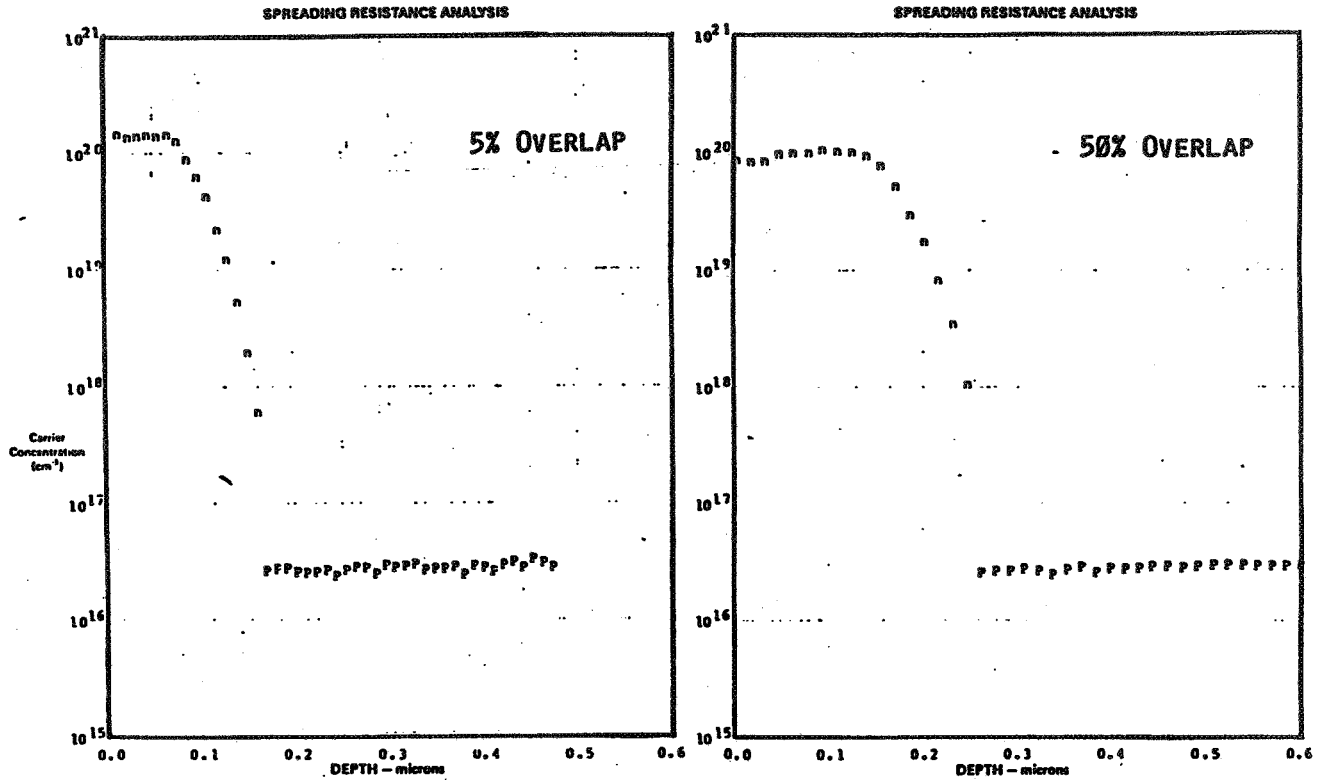
PRECEDING PAGE BLANK NOT FILMED

PROCESS DEVELOPMENT



ORIGINAL PAGE IS
OF POOR QUALITY

PROCESS DEVELOPMENT



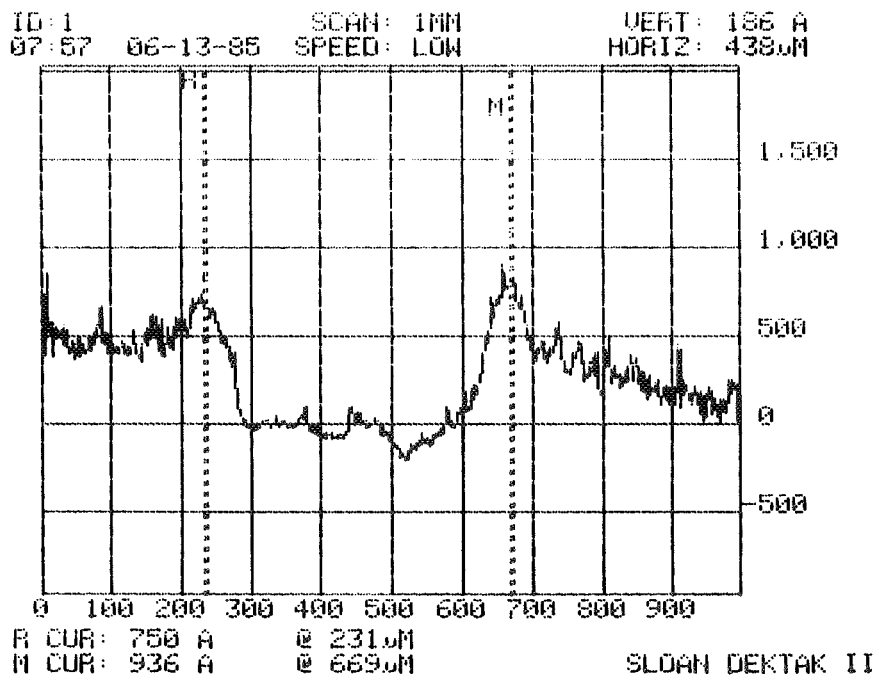
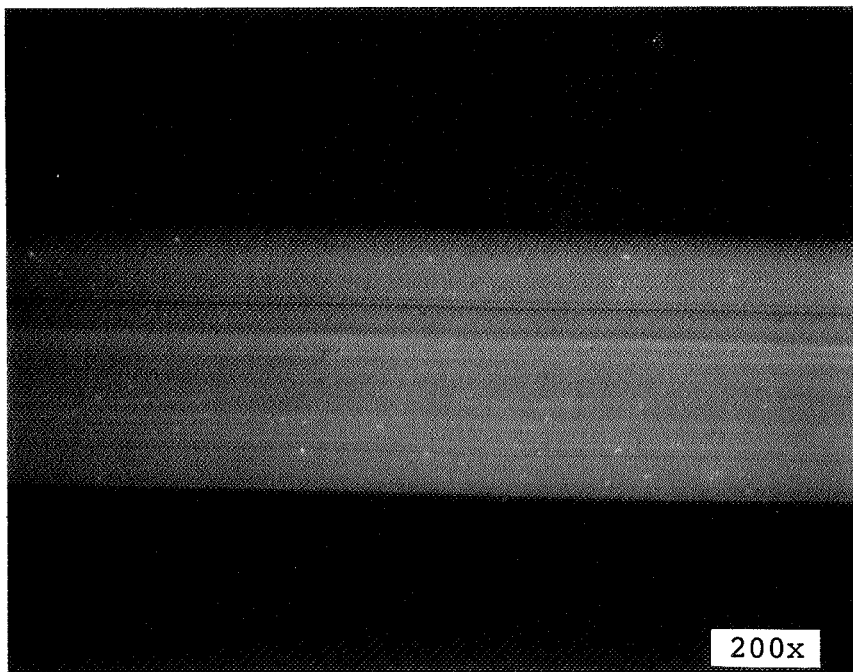
JUNCTION DEPTH PROFILES OF 1.4 J/CM² LASER-ANNEALED SAMPLES WITH 5% AND 50% OVERLAP.

(RESULTS FROM COLLABORATIVE PROJECT BETWEEN ARCO SOLAR AND OAK RIDGE NATIONAL LABORATORY)

PROCESS DEVELOPMENT

ORIGINAL PAGE IS
OF POOR QUALITY





DEKTAk MEASUREMENT ACROSS THE DEPOSITED
METAL LINE. NOTE THE VALLEY IS BELOW
THE WAFER SURFACE.

PROCESS DEVELOPMENT

III. SURFACE PASSIVATION

CONDITIONS: ARF AT 198 NM, OUTPUT ENERGY - MAX

CHAMBER PRESSURE -6-10 TORR, BEAM PARALLEL TO WAFER SURFACE.

CHEMICAL REACTION: $\text{SiH}_4 + 4\text{N}_2\text{O} \xrightarrow{h\nu} \text{SiO}_2 + 2\text{H}_2\text{O} + 4\text{N}_2$

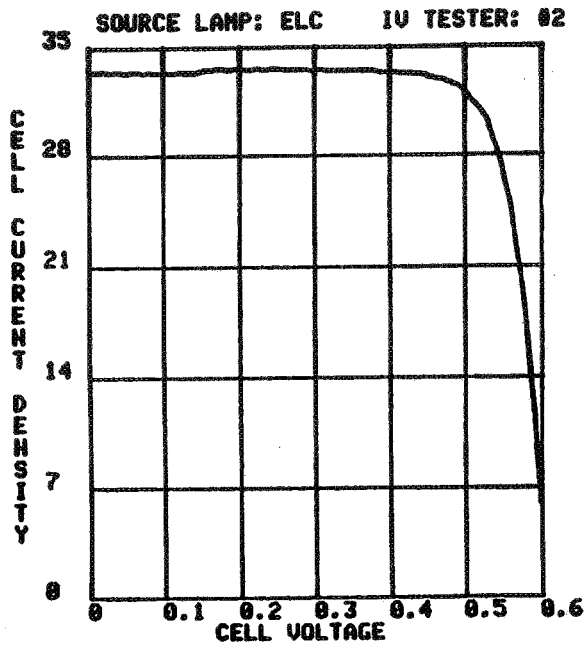
DEPOSIT RATE -600°-800°A/MIN

(EXPERIMENT TO BE PERFORMED)

Summary of Achievements

1. BATCH MODE LASER ANNEALING ACCOMPLISHED ON 50 2"x2" Cz WAFERS.
BEST CELL EFFICIENCY AFTER AR COATING IS 16.1% (WITHOUT BSF).
SPECTRAL RESPONSE IS SUPERIOR TO COMMERCIAL THERMALLY DIFFUSED CELL (WITH BSF) IN BLUE WAVELENGTH.
LOWER V_{OC} IN LASER ANNEALED WAFER IS DUE TO LASER BEAM EDGE DAMAGE.
2. LCVD TUNGSTEN LINES ON SILICON SURFACE SUCCESSFULLY DEPOSITED WITH GOOD ADHESION.

PROCESS DEVELOPMENT



SINGLE/POLY
 LIGHT IV AT 25C
 OPERATOR: D WONG
 CELL: ASEC LA 03 A
 Date/time: 18-JUN-85 12:36:57

AREA: 4.00 (sq.cm)

Isc: 0.134 (amps)
 Jsc: 33.50 (ma/sq)
 Voc: 0.609 (volts)

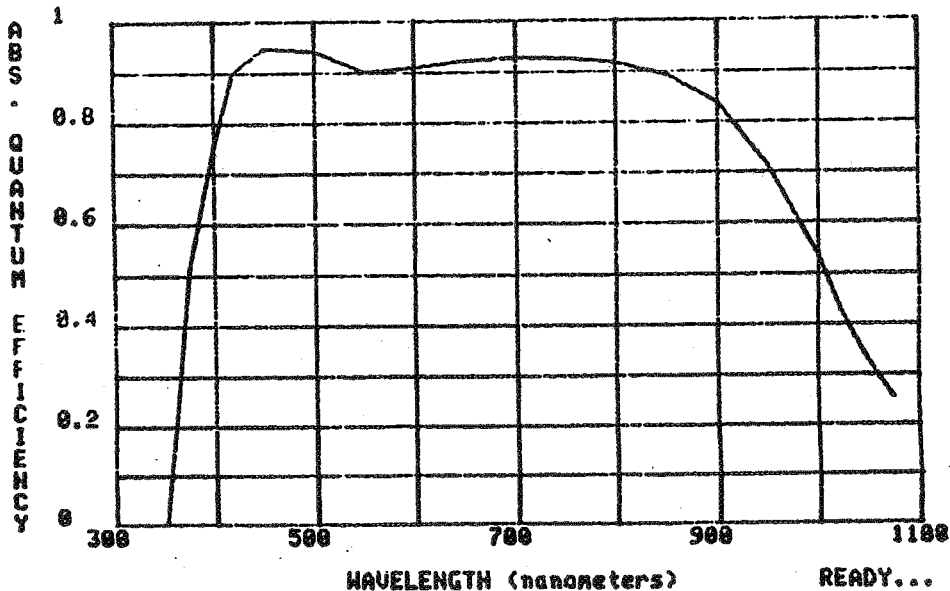
Ipn: 0.125 (amps)
 Jpn: 31.36 (ma/sq)
 Vpn: 0.514 (volts)

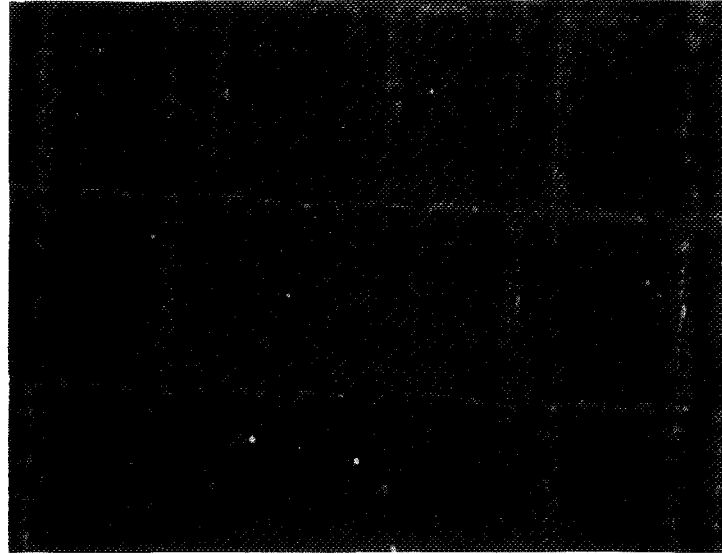
Pn: 0.064 (watts)
 Cff: 78.99 %
 Eff: 16.11 %

ASEC CONTACTS AND A/R
 LASER ANNEALED
 SURFACE DIRTY, HEAT TREATED

B62 LASER ANNEALED @
 1.47 J/cm²

Sample: ASEC METALIZATION, HEAT TREATED #3
 Voltage: 0.000 Volts Light Bias: N
 Date/time: 18-JUN-85 15:45:44 Operator: D WONG
 System Calibrated 18-JUN-85 15:21:06 Standard Cell #325





DAMAGES AT THE LASER BEAM EDGES
THAT LED TO V_{OC} DEGRADATION.

Problems

1. JUNCTION FORMATION

PROCESS EXPENSIVE AND TIME-CONSUMING. CELL EFFICIENCY MATCHES BUT IS NOT HIGHER THAN CONVENTIONAL THERMAL PROCESS.

2. UNABLE TO PROCESS LARGE AREA (5") CELLS DUE TO LACK OF ION IMPLANT FACILITY.

3. METALLIZATION

SLOW PROCESS. SILVER PLATING ON TUNGSTEN IS QUESTIONABLE.

4. PASSIVATION

CAN CVD SiO_2 DEACTIVATE THE DANGLING SILICON BONDS ON THE SURFACE?

EXCIMER LASER ANNEALING FOR FABRICATION OF LOW-COST SOLAR CELLS

SPIRE CORP.

M.B. Spitzer
A.C. Greenwald
S.J. Hogan

Program Goal

TO DETERMINE IF PULSED EXCIMER LASER ANNEALING (PELA) IS COST EFFECTIVE COMPARED TO BASELINE PROCESS.

BASELINE PROCESS

CLEAN
DRY
DIFFUSE JUNCTION
ALUMINUM BSF
CLEAN
PRINT Ag BACK
PRINT Ag FRONT
LASER CUT
TEST AND SORT

LASER PROCESS

CLEAN
DRY
ION IMPLANT
LASER ANNEAL
PRINT Ag BACK
PRINT Ag FRONT
LASER CUT
TEST AND SORT

Objectives

- BUILD AN EXCIMER LASER PULSED ANNEAL APPARATUS
- DEVELOP ANNEAL PROCESSING FOR HIGH EFFICIENCY CELLS
- FABRICATE 300 SOLAR CELLS
- PERFORM ECONOMIC ANALYSIS

PROCESS DEVELOPMENT

Laser-Annealed AR-Coated Cells

<u>CELL</u>	<u>LOT</u>	<u>ρ</u> <u>(Ω cm)</u>	<u>V_{oc}</u> <u>(mV)</u>	<u>J_{sc}</u> <u>(mA/cm²)</u>	<u>FF</u> <u>(%)</u>	<u>Eff</u> <u>(%)</u>
4615-4d	SW-27	0.34	616	31.2	80.2	15.4
4615-8e	WA70055	0.31	614	31.7	79.9	15.6
4615-12d	WA70055	0.17	617	30.4	80.2	15.0
4615-16a	WA20820	0.34	616	31.2	80.0	15.4
4615-20b	WA20979	2.2	592	32.0	79.5	15.1

NOTES: INSOLATION WAS SIMULATED AM1, 100mW/cm². T=28°C. A=4cm².

Advantages and Disadvantages of Laser Annealing

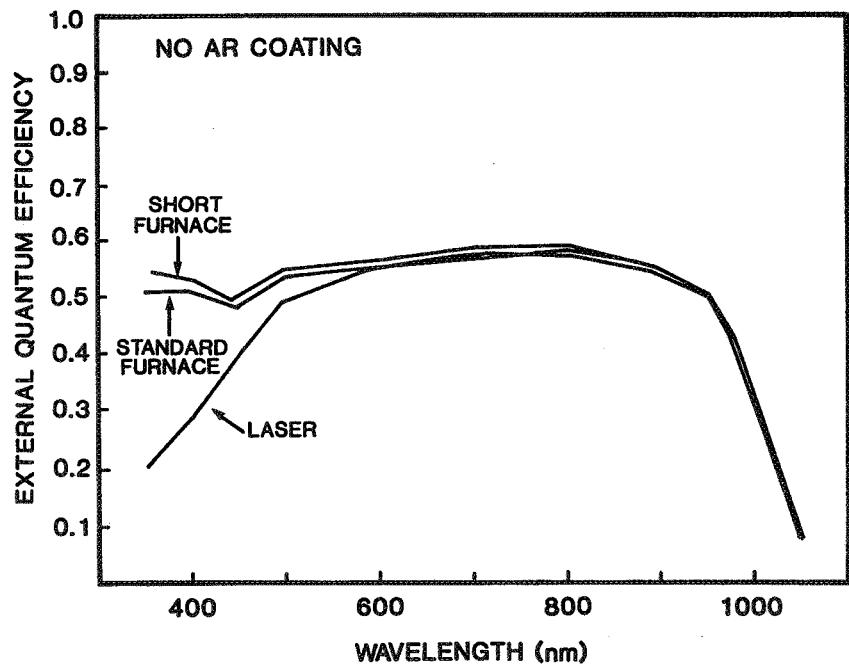
- RAPID DRY PROCESSING
- NO HEATING OF THE WAFER
- TEXTURED WAFERS DIFFICULT TO ANNEAL
- NOT COMPATIBLE WITH SiO₂ PASSIVATION

PROCESS DEVELOPMENT

Best-Cell Comparison of Laser Annealing With
Furnace Annealing (No AR Coatings)

<u>CELL</u>	<u>ANNEAL</u>	<u>V_{oc}</u> <u>(mV)</u>	<u>J_{sc}</u> <u>(mA/cm²)</u>	<u>FF</u> <u>(%)</u>	<u>Eff</u> <u>(%)</u>
4615-4d	LASER	607	22.6	79.5	10.9
4524-13e	SHORT FURNACE	612	23.6	81.4	11.8
4524-9c	STANDARD FURNACE	615	23.9	82.0	12.0

NOTES: INSOLATION WAS SIMULATED AM1, 100 mW/cm². T=28°C. A=4cm².

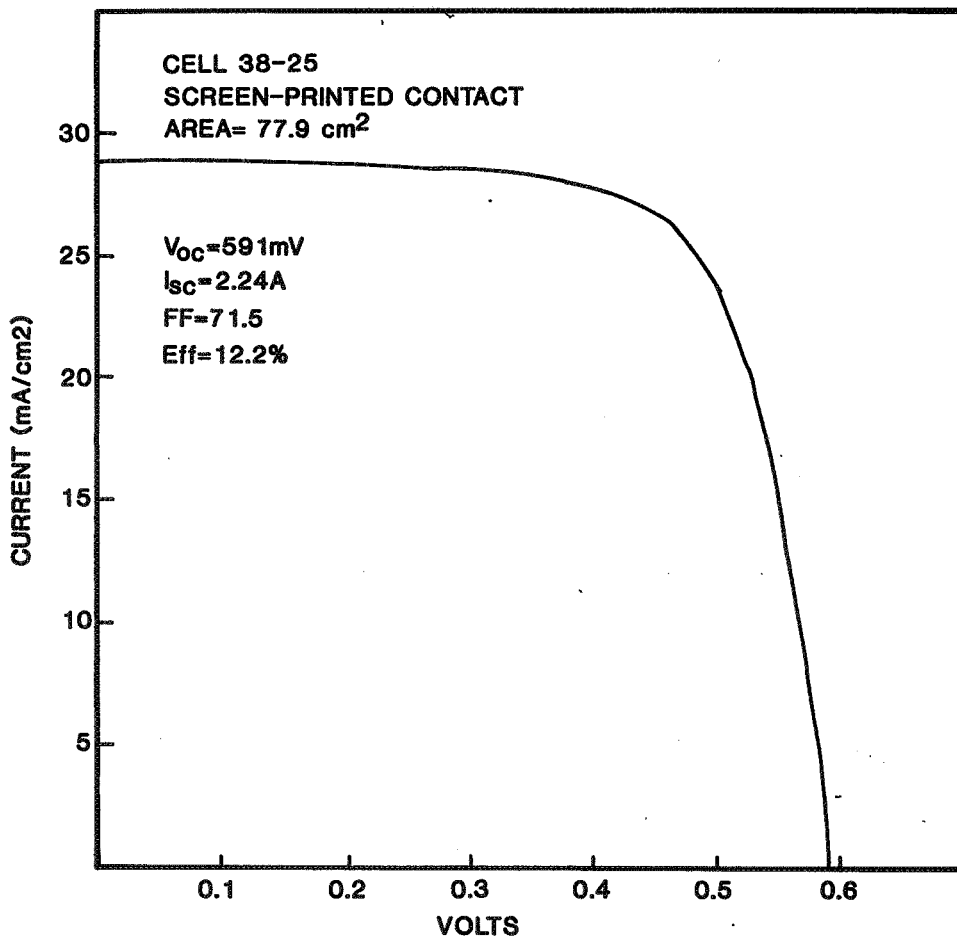


PROCESS DEVELOPMENT

Large-Area AR-Coated Solar Cells

<u>NO. OF CELLS</u>	<u>METALLIZATION</u>	<u>ANNEAL</u>	<u>V_{oc} (mV)</u>	<u>J_{sc} (mA/cm²)</u>	<u>FF (%)</u>	<u>Eff (%)</u>
7	PRINTED	LASER	589	27.1	72.8	11.5
7	PRINTED	FURNACE	590	28.9	71.5	12.1
4	EVAPORATED	LASER	590	28.9	77.9	13.3
5	EVAPORATED	FURNACE	591	30.8	77.4	14.1

NOTES: AREA OF EVAPORATED CELLS IS 53cm².
 AREA OF SCREEN-PRINTED CELLS IS 77.9cm².
 INSOLATION WAS AM1,100mW/cm². T=28°C



PROCESS DEVELOPMENT

Excimer-Laser-Annealed Solar Cells

<u>CONTACT</u>	<u>NO. OF CELLS</u>	<u>V_{oc} (mV)</u>	<u>J_{sc} (mA/cm²)</u>	<u>FF (%)</u>	<u>Eff (%)</u>	<u>Effx1.4 (%)</u>
EVAPORATED (53cm ²)	92	580 (3)	21.2 (0.3)	78.1 (0.6)	9.6 (0.2)	13.4 (0.3)
PRINTED (77.9cm ²)	25	580 (2)	19.9 (0.3)	71.0 (2.0)	8.2 (0.3)	11.5 (0.4)

NOTES: INSOLATION WAS AM1, 100mW/cm². T=28°C.

Summary of Economic Analysis

<u>PROCESS</u>	<u>COST-PER-WAFER (1985\$)</u>
ION IMPLANT PHOSPHORUS (SPI-ION 1000)	0.18
TUBE FURNACE ANNEAL	0.07
BELT FURNACE ANNEAL	0.035
EXCIMER LASER	0.05

1MW/SHIFT, 3 SHIFTS/DAY, 90% YIELD.

PROCESS DEVELOPMENT

Principal Findings

- (1) **EXCIMER LASER ANNEAL IS SATISFACTORY WHEN APPLIED TO POLISHED WAFERS. ANNEALING OF TEXTURED WAFERS REQUIRES FURTHER WORK.**
- (2) **THE 50 WATT EXCIMER LASER IS CAPABLE OF HIGH THROUGHPUT PROCESSING.**
- (3) **LASER UNIFORMITY IS SUFFICIENT.**
- (4) **SCREEN-PRINTED CONTACTS CAN BE APPLIED TO EXCIMER-LASER-ANNEALED WAFERS.**
- (5) **ANALYSIS INDICATES THAT THE LASER MUST PRODUCE BETTER CELLS THAN THE FURNACE TO BE ECONOMICALLY COMPETITIVE.**

AMORPHOUS METALLIC FILMS
IN SILICON METALLIZATION SYSTEMS
CALIFORNIA INSTITUTE OF TECHNOLOGY

Frank So
Elzbieta Kolawa
Marc-A. Nicolet

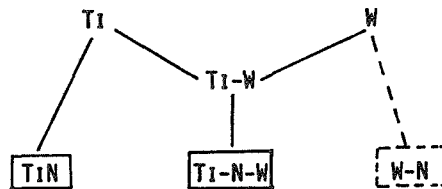
Previous Findings

AMORPHOUS BINARY METALLIC ALLOYS (E.G. NI-W, W-ZR):

- CRYSTALLIZATION TEMPERATURE $T_c = 650^\circ\text{C}$ (NI-W),
 900°C (W-ZR).
- REACT WITH SI SUBSTRATE AND METAL OVERLAYERS
(E.G. AL, AG, AU) BELOW T_c .
- USEFUL AS DIFFUSION BARRIERS UP TO $\sim 500^\circ\text{C}$ WITH
AL OVERLAYER.
- ADDING N SUPPRESSES REACTION WITH AL UP TO $\sim 550^\circ\text{C}$.

Amorphous W-N

MOTIVATION:

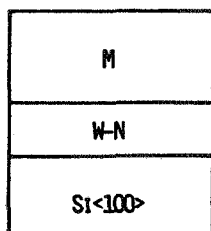


- SPUTTERED $\text{Ti}_{10}\text{W}_{90}$ COMMONLY USED DIFFUSION BARRIER.
- ADDING N IMPROVES BARRIER FOR SI/TI-N-W/AU.
- SPUTTERED TiN WELL STUDIED, SUCCESSFUL.
- STUDY W-N.

PROCESS DEVELOPMENT

Experimental Procedures

- SUBSTRATE: SI <100>, HIGH RESISTIVITY (900 Ω -CM), AND SiO₂.
- BARRIER LAYER W-N: R.F. SPUTTERING; 400W; 10MTORR (AR + N₂); N₂ CONCENTRATION: 0, 5, 10, 20, 40, 80%; \sim 900 Å.
- METAL OVERLAYER M: R.F. SPUTTERED AL, AG, AU WITHOUT BREAKING VACUUM; 1000 - 4000 Å.
- VACUUM ANNEALING: $\leq 7 \times 10^{-7}$ TORR; 400-900°C, 30 MIN.
- CHARACTERIZATION: RBS, X-RAY DIFFRACTION; SHEET RESISTANCE, SEM, AES.



M = AL, AG, AU

Figure 1

Sketch of W-N Phase Diagram Including Metastable Forms

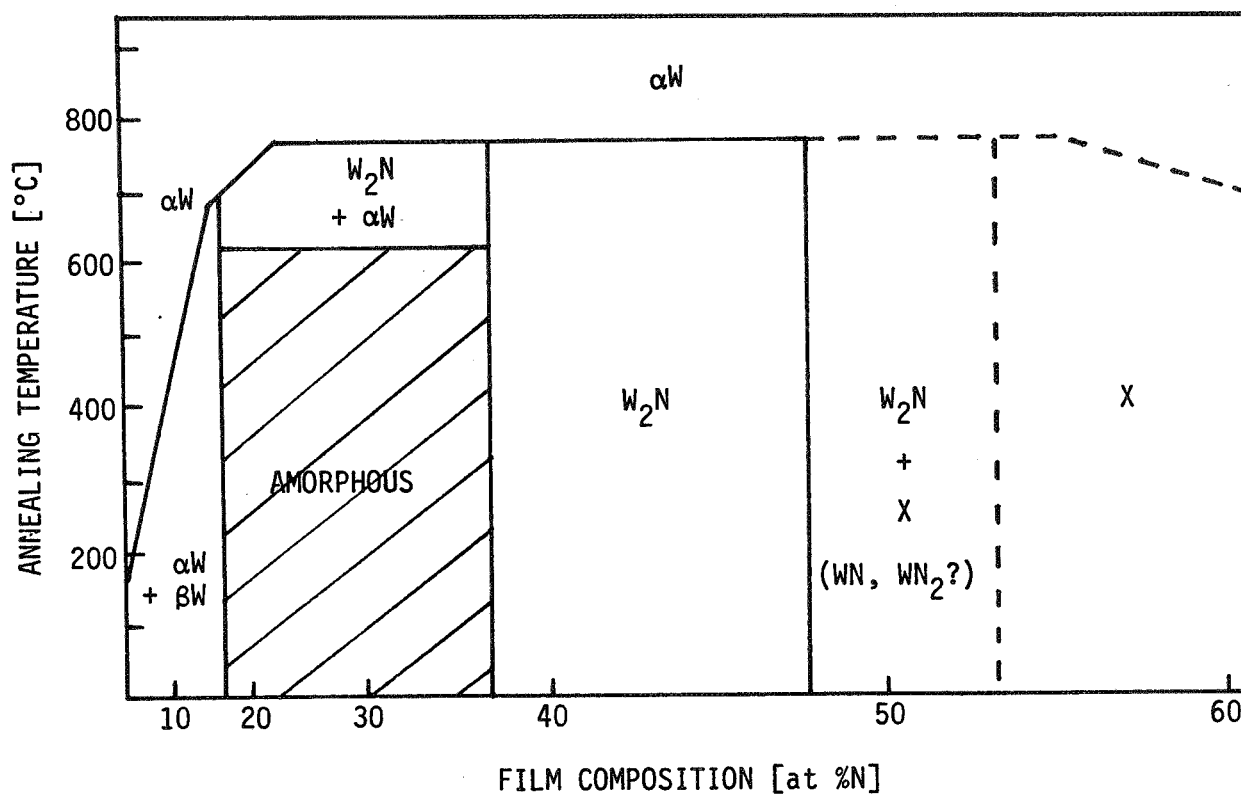
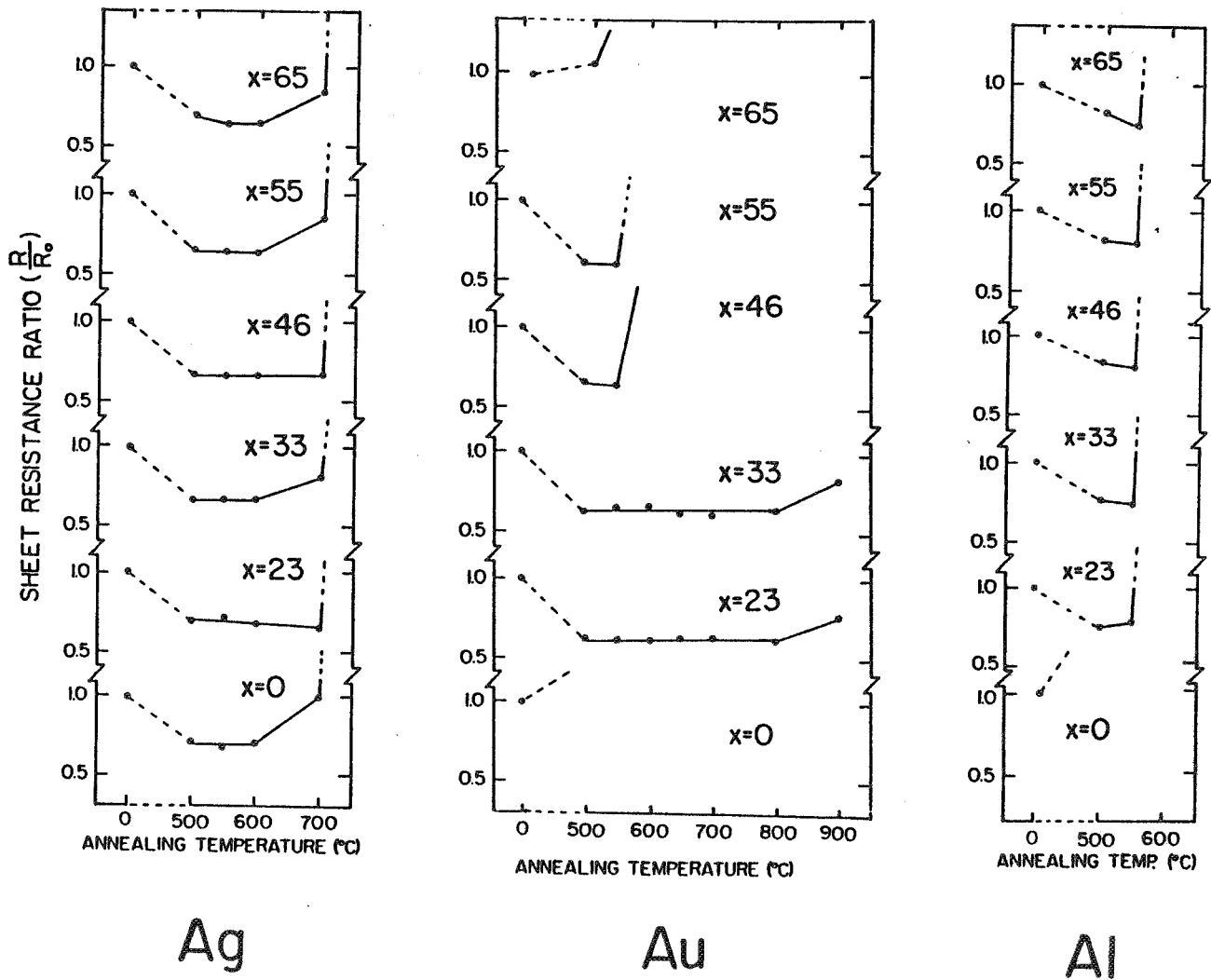


Figure 2

Normalized Sheet Resistances of $Si/W_{100-x}N_x/Metal$



NORMALIZED SHEET RESISTANCES OF $Si/W_{100-x}N_x/M$
 (M = AL, AG, AU) SAMPLES AS A FUNCTION OF ANNEALING
 TEMPERATURE (30 MIN).

PROCESS DEVELOPMENT

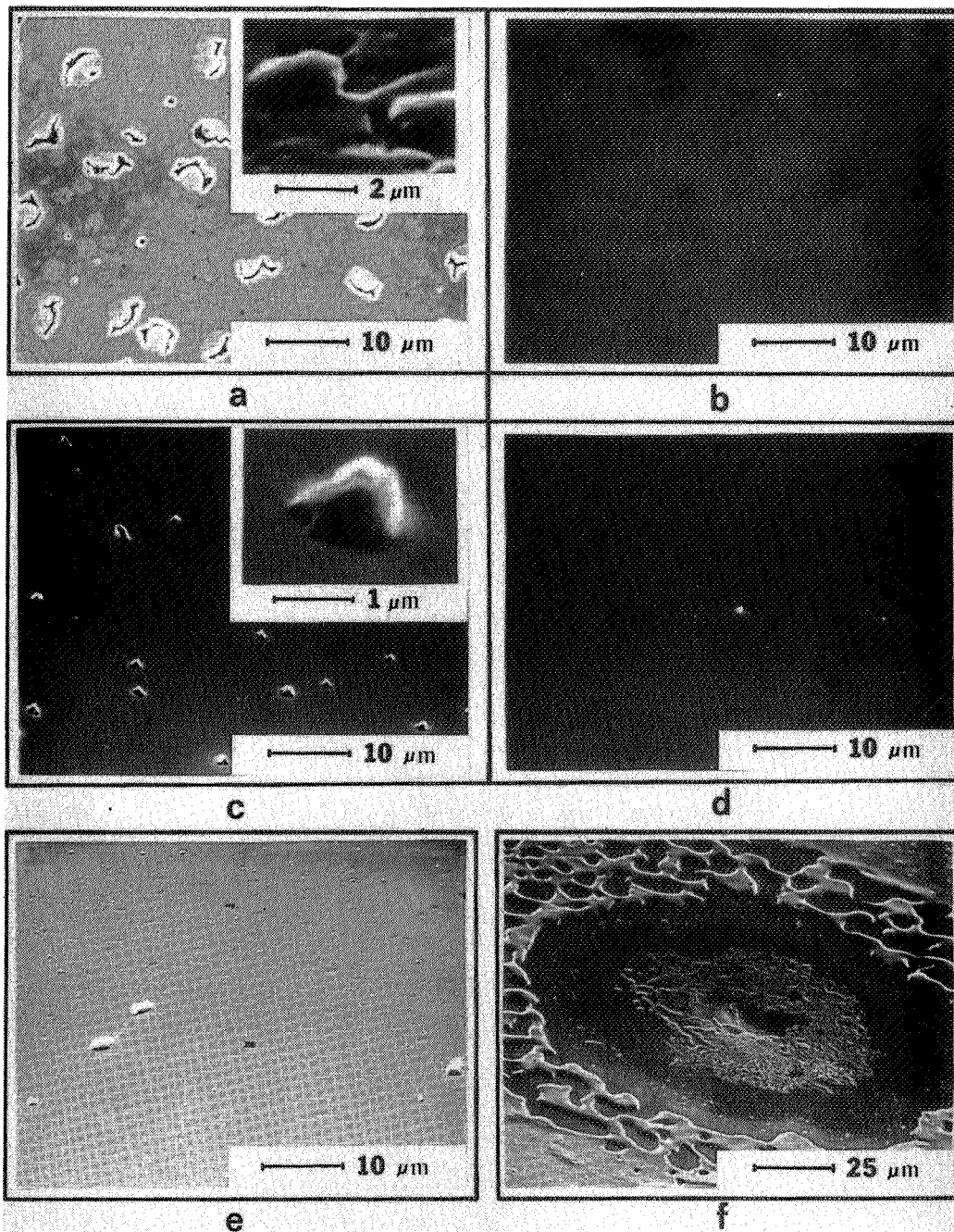
Observations on Figure 2

- PURE W ($x = 0$) FAILS BELOW 500°C, 30 MIN FOR AU, AL.
- FOR AG AND AL: AMORPHOUS AND POLYCRYSTALLINE W-N EQUALLY GOOD.
- FOR AU: ONLY AMORPHOUS W-N IS GOOD.
- FAILURE MODE: DELAMINATION → LOCALIZED CHEMICAL INTERACTION → LARGE SCALE INTERMIXING.

Conclusions

- GOOD BARRIER BETWEEN SI <100> AND
 - AG: $\sim 20 < x < \sim 70$ UP TO 700°C, 30 MIN.
 - AU: $\sim 20 < x < \sim 40$ UP TO 800°C, 30 MIN.
 - AL: $\sim 20 < x < \sim 70$ UP TO 550°C, 30 MIN.

Figure 3

ORIGINAL PAGE IS
OF POOR QUALITY

SEM micrographs of annealed Si/W-N/metal samples before and after chemical etching of the metal overlayer. (A) Blistering and fracturing is seen in the Si/W₄₅N₅₅/Ag sample after annealing at 700°C. (B) Etching of Ag removes the characters. (C) Blistering is seen in the Si/W₇₇N₂₃/Au sample after annealing at 600°C. (D) Etching of Au removes the characters. The few characters of the Si/W₆₇N₃₃/Al sample annealed at 55°C (E) are also removed by etching Al (not shown). (F) A typical localized failure point observed in Si/W-N/Au (and Si/W-N/Al) samples annealed above the eutectic temperature of the overlayer with silicon.

PROCESS DEVELOPMENT

Amorphous Bilayers

AL METALLIZATION SCHEME; AT 550°C

Si/W-N/AL	STABLE
Si/W-Zr/AL	NOT STABLE
Si/W-Zr/W-N/AL	NOT STABLE
Si/Ti/W-N/AL	NOT STABLE
Si/TiN/W-N/AL	STABLE

POSSIBLE EXPLANATION:

- Ti (OR Zr) DEPRIVES W-N OF N UPON ANNEALING.

NEED AES FOR N PROFILING.

Outlook

QUESTIONS:

- FOR $\sim 20 < x < \sim 40$: ROLES OF N AND MICROSTRUCTURE IN INHIBITING Si/W-N/AU INTERDIFFUSION.
- ROLE OF SUBSTRATE BIAS AND BASE PRESSURE IN SPUTTERING CHAMBER.
- WHY DOES Ti CAUSE THERMAL INSTABILITY IN Si/Ti/W-N/AL AT 550°C?

FUTURE WORK:

- TEST AMORPHOUS BARRIERS ON SHALLOW JUNCTIONS.
- TEM STUDY OF W-N FILMS.
- AMORPHOUS BILAYERS.

MOD SILVER METALLIZATION: SCREEN PRINTING AND INK-JET PRINTING

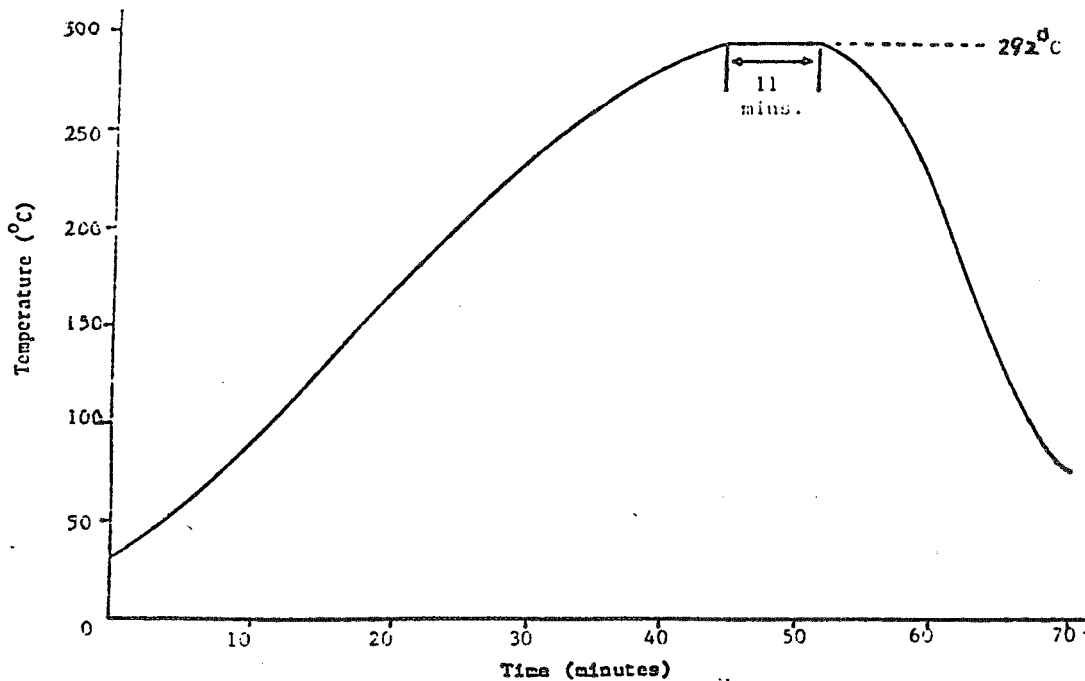
PURDUE UNIVERSITY

R.W. Vest
G.M. Vest

Experimental Variables

1. Ink Chemistry
2. Deposition Parameters
3. Time-Temperature Processing

Time-Temperature Profile for Standard Firing Sequence No. 1



PRECEDING PAGE BLANK NOT FILMED

PROCESS DEVELOPMENT

Ink Chemistry

1. Silver Compound
Ag Neodecanoate
2. Adhesion Agent
3. Solder Leach Resistant Agent
4. Solvent(s)
 - a. Screen Printing
Low Boiling - Benzene
High Boiling - Neodecanoic
Acid: Butyl Carbitol
Acetate (2:1)
 - b. Ink Jet Printing
Low Boiling

PROCESS DEVELOPMENT

Properties of Metallo-Organic Base Metal Oxide Binder Compounds and Those of Silver Inks Formulated with Them.

Binder Compound	T _D (°C)	w/o Product	T _D for 97/3 Ink (°C)	Comments
Bismuth 2-ethylhexanoate in benzene	340	14.4	310	Smooth ink decomposition with all but 1 w/o decomposed by 270°C.
Chromium (II) 2,4-pentanedionate solid	270 ^(a)	4.2	318	Definite 2-stage ink decomposition occurs at 232°C.
Nickel 2-ethylhexanoate in benzene	323	5.0	292	All but 3.6 w/o decomposed by 232°C. Possible 2-stage decompositing occurring.
Cobalt 2-ethylhexanoate in benzene	292	8.4	283	2-stage ink decomposition occurs at 243°C and 283°C, although its not as severe as in Ag/Cr ink.

(a) Except for 1 w/o, which decomposed by 365°C.

PROCESS DEVELOPMENT

Fired Front Contact Properties of Inks with Four Different Compounds Added for Potential Adhesion Promotion.

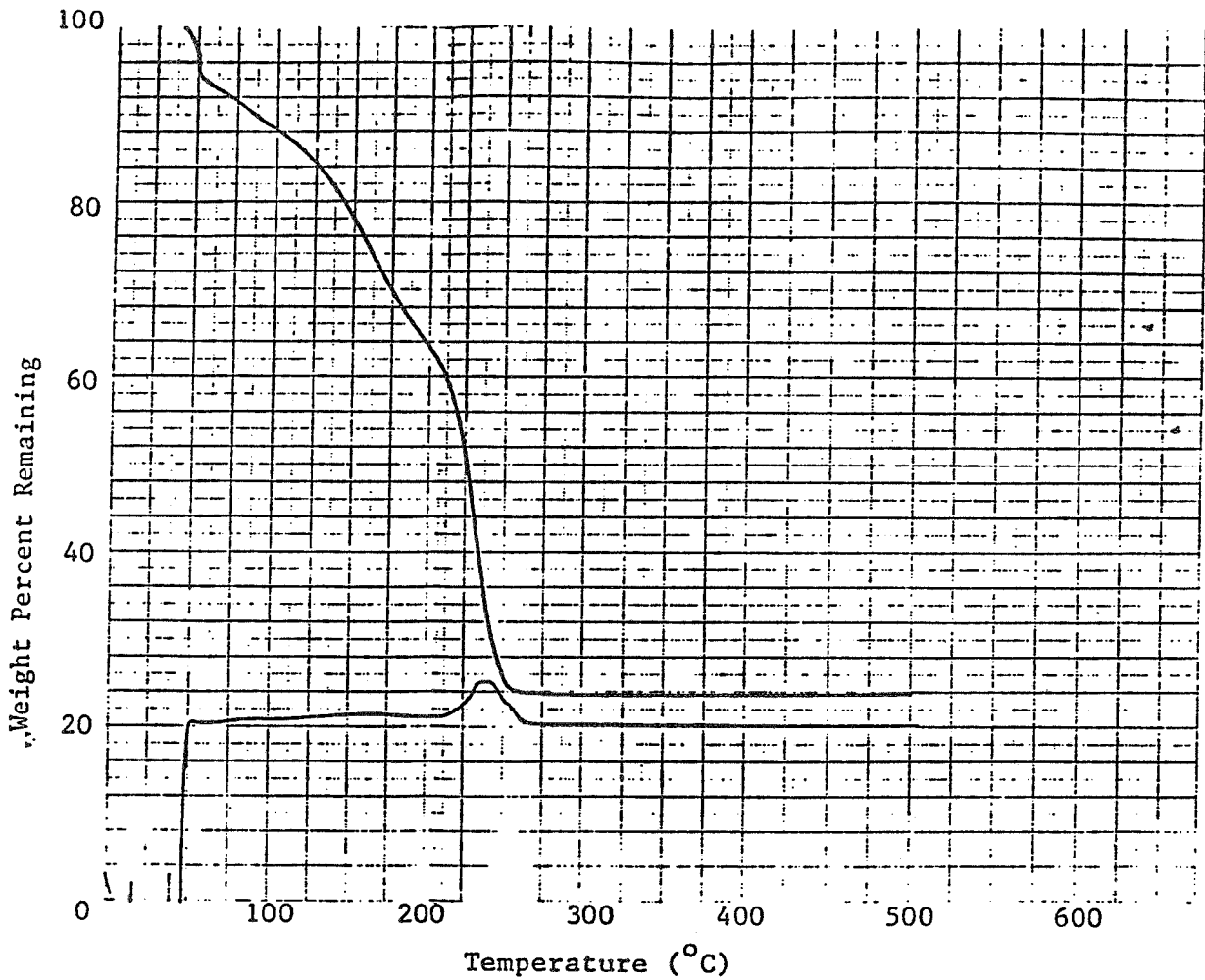
Ink	Fired Film Appearance	Line Defin.	Sheet Resistance ($m\Omega/sq \pm \sigma$)			Initial Adhesion
			# of Films	Initial Value	Value After 60 sec. Spike at 800 °C	
Ag/Bi (SPC3-3A)	silver with copperish tint	A	16	40.1 ⁺ -3.9	24.9 ⁺ -1.5	excellent
Ag/Cr	dark silver/grey	A/B	7	89.0 ⁺ -3.8	51.2	good to excellent
Ag/Ni	dark with purple tint	A	9	157.7 ⁺ -7.5	91.3	excellent
Ag/Co	dark with greenish yellow tint	A	9	>860	98.3	fair to good

PROCESS DEVELOPMENT

Firing Study Results for Bismuth Oxide Content Optimization

Ink ^(a) Chemistry	# of Layers	Line Defin.	Sheet Resist. (mΩ/sq)	Initial Adhesion
95% Ag 5% Bi	1	A	57.9	Excellent
95% Ag 5% Bi	2	A	32.3	One half of bus bar poor. Excellent elsewhere.
97% Ag 3% Bi	1	A	40.3	Excellent
97% Ag 3% Bi	2	A/B	24.6	Excellent, small piece of bus bar removed.
99% Ag 1% Bi	1	A/B	38.8	Excellent
99% Ag 1% Bi	2	B	21.1	One half of bus bar poor. Excellent elsewhere.

(a) Based on expected theoretical fired film composition which is not verified analytically.



Thermogram of ink SC-10 at 10°C/minute

Important Properties

Theor. Fired Film Composition: 99 wt.% Ag - 1 wt.% Bi

T_D : 257°C

Inorganic Content: 23.6 wt. %

PROCESS DEVELOPMENT

Fired Film Thickness Values and Resistivity Calculated Values.

Film I.D.	Average Film Thickness (μm)			Sheet Resist. ($\mu\Omega/\text{sq}$)	Resistivity ($\mu\Omega\text{-cm}$)
	Bus Bar	Finger	Overall Average		
1 Layer Pure Silver	1.08	0.62	7.6×10^{-5}	2.62×10^4	1.99
1 Layer 1 w/o Bi	0.75	0.53	5.9×10^{-5}	3.88×10^4	2.30
1 Layer 3 w/o Bi	1.21	0.58	7.7×10^{-5}	4.03×10^4	3.11

PROCESS DEVELOPMENT

Summary of the Effects of 60 Second Thermal Spiking.

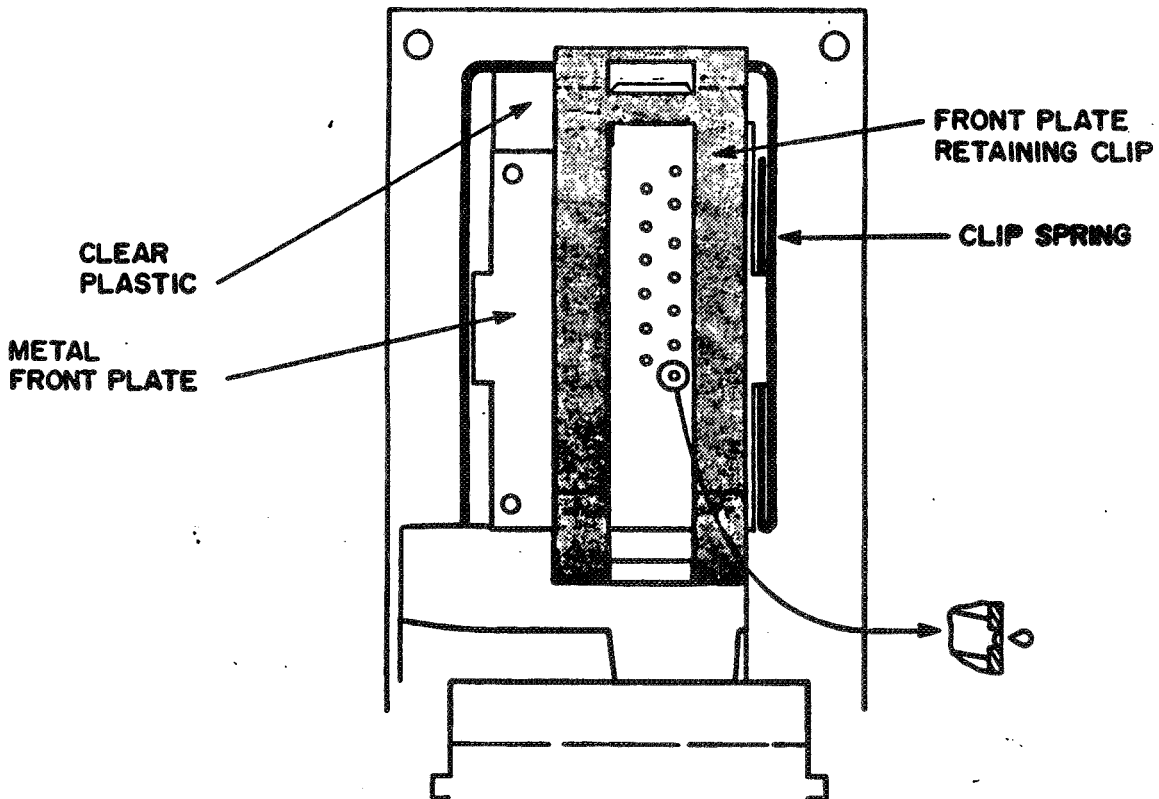
Bismuth Content (wt. %)	Spiking Temp. (°C)	Initial Sheet Resist. (mΩ/sq)	Final Sheet Resist. (mΩ/sq)	Δ Sheet Resist. (mΩ/sq)	Adhesion Effects	Photovoltaic Response Improvement
5	600	57.8	27.1	30.7	Good before spiking. Excellent after spiking.	Slight Negative
5	700	61.0	26.9	34.1	Same as Above	Very Positive
5	750	59.2	27.1	32.1	Same as Above	Very Positive
5	800	53.6	25.7	27.9	Same as Above	Very Positive
3	600	41.4	27.5	13.9	Excellent Before & After Spiking.	None
3	700	39.6	26.0	13.6	Same as Above	Slight Negative
3	750	37.7	26.5	11.2	Same as Above	Positive
3	800	37.3	24.9	12.4	Same as Above	Positive
1	600	37.4	26.1	11.3	Excellent Before & After Spiking.	Slight Positive
1	700	37.8	24.2	13.6	Same as Above	Positive
1	750	38.0	27.9	10.1	Same as Above	Very Positive
1	800	36.4	28.6	7.8	Same as Above	Very Positive

PROCESS DEVELOPMENT

Photovoltaic Evaluation of MOD Silver (1 w/o Bi) Metallized Solar Cells Without AR Coating.

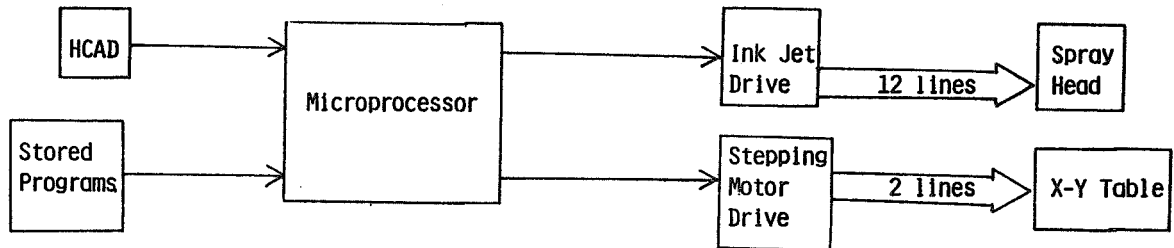
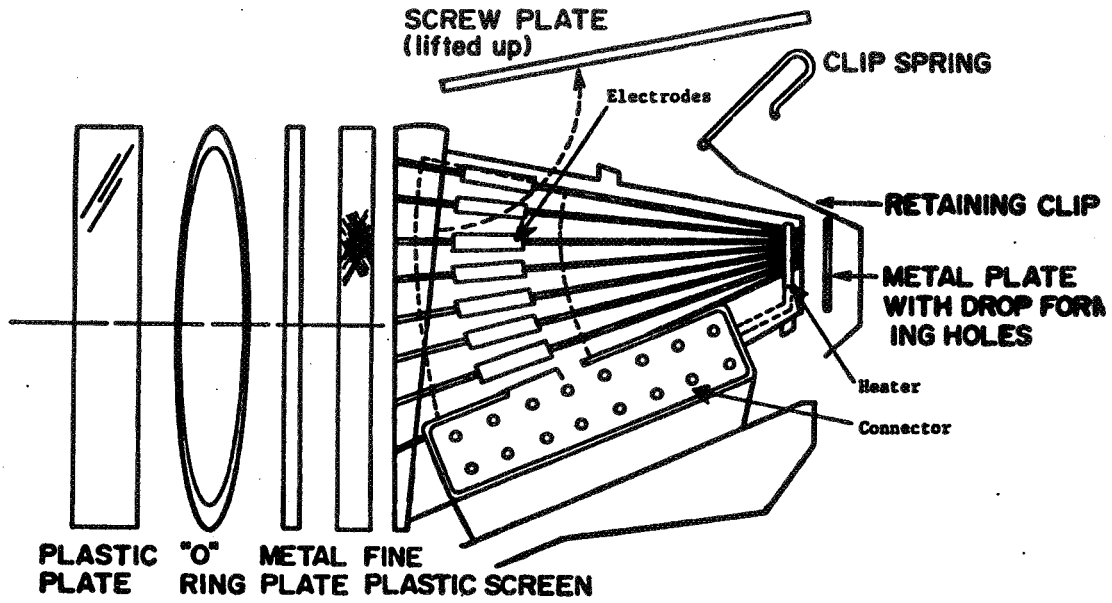
Cell Description	V_{oc} (mV)	I_{sc} (mA)	Efficiency (%)	Fill Factor	Series Resist. (ohms)	Shunt Resist. (ohms)	Sheet Resist. ($m\Omega/sq$)
Single Layer MOD Silver	530.4	72.6	6.1	0.633	1.171	99.4	39
Two Layer MOD Silver	522.6	66.8	3.5	0.401	2.658	49.8	21

Nozzle Assembly (Front View)

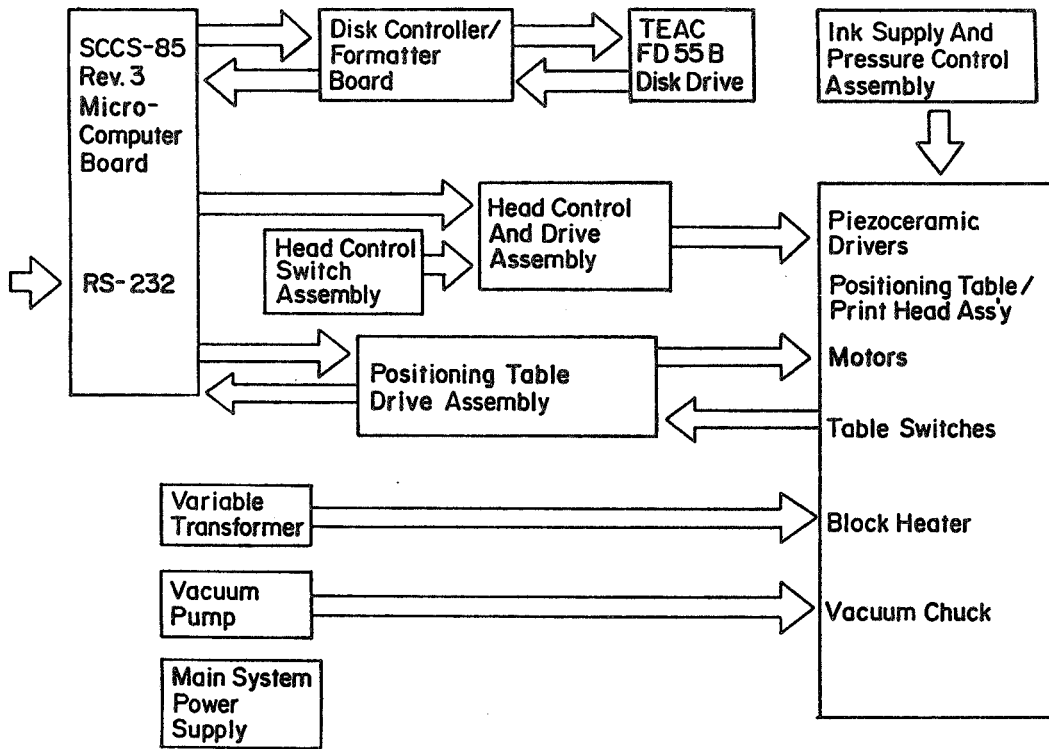


PROCESS DEVELOPMENT

Nozzle Assembly (Side View)



Ink-Jet Printing System



Ink Requirements

1. No Particulates
2. Low Viscosity
3. High Surface Tension
4. High Inorganic Content
5. Non Clogging
6. Stable

PROCESS DEVELOPMENT

Ink-Jet Printing Studies

Ink Parameters

1. viscosity
2. surface tension
3. metal content
4. solvent vapor pressure

Printer Parameters

1. pulse voltage
2. pulse frequency
3. ink pressure
4. nozzle diameter
5. nozzle-substrate separation

Substrate Parameters

1. velocity
2. temperature

Firing Parameters

1. heating rate
2. maximum temperature
3. time at maximum temperature

Solvents Evaluated for Ink-Jet Printing

Solvent	B.P. (°C)	Comments
xylene	137	Poor line definition for thick prints.
toluene	111	Poor line definition for very thick prints
cyclohexane	80.7	Voids in prints
benzene	80	Good prints
hexane	69	Clogging
tetrahydrofuran	66	Clogging

PROCESS DEVELOPMENT

Theory

w = dry film width

t = dry film thickness

$$tw = C \left(\frac{f}{s} \right) v$$

C = constant for a given ink and printer

f = drop frequency

s = substrate speed

v = velocity of ink in nozzle

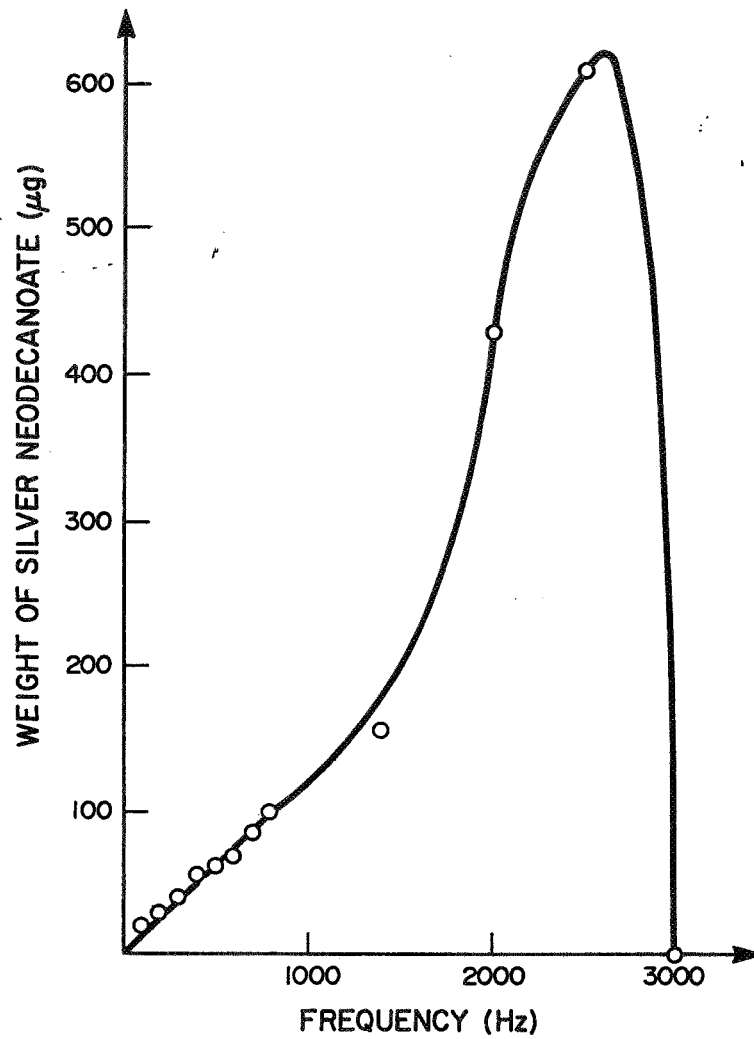
$v = v(n, \gamma, V)$ for a given printer

n = ink viscosity

γ = ink surface tension

V = input voltage

PROCESS DEVELOPMENT



Summary

1. Screen printed MOD Ag films with low porosity and excellent adhesion can be formed on Si below 300°C.
2. The photovoltaic response is promising, but the contact resistance must be reduced.
3. Excellent line definition can be achieved with ink jet printed MOD inks.

PROCESS RESEARCH OF NON-Cz MATERIAL
WESTINGHOUSE ELECTRIC CORP.

Robert B. Campbell

Contract Information

**OBJECTIVE: INVESTIGATE HIGH-RISK, HIGH PAY-OFF IMPROVEMENTS TO WESTINGHOUSE
BASELINE SEQUENCE**

TIME PERIOD: JANUARY 1985 - AUGUST 1985

Contract Tasks

- INVESTIGATE EXCIMER LASER DRIVE OF LIQUID DOPANTS IN DENDRITIC WEB SILICON
- CONDUCT PROCESS SENSITIVITY STUDIES
- DEVELOP COST ANALYSIS (FORMAT A's)
- INVESTIGATE OTHER ADVANCED TECHNIQUES FOR JUNCTION FORMATION

Potential Benefits

- FEWER PROCESSING STEPS
- MORE RAPID PROCESSING
- LESS COSTLY PROCESSING
- MORE UNIFORM CELL PARAMETERS

C-6

PROCESS DEVELOPMENT

Junction Formation Using an Excimer Laser

APPROACH

HEAT SURFACES OF WEB WITH LASER TO DIFFUSE LIQUID DOPANTS

CONDITIONS

WAVELENGTH - 3080 nm

POWER INPUT TO WEB - 0.5 to 2.5 Joules/cm²

EXPERIMENT

DRIVE B, P, AND AL INTO BOTH N-TYPE AND P-TYPE WEB

LASER PROCESSING CARRIED OUT AT SPECTRA TECHNOLOGY, BELLEVUE, WA,

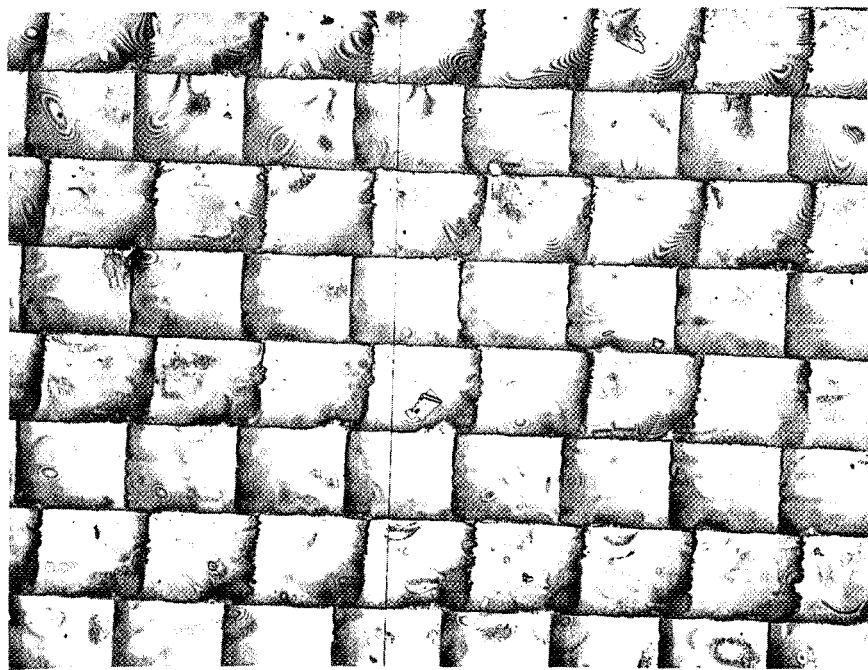
Results: Excimer Laser

- JUNCTION CHARACTERISTICS
 - N⁺N OR N⁺P (PHOS. DOPED) $C_0 = 10^{19}/\text{cm}^2$ $X_j = 0.2 - 0.25 \mu\text{m}$
 - P⁺N OR P⁺P (B DOPED) ESSENTIALLY NO JUNCTION
 - P⁺P (AL DOPED) ESSENTIALLY NO JUNCTION
- CELL PROPERTIES
 - P TYPE WEB, $\eta_{\text{max}} = 9.6\%$ - DUE TO HIGH RESISTANCE BACK CONTACT (BOTH B & AL BSF)
 - N TYPE WEB, $\eta_{\text{max}} < 1\%$ - POOR B DOPED EMITTER
- ANNEALING UP TO 800°C IMPROVES CELL PROPERTIES
- NO CROSS-CONTAMINATION NOTED
- CRYSTAL PAIRS PROCESSED BASELINE SEQUENCE - $\eta = 14\%$ (TOTAL LIQUID SYSTEM)

Sample 18A, p-Base Web, Al BSF 1.5 J/cm²



Sample 14B, p-Base Web, Boron BSF 2.0 J/cm²



PROCESS DEVELOPMENT

Summary of Data

PROCESS	AVG. EFF. (%)
1. WESTINGHOUSE BASELINE - DIFFUSION WITH TOTAL LIQUID SYSTEM (P100 & B150)	14.0
2. P100 FRONT JUNCTION - LASER DRIVE B150 BACK JUNCTION - DIFFUSED	13.2
3. P100 FRONT JUNCTION - DIFFUSED B150 BACK JUNCTION - LASER DRIVE	10.0
4. P100 FRONT JUNCTION - DIFFUSED B150 BACK JUNCTION - LASER DRIVE BACK SURFACE DAMAGED	11.0
5. P100 FRONT JUNCTION - LASER DRIVE B150 BACK JUNCTION - LASER DRIVE	8.6
6. P100 FRONT JUNCTION - LASER DRIVE B150 BACK JUNCTION - LASER DRIVE ANNEAL 700°C - 1 HR IN N ₂	9.6

Dark I-V Data on Selected Cells

Process and Cell ID	Eff. (%)	R _s (Ωcm ²)	R _{sh} (K Ωcm ²)	J01 (A/cm ²)	J02 (A/cm ²)	Diffusion Length* (μm)
11-1 Total laser process + 700°C anneal	10.1	.68	22	4.7 x 10 ⁻¹¹	1.8 x 10 ⁻⁶	26
12-2 Total laser process	8.1	.88	6	1.5 x 10 ⁻¹⁰	6.4 x 10 ⁻⁶	19
68-1 Laser drive front junction, diffused BSF	13.2	.68	1.0	1.3 x 10 ⁻¹¹	2.5 x 10 ⁻⁶	36

Front Junction Dopant - P100

Back Junction Dopant - B150

*L_n measured by surface photovoltage technique.

PROCESS DEVELOPMENT

Conclusions: Excimer Laser Processing

- FRONT JUNCTION (PHOSPHORUS DIFFUSED) SATISFACTORY FOR SOLAR CELLS.
- BACK JUNCTION SHALLOW DUE TO SLIGHT PENETRATION OF BORON OR ALUMINUM.
RESULTS IN HIGH SERIES RESISTANCE IN CELLS.
- FURTHER TESTS TO BE CARRIED OUT ON LOW RESISTIVITY MATERIAL.

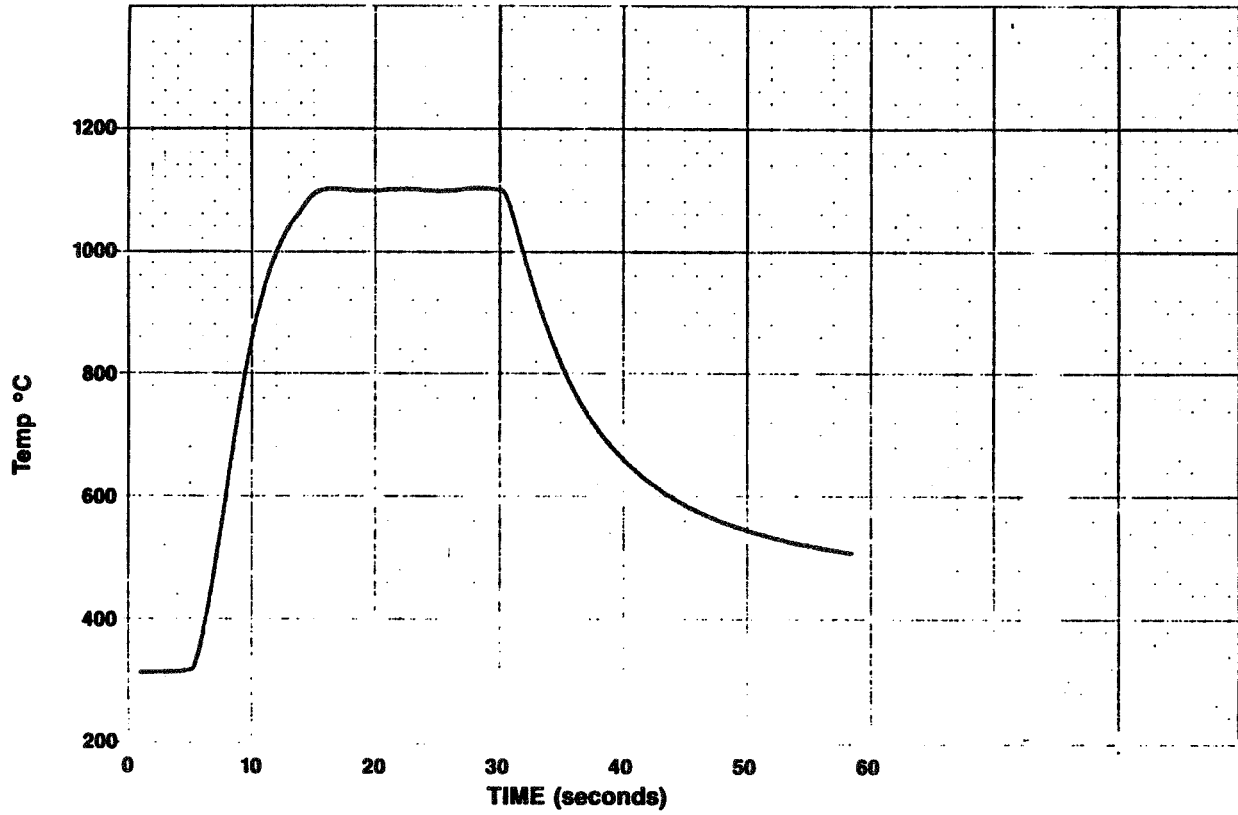
Junction Formation Using a Directed Heat Source

- WEB STRIPS COATED WITH LIQUID DOPANTS (BOTH SIDES) AND
HEATED IN A TUNGSTEN-HALOGEN FLASH LAMP
- NOMINAL TIME - 15 SEC.
NOMINAL TEMPERATURE - 1100°C
- JUNCTIONS FORMED SIMULTANEOUSLY ON BOTH SIDES OF WEB STRIP
- N^+PP^+ AND P^+NN^+ CELLS FABRICATED
- NO CROSS-CONTAMINATION NOTED
- WORK CARRIED OUT COURTESY OF AG ASSOCIATES, PALO ALTO, CA

PROCESS DEVELOPMENT

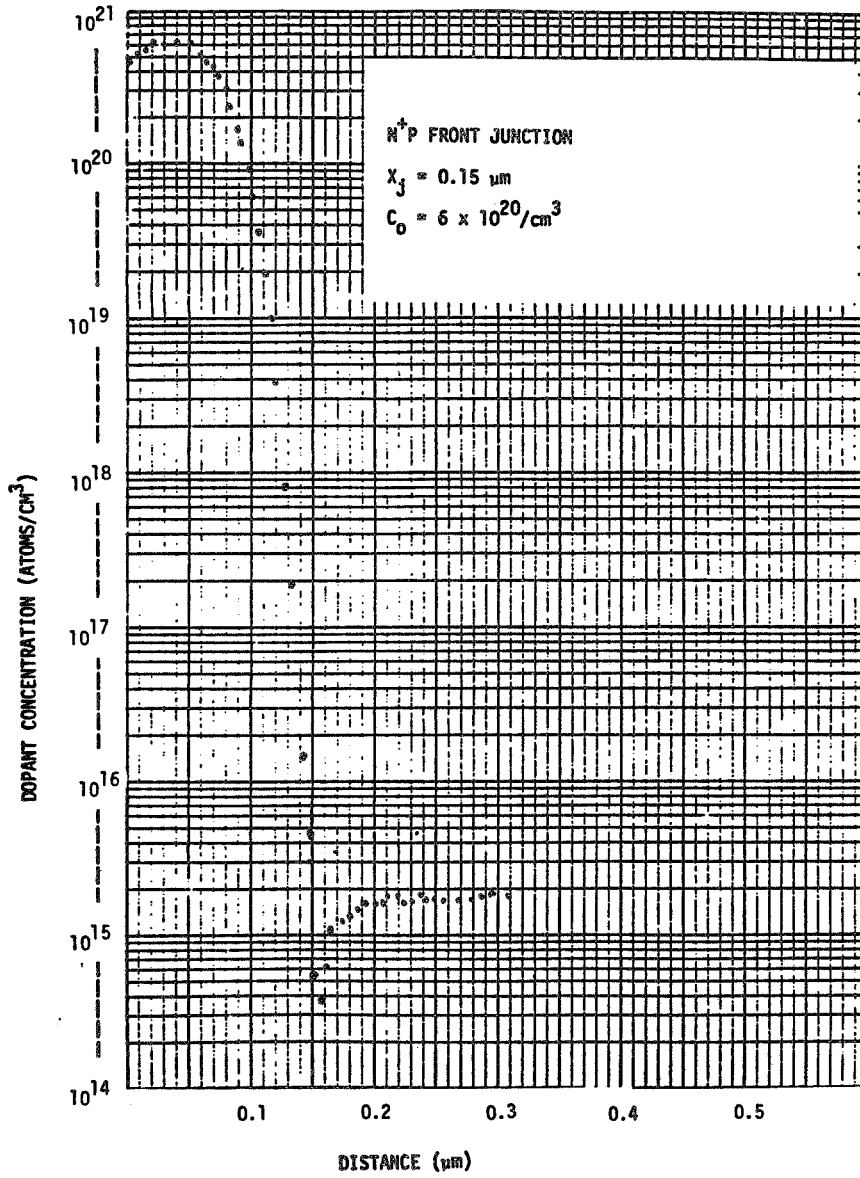
Heat Pulse Temperature-Time Profile

Sample No. WESTINGHOUSE - DENDRITIC WEB



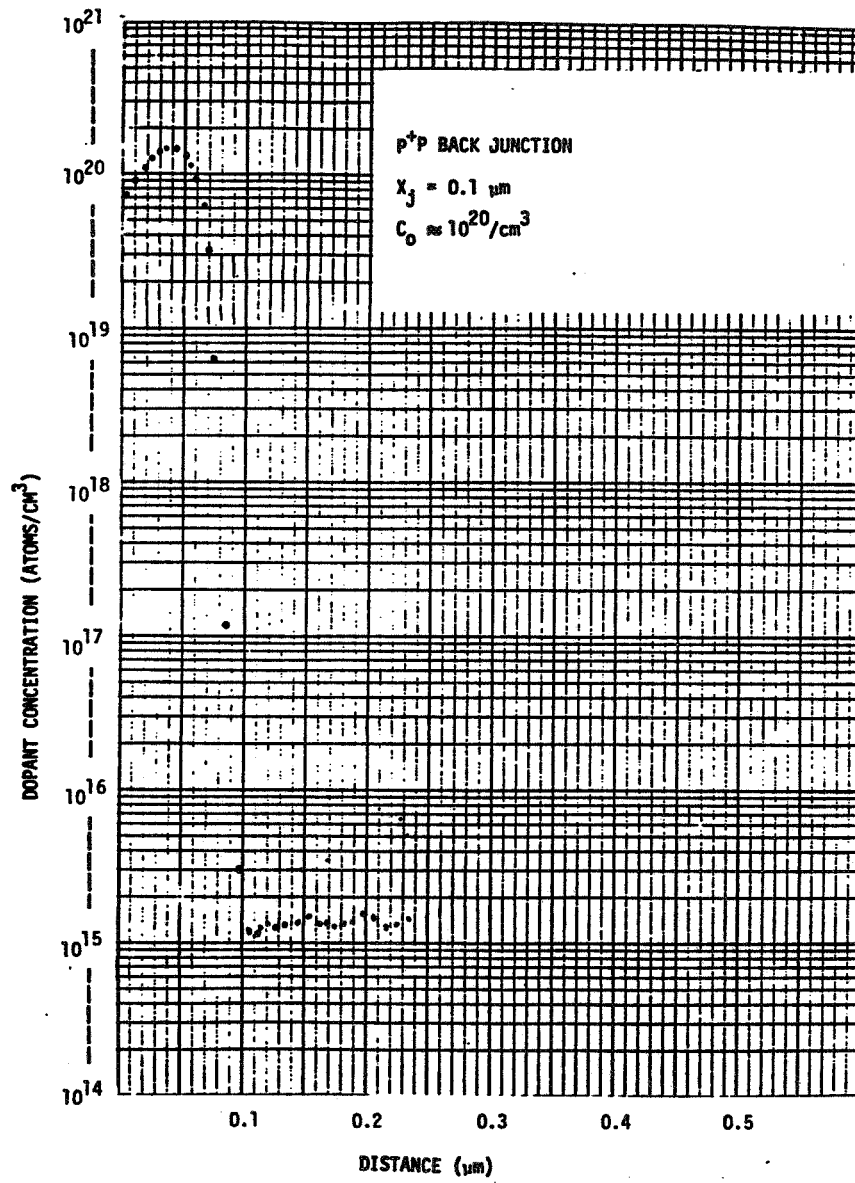
AG Associates 1052 Elwell Ct. Palo Alto, CA 94303 415-961-6823

Heat Pulse Simultaneous Junction Formation



PROCESS DEVELOPMENT

Heat Pulse Simultaneous Junction Formation



PROCESS DEVELOPMENT

Simultaneous Junction Formation Using Heat Pulse:
Representative Data

<u>CELL ID</u>	<u>COND. TYPE</u>	<u>Res (Ωcm)</u>	<u>Voc (V)</u>	<u>J_{sc} ($\frac{\text{mA}}{\text{cm}^2}$)</u>	<u>FF</u>	<u>EFF.</u>	<u>COMMENTS</u>
8A	P	4	.497	23.8	.76	9.0	AS DIFFUSED
8B	P	4	.541	29.1	.78	12.3	800°C ANNEAL
6A	N	1	.556	24.9	.78	10.8	AS DIFFUSED
6B	N	1	.578	30.5	.75	13.2	800°C ANNEAL
7A	N	1	.561	26.6	.79	11.8	AS DIFFUSED
7B	N	1	.601	32.9	.77	15.0	800°C ANNEAL

Dark I-V Data

<u>SAMPLE</u>	<u>TREATMENT</u>	<u>J₀₂ ($\frac{\text{A}}{\text{cm}^2}$)</u>	<u>Ln (μm)</u>
7A	AS TREATED	6.6×10^{-12}	63
7B	ANNEALED 800°C	1.4×10^{-12}	320

N-TYPE SAMPLES FROM SAME WEB CRYSTAL

PROCESS DEVELOPMENT

Conclusions: Directed Heat-Source Junction Formation

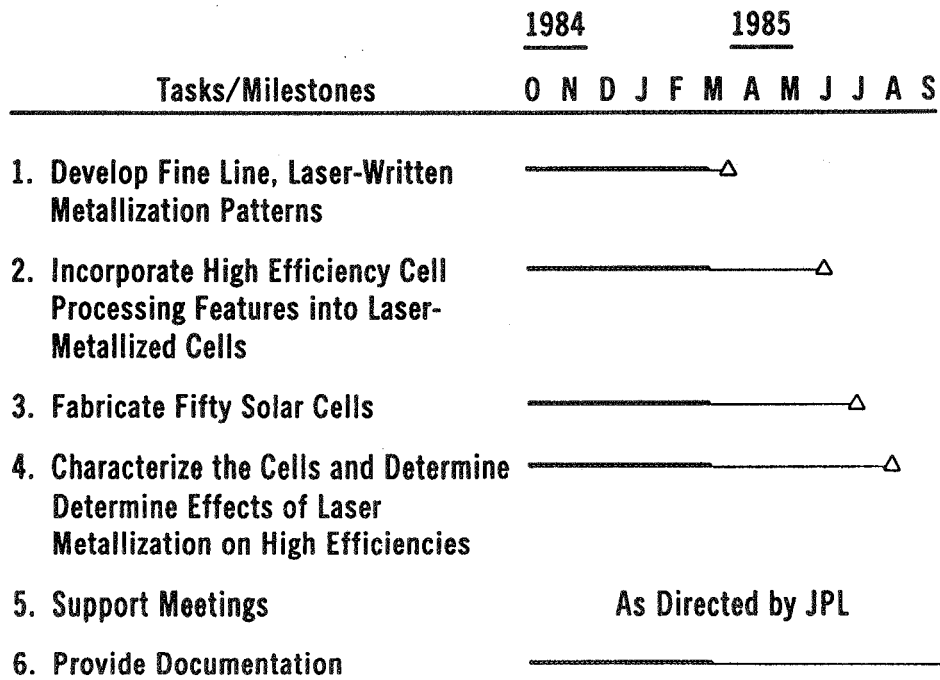
- SIMULTANEOUS DIFFUSION POSSIBLE WITHOUT CROSS-CONTAMINATION
- ANNEALING REQUIRED AFTER JUNCTION FORMATION TO ACHIEVE HIGHEST EFFICIENCY
- A DETAILED STUDY REQUIRED TO OPTIMIZE HEAT PULSE PARAMETERS (TIME/TEMP/COOLING RATE)

LASER-ASSISTED SOLAR-CELL METALLIZATION PROCESSING

WESTINGHOUSE ELECTRIC CORP.

A. Rohatgi
 P.G. McMullin
 P. Rai-Choudhury

Milestone Chart

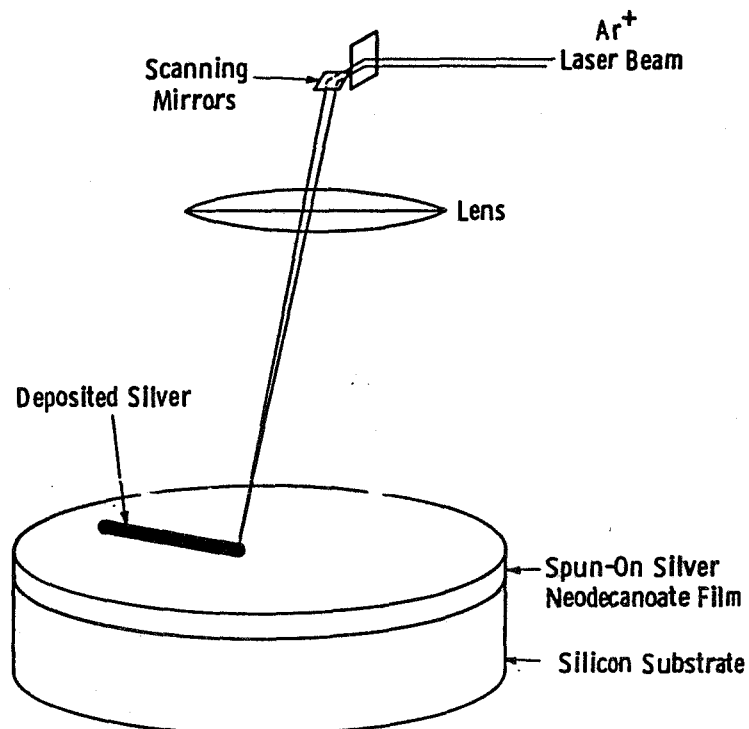


PROCESS DEVELOPMENT

Potential Advantages of Laser Deposition Techniques for Photovoltaic Systems

- High Resolution
- No Photolithography
- Clean And Contamination - Free
- In-Situ Sintering
- Low Contact Resistance

Laser Pyrolysis of Spun-on Metallo-Organic Film



Sample Base Temperature 75°C

Focussed Laser Spot Decomposes Spun-On Film

Silver Metallization Patterns are Formed by Direct-Writing

PROCESS DEVELOPMENT

Lighted I-V Data for Baseline Cells

Cell I.D.	Short-Circuit Current (mA)	Open-Circuit Voltage (V)	Fill Factor	Efficiency (%)
B-202	34.3	0.572	0.704	13.8
B-203	34.4	0.508	0.764	13.3
B-205	37.0	0.581	0.682	14.7
M-206	36.6	0.578	0.719	15.2
M-207	36.5	0.579	0.738	15.6
M-208	36.3	0.581	0.701	14.8
M-210	34.2	0.578	0.749	14.8
M-211	30.1	0.566	0.570	9.7
M-212	24.5	0.574	0.737	10.4
M-214	34.5	0.574	0.670	13.3
Best Cell	36.5	0.579	0.738	15.6
Average Cell	33.8	0.569	0.703	13.6
Worst Cell	30.1	0.566	0.570	9.7

Lighted I-V Data for Laser-Metallized Cells

Cell I.D.	Short-Circuit Current (mA)	Open-Circuit Voltage (V)	Fill Factor	Efficiency (%)
LM-102	32.6	0.569	0.753	14.0
LM-103	32.0	0.571	0.751	13.7
LM-106	33.2	0.572	0.777	14.8
LM-107	33.1	0.573	0.770	14.6
LM-108	33.3	0.576	0.752	14.4
LM-109	34.1	0.576	0.763	15.0
LM-110	34.2	0.575	0.775	15.3
LM-111	33.7	0.572	0.774	14.9
LM-112	33.9	0.571	0.774	15.0
LM-114	34.0	0.575	0.766	15.2
LM-115	34.2	0.579	0.766	15.2
LM-514	35.6	0.586	0.755	15.7
LM-515	36.1	0.589	0.776	16.5
Best Cell	36.1	0.589	0.776	16.5
Average Cell	33.9	0.576	0.766	15.0
Worst Cell	32.0	0.571	0.751	13.7

PROCESS DEVELOPMENT

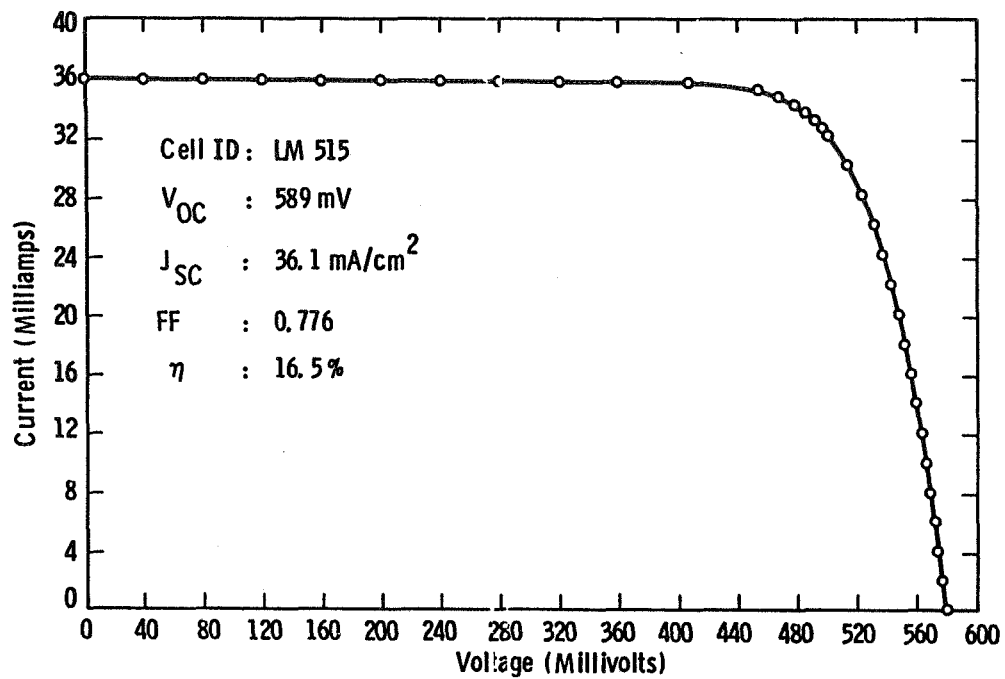
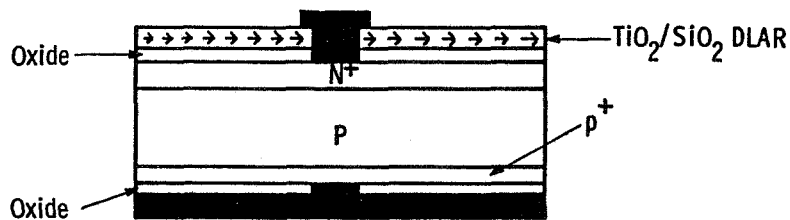


Fig. 14—Lighted I-V characteristic of AR-coated, laser-metallized cell, LM-515, with a cell efficiency of 16.5%



PROCESS DEVELOPMENT

Line Widths as a Function of Laser Power
Before and After Electroplating

Laser Power (W)	Linewidths (μm)		
	Before Film Rinse	After Film Rinse	After 40 Min. Electroplating
8	80	85	90
6	80	80	85
4	70	70	75
2	60	65	70
1	60	50	50

*80 mm Lens, 100 gms of Ag Neodecanoate in 100 c.c. Xylene

Line Widths as a Function of Laser Power With 50 mm Lens Before and After Film Rinse

Laser Power (W)	Linewidth (mm)	
	Before Film Rinse	After Film Rinse
8.50	85	60
7.50	75	65
6.90	75	60
6.36	75	60
5.70	70	60
4.92	70	55
4.14	65	50
3.30	60	50
2.55	55	40
1.80	50	40
1.20	45	30
0.66	25	20

PROCESS DEVELOPMENT

Approaches in Progress for Achieving Higher Efficiency in Laser-Metallized Cells

- Surface Passivation
 - (a) 100 Å Passivating Oxide
 - (b) 30 Å Tunnel Dielectric
- Reduction of Line Width
 - (a) Modifying Focussing Optics
 - (b) Reduced Laser Power
 - (c) Silver Concentration in Silver Neodecenoate Solution
- High Quality Float Zone Silicon
 - (a) 0.25 Ω-cm
 - (b) Capable of Giving >18% Efficient Cells by Conventional Processing

Laser-Metallized Solar Cells Using Low-Resistivity Float-Zone Silicon (First Run)

	V_{oc} (Volts)	J_{sc} mA/cm ²	FF	η %	R_s Ω-cm ²	R_{sh} KΩ-cm ²	$J_{01} \times 10^{12}$ A/cm ²	$J_{02} \times 10^6$ A/cm ²
#16	.589	32.9	.778	14.8	.53	294	2.4	1.8
#8	.585	33.4	.767	15.0	.70	97	2.0	1.2
#7	.585	33.5	.759	14.9	.67	16	2.7	3.6
#6	.590	33.7	.766	15.3	.61	151	2.1	2.1
*# Hify 16-4	.621	36.7	.804	18.4	.56	150	0.05	1.0

*Best Cell Fabricated on This Material By Conventional Lithography/Evaporation Process

MICROWAVE-ENHANCED THIN-FILM DEPOSITION

SUPERWAVE TECHNOLOGY, INC.

S. Chitre

Superwave Technology 956828

DEMONSTRATION OF FEASIBILITY OF DEPOSITING SEMICONDUCTOR LAYERS
USING MICROWAVE ENHANCED PLASMA TECHNIQUES.

RATIONALE:

MICROWAVE ENHANCED CHEMICAL VAPOR DEPOSITION (MECVD) OF PASSIVATION
COATINGS HAS THE POTENTIAL ADVANTAGES OF:

(1) HIGHER ELECTRON PLASMA DENSITY $10^{13}/\text{cm}^2$ vs $10^9/\text{cm}^2$ FOR RF
BECAUSE

WHERE ω_p IS 2.45 GHz INSTEAD OF 13.56 MHz.

- (2) LONG LIFE TIME IN SPECIES WHICH ALLOW REACTION CHAMBER AND
PLASMA GENERATION CHAMBER TO BE SEPARATED.
- (3) MORE CONTROL OF DEPOSITION KINETICS WITH LESS DAMAGE TO
SUBSTRATE.
- (4) CONTROLLING FILM GRADIENTS OR DOPING PROFILES
- (5) LOWER POWER REQUIREMENTS
- (6) LOWER REACTIVE GAS CONSUMPTION

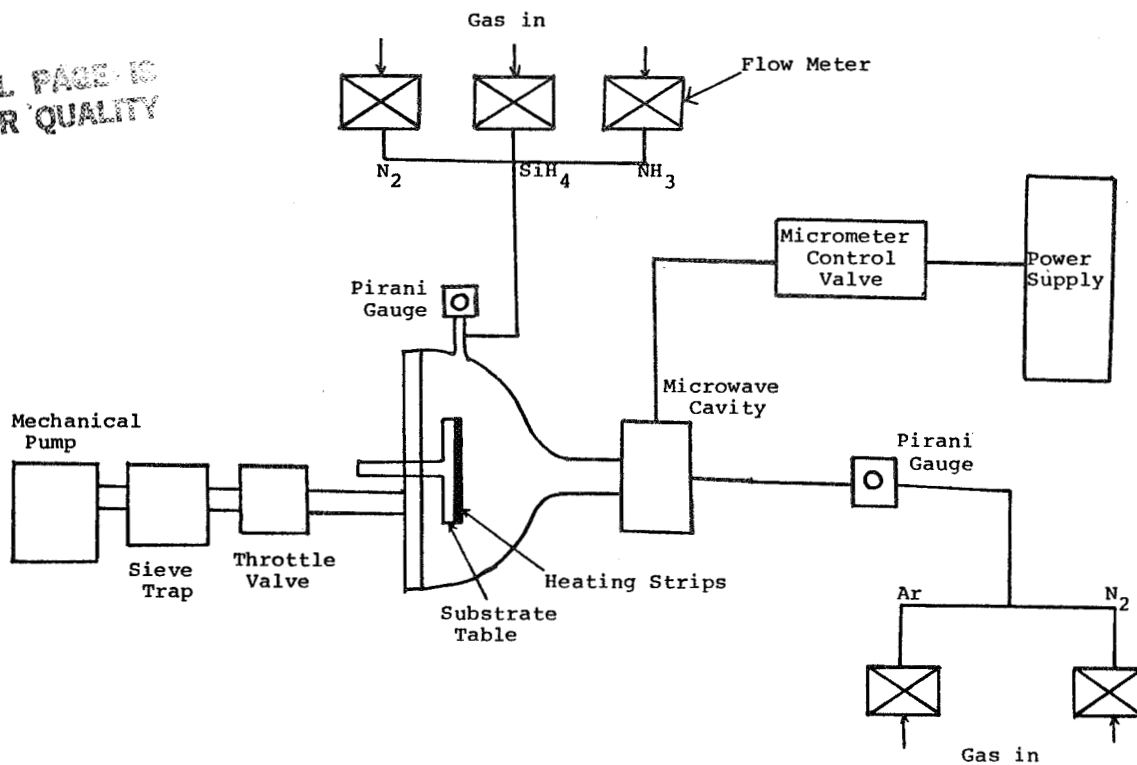
Objective

DESIGN, FABRICATE AND DEMONSTRATE A MICROWAVE ENHANCED CVD SYSTEM
TO SHOW FEASIBILITY OF DEPOSITING SILICON NITRIDE.

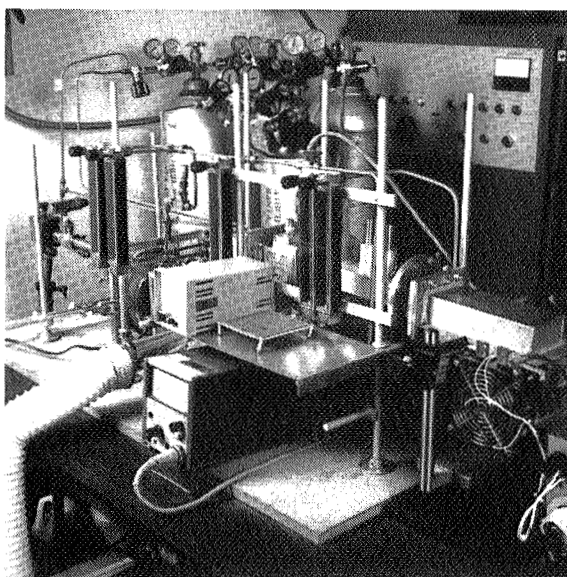
PROCESS DEVELOPMENT

Microwave Deposition System

ORIGINAL PAGE IS
OF POOR QUALITY



Microwave Enhanced Plasma System



PROCESS DEVELOPMENT

Status

- CONTRACT IS COMPLETE
- FEASIBILITY HAS BEEN DEMONSTRATED
- FUNDING PROBLEMS FOR FOLLOW-ON FOR FURTHER DEVELOPMENT

N86 - 29387

LIFE-CYCLE COSTS OF HIGH-PERFORMANCE CELLS

JET PROPULSION LABORATORY

Ron Daniel
Dale Burger
Leonard Reiter

Introduction

- **Value of PV system must include all costs and revenues associated with the system over its lifetime**
- **Methodology used in this study determines:**
 - (1) **The value of improvements to the lifetime power output of a PV system**
 - (2) **How much additional expense could be added during cell and module fabrication to achieve that added performance**
- **How does the initial cost relate to the final value?**

Study Activities

- **To compare the NPV of the life-cycle cost of four PV module production technologies**
 - (1) **1985 MY SOA Cz at 5 MW annual prod.**
 - (2) **1992 MY SOA Cz at 25 MW annual prod.**
 - (3) **1992 MY high-eff. Cz at 25 MW annual prod.**
 - (4) **1992 MY high-eff. web at 25 MW annual prod.**
- **Look at various module and system configurations:**
 - **Large and standard module size**
 - **Series — parallel circuitry**
 - **Cross strapping**
 - **Bypass diodes around each cell**
 - **Series — parallel modules**
 - **Bypass diodes around each series block, module and parallel module group**
- **Module replacement**
 - **Cell failure (opens only; 1 per 10,000 per year), causing module back bias of 0.5 volt**

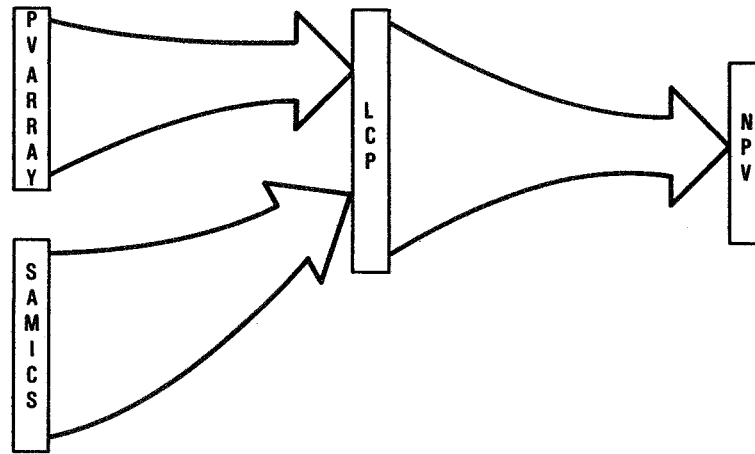
PRECEDING PAGE BLANK NOT FILMED

PROCESS DEVELOPMENT

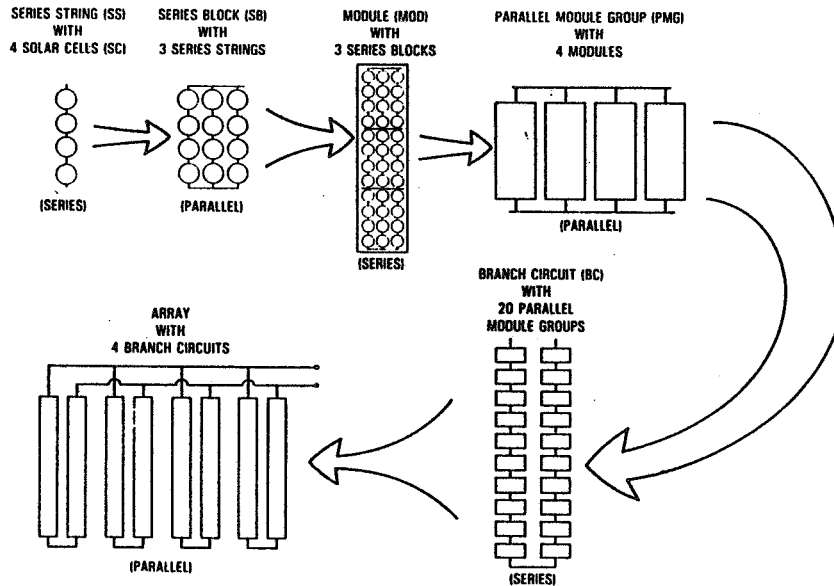
Methodology

- Use three PA&I-developed simulation models
 - PVARRAY – system array performance
 - SAMICS – simulated module manufacturing industry
 - LCP – simulates the energy output, cost and value of a PV power plant over its useful lifetime

PV Array Design Economic Evaluation Methodology



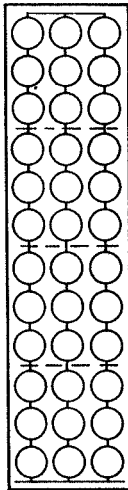
PVARRAY Terminology



PROCESS DEVELOPMENT

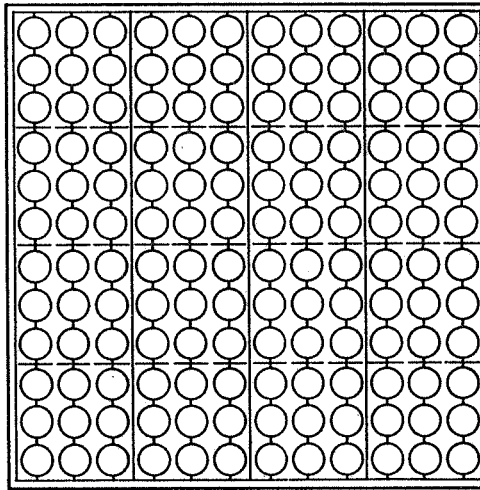
PVARRAY Module Configurations

**STANDARD
MODULE**



**12SC, 3SS
OR
3SC, 3SS, 4SB
(W/CROSS STRAPS)**

**LARGE
MODULE**



**12SC, 12SS
OR
3SC, 12SS, 4SB
(W/CROSS STRAPS)**

Input Parameters

LCP

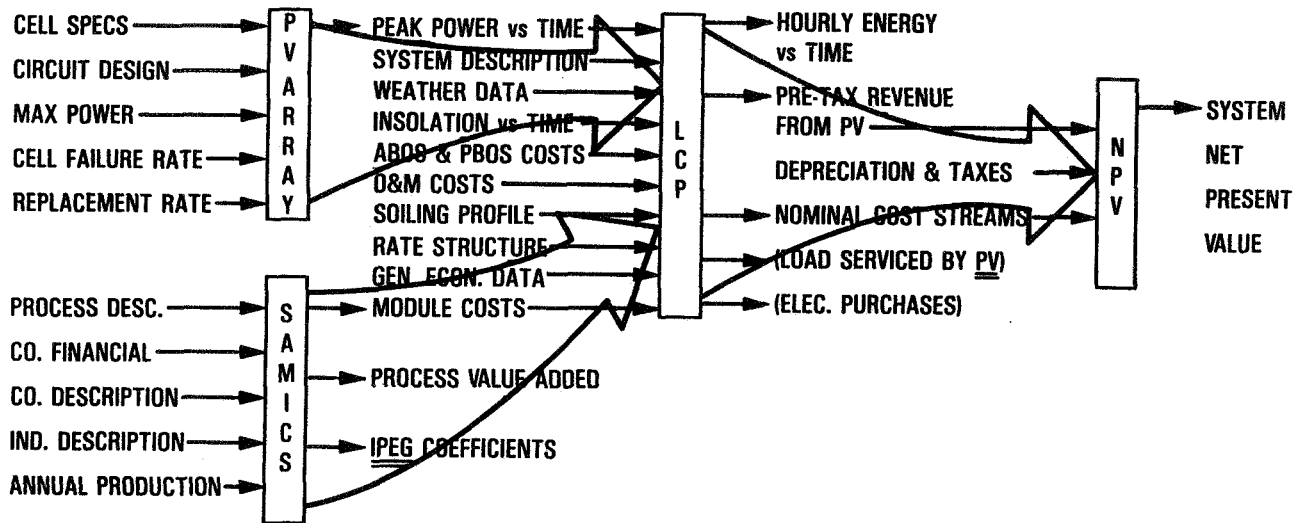
Mfg. yr	1985	1992
ABOS (\$/m²)	115	60
PBOS (\$/kW)	600	150
O&M (\$/m²/yr)	1.30	1.30

Rate Structure (¢/kWh) — 8.5 peak, 7.1 mid-peak, 6.0 off-peak
Insulation — 2300 kWh/yr

NPV

Inflation rate — 5%
Discount rate — 9%
Depreciation — 15-yr life

PROCESS DEVELOPMENT



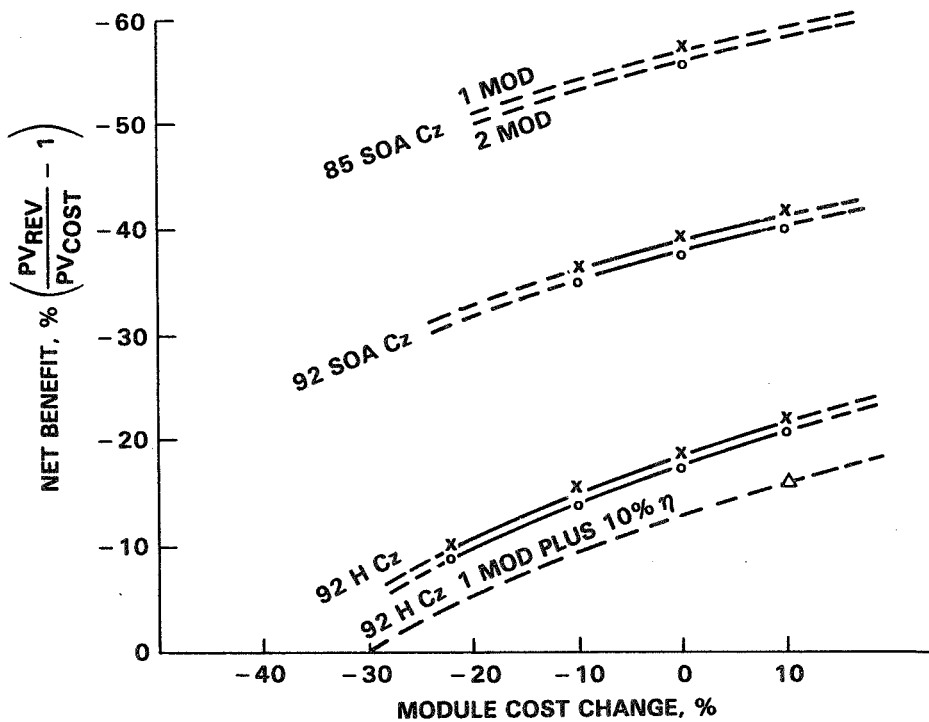
SAMICS: SOLAR ARRAY MANUFACTURING INDUSTRY COSTING STANDARDS

LCP: LIFETIME COST AND PERFORMANCE MODEL

PROCESS DEVELOPMENT

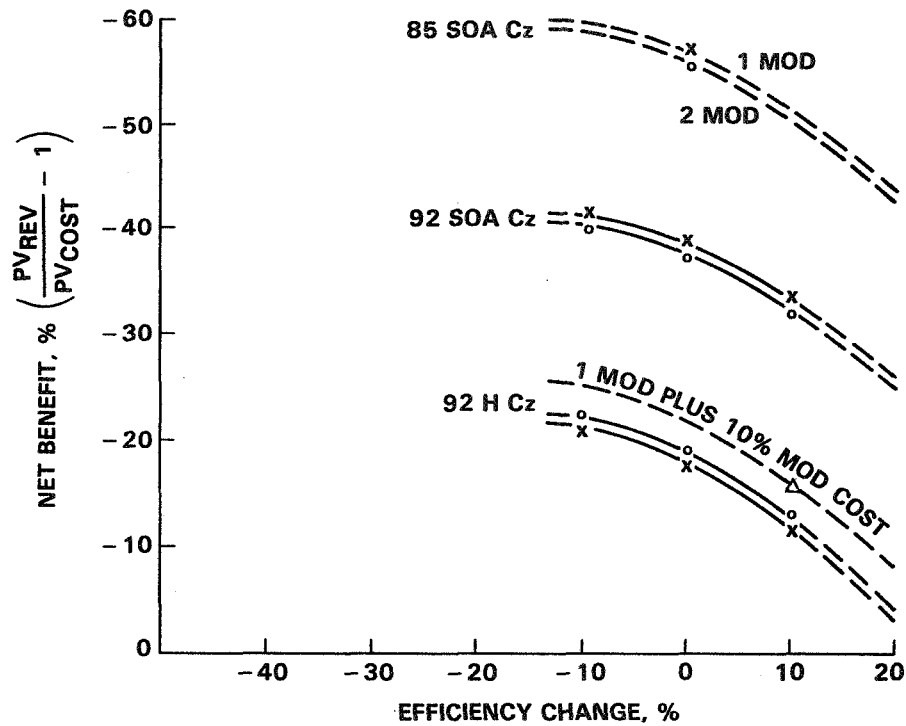
	SOA Cz		High-Efficiency Cz
	1985	1992	1992
Mfg. yr			
Mod. Size	1.2 x 1.2 m	1.2 x 1.2 m	1.2 x 1.2 m
Cell Eff.	11.9%	11.9%	18.7%
Mod Eff.	9.5%	9.5%	16.2%
W _p /Mod.	147	147	233
Annual Prod.	5 MW	25 MW	25 MW
Si Cost, 82\$	\$34 /kg	\$18/kg	\$18/kg
Value Added			
\$/W _p	3.52	2.40	1.65
\$/m ²	359	245	267

Sensitivity of Net Benefit to Module Cost Change



PROCESS DEVELOPMENT

Sensitivity of Net Benefit to Efficiency Change



Summary

- Models PVARRAY, SAMIS and LCP provide a tool for evaluating PV technologies and PV systems
- Two evaluation rankings possible, system performance and NPV
- Can identify system and performance tradeoffs

Preliminary Conclusions:

- Parallel redundancy recommended
- For large modules, value of bypass diodes is marginal
- High efficiency and lower module cost are needed for PV to be economically attractive

Future Work

- **High-efficiency web**
- **Standard-size modules (0.30 × 1.2 m)**
- **Cross strapping**
- **Diodes around series blocks and individual cells**
- **A look at several specific processes and their effects on module cost and efficiency**

SAMICS ON THE IBM PC

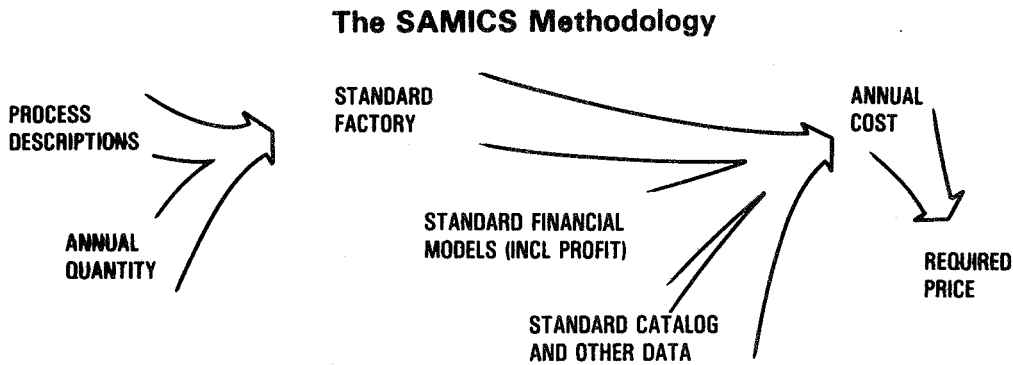
JET PROPULSION LABORATORY

R. Chamberlain

SAMICS

Solar Array Manufacturing Industry Costing Standards consist of

- Std catalog of input prices
- Std process description format
- Std factory design & staffing
- Std financial parameters
- Std methodology for computing required product price

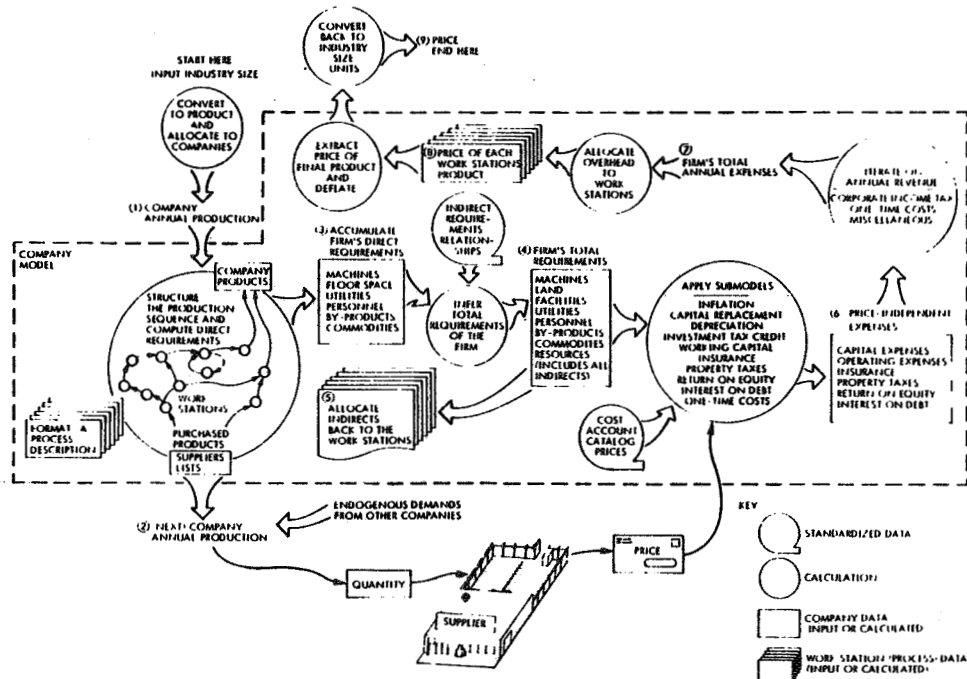


SAMIS and IPEG both implement this methodology

PRECEDING PAGE BLANK NOT FILMED

SAMIS

Standard Assembly-Line Manufacturing Industry Simulation



Complete implementation of all SAMICS non-linearities

Calibrates IPEG assumptions

Does catalog look-ups and interpolations and all bookkeeping

Can vary anything

PROCESS DEVELOPMENT

IPEG

Improved price estimation guidelines

PRICE × QUAN =

$C_1 \times EQPT + C_2 \times SQFT + C_3 \times DLAB + C_4 \times (MATS + UTIL)$

**Kinds and relative proportions of indirect requirements are fixed
(by a calibrating SAMIS run)**

**Coefficients provide rules of thumb but are derived from financial
parameters, not input**

**Bookkeeping needed to get EQPT, SQFT, DLAB, MATS, UTIL
from process descriptions; IPEG does not read process
design changes**

IPEG2 = "Back of the envelope"

PC-IPEG responds immediately — can vary financial parameters

ENCAPSULATION PROCESSING AND MANUFACTURING YIELD ANALYSIS

SPRINGBORN LABORATORIES, INC.

P. Willis

Goals

- UNDERSTAND THE RELATIONSHIPS BETWEEN:
 - FORMULATION VARIABLES
 - PROCESS VARIABLES
- DEFINE CONDITIONS REQUIRED FOR OPTIMUM PERFORMANCE
- RELATE TO MODULE RELIABILITY
- PREDICT MANUFACTURING YIELD
- PROVIDE DOCUMENTATION TO INDUSTRY

PRECEDING PAGE BLANK NOT FILMED

PROCESS DEVELOPMENT

Material Variables

LAMINATION POTANTS

- ETHYLENE/VINYL ACETATE (EVA)
- ETHYLENE/METHYL ACRYLATE (EMA)

CASTING POTANTS

- ALIPHATIC POLYURETHANE (PU)

ADHESIVES/PRIMERS

- THREE BASIC PRIMER SYSTEMS

COVER FILMS

- TEDLAR, ACRYLICS, FEP

FORMULATION VARIABLES:

TYPE AND AMOUNT OF:

- CURING AGENTS (PEROXIDES)
- ANTIOXIDANTS
- ULTRAVIOLET SCREENERS
- ULTRAVIOLET STABILIZERS (HALS)
- SELF PRIMING AGENTS

STORAGE CONDITIONS:

- TIME, TEMPERATURE, HUMIDITY, LIGHT
AIR EXPOSURE

QUALITY CONTROL:

- DETERMINE ANALYTICAL METHODS TO VERIFY
COMPOSITION
- PUBLISH QC SPECIFICATIONS FOR MATERIAL
CERTIFICATION

PROCESS DEVELOPMENT

Process Variables

(VACUUM BAG LAMINATION)

- AMBIENT CONDITIONS:
 - TEMPERATURE
 - HUMIDITY
 - BAROMETRIC PRESSURE
- VACUUM PRESSURE (INITIAL) AND TIME OF EVACUATION
- TEMPERATURE - - RATE OF RISE
- TEMPERATURE - - ULTIMATE
- DWELL TIME, AT TEMPERATURE
- RATE OF COOLING
- TIME/TEMPERATURE/PRESSURE INTER-RELATIONSHIP

(CASTING LIQUID SYSTEMS)

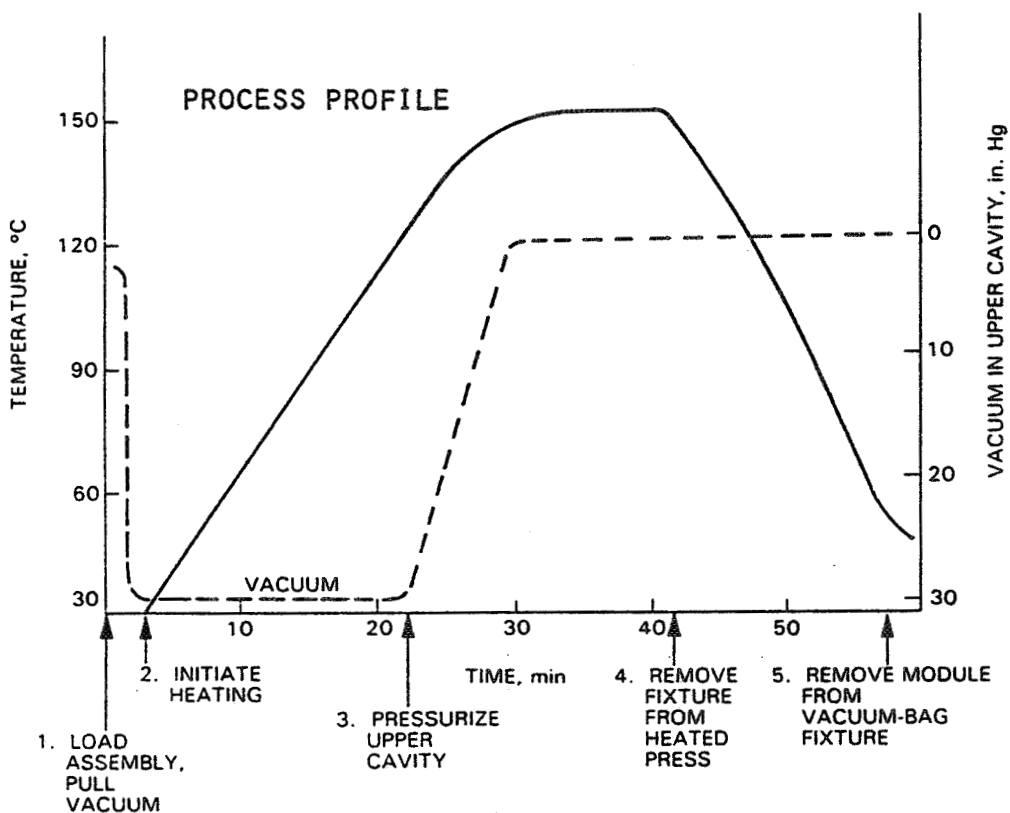
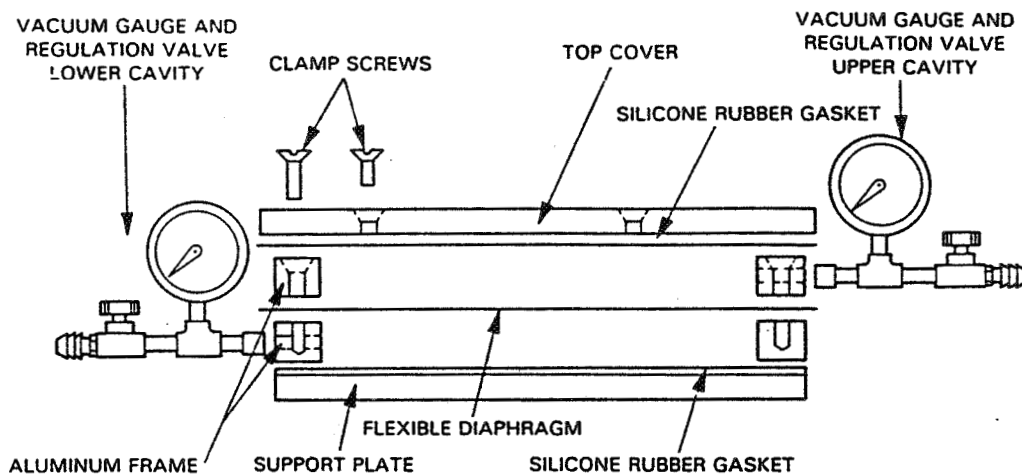
ABOVE VARIABLES, PLUS:

- 2 COMPONENT MIX TIME
- DEGASSING PRESSURE
- PUMP AND FILL TIMES
- MIX UNIFORMITY
- GEL TIME

PROCESS DEVELOPMENT

Process Equipment

EXPERIMENTAL LAMINATOR



- MICROPROCESSOR CONTROLLED EXPERIMENTAL LAMINATOR CONSTRUCTED
- STUDIES STARTED ON PROCESSING PROFILES
 - RATE OF HEATING (HOW SLOW, HOW FAST ?)
 - VACUUM TIMING
 - RATE OF COOLING

PROCESS DEVELOPMENT

Quality and Performance Criteria

- METHOD:
- PREPARE TEST MODULES AND/OR OTHER TEST SPECIMENS WITH CHANGE IN SIGNIFICANT VARIABLE(S)
 - DETERMINE THE EFFECT

<u>COMPONENT</u>	<u>CRITERION</u>	<u>TEST</u>
POTTANT	ADEQUATE CURE	PERCENT GEL THERMAL CREEP
	TRAPPED BUBBLES	VISUAL
	DISCOLORATION	VISUAL
CELLS	BREAKAGE	VISUAL, RESISTANCE
	INTERCONNECT	RESISTANCE
	REGISTRATION	VISUAL
COVER FILMS	TEARS/PUNCTURES	VISUAL
	WARPING/SHRINKAGE	VISUAL
GLASS (SUPERSTRATE)	FRACTURE	VISUAL
ADHESION	BOND STRENGTH	PEEL TEST
	ENDURANCE	WATER SOAK (50°C)

NEED TO DECIDE ON:

- STANDARD TEST SPECIMEN(S)
- STANDARD TEST PROTOCOL
- UNIFORM DATA SETS

PROCESS DEVELOPMENT

Data Analysis

- STATISTICAL ANALYSIS COMPLICATED BY LACK OF UNIFORMITY IN DATA TYPE

- TWO TYPES OF DATA:

DISCRETE (PASS/FAIL)

CELL FRACTURE
INTERCONNECT BREAKAGE
TRAPPED BUBBLES
THERMAL CREEP
GLASS FRACTURE

CONTINUOUS

GEL CONTENT
PEEL STRENGTH
STABILIZER LOSS

FOR CONTINUOUS DATA TYPES:

- TWO LEVEL FACTORIAL EXPERIMENTS (MOST INFORMATION, FEWEST EXPERIMENTS)
- NO. EXPERIMENTS = 2^K , K = NO. VARIABLES
- DETERMINES EFFECT OF SINGLE VARIABLE AT TWO LEVELS
- DETERMINES FACTOR INTERACTIONS (SEVERAL VARIABLES)
- PERMITS RANKING OF VARIABLES ACCORDING TO MAGNITUDE OF EFFECT
- LINEAR ANALYSIS POSSIBLE FOR SUBSEQUENT PREDICTIVE CAPABILITY

FOR DISCRETE DATA TYPES:

- DETERMINE "X SUCCESSES IN N TRIALS" FOR SUITABLY LARGE SAMPLE
- SCATTER PLOT - FOR FIRST ESTIMATE OF ACCEPTABLE PROCESSING RANGE
- BINOMIAL DESTRIUTION - DETERMINE PROBABILITY OF FAILURE

IN GENERAL:

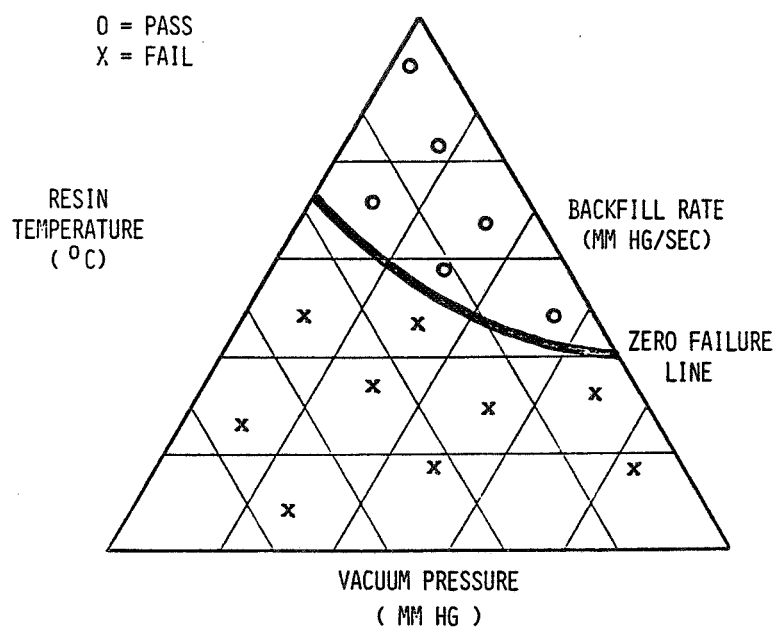
1. DETERMINE THE DOMINANT FAILURE MODE
2. DETERMINE VARIABLE(S) RESPONSIBLE
3. DETERMINE EXPERIMENTAL CONDITIONS THAT RESULT IN A RANGE OF FAILURES
4. DETERMINE THE MEAN AND STANDARD DEVIATION OF THE DISTRIBUTION
5. USE PROBABILITY DISTRIBUTION FUNCTION TO CALCULATE PROBABLE FAILURE AT OTHER STRESS LEVELS

PROCESS DEVELOPMENT

Manufacturing Practice: Discrete Variables

- PREPARE GRAPHICAL INTERPRETATION OF DATA
- DETERMINE " TOLERABLE FAILURE " LEVEL
- DEFINE BOUNDRY CONDITIONS FOR DEFECT-FREE MANUFACTURING (FIRST ESTIMATE)

EXAMPLE: CELL BREAKAGE

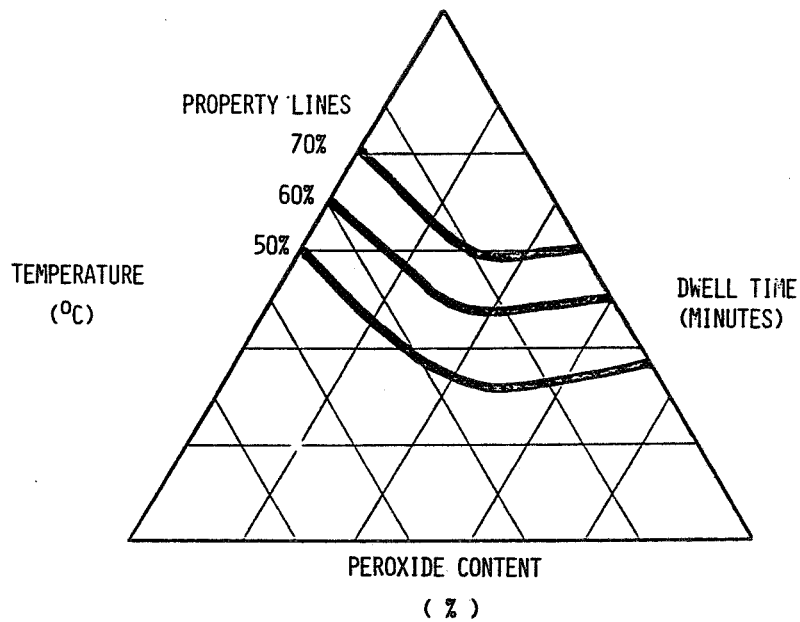


PROCESS DEVELOPMENT

Manufacturing Practice: Continuous Variables

- GRAPHICAL PRESENTATION ALSO GOOD FOR CONTINUOUS VARIABLES
- PROVIDES BOUNDRIES FOR PROCESS/FORMULATION VARIABLES BASED ON CRITERIA OF ACCEPTABILITY
- EASILY USED IN MANUFACTURING PRACTICE

EXAMPLE: PERCENT GEL
(DEGREE OF CURE)



PROCESS DEVELOPMENT

Formulation Sensitivity

- UV SCREENERS AND OTHER STABILIZERS - SLOW DOWN CURE RATE SLIGHTLY. NO ENORMOUS DIFFERENCE BETWEEN TYPES
- ANTIOXIDANTS CAN HAVE MAJOR EFFECT ON CURE, NOT USED/UNNECESSARY

CURE VERSUS PEROXIDE CONTENT
(TIME TO GEL CONTENT >65%, MINUTES)

	<u>EVA 9918</u>			
	<u>130°</u>	<u>140°</u>	<u>150°</u>	<u>160°</u>
LUPERSOL 101:				
1.5%	NC	20	10	5
0.5%	NC	30	20	10

	<u>EVA 15295</u>			
	<u>130°</u>	<u>140°</u>	<u>150°</u>	<u>160°</u>
LUPERSOL TBEC:				
1.5%	8	<5	3	1
0.5%	NC	10	5	<5

(NC = NO CURE)

- ONE THIRD THE STANDARD PEROXIDE CONCENTRATION DOUBLES THE REQUIRED TIME
- EVA FORMULATIONS NOT SENSITIVE TO MINOR VARIATIONS ON PEROXIDE CONTENT

PROCESS DEVELOPMENT

Process Sensitivity

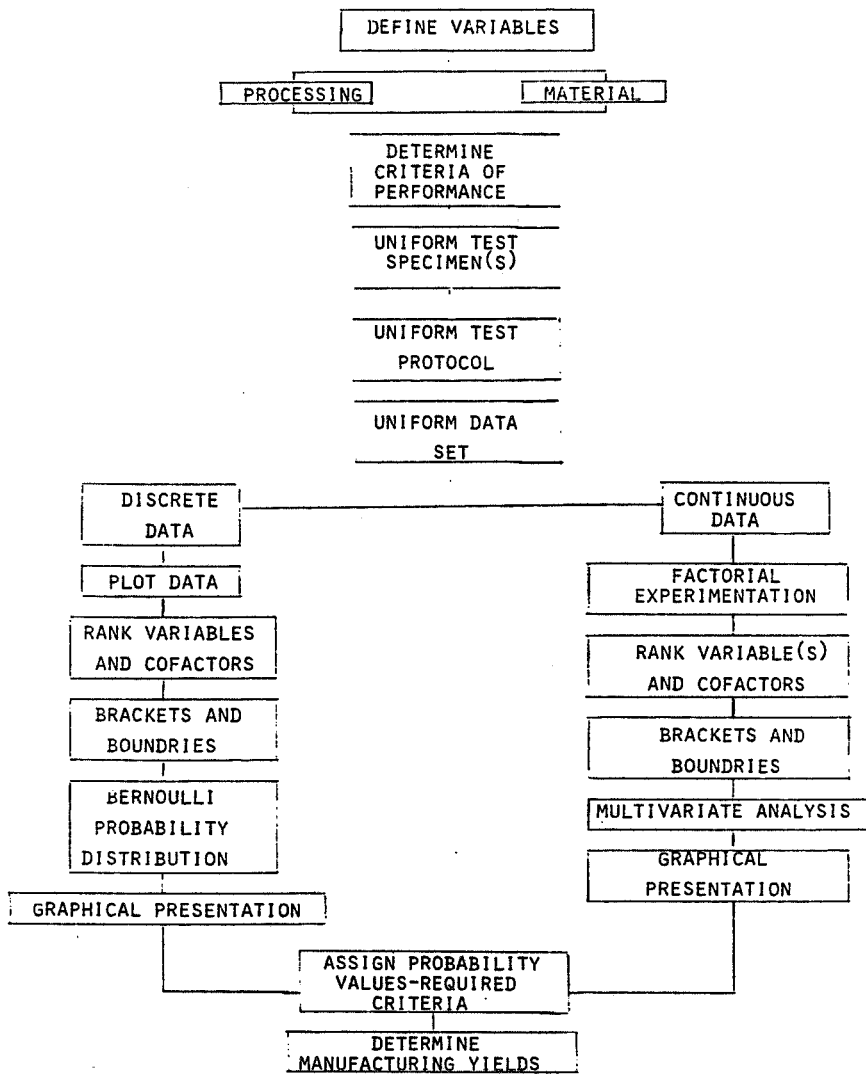
EVA STORAGE / AIR EXPOSURE

	<u>EVA NUMBER</u>	
	<u>9918</u>	<u>15295</u>
PEROXIDE:	LUPERSOL 101	LUPERSOL TBEC
CURE	150° / 20 MIN	150° / 5 MIN
CONDITIONS:	140° / 20 MIN	140° / 5 MIN

<u>AIR EXPOSURE</u>	<u>GEL CONTENTS:</u>	
CONTROL, 0	80 % 64 %	93 % 91 %
24 HOURS	82 % 71 %	85 % 78 %
48 HOURS	78 % 0 %	81 % 72 %
72 HOURS	70 % 0 %	83 % 82 %
168 HOURS (ONE WEEK)	0 % 0 %	70 % 0 %

- EVA FORMULATIONS STRONGLY AFFECTED BY AIR EXPOSURE. AIR EXPOSURE .
- FORMULATION WITH TBEC PEROXIDE MUCH LESS AIR SENSITIVE
- EVA STORED IN ROLL FORM - APPEARS TO HAVE LONG STORAGE LIFE
- CUT EVA SHEET ONLY BEFORE USE, DISCARD FIRST WRAP OF ROLL

JPL Process Sensitivity Analysis



PROCESS DEVELOPMENT

Conclusions

- EVA FORMULATIONS RELATIVELY INSENSITIVE TO QUANTITY OF PEROXIDE BUT VERY SENSITIVE TO AIR EXPOSURE
- UNWRAP/CUT EVA JUST BEFORE MODULE MANUFACTURING - LIMIT AIR EXPOSURE

Accomplishments

- ANALYTICAL METHODS DEVELOPED FOR PEROXIDE CONTENT
- MICROPROCESSOR CONTROLLED EXPERIMENTAL LAMINATOR CONSTRUCTED
- EXPERIMENTAL TEST METHODOLOGY DEVELOPED (FIRST CUT)
- REVISED EVA PRODUCT BROCHURE AVAILABLE INCLUDES " TROUBLE SHOOTING " SECTION

Future Work

- DETERMINE DOMINANT FAILURE MODES
- CONVERT DATA TO PRACTICAL ENGINEERING FORMAT
- RELATE DATA TO MANUFACTURING YIELD
 - ASSIGN PROBABILITY OF FAILURE
 - NORMAL DISTRIBUTION (?)
 - WEIBUL (?)

ADVANCED SILICON SHEET

Anthony Briglio, Jr., Chairman

Ten presentations were made at this session covering research on silicon-shaped sheet technology.

JPL reported highlights of the FSA-sponsored Silicon Ribbon Stress/Strain Workshop that was held January 23 and 24, 1985, at the Mobil Solar Energy Corp., Waltham, Massachusetts. The presentations and discussions were aimed at acquiring a generic understanding of the sources of stress, deformation, and structural characteristics occurring during the growth of silicon ribbon.

Westinghouse Electric Corp. reported on its program to develop the technology of the silicon dendritic-web ribbon growth process. The effort is being concentrated on the area rate and quality requirements necessary to meet the JPL/DOE goals for terrestrial PV applications.

JPL described progress made in the study of defect characterization of silicon dendritic-web ribbon, using chemical etching combined with optical microscopy, as well as the electron-beam-induced current (EBIC) technique.

Cornell University reported progress on the electrical, structural, and chemical characterization of silicon sheet material. In the study on high-temperature deformation of Westinghouse dendritic-web ribbon, experimental creep tests were performed at Mobil Solar Energy Corp. in four-point bending under constant load conditions, and unusual behavior was observed. Also, measurements of oxygen content in web ribbon were made.

In the study of stress/strain relationships in silicon ribbon, the University of Kentucky calculated numerous solutions for stresses, strain rates, and dislocation densities through the use of the Sumino model. It has been concluded that many cases of failure of computer solutions to converge are analytical manifestations of shear bands (Luder's bands) observed in experiments.

Mobil Solar Energy Corp. reported on stress and efficiency studies on sheet silicon. It was found that the bulk diffusion length of stressed float zone (FZ) and Czochralski (Cz) silicon is limited by point defect recombination to about 20 μm in dislocation-free regions after high-temperature heat treatment and stress application.

Energy Materials Corp. reported on progress in developing a low-angle silicon sheet growth method (LASS) growth process. A video recording of ribbon growth at a pull speed of 40 cm/min was shown, including an example in which both dendritic and planar growth occur simultaneously in the same ribbon.

The Massachusetts Institute of Technology discussed the study of high-speed growth of silicon sheet in inclined-meniscus configurations. It was concluded that the maximum growth rates in vertical and inclined growth are set by thermal-capillary limits.

ADVANCED SILICON SHEET

The Solar Energy Research Institute reported on its study of silicon sheet material requirements for high-efficiency solar cells. Research continued on obtaining long-lifetime single-crystal FZ silicon and on understanding and reducing the mechanisms that limit the achievement of long lifetimes.

The University of Illinois at Chicago presented results of the program on developing an understanding of the basic mechanisms of abrasion and wear of silicon and on the non-destructive measurement of residual stresses in sheet silicon. Experiments were conducted at various temperatures and in the presence of various fluids. In abrasive wear, it was shown that dislocations, microtwins, and cracks are generated beneath the contact surface. Residual stresses in ribbon produced by Mobil Solar Energy Corp. by the EFG process were measured by use of a shadow moiré interferometry technique.

SILICON RIBBON STRESS/STRAIN WORKSHOP

MOBIL SOLAR ENERGY CORP.

M. H. Leipold

Program Relevance of Workshop

Provide generic understanding of the sources of stress, deformation and structural characteristics occurring during the growth of silicon ribbon

Technical value:

Encourage interaction among researchers studying sources and effects of deformation and structure during growth of silicon ribbon

Previous meetings:

November 8-9, 1983, Mobil Solar Energy Corp.
January 10-10, 1984 Westinghouse Electric Corp.

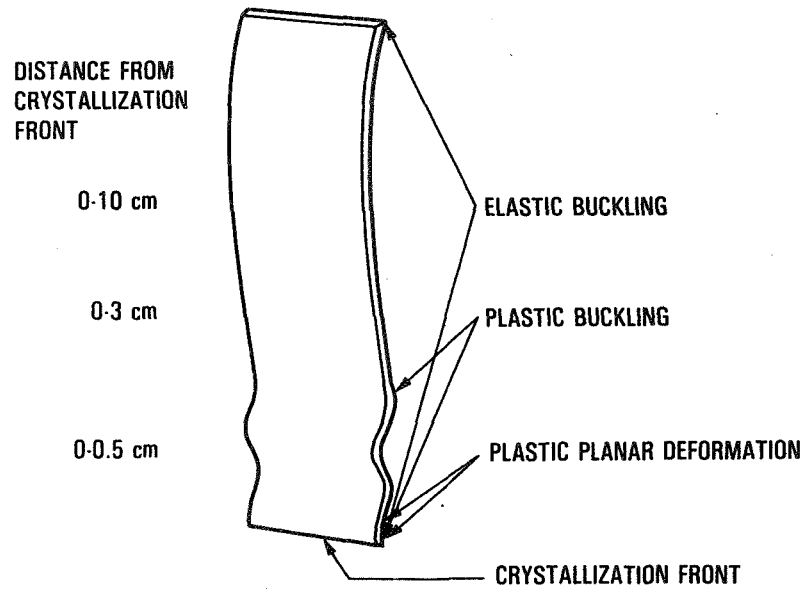
Wednesday 23, January 1985

8:30 AM	Opening	- M. Leipold
8:45	Stress/Strain Modeling	- O. Dillon, University of Kentucky
9:30	Defect Mapping in Silicon Sheet	- R. De Angelis, University of Kentucky
10:15	Coffee break	
10:30	Failure Analysis of Silicon Sheet	- T. O'Donnell, JPL
11:15	Silicon Materials Tests	- W. Phillips, JPL
12:00 Noon	Lunch	
2:00	Stress/Strain Analysis Program	- R. Seidensticker, Westinghouse
2:45	Coffee break	
3:00	Lateral Temperature Modeling of Web	- R. Sekerka, Carnegie-Mellon Institute
3:45	Plastic Deformation in Web Material	- L. Cheng, JPL

Thursday 24, January 1985

8:45 AM	Stress/Strain Analysis	- J. Kalejs, Mobil Solar
9:30	Heat Flow Model	- R. Brown, MIT
10:15	JPL Stress/Strain Program	- B. Wada, JPL
12:00 Noon	Lunch	
1:00	Discussion on Future Research Activities	
2:30	Wrap-up Discussion by DOE, SERI, JPL	

ADVANCED SILICON SHEET



Elastic Buckling

- Analytical method generally available
- Limitations
 - Thermal profile
 - Elastic properties
 - Specific buckling mode not easily predictable
- Reasonable agreement
 - Theory — experiment
 - Various analytical approaches

Plastic Buckling

- Analytical development proceeding
- Limitations
 - Range of analysis limited
 - Availability of mechanical data for Si
 - Thermal profile
- Agreement
 - Experimental confirmation not available

Plastic In-Plane Deformation

- Analytical development proceeding
- Limitations
 - Thermal profile very poorly known
 - Limited distance
 - Mechanical work
 - Availability of data for Si
- Agreement
 - Basically none

Summary

- Progress continues for models to describe mechanical aspects of ribbon growth, but answer not yet at hand
- Comparison and integration of various approaches under way
- Experimental confirmation of many elements not yet begun

ADVANCED DENDRITIC WEB GROWTH DEVELOPMENT

WESTINGHOUSE ELECTRIC CORP.

R. H. Hopkins

Advanced Silicon Sheet Task

<p>Technology Single Crystal Ribbon Growth</p>	<p>Report Date 6/19/85</p>
<p>Approach Silicon Dendritic Web Growth</p> <p>Contractor Westinghouse Electric Corporation Advanced Energy Systems Division JPL Contract 955843</p>	<p>Status</p> <ul style="list-style-type: none"> • Model-Driven Low Stress Design Led to Record Web Width - 6.7 cm • New Length Record with Continuous Replenishment - 7.5 m (4.1 cm Width) • Area Rates - 8 cm²/min (1.5 m) - 13 cm²/min Short Lengths • 5 cm Wide Webs Grown Regularly • Sensor for Closed Loop Control Based on Dendrite Thickness Demonstrated • Software and Hardware Elements for Closed Loop Control Completed • Plastic Flow Modeling Initiated for Stress Reduction
<p>Goals For 1985</p> <p>Demonstrate</p> <ul style="list-style-type: none"> • Area Growth Rate of 13 cm²/min (2 m Length) • Area Growth Rate of 16 cm²/min (2 m Length) • Closed Loop Growth Control System 	

Outline

Introduction — — — — — R. H. Hopkins

- Goals
- Organization

Closed Loop Web Growth System Development

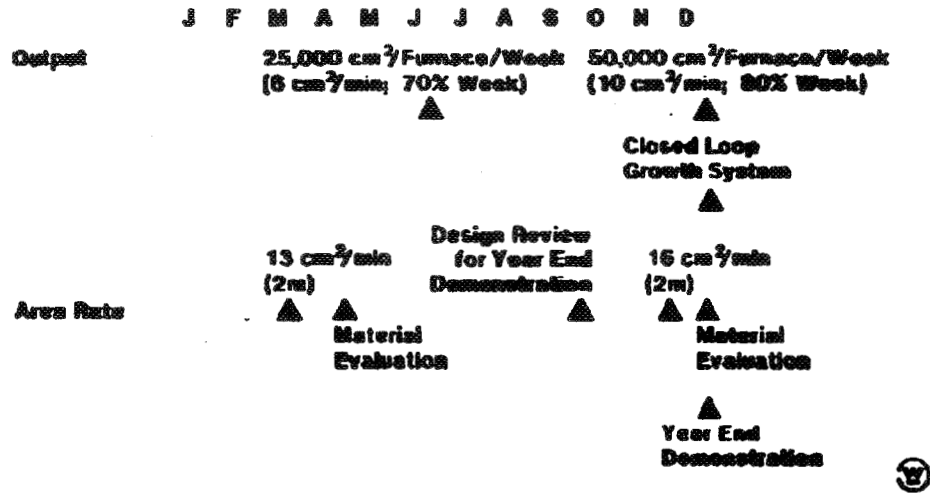
- Dendrite Thickness Monitor
- Closed Loop Control System
- System Monitoring

Stress Reduction for High Area Rate Growth

- Far Stress
- Near Stress

Plastic Deformation — — — — — J. Spitznagel

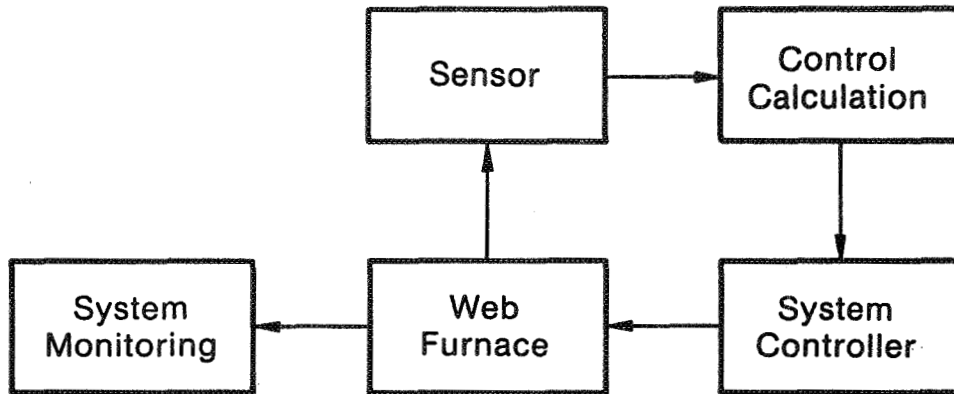
Web Technology Development
1985 Milestones



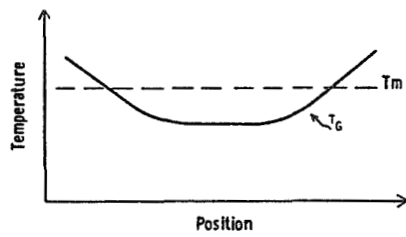
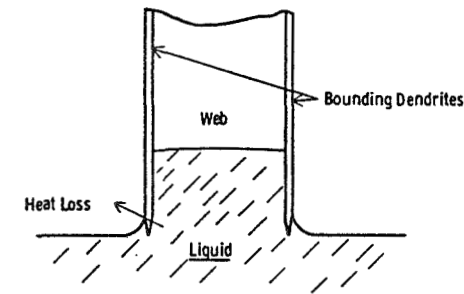
Web Technology Development

Output Team - G.E. Duncan		
	<u>Goals</u>	<u>Date</u>
System Performance Task	25,000 cm ² /Furnace/Week	6/30/85
F.A. Pietrowski	50,000 cm ² /Furnace/Week	12/31/85
Continuous Replenishment Task	Closed-Loop Growth Control	12/31/85
F.A. Pryzwarty		
Instrumentation and Control Task		
J.R. Eason		
Area Rate Team - R.H. Hopkins		
	<u>Goals</u>	<u>Date</u>
Modeling and Analysis Task	13 cm ² /min (2m)	3/31/85
R.G. Seidensticker	16 cm ² /min (2m)	12/31/85
Experiment Concept and Evaluation Task		
J.P. McHugh		
Component Design and Implementation Task		
R.P. Sprague		
Characterization Task		
J. Spitznagel		
Information Management - E.L. Kochke		

Closed Loop Web Growth System

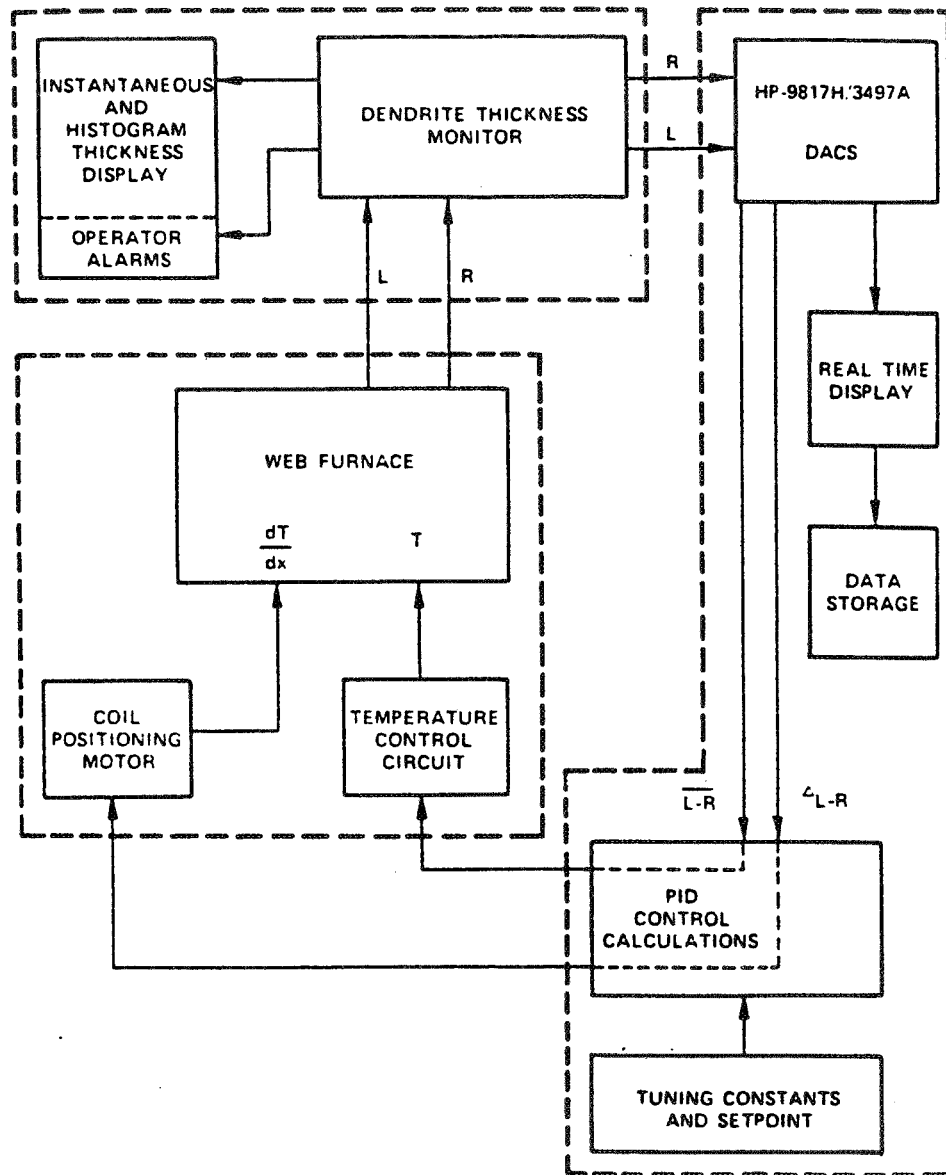


Web Growth Control



- Growth Temperature, T_G - Control Furnace Temperature
- Lateral Symmetry - Control Coil Position

Closed-Loop Control System

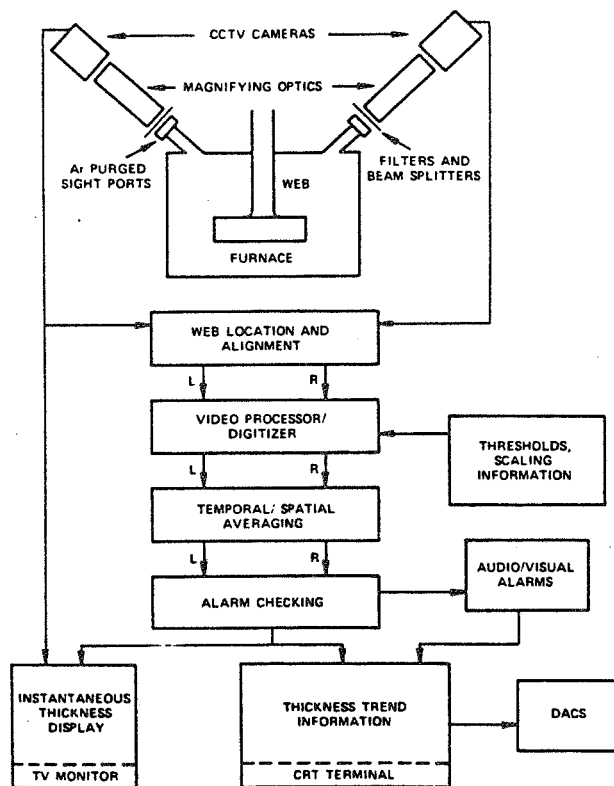


Basis for Web Closed-Loop Control


Dendrite Thickness Controlled Through Digital Feedback Loop

- DTM Provides Input to Two Uncoupled P-I-D Control Equations
 - Average L-R Thickness Controls Temperature
 - Thickness Difference Controls Spatial Temperature Distribution
- RF Coil Position (Left-Right) Adjusted Through PID Output to Motorized Stage for dT/dx Changes
- Temperature (RF Power) Adjusted By Biasing Light Pipe Input to Analog Temperature Controller (Based on PID Control Output)

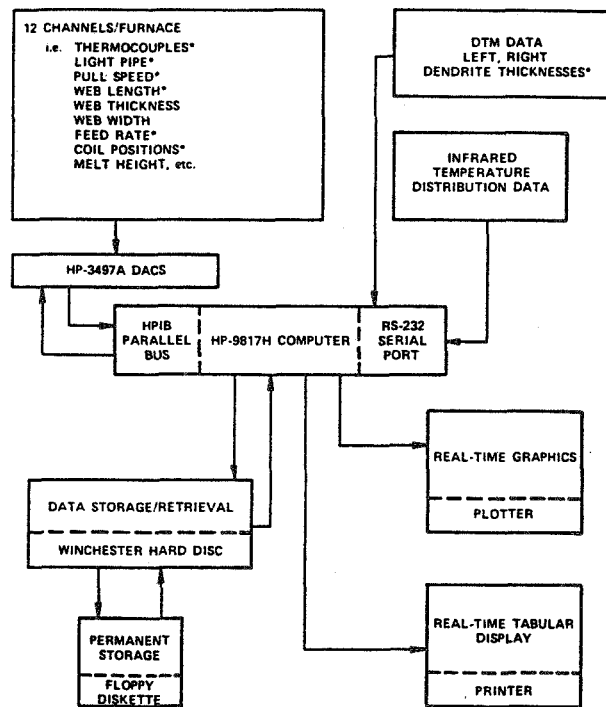
Dendrite Thickness Monitor



Dendrite Thickness Monitor (DTM)

- View-719 VidiconType Dimension Inspection System
-  Developed Application Software
 - Visual Display for Operator in Manual Mode
 - Input to Control System in Automatic Mode
- Automatic Calibration and Dendrite Tracking
- Gas Purged Viewport System on Furnace Provides Clean Sightpath
- 50 Microns (1 PIXEL) Resolution; with Software Averaging, Repeatability ~ 10 Microns

Data Acquisition System

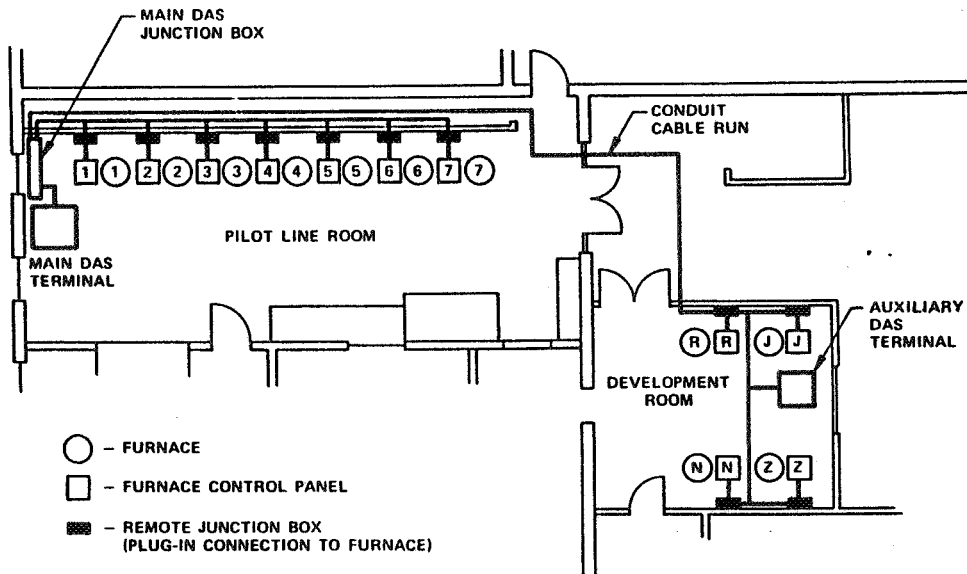


*CURRENTLY AVAILABLE

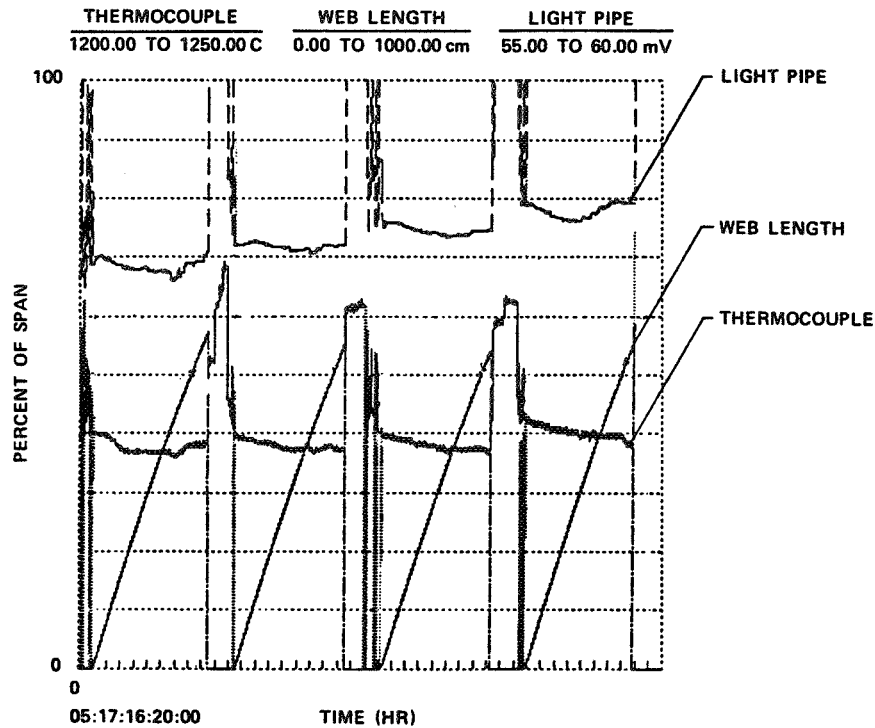
Data Acquisition System (DAS)

- Based on HP-9817H Computer with HP-3497A Data Acquisition System
- Hardware Configuration Allows Maximum of 12 Data Channels Per Furnace
- Anticipated Storage Capacity ~1 Week of Data for 11 Furnaces
- Real-Time Graphics or Tabular Display
- Variable Sampling Rate Data Storage with Time Compression/Expansion Capability on Recalled Graphics Display

Data Acquisition Cabling Plan



Monitoring with Real-Time Data Acquisition System



Closed-Loop Development Status

- DTM Tests Successful
 - Operator Acceptance for Manual Operation
 - Adequate Resolution
 - Reduced Terminations/Longer Webs
- Dendrite Thickness Data Compatible with Control Function
- Software for P.I.D. Control Algorithm Complete
- Computer Controlled Coil Positioner and Temperature Control Demonstrated
- Software for Dual Furnace Operation of DTM Complete
- Cabling of Furnaces for Data Acquisition and Monitoring Complete

Area Rate

TECHNICAL ISSUES

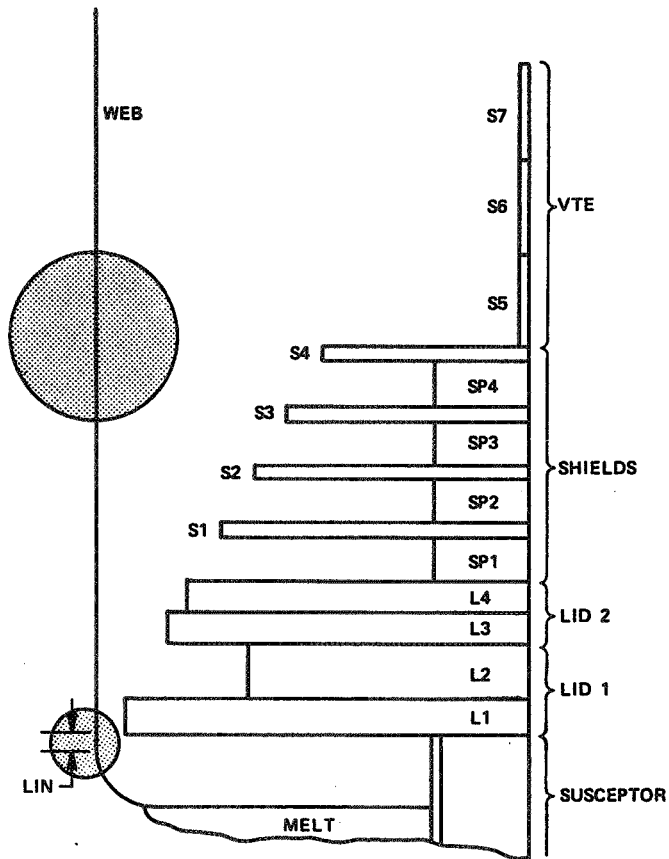
1. Low Stresses —→ Wide Crystals

- Far Stress
- Near Stress

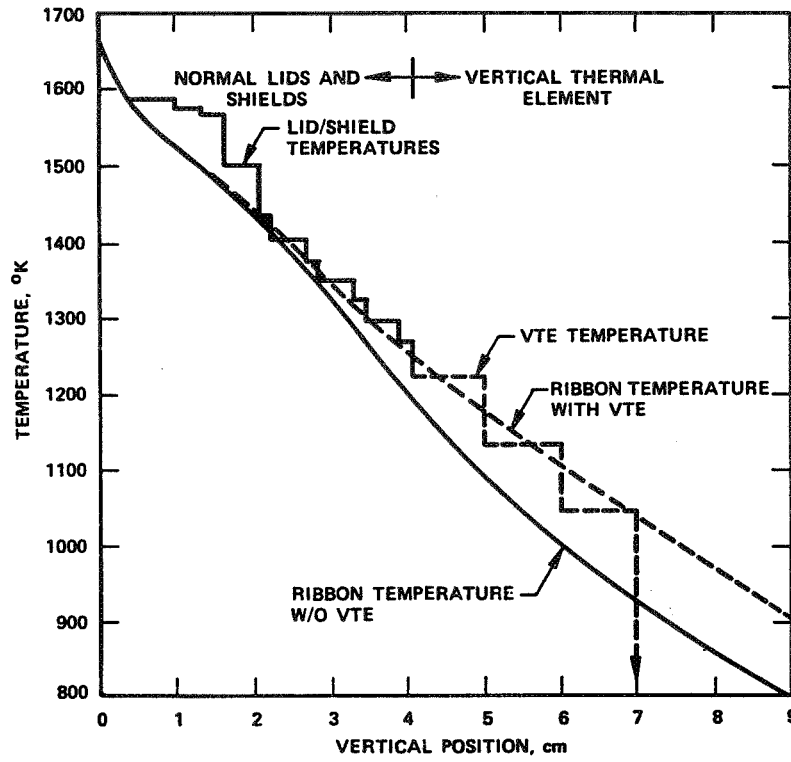
2. Maximum Interface Heat Loss —→ High Speed

- Growth Stability with Deep Melts
- Stress Trade-Offs

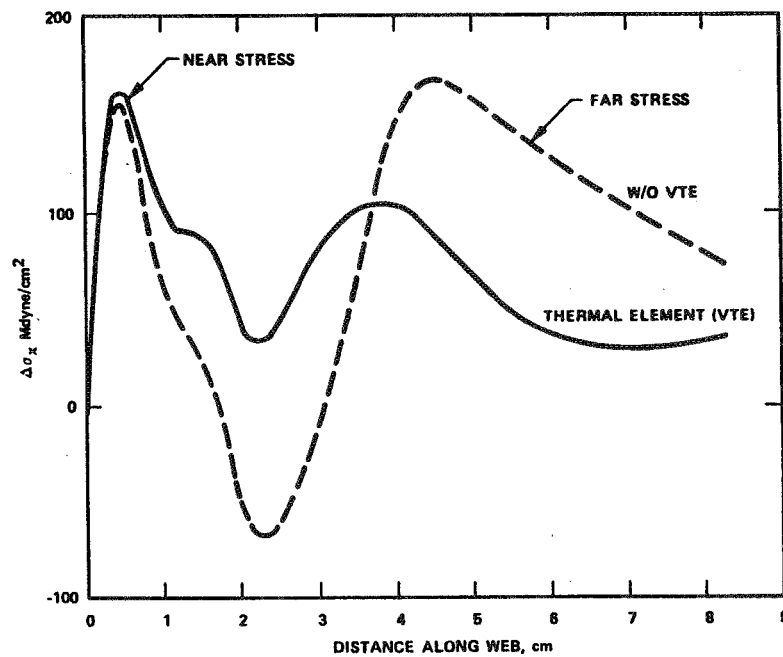
Schematic Growth Configuration (for modeling)



Calculated Web Thermal Profiles

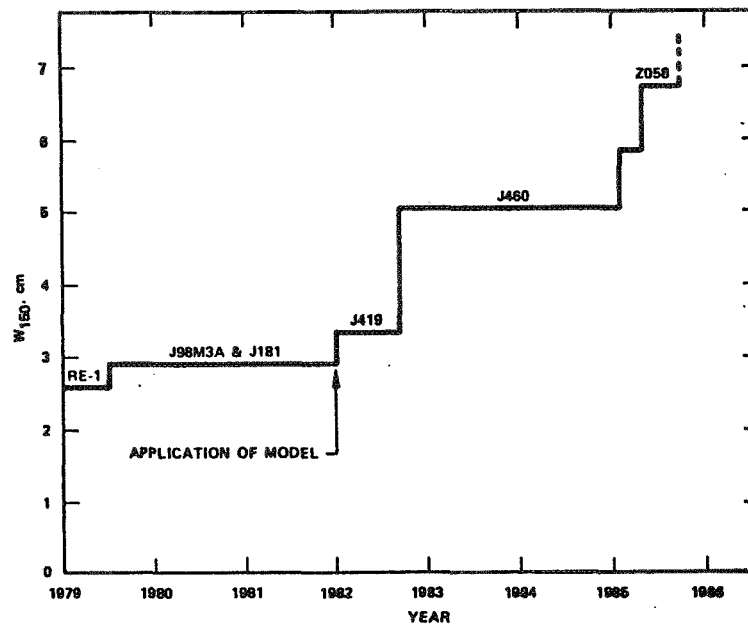


Far Stress Reduction by Thermal Element Above Shield Stack



ADVANCED SILICON SHEET

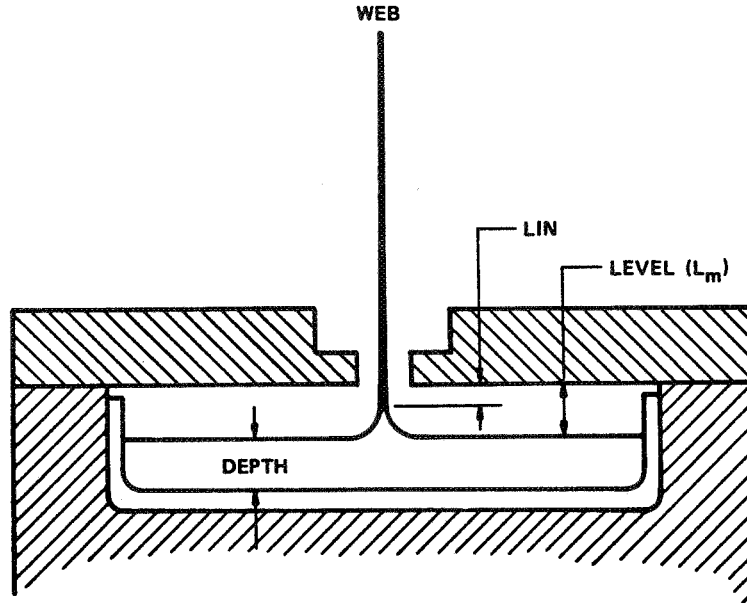
Undeformed Web Width



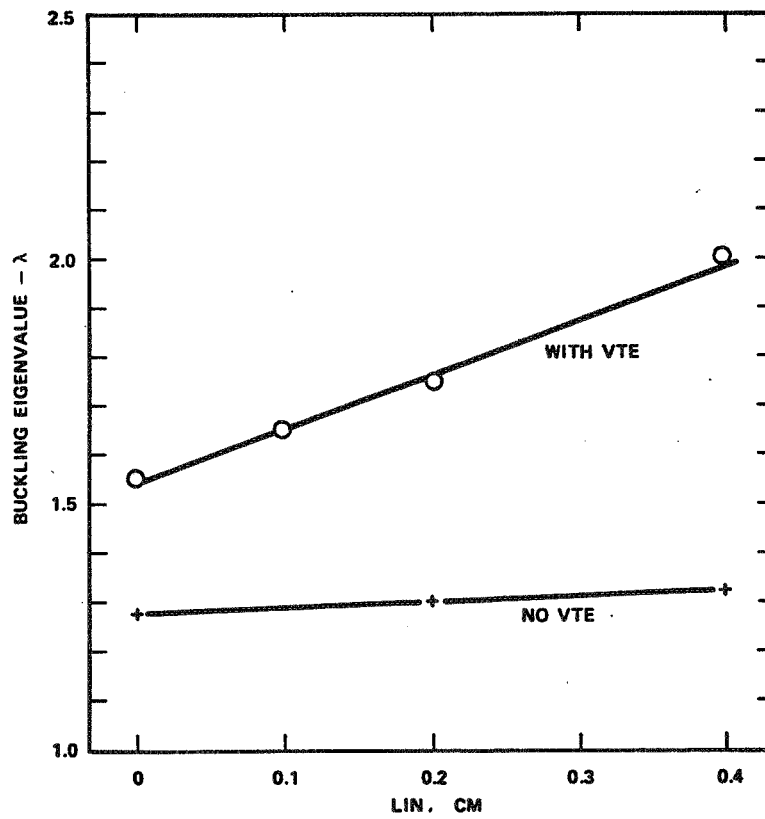
Recent Wide Web Crystals

CRYSTAL	W (cm)	t (μm)	V (cm ² /min)	Area Rate (cm ² /min)
N126-14	5.0	210	1.13	5.6
N127-3	5.6	170	1.13	6.3
N127-4	5.0	140	1.43	7.1
Z058-4	5.8	160	1.05	6.1
Z059-2	5.0	135	1.13	5.6
N128-15	4.9	75	1.88	9.2
N128-16	5.2	95	1.65	8.6
N128-19	5.2	130	1.43	7.4
Z060-14	4.5	135	1.57	7.1
R483-10	4.8	145	1.38	6.6
N130-11	5.4	140	1.28	6.9
R485-7	4.8	105	2.04	9.8
N132-2	4.7	145	1.28	6.0
R486-12	5.0	210	1.38	6.9
R486-13	4.8	150	1.38	6.6
N132-2	4.7	145	1.28	6.0
Z063-2	5.5	130	1.35	7.4
			2.10	11.5
J55-13	5.2	125	1.29	6.7
J551-15	5.5	150	1.02	5.6
J552-1	6.7	...	1.29	8.1
J554-1	5.4	170	1.15	6.2
J554-2	5.3	165	1.15	6.1
J555-1	5.0	205	1.15	5.8
		65	2.65	13.3
J55-6	5.2	150	1.15	6.0
J557-2	5.3	170	1.29	6.9
J557-5	6.4	190	1.15	7.4
J557-6	5.0	160	1.15	5.8
J557-7	5.3	165	1.15	6.1
J559-8	5.0	170	1.15	5.8
J560-2	6.0	155	1.15	6.9
N141-1	5.2	150	1.28	6.7
Z066-7	5.0	140	1.22	6.1
Z069-1	4.8	170	1.31	6.3
Z069-8	4.8	165	1.22	5.9
Z070-17	4.8	135	1.31	6.3
N142-3	4.8	120	1.28	6.1
R492	5.1	155	1.11	5.7

Melt Geometric Parameters

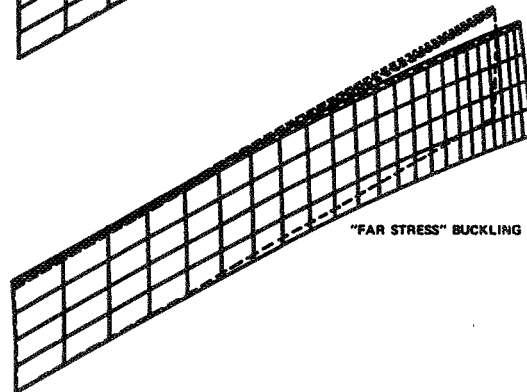
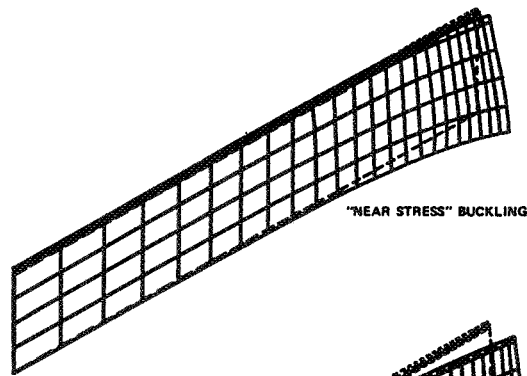
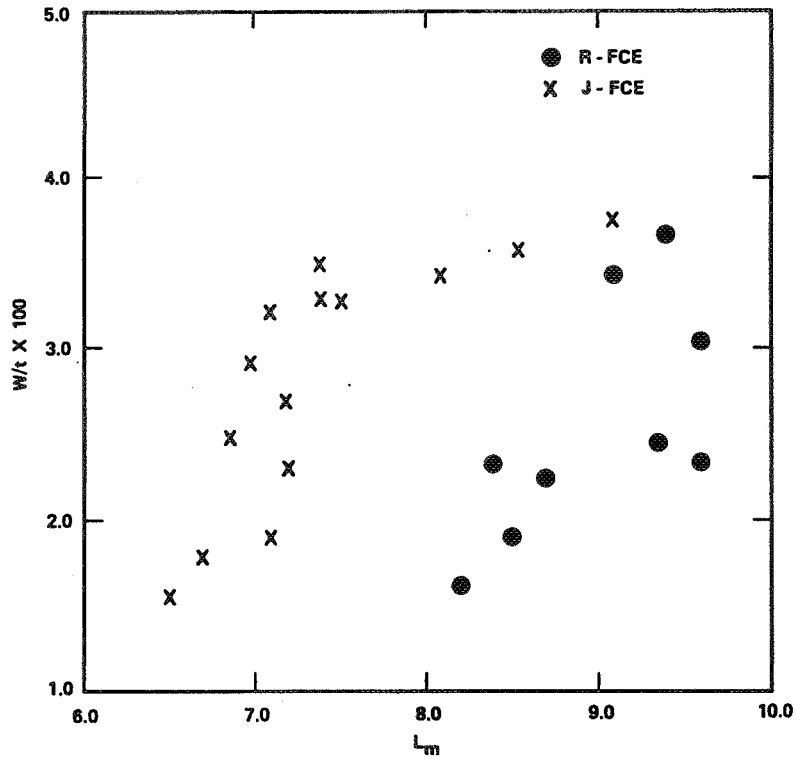


Variation in Web Buckling Eigenvalue with Crystal-Liquid Interface Position



ADVANCED SILICON SHEET

Normalized Buckling Width Versus Melt Level



Near Stress Reduction

APPROACHES

Model

- Direct Stress Calculation from Hypothetical Lid Design
- General Analysis from Synthetic Temperature Profiles
- Guidance from Effective Ambient Temperature Calculation

Fabricate and Test Lids

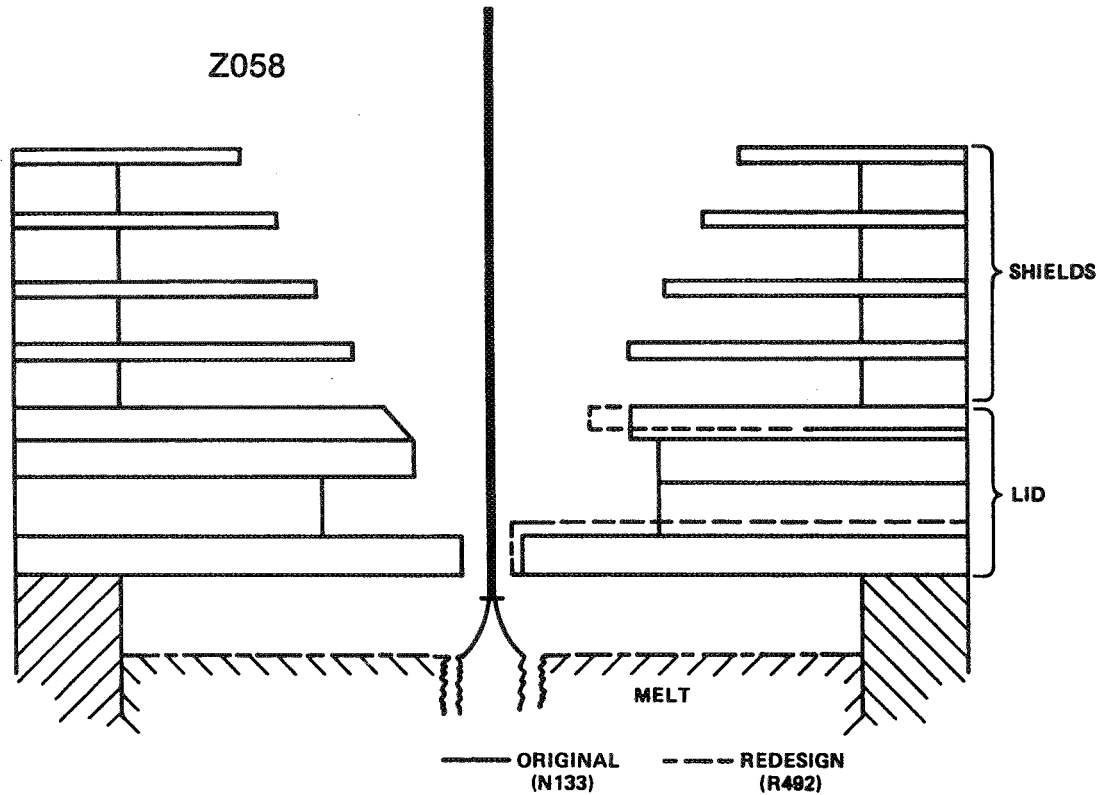
Evaluate Parametric Effects on Crystal Quality

Modeling New Lids for Interface Stress Reduction

(LIN = 0)

<u>Model Case</u>	<u>Remarks</u>	<u>V Web (cm/min)</u>	<u>σ_y (0) (Md/cm²)</u>	<u>$\Delta\sigma_x$ (near) (Md/cm²)</u>
J460	Baseline	1.53	-645	155
New 1 (N-133)	Std. T's	1.53	-612	145
New 1 (N-133)	Hotter Cavity	1.52	-591	139
New 1 (N-133)	Hot/Deeper Cavity	1.48	-581	140

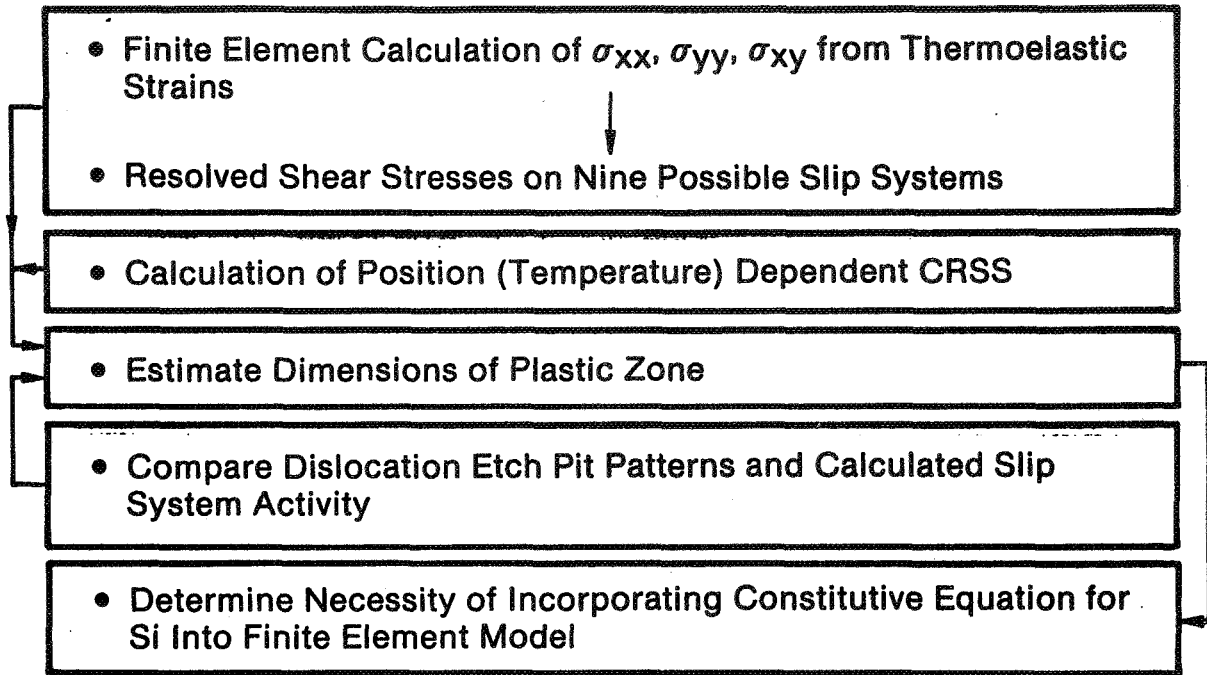
Lid Designs for Interface Stress Reduction



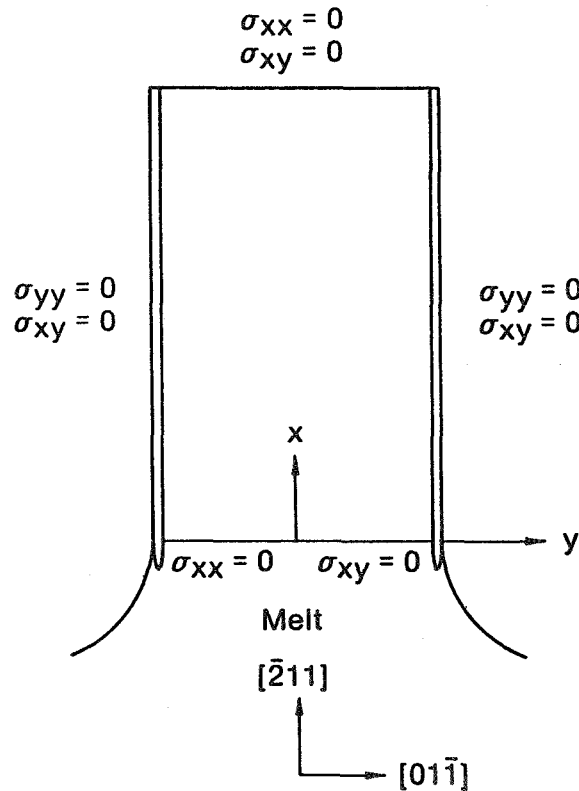
Typical Web Etch Pit and Stress Data

Growth Configuration	J435	Z058 (Far Stress Control)	R492 (Near Stress Control)
Residual Stress (Mdyn/cm ²)	20-40 (Tensile)	<10 (T and C)	<10 (Compressive)
Etch Pit Density (cm ⁻²)	20-40K	~3K	<5K

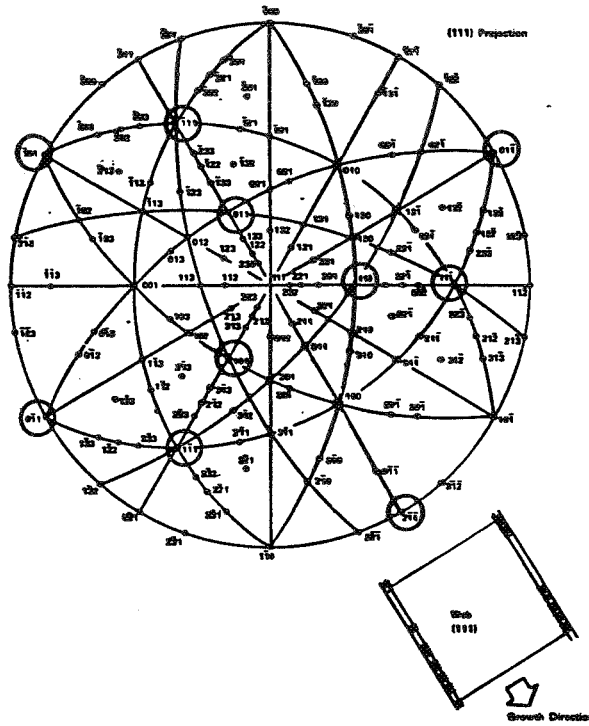
Plasticity Effects in Web Growth



Web Geometry



Web Slip Systems



Calculation of Resolved Shear Stresses

$$\sigma_{ij} = a_{ix} a_{jx} \sigma_{xx} + [a_{ix} a_{jy} + a_{iy} a_{jx}] \sigma_{xy} + a_{iy} a_{jy} \sigma_{yy}$$

Where

a_{ix} = Cosine of Angle Between Normal to Slip Plane and $[2\bar{1}\bar{1}]$

a_{jx} = Cosine of Angle Between Slip Direction and $[2\bar{1}\bar{1}]$

a_{iy} = Cosine of Angle Between Normal to Slip Plane and $[01\bar{1}]$

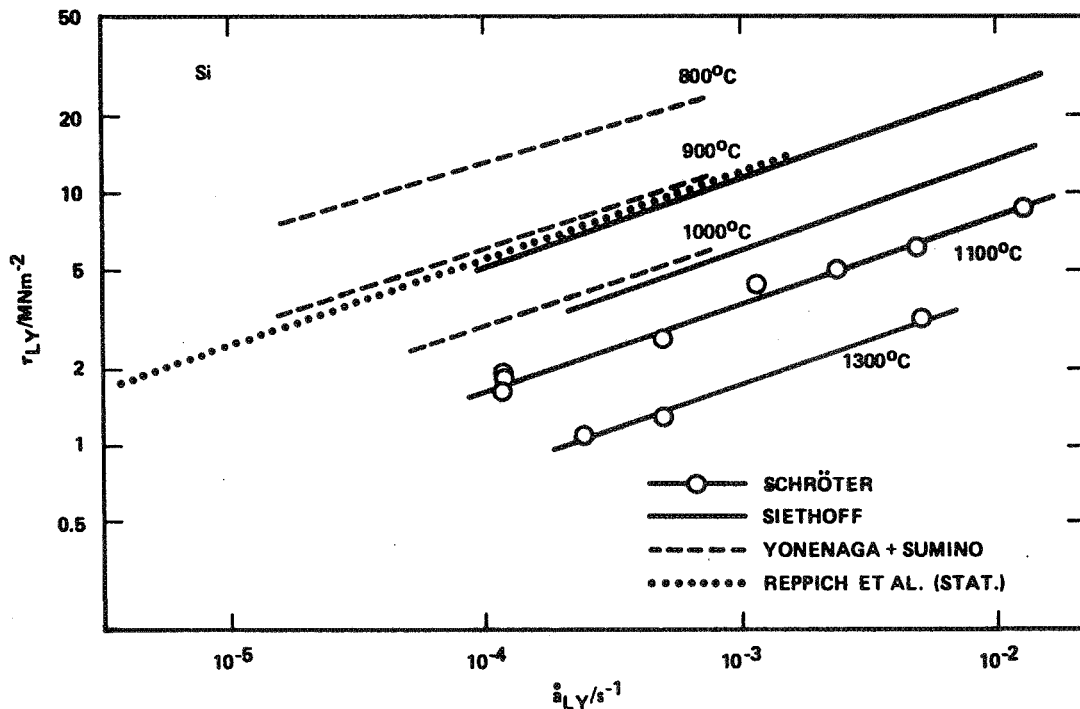
a_{jy} = Cosine of Angle Between Slip Direction and $[01\bar{1}]$

ADVANCED SILICON SHEET

Resolved Shear Stresses for Single Crystal (111) Web Silicon

<u>Plane</u>	<u>Direction</u>	<u>Resolved Shear Stress</u>
(1 $\bar{1}\bar{1}$)	[011]	$-0.272 \sigma_{XX} + 0.470 \tau_{XY}$
(1 $\bar{1}\bar{1}$)	[110]	$0.136 \sigma_{XX} - 0.408 \sigma_{YY}$
(1 $\bar{1}\bar{1}$)	$\bar{1}$ [01]	$-0.408 \sigma_{XX} + 0.471 \tau_{XY} + 0.408 \sigma_{YY}$
(11 $\bar{1}$)	[011]	$-0.272 \sigma_{XX} - 0.470 \tau_{XY}$
(11 $\bar{1}$)	[101]	$0.136 \sigma_{XX} - 0.943 \tau_{XY} - 0.408 \sigma_{YY}$
(11 $\bar{1}$)	$\bar{1}$ [10]	$-0.408 \sigma_{XX} - 0.471 \tau_{XY} + 0.816 \sigma_{YY}$
($\bar{1}$ 11)	[110]	$-0.272 \sigma_{XX} - 0.471 \tau_{XY}$
($\bar{1}$ 11)	[101]	$-0.272 \sigma_{XX} + 0.471 \tau_{XY}$
($\bar{1}$ 11)	[0 $\bar{1}$ 1]	$0.943 \tau_{XY}$

Lower Yield Stress as a Function of Strain Rate in FZ and Cz Silicon



Critical Resolved Shear Stress Criterion for First Iteration

$$\dot{\epsilon}_{avg} = \frac{\partial(\alpha T)}{\partial t}$$

$$\simeq 5 \times 10^{-5} \text{ s}^{-1}$$

$$\tau_{LY} = 1.505 \times 10^{-3} \text{ EXP } [9283/T]$$

τ_{LY} = Shear Stress at Lower Yield Point in MPa

T = Web Temperature, °K (T ≥ 1000K)

<u>T°K</u>	<u>τ_{LY} (MPa)</u>
1073 (800°C)	8.6
1173 (900°C)	4.1
1273 (1000°C)	2.2
1373 (1100°C)	1.3
1573 (1300°C)	0.55

Problems/Concerns

- (1) Reduction in Interface Stress for High Speed Growth Requires Analytical and Experimental Effort: Calendar Year Schedule is Ambitious
- (2) Uncertainties in High Temperature Properties of Silicon Impact Stress Modeling

DEFECT CHARACTERIZATION OF SILICON DENDRITIC
WEB RIBBONS

JET PROPULSION LABORATORY

Li-Jen Cheng

Contents

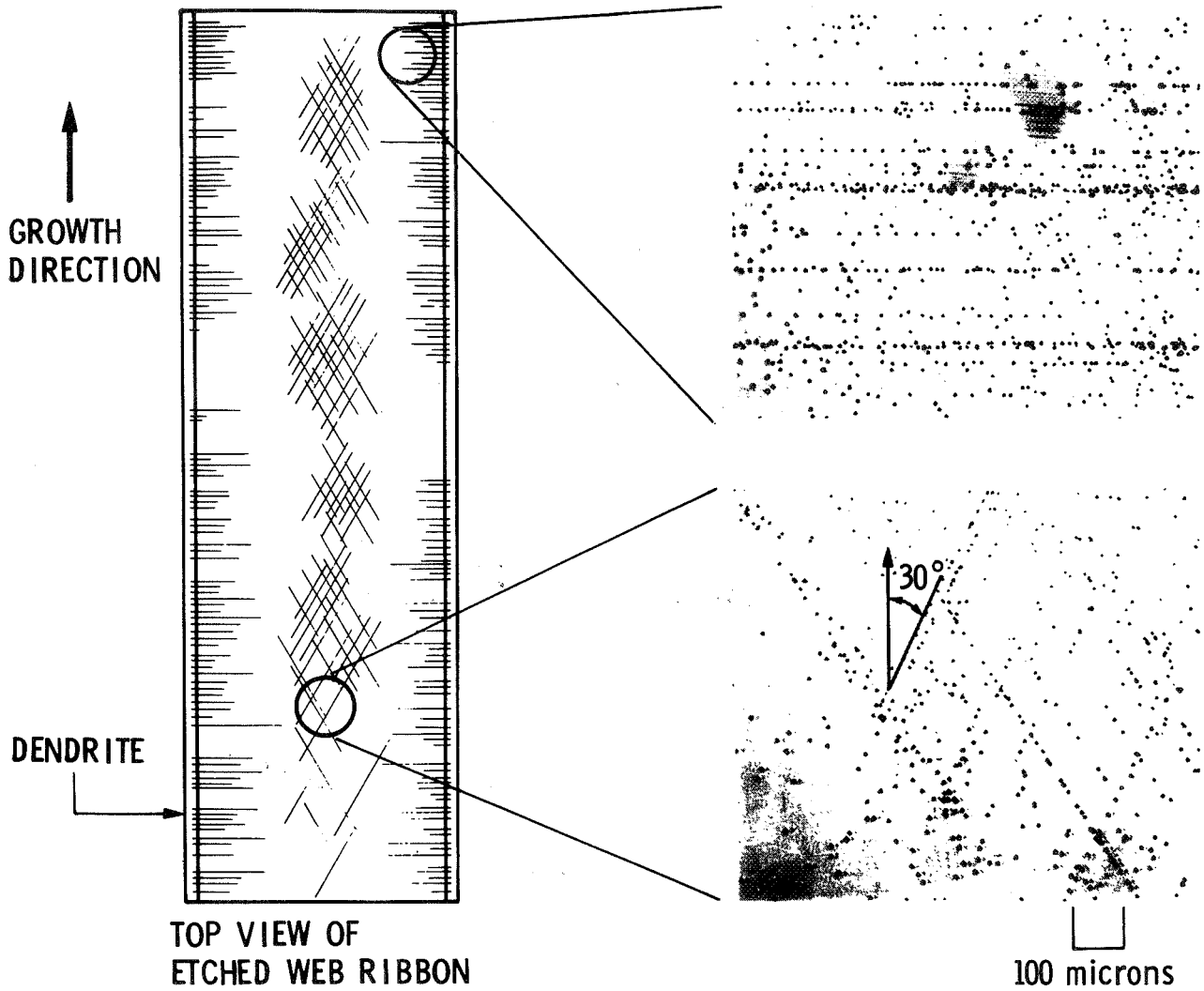
- * Etch Pit Distribution

- * Cross-Section EBIC

- * Thermal Annealing Effect on
Carrier Lifetime

PRECEDING PAGE BLANK NOT FILMED



ADVANCED SILICON SHEET



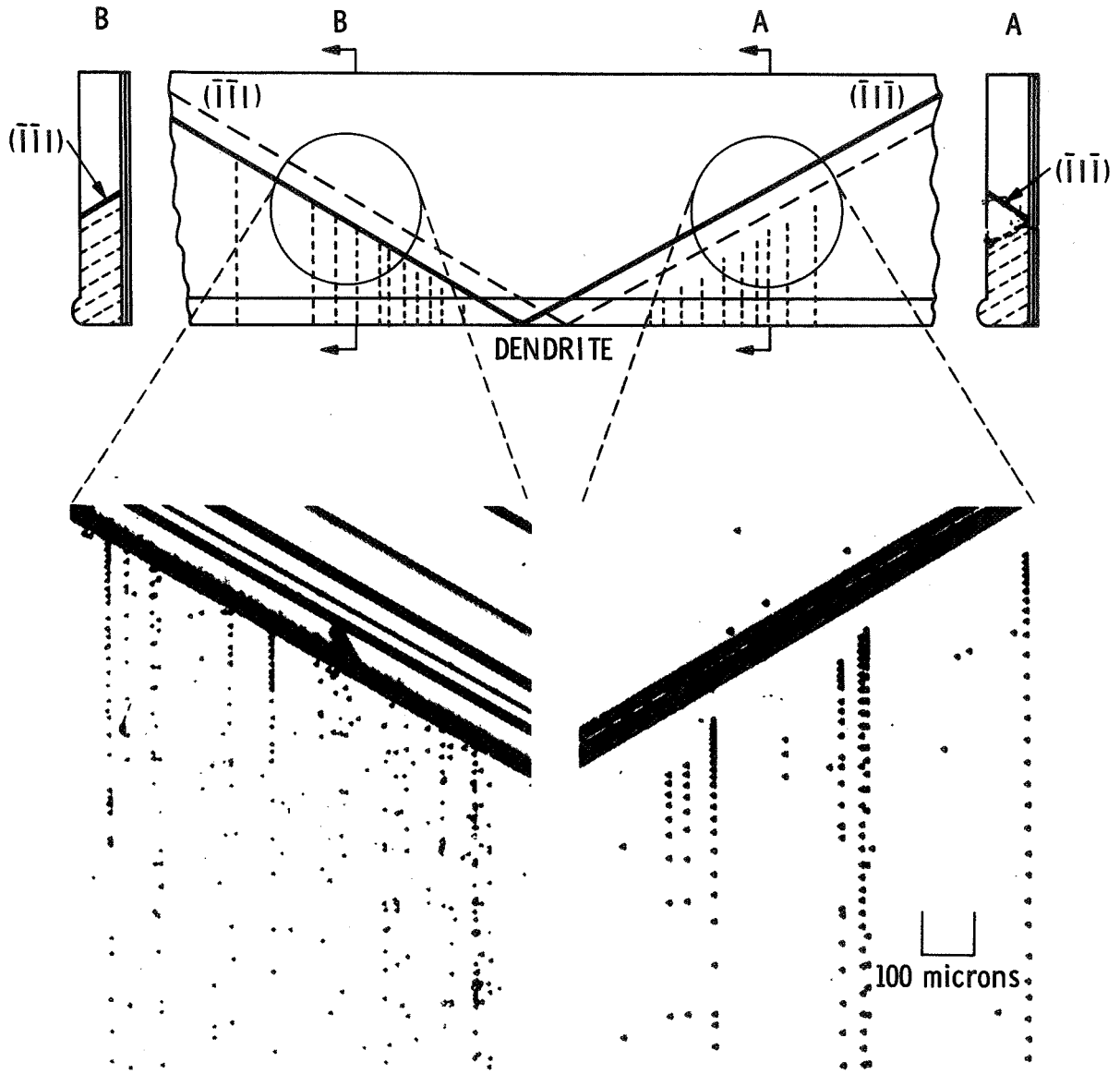
Patterns of Etch Pits on Web Ribbon Surface
Due to Dislocations

ORIGINAL PAGE IS
OF POOR QUALITY

Possible Movement of Three Major Slip Planes Under Stress

NATURE OF STRESS	DIRECTION WITH RESPECT TO GROWTH AXIS	INTERCEPTS ON WEB SURFACE
TENSILE	PARALLEL, σ_{xx} PERPENDICULAR, σ_{yy}	
SHEAR	PARALLEL, σ_{yx} PERPENDICULAR, σ_{xy}	

ADVANCED SILICON SHEET



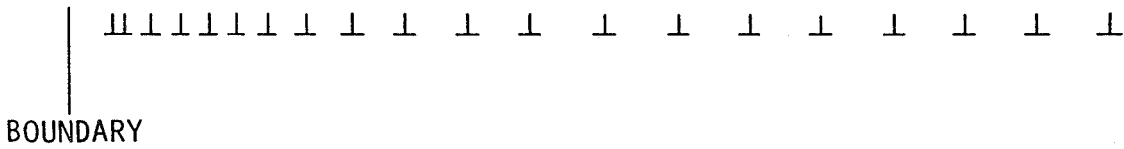
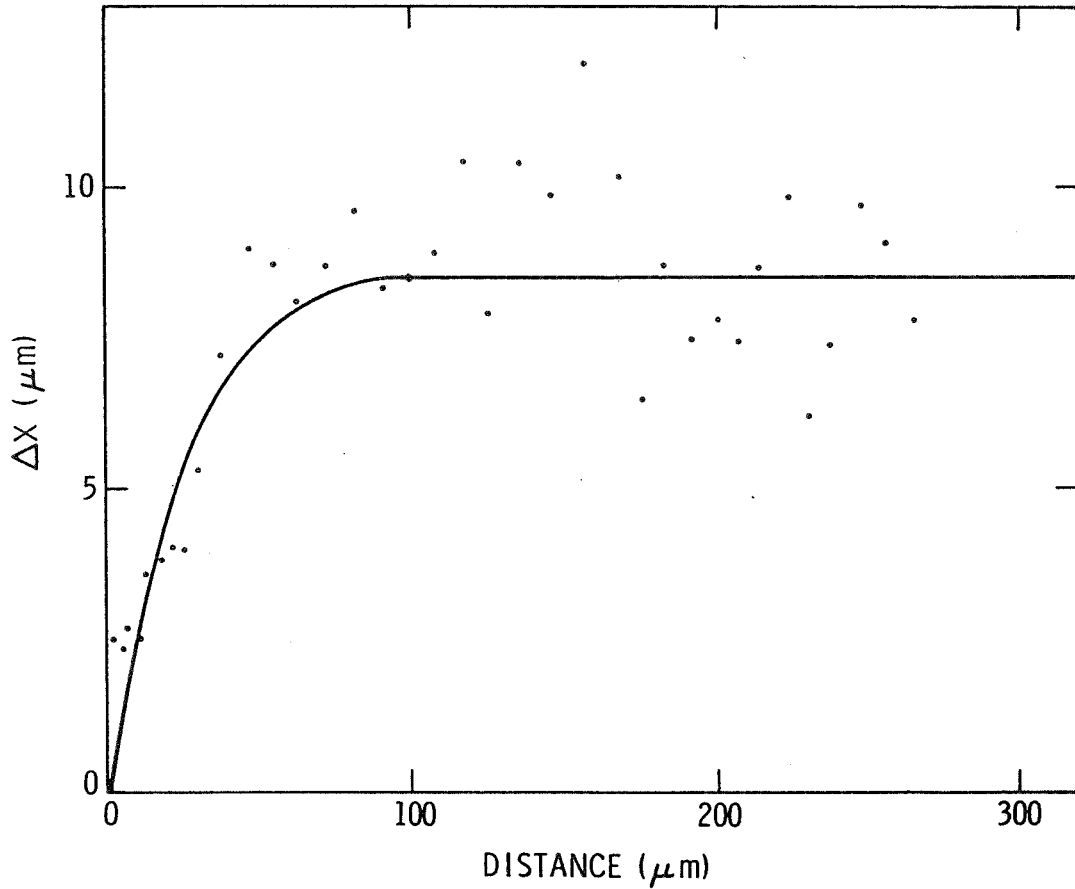
— INTERCEPTS OF $(\bar{1}\bar{1}\bar{1})$ AND (111)
TWIN BOUNDARIES WITH THE
RIBBON SURFACE

- - - INTERCEPTS OF $(\bar{1}\bar{1}\bar{1})$ AND (111)
TWIN BOUNDARIES WITH
THE TWIN PLANE

- - - - - ETCH PIT LINES DUE TO SLIP
DISLOCATIONS $[101]$

==== THE TWIN PLANE IN THE CENTER OF
THE RIBBON PARALLEL
TO THE SURFACE

ADVANCED SILICON SHEET



TOTAL STRESS ON THE FIRST DISLOCATION DUE TO THE PRESENCE OF NEIGHBORING DISLOCATIONS ALIGNING ALONG x DIRECTION

$$\sigma_{xy}^{tot} = \frac{\mu b}{2\pi(1-\gamma)} \sum_i \frac{1}{x}$$

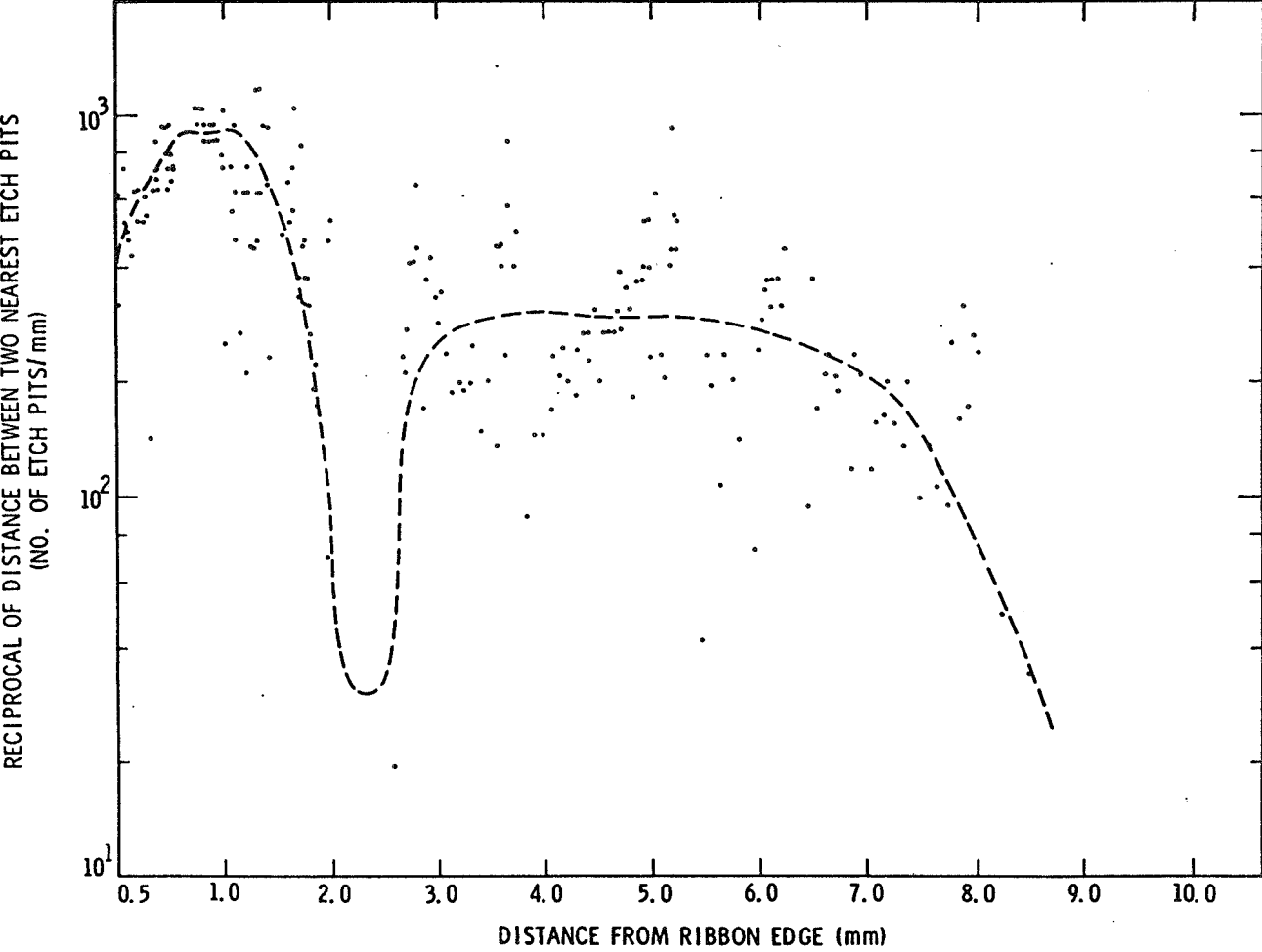
EXPERIMENTAL DATA

$$\sigma_{xy}^{tot} \text{ (AT THE PILEUP)} = 1.07 \times 10^8 \text{ dynes/cm}^2 \text{ (} 1.55 \times 10^3 \text{ PSI)}$$

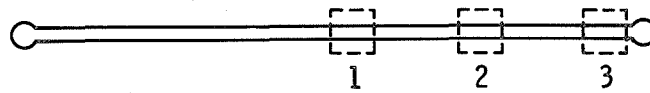
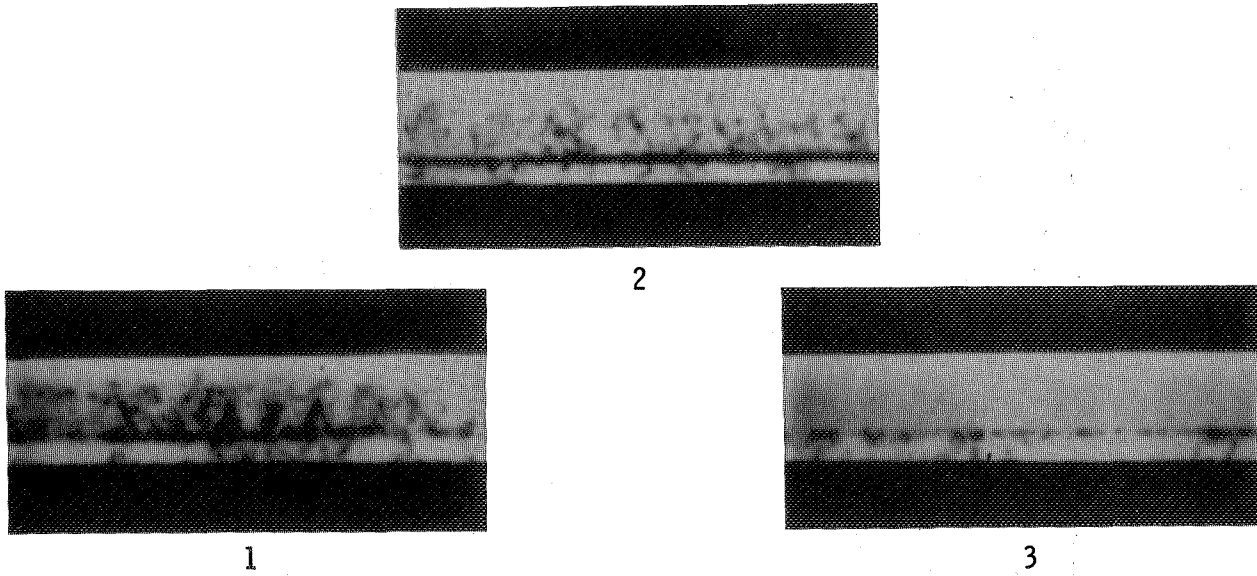
USING $\gamma = 20 \text{ PSI}$

$$\mu = \frac{\gamma}{2(1-\gamma)} = 9.57 \times 10^{11} \text{ dynes/cm}^2$$

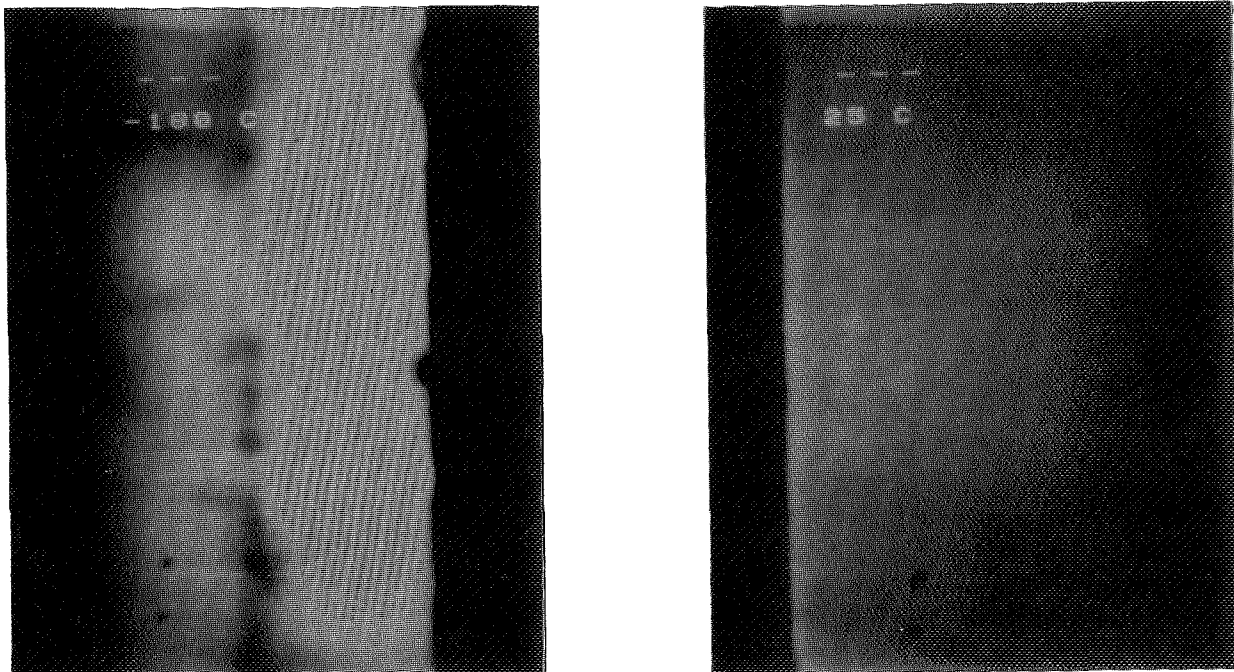
ADVANCED SILICON SHEET



Cross-Section EBIC in As-Grown Web Ribbons (taken at room temperature)

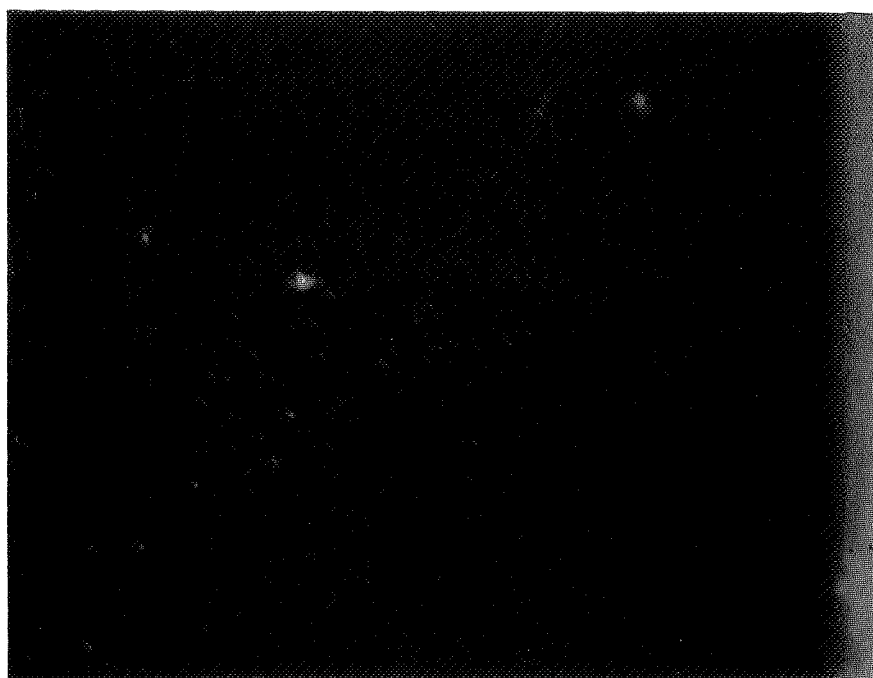


Temperature Dependence of EBIC in Diffused Silicon Web Ribbon



ADVANCED SILICON SHEET

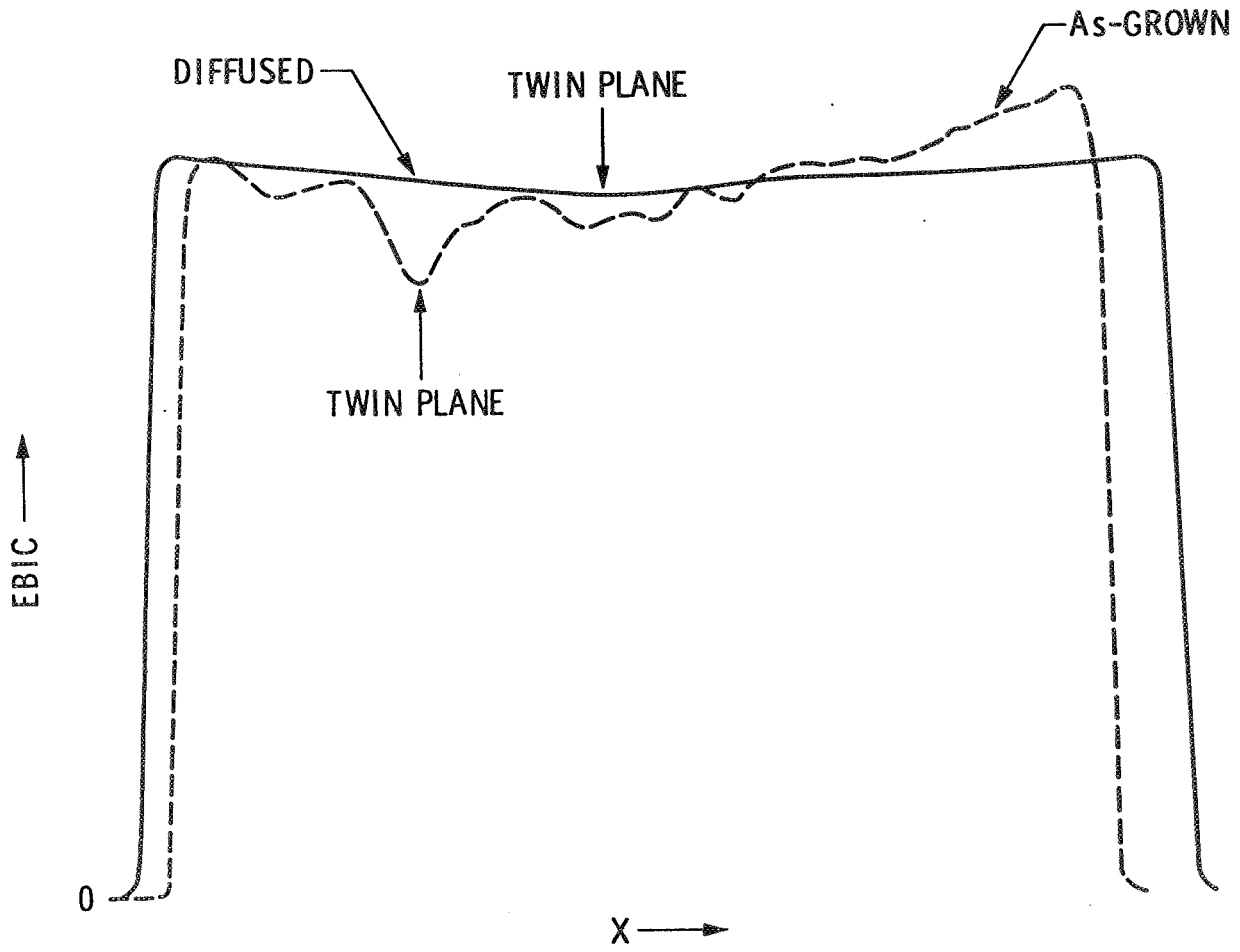
SEM Picture of Etched Cross-Section of Silicon Web Ribbon



┌──────────────────┐
DENUDED
ZONE ↑
SURFACE

ORIGINAL PAGE IS
OF POOR QUALITY

Effect of Diffusion



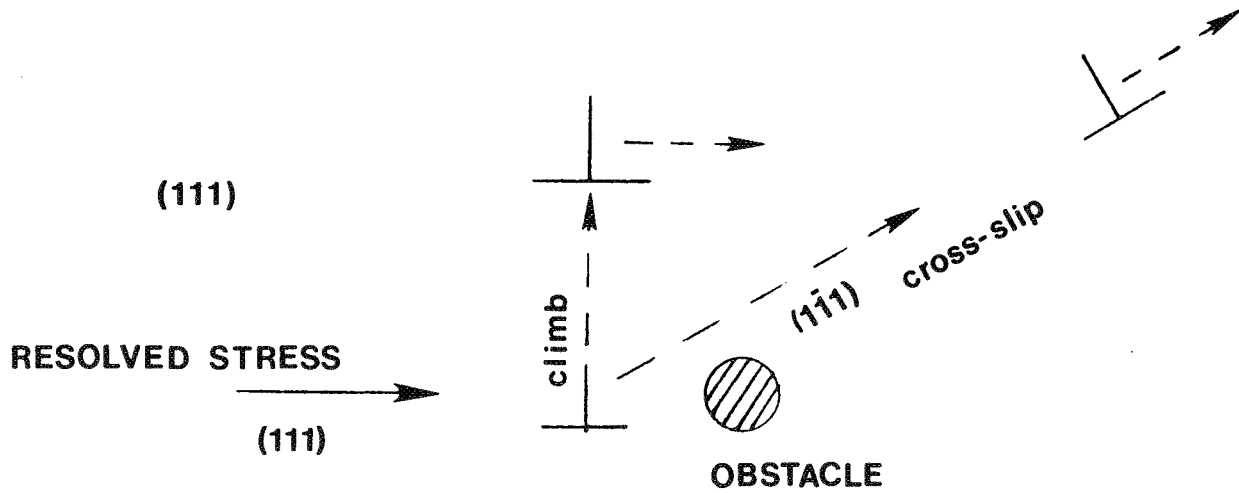
ELECTRICAL, STRUCTURAL, AND CHEMICAL CHARACTERIZATION OF SILICON SHEET MATERIALS

CORNELL UNIVERSITY

D. G. Ast
S. L. Hyland

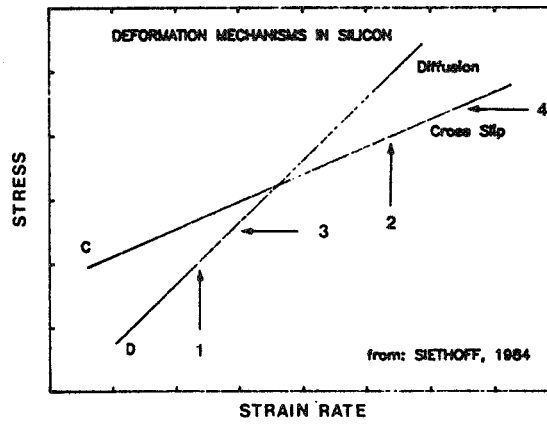
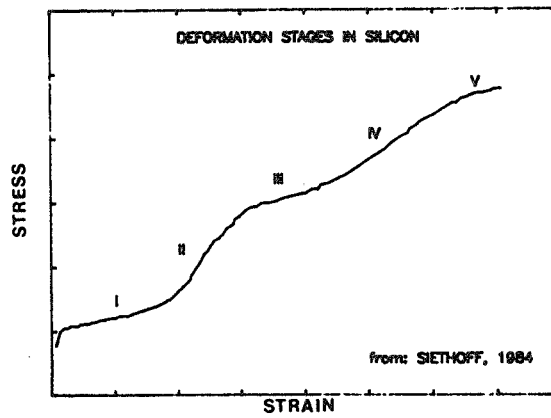
Study of Stress in Web Silicon Ribbons
Using High-Temperature Creep Experiments

Dislocation Motion Around an Obstacle

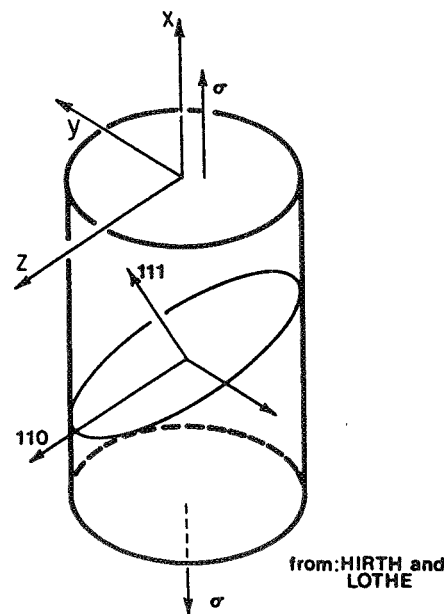


PRECEDING PAGE BLANK NOT FILMED

Deformation in Silicon



Resolving Applied Stress on a Dislocation

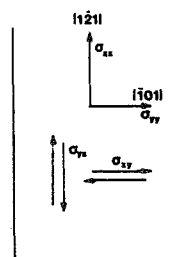


Calculation of Slip Systems

STRESS	ACTING ON		SCHMIDT FACTOR
	PLANE	DIRECTION	
σ_{xx} $\bar{1}\bar{2}1$	$\bar{1}\bar{1}\bar{1}$	$10\bar{1}$	0
		$0\bar{1}1$	0.2722
		110	0.2722
	$1\bar{1}\bar{1}$	110	-0.1361
		$0\bar{1}1$	0.4082 *
		101	0.2722
	$\bar{1}\bar{1}1$	$1\bar{1}0$	0.4082 *
		011	-0.1361
		101	0.2722
	111	$\bar{1}01$	0
		$1\bar{1}0$	0
		$0\bar{1}1$	0
σ_{yy} $\bar{1}01$	$\bar{1}\bar{1}\bar{1}$	$0\bar{1}1$	-0.4082
	$\bar{1}\bar{1}1$	$1\bar{1}0$	-0.4082
σ_{xy} OR σ_{yx}	$\bar{1}\bar{1}\bar{1}$	$10\bar{1}$	0.9428

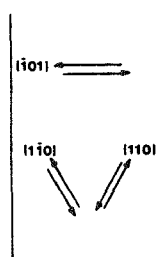
Resultant Stresses

APPLIED STRESS



RESULTING FROM

SHEAR STRESS

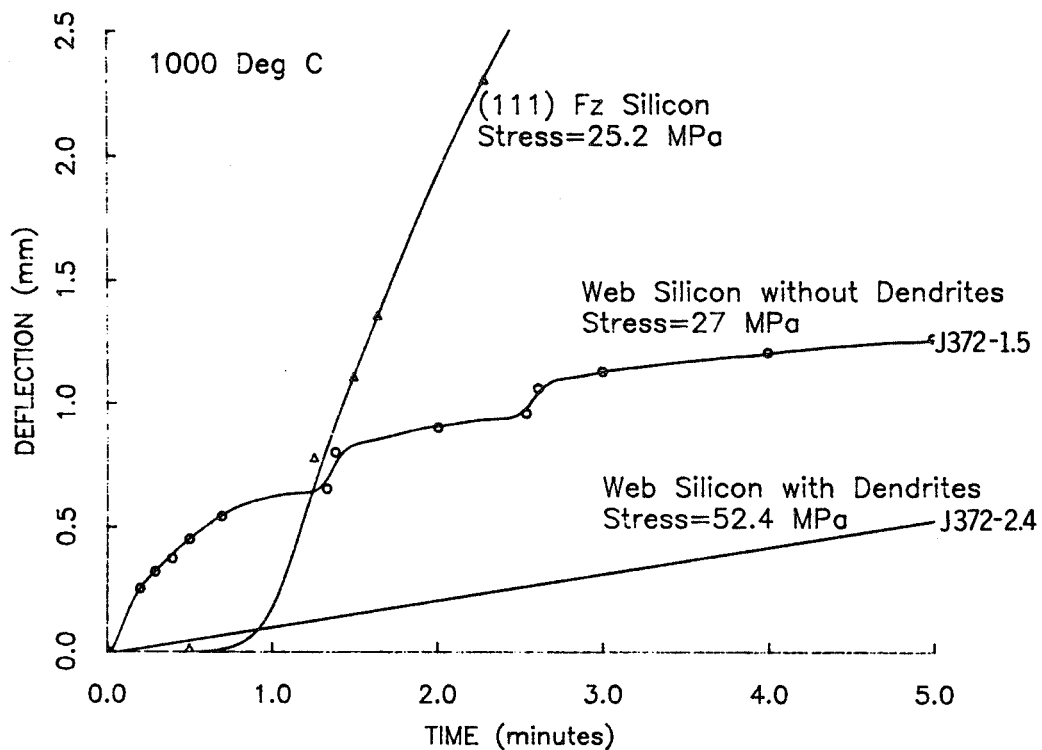


σ_{xy} OR σ_{yx}

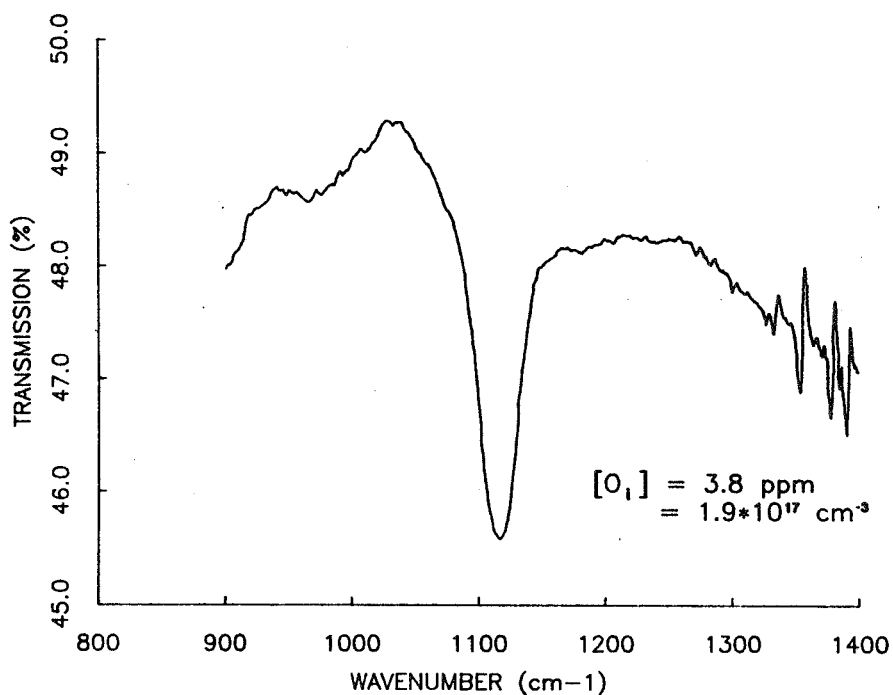
σ_{xx} OR σ_{yy}

ADVANCED SILICON SHEET

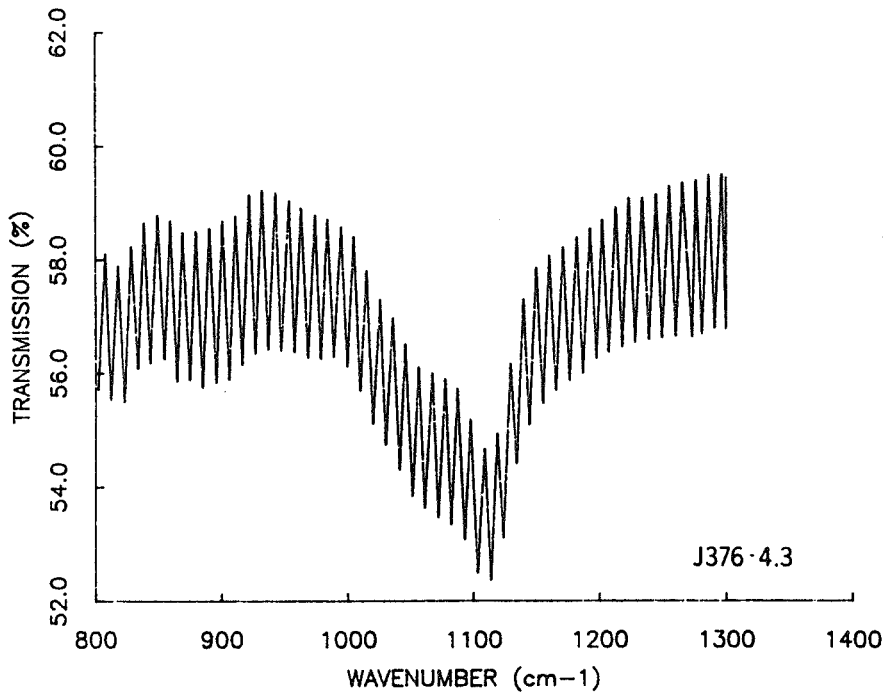
Deflection Versus Time for Four-Point Bending



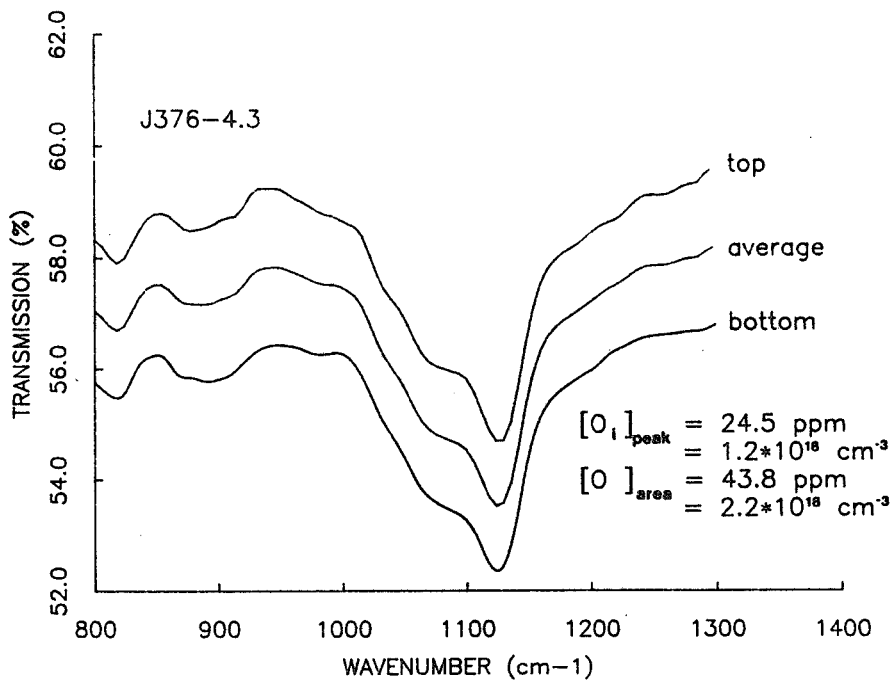
IR Transmission Versus Wavenumber for Czochralski Silicon



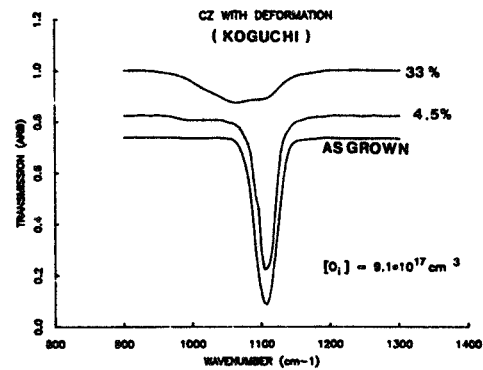
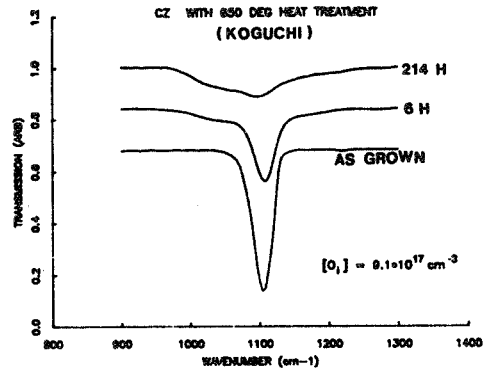
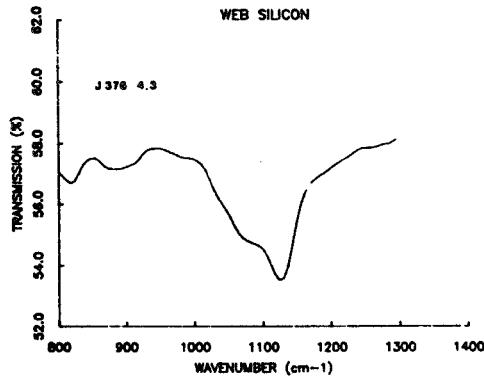
IR Transmission Versus Wavenumber for Web Silicon



IR Transmission Versus Wavenumber for Web Silicon



IR Transmission Versus Wavenumber



Conclusions

Creep behavior of Web is very different from any seen for single crystal silicon.

Perhaps modeled between single crystal and polycrystalline

Perhaps related to stress in the ribbon.

Oxygen level in Web silicon is near the saturation level at the melting point of silicon.

Interstitial oxygen is only about 1/2 the total oxygen content.

The rest of the oxygen is in a state close to that of interstitial oxygen that is affected by its environment.

ANALYSIS OF SILICON STRESS/STRAIN RELATIONSHIPS

UNIVERSITY OF KENTUCKY

O. Dillon

$$\dot{\epsilon}_{ij} = \frac{(1+\nu)}{E} \dot{\sigma}_{ij} - \frac{\nu \dot{\sigma}_{kk} \delta_{ij}}{E} + \dot{\epsilon}_{ij}^{PL} \tag{1}$$

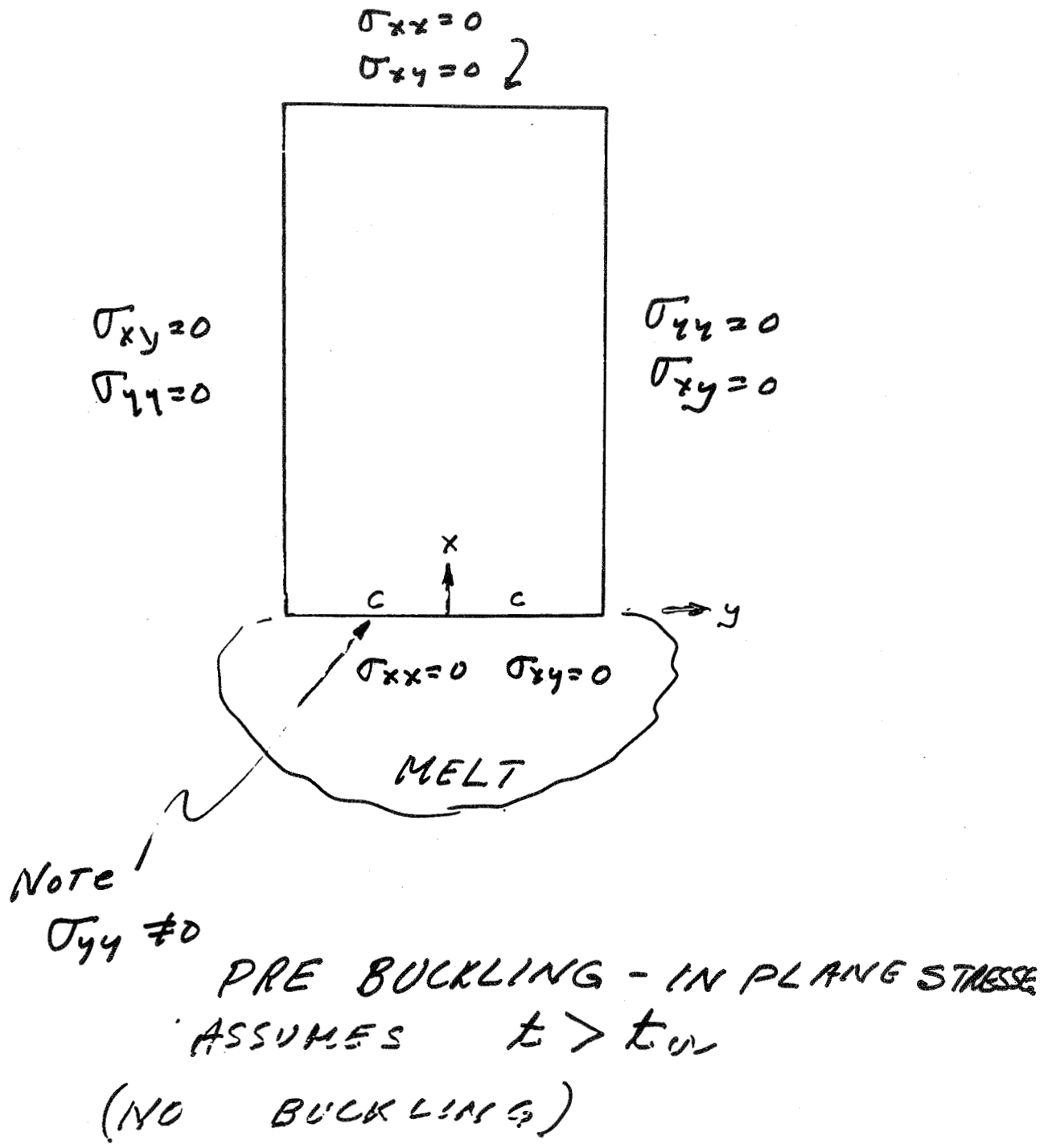
where the inelastic strain rate tensor $\dot{\epsilon}_{ij}^{PL}$ is the plastic strain rate and is

$$\dot{\epsilon}_{ij}^{PL} = f S_{ij} \tag{2}$$

where S_{ij} are the deviatoric stress components and where

$$f = \frac{bB}{\tau_0 m} N_m (\sqrt{J_2} - D\sqrt{N_m}) \frac{e^{-Q/kT}}{\sqrt{J_2}} \tag{3}$$

ADVANCED SILICON SHEET



ADVANCED SILICON SHEET

$$\nabla^2(\sigma_{xx} + \sigma_{yy}) = -\alpha E \nabla^2 T + \frac{1}{\nu} \int_0^x \left(\frac{\partial^2 \epsilon_{xx}^{PL}}{\partial y^2} + \frac{\partial^2 \epsilon_{yy}^{PL}}{\partial x^2} - 2 \frac{\partial^2 \epsilon_{xy}^{PL}}{\partial x \partial y} \right) E \, du \quad (8)$$

$$\sigma_{xx} = \frac{2}{f} \left[\epsilon_{xx}^{oc} + \frac{1}{2} \epsilon_{yy}^{oc} - z \frac{\partial^2 w^c}{\partial x^2} - \frac{z}{2} \frac{\partial^2 w^c}{\partial y^2} \right]$$

where w^c is the creep (viscoplastic) portion of the transverse displacement.

The moment intensity is related to the stress by the basic definition.

$$M_{xx} = - \int_{-h/2}^{h/2} \sigma_{xx} z \, dz$$

The "elastic moment" M_{xx}^e is then

$$M_{xx}^e = \frac{Eh^3}{12(1-\nu^2)} \left[\frac{\partial^2 w^e}{\partial x^2} + \nu \frac{\partial^2 w^e}{\partial y^2} \right] \quad (5)$$

while the corresponding "inelastic" moment component is

$$M_{xx}^c = \frac{1}{f} \left[\frac{\partial^2 w^c}{\partial x^2} + \frac{1}{2} \frac{\partial^2 w^c}{\partial y^2} \right] \frac{h^3}{12} \quad (6)$$

Since the moments are the same, the displacements are clearly related by

$$\frac{\partial^2 w^c}{\partial x^2} = \frac{fE}{(1-\nu^2)} \frac{\partial^2 w^e}{\partial x^2} \quad (7)$$

$$\begin{aligned} D \nabla^4 w^e &= N_{xx}^o \frac{\partial^2 w^e}{\partial x^2} + 2N_{xy}^o \frac{\partial^2 w^e}{\partial x \partial y} + N_{yy}^o \frac{\partial^2 w^e}{\partial y^2} \\ &+ \frac{f E h^3}{12(1-\nu^2)} \left[N_{xx}^o \frac{\partial^2 w^e}{\partial x^2} + 2N_{xy}^o \frac{\partial^2 w^e}{\partial x \partial y} + N_{yy}^o \frac{\partial^2 w^e}{\partial y^2} \right] \quad (9) \end{aligned}$$

$$w^e(x,y,t) = g(t)W(x,y) \quad (10)$$

and obtain

$$\ddot{g} - \lambda^2 g = 0 \quad (11)$$

for the time part and

$$D \nabla^4 W = N_{\alpha\beta}^0 \left(1 + \frac{f F}{12(1-\nu^2)\lambda^2} \right) \frac{\partial^2 W}{\partial x_\alpha \partial x_\beta} \quad (12)$$

Hence one can see that the inelastic material behavior results in buckling very much like the elastic case but with the pseudo in plane forces given by

$$N_{\alpha\beta}^0 \left(1 + \frac{f E}{12(1+\nu^2)} \frac{1}{\lambda^2} \right) \quad (13)$$

The separation parameter λ^2 in Eq (13) reflects how "fast" the lateral deflections grow from some initial value. Clearly the presence of $f(x,y)$ in the numerator of Eq (13) makes simple interpretation impossible for λ^2 except as given in Eq (11).

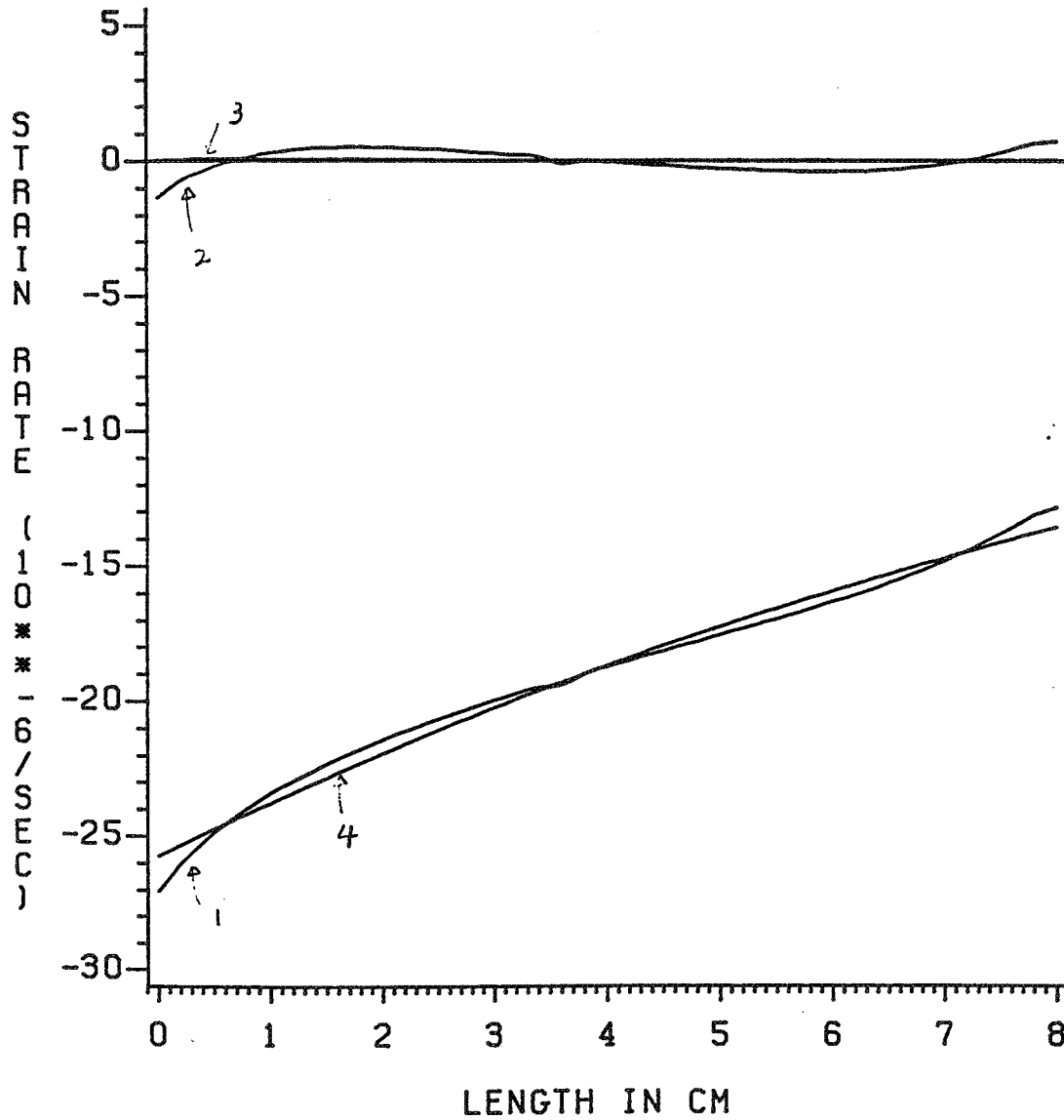
To obtain values for λ^2 , we use a Galerkin method on Eq (12) and find that

$$\lambda^2 = \frac{2 h_{cr}^3 \iint f E^2 \nabla^4 W W \, da}{3(h^3 - h_{cr}^3) \iint E \nabla^4 W W \, da} \quad (14)$$

ADVANCED SILICON SHEET

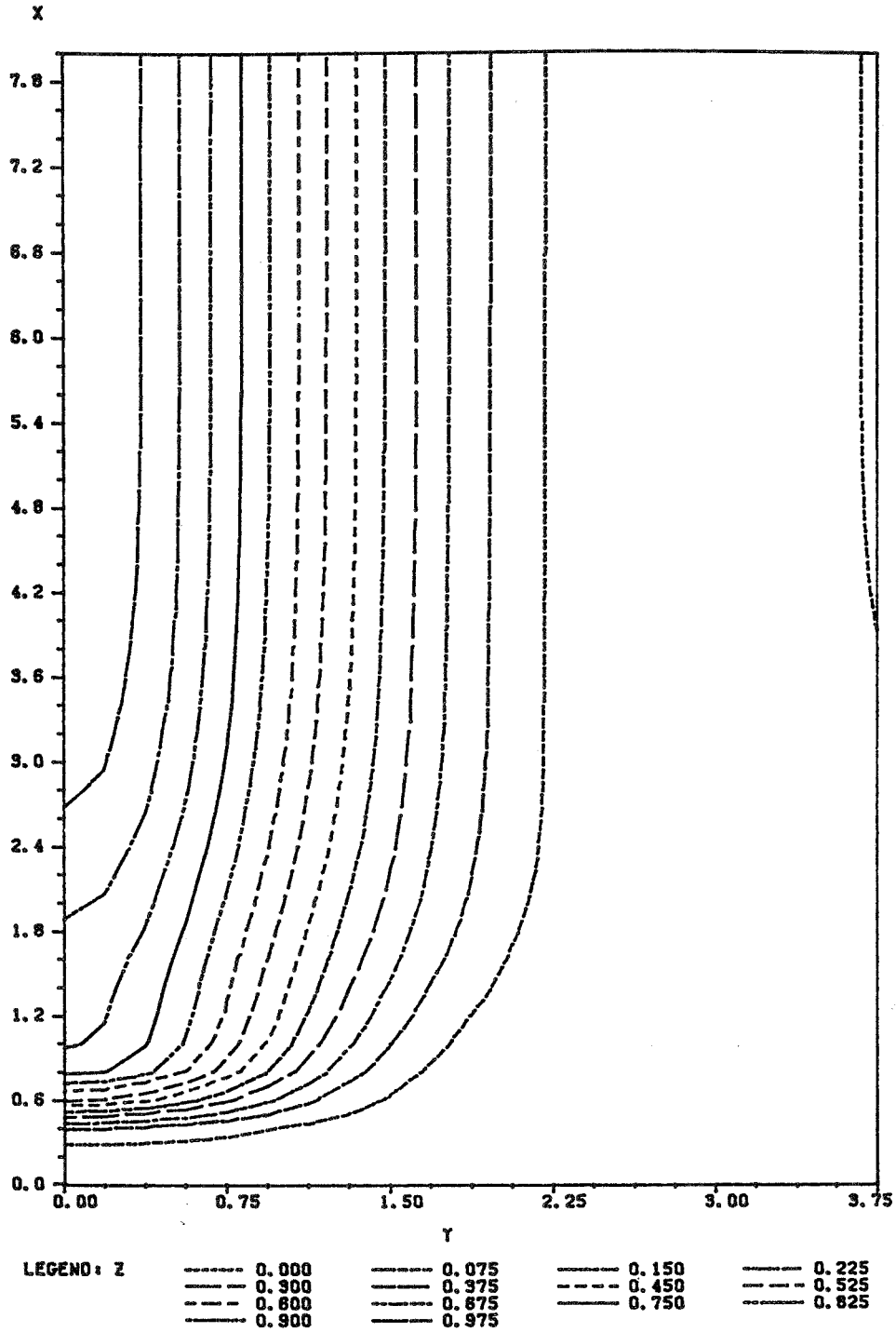
Normal Strain Rate XX Along Y = 0 (Centerline)
for $T = 1440 * \text{Exp}(-0.08X)$ Width = 6.0 CM

LINE 1 IS TOTAL, LINE 2 IS ELASTIC, LINE 3 IS PLASTIC AND LINE 4 IS THERMAL STRAIN RATE



ADVANCED SILICON SHEET

The Dislocation Density Contour Plot
 for $T = 1440 \cdot \text{Exp}(-0.08X)$
 Unit of X and Y = CM, Unit of Z = 10^3 Per CM^2



ADVANCED SILICON SHEET

$$6 \text{ cm} \times 6 \text{ cm}$$

$$T = T_w$$

The results are

N_o/cm^2	$N_f \text{ max} /cm^2$	$\sigma_{yy} \text{ max} \text{ MPa}$	$\sigma_{xx} \text{ max} \text{ MPa}$	$t_2^{cr} \text{ mm}$	$t_2^{cr} \text{ m}$
.3	2497	-22.64	15.23	.1936(c)	.1375(t)
.15	1092	-22.65	15.99	.1965(c)	.1388(t)
.01	266	-23.69	17.1	.1982(c)	.1394(t)

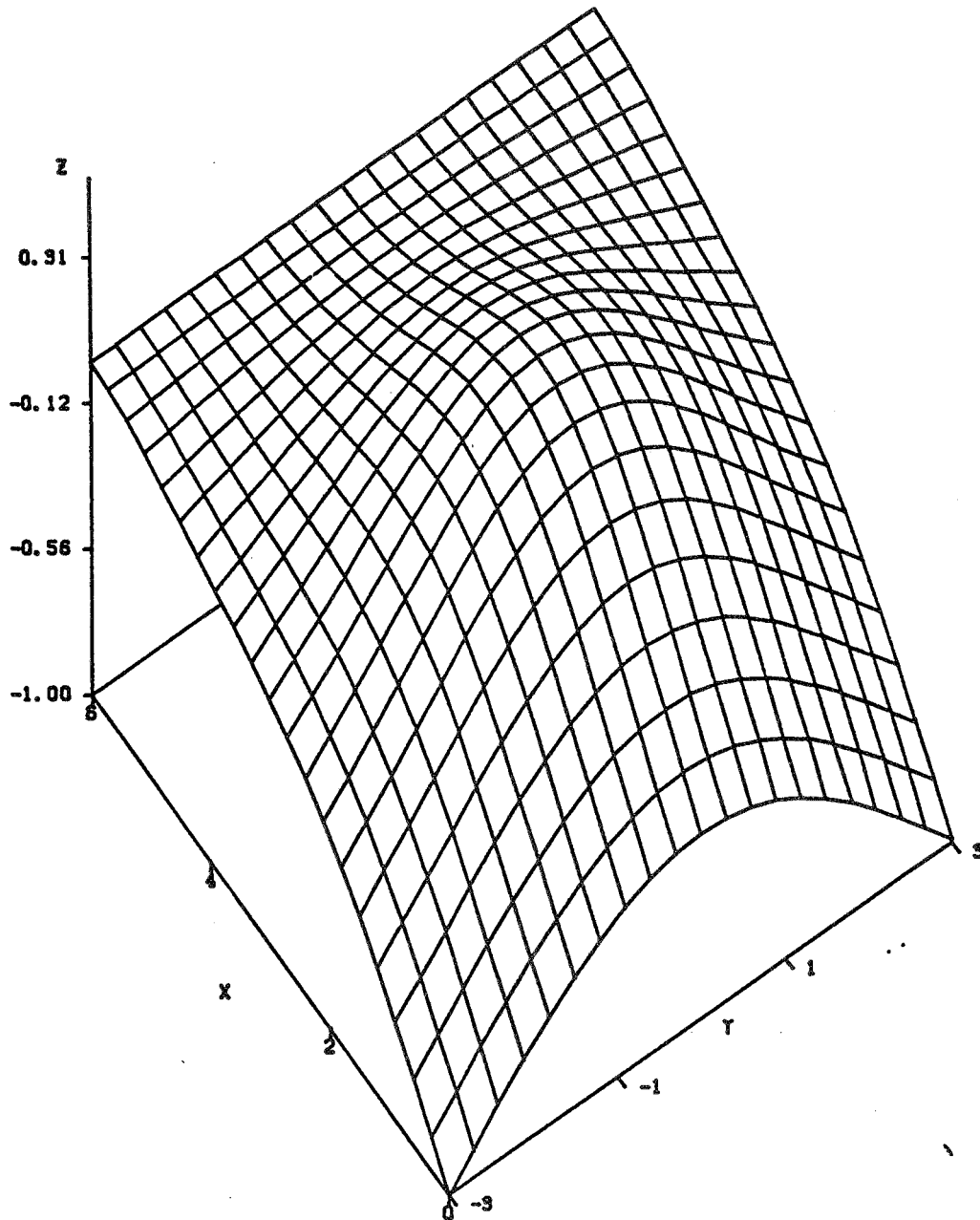
	D>10D	Larger backstress			
.3	1811	-22.64	15.41	.1948(c)	.1381(t)

Table I

C-7

ADVANCED SILICON SHEET

The 20th Elastic Buckling Mode
for Westinghouse Temperature Profile
Critical Thickness = 0, 19817 MM
Unit of X and Y = CM



ADVANCED SILICON SHEET

Mode	hcr (mm)	λ^2 (sec ⁻¹)	
1	.1936	+.06668	critical case
2	.1375	+.01124	
3	.1132	+.00742	
4	.1061	+.00452	
5	.0893	+.00365	
6	.08503	+.00153	
7	.07565	+.00698	
8	.06755	+.00117	
9	.06644	+.006555	
10	.04985	-.0000416	
11	.04086	+.0000832	

$T = T_w$

$N_0 = .3/\text{cm}^2$

6cm x 6cm

ADVANCED SILICON SHEET

Mode	hcr (mm)	λ^2 (sec ⁻¹)	
1	.1965	+.02937	critical case
2	.1388	+.004919	
3	.1099	+.003094	
4	.1074	+.0018414	
5	.09146	+.0016733	
6	.08562	+.000734	
7	.076924	+.001504	
8	.069808	+.000597	
9	.06800	+.000367	
10	.062011	+.006800	

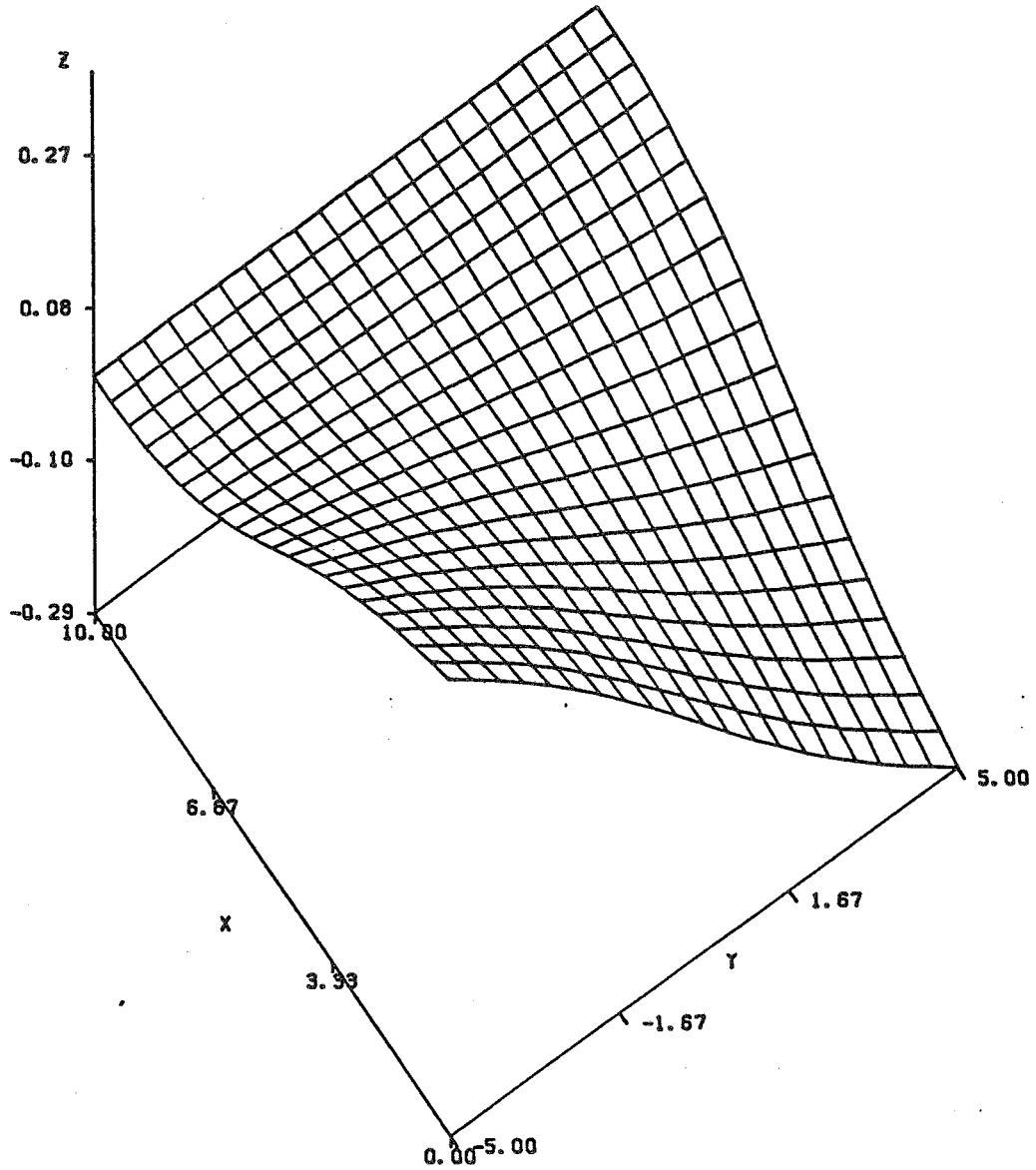
$$T = T_w$$

$$N_0 = .15/\text{cm}^2$$

6cm x 6cm

ADVANCED SILICON SHEET

The First Positive Buckling Mode
for Westinghouse Temperature Profile
Critical Thickness = 0.76154 MM
Unit of X and Y = CM



ADVANCED SILICON SHEET

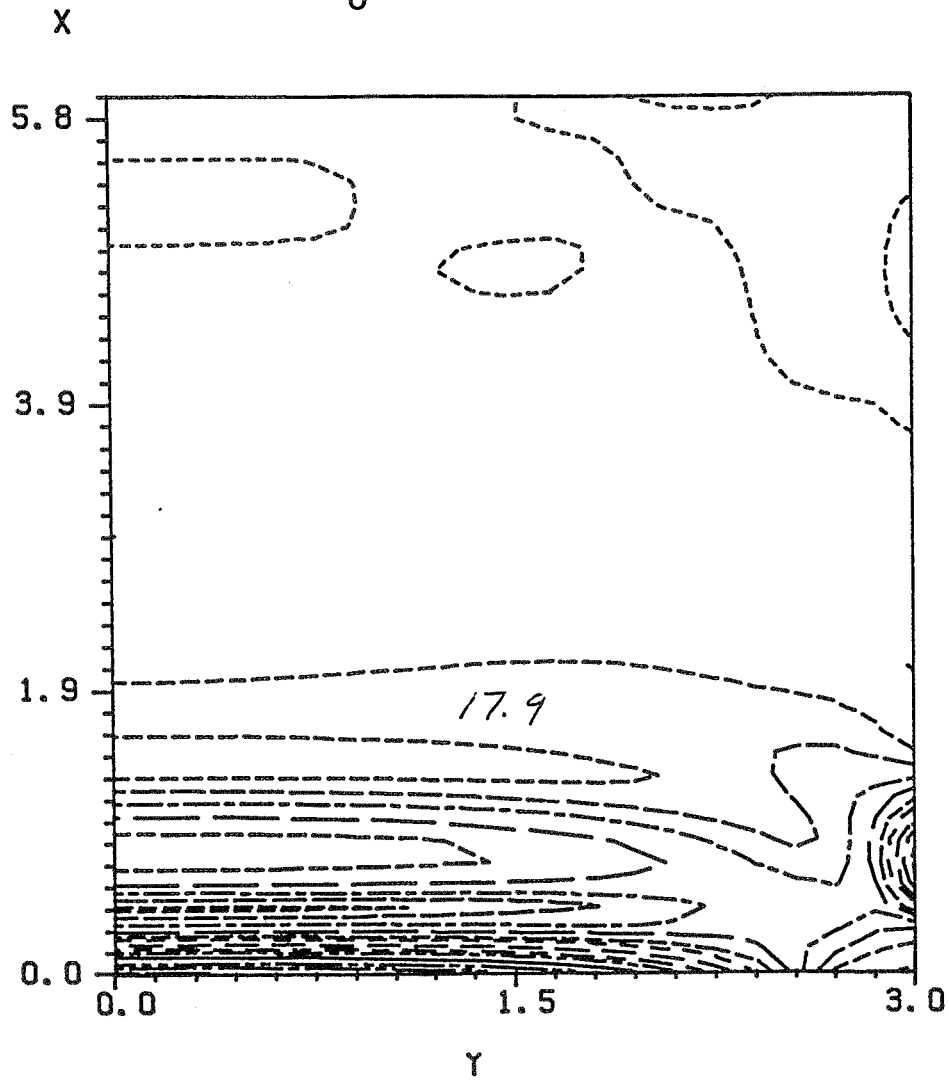
Mode	hcr (mm)	$\lambda^2 \text{sec}^{-1}$	
1	.4204	-1.706×10^{-3}	
2	.3872	-7.164×10^{-3}	
3	.3346	-5.623×10^{-4}	
4	.3080	$+2.8909 \times 10^{-3}$	
5	.2789	$+4.9641 \times 10^{-3}$	critical case
6	.2663	-7.8054×10^{-4}	
7	.2337	$+2.3418 \times 10^{-4}$	
8	.2281	-1.1527×10^{-3}	
9	.2044	-6.0790×10^{-4}	
10	.1974	$+1.2900 \times 10^{-4}$	
11	.1801	-2.0870×10^{-4}	
12	.1724	$+1.0930 \times 10^{-4}$	

T = Modified EFG
 $N_0 = 2 \times 10^{-7} / \text{cm}^2$
 6cm x 6 cm

Run V-0545
 8 June

The Effectiveness Stress Contour Plot
for Modified EFG Profile
Unit of X and Y = CM, Z = MPA

$$N_0 = 2 \times 10^{-7} / \text{cm}^2$$



LEGEND: Z

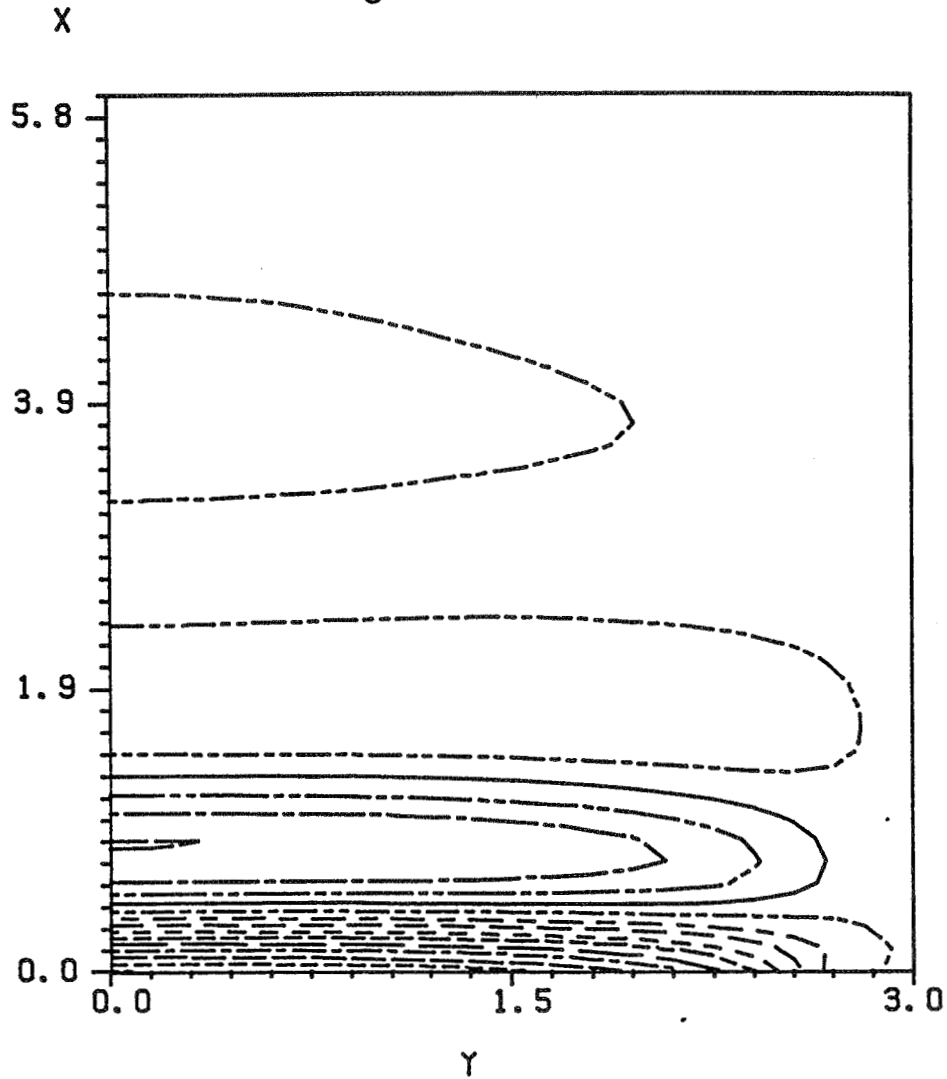
-----	1.5	-----	17.9
-----	34.3	-----	50.7
-----	67.1	-----	83.5
-----	99.9	-----	116.3
-----	132.7	-----	149.1
-----	165.5	-----	181.9
-----	198.3	-----	214.7

ADVANCED SILICON SHEET

The Normal Stress YY Contour Plot
for Modified EFG Profile

Unit of X and Y = CM, Z = MPA

$$N_0 = 2 \times 10^{-7} / \text{cm}^2$$

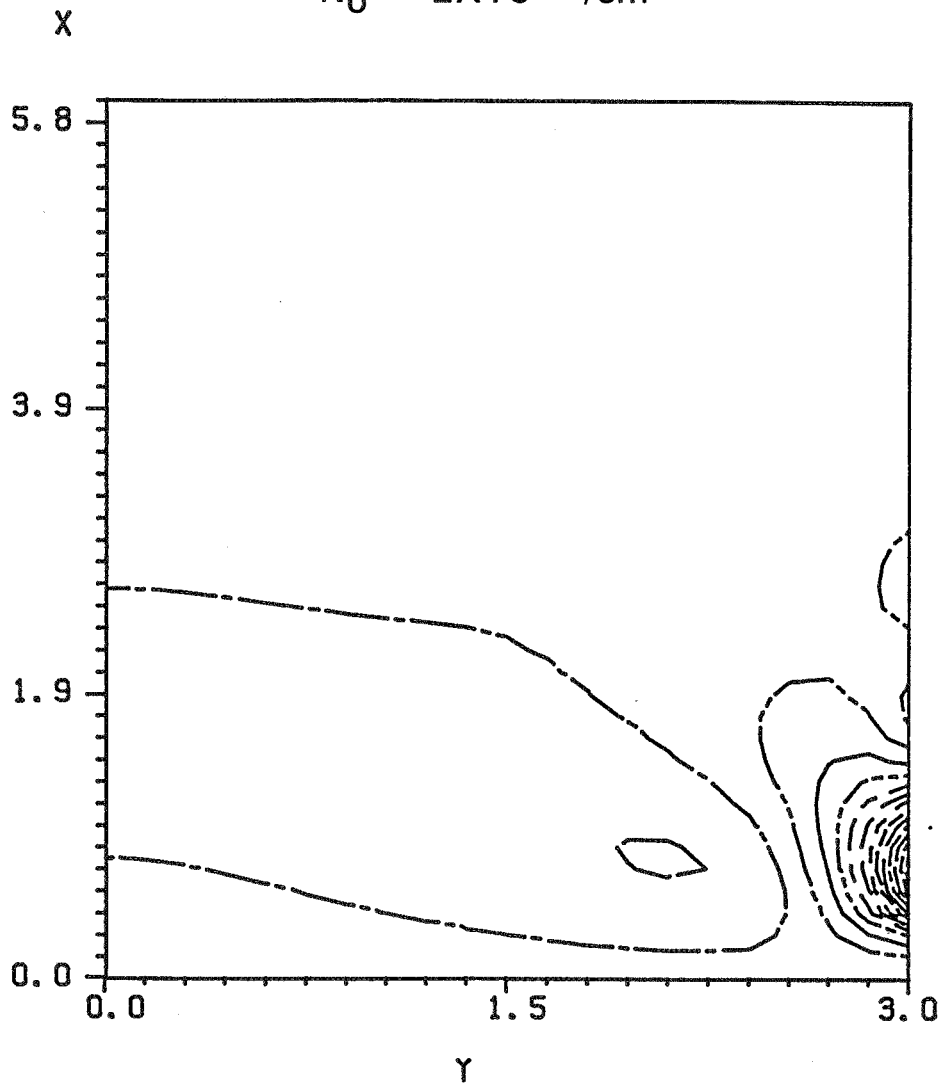


LEGEND: Z

-----	-215.4	-----	-191.8
-----	-168.2	-----	-144.6
-----	-121.0	-----	-97.4
-----	-73.8	-----	-50.2
-----	-26.6	-----	-3.0
-----	20.6	-----	44.2
-----	67.8	-----	91.4

The Normal Stress XX Contour Plot
for Modified EFG Profile
Unit of X and Y = CM, Z = MPA

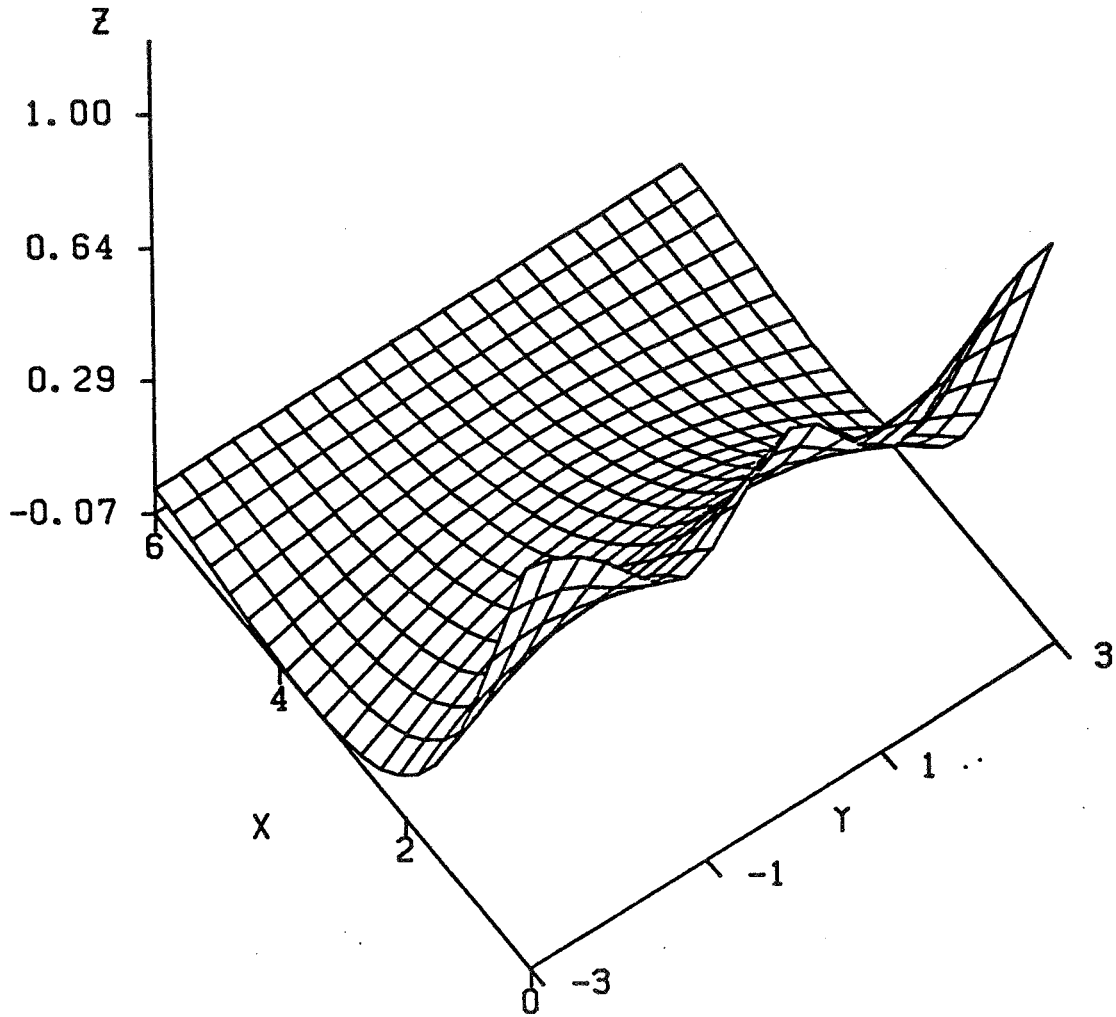
$$N_0 = 2 \times 10^{-7} / \text{cm}^2$$



LEGEND: Z	-----	-150.0	-----	-137.3
	=====	-124.6	-----	-111.9
	=====	-99.2	-----	-86.5
	-----	-73.8	-----	-61.1
	-----	-48.4	-----	-35.7
	=====	-23.0	-----	-10.3
	-----	2.4	=====	15.1

ADVANCED SILICON SHEET

The 13th Buckling Mode
for Modified EFG Profile
Critical Thickness = 0, 027877 MM
Unit of X and Y = CM



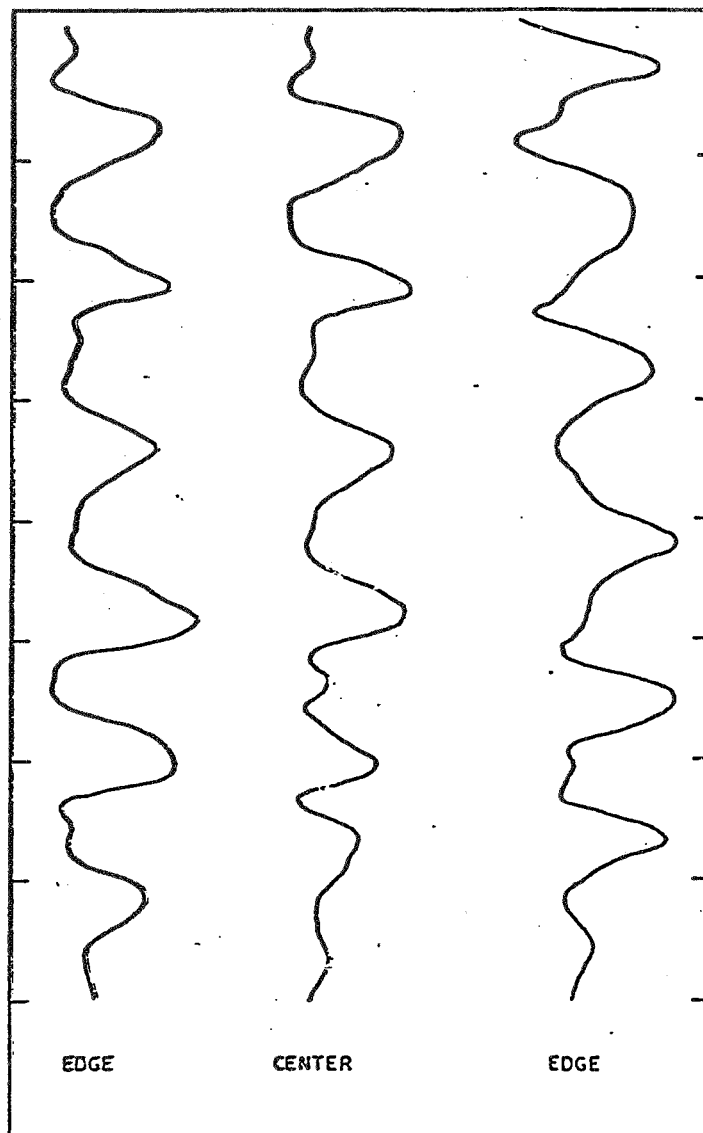


Fig. 1. Surface profile traces illustrating typical edge buckling for ribbon no. 18-102-2 grown at a speed of 3.0 cm/min. Traces are taken along the growth direction, with respect to the width dimension as marked.

MAR 1979

ADVANCED SILICON SHEET

for the case of a 6 cm x 6 cm ribbon pulled at $v_0 = .0005$ m/sec. The results are shown in Table III.

M /cm	N_0 cm/2	N_{f2} /cm ²	N_{fel} /cm ²	$\sigma_{yy_{max}}$ MPa	L_u mm
1.75	.5	Diverge	4.65×10^8	-151.1*	.4698 *
1.0	.3	Diverge	3.175×10^8	-101.7*	
.25	.3	Diverge	$.5941 \times 10^4$	- 17.4*	
.240625	.3	1.06×10^4	$.3137 \times 10^4$	- 17.8	
.2375	.3	1984	$.2527 \times 10^4$	- 16.8	.21364
.225	.3	963	1049	- 15.0	
.200	.3	173	174	- 12.1	.29581

Table III

The * in the last column indicates these are the elastic stresses, because plastic ones are not obtained.

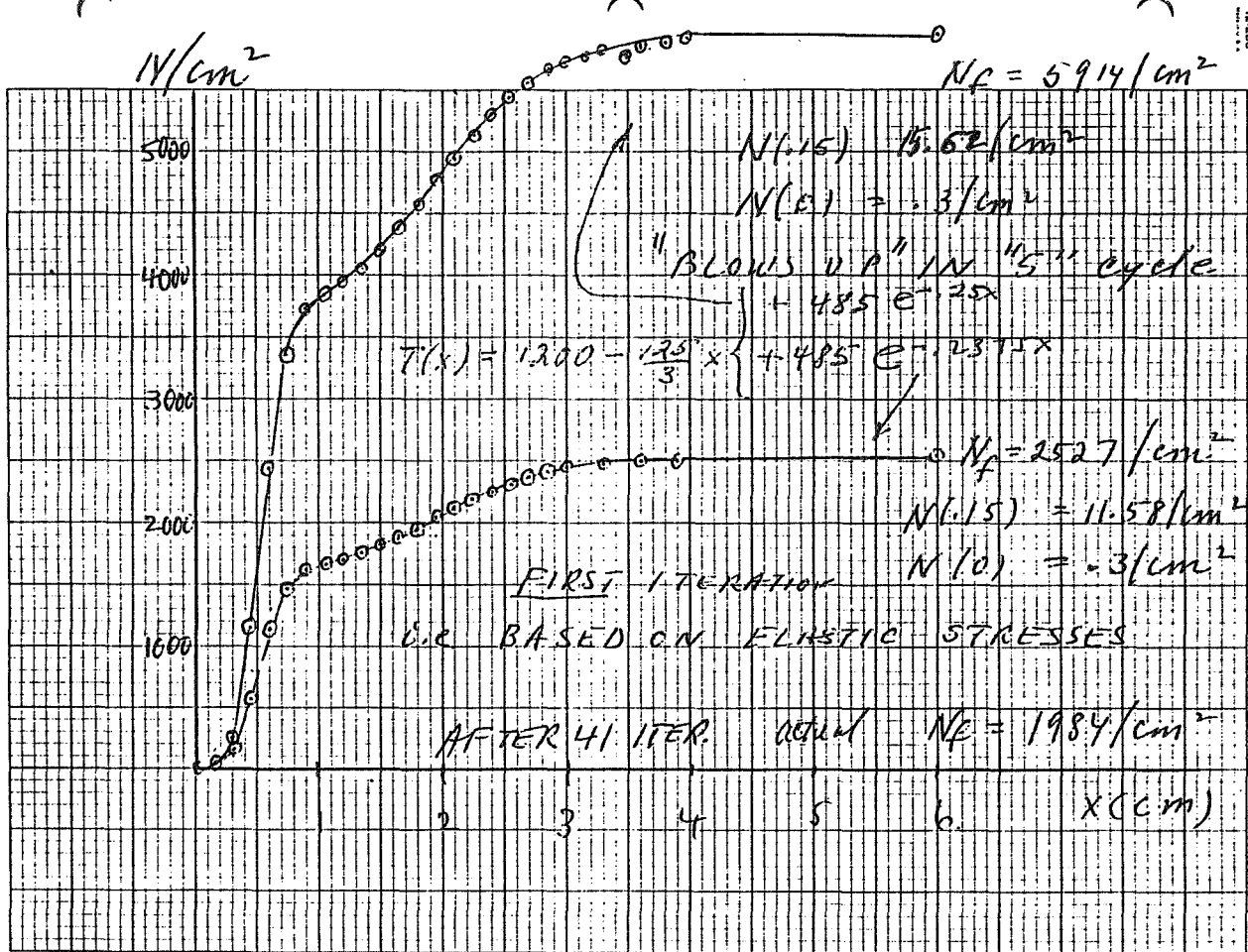
$$T_{NEFG} = 1200 - \frac{125x}{3} + 485e^{-1.75x}$$

This led to divergent solutions under conditions when the Westinghouse profile did not. With this situation in mind we considered the family of thermal profiles, defined by

$$T(x) = 1200 - \frac{125x}{3} + 485 e^{-Mx}$$

ORIGINAL PAGE IS
OF POOR QUALITY

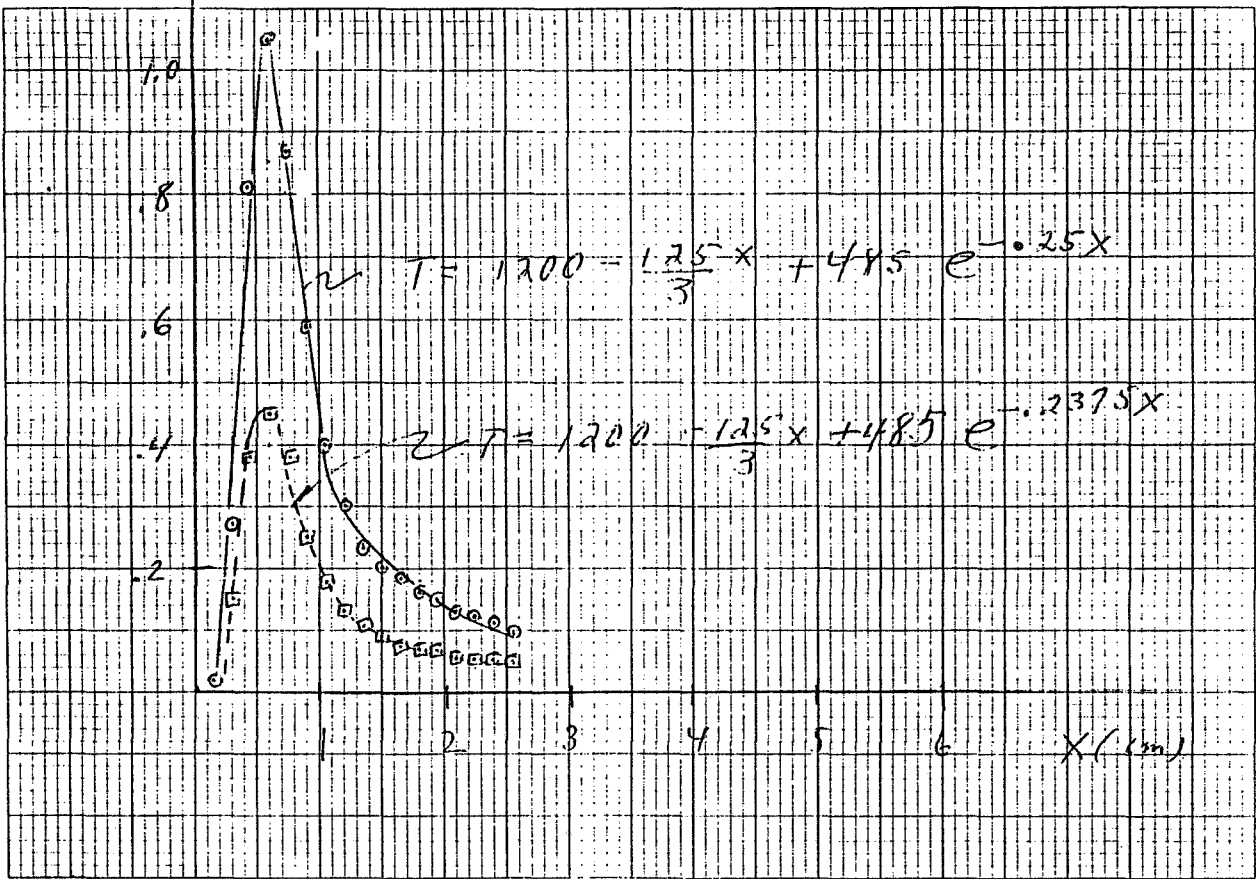
10 Squares to the Inch



$N_0 = 3/cm^2$

10 Squares to the Inch

$\sum_{xx}^{m} \times 10^5$



ADVANCED SILICON SHEET

Really New Science

Dislocations as part of the stress analysis.
That is $N \neq$ constant!

New

Creep buckling (lowest mode does not dominate!)

Practical

Elastic very useful

Plastic - residual stress

$\tau_{cr} \doteq \tau_{cr}$ (elastic)

Keep N small

Very sensitive

(ala melting)

STRESS STUDIES IN EDGE-DEFINED FILM-FED GROWTH OF SILICON RIBBONS

MOBIL SOLAR ENERGY CORP.

J. Kalejs

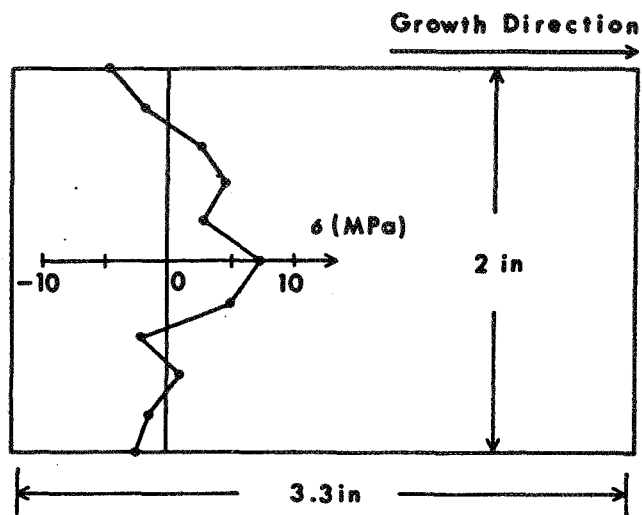
TECHNOLOGY ADVANCED MATERIALS RESEARCH TASK	REPORT DATE JUNE 19, 1985
APPROACH STRESS AND EFFICIENCY STUDIES IN EFG CONTRACTOR MOBIL SOLAR ENERGY CORPORATION, CONTRACT NUMBER 956312	STATUS <ul style="list-style-type: none"> ● HORIZONTAL TEMPERATURE VARIATIONS CAN GIVE STRESS REDUCTIONS, BUT NOT SUFFICIENT TO OVERCOME CREEP LIMITATIONS ON GROWTH SPEED IN VERTICAL MODE. ● QUANTITATIVE HIGH RESOLUTION EBIC ANALYSIS DEVELOPED: <ul style="list-style-type: none"> - EBIC STUDIES DEMONSTRATE POINT DEFECT LIMITATIONS ON DIFFUSION LENGTH IN FZ AND CZ SILICON HEAT TREATED AND STRESSED ABOVE 1200°C AND COOLED RAPIDLY. NO DEPENDENCE ON OXYGEN OR CARBON LEVELS. SIMILAR RESULTS FOR EFG SHEET. ● LOW RESISTIVITY AS-GROWN EFG MATERIAL DIFFUSION LENGTHS IMPROVED BY GALLIUM OVER BORON DOPANT.
GOALS <ul style="list-style-type: none"> ● TO DEFINE MINIMUM STRESS CONFIGURATION FOR SILICON SHEET GROWTH. ● TO QUANTIFY DISLOCATION ELECTRICAL ACTIVITY AND LIMITS ON CELL EFFICIENCY. ● TO STUDY BULK LIFETIME DEGRADATION DUE TO INCREASE IN DOPING LEVELS. 	

Low-Stress EFG Configurations

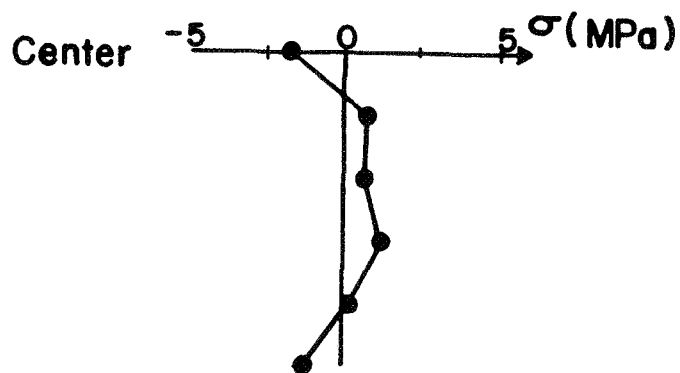
- STRESS, DISLOCATION DENSITIES REDUCED ONLY AT EXPENSE OF GROWTH SPEED CAPACITY:
 - FOR INTERFACE GRADIENTS $\leq 1000^{\circ}\text{C}$, SPEED IS LIMITED TO 1-1.5 CM/MIN.
 - $N_D \leq 1 \times 10^5/\text{cm}^2$, LÜDERS STRAIN OCCURRENCE ELIMINATED, RESIDUAL STRESS IS REDUCED.
- HORIZONTAL GRADIENT MODELING SHOWS SOME PROMISE FOR STRESS MANIPULATION BELOW 1200°C TO 900°C, WHERE CREEP IS STILL SIGNIFICANT, BUT WILL NOT ALLOW SPEED CAPACITY INCREASES.
- INCLINED INTERFACE GROWTH APPEARS TO BE ONLY ALTERNATIVE TO OVERCOME HIGH TEMPERATURE CREEP LIMITATION.

PRECEDING PAGE BLANK NOT FILMED

ADVANCED SILICON SHEET



HIGH STRESS, 2 CM/MIN, $N_D \sim 10^6$ TO 10^7 /CM²



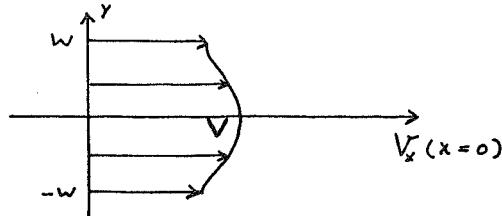
LOW STRESS, 1 CM/MIN, $N_D \leq 1 \times 10^5$ /CM²

New Interpretation of Stress-Strain Effects in High-Speed Sheet Growth (J. W. Hutchinson, Harvard University)

■ NON-THERMAL INELASTIC STRAIN CONTRIBUTES TO INTERFACE VELOCITY NONUNIFORMITY

$$\epsilon_{TOT} = \epsilon^E + \epsilon^I + \epsilon^T$$

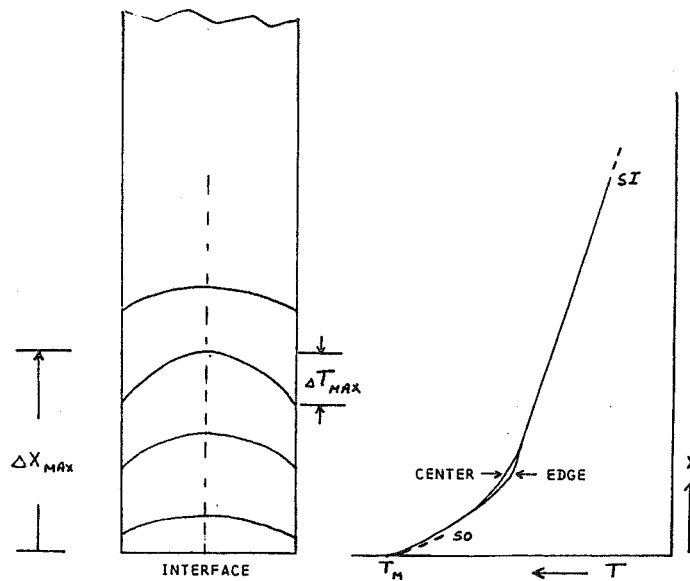
$$\epsilon^I = \underbrace{\epsilon^C}_{\text{CREEP STRAIN}} + \underbrace{\epsilon^M}_{\text{MISFIT STRAIN}}$$



VELOCITY PROFILE ACROSS STRIP AT $x = 0$

■ IMPLICATIONS OF VELOCITY NONUNIFORMITY ON INTERFACE SHAPE, STRUCTURE UNKNOWN.

Stress Analysis with Horizontal Temperature Gradients



■ HIGH CREEP CONDITION, $v = 3$ CM/MIN, WIDTH OF 5 CM.

■ PARABOLIC HORIZONTAL PROFILE:

- HORIZONTAL INTERFACE PROFILE.
- PEAK DIFFERENCE ΔT_{MAX} OCCURS AT DISTANCE ΔX_{MAX} FROM INTERFACE.

ADVANCED SILICON SHEET

Maximum Residual (Room Temperature) Stress (MPa) for Horizontal Temperature Field Variations

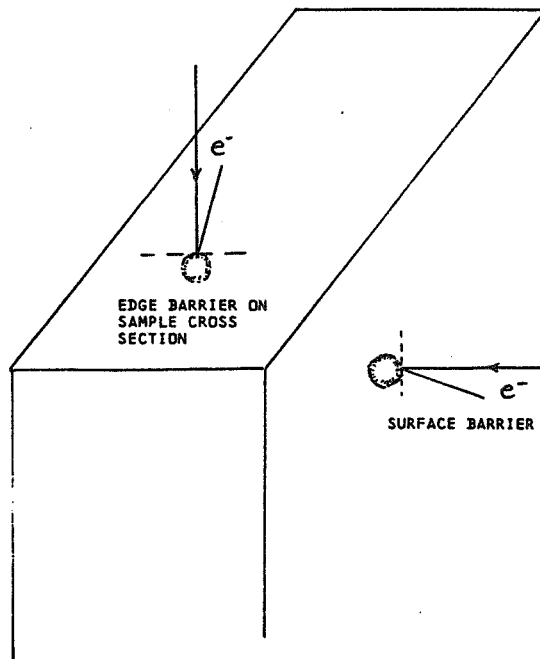
A) $S_0 = 500^{\circ}\text{C}/\text{cm}$, $S_1 = 60^{\circ}\text{C}/\text{cm}$

ΔX_{MAX} (CM)	ΔT_{MAX}				
	0	50	100	150	200
0.5	67.0	63.0			
1.0	67.0	62.8	59.9		
2.0	67.0	69.6	77.4	85.6	84.0
3.0	67.0	68.8	74.5		

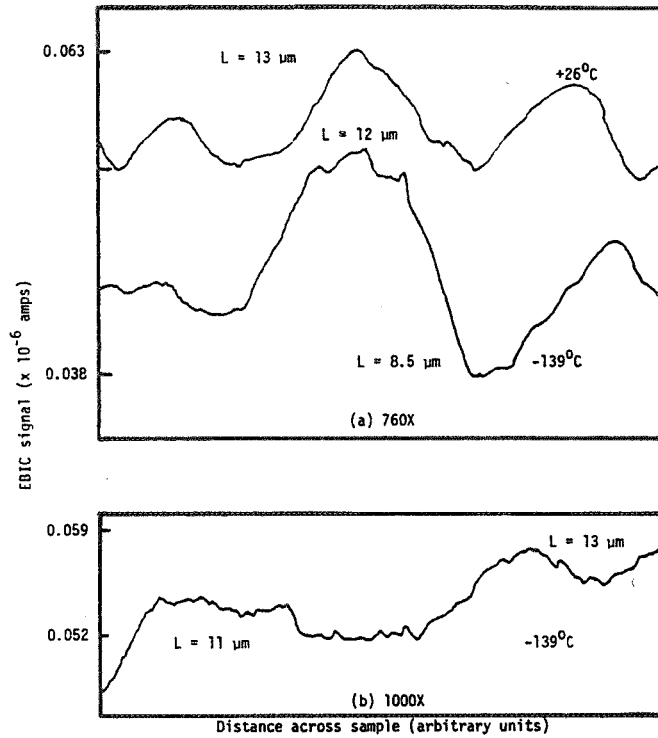
B) $S_0 = 1250^{\circ}\text{C}/\text{cm}$, $S_1 = 40^{\circ}\text{C}/\text{cm}$

ΔX_{MAX} (CM)	ΔT_{MAX}				
	0	50	100	200	300
0.5	474	486	501		
1.0	474	472	470		
2.0	474	460	446		
3.0	474	459	444	415	387
5.0	474	463	453	433	414

EBIC Measurement Configurations



- ⊗ DESIRE HIGH RESOLUTION ON L MEASUREMENT.
- ⊙ RELATE SAMPLE INHOMOGENEITIES IN L TO BULK L (LARGE AREA MEASUREMENT).



High magnification EBIC line scans in stressed carbon-rich (111) C2 silicon.

High-Resolution EBIC Results

- LARGE DIFFERENCES FOUND BETWEEN SURFACE AND EDGE CROSS SECTION MEASUREMENTS OF DIFFUSION LENGTH BY EBIC.
- DIFFERENCE ATTRIBUTED TO ABILITY TO RESOLVE DIFFUSION LENGTH INHOMOGENEITIES IN NEAR-SURFACE REGIONS OF STRESSED SAMPLES AT $\geq 500X$.
- CAUTION MUST BE EXERCISED IN INTERPRETATION OF EDGE CROSS SECTION EBIC MEASUREMENTS DUE TO GEOMETRICAL EFFECTS IN ADDITION TO MATERIAL INHOMOGENEITIES.

ADVANCED SILICON SHEET

EBIC Characterization

● SCOPE OF THE PRESENT STUDY:

- CZ SILICON OF VARIOUS CARBON LEVELS AND FZ SILICON STRESSED ABOVE 1200°C, AND EFG SHEET.

- CRYSTAL GROWTH FURNACE 17 AND SEALED, EVACUATED QUARTZ AMPOULE ANNEALS.

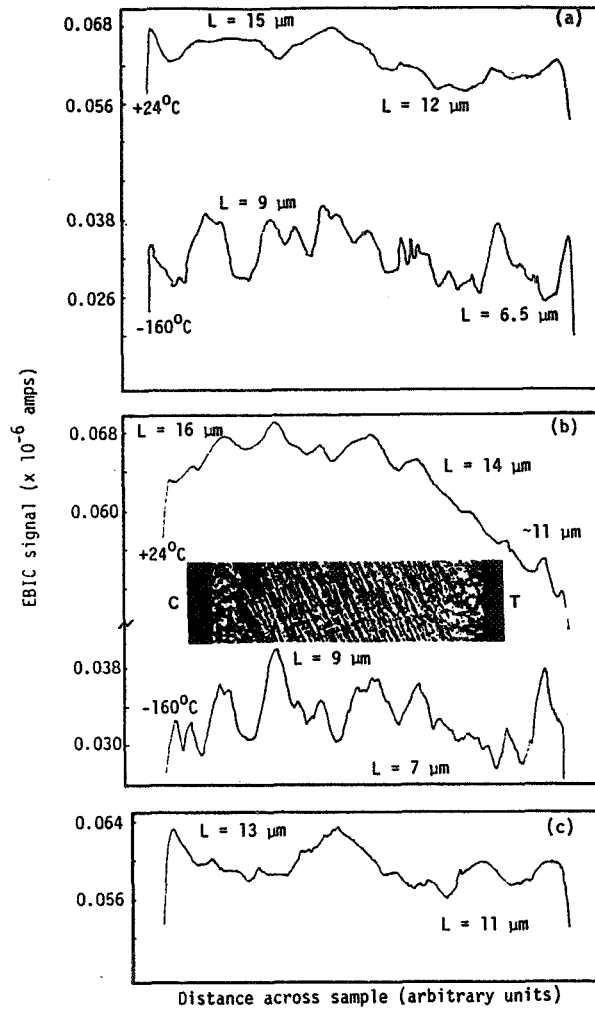
● DISLOCATION DENSITY DEPENDENCE OF L WITH N_D UP TO $\sim 1 \times 10^7/\text{cm}^2$.

- EFFECT OF POST-DEFORMATION ONE-HOUR ANNEALS AT 575°C AND 850°C.

FZ and Cz Silicon Wafer Description for Samples Stressed at 1370°C in Four-Point Bending

Sample	O_i (cm^{-3})	C_s (cm^{-3})	N_D (As-Grown) (cm^{-2})	Stress (MPa)	N_D^C (cm^{-2})	N_D^E (cm^{-2})
(111) FZ (#15)	$<10^{16}$	$<10^{16}$	0	8	1×10^6	$<10^4$
(111) FZ (#17)	$<10^{16}$	$<10^{16}$	0	14	1×10^7	5×10^4
(100) CZ (#25)	$\sim 10^{18}$	$<10^{16}$	0	14	$\sim 10^7$	$<5 \times 10^4$
(111) CZ (#9)	$\sim 10^{18}$	4×10^{17}	$\sim 10^4$	7	$\sim 10^6$	2×10^4

ADVANCED SILICON SHEET



EBIC line scans for stressed FZ silicon sample #17C in central high dislocation density ($\sim 1 \times 10^7/\text{cm}^2$) region: (a) after four-point bending at 1370°C; (b) after one-hour anneal at 575°C; (c) after one-hour anneal at 850°C.

Observations

- ANNEALS ABOVE 1200°C IN EVACUATED QUARTZ AMPOULE IN QUARTZ TUBE FURNACE AND CRYSTAL GROWTH FURNACE HAVE SIMILAR EFFECTS IN DEGRADING L.
- L IS 15-25 MICRONS IN DISLOCATION-FREE REGIONS; DISLOCATIONS UP TO $\sim 1 \times 10^7/\text{cm}^2$ DEGRADE IT TO 10-15 MICRONS.
- SUBSEQUENT ONE-HOUR ANNEALS AT 575°C AND 850°C RAISE L BY FACTOR OF TWO AT BEST (MUCH BELOW STARTING L ~ 150 MICRONS).
- L VALUES ARE INDEPENDENT OF OXYGEN AND CARBON CONCENTRATIONS, AND SIMILAR TO EFG AS-GROWN MATERIAL.

Conclusions

- L IS POINT DEFECT LIMITED TO RANGE OF ABOUT 20 MICRONS AND IS FIXED BY COOLING RATE FROM HIGH TEMPERATURES.
- IN-DIFFUSION OF SLOW DIFFUSING IMPURITIES RULED OUT -- NO GRADIENTS.
- IF IN-DIFFUSION BY IRON OCCURS, DISLOCATIONS, CARBON AND OXYGEN DO NOT PRODUCE SIGNIFICANT GETTERING WITH ANNEALING FOR ONE HOUR AT 575⁰C AND 850⁰C.

Comparison of Boron and Gallium-Doped EFG Material As-Grown Quality as a Function of Resistivity

<u>RESISTIVITY (OHM-CM)</u>	<u>DOPANT TYPE</u>	<u>SPV L (MICRONS)</u>
UNDOPED (> 15)		40-60
5	BORON	38
	GALLIUM	70
1	BORON	40
	GALLIUM	55
0.2	BORON	27
	GALLIUM	45

Future Work

- EBIC STUDIES OF FZ SILICON STRESSED AT 600-1000°C, COOLED UNDER LOAD
 - SUGGESTION IS THAT DISLOCATION ELECTRICAL ACTIVITY MAY DIFFER WHEN COOLED WITH AND WITHOUT STRESS.
 - USE INFORMATION TO HELP IDENTIFY TEMPERATURE OF GENERATION OF DISLOCATIONS IN EFG SHEET-STRESS CONDITIONS.
 - PHOSPHORUS GETTERING (900°C) RESPONSE.
- CONTINUED CHARACTERIZATION AND COMPARISON OF LOW RESISTIVITY BORON AND GALLIUM DOPANT EFFECTS.
- MODELING OF HORIZONTAL TEMPERATURE PROFILES IN SHEET GROWTH.
- EXAMINATION OF FEASIBILITY OF INCLINED INTERFACE EFG FOR STRESS REDUCTION.

**ANALYSIS OF HIGH-SPEED GROWTH OF SILICON SHEET
IN INCLINED-MENISCUS CONFIGURATION**

MASSACHUSETTS INSTITUTE OF TECHNOLOGY

P. D. Thomas

R. A. Brown

Goals

USE TWO-DIMENSIONAL THERMAL-CAPILLARY MODEL
TO IDENTIFY RATE AND PROCESSING LIMITS FOR
GROWTH OF THIN SILICON SHEETS.

RESULTS FOR VERTICAL AND INCLINED DIE-DEFINED
GROWTH SYSTEMS

PRECEDING PAGE BLANK NOT FILMED

Important Results

1. MAXIMUM GROWTH RATE IN VERTICAL SYSTEM IS SET BY THERMAL-CAPILLARY LIMIT BEYOND WHICH STEADY GROWTH IS IMPOSSIBLE
 - LIMITS GROWTH RATE IN DIE-DEFINED SYSTEMS (EFG)
 - OF SECONDARY IMPORTANCE IN FREE-MENISCUS GEOMETRIES (DENDRITIC WEB, EDGE-SUPPORTED)

2. VERTICAL GROWTH IS QUALITATIVELY MODELLED BY ONE-DIMENSIONAL HEAT TRANSFER
 - LATERALLY UNIFORM TEMPERATURE
ALMOST FLAT MELT/CRYSTAL INTERFACE

3. ONE-DIMENSIONAL MODEL IS VALID FOR A WIDE RANGE OF AMBIENT CONDITIONS

4. THERMAL-CAPILLARY LIMITS EXIST FOR INCLINED GROWTH SYSTEMS

Thermal-Capillary Model, Heat Transfer

$L^* = 0.025 \text{ cm}, T^* = 1683^\circ\text{K}$

CONDUCTION DOMINATED

$K_1 \nabla^2 T = 0 \quad (\text{MELT})$

$K_2 \nabla^2 T - \rho E (\underline{V} \cdot \nabla T) = 0 \quad (\text{CRYSTAL})$

BOUNDARY CONDITIONS

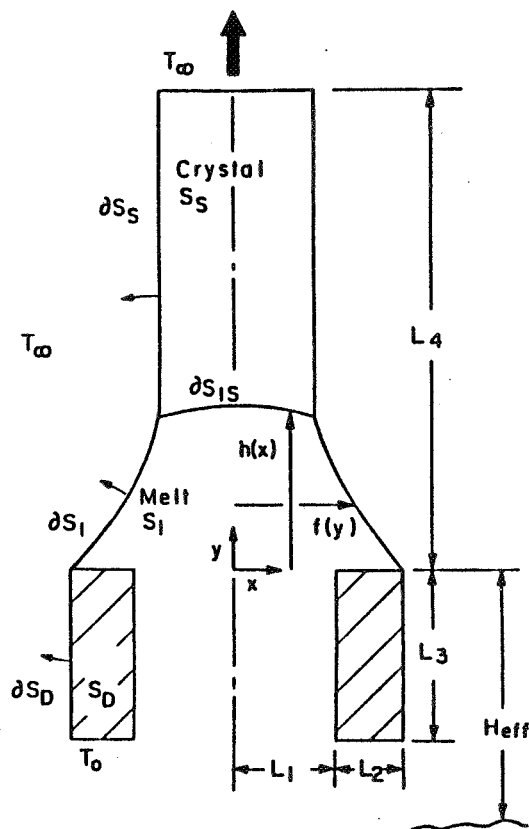
$-\underline{N} \cdot \underline{K} \nabla T = Bi(T - T_A) + R(T^4 - T_A^4)$

$T|_{y=-L_3} = T_0$

$T|_{y=h(x)} = 1.0$

$T|_{y=\infty} = T_\infty$

$\underline{N} \cdot \underline{K}_2 \nabla T - \underline{N} \cdot \underline{K}_1 \nabla T = \rho E \underline{S} T (\underline{N} \cdot \underline{V})|_{y=h(x)}$



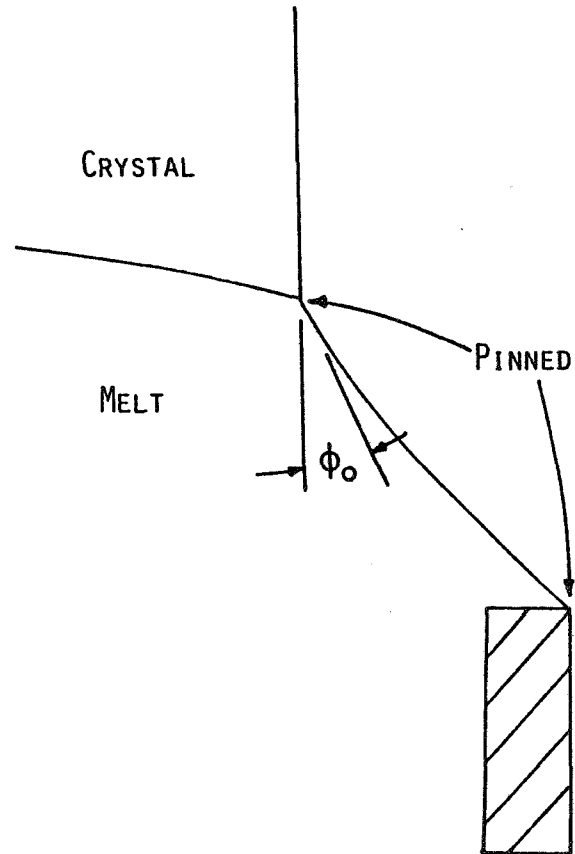
Thermal-Capillary Model, Capillarity

MENISCI

$$2\mathcal{H} = Bo(\gamma + H_{EFF})$$

BOUNDARY CONDITIONS

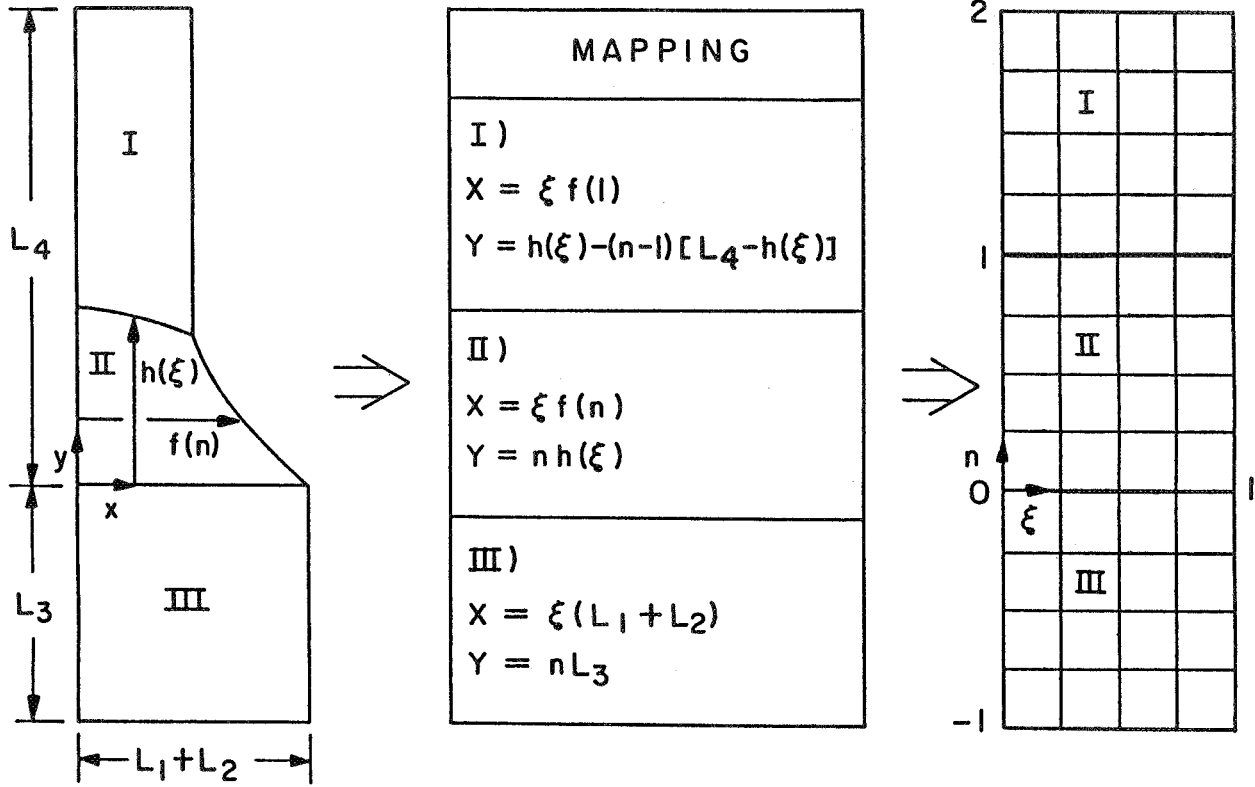
- PINNED AT DIE
- PINNED AT CRYSTAL
- STEADY STATE ANGLE, $\phi_0 = 11^\circ$
USED TO DETERMINE THE
CRYSTAL THICKNESS



Characteristics of Isotherm/Newton Method

- GALERKIN/FINITE-ELEMENT APPROXIMATIONS TO
 - TEMPERATURE FIELD IN EACH PHASE
 - MELT/CRYSTAL INTERFACE SHAPE
 - MELT/GAS MENISCI
- SIMULTANEOUS CONVERGENCE IN ALL VARIABLES

Mapping from Real Coordinates to a Unit Domain



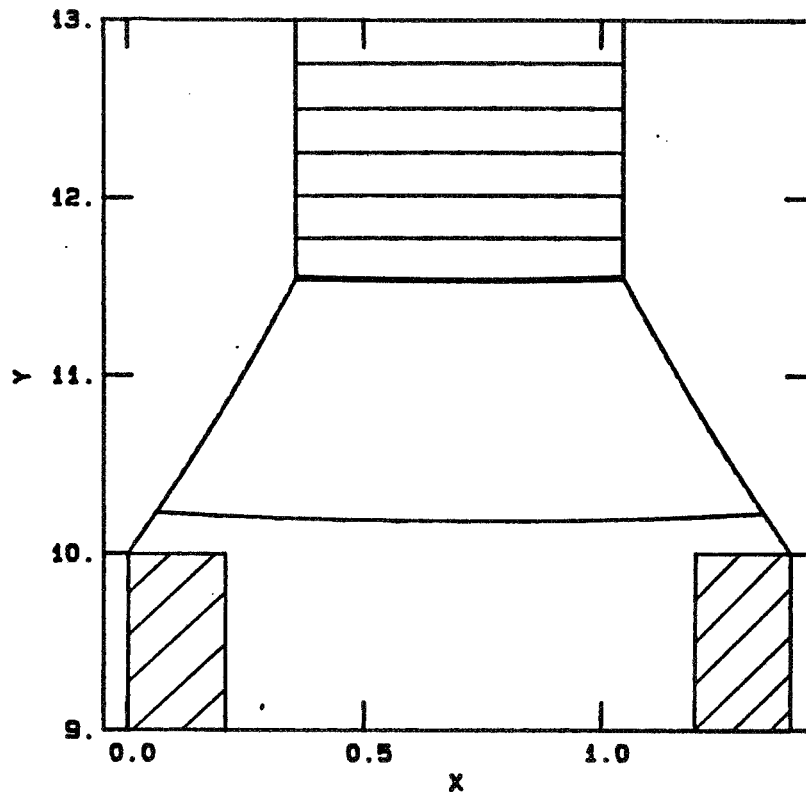
ADVANCED SILICON SHEET

Sample Result for Die-Defined System

$V = 1.5 \text{ cm/MIN}$

UNIFORM AMBIENT, $T_{\infty} = 0.2 \text{ (340}^{\circ}\text{K)}$

ISOTHERMS 5° APART



- UNIFORM ISOTHERMS POINT TO 1D TEMPERATURE FIELD

ADVANCED SILICON SHEET

One-dimensional model is based on:

- LATERALLY AVERAGED TEMPERATURE

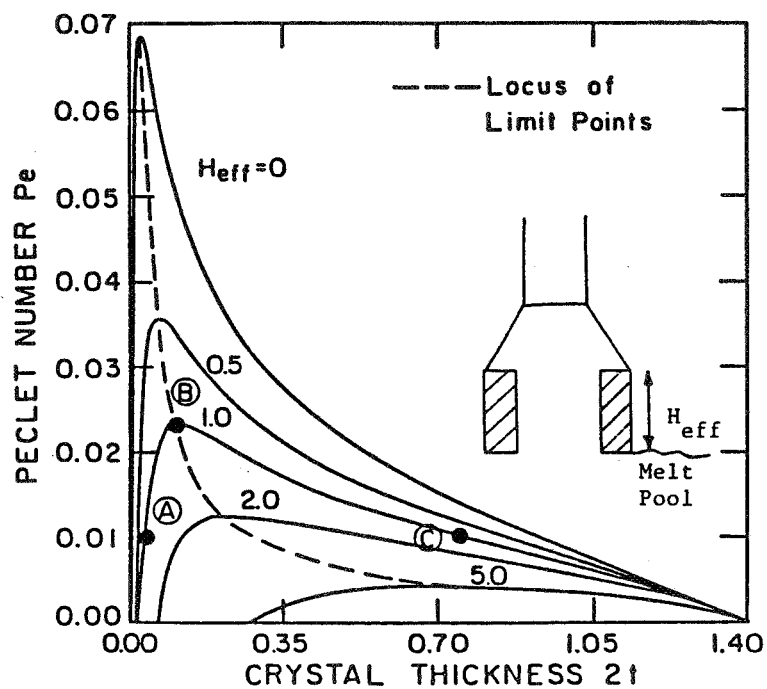
$$\hat{T}(Y) = T(X, Y) \quad \text{AT } X = \dagger$$

- CONDUCTION DOMINATES OVER RADIATION

$$\frac{H \dagger}{K} \ll 1$$

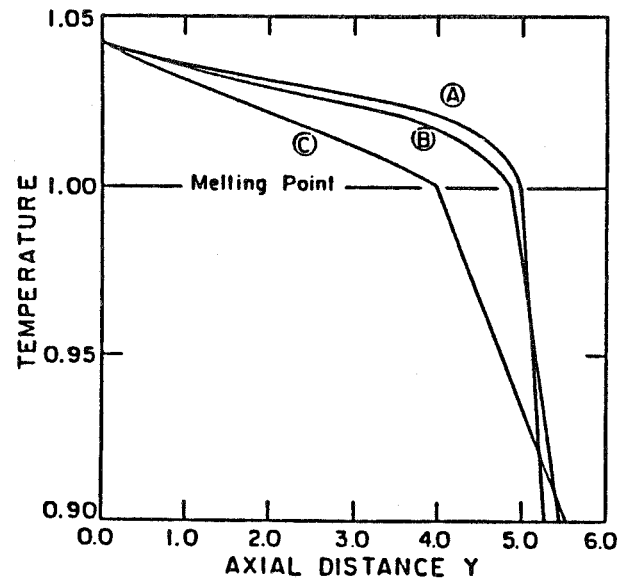
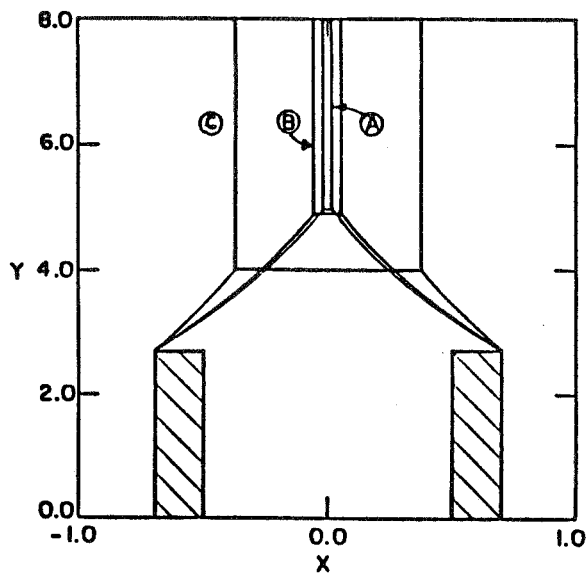
H = EFFECTIVE HEAT TRANSFER COEFFICIENT

Maximum Growth Rate in Die-Defined System is Determined by Limit Points

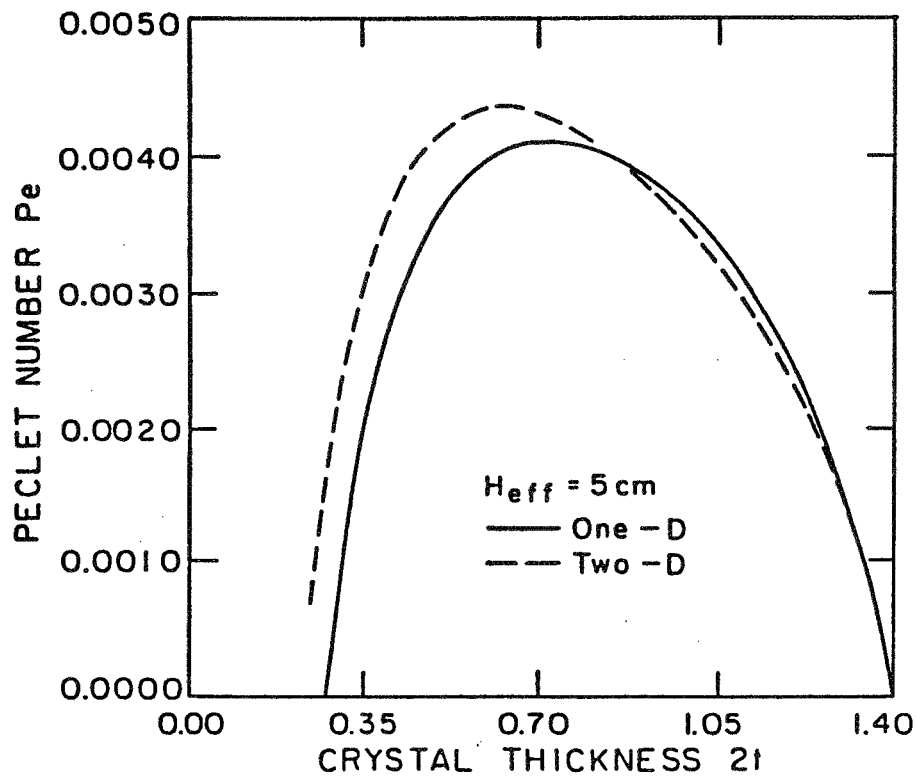


ADVANCED SILICON SHEET

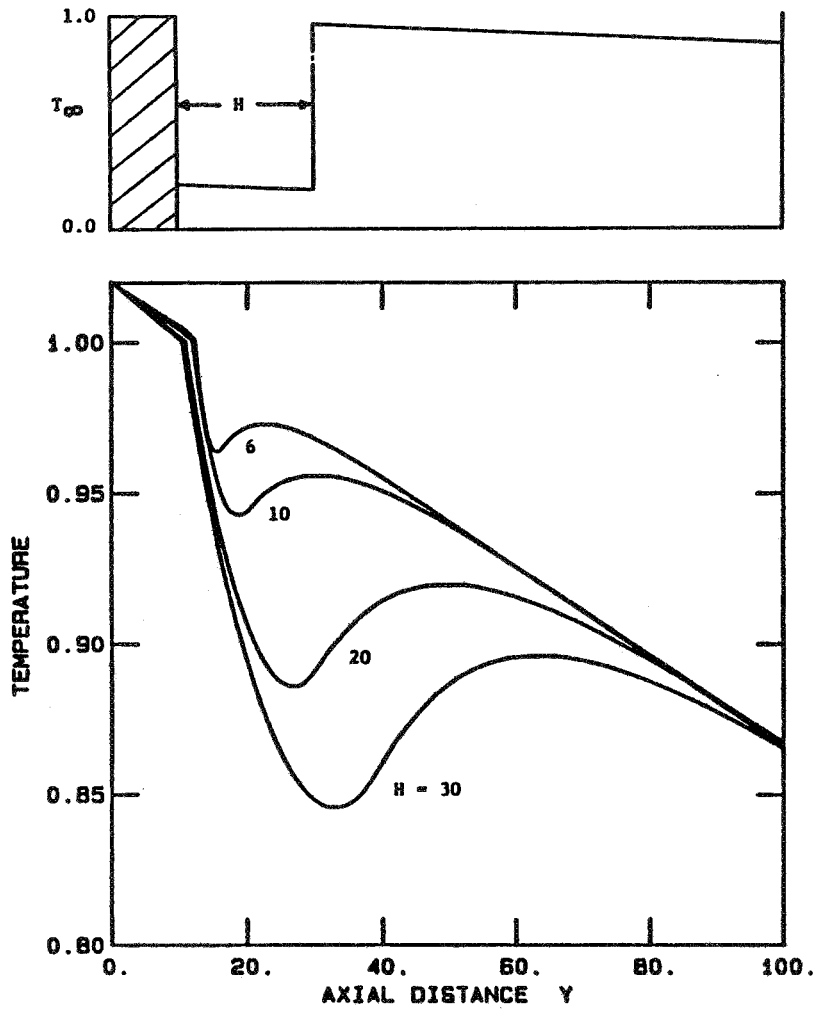
At the Limit Point, the Sensible Heat Cannot be Funneled Quickly Enough from the Melt into the Crystal



Results of One- and Two-Dimensional Models are Qualitatively Similar

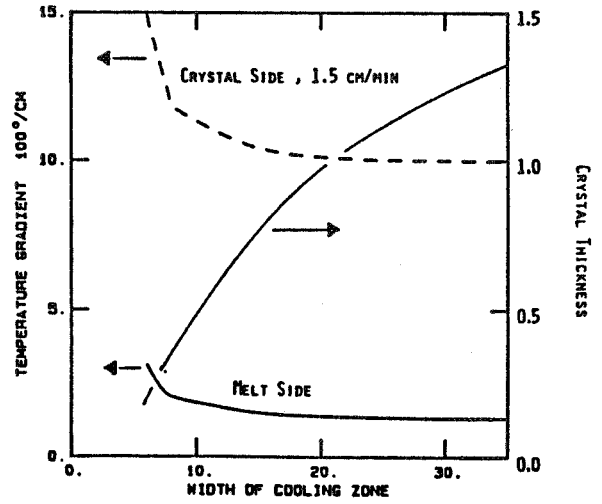
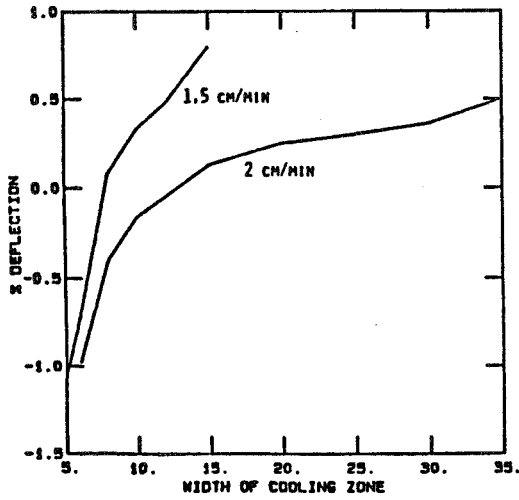


How Important is the Ambient Temperature Profile?



ADVANCED SILICON SHEET

Deflection of Mel/Crystal Interface is Small
(Temperature Gradient Almost Constant Except at Small Thicknesses)

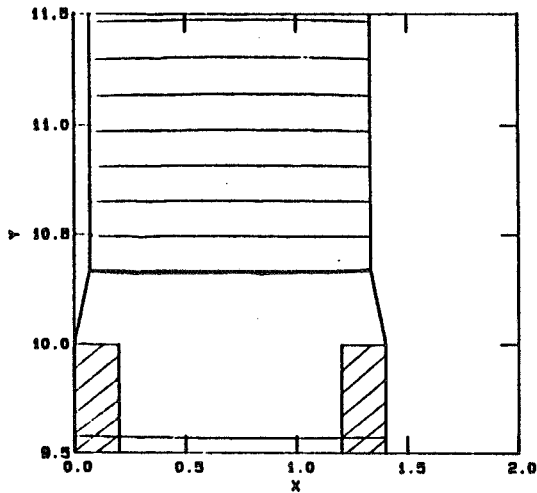


Inclined Growth for Uniform Ambient

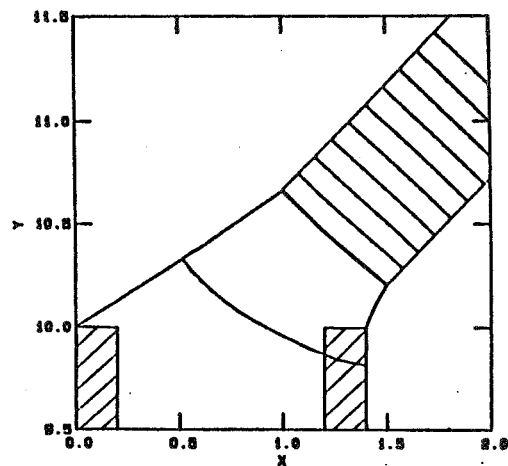
$T = 5^{\circ}\text{K}$ FOR ISOTHERMS

$V = 1.5$ CM/MIN

- ISOTHERMS ARE PERPENDICULAR TO DIRECTION OF GROWTH

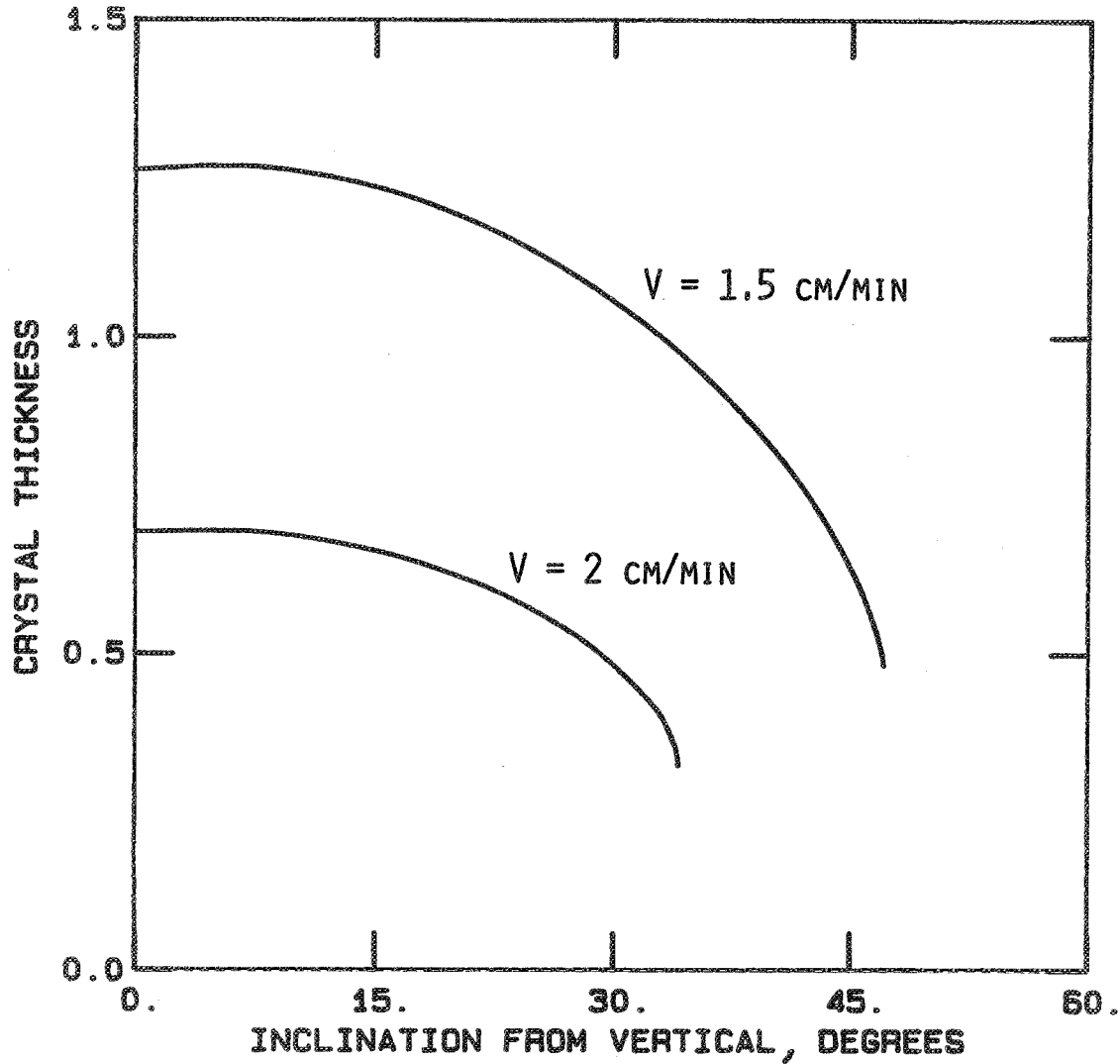


$\theta = 0^{\circ}$



$\theta = 45^{\circ}$

Effect of Inclination on the Crystal Thickness



Summary

- MAXIMUM GROWTH RATE IN VERTICAL AND INCLINED SYSTEMS IS SET BY THERMAL-CAPILLARY LIMITS
- MELT/CRYSTAL INTERFACE IS FLAT
- VERTICAL GROWTH IS QUALITATIVELY MODELLED BY ONE-DIMENSIONAL HEAT TRANSFER

HIGH-PURITY SILICON CRYSTAL GROWTH INVESTIGATIONS

SOLAR ENERGY RESEARCH INSTITUTE

T. F. Cizek
J. L. Hurd
T. Schuyler

Goals

- A. OPTIMIZE DOPANTS AND MINORITY CARRIER LIFETIME IN FZ MATERIAL
- B. IMPROVE THE CONTROL OF LIFETIME DEGRADATION MECHANISMS
(IMPURITIES, THERMAL HISTORY, POINT DEFECTS, SURFACE EFFECTS)
- C. CHARACTERIZE LIFETIME-RELATED CRYSTALLOGRAPHIC DEFECTS
(VIA X-RAY TOPOGRAPHY AND OTHER METHODS)

Recent Emphasis

- A. INSTALLATION OF RESIDUAL GAS ANALYSIS (RGA) ON FLOAT-ZONING FURNACE
- B. IMPLEMENTATION OF MINORITY CARRIER LIFETIME MEASUREMENTS
- C. DEVELOPMENT OF POINT DEFECT DECORATION PROCEDURES
- D. X-RAY TOPOGRAPHY AND EBIC CHARACTERIZATION OF WEB AND FZ CRYSTALS
- E. CALCULATIONS FOR PURIFICATION BY BOTH EVAPORATION AND SEGREGATION
- F. INVESTIGATION OF THE DEPENDENCE OF LIFETIME ON CRYSTAL COOLING RATE
(BOTH DISLOCATED AND DISLOCATION-FREE CRYSTALS)
- G. GROWTH OF P-TYPE, HEAVILY Ga-DOPED CRYSTALS WITH HIGH LIFETIMES

PRECEDING PAGE BLANK NOT FILMED

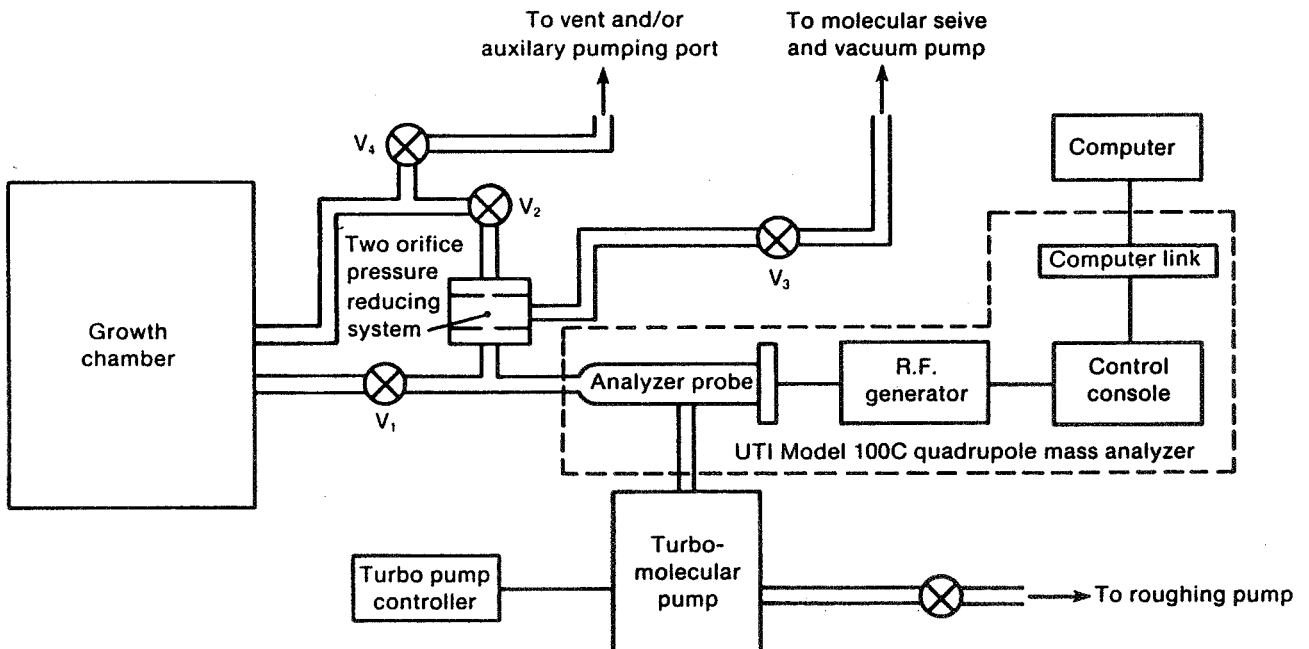
Current Potential Uses of RGA in High-Purity Silicon Growth

Qualitative:

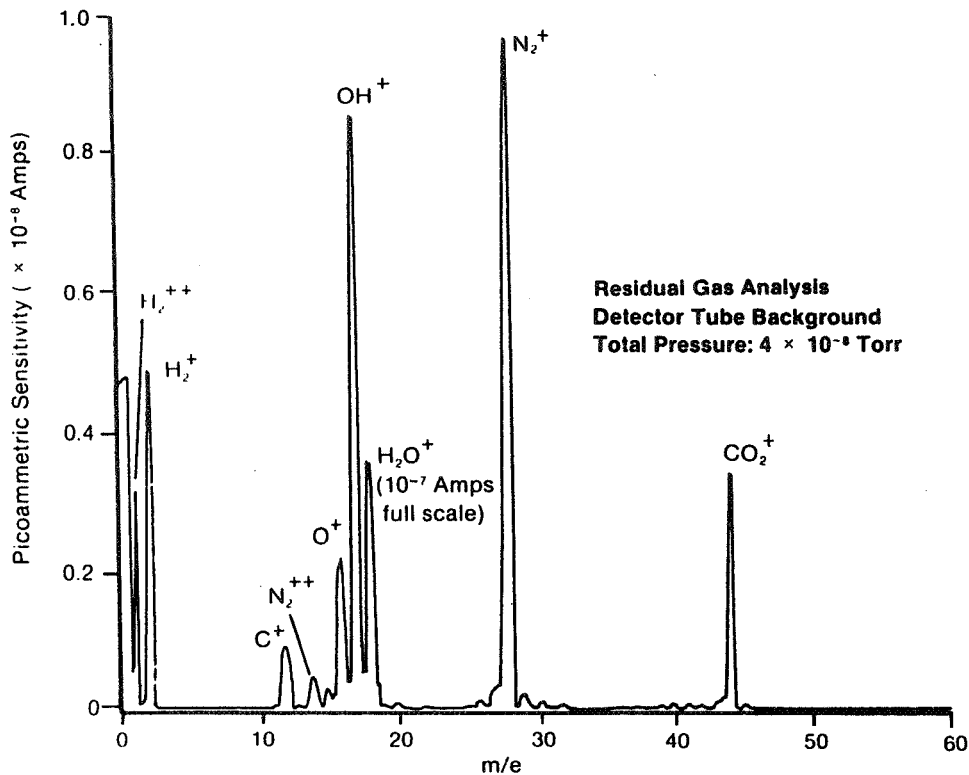
1. Leak checking with growth chamber under argon pressure or under vacuum with helium gun.
2. Run-to-run comparisons of purity levels and location of impurity sources.

Quantitative:

1. Detection of evaporated growth zone impurities in vacuum.
2. Analysis of trace gas impurities in 1-3 Atm. growth ambient.
3. Verification of argon supply purity.



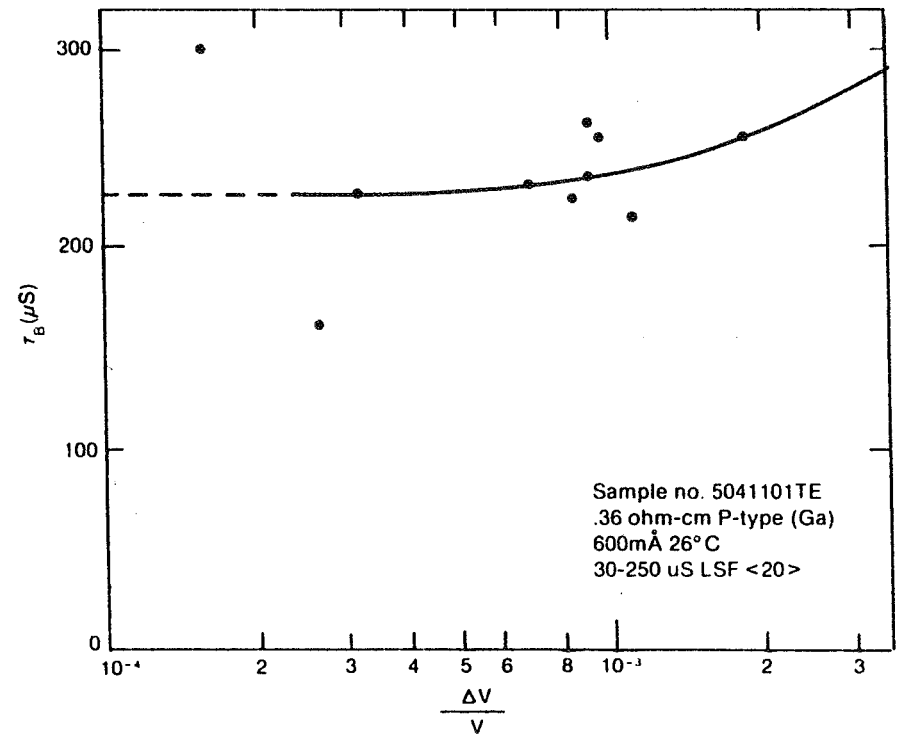
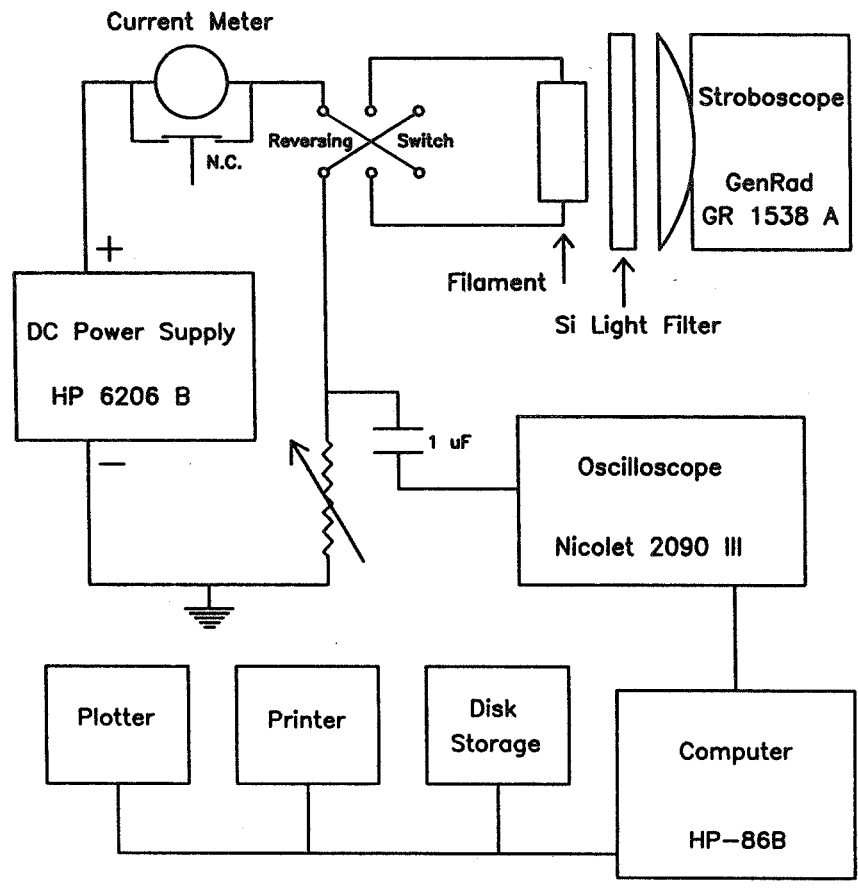
ADVANCED SILICON SHEET



Minority Carrier Lifetime Measurements in Low Resistivity (<1 ohm-cm) Silicon

1. High current density at low applied voltages.
 - a. Reduction of applied voltage.
 - b. Control of sample temperature.
 - c. Increased series resistor power ratings.
 - d. Reduction of series R/sample R ratio.
2. Low PCD signal amplitude.
 - a. Increased flash tube intensity by using an extra capacitor.
 - b. Increased sample length.
3. Larger effect of noise on smaller PCD signal.
 - a. Computer averaging of 20 to 100 oscilloscope traces.

ADVANCED SILICON SHEET

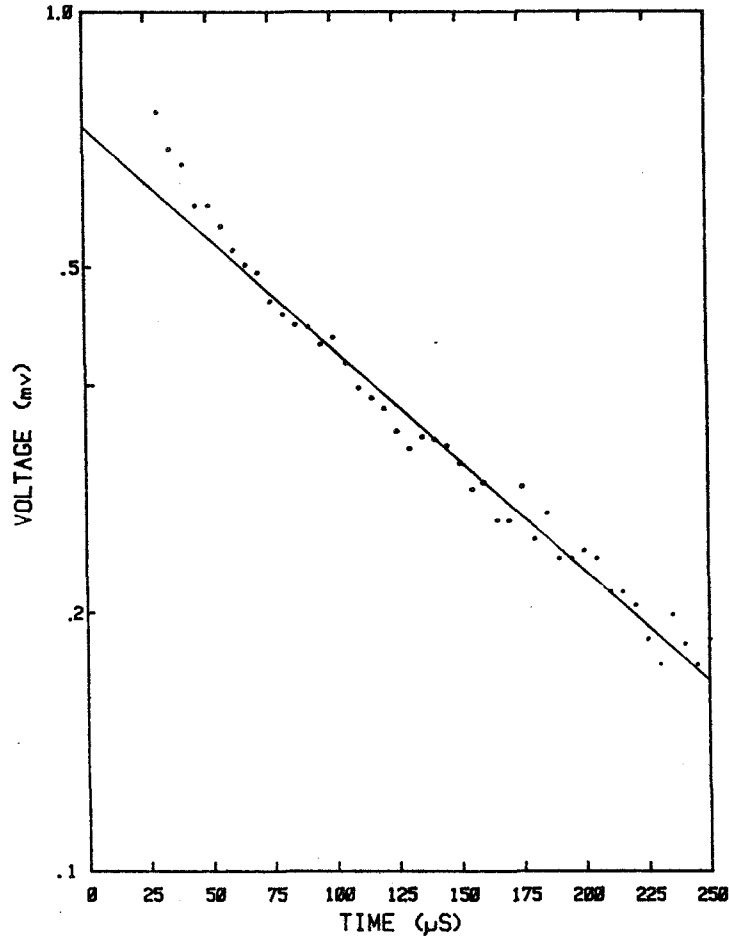


Sample number: 5041101TE Date: 5/13/85 Total of 20 traces averaged.

Peak voltage: .7656mV $\Delta V/V$: $1.06E-3$ at 30 μ S
FILAMENT LIFETIME= 168 BULK LIFETIME= 214 μ S
Sample dimensions HxWxL= 7.5 7.5 27 OR Diameter= 0 Rs=1275.6

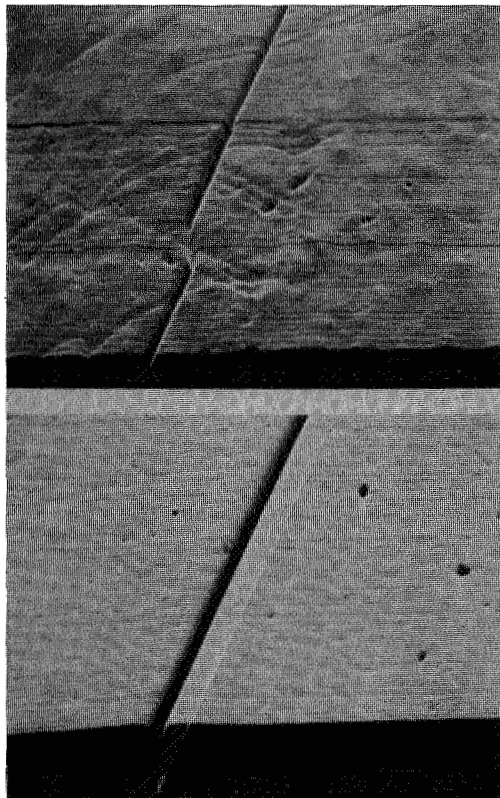
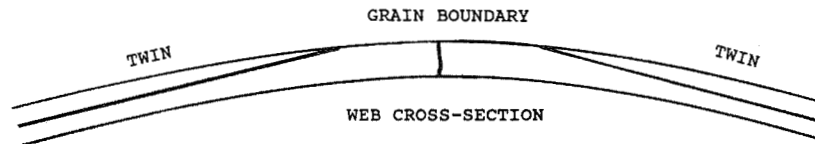
Measurement temperature= 26 Sample current= 300
Resistance: 2.5 Voltage: .72 Resistivity: .36 Type: P
Series R: 10.4 Maximum series current: 693
Predicted V at 2000 μ S is: $4.97E-6$

Plot for points from t=30 to 250 μ S
LSF Done 32.8 Minutes
LTPLOT



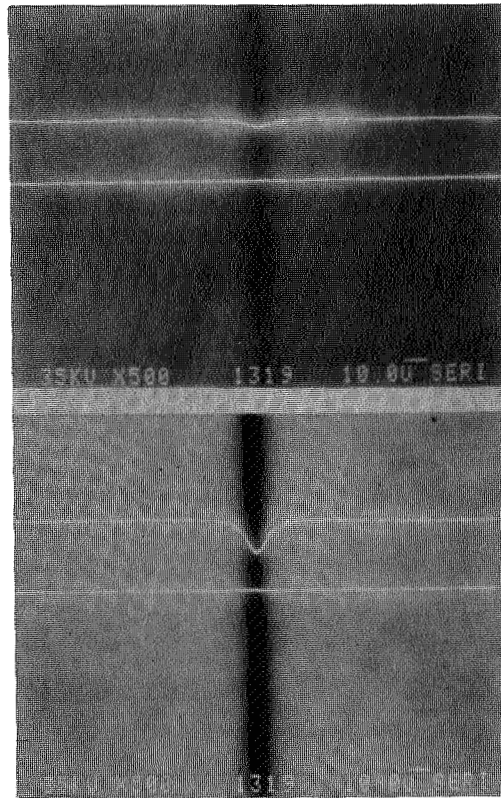
Procedure for Copper Decoration

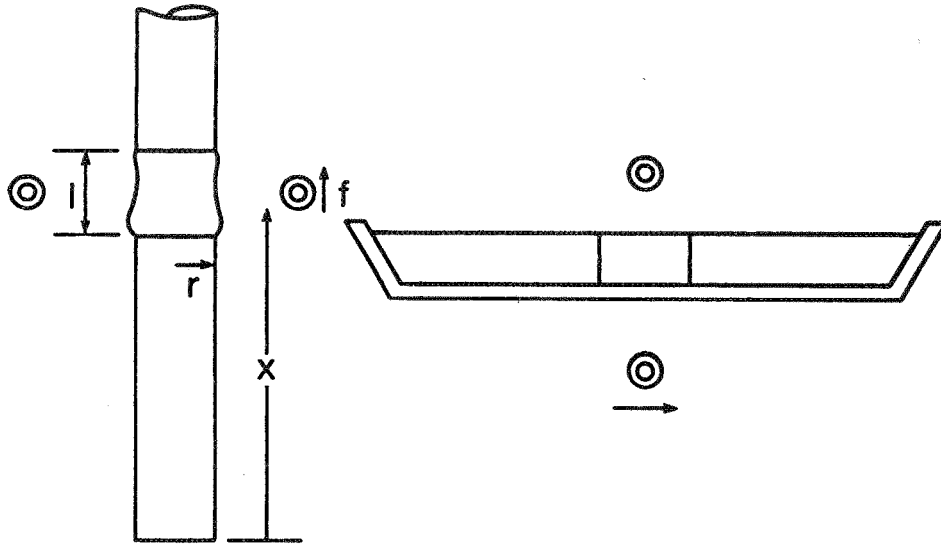
1. ETCH 1 CM THICK SAMPLE IN NaOH
2. APPLY SATURATED, HOT CuSO_4 /WATER TO WARM SAMPLE
3. HEAT TO 850°C FOR 1 HR.
4. COOL TO 750°C OVER A 4 MIN. PERIOD
5. COOL TO 400°C OVER A 2 MIN. PERIOD
6. COOL TO 200°C OVER A 4 MIN. PERIOD
7. COOL TO $<50^\circ\text{C}$ OVER A 4 MIN. PERIOD
8. REMOVE A THIN WAFER ABOUT 2 MM FROM SURFACE OF SAMPLE



<-TWIN->

<-GRAIN->
BOUNDARY





$$C_n(x)/C_o = (k/(k+g))^n [1 - (1-k-g)Z_n e^{-(k+g)x}]$$

where

$$Z_n = n - \sum_{s=1}^{n-1} (n-s)(k+g)^{s-1} e^{-s(k+g)} ((s+x)^{s-2} / s!) \{ (s-1)x + (s+x)[1 - (k+g)x] \}$$

and

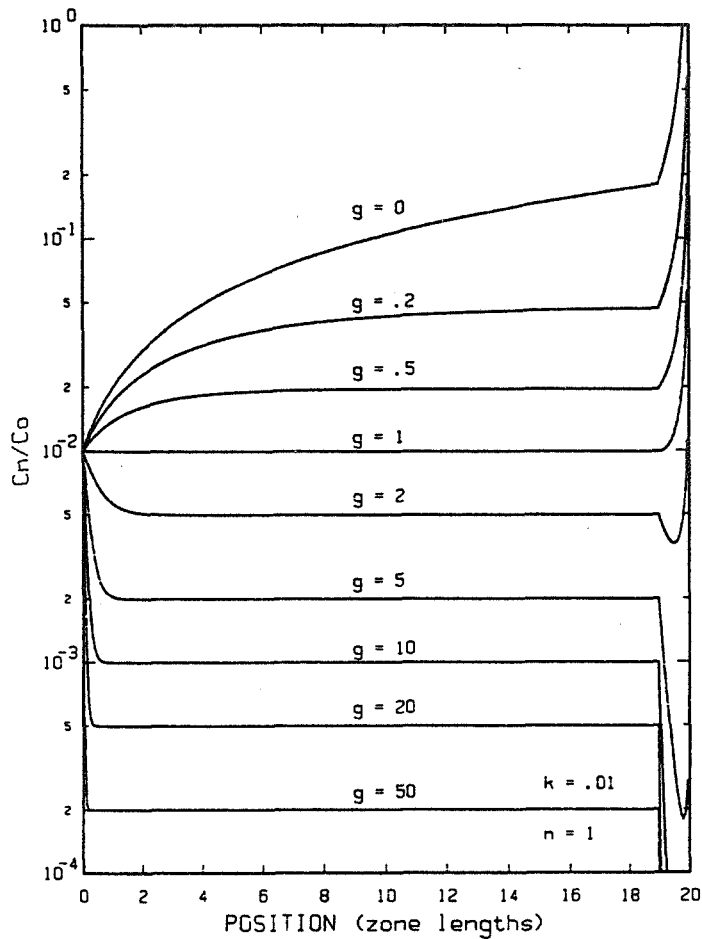
- n = number of zone passes
- k = effective segregation coefficient
- g = effective evaporation coefficient
- x = position in units of zone length
- C_o = original uniform impurity concentration
- C_n(x) = impurity concentration at x after n passes.

In the last zone (or for normal freezing):

$$C_n(x) = C_n(N-1)(N-x)^{(k-1)} e^{-g[x-(N-1)]}$$

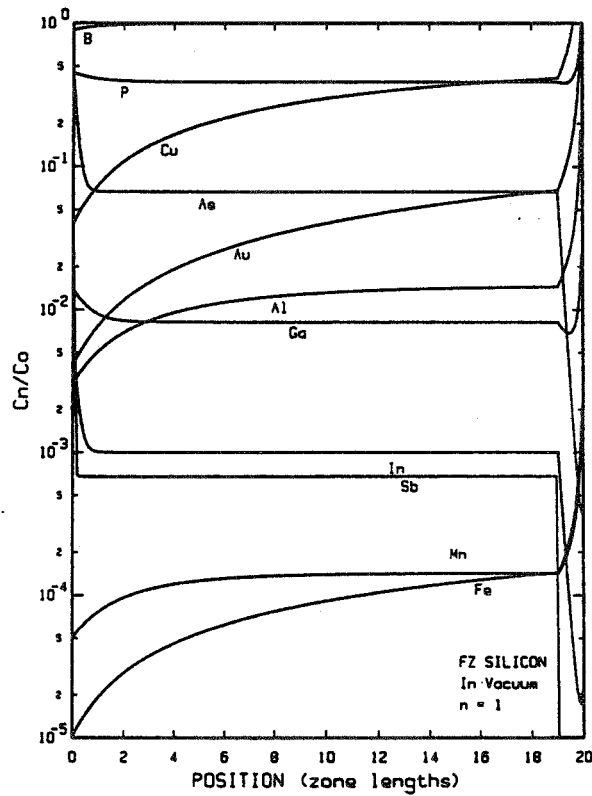
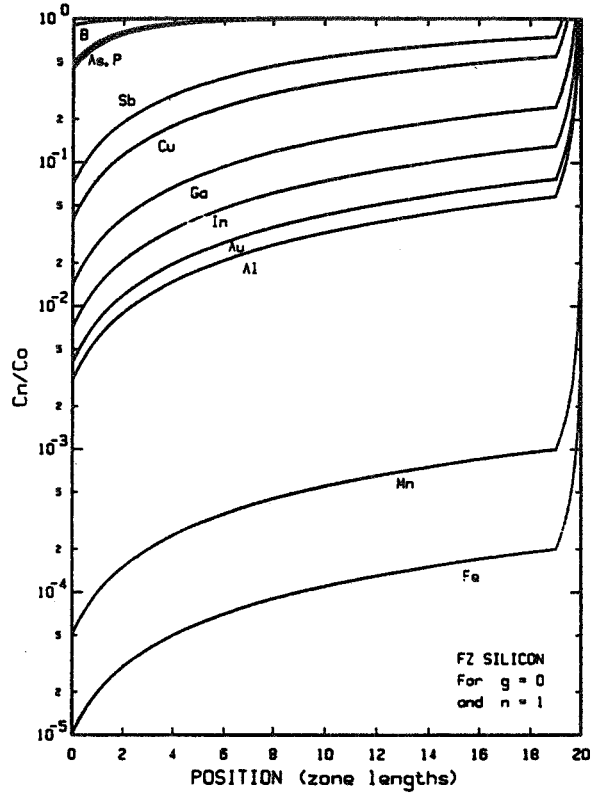
where $N-1 < x < N$ and $N =$ ingot length in zone length units.

ADVANCED SILICON SHEET

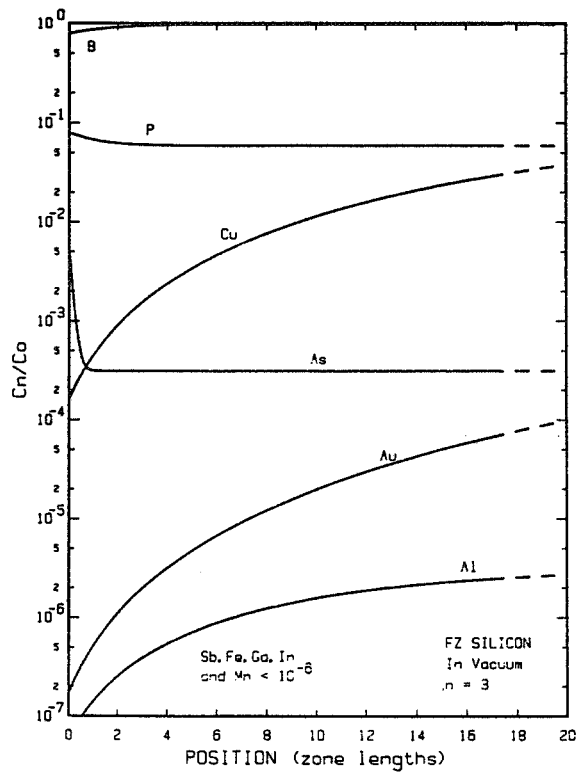
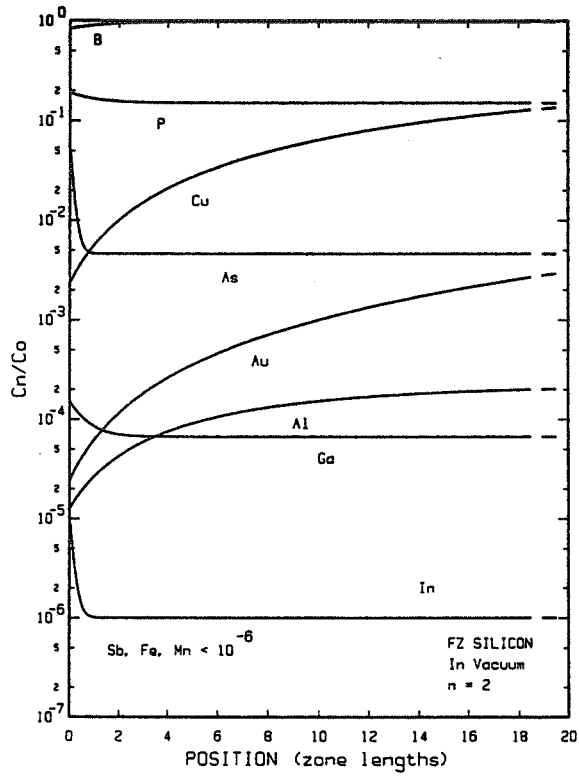


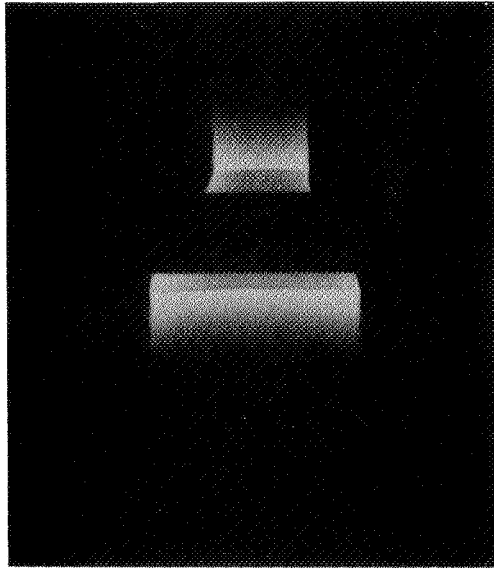
Impurity in Silicon	Effective Segregation Coefficient	Effective Evaporation Coefficient
Aluminum	0.003 (a)	0.2 (e)
Antimony	0.07 (a)	100 (e)
Arsenic	0.5 (a)	7 (e)
Boron	0.9 (a)	0.007 (e)
Copper	0.04 (b)	0.035 (b)
Gallium	0.014 (a)	1.7 (e)
Gold	0.004 (b)	0.012 (b)
Indium	0.007 (a)	7 (e)
Iron	0.00001 (c)	0.035 (e)
Manganese	0.00005 (c)	0.35 (e)
Phosphorus	0.45 (d)	0.71 (d)

ADVANCED SILICON SHEET

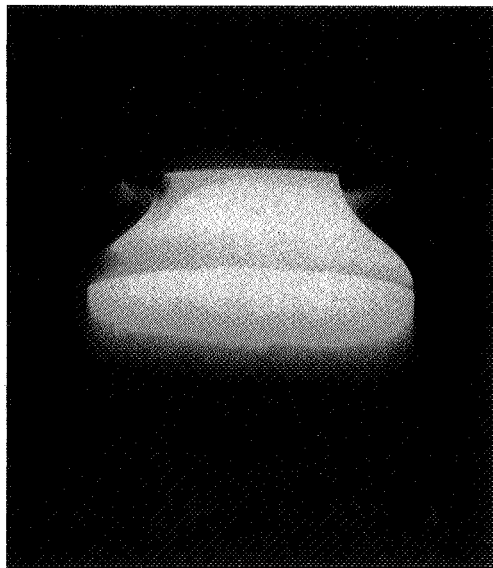


ADVANCED SILICON SHEET





Growth configuration for studying minority carrier lifetime as a function of crystal cooling rate after solidification



Growth of a 34 mm diameter [100] dislocation-free FZ crystal

Gallium Doping

ORIGINAL PAGE IS
OF POOR QUALITY

$$m = WCV/kL_A$$

WHERE

m = MASS OF PURE GALLIUM APPLIED TO SEED END OF INGOT

W = ATOMIC WEIGHT OF GALLIUM

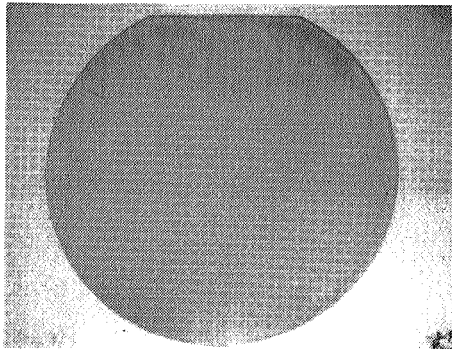
C = DESIRED UNIFORM DOPANT CONCENTRATION IN CRYSTAL

V = ZONE MELT VOLUME

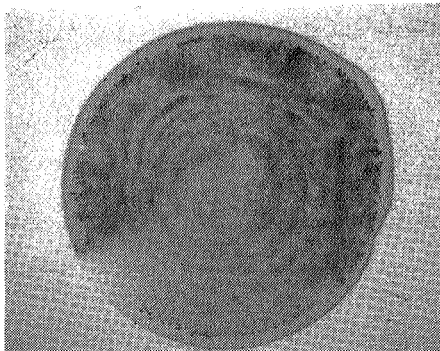
k = EFFECTIVE SEGREGATION COEFFICIENT OF Ga IN Si

L_A = AVOGADRO'S NUMBER

m IS ABOUT 6 mg FOR A 0.3 OHM-CM, 34 mm DIAMETER CRYSTAL



(220) X-ray topograph (nuclear emulsion plate) of a dislocation-free, 0.34 Ohm-cm, Ga-doped, (100) wafer from a float-zoned, [100] crystal with minority carrier recombination lifetime >200 microseconds



(422) X-ray topograph (DEF-5 film) of a copper-decorated vacuum float-zoned, dislocation-free (111) silicon wafer

ADVANCED SILICON SHEET

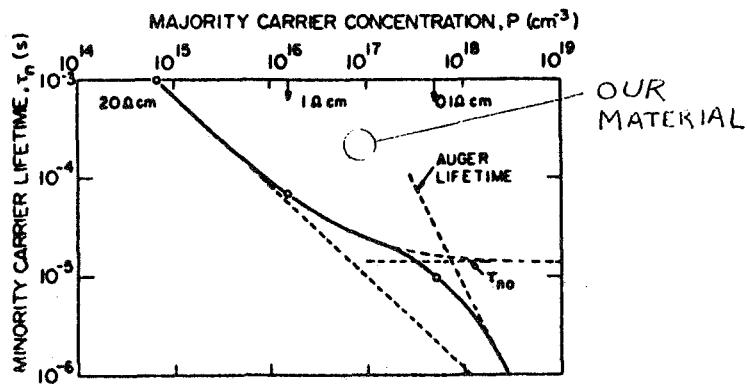
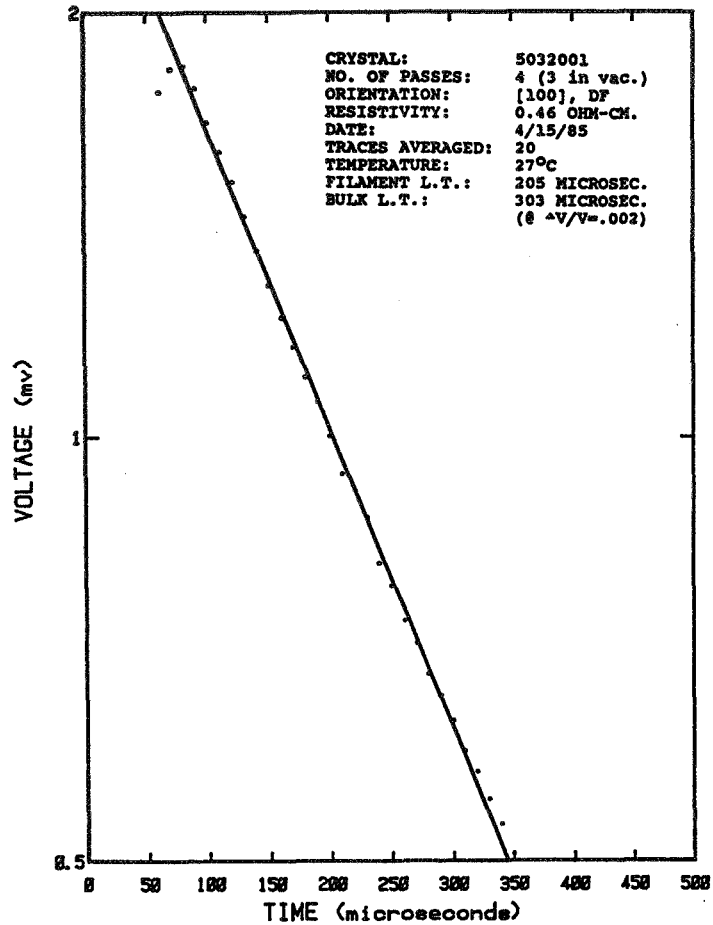
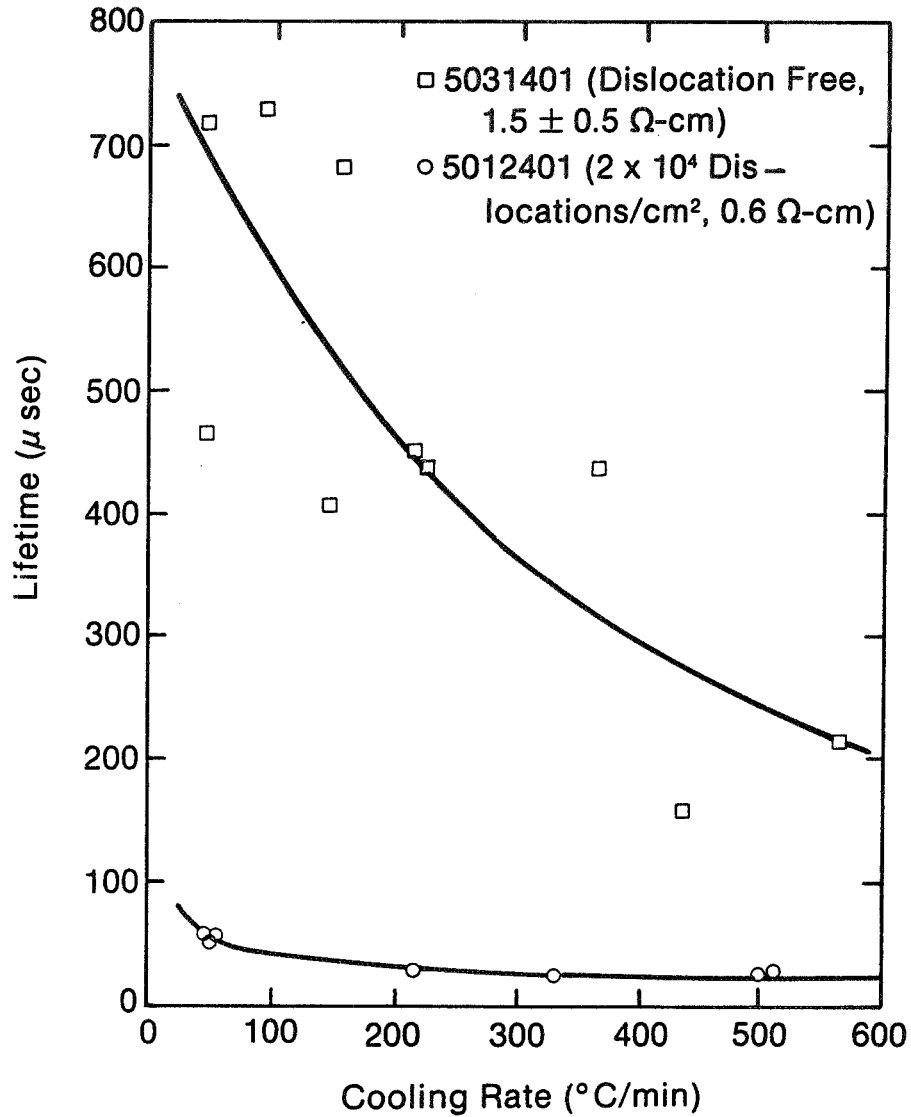


Fig. 3. The minority-carrier lifetime versus majority-carrier concentration relationship used for p-type material. For n-type material the Auger cutoff is shifted slightly towards lower concentrations. Otherwise, τ_p is taken as identical to τ_n . The three circles indicate the points determined by the experts group (see Acknowledgment).
 (from welf)

ADVANCED SILICON SHEET



Future Plans

- A. INVESTIGATE DOPANT SPECIES EFFECTS ON MINORITY CARRIER LIFETIME
- B. INVESTIGATE FEED ROD CLEANING EFFECTS ON MINORITY CARRIER LIFETIME
- C. INVESTIGATE SURFACE PROXIMITY EFFECTS ON MINORITY CARRIER LIFETIME
- D. GROW AND CHARACTERIZE HIGH-LIFETIME, HEAVILY-DOPED, FZ CRYSTALS

SILICON SHEET SURFACE STUDIES

UNIVERSITY OF ILLINOIS AT CHICAGO

S. Danyluk

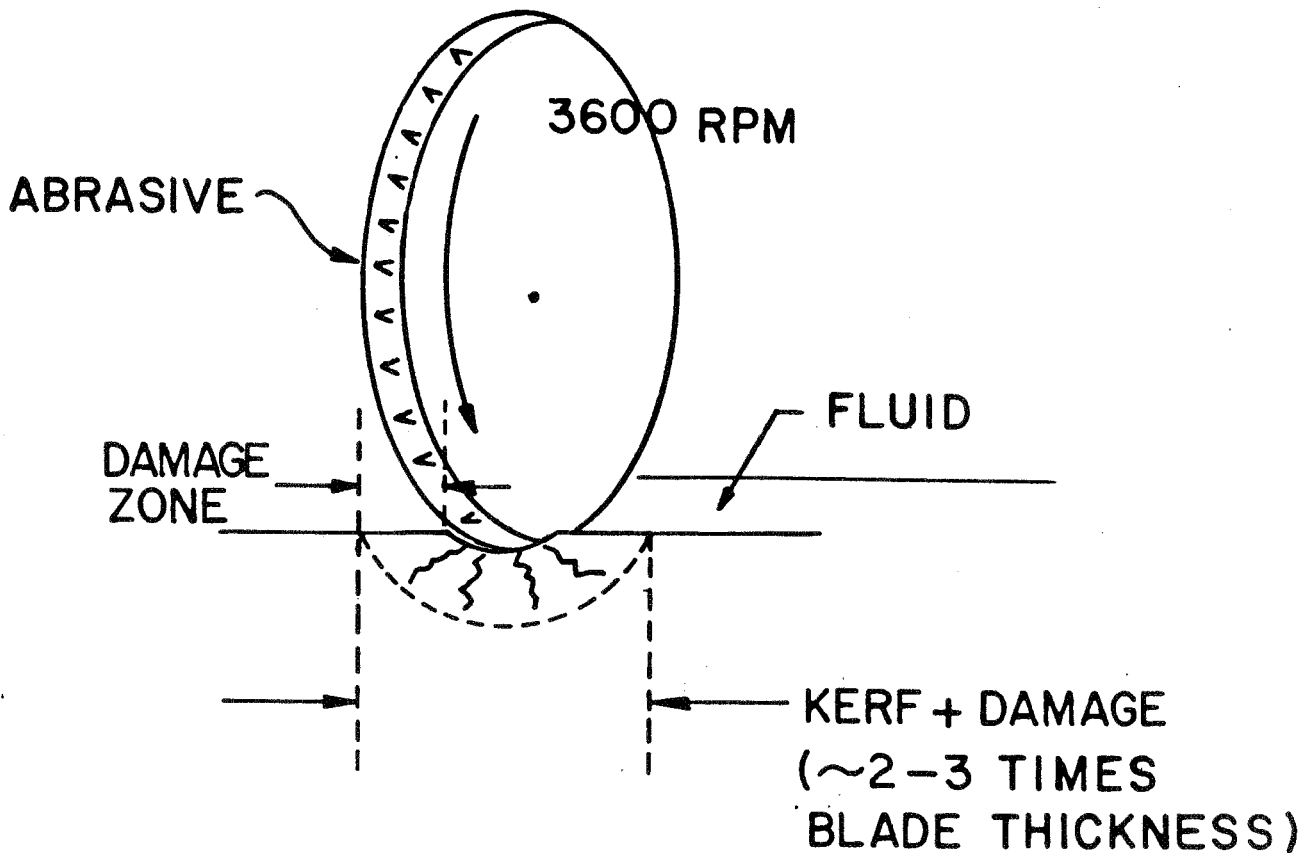
Abrasion and Wear
of Silicon in Fluids

Measure Wear Rate
(in fluids)
Determine Mechanism
of Wear
Develop Model

Non-destructive
Determination of Residual
Stresses in Sheet Silicon

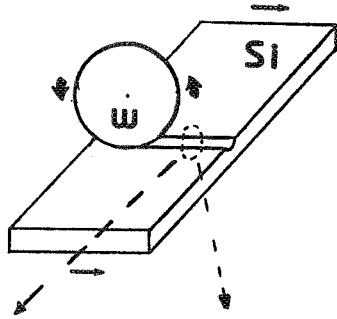
Develop experimental
technique
Perform Analysis
Determine σ_{RS} in
WEB, EFG sheet

OD Sawing (Dicing)

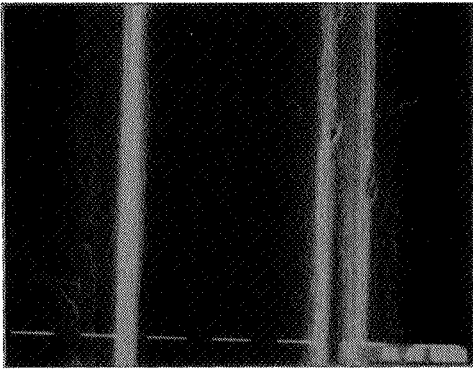


ADVANCED SILICON SHEET

Grinding of Silicon Single Crystal



ORIGINAL PAGE IS
OF POOR QUALITY



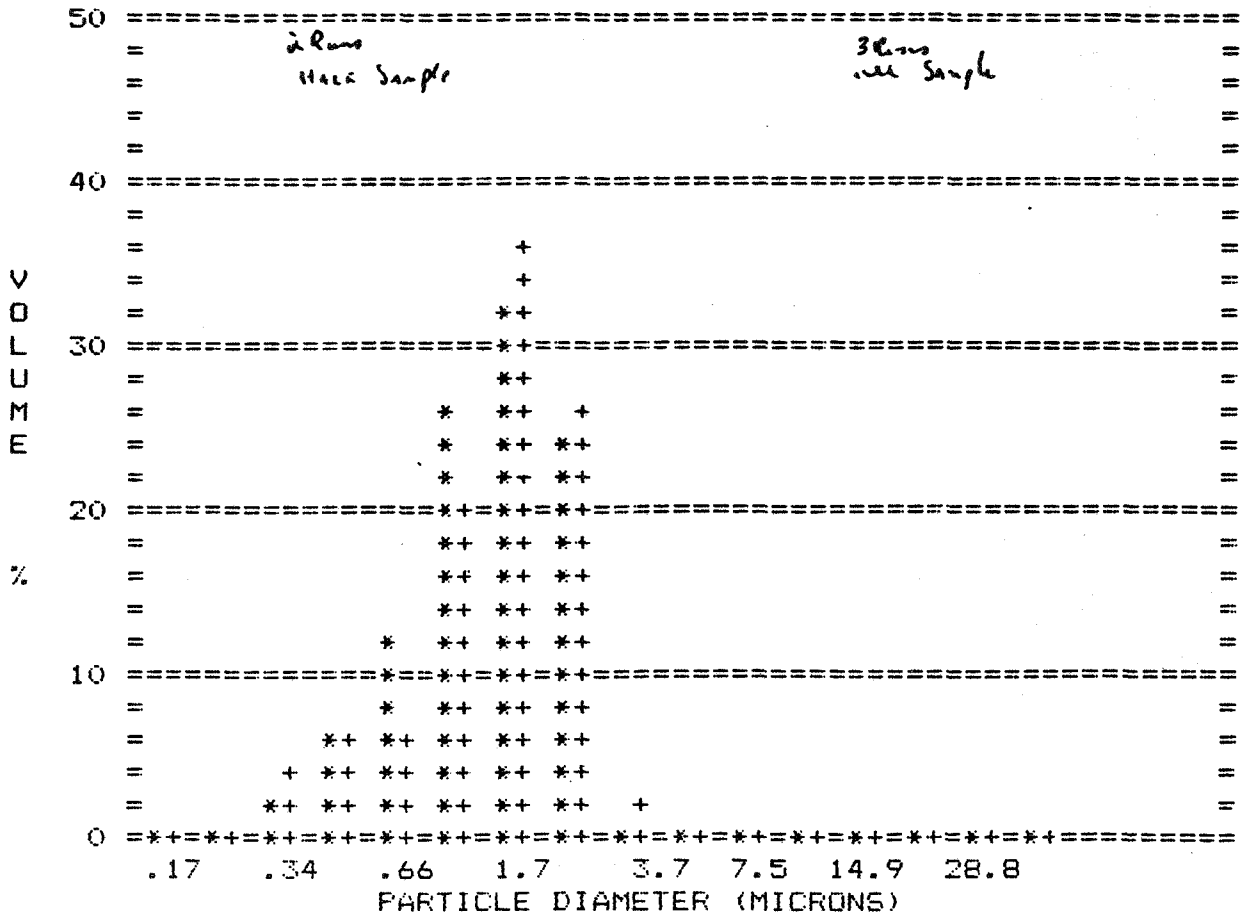
(a) P type (100), RPM: 1000, Depth of cut: .002", Feed rate: .7"/min., Blade thickness: .0010"



(b) Higher magnification of (a)

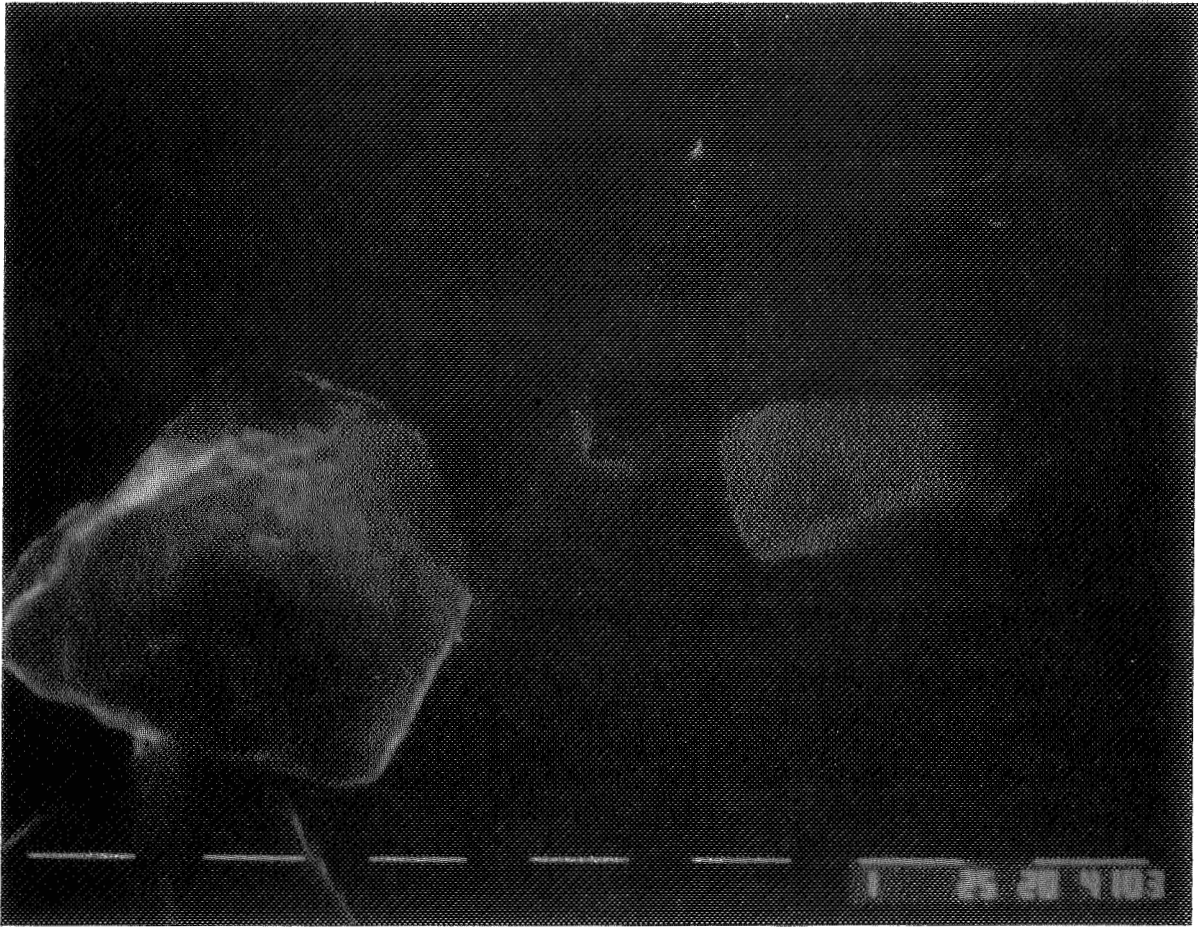
ADVANCED SILICON SHEET

PARTICLE SIZE DISTRIBUTION, DIFFERENTIAL * CURRENT
 CURRENT IS MEAN OF 2 RUNS + COMPARISON
 * SIP 1000 + SIP 1000



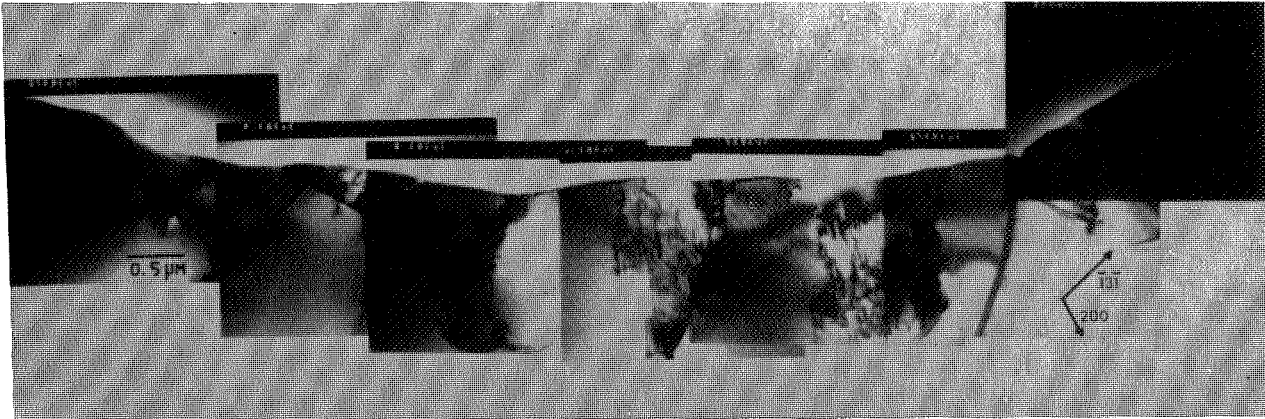
* Grinding condition of silicon

rpm : 1000, depth of cut : .005", feed rate : 1.5"/min.
 room temperature, without fluids

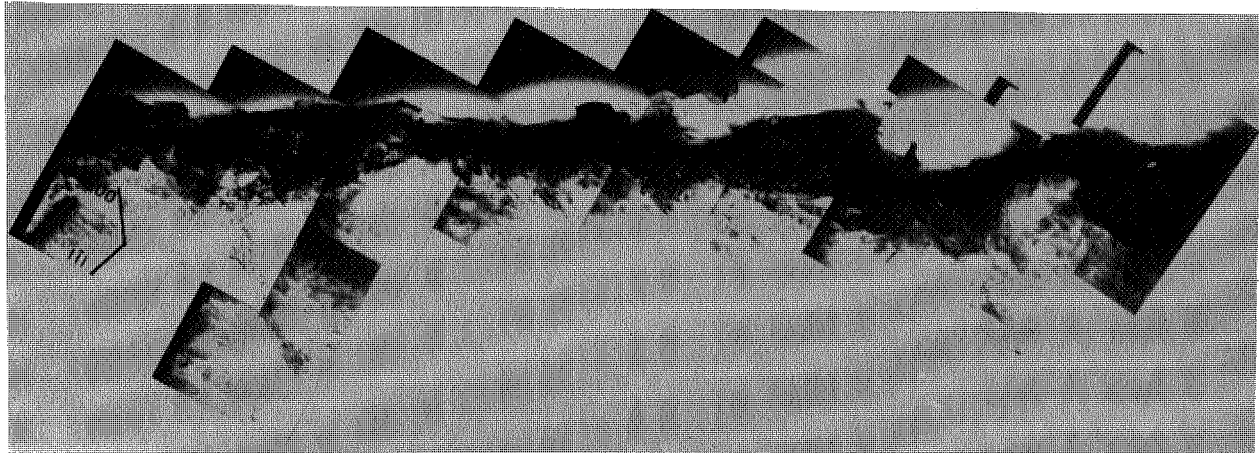


Diamond Grit of Dicing wheel, Series 401,
Micro Automation, blade thickness .0006-.0008"

ORIGINAL PAGE IS
OF POOR QUALITY

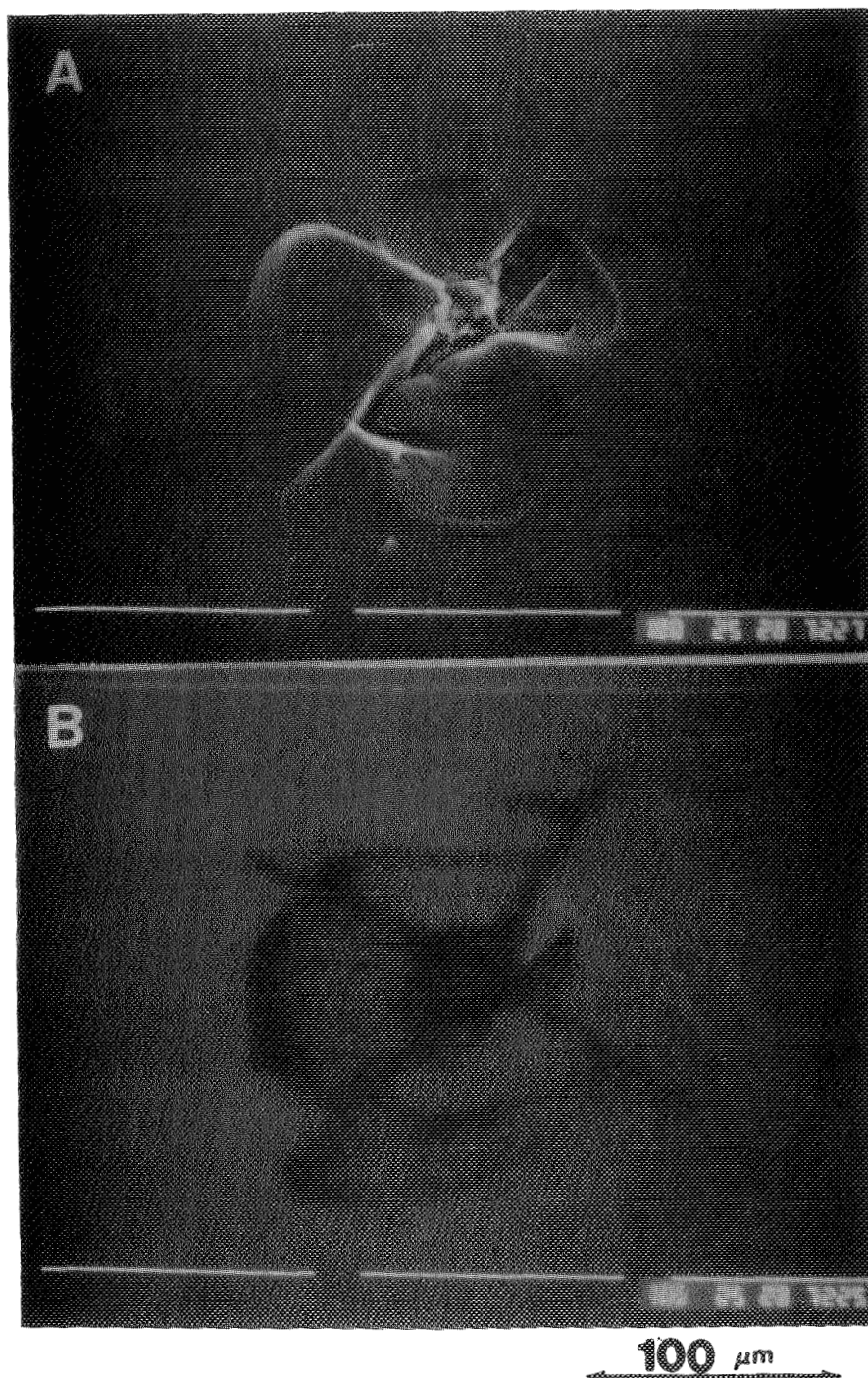


TEM micrograph of a scratch groove in p-type Cz silicon abraded in ethanol. The load on the pyramid diamond was 0.5 N and the scratching speed was 1.1 cm/s.



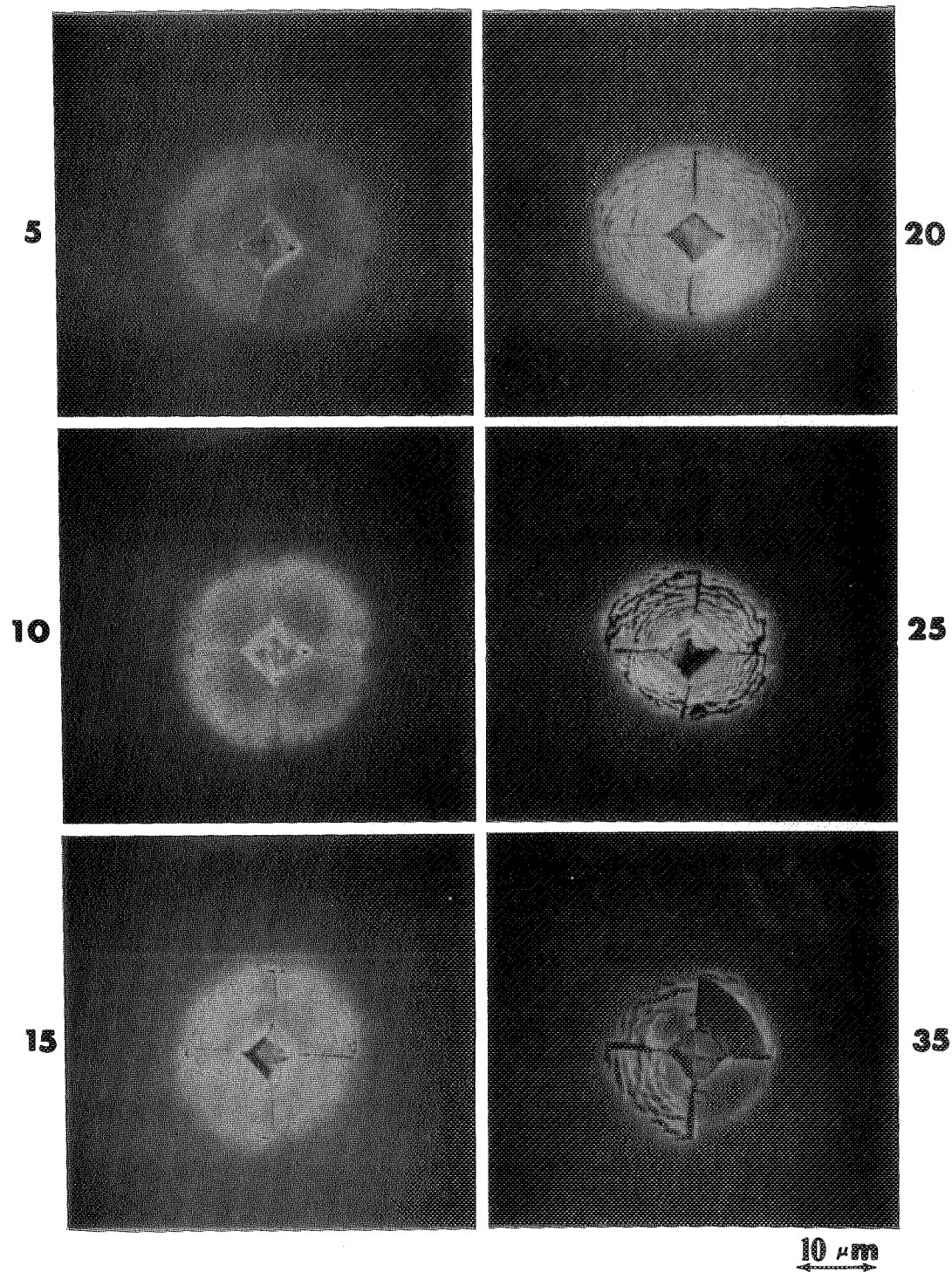
TEM micrograph of a scratch groove in p-type Cz silicon abraded in de-ionized water. The load on the abrading pyramid diamond was 0.5 N and the scratching speed was 1.1 cm/s.

ADVANCED SILICON SHEET



(A) Secondary electron image (SEI) and
(B) electron beam induced current (EBIC) image
of a pyramidal indentation in a (100) n-type silicon.
The indentation load was 9.8N.

ORIGINAL PAGE IS
OF POOR QUALITY



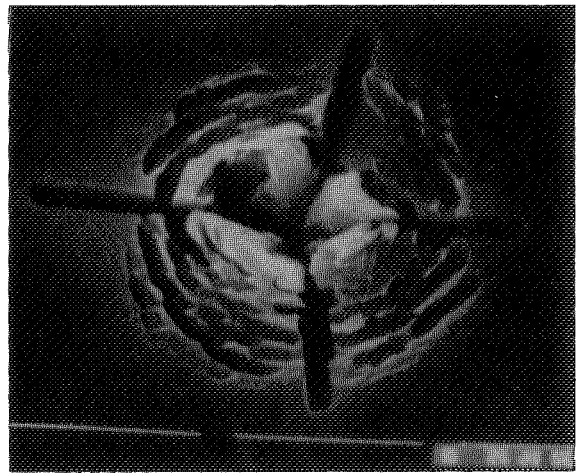
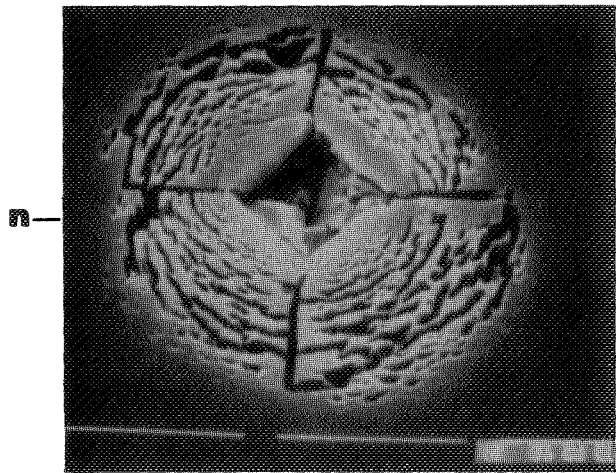
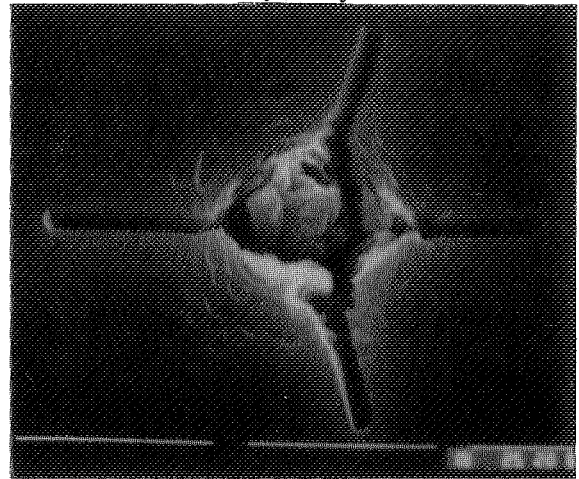
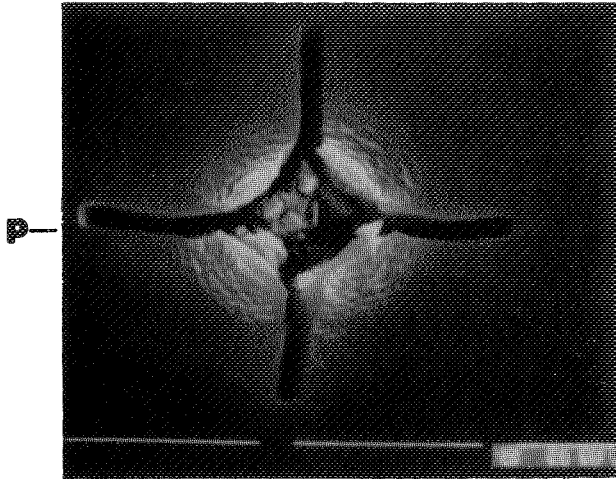
SEM micrographs of indentations as function of Sirtl etching time(s). The indentations of (100) n⁻ type Cz silicon were made in 10⁻³ M/I NaI.

ADVANCED SILICON SHEET

ORIGINAL PAGE IS
OF POOR QUALITY

(100)

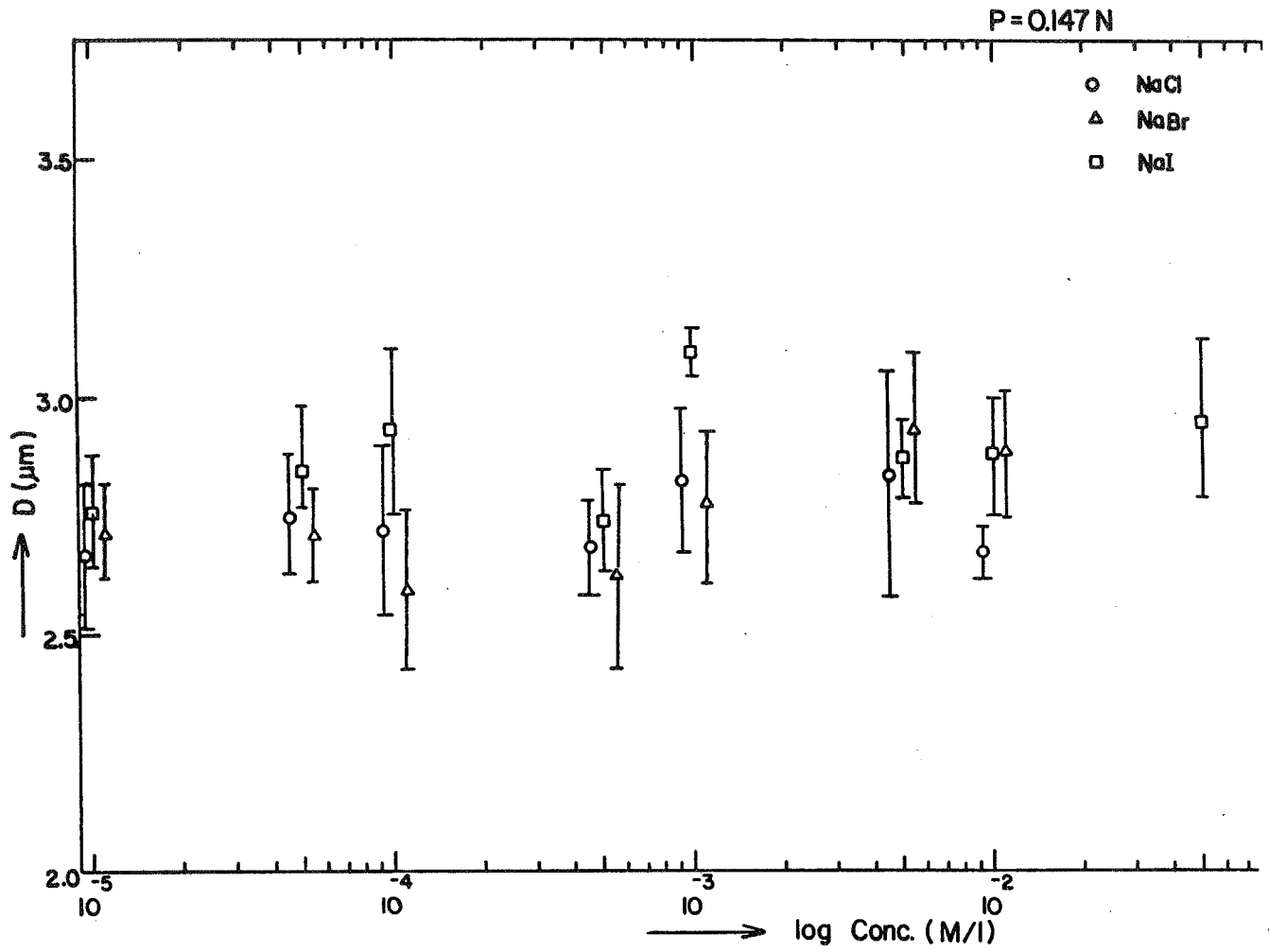
(111)



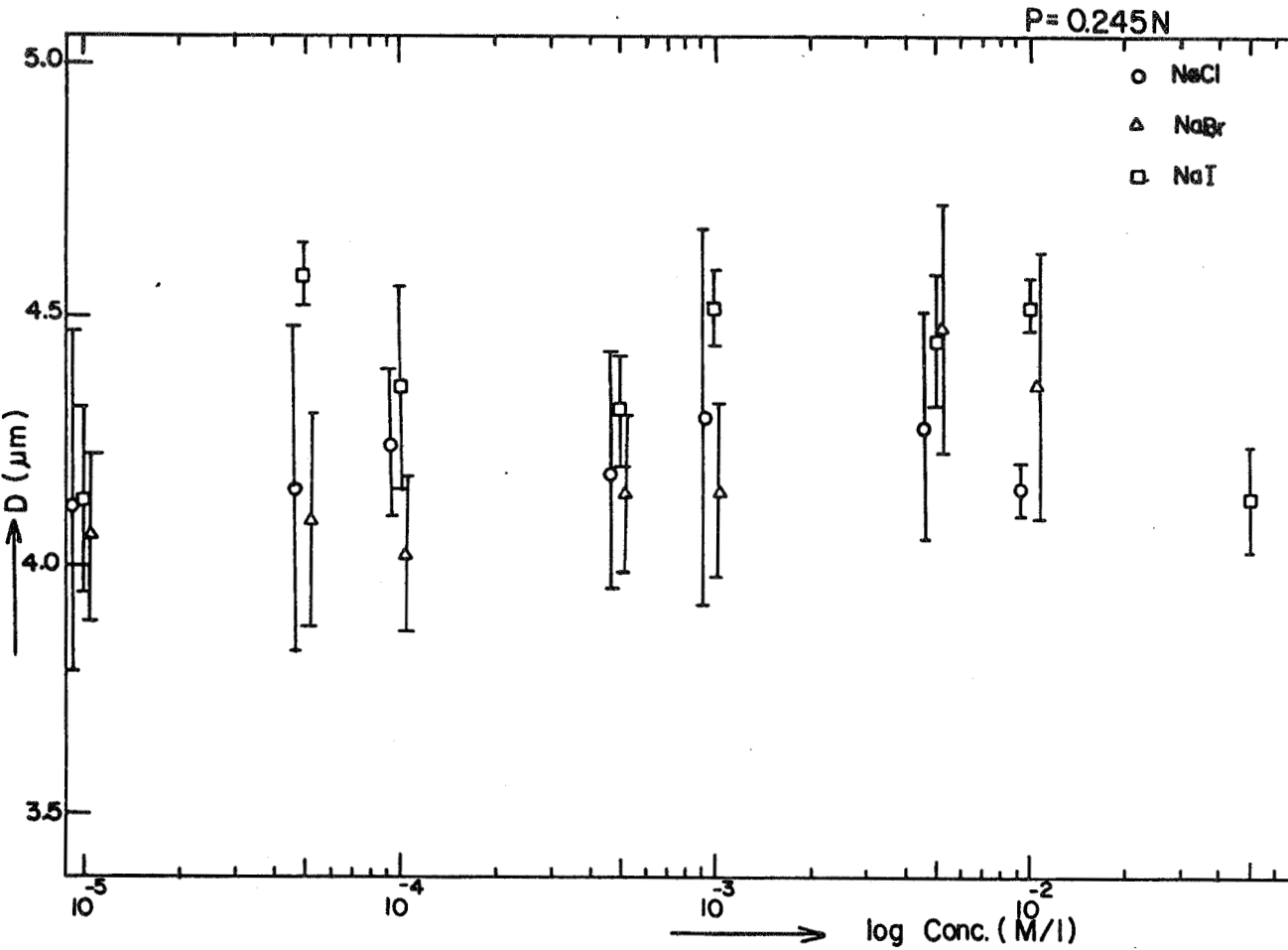
← 10 μm →

SEM micrographs of indentations ($P=0.49\text{N}$, Sirtl etch for 25 s.)
The indentations of (100), (111) p- and n-type Cz silicon were made
in 10^{-3}M/l NaI .

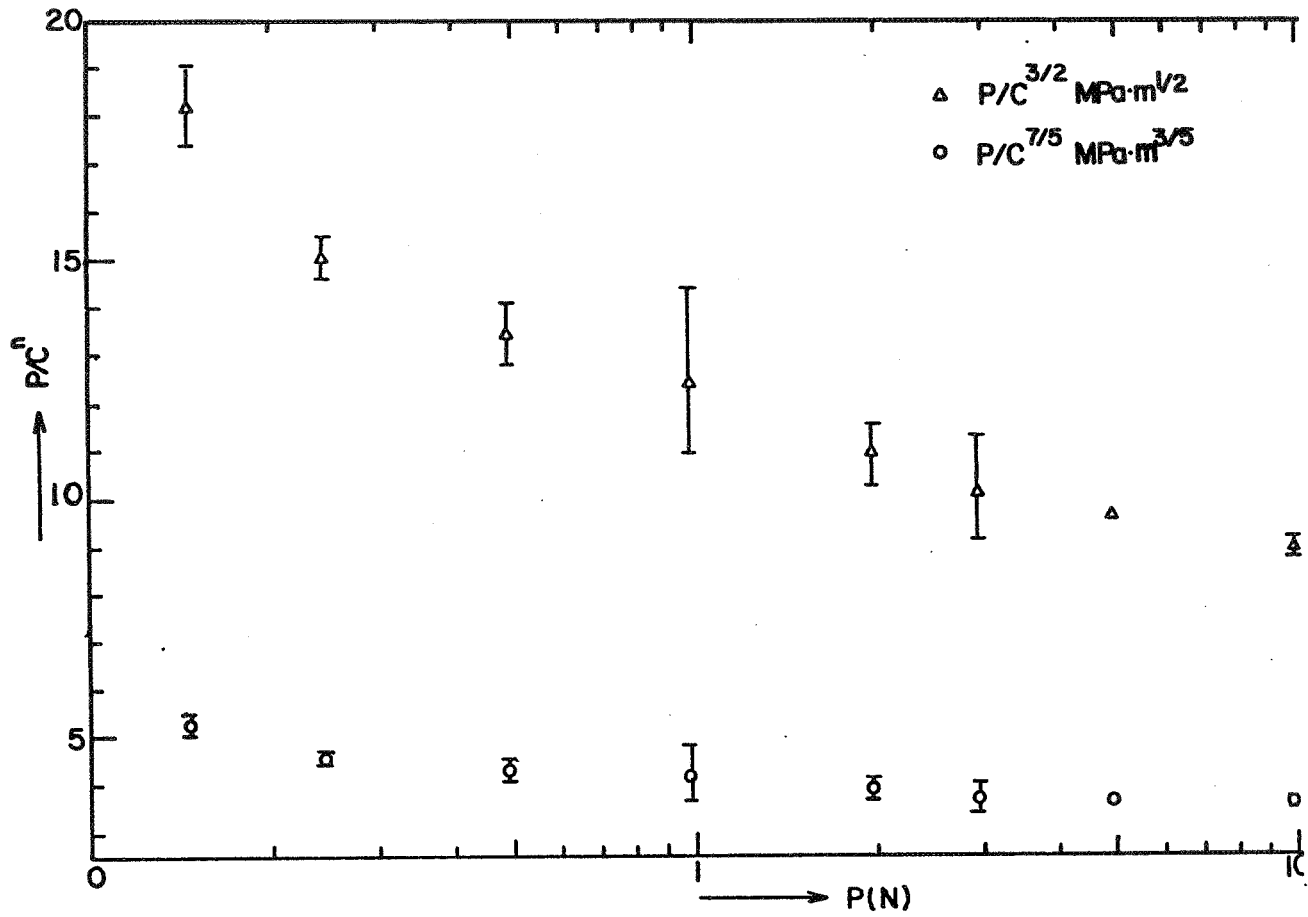
ADVANCED SILICON SHEET



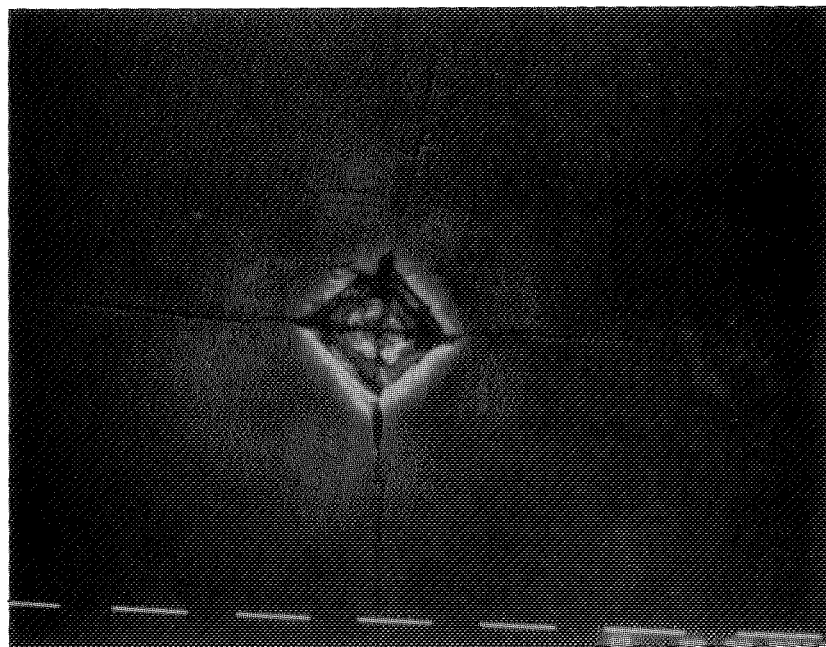
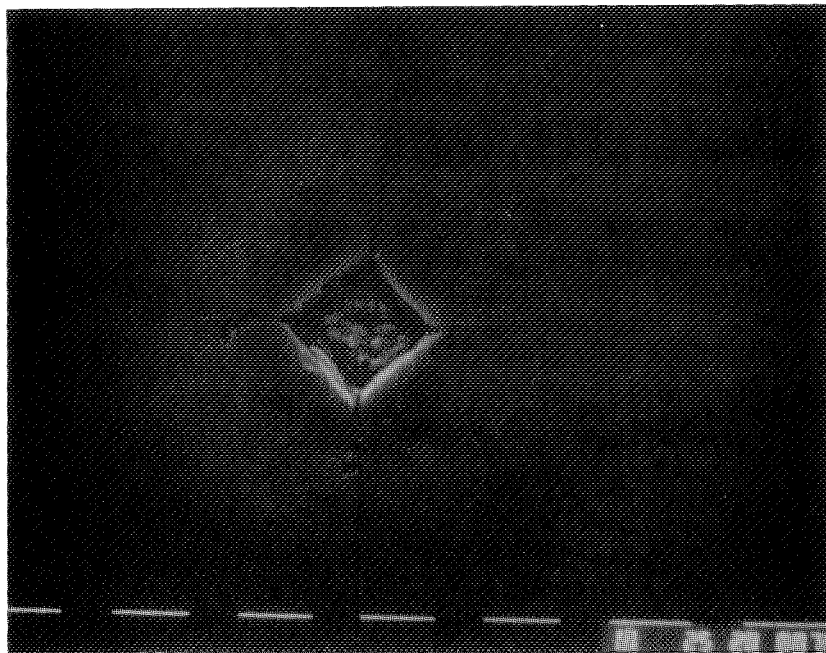
ADVANCED SILICON SHEET



ADVANCED SILICON SHEET

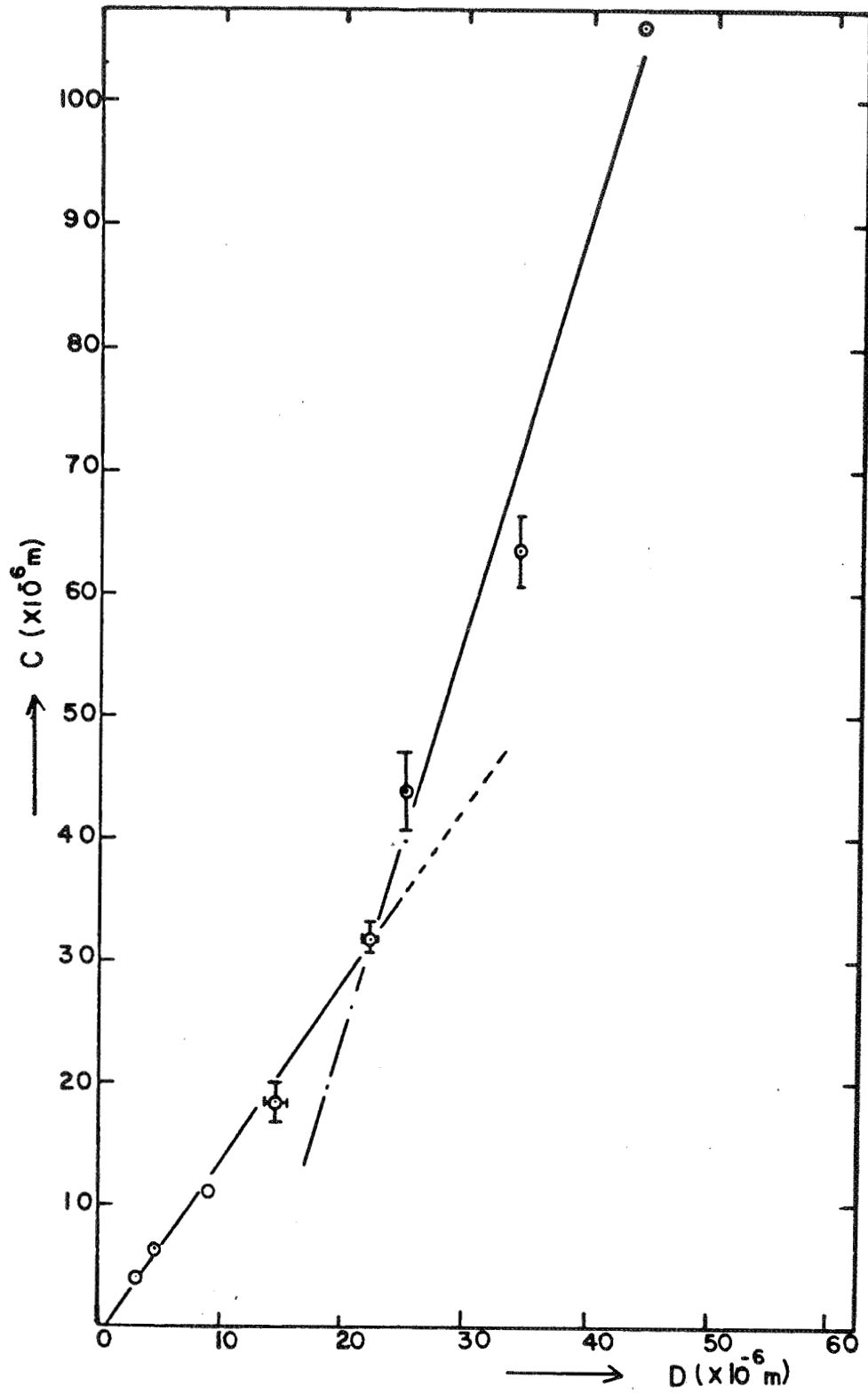


ORIGINAL PAGE IS
OF POOR QUALITY

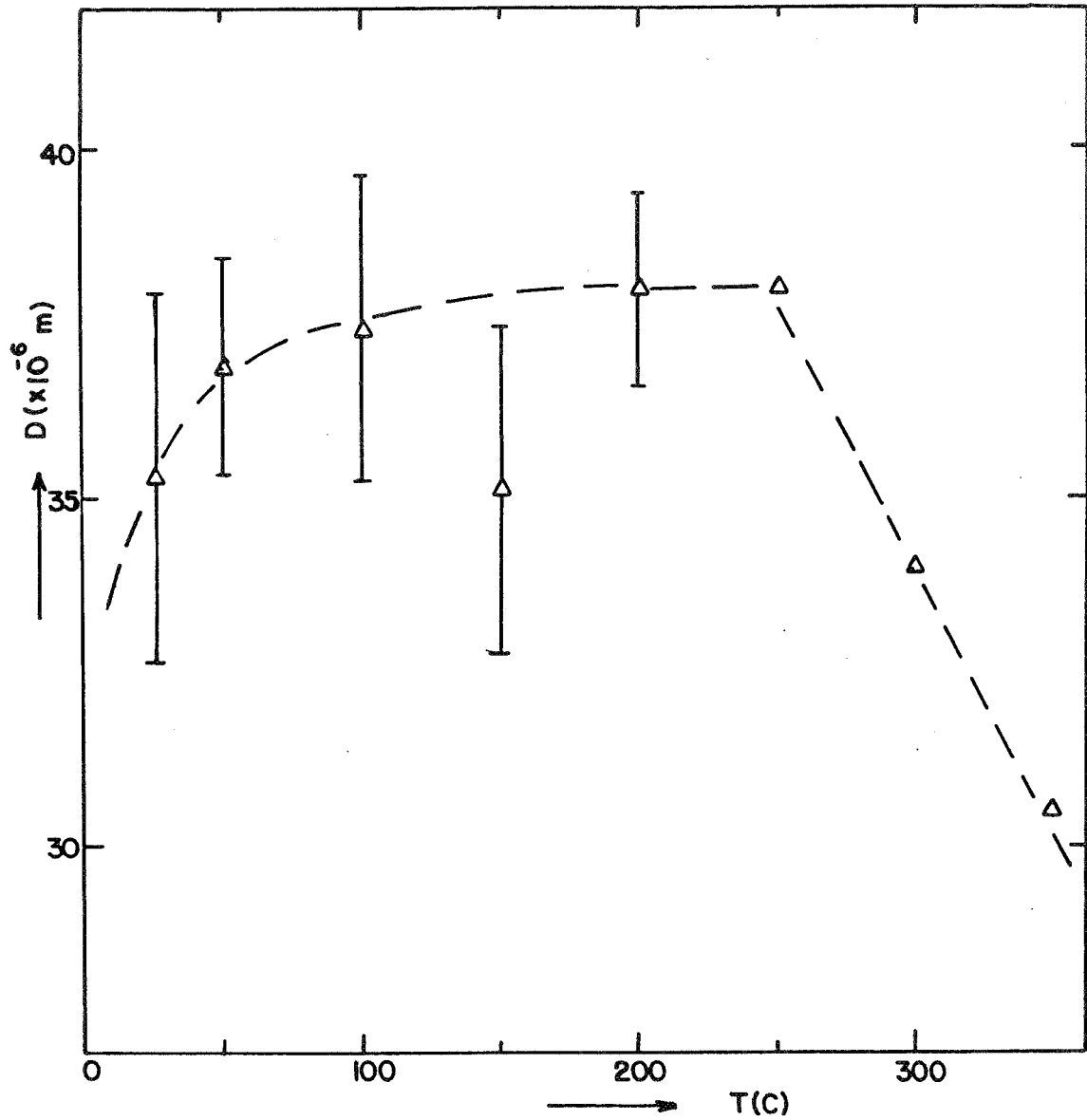


20 μm

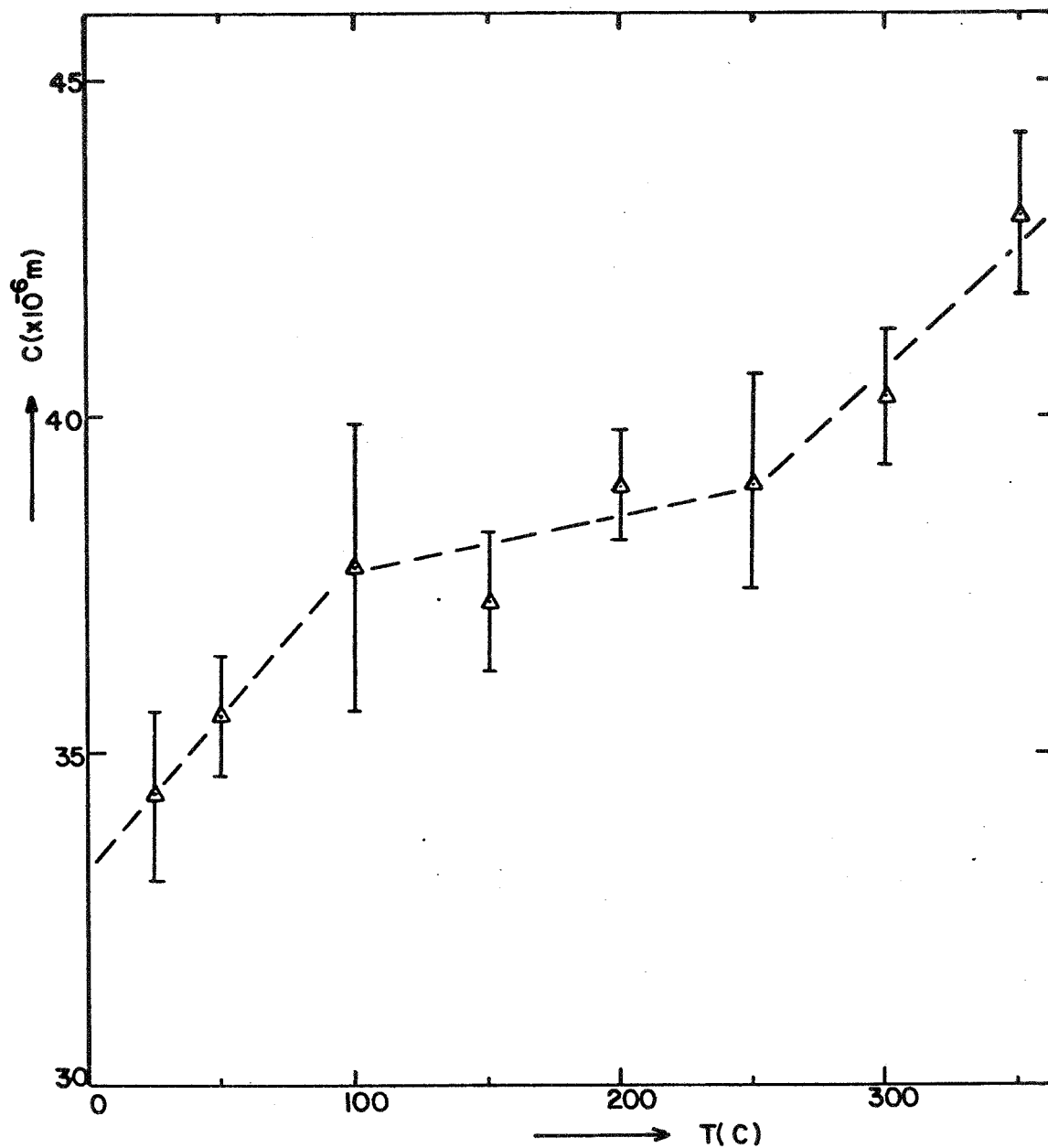
SEM micrographs of indentation for (100) n-type silicon. The indentations were made with a load of 1.98N at 350°C, and etched in dilute Sirti solution for 15s.



ADVANCED SILICON SHEET



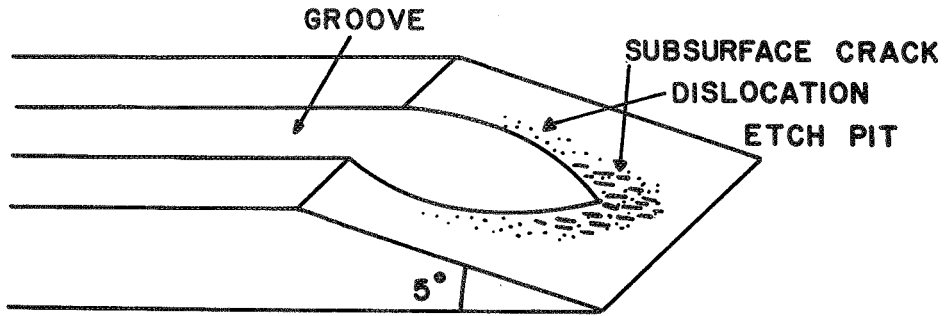
Damage size as a function of temperature for (100) n-type Cz silicon under a load of 1.98N.



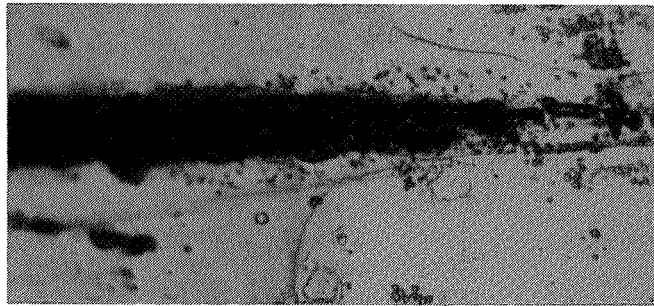
Radial crack length as a function of temperature for (100) n-type Cz silicon under a load of 1.98N.

ADVANCED SILICON SHEET

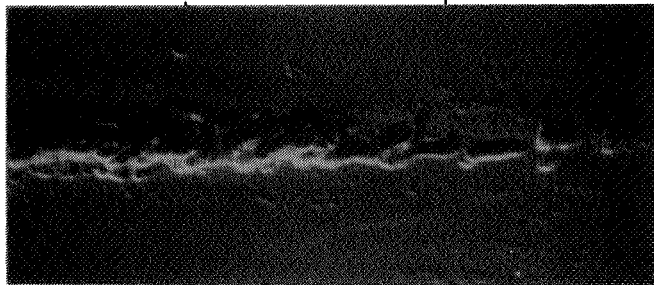
ORIGINAL PAGE IS
OF POOR QUALITY



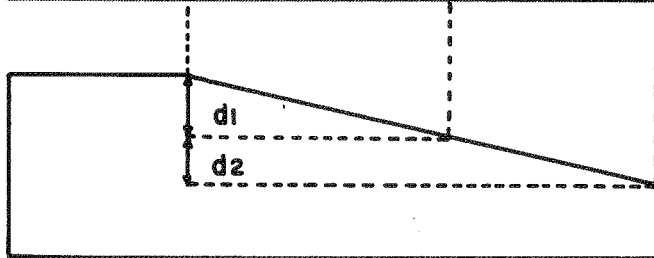
- 10 SCRATHES IN DI H₂O
- ANNEALED AT 750°C FOR 1 HR



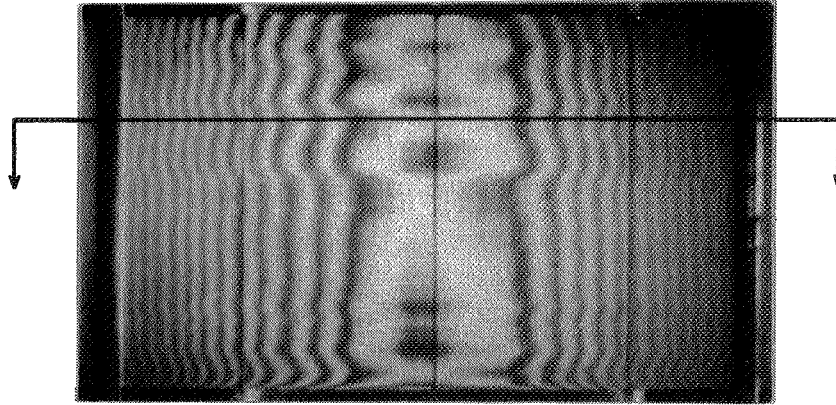
OPTICAL



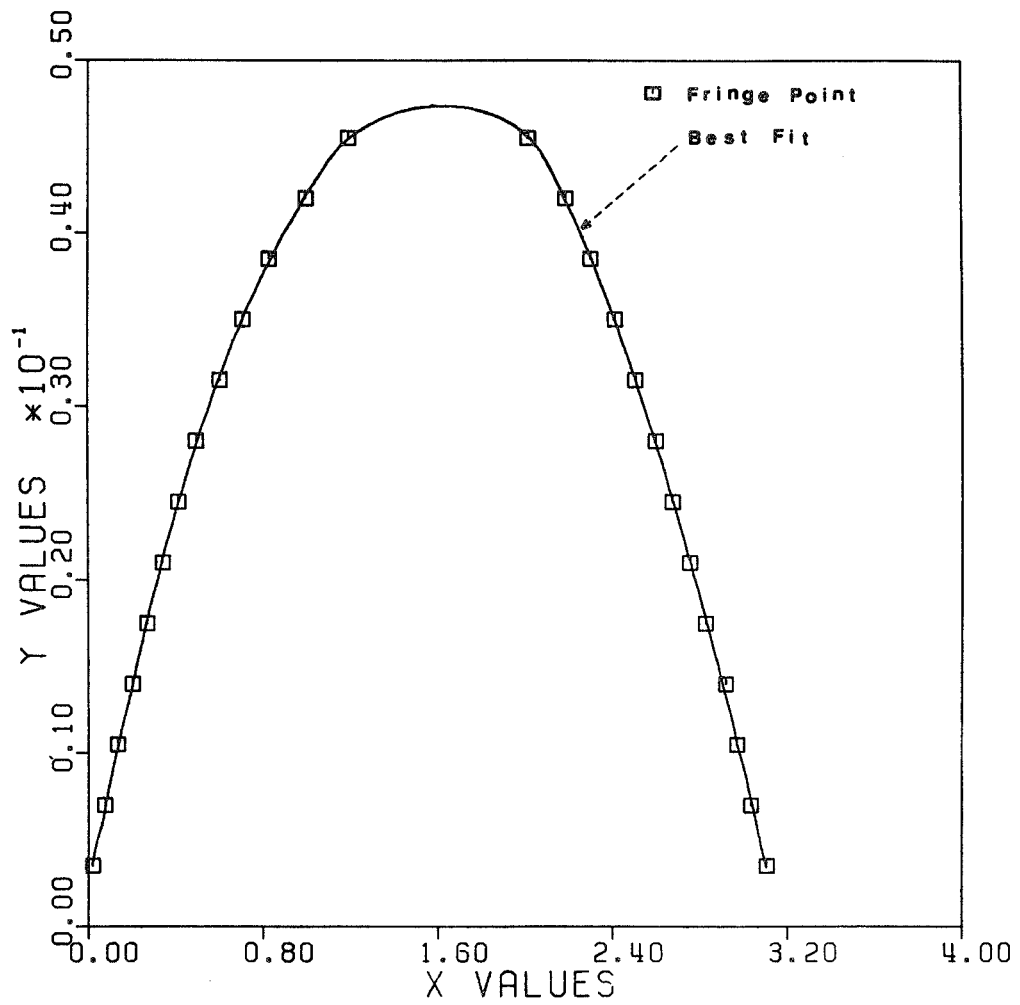
SEM
(BSE MODE)



d1 : DEPTH OF GROOVE
d2 : DEPTH OF DAMAGE



HIGH STRESS (1.4 lb)



DEFLECTION

ADVANCED SILICON SHEET

Best Fit Polynomial

$$Y = -0.001 X^8 + 0.005 X^7 - 0.019 X^6 + 0.04 X^5 - 0.038 X^4 + 0.015 X^3 - 0.023 X^2 + 0.061 X + 0.004$$

Deflection (Cubic Spline)

0.0300 0.0317 0.0319 0.0311 0.0291

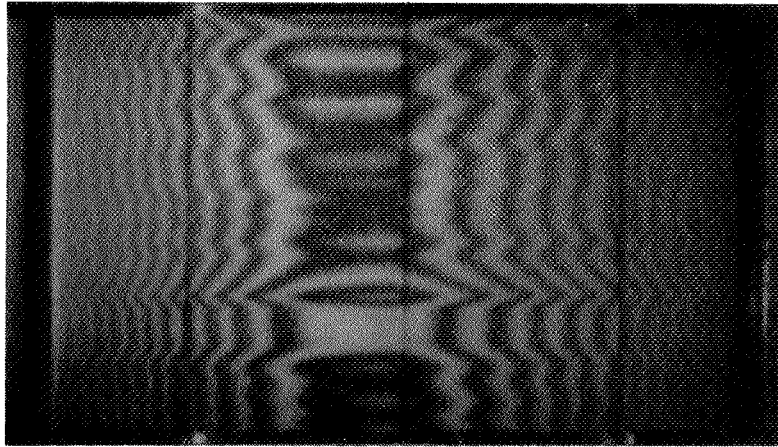
Second Derivative (Cubic Spline)

0.0529 0.0363 0.0248 0.0344 0.0441

Residual Stress

-8.547 -7.720 -7.670 -7.856 -8.545

	0.6	0.8	1.0	1.2	1.4
1	-8.045	-7.694	-7.604	-7.662	-8.248
2	-8.146	-7.621	-7.628	-7.825	-8.478
3	-8.547	-7.720	-7.670	-7.866	-8.545
4	-8.132	7.314	7.417	7.543	7.817
5	7.689	7.553	7.581	7.706	8.085
6	7.735	7.516	7.481	7.635	8.009
7	-8.369	-7.743	7.446	7.499	8.190
8	-8.208	-7.764	-7.540	-7.817	-8.403
9	-8.109	-7.763	-7.636	-8.265	-8.924
10	-7.801	-7.492	-7.485	-7.648	-8.250



High Stress (1.8 lb)

	0.4	0.6	0.8	1.0	1.2	1.4
1	-8.920	-7.827	-7.765	-7.791	-8.065	-8.623
2	-8.235	-7.692	7.140	7.171	7.337	-8.577
3	-8.179	-7.615	-7.527	-7.789	-7.921	-8.443
4	7.712	7.419	7.283	-8.156	-7.859	-8.407
5	8.132	7.690	7.518	7.410	7.581	7.718
6	7.969	6.470	7.413	7.433	7.673	7.465
7	8.046	7.767	7.483	7.593	7.945	8.442
8	-8.059	-7.598	-7.344	-7.389	-7.576	-8.110
9	-7.924	-7.200	-7.182	-7.592	-7.378	7.074
10	-8.780	-8.064	6.807	6.909	8.076	-9.062

Residual Stress Distribution

MODULE DEVELOPMENT AND ENGINEERING SCIENCES

Melvin I. Smokler, Chairman

M. Spitzer, of Spire Corp., described Spire progress on the development of a high-efficiency module. The effort includes development of high-efficiency cells using crystalline silicon wafers made from FZ silicon. Module-size cells, 53² cm in area, have been fabricated with efficiency of 18%.

R. Sugimura, of JPL, reported that new materials have been developed which show promise of fabricating modules that can pass the Underwriter Laboratories Class A burning-brand test for fire-ratable solar cell modules.

D. Otth, of JPL, reviewed the development of a qualification test for modules bypass diodes. Diode junction temperature is measured, indirectly, under laboratory ambient conditions, and extrapolated to field conditions. Criteria are given for diode reliability.

R. Mueller, of JPL, reported the development of the capability for measurement under global irradiance spectral distribution. He also described the status of the international round robin of reference cell measurements managed by the Commission of European Communities (CEC).

J. Lathrop, of Clemson University, discussed the work at Clemson on reliability testing of solar cells. Results are given on initial temperature and humidity tests of amorphous silicon devices.

Q. Kim, of JPL, presented results obtained in applying the unique characteristics of the solar-cell laser scanner to investigate the defects and quality of amorphous silicon cells.

D. Burger, of JPL, described the application of PVARRAY, a software program for design of PV arrays. Results of sample parametric studies on array configurations were presented.

PRECEDING PAGE BLANK NOT FILMED

HIGH-EFFICIENCY MODULE DESIGN

SPIRE CORP.

M.B. Spitzer

Principal Results

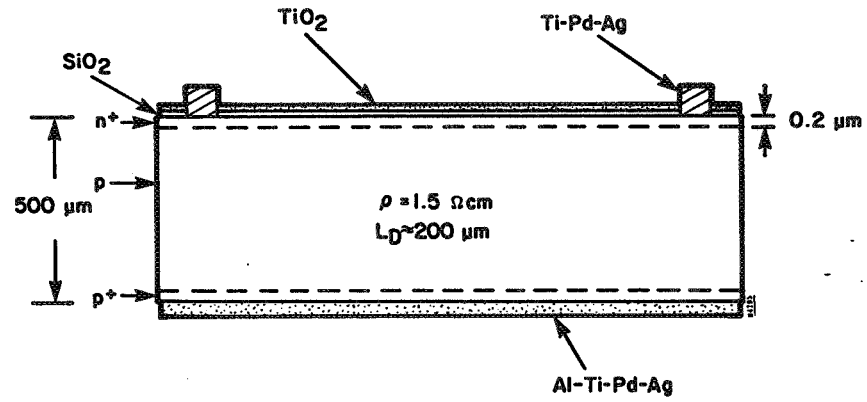
- FABRICATED MODULE WITH HIGH SUB-BANDGAP REFLECTIVITY AND EFFICIENCY OF 13.7%.
- FABRICATED LARGE-AREA CELLS WITH EFFICIENCY OVER 18%.

Objectives

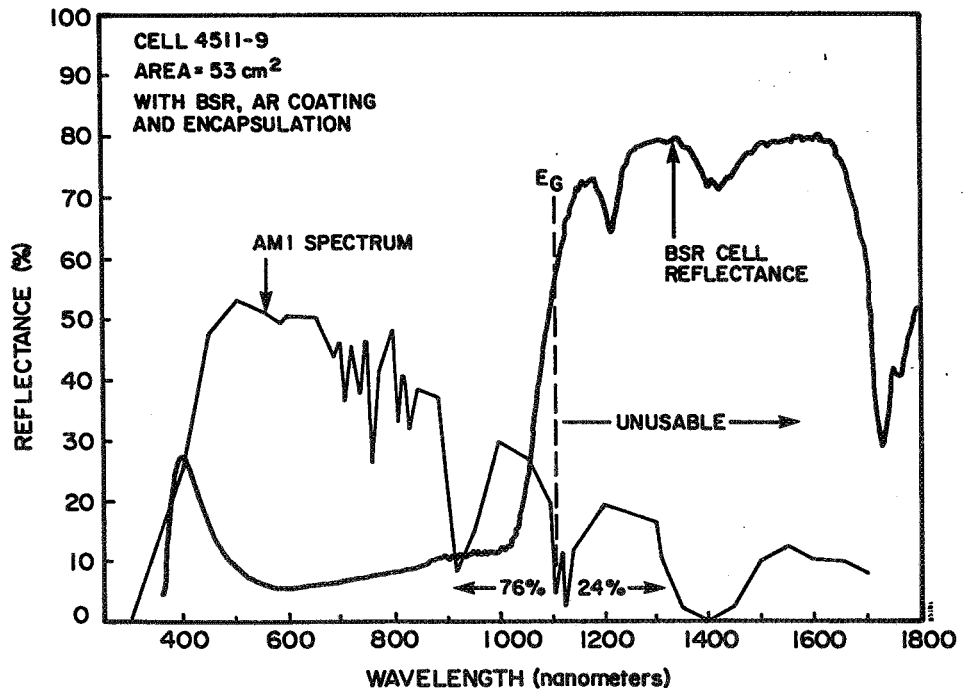
- FABRICATION OF MODULES WITH EMPHASIS ON REDUCED OPERATING TEMPERATURE.
- FABRICATION OF HIGHLY EFFICIENT MODULES.
- EVALUATION OF POSSIBLE TRADE-OFF BETWEEN HIGH EFFICIENCY AND LOW NOCT.

PRECEDING PAGE BLANK NOT FILMED

Cell Design



- AI USED FOR BSR
- SiO₂ USED TO PASSIVATE SURFACE
- p⁺ SIMPLE OHMIC CONTACT (NOT BSF)
- NO EDGE PASSIVATION USED



Assembly Performance

**(AM1.5, 100 mW/cm², T= 25°C)
Tested by JPL**

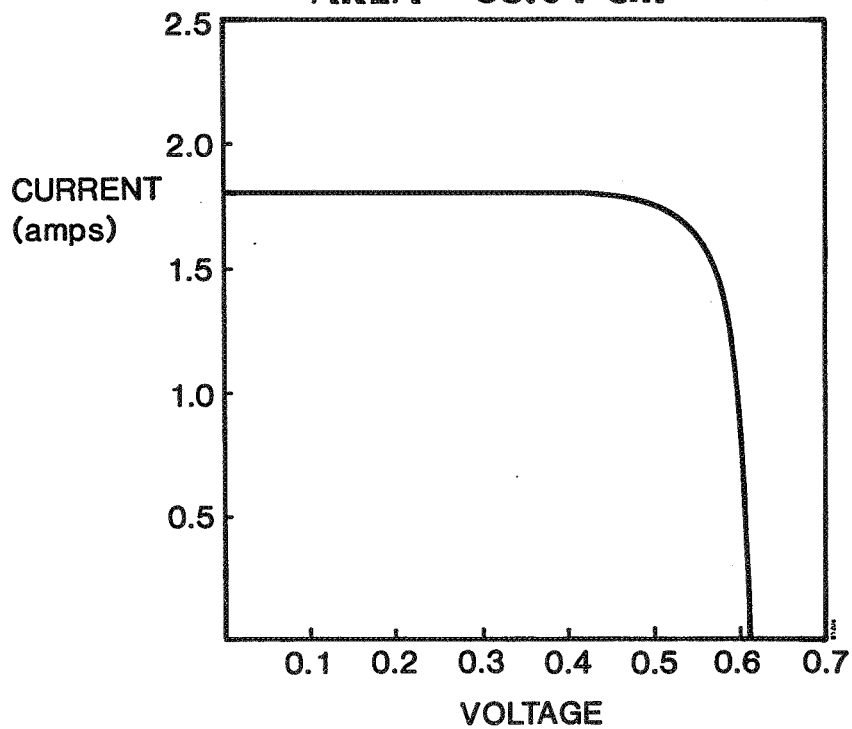
Eff = 17.1%

V_{oc} = 611 mV

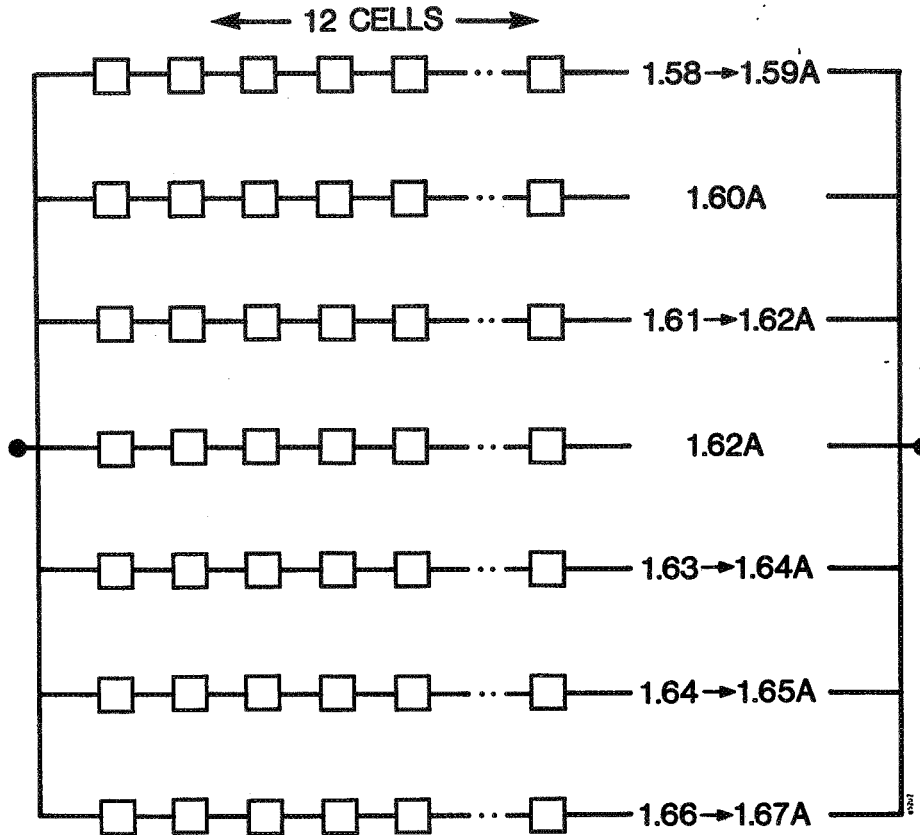
J_{sc} = 34 mA/cm²

FF = 82.5%

AREA = 53.04 cm²



Module Circuit and Mismatch Loss



**I_{mp} OF EACH CELL WITHIN
1% OF THE STRING AVERAGE.**

**ALL STRINGS HAVE ΣV_{mp}
of $6.053 \pm .001$ mV.**

AVE. Eff = 15.4%

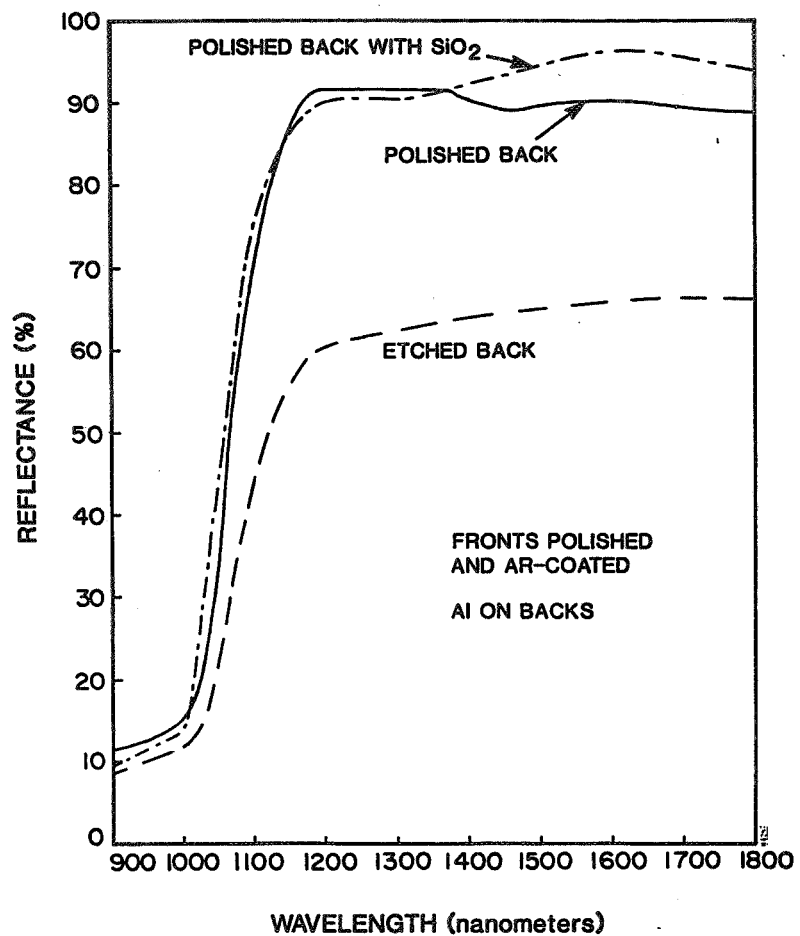
Options in Cell Design

- POLISHED VERSUS TEXTURE
 - POLISHED YIELDS BEST SUB-BANDGAP REFLECTION
 - TEXTURE YIELDS LOWER OVERALL REFLECTION

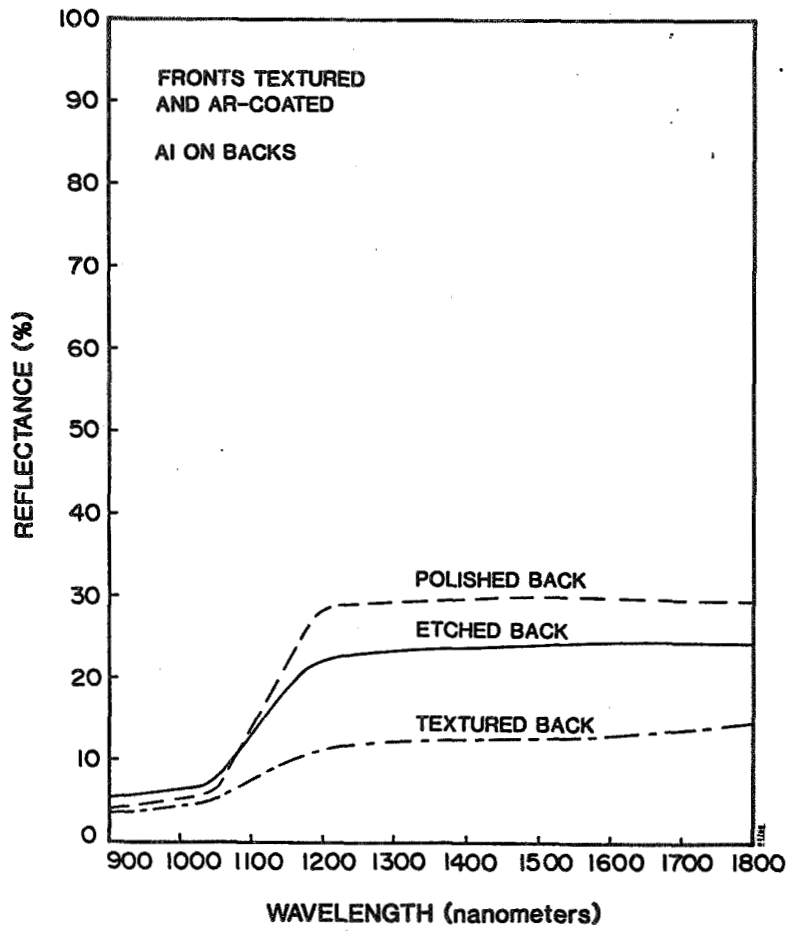
- LOW RESISTIVITY SILICON ($\sim 0.3\Omega\text{cm}$)
 - HIGHER V_{oc} POSSIBLE
 - REQUIRES PRECISE DOPING

- REDUCE THICKNESS, ADD BACK PASSIVATION
 - YIELDS PROBLEMS?
 - REQUIRES PRECISE DOPING
 - OFFERS HIGHER EFFICIENCY

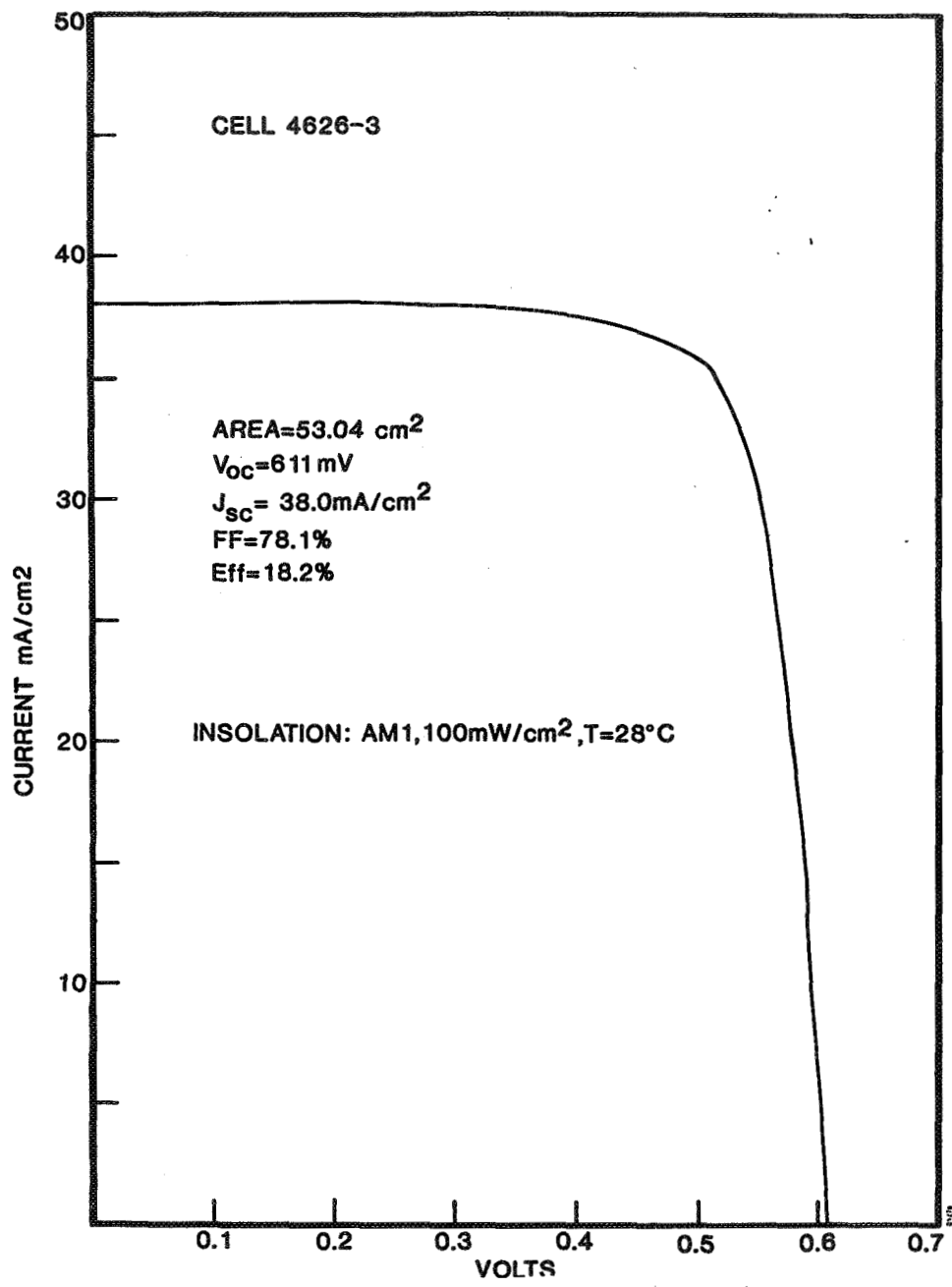
MODULE DEVELOPMENT AND ENGINEERING SCIENCES



MODULE DEVELOPMENT AND ENGINEERING SCIENCES



MODULE DEVELOPMENT AND ENGINEERING SCIENCES



Furnace-Annealed Texture-Etched Large-Area Cells

<u>V_{oc}</u> <u>(V)</u>	<u>I_{sc}</u> <u>(A)</u>	<u>J_{sc}</u> <u>mA/cm²</u>	<u>FF</u> <u>(%)</u>	<u>Eff</u> <u>(%)</u>
0.610	2.001	37.7	77.5	17.8
0.611	2.018	38.0	78.1	18.2
0.606	1.986	37.4	77.5	17.6
0.602	1.933	36.5	78.1	17.1
0.610	2.016	38.0	78.4	18.2
0.604	1.965	37.1	77.7	17.4
0.610	2.011	37.9	77.7	18.0
0.609	2.028	38.2	77.5	18.1
0.609	2.014	38.0	76.5	17.7
0.609	2.013	38.0	77.9	18.0
0.611	2.026	38.2	77.8	18.2
0.606	1.964	37.0	77.8	17.5
0.608	1.985	37.4	76.9	17.5
0.607	2.018	38.0	76.2	17.6
0.611	2.033	38.3	77.4	18.1
0.606	1.980	37.3	77.4	17.5
0.609	2.022	38.1	77.5	18.0
0.609	2.011	37.9	78.3	18.1
0.610	2.029	38.2	77.0	18.0
0.607	1.984	37.4	77.5	17.6
0.601	1.930	36.4	76.6	16.7
0.603	1.959	36.9	76.2	17.0
0.608	1.997	37.6	77.4	17.7
0.003	0.031	0.6	0.6	0.4

NOTES: AREA=53cm². T=28 C. INSOLATION
WAS SIMULATED AM1, 100mW/cm².

Projections for Module Made of Texture-Etched Cells

	POLISHED CELLS (ACTUAL)	TEXTURED CELLS (PROJECTED)
AVERAGE CELL EFFICIENCY	15.4%	17.7%
PACKING FACTOR (90%)	13.9%	15.9%
INTERCONNECT LOSSES (1.4%)	13.7%	15.7%

Conclusions

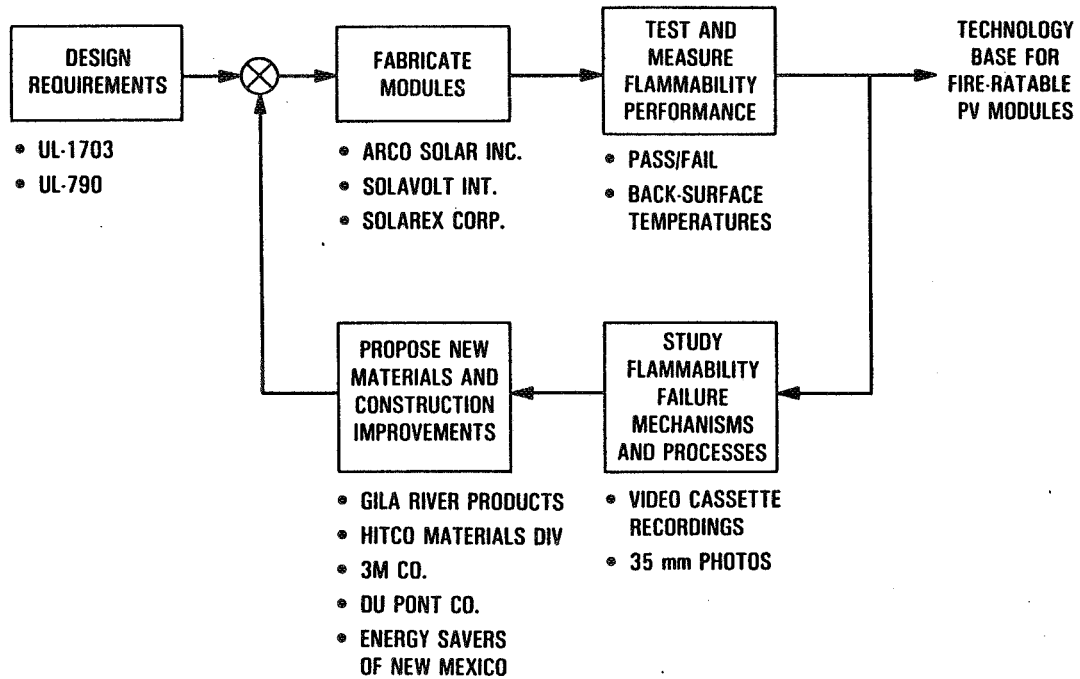
- BSR CELLS OFFER HIGH REFLECTION OF SUB-BANDGAP PHOTONS.
- ENCAPSULATED CELL EFFICIENCY OF 17.1% HAS BEEN ACHIEVED, WITH A 53cm² CELL (MEASURED AT JPL).
- MODULE EFFICIENCY OF 13.7% HAS BEEN ACHIEVED, NOCT IS 45°C (MEASURED AT JPL).
- TEXTURED CELL EFFICIENCY OF 18.2% HAS BEEN ACHIEVED WITH A 53cm² CELL.
- MODULE EFFICIENCY GREATER THAN 15% IS REALISTIC IN THE VERY NEAR FUTURE.

MODULE FLAMMABILITY RESEARCH

JET PROPULSION LABORATORY

R. S. Sugimura
D. H. Otth

Approach



Tests for Fire Resistance of Roof Covering Materials (UL-790)

Fire Rating	Spread-of-Flame Test			Burning-Brand Test		
	Flame Temperature, °F	Flame Application Time, min	Allowable Flame Spread Distance, ft	Brand Size, in.	Brand Ignition Temperature, °F	Approximate Peak Module Temperature, °F
Class A	1400	10	≤ 6	12 x 12 x 2½	1630	1900
Class B	1400	10	≤ 8	6 x 6 x 2½	1630	1400
Class C	1300	4	≤ 13	1½ x 1½ x 25/32	—	—

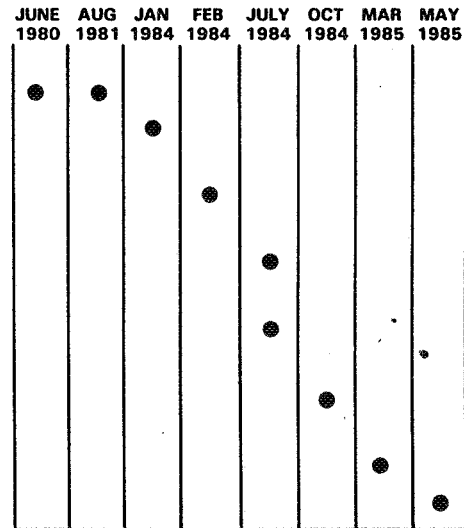
Spread-of-flame test – distance that flame has spread. No flaming or glowing brands of roof material

Burning-brand test – until flame, glow and smoke disappear. No sustained flaming on underside, production of flaming, or glowing brands of roof material

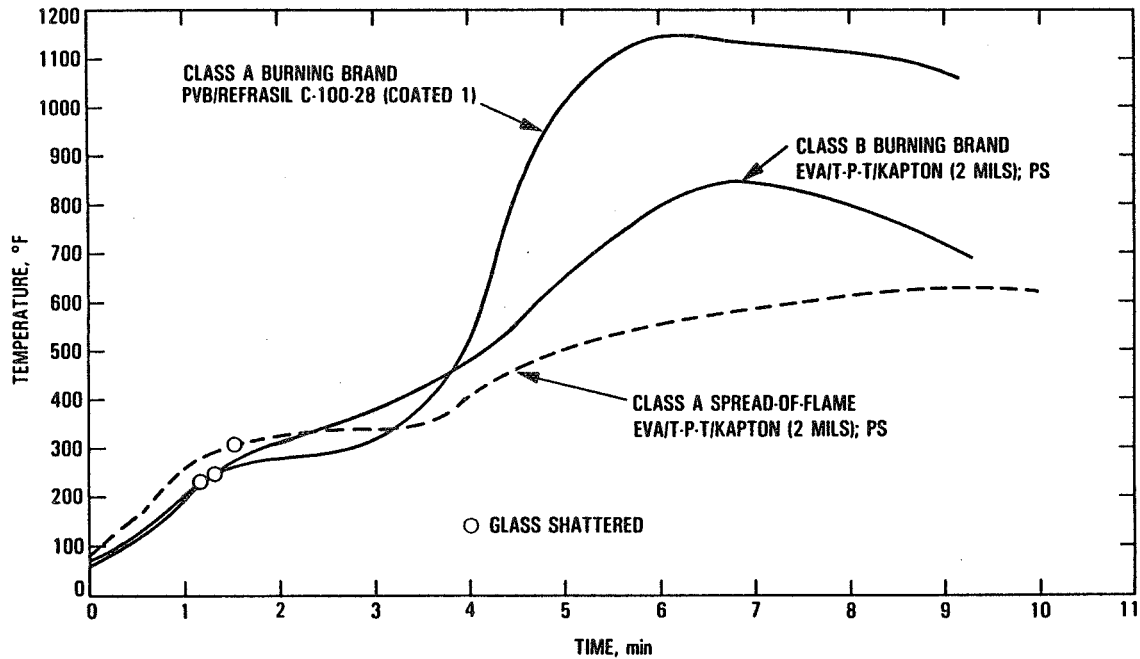
Chronological Overview

Test phases

- Exploratory (uninstrumented)
- Diagnostic (instrumented)
- Experimental modules:
 - Characterize Burning Brand, Class B
 - Identify lower-cost materials, Burning-Brand, Class B
 - Characterize Spread-of-Flame, Classes A and B
 - Characterize Burning-Brand, Class A
 - Identify lower-cost materials, Burning-Brand, Class A
 - Assess impact on module edges



Module Back-Surface Temperature History



Flammability Test Highlights

Pottant ^a	Back-Cover Configuration ^b	Flame	"B" Brand	"A" Brand
EVA EVA	T-P-T/Kapton (2 mils); PS T-P-T/Kapton (2 mils); TS	●	● ○	○
EVA PVB	Kapton (2 mils) Kapton (2 mils)	●	● ○	
EVA EVA	Al (3 mils) in. 4-layer laminate T-P-T/SS (2 mils)		● ●	○ ●
EVA EVA EVA EVA	T-P-T/FG; TS T-P-T/FG; PS FG - Silicone rubber (1 side) FG - Neoprene rubber (1 side)	● ●	● ○ ● ●	
EVA, PVB	Refrasil FG (15 mils) - Z-mix (1 side)			●
EVA, S, PVB	FG (24 mils) - Z-mix (1 side)			●
EVA, S, PVB	FG (13 mils) - Z-mix (1 side)			●
EVA, S, PVB	FG (7 mils) - Z-mix (2 sides)			●

● = passed ○ = failed

^aEVA - ethylene vinyl acetate; PVB - polyvinyl butyral; S - Pottant S (Solavolt Int.)

^bT-P-T - Tedlar-polyester-Tedlar; PS - pressure sensitive; TS - Thermoset; SS - stainless steel; FG - fiberglass; Al - aluminum; Z-mix - proprietary HITCO coating

Candidate Materials for Fire-Ratable Modules

Back-Cover Material Description ^a	Manufacturer	≈ \$/ft ²
Class B		
Kapton (2 mils)	DuPont 200H	0.75
Vonar/Surmat/Conbond 1560/T (4 mils)	DuPont	—
FG (4 mils) — red silicone rubber (1 side)	3M SRG-0607 1/c	1.08-0.76
FG (4 mils) — Neoprene rubber (1 side)	3M FGN-0605 1/c	0.80-0.64
Mylar/Al (0.7 mils)/rubberized back coat	Spire Block IV	—
Al (3 mils) in 4-layer laminate	—	—
T (1½ mils) — Mylar (5 mils) — Al (0.5 mils) — EVA (4 mils)	Gila River — Solar 2	0.80
T (1½ mils) — FG (8 mils — epoxy) — T (1½ mils) ^b	Gila River — Solar 5	—
Class A		
Refrasil (15 mils) — Z-mix (1 side)	HITCO C100-28 w/Z-mix	2.22
FG (24 mils) — Z-mix (1 side)	HITCO 1584 w/Z-mix	1.42
FG (13 mils) — Z-mix (1 side)	HITCO 1582 w/Z-mix	1.12
FG (7 mils) — Z-mix (2 sides)	HITCO Solar-Tex	0.63-0.73 ^c
Stainless steel foil (2 mils)	—	0.45

^a T — Tedlar; FG — fiberglass; Al — aluminum; EVA — ethylene vinyl acetate

^bPossible candidate for Class A. ^cPrice varies according to color: black/black; white/white; black/white

Summary

- Fire-resistant module designs require special high-temperature materials and constructions to achieve Class B and Class A ratings
- Synergisms exist between back-surface materials and module configuration
 - Amount of pottant
 - Type of adhesive
 - Edge seals

Future Work

- Test durability and reliability performance of selected candidates
- Test module edge-seal materials and configurations

DEVELOPMENT OF DESIGN CRITERIA AND A QUALIFICATION TEST FOR BYPASS DIODES

JET PROPULSION LABORATORY

D. H. Otth

Objectives

- Define specific design criteria for bypass diodes in PV applications to ensure acceptable field reliability
- Develop a qualification test for assessing conformance to design criteria
 - Diodes integral with module
 - Externally mounted diodes
- Use test procedure to assess diode and heat-sink adequacy in a variety of modules and refine the qualification test

Design Criteria

DIODE JUNCTION TEMPERATURE ALLOWABLES

DIODE TYPE	MAXIMUM ALLOWABLE JUNCTION TEMPERATURE	DERATED TEMPERATURE FOR LONG-TERM RELIABILITY
p-n	175°C	125°C
Schottky	125°C	75°C
APPLICABLE FIELD CONDITIONS	100 mW/cm ² 40°C 1.5 I _{sc}	100 mW/cm ² 40°C 1.0 I _{sc}

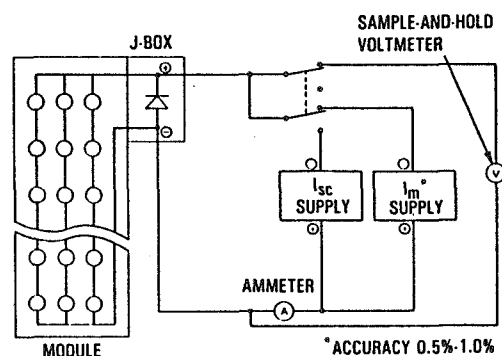
Qualification Test Approach

- Develop test to determine diode junction temperature in situ using readily available laboratory test instruments
 - Use diode forward-voltage drop versus temperature to sense junction temperature
 - Extrapolate temperature to 100 mW/cm², 40°C field thermal conditions from laboratory temperature using NOCT relationships

Method for Assessing Design Conformance

- (1) Simulate field thermal conditions by heating module front surface with IR radiant heaters to obtain predicted module temperature rise above ambient for 100 mW/cm² irradiance
- (2) Apply test current 1.5 I_{SC} or 1.0 I_{SC} to diode until thermal equilibrium is reached
- (3) Sense the diode junction temperature (T_j) by measuring forward voltage drop across junction at a fixed, known current level (I_m)
Oven characterization tests used to obtain diode temperature vs voltage drop curve
- (4) Compute junction temperature under 40°C ambient conditions as T_j + 40°C minus the test environment ambient temperature (i.e., T_{Room})

Test Circuit for Measuring Bypass Diode Junction Temperature



Junction Temperature Assessments of Various Heat-Sinked Bypass Diodes for 100 mW/cm², 40°C Field Conditions

Module and Heat-Sink Design			Derated Temp (T _j) _D (125°C Limit)		Max Operating Temp (T _j) _{max} (175°C Limit)	
Module Type	P-n Diode Location	NOCT °C	1.0 I _{sc} A	(T _j) _D °C	1.5 I _{sc} A	(T _j) _{max} °C
A	Across Terminals, in Junction Box	46	2.27	83	3.40	105
B	Bracket in Junction Box	54	12.02	122	—	—
C	P-C Board in Junction Box	49	5.30	186	7.95	234
D	Module Frame	56	6.80	140	10.30	185
E	Bracket in Junction Box	47	5.3	130	7.95	169
F	Across Terminals, in Potted J-Box	51	1.44	57	2.16	79
G	Across Bus Bar Ends in Laminate Assembly	47	7.1	234	—	—
H	External Assembly Diode	—	1 X 60	91	1 X 90	128
		—	2 X 60	102	2 x 90	142

Conclusions

- Proposed qual test worked well with a wide variety of bypass diode mounting configurations
- Wide variability of performance obtained from module/diode test set
 - 3 devices: junction temperatures well below limits
 - 2 devices: close to limits, i.e., 1 marginally under and 1 marginally over
 - 3 devices: well beyond the limits
- Diodes meeting the 125°C derated limit at 1.0 I_{sc} easily passed the 175°C maximum operating temperature limit at 1.5 I_{sc}
 - Derated junction temperature limit of 125°C is the more stringent design criterion
- Properly heat-sinked diodes can easily meet the design criteria

MODULE DEVELOPMENT AND ENGINEERING SCIENCES

Future Work

- **Continue to refine steps in test method to establish a detailed qualification test procedure**
- **Include bypass diode performance criteria and test procedure in Block VI module design and test specification**

DEVELOPMENT OF AM 1.5 GLOBAL MEASUREMENT PROCEDURES AND INTERNATIONAL CELL MEASUREMENT ROUND ROBIN

JET PROPULSION LABORATORY

R. Mueller

Spectral Irradiance (JPL Unfiltered LAPSS)

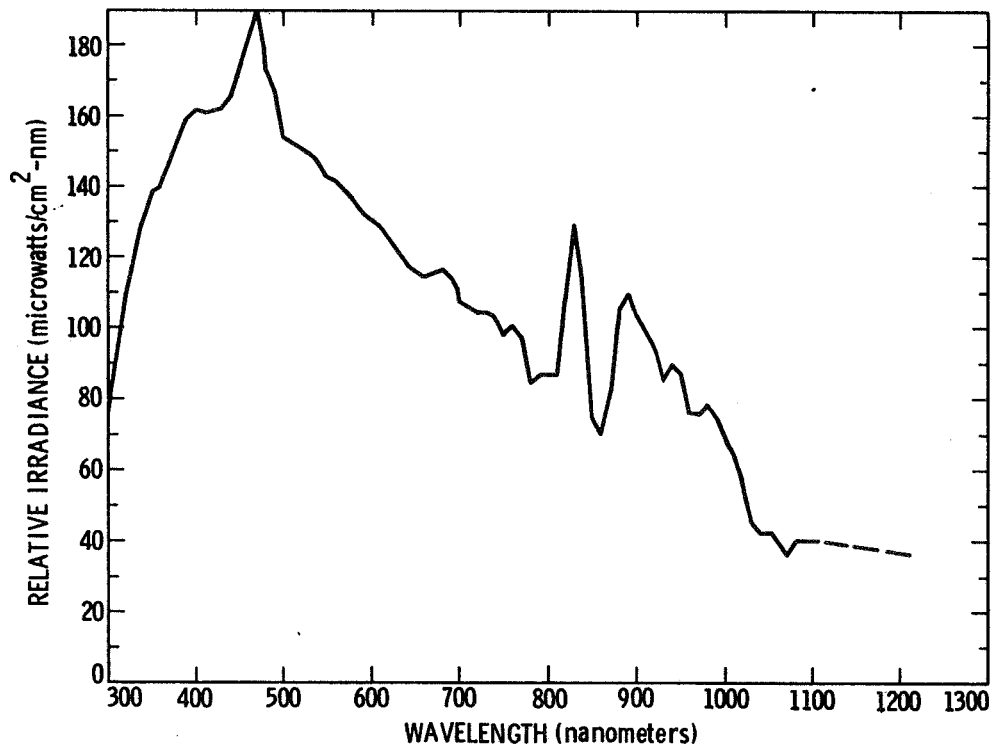


FIGURE 1

Spectral Irradiance (AM 1.5 Direct LAPSS Versus ASTM AM 1.5 Direct)

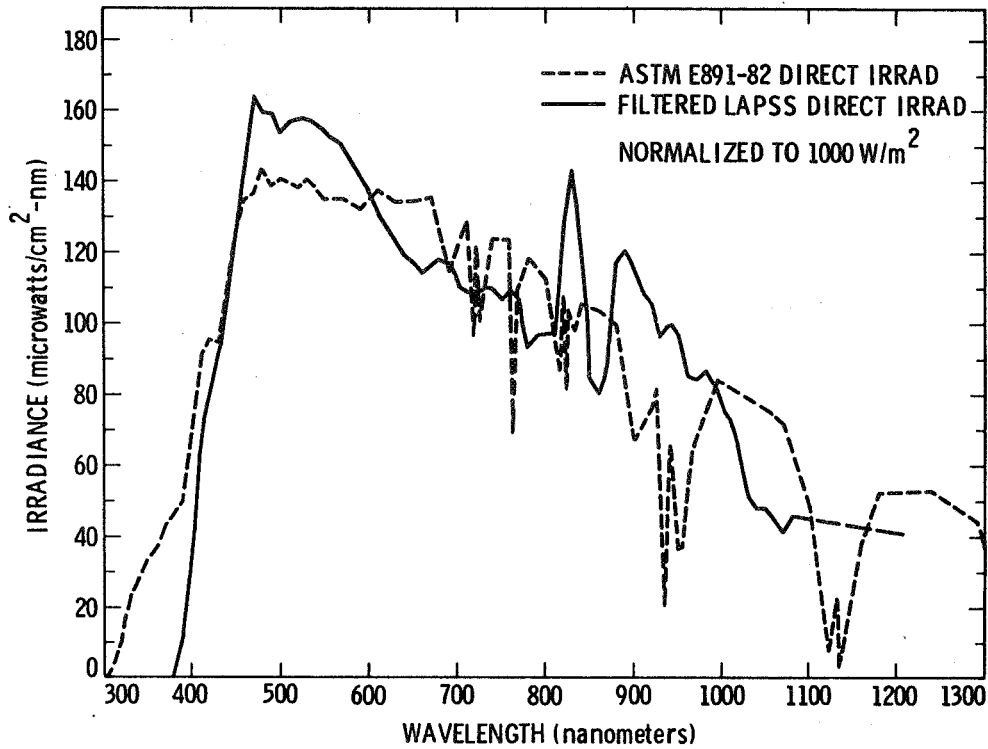


FIGURE 2

Spectral Distribution of Irradiance Performance
 JPL AM 1.5 Direct Filtered LAPSS (0.4 to 1.1 μm)

PERCENT OF TOTAL IRRADIANCE BETWEEN 0.4 μm AND 1.1 μm
 FOR NORMALIZED IRRADIANCE CURVES

WAVELENGTH INTERVAL, μm	(1) ASTM E 891-82 AM 1.5 DIRECT SPECTRUM	(2) JPL AM 1.5 DIRECT FILTERED LAPSS	RATIO (2) / (1)
0.4 to 0.5	16.0	15.8	0.989
0.5 to 0.6	18.6	20.2	1.085
0.6 to 0.7	18.0	16.1	0.893
0.7 to 0.8	15.5	14.0	0.905
0.8 to 0.9	13.3	14.4	1.083
0.9 to 1.1	18.6	19.5	1.046

Airmass 1.5 Global Measurement Procedure

1. TYPE II (SECONDARY) CALIBRATION USING ASTM 130
2. LIGHT SOURCE IS THE JPL AM 1.5 GLOBAL FILTERED LAPSS
3. PRIMARY REFERENCE CELL CALIBRATED IN DIRECT NORMAL SUNLIGHT BY COMPARISON TO A NORMAL INCIDENCE PYRHELIOMETER USING ASTM 130
4. CALIBRATION VALUE OF PRIMARY REFERENCE CELL ADJUSTED MATHEMATICALLY TO THE ASTM E 892-82 GLOBAL SPECTRUM
5. TEMPERATURE OF PV DEVICE AND REFERENCE CELL ARE CONTROLLED

Adjustment of Primary Reference Cell (Direct Normal Calibration, DV_d , for a Global Calibration, DV_g)

$$CV_g = CV_d \frac{\int E_g(\lambda) R_r(\lambda) d\lambda \cdot \int E_d(\lambda) d\lambda}{\int E_d(\lambda) R_r(\lambda) d\lambda \cdot \int E_g(\lambda) d\lambda}$$

WHERE:

$E_d(\lambda)$ IS THE ABSOLUTE SPECTRAL IRRADIANCE FOR AM 1.5 DIRECT NORMAL, ASTM E 891-82

$E_g(\lambda)$ IS THE ABSOLUTE SPECTRAL IRRADIANCE FOR AM 1.5 GLOBAL, ASTM E 892-82

$R_r(\lambda)$ IS THE SPECTRAL RESPONSE OF THE PRIMARY REFERENCE CELL

Why Use Secondary Calibration in JPL LAPSS?

1. PRIMARY CALIBRATION IN SUNLIGHT VERY TIME CONSUMING
2. ONLY A LIMITED SUNLIGHT CALIBRATION OF A PRIMARY REFERENCE CELL IS NECESSARY
3. THE JPL LAPSS IS FILTERED TO CLOSELY MATCH THE AM 1.5 GLOBAL SPECTRUM
4. TEMPORAL STABILITY OF THE FILTERED LAPSS IS EXCELLENT
5. PRIMARY REFERENCE CELL NOT REQUIRED TO BE SPECTRALLY MATCHED TO THE PV DEVICE BEING CALIBRATED
6. LOWER COST AND MORE TIMELY METHOD FOR PROVIDING REFERENCE CELLS

Spectral Irradiance (AM 1.5 Global LAPSS Versus ASTM AM 1.5 Global)

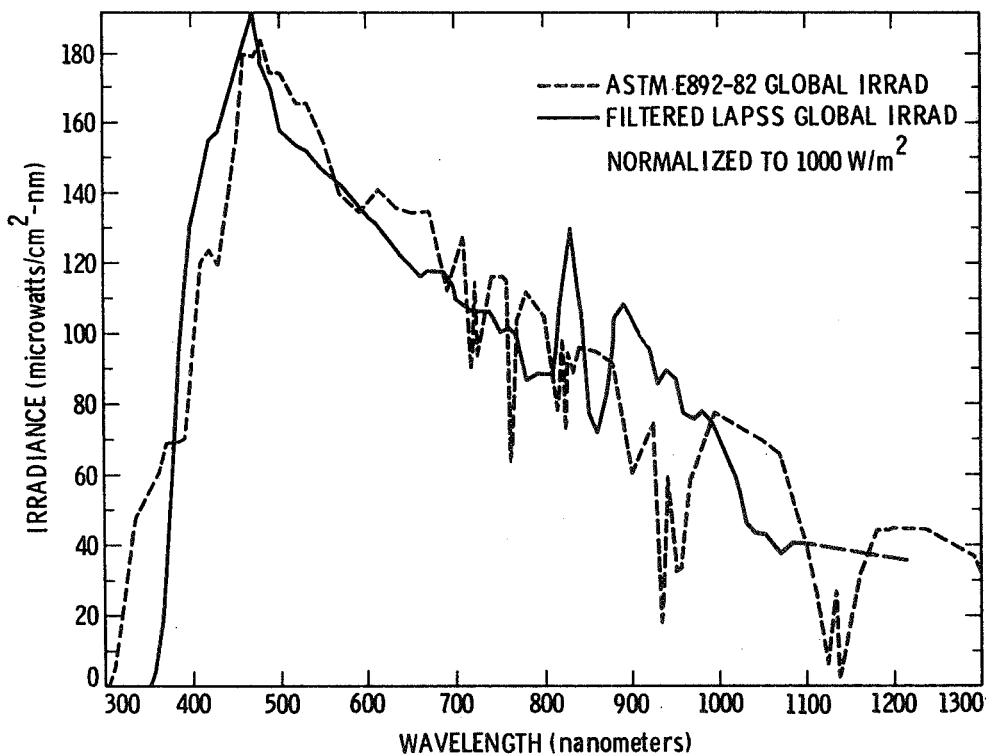


FIGURE 3

Spectral Distribution of Irradiance Performance
 JPL AM 1.5 Global Filtered LAPSS (0.35 to 1.1 μm)

PERCENT OF TOTAL IRRADIANCE BETWEEN 0.4 μm AND 1.1 μm
 FOR NORMALIZED IRRADIANCE CURVES

WAVELENGTH INTERVAL, μm	(1) ASTM E 892-82 AM 1.5 GLOBAL SPECTRUM	(2) JPL AM 1.5 GLOBAL FILTERED LAPSS	RATIO (2) / (1)
0.4 to 0.5	20.0	21.8	1.090
0.5 to 0.6	20.4	19.3	0.946
0.6 to 0.7	17.5	16.0	0.914
0.7 to 0.8	14.3	13.2	0.923
0.8 to 0.9	11.8	12.9	1.093
0.9 to 1.1	16.0	16.8	1.050

Spectral Distribution of Irradiance Performance
 JPL AM 1.5 Global Filtered LAPSS (0.4 to 1.1 μm)

PERCENT OF TOTAL IRRADIANCE BETWEEN 0.35 μm AND 1.1 μm
 FOR NORMALIZED IRRADIANCE CURVES

WAVELENGTH INTERVAL, μm	(1) ASTM E 892-82 AM 1.5 GLOBAL SPECTRUM	(2) JPL AM 1.5 GLOBAL FILTERED LAPSS	RATIO (2) / (1)
0.35 to 0.4	4.3	3.8	0.884
0.4 to 0.5	19.1	21.0	1.099
0.5 to 0.6	19.5	18.5	0.949
0.6 to 0.7	16.8	15.4	0.917
0.7 to 0.8	13.7	12.7	0.927
0.8 to 0.9	11.3	12.4	1.097
0.9 to 1.1	15.3	16.2	1.059

MODULE DEVELOPMENT AND ENGINEERING SCIENCES

CEC Round Robin

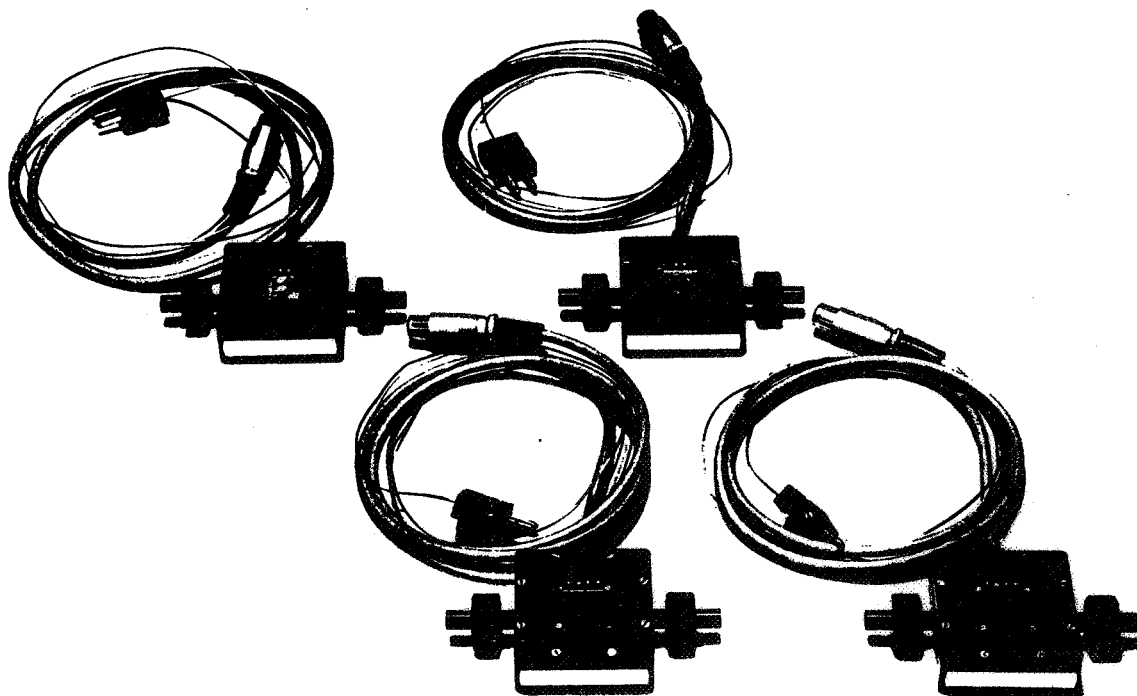
MANAGED BY: COMMISSION OF THE EUROPEAN COMMUNITIES
JOINT RESEARCH CENTRE
ISPRA ESTABLISHMENT
21020 ISPRA (VARESE) ITALY

OBJECT: TO RESOLVE DISAGREEMENT IN MEASUREMENTS

REFERENCE CELLS PROVIDED BY:

4 CELLS	AMORPHOUS SILICON	JMI (JAPAN MACHINERY & METALS INSPECTION INSTITUTE)
5 CELLS	MONO & POLYCRYSTALLINE	ENEA (NUCLEAR & ALTERNATIVE ENERGY AGENCY), ITALY
2 CELLS	POLYCRYSTALLINE SILICON	AEG (TELEFUNKEN) GERMANY
3 CELLS	MONOCRYSTALLINE SILICON	PW (PHOTOWATT ORGANIZATION), FRANCE
4 CELLS	MONO & POLYCRYSTALLINE	JPL (JET PROPULSION LABORATORY), USA

18 CELLS TOTAL



ORIGINAL PAGE IS
OF POOR QUALITY



CEC Round Robin Measurements Timetable

UNTIL AUG 7, 1984	JRC (JOINT RESEARCH CENTRE) ISPRA, ITALY
AUG 15 - SEPT 15, 1984	RAE (ROYAL AIRCRAFT ESTABLISHMENT), UNITED KINGDOM
SEPT 15 - OCT 15, 1984	CNES (NATIONAL CENTRE FOR SOLAR ENERGY), FRANCE
OCT 15 - NOV 15, 1984	ENEA (NUCLEAR AND ALTERNATIVE ENERGY AGENCY), ITALY
NOV 15 - DEC 15, 1984	DFVLR (RESEARCH & EXPERIMENT INSTITUTE FOR AIR & SPACE TRAVEL), GERMANY
JANUARY 1985	NRC (NATIONAL RESEARCH CENTRE), CANADA
FEBRUARY 1985	JPL (JET PROPULSION LABORATORY), USA
MARCH 1985	JMI (JAPAN MACHINERY & METALS INSPECTION INSTITUTE), JAPAN
APRIL 1985	JRC (JOINT RESEARCH CENTRE) ISPRA, ITALY

MODULE DEVELOPMENT AND ENGINEERING SCIENCES

Summary of the JPL Global I_{sc} Values for Summit Round Robin Cells (In mA @ 100 mW/cm² Irradiance)

CELL NUMBER		COLUMN NUMBER AND IRRADIANCE SPECTRUM (SEE COLUMN NOTES BELOW)				
RRC CELL*	JPL REF. CELL	(1) JPL LAPSS GLOBAL	(2) JPL LAPSS GLOBAL	(3) E892-82 (GLOBAL)	(4) E892-xx (GLOBAL)	(5)† IEC (GLOBAL)
1	SS1439B	23.83	23.83	23.90	23.53	23.81
2	SS1439B	24.10	24.10	24.19	23.80	24.09
3	SS1439B	24.81	24.81	24.83	24.43	24.72
4	SS1439B	22.96	22.96	23.08	22.67	22.94
5	SS1440	105.7	105.0	106.2	106.8	108.1
6	SS1440	104.3	103.6	104.8	105.4	106.7
7	SS1440	99.9	99.9	100.6	101.4	102.6
8	SS1440	108.2	108.2	109.7	110.2	111.5
9	SS1440	99.0	97.6	98.4	98.9	100.1
10	SS1440	108.4	106.7	107.6	108.1	109.4
11	SS1440	114.3	114.2	115.5	115.9	117.3
12	SS1440	112.7	111.8	112.6	112.9	114.2
13	SS1440	110.9	110.2	111.0	111.4	112.7
14	SS1440	111.3	110.5	111.3	111.6	112.9
15	SS1440	135.3	135.4	135.5	135.4	137.1
16	SS1440	95.4	95.4	96.0	96.7	97.8
17	SS1440	131.7	131.8	131.8	132.0	133.5
18	SS1440	100.0	100.0	101.3	101.9	103.1

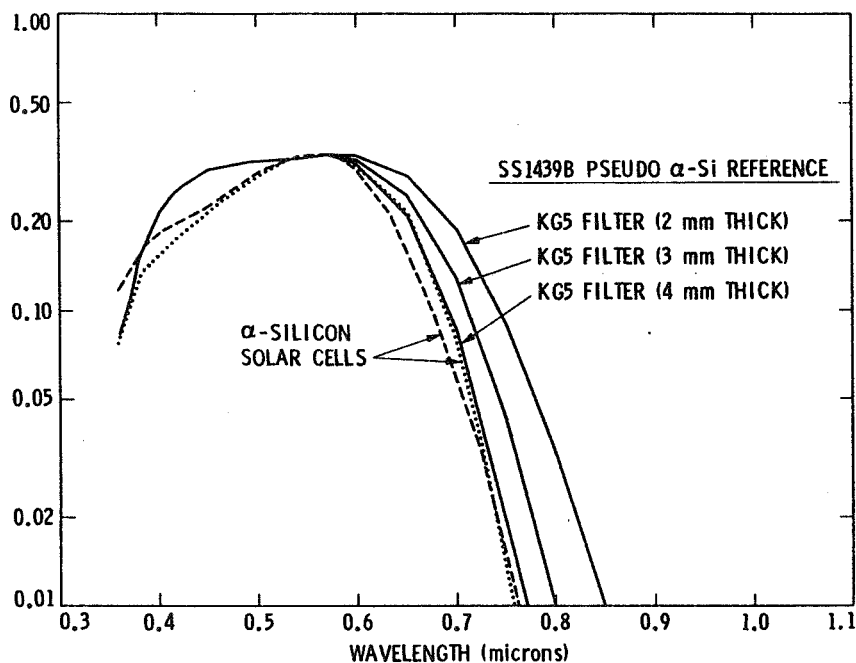
COLUMN NO. I_{sc} EVALUATION METHOD

- (1): MEASUREMENT WITH FILTERED JPL LAPSS SIMULATING ASTM E892-82 SPECTRUM (GLOBAL)
- (2): SAME AS (1) EXCEPT RRC CELL PREVIOUSLY EXPOSED TO SUNLIGHT FOR FIVE MINUTES
- (3): COMPUTATION BY SPECTRAL MISMATCH CORRECTION OF VALUE IN COLUMN (2) TO THE ASTM E892-82 SPECTRUM (GLOBAL)
- (4): COMPUTATION BY SPECTRAL MISMATCH CORRECTION OF VALUE IN COLUMN (2) TO A PROPOSED 1985 REVISION OF ASTM E892-82 SPECTRUM (GLOBAL)
- (5): COMPUTATION BY SPECTRAL MISMATCH CORRECTION OF VALUE IN COLUMN (2) TO THE IEC SPECTRUM (GLOBAL)

* CELLS 1 THROUGH 4 ARE AMORPHOUS SILICON. CELLS 5 THROUGH 18 ARE CRYSTALLINE SILICON.

† THE VALUES IN COLUMN (5) ARE THE JPL CALIBRATION VALUES FOR THE SUMMIT ROUND ROBIN CONDITIONS.

Comparison of Relative Spectral Response

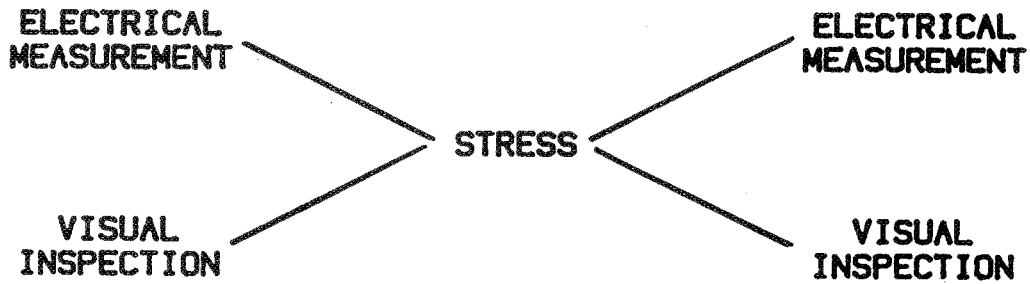


AMORPHOUS-SILICON CELL RELIABILITY TESTING

CLEMSON UNIVERSITY

J. W. Lathrop

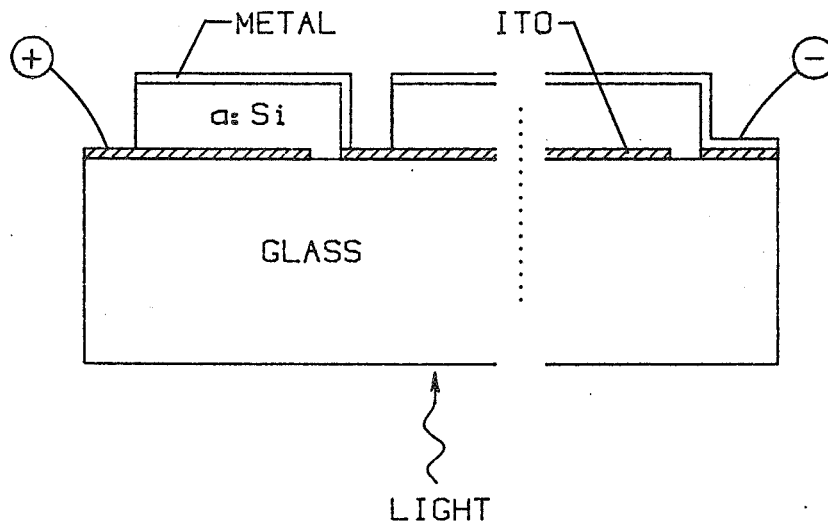
Accelerated Stress Test Methodology



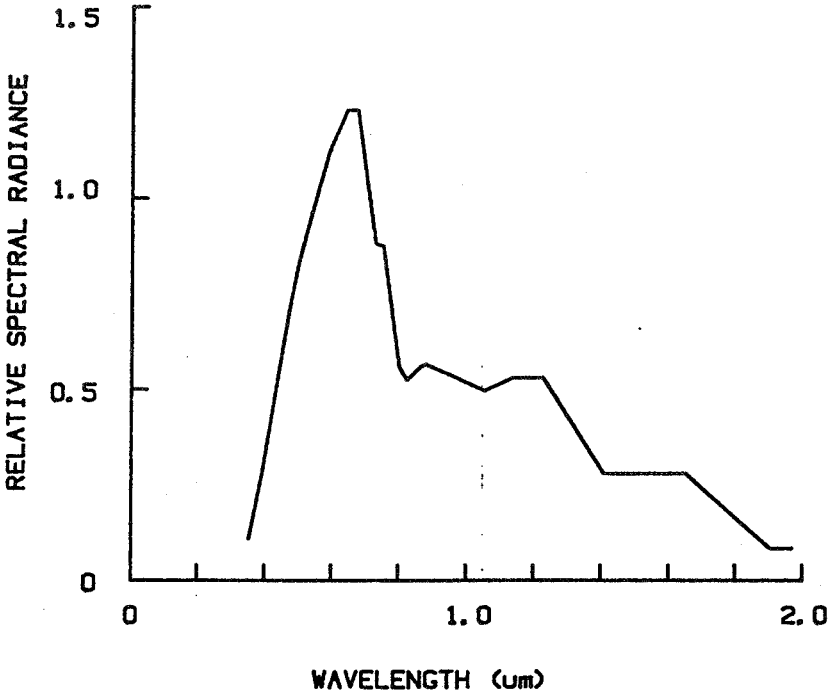
Amorphous-Silicon Problem Areas

MEASUREMENT -- REFERENCE CELL
INSPECTION -- SURFACE ANALYSIS METHODS
STRESS -- TEST SCHEDULE

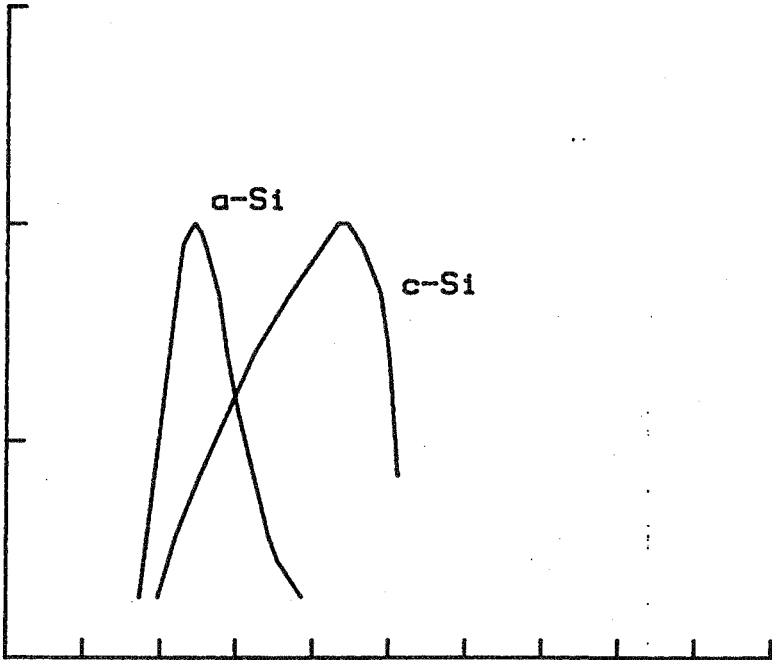
Schematic Diagram of Amorphous-Silicon Monolithic Solar Panel



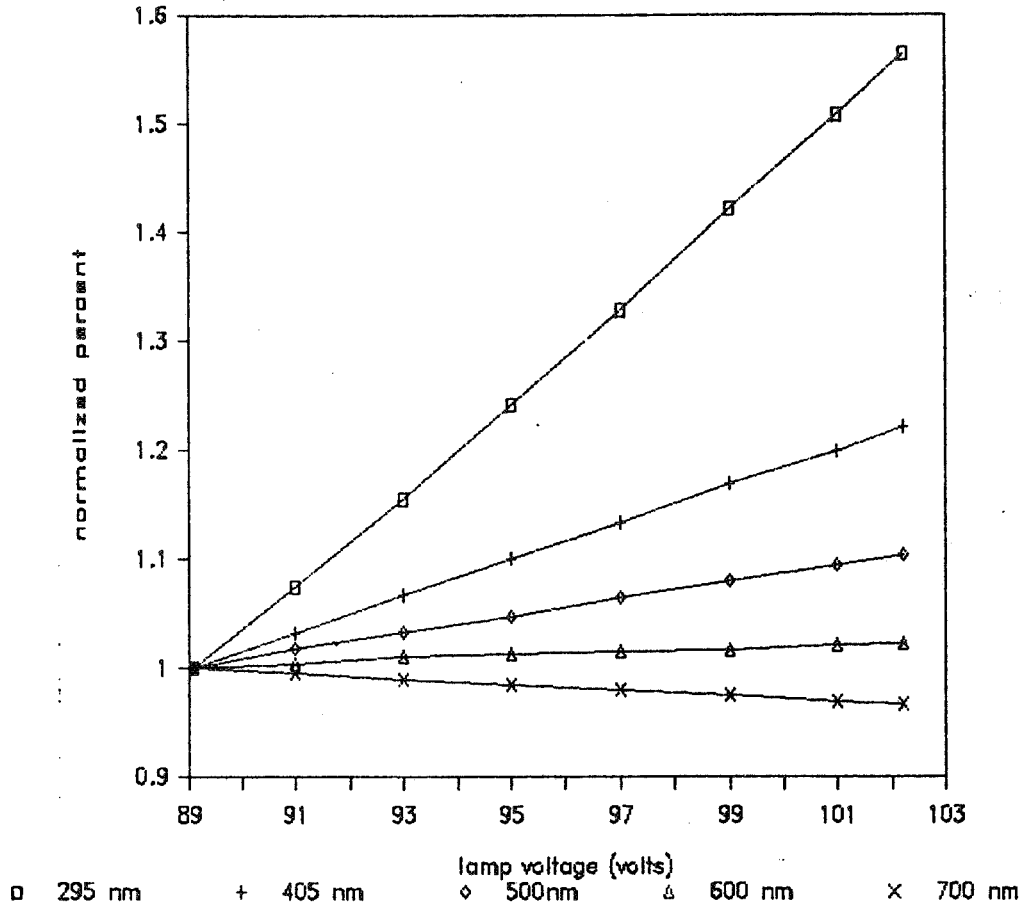
Relative Spectral Distribution of ELH Lamp



Relative Spectral Response



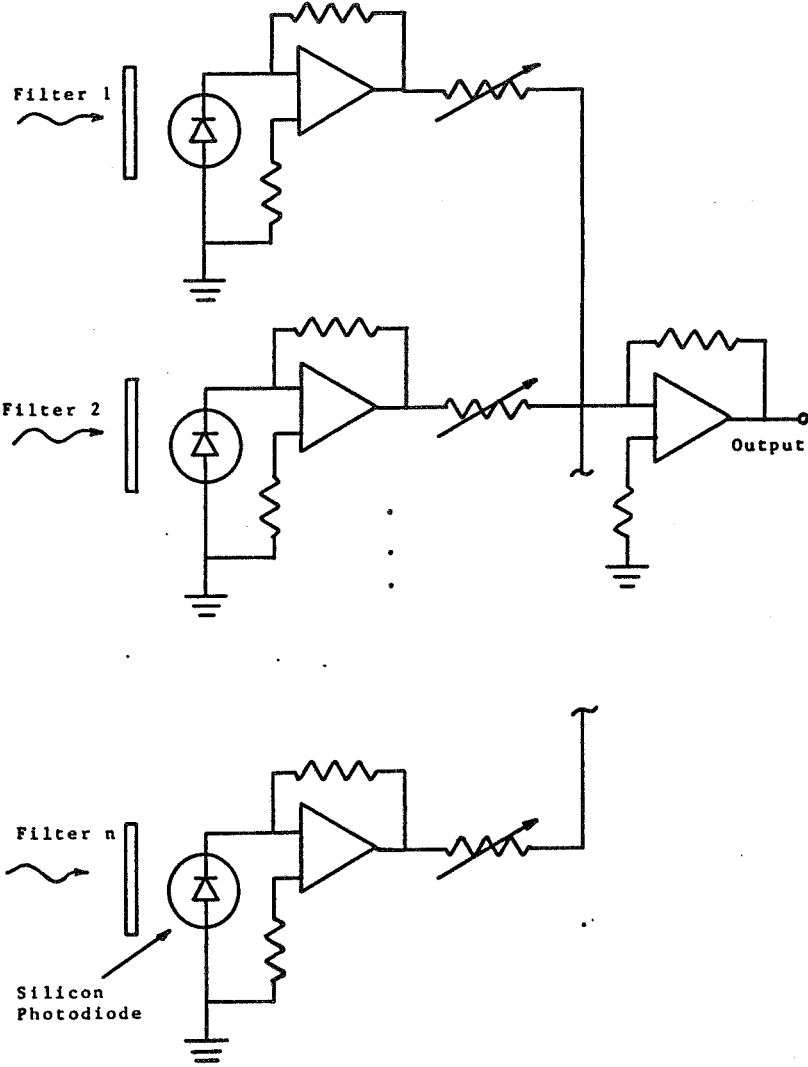
ELH Spectral Content Versus Lamp Voltage



Calibration and Measurement Procedures for Crystalline Cells

	RADIATION TYPE	SOURCE INTENSITY	SOURCE SPECTRAL DIST.	CELL	I(out)
CALIBRATION	NATURAL	1-SUN	1-SUN	SMALL REFERENCE	I_o
	ELH	A	B	SMALL REFERENCE	I_o
	ELH	A	B	FULL STANDARD	I_s
MEASUREMENT	ELH	A'	B'	FULL STANDARD	I_s

Simulated Amorphous Reference Cell



Calibration and Measurement Procedures for Crystalline Cells

	RADIATION TYPE	SOURCE INTENSITY	SOURCE SPECTRAL DIST.	CELL	I(out)
CALIBRATION	NATURAL	1-SUN	1-SUN	SMALL REFERENCE	I_o
	ELH	A	B	SMALL REFERENCE	I_o
	ELH	A	B	FULL STANDARD	I_s
MEASUREMENT	ELH	A'	B'	FULL STANDARD	I_s

Calibration and Measurement Procedures for Amorphous Cells

	RADIATION TYPE	SOURCE INTENSITY	SOURCE SPECTRAL DIST.	CELL	I(out)
SPECTRAL CALIBRATION	ELH	A	B	MFG SAMPLE	$I(1)...I(n)$
	ELH	A	B	SI DIODE REF	$I(1)...I(n)$
INTENSITY CALIBRATION	NATURAL	1-SUN	1-SUN	MFG SAMPLE	I_o
	ELH	A'	B'	MFG SAMPLE	I_o
	ELH	A'	B'	SI DIODE REF	I_s
MEASUREMENT	ELH	A''	B''	SI DIODE REF	I_s

MODULE DEVELOPMENT AND ENGINEERING SCIENCES

IN GENERAL,

$$j = \int_{\text{spectrum}} I(\lambda) \cdot R(\lambda) d\lambda$$

where j = short circuit current density (A/cm^2)
 $I(\lambda)$ = illumination intensity ($W/cm^2/\mu m$)
 $R(\lambda)$ = solar cell response (A/W)

FOR AN a-Si CELL

$$j(a) = I(\lambda_1) R_a(\lambda_1) \Delta\lambda + I(\lambda_2) R_a(\lambda_2) \Delta\lambda + \dots + I(\lambda_n) R_a(\lambda_n) \Delta\lambda$$

FOR A c-Si CELL

$$j(c) = I(\lambda_1) R_c(\lambda_1) \Delta\lambda + I(\lambda_2) R_c(\lambda_2) \Delta\lambda + \dots + I(\lambda_n) R_c(\lambda_n) \Delta\lambda$$

THE PROGRAMMABLE REFERENCE CELL CONSISTS OF n BAND PASS ($\Delta\lambda$) FILTERED DIODES, EACH HAVING A SEPARATE AMPLIFIER (GAIN = A). THE SHORT CIRCUIT CURRENT FROM EACH DIODE IS ADDED TO GIVE A TOTAL CURRENT VALUE OF:

$$i(P) = A_1 I(\lambda_1) R_c(\lambda_1) \Delta\lambda + A I(\lambda_2) R_c(\lambda_2) \Delta\lambda + \dots + A_n I(\lambda_n) R_c(\lambda_n) \Delta\lambda$$

IF THE AMPLIFIER GAINS ARE ADJUSTED IN THE COMPUTER SUCH THAT

$$A_n = C \cdot R_a(\lambda_n) / R_c(\lambda_n)$$

WHERE C IS A CONSTANT SUCH THAT $i(P)$ = CURRENT UNDER 1-SUN ILLUMINATION. THEN

$$i(P) = C \cdot j(a)$$

AND THE FILTERED DIODE ARRAY WILL ACT AS A SIMULATED REFERENCE CELL.

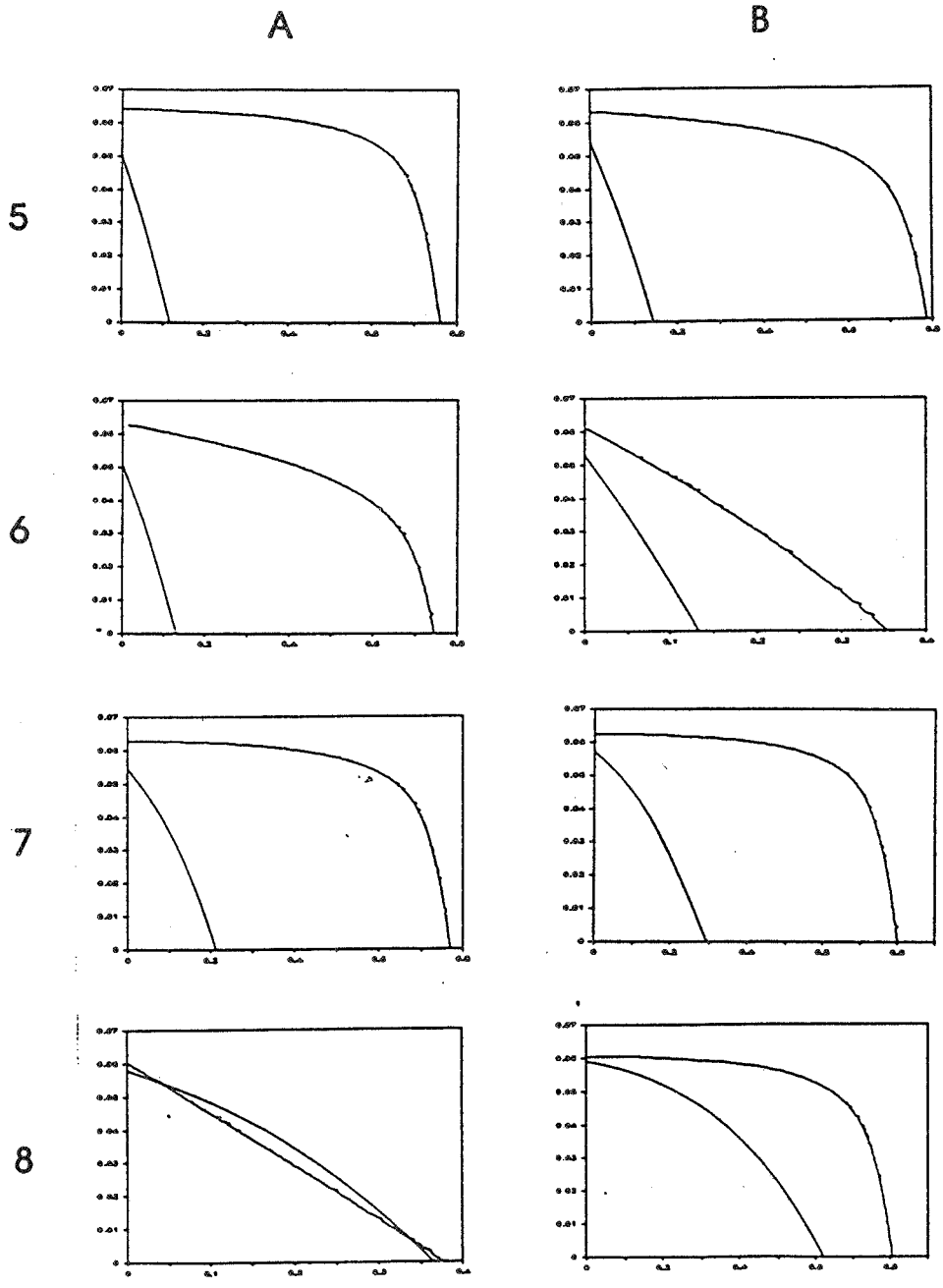
CALIBRATION REQUIRES DETERMINING:

- 1) SPECTRAL RESPONSE RATIOS OF FILTERED SILICON DIODES AND UNKNOWN CELL
- 2) VALUE OF CONSTANT, C .

ACCURACY OF CALIBRATION WILL DEPEND ON THE NUMBER OF DIODES USED AND THE WIDTH OF THE BAND PASS FILTERS.

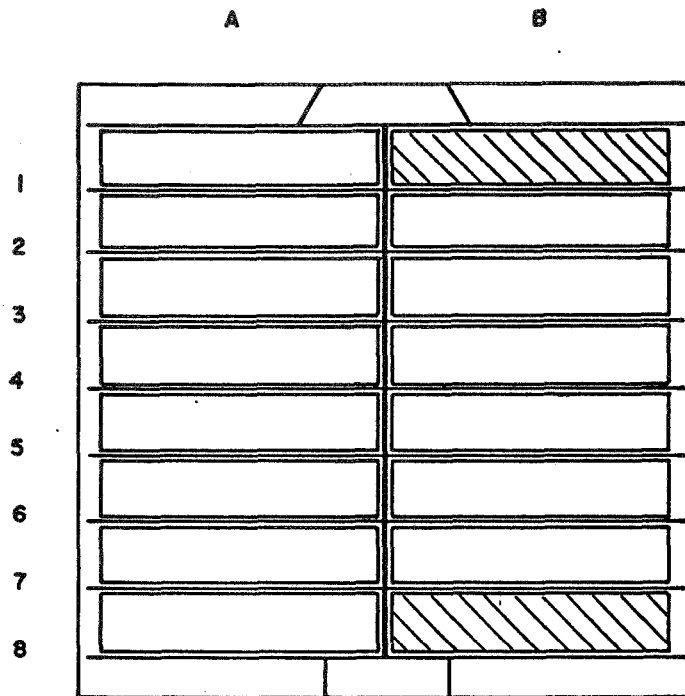
BECAUSE OF ITS SMALL AREA, THE SIMULATED REFERENCE CELL DOES NOT PERFORM SPATIAL AVERAGING. HENCE UNIFORM ILLUMINATION IS REQUIRED.

Initial and After 140°C Step for Amorphous-Silicon Cells

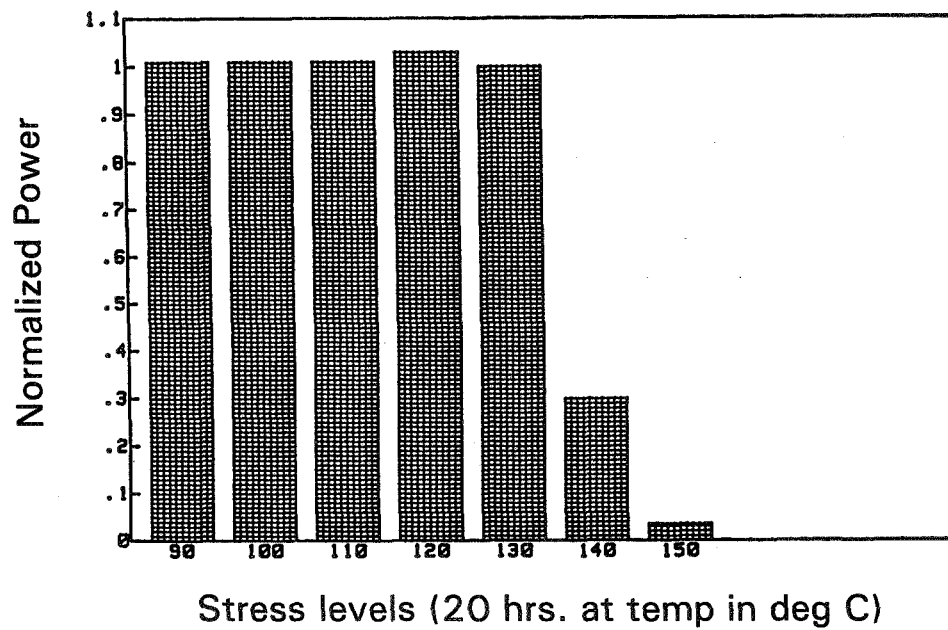


MODULE DEVELOPMENT AND ENGINEERING SCIENCES

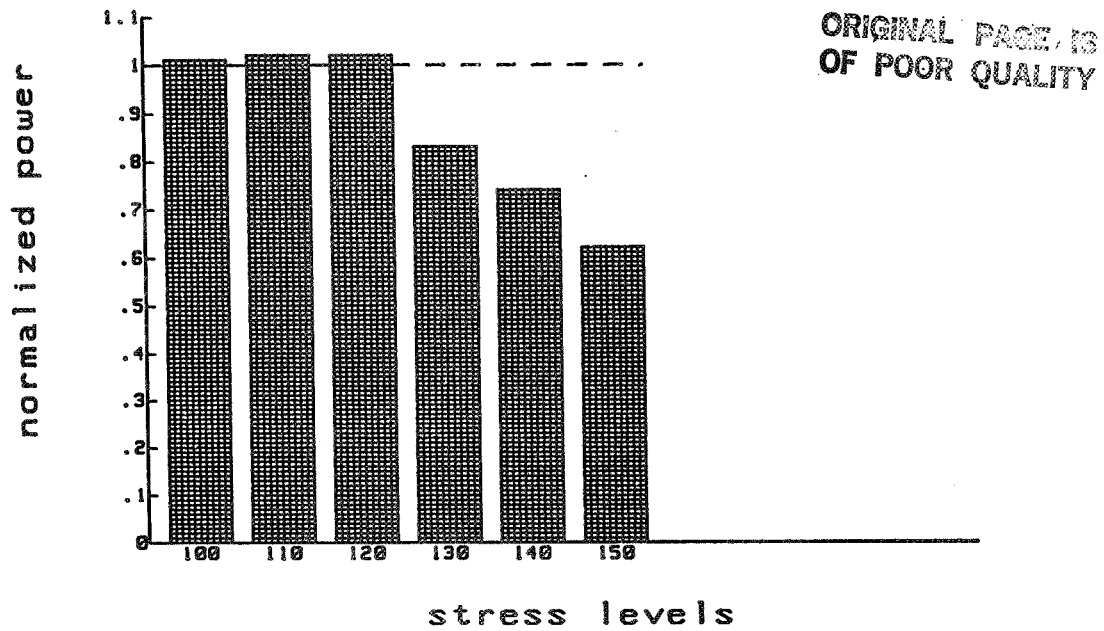
Diagram of Step Stress Submodule Showing Location of Two "Bad" Cells



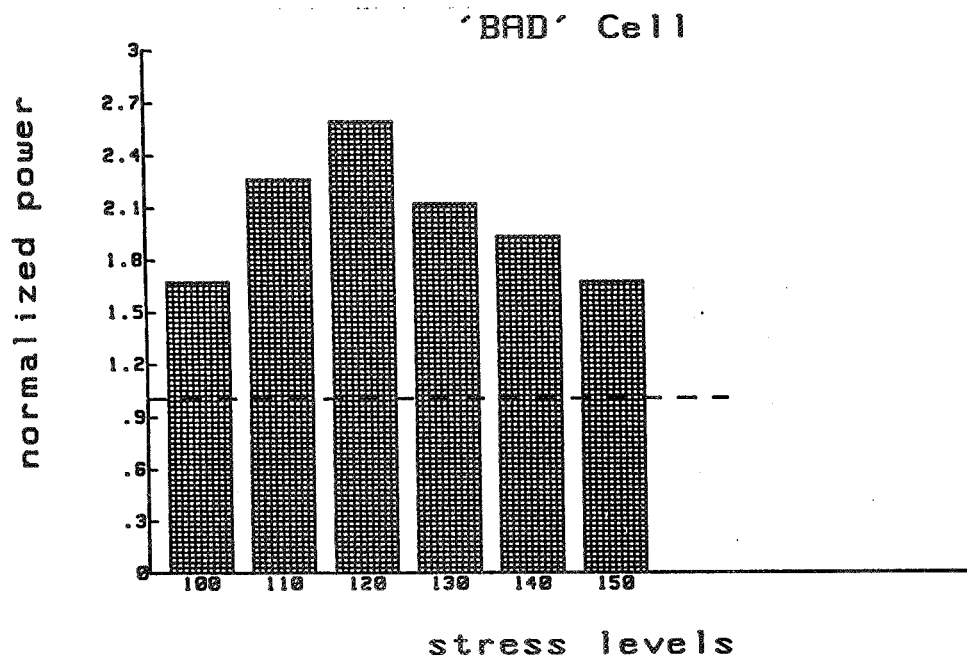
Temperature Step Stress



Temperature Step Stress: "Good" Cell
(20 h at Temperature in Degree C)



Temperature Step Stress: "Bad" Cell
(20 h at Temperature in Degree C)



Temperature Step Stress

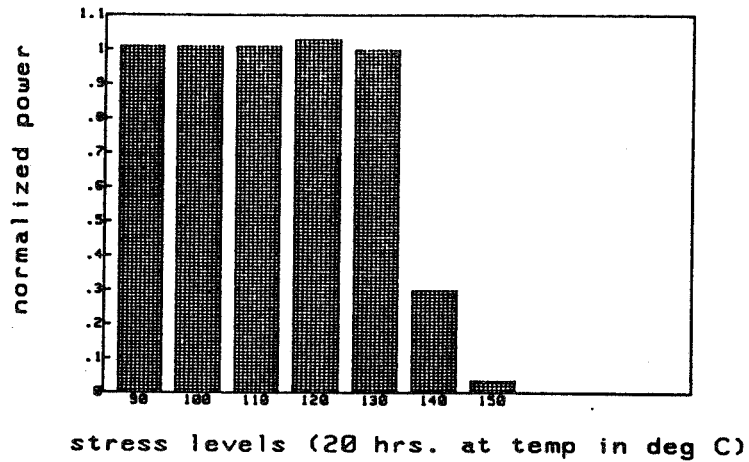


Figure 1. Average Normalized Power Output as a Function of Stress Level Temperature for 16 Amorphous Silicon Solar Cells.

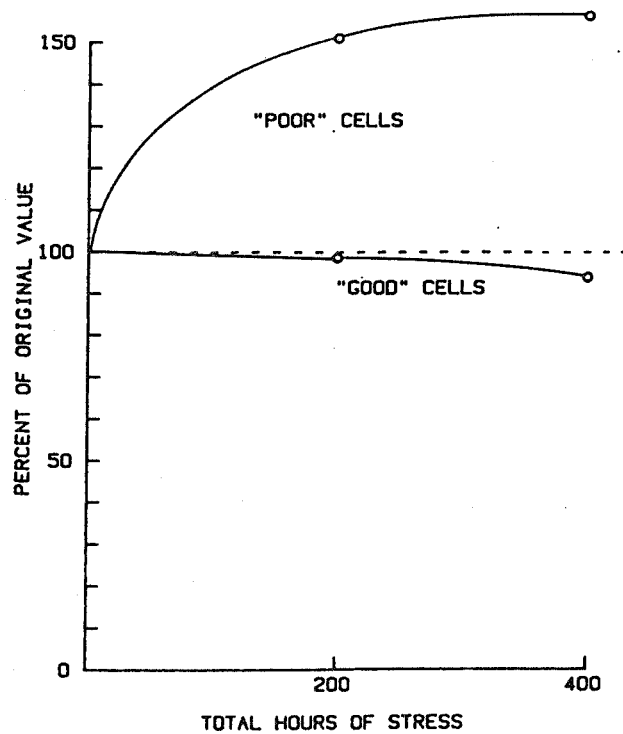


Figure 2. Average Normalized Power Output of Amorphous Silicon Solar Cells as a Function of 85/85 Stress Time.

PHOTOCURRENT IMAGES OF AMORPHOUS-SILICON SOLAR-CELL MODULES

JET PROPULSION LABORATORY

Q. Kim
A. Shumka
J. Trask

State of the Art of a-Si Solar Cells

PERFORMANCE OF BEST REPORTED SINGLE JUNCTION P-I-N AMORPHOUS SILICON SOLAR CELLS

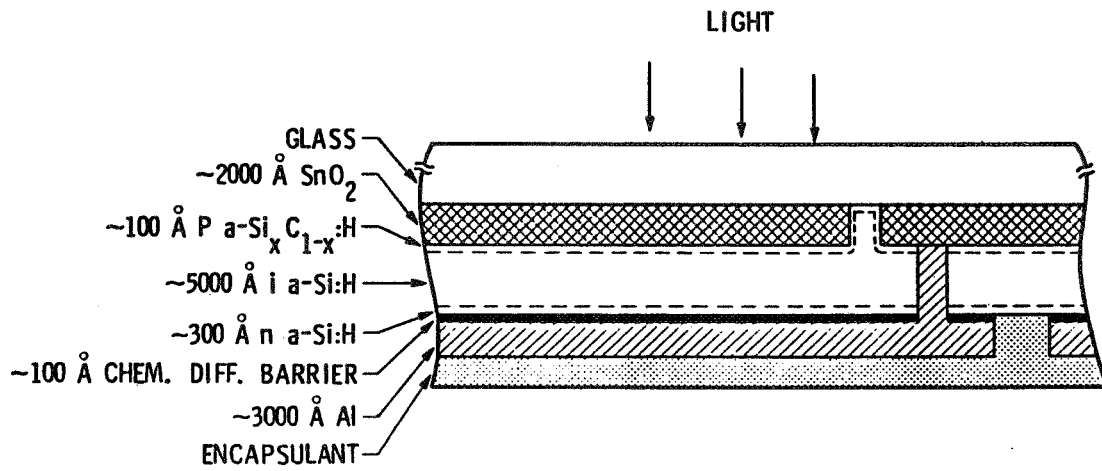
	V_{oc} mV	J_{sc} mA/cm ²	FF %	EFF. %
BEST INDIVIDUAL PARAMETERS	950	16.70	74.0	11.70
• HIGH CONVERSION EFFICIENCY:	7.4 - 11.7%			
• DIFFERENT DEVICE STRUCTURES:	p - i - n n - i - p			
• DIFFERENT FABRICATION PROCESS:	GLOW DISCHARGE REACTIVE SPUTTERING CHEMICAL VAPOR DEPOSITION			

Commercial Modules

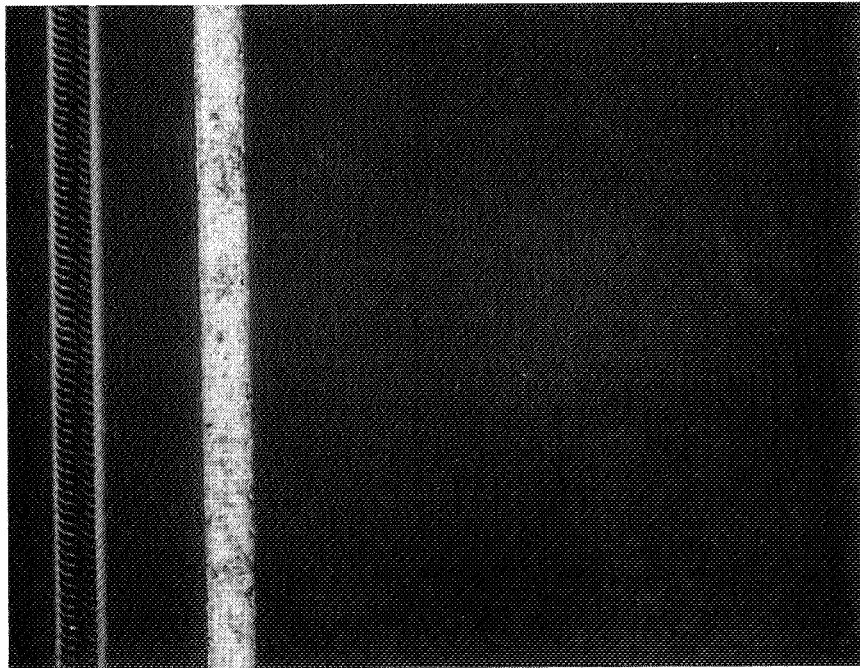
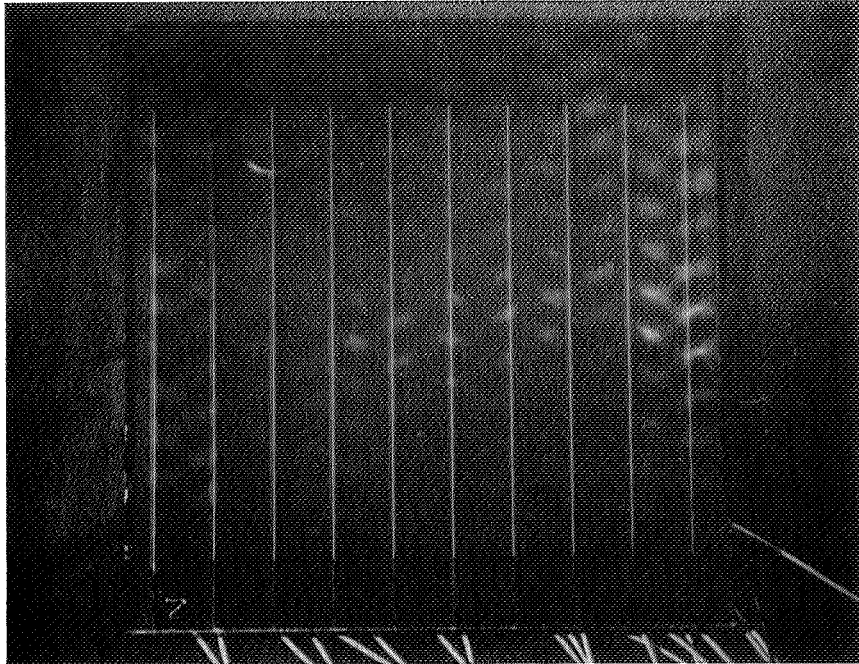
MANUFACTURERS	V_{oc} mV	J_{sc} mA/cm ²	FF	EFF. %
A	0.726	9.59	0.572	3.99
B	0.869	12.60	0.666	7.33
C	0.674	13.20	0.717	6.35

MODULE DEVELOPMENT AND ENGINEERING SCIENCES

a-Si:H Solar-Cell Structure With Enlarged Section of
Electrode Coupling Portion of Integrated a-Si Cell

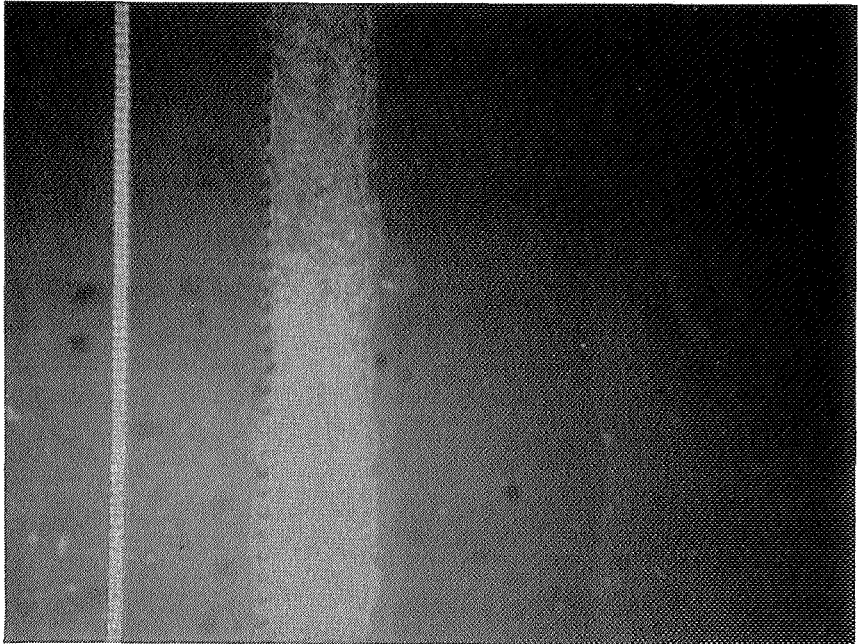
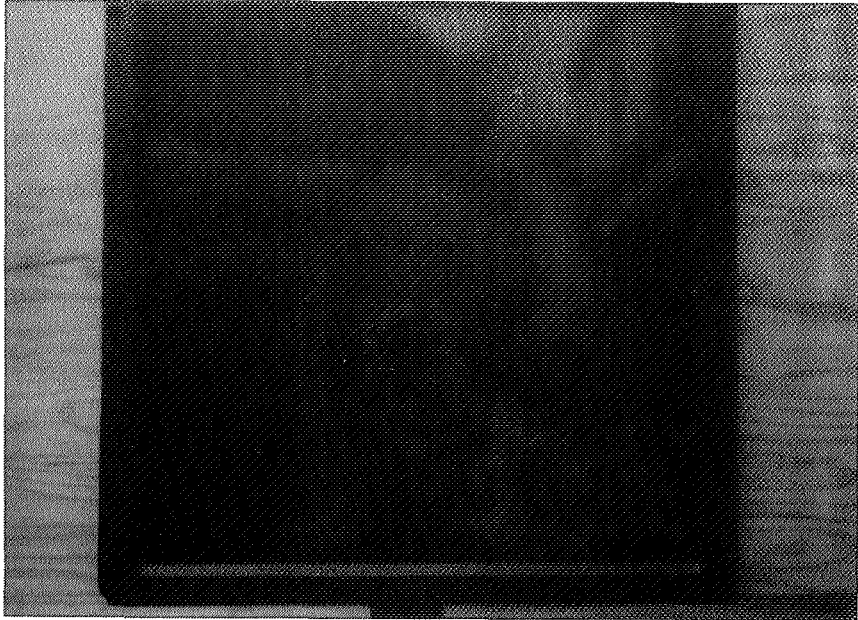


Module A and Its Cell InterCoupling

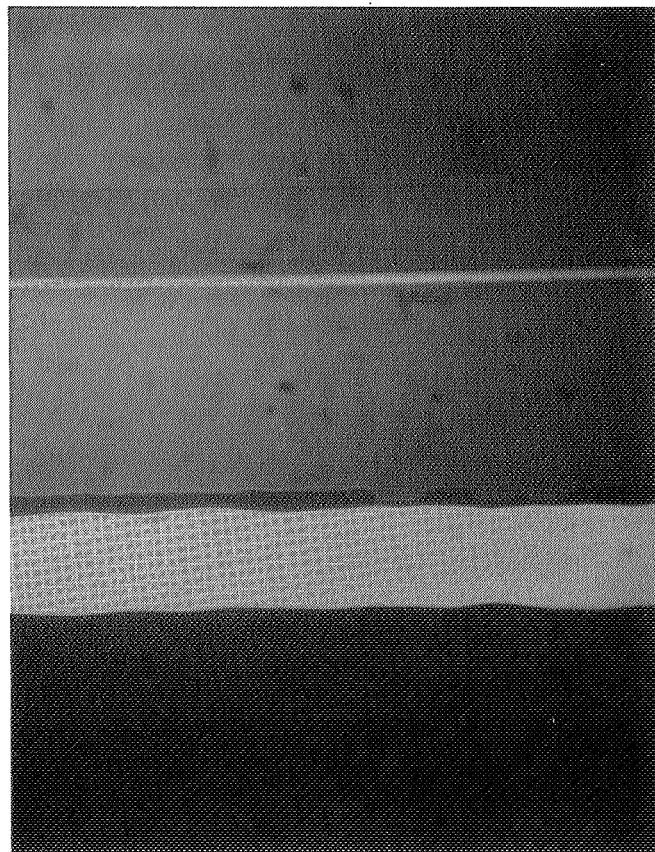
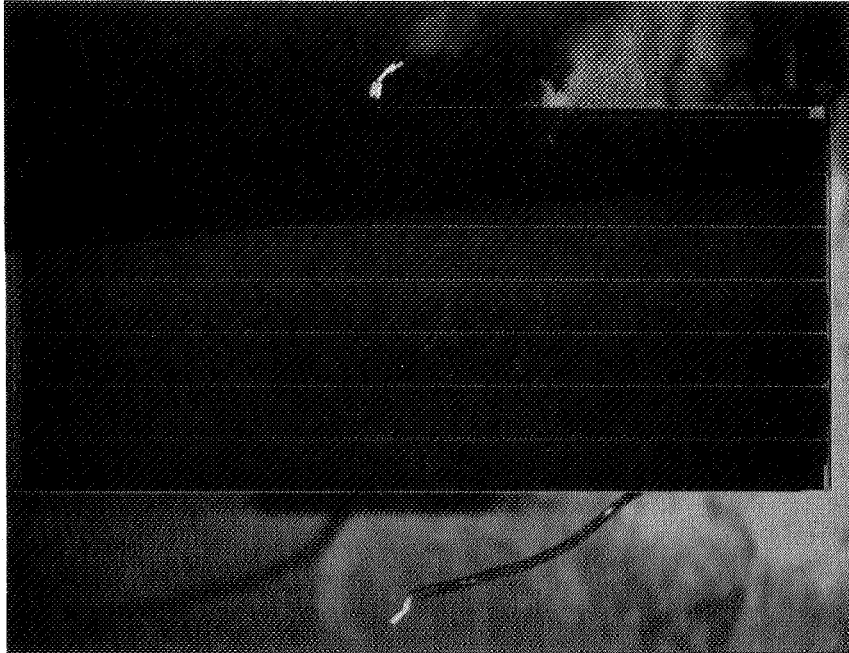


MODULE DEVELOPMENT AND ENGINEERING SCIENCES

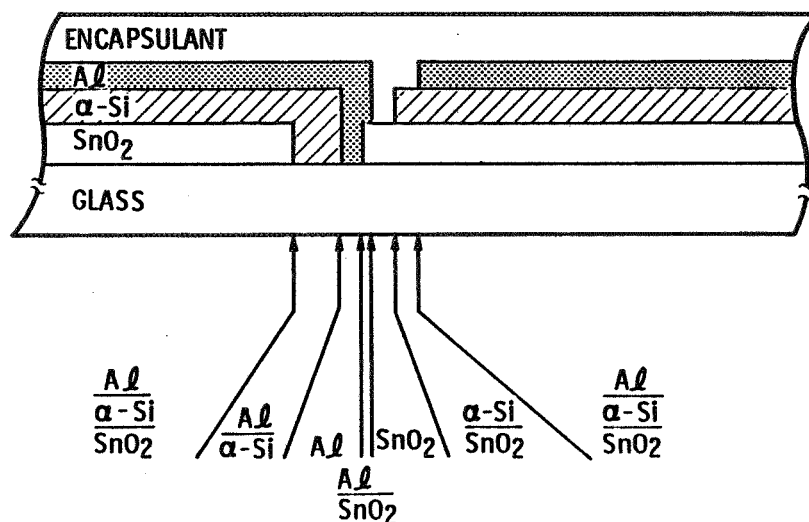
Module B and Its Cell Intercoupling



Module C and Its Cell Intercoupling



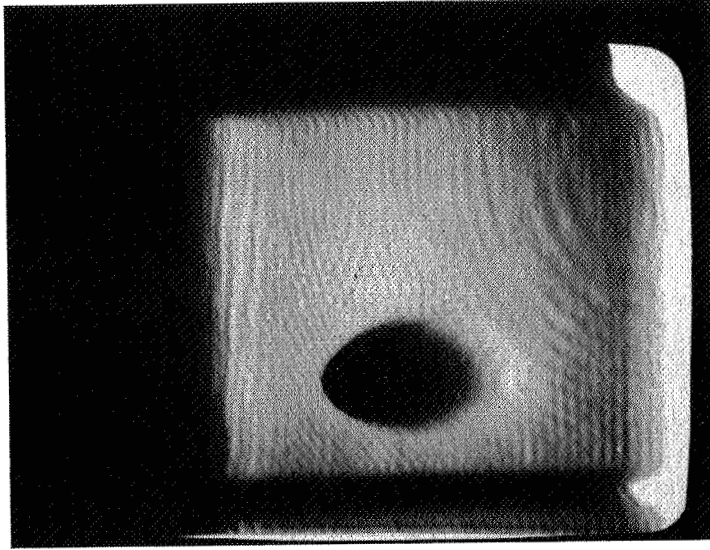
a-Si:H Solar-Cell Structure With Enlarged Section of Masked Cell Interconnecting Portion



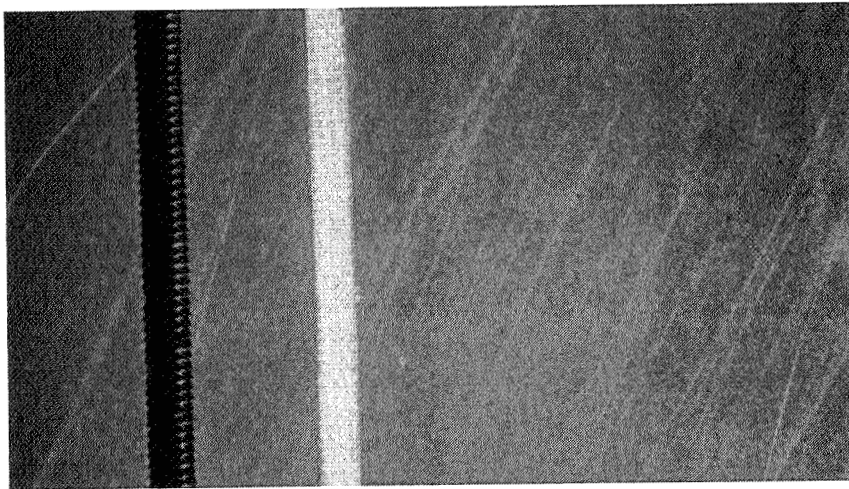
Failure Modes

- ELECTRICAL SHORTS
- FILM INHOMOGENITY
- CELL INTER-COUPLING WORKMANSHIP
- EFFICIENCY DEGRADATION
- WEATHERING DUE TO:
 - TEMPERATURE
 - HUMIDITY
 - CORROSION
 - ETC.

Electrical Short

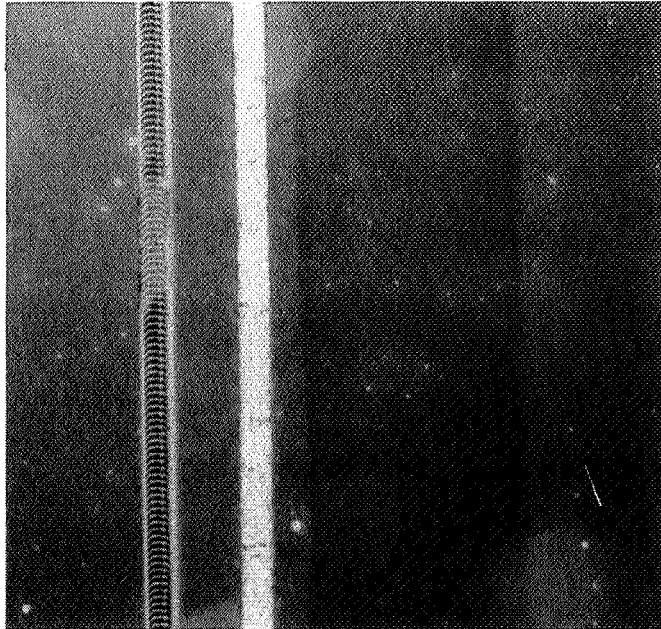


Masking Problem

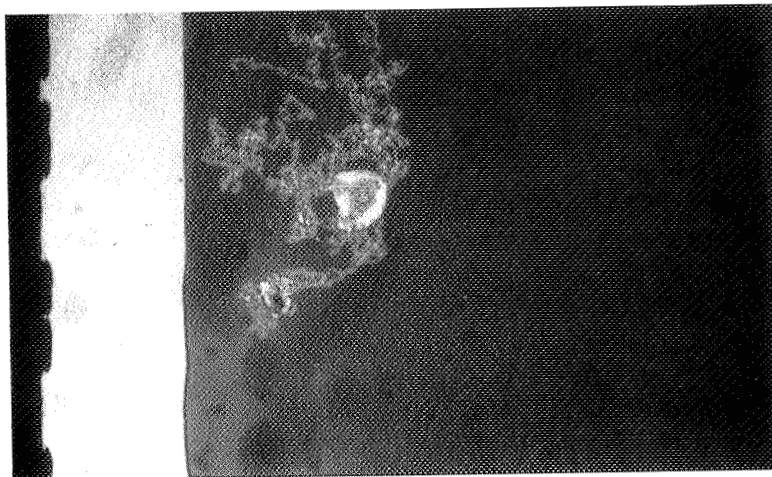
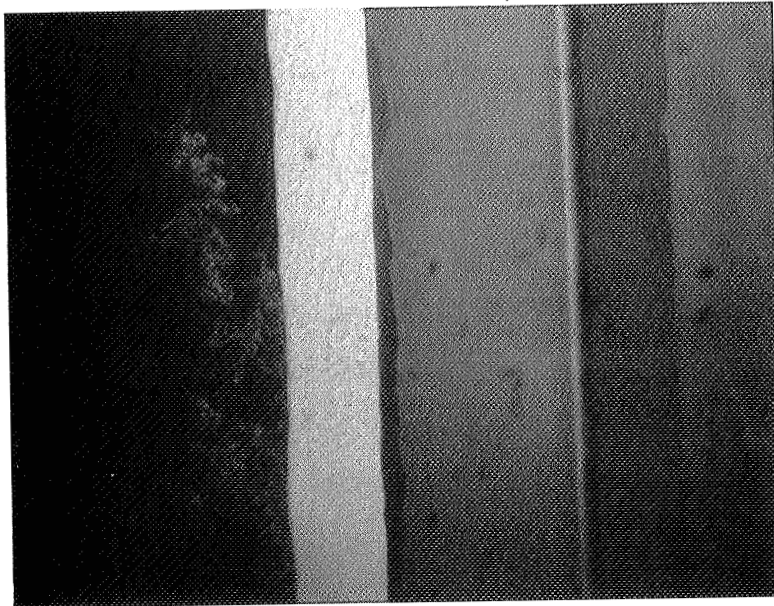
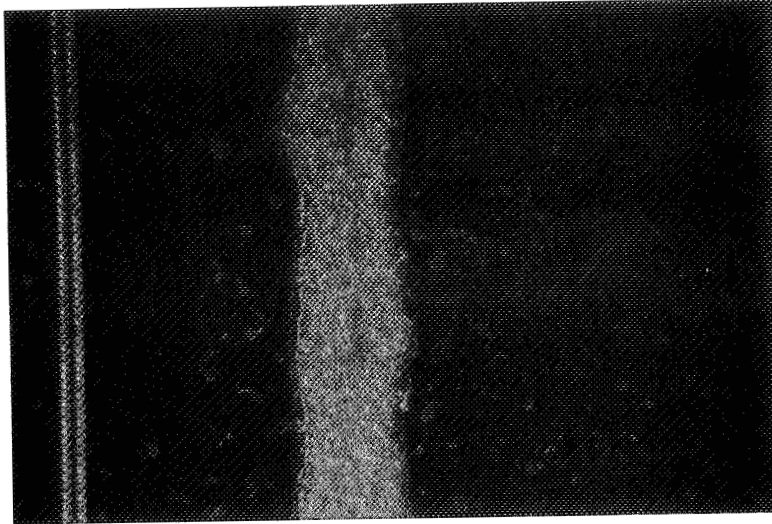


MODULE DEVELOPMENT AND ENGINEERING SCIENCES

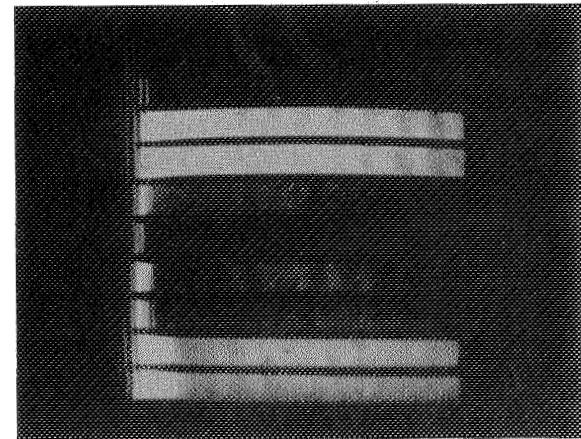
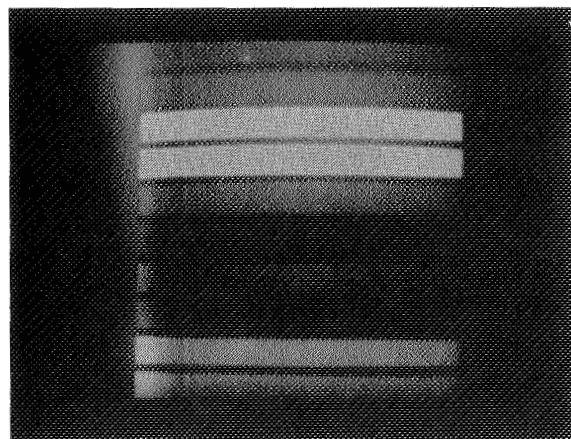
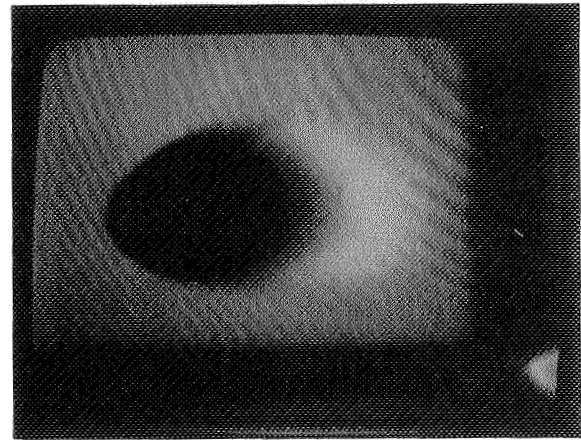
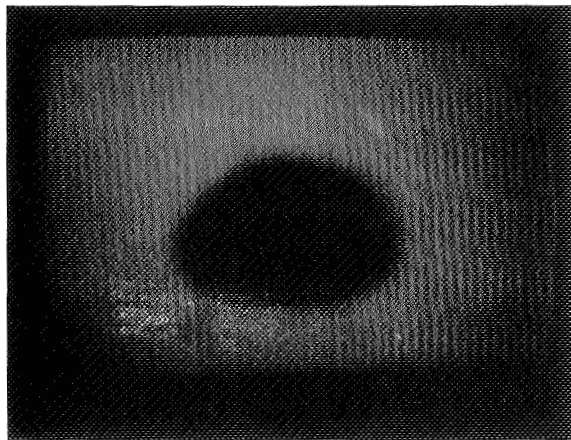
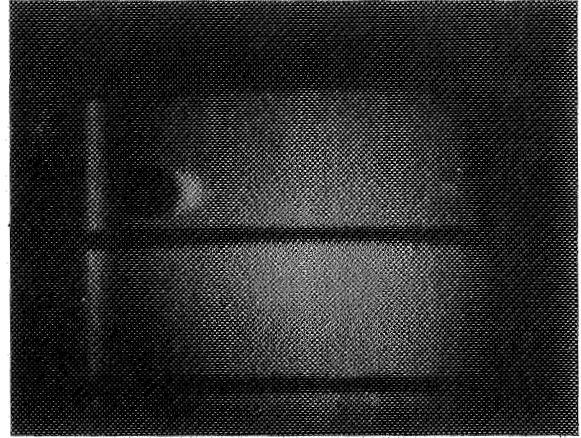
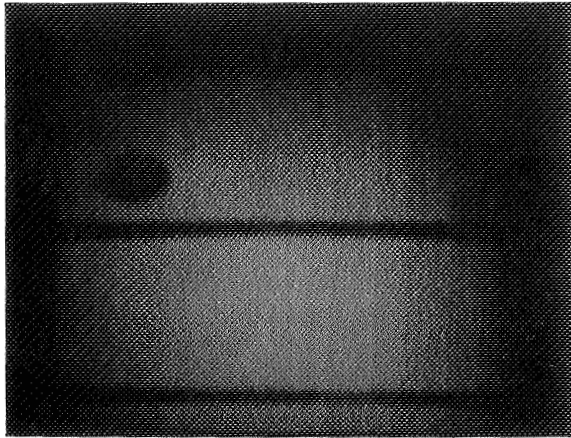
Non-Uniform Laser Scribing



Masking Workmanship



Y-Modulation for Better Display

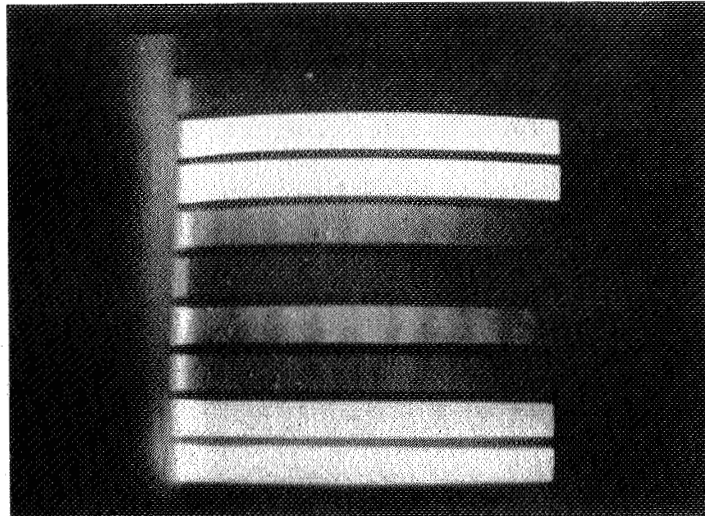


NORMAL

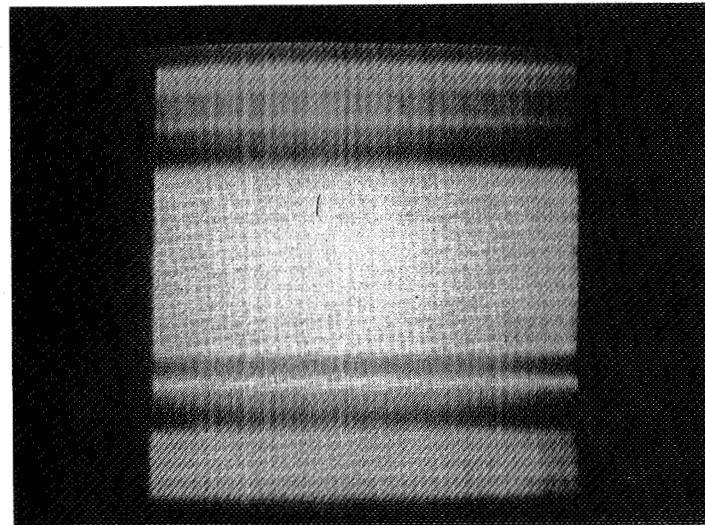
Y-MODULATED

Solar-Cell Laser Scanner Images

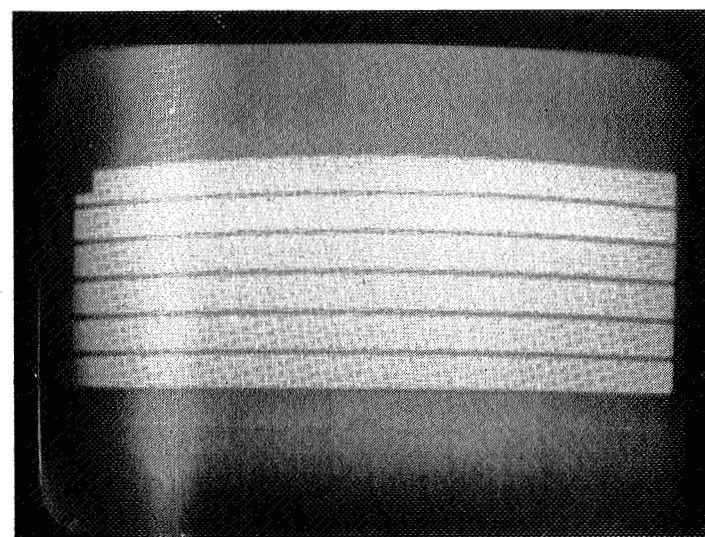
MODULE A



MODULE B



MODULE C

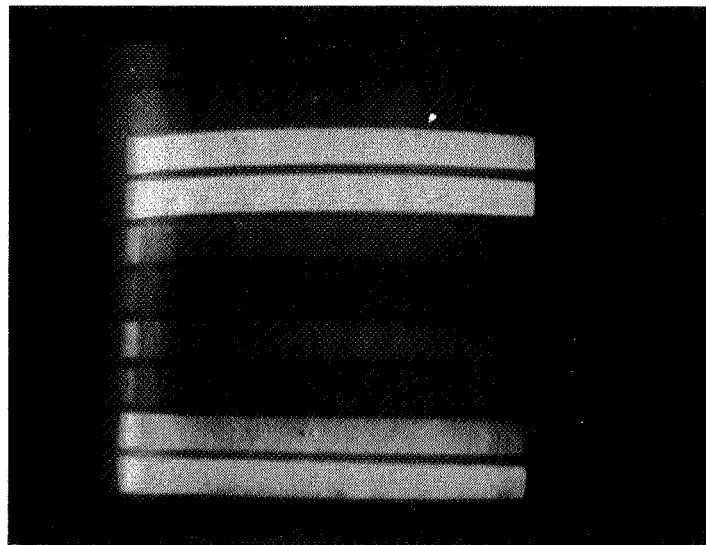


MODULE DEVELOPMENT AND ENGINEERING SCIENCES

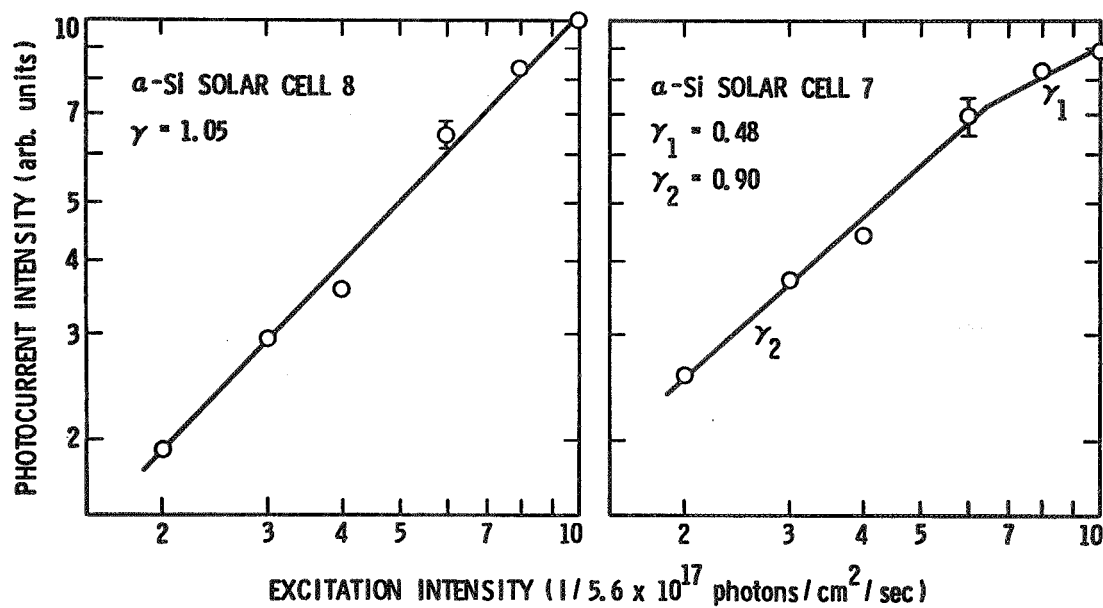
Effects of Excitation Intensity on Photocurrent Response

- PROCESS V.S. CELL QUALITY
- NONDESTRUCTIVE DIAGNOSIS ON PROCESSING PARAMETERS

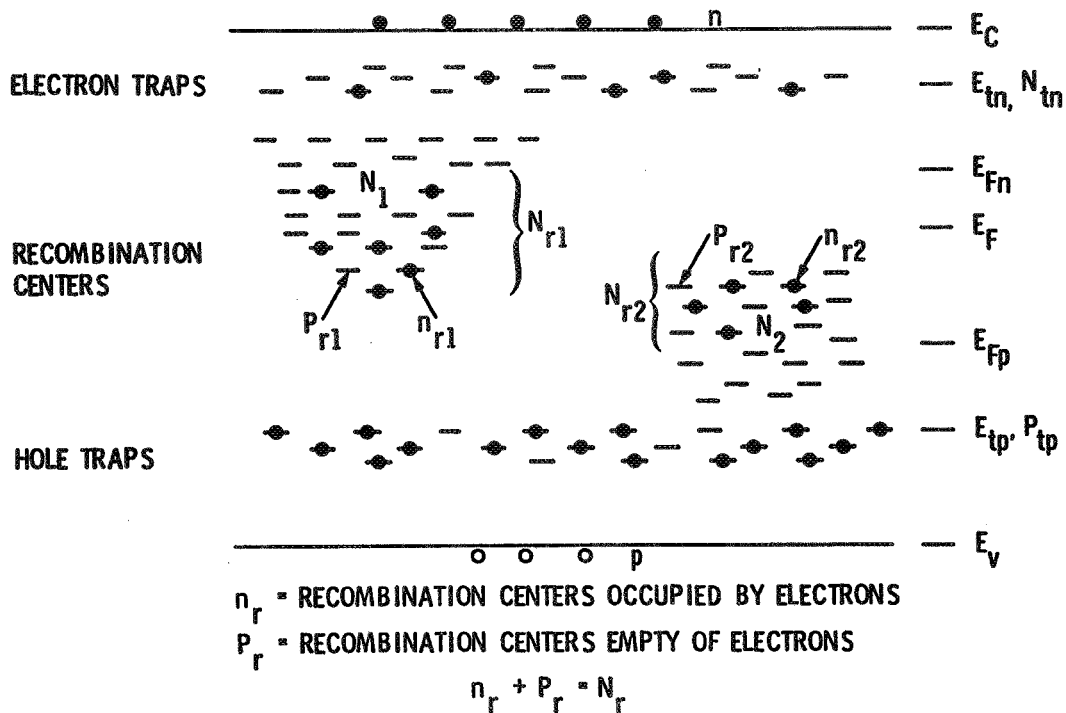
SCLS Image of Module 1 Using 4579 Å Argon Laser Line



Photocurrent Dependence on Excitation Intensity



Schematic Energy-Band Diagram and Distribution of Gap States in a-Si:H



Free Carrier Electron Transport Model

$1 \geq \gamma \geq \frac{1}{2}$: MONOMOLECULAR RECOMBINATION

$$I \propto F^\gamma$$

$\gamma = \frac{1}{2}$: BIMOLECULAR RECOMBINATION

(DIRECT RECOMBINATION BETWEEN EITHER
FREE OR TRAPPED CARRIERS)

Whisker Signal

- DEVICE PARAMETER RELATED
- PROCESS RELATED

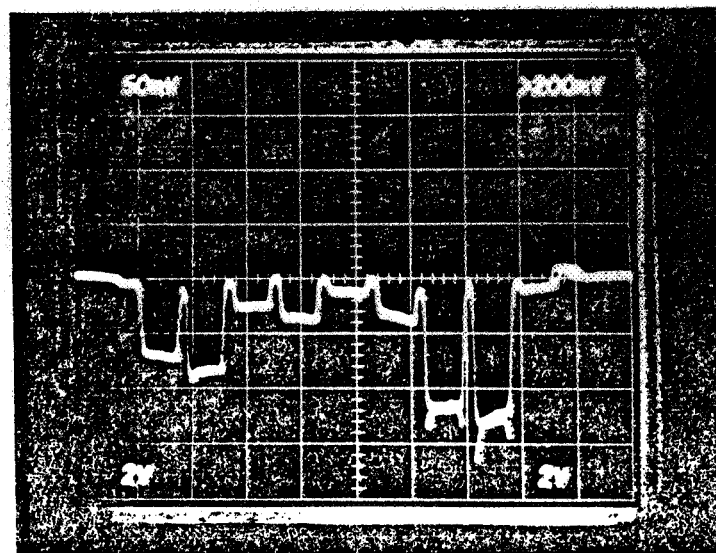
Conclusion

- SOLAR CELL LASER SCANNER CAN BE EFFECTIVELY USED TO NONDESTRUCTIVELY TEST NOT ONLY ACTIVE DEFECTS BUT ALSO THE CELL QUALITY AND INTEGRITY OF ELECTRICAL CONTACTS.

Plans for a-Si Solar Cells

- UPGRADE SCLS CAPABILITY TO PROBE PHOTOCURRENT RESPONSE IN DIFFERENT LAYERS OF THE DEVICE.
- EVALUATE AND CHARACTERIZE MODULE DEGRADATIONAL PHENOMENA IN THIN-FILM AMORPHOUS SILICON SOLAR CELLS WITH PARTICULAR EMPHASIS ON MICRO AND MACROSCOPIC DEFECTS/FLAWS.
- DEVELOP METHODS TO ANALYZE FAILURE MODES RESULTING FROM DEGRADATION DUE TO ENVIRONMENTAL EFFECTS SUCH AS OPTICAL, THERMAL, MECHANICAL AND MOISTURE.
- ANALYZE CELL INTER-COUPPLINGS.

Photocurrent Signal of Module 1 Across the Nine Cells in Series Coupled Module Scanned by a He-Ne Laser (3.0 mW)



AMORPHOUS-SILICON MODULE HOT-SPOT TESTING

JET PROPULSION LABORATORY

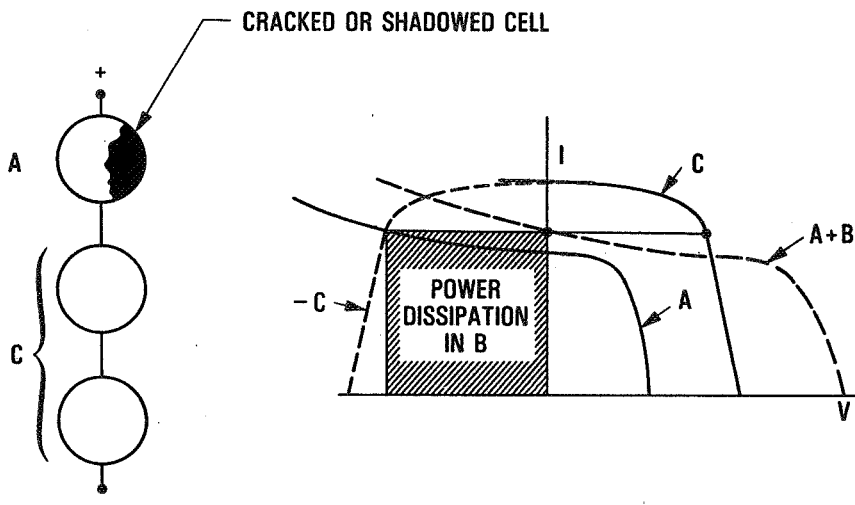
C. C. Gonzalez

Background

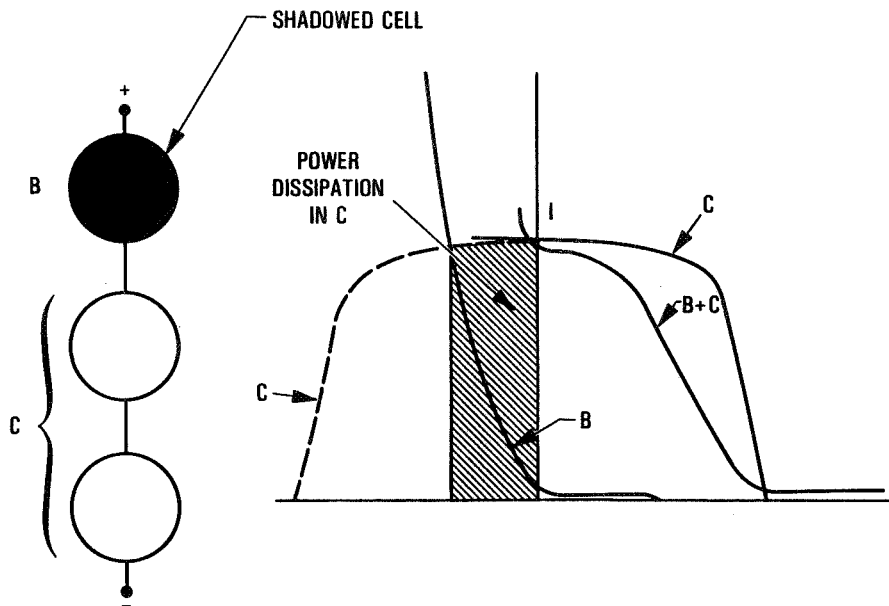
- Hot-spot heating occurs when cell short-circuit current is lower than string operating current
 - Cell goes into reverse bias and absorbs power (= reverse-bias voltage x cell current)
 - Reverse-bias voltage is proportional to the number of cells in series with the affected cell
 - It is necessary to limit reverse-bias voltage by means of bypass diodes

- Nonuniform heating over cell area leads to increased temperature for same power dissipation

Visualization of Hot-Spot Cell Heating with High-Shunt Resistance Cell



Visualization of Hot-Spot Cell Heating with Low-Shunt Resistance Cell



Key Lessons from Crystalline Silicon

- **Maximum allowable temperature for encapsulants: 120°C to 140°C**
- **Temperature very dependent on cell-to-cell shunt-resistance differences**
- **Lateral heat transfer from hot spot is important**
- **Common failure at high heat levels is cell shorting**
- **Typical crystalline-silicon module requires bypass diodes around every 12 to 18 cells**
- **Heating is highly non-linear function of applied current and voltage**
 - **Non-linear reverse I-V characteristic**
 - **Changing shunt-resistance with temperature**
 - **Changing hot-spot area with temperature**

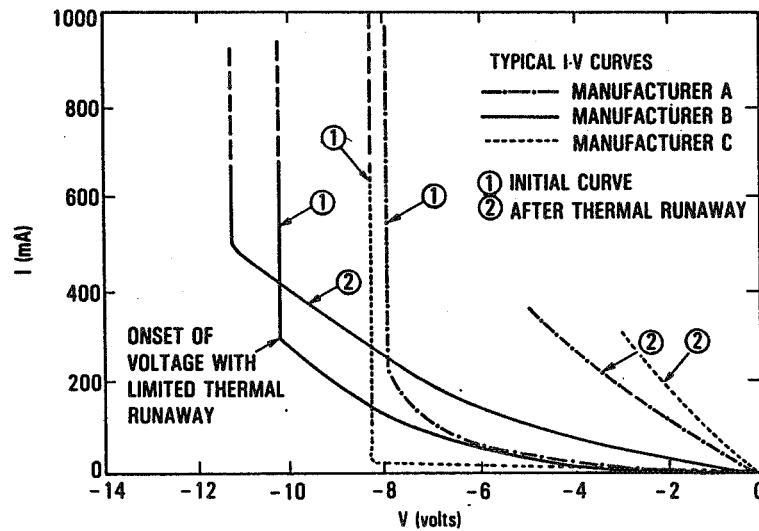
Amorphous-Cell Hot-Spot Testing Objectives

- To develop the techniques required for performing reverse-bias testing of amorphous cells
- To quantify the response of amorphous cells to reverse biasing
- To develop guidelines for reducing hot-spot susceptibility of amorphous modules
- To develop a qualification test for hot-spot testing of amorphous modules

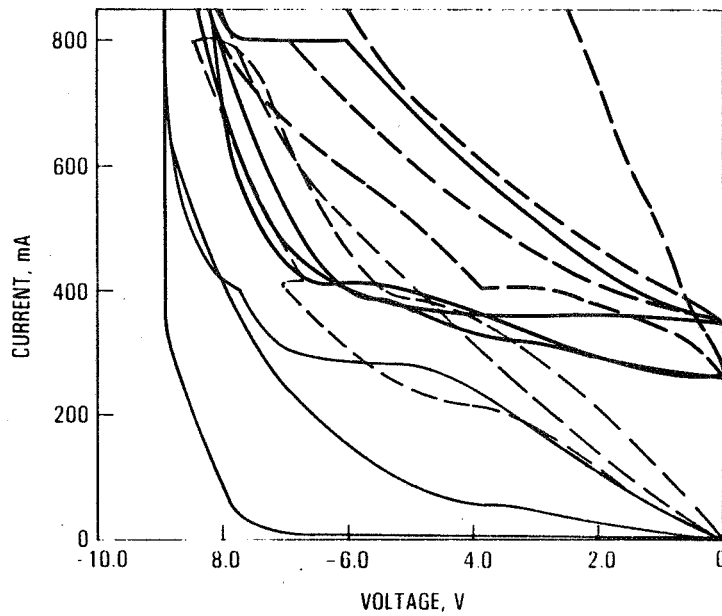
Approach

- Amorphous cells tested using two techniques
 - First is equivalent to that used in hot-spot testing of crystalline cells
 - Hot-spot temperature monitored using IR camera
 - Reverse-bias I-V curve plotted as test is conducted
 - Second consists of pulsed reverse-bias voltage ranging in duration from 0.01 to 100 milliseconds
 - I-V curve plotted after each pulse

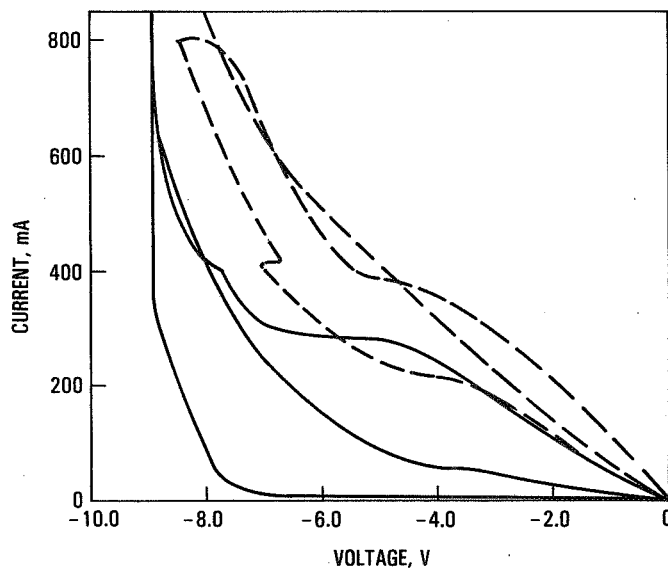
Amorphous-Cell Second-Quadrant I-V Curves



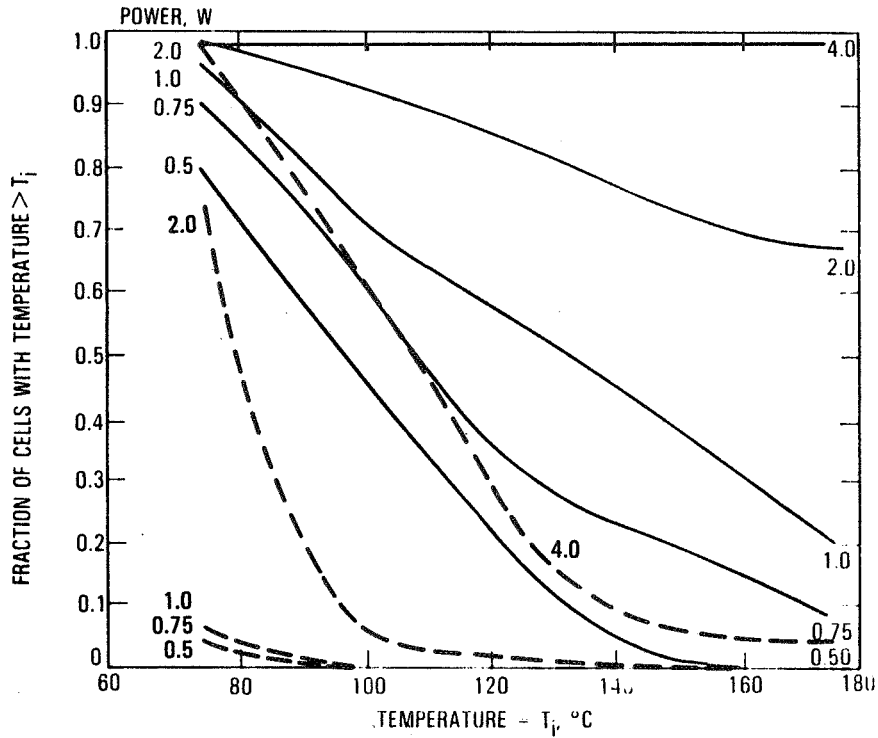
Amorphous-Module Cell-Reverse Quadrant I-V Curves
Illuminated Cells



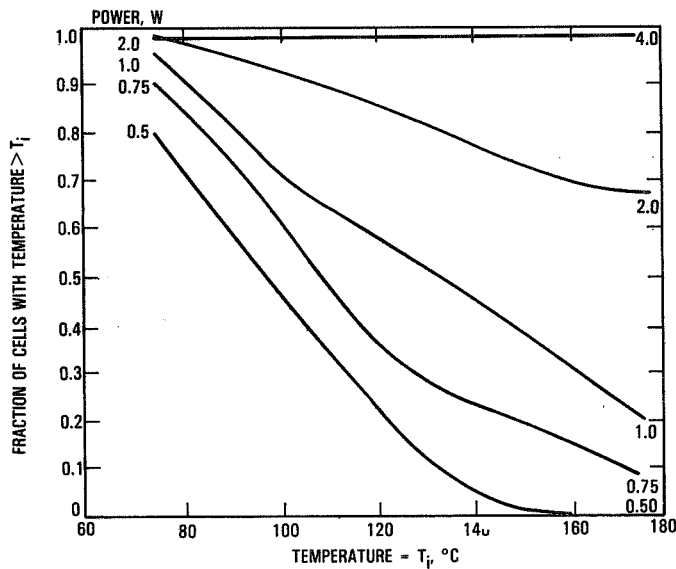
Amorphous-Module Cell-Reverse Quadrant I-V Curves
Unilluminated Cells



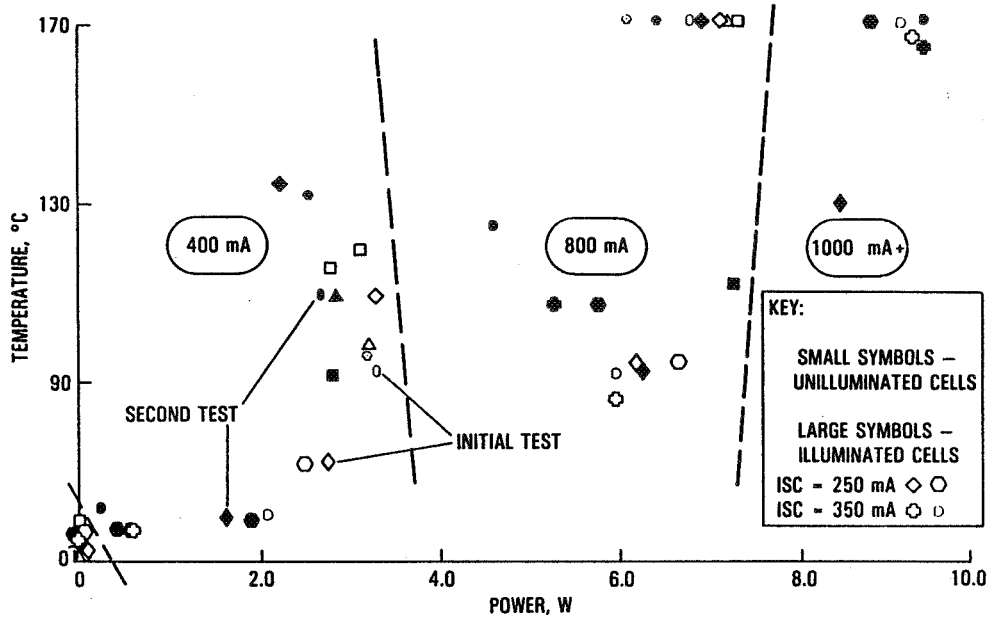
Fraction of Cells Reaching a Given Temperature as a Function of Power Dissipated
(Modules)



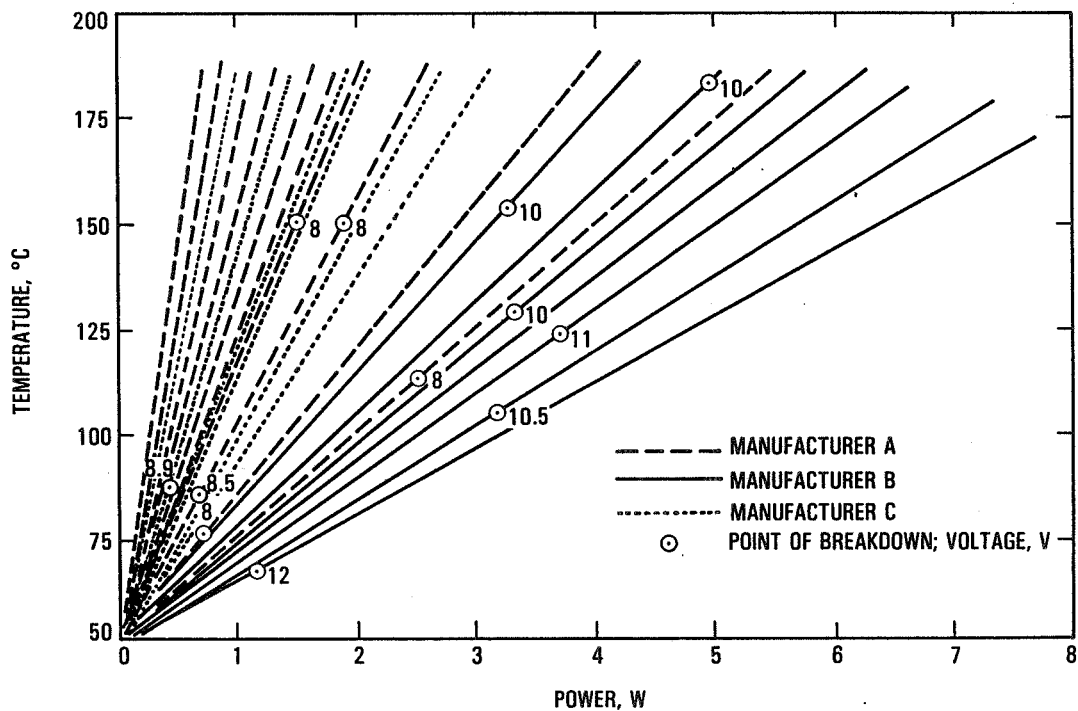
Fraction of Cells Reaching a Given Temperature as a Function of Power Dissipated
(Submodules)



Hot-Spot Temperature Versus Power for Cells in Encapsulated Module
(Test Current Equal to 1, 2, and 2 + Cell I_{SC})



Hot-Spot Temperature Versus Power
(Unencapsulated Amorphous-Silicon Submodules, No Illumination)



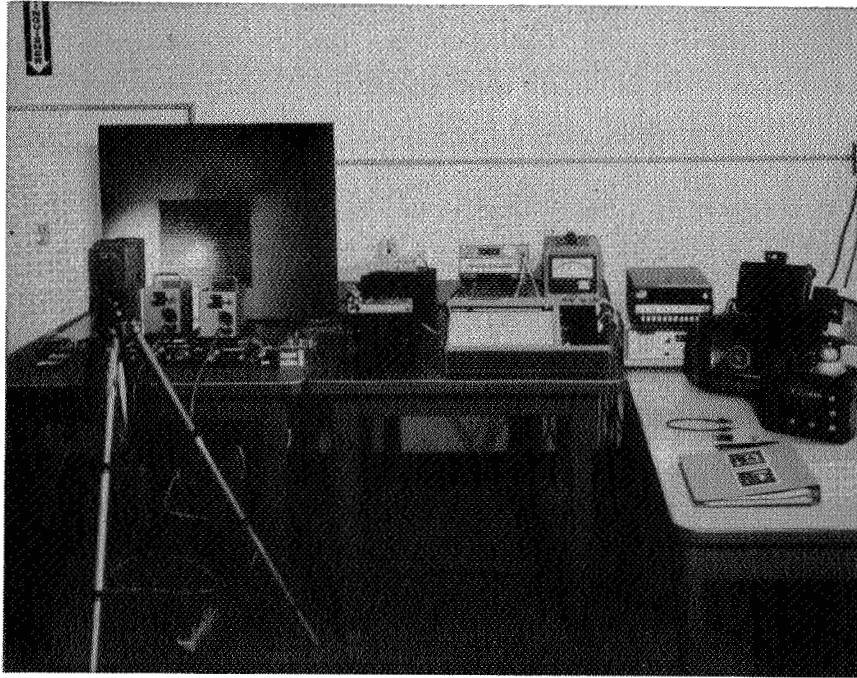
Hot-Spot Qualification Test

- **Hot-spot qualification test performed on one module type**
- **Same procedure and equipment as for crystalline cells**
 - **100-hour cyclic test**
 - **Treated as low-shunt-resistance cell (Type B)**
 - **Test performed in absence of illumination**
 - **Test current is module short-circuit current**
 - **Module temperature raised to field environment (45°C to 50°C)**

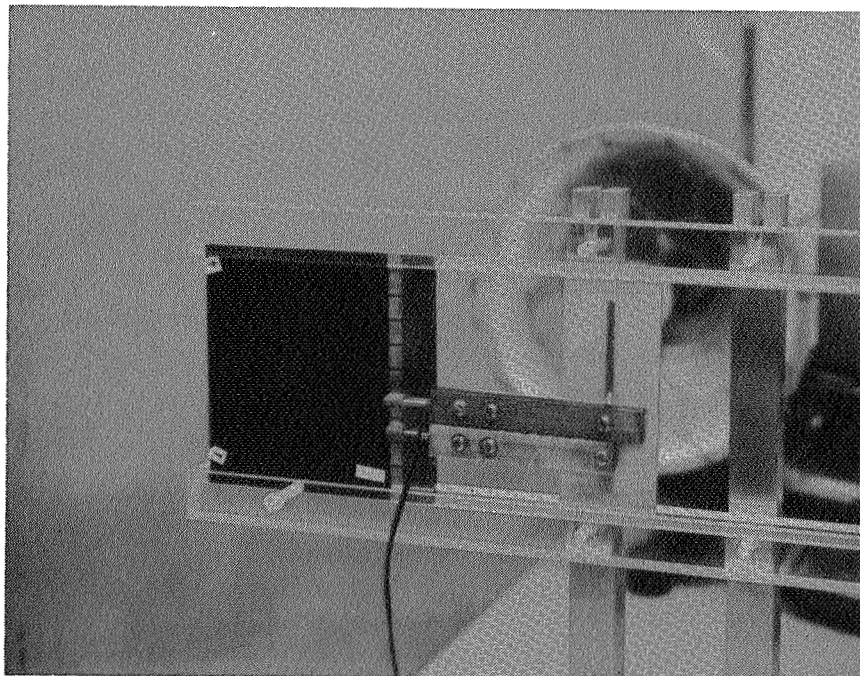
Results and Conclusions

- **Amorphous cells undergo hot-spot heating similarly to crystalline cells**
 - **Shunt resistance levels similar**
 - **Tolerance to heating level similar**
- **Comparison of results obtained with submodules versus actual module indicate heating level lower in latter**
 - **Module structure contains thick (relative to front surface) glass substrate not present in submodules**
- **Module design must address hot-spot heating**
 - **Heat-sinking cells**
 - **Use of bypass diodes**
 - **Use of smaller solar cells (lower maximum current)**
- **Hot-spot qualification test conducted on module**
 - **Module passed test with no instabilities**
 - **Minor cell erosion occurred that is characteristic of amorphous cells**

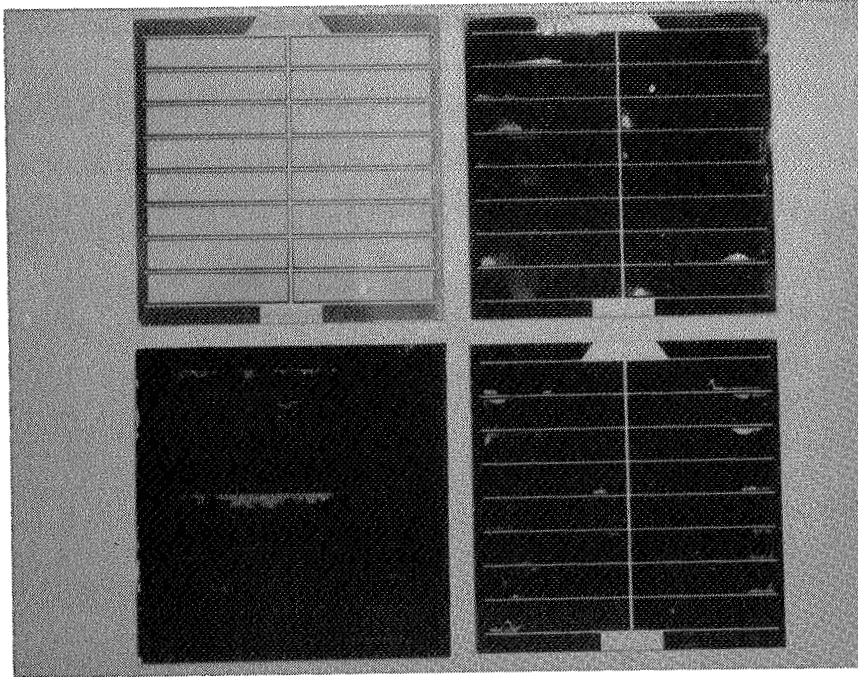
Hot-Spot Test Set-Up



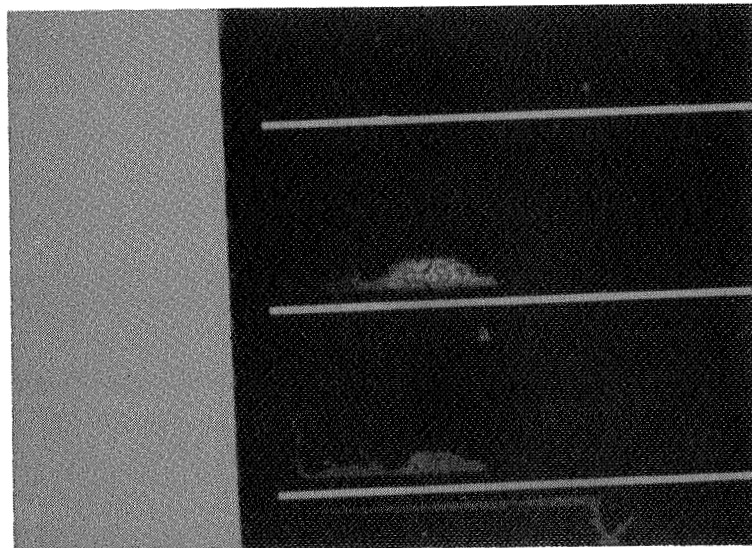
Test Set-Up for Submodule Using Conductive Elastomeric Material



Results of Hot-Spot Testing of Four Submodules

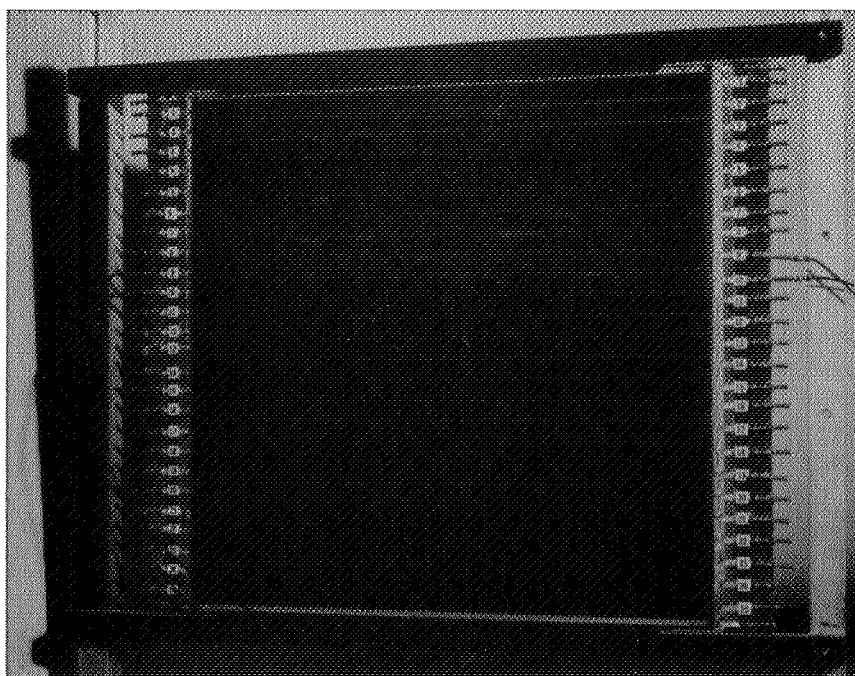


Close-up View of Hot-Spot Area



MODULE DEVELOPMENT AND ENGINEERING SCIENCES

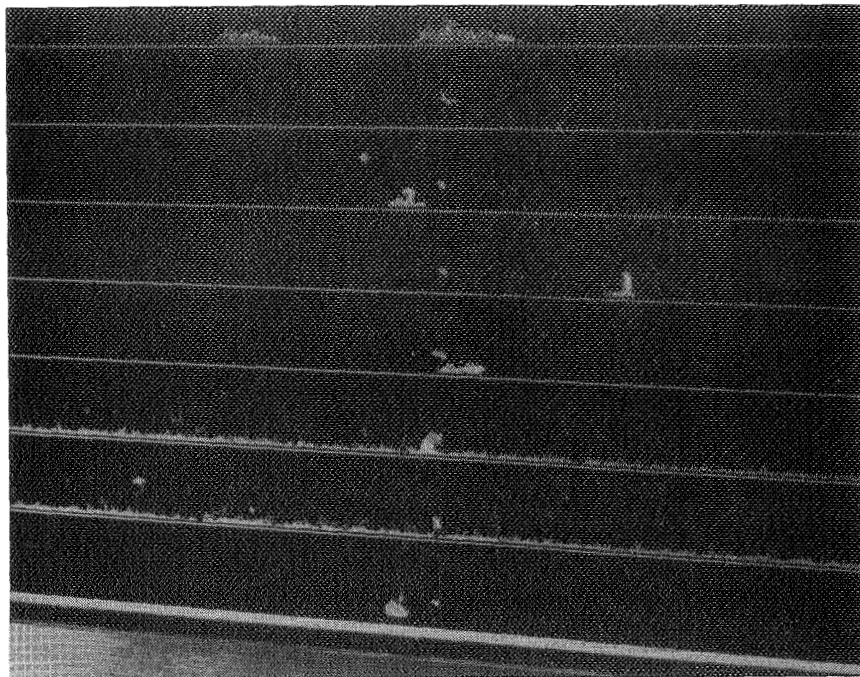
Front Side of Arco Test Module



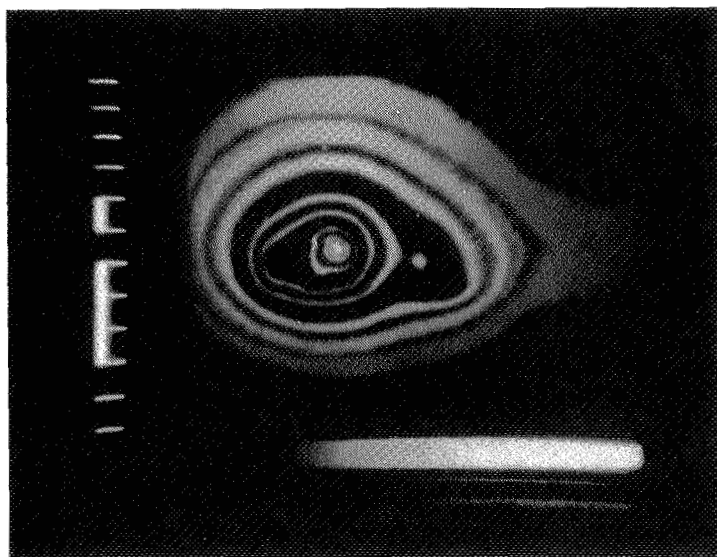
**Back Side of Arco Test Module Showing
Added Conductive Ribbon Attached with Conductive Epoxy**



Close-up of Arco Test Module Showing Results of Hot-Spot Testing

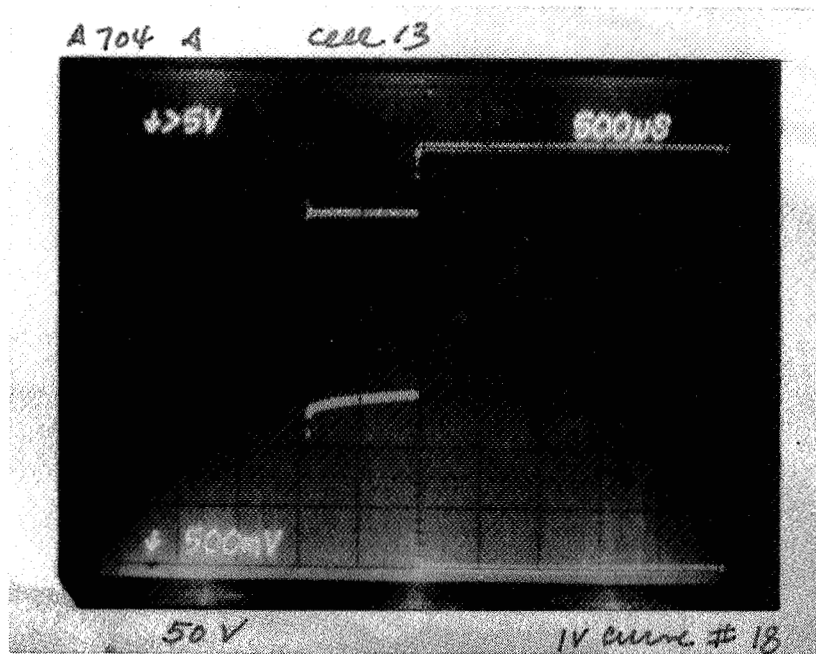


Hot-Spot Recorded on IR Monitor Using Time-Lapse Photography



MODULE DEVELOPMENT AND ENGINEERING SCIENCES

Ocilloscope Trace of Pulse-Reverse Bias Testing



ORIGINAL PAGE IS
OF POOR QUALITY

PVARRAY: A SOFTWARE TOOL FOR PHOTOVOLTAIC ARRAY DESIGN

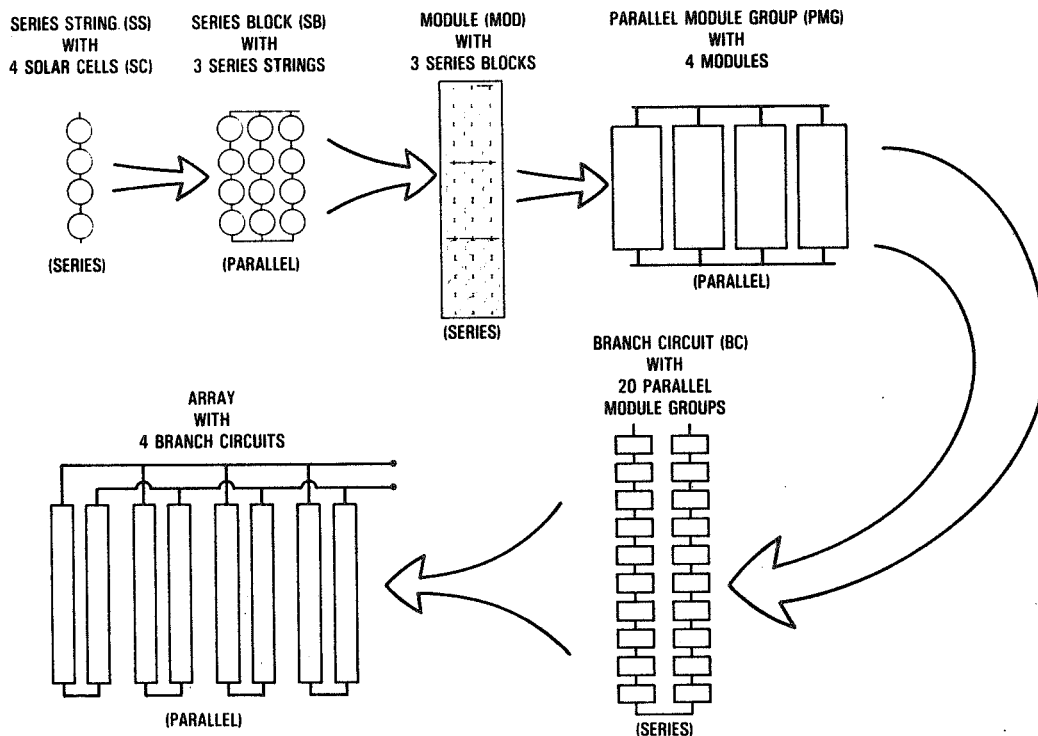
JET PROPULSION LABORATORY

Dale R. Burger

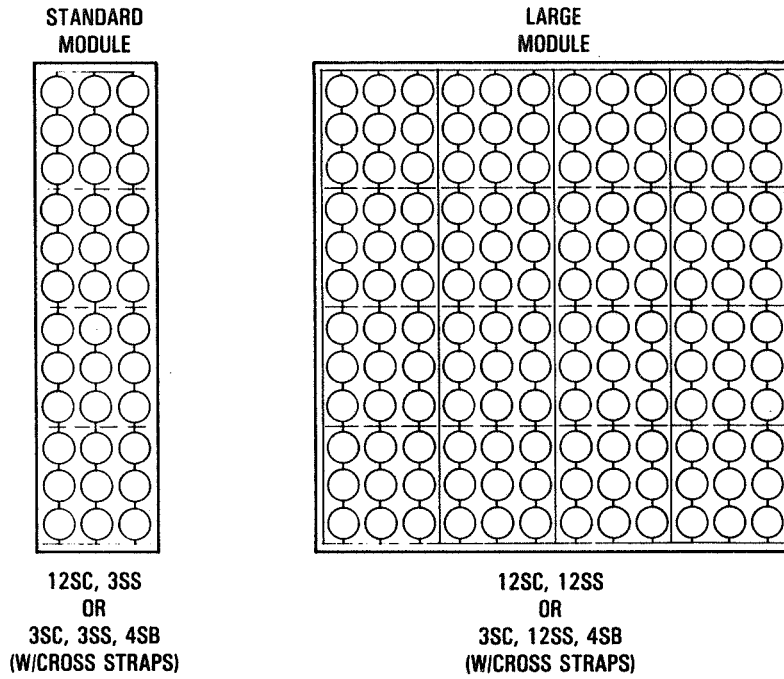
Background

- Part of a PV costing system
 - SAMIS-PC (module cost)
 - PVARRAY (array performance)
 - LCP (life-cycle cost/performance)
- Funded by PA&I

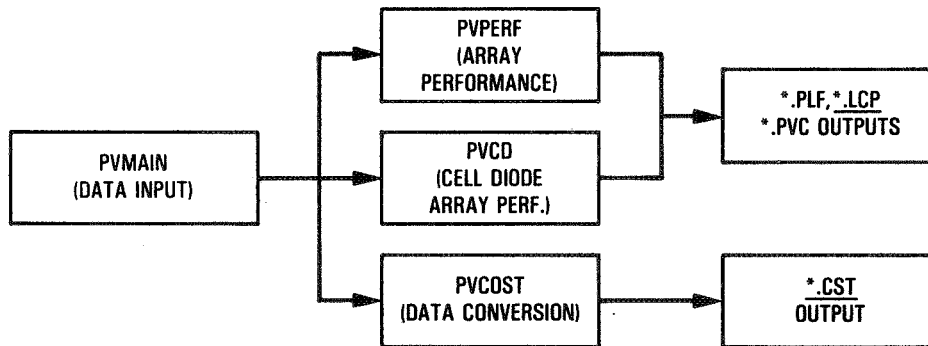
PVARRAY Terminology



PVARRAY Module Configurations



PVARRAY Flow Chart



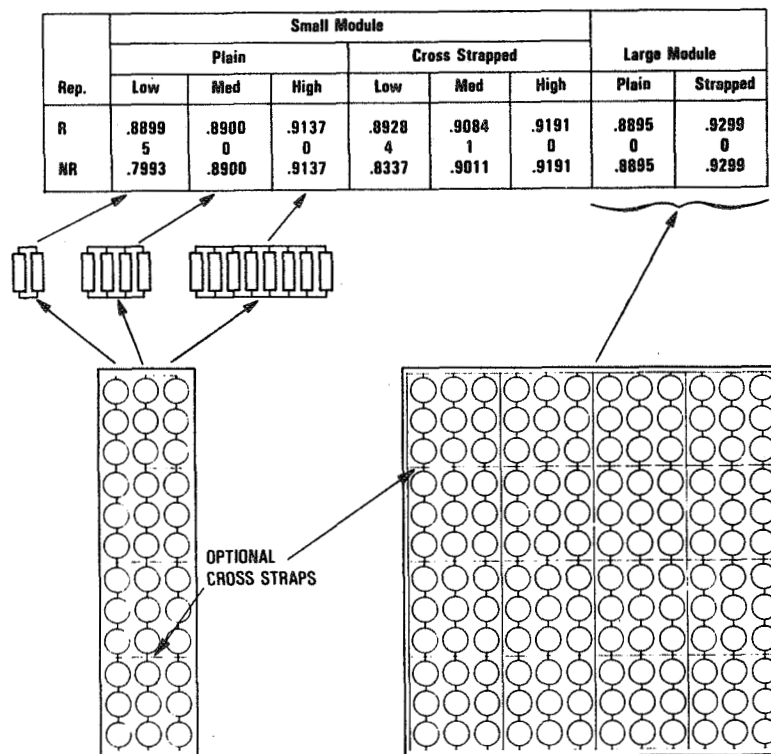
Array Analysis

- Fixed number of cells at 11520
- Fixed random number seed as 2560 which gave large number of early failures
- Ignored certain array design problems
 - Shadowing
 - Hot-spot heating
 - Shorts

Assumptions and Caveats

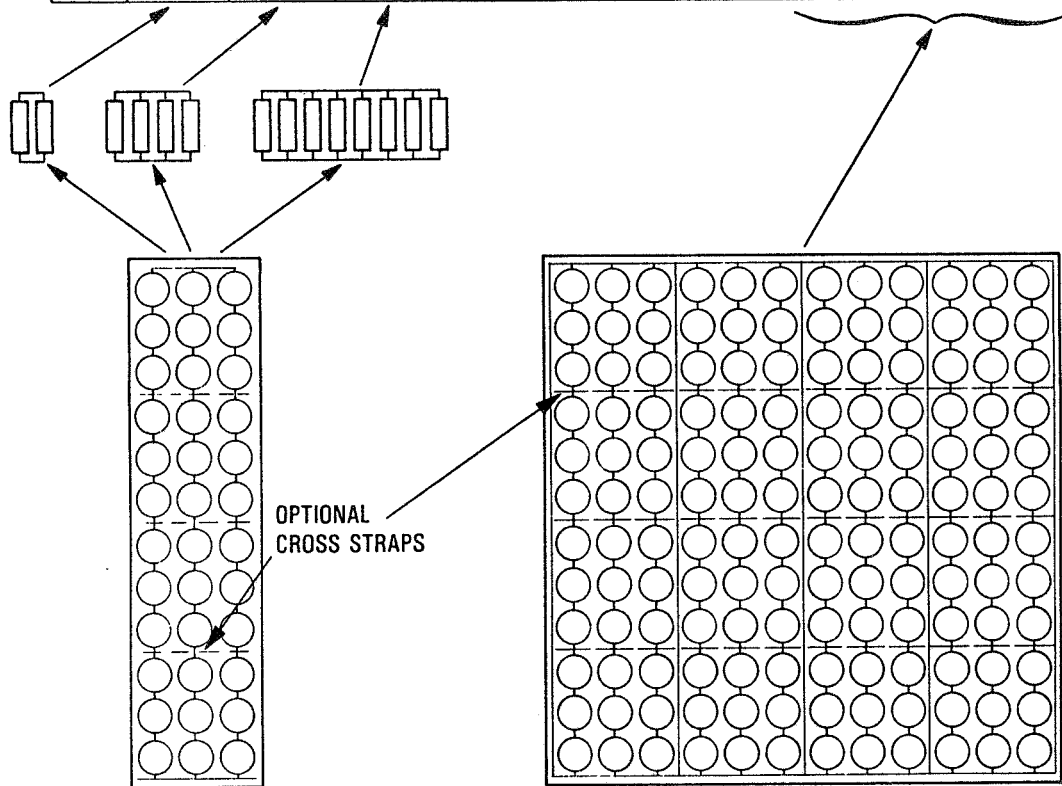
- Parallel redundancy
- Diode placement
- Replacement strategy
- High-efficiency cells

Parallel Redundancy, No Diodes



Parallel Redundancy, Module Diodes

Rep.	Small Module						Large Module	
	Plain			Cross Strapped (4D)			Plain	Strapped (4D)
	Low	Med	High	Low	Med	High		
R	1.000	.8912	.9144	(Note 1)	(Note 1)	(Note 1)	.8915	(Note 1)
NR	34	1	0	.8793	.9071	.9243	1(4)	.9385
NR	.8684	.8900	.9144				.8902	.9385



MODULE DEVELOPMENT AND ENGINEERING SCIENCES

Diode Placement

Diode Location	Rep.	Small Module						Large Module	
		Plain			Cross Strapped			Plain	Strapped
		Low	Med	High	Low	Med	High		
Around Group	R	1.000 34	.8931 2	.9144 0	1.000 34	.9369 4	.9217 0	.9166 4(16)	.9299 0
	NR	.8655	.8900	.9144	.8744	.9011	.9217	.8895	.9299
Around Module	R	1.000 34	.8912 1	.9144 0	(Note 1)	(Note 1)	(Note 1)	.8915 1(4)	(Note 1)
	NR	.8684	.8900	.9144				.8902	
Around Block	R				1.000 34	1.000 34	.9783 17		.9658 3(12)
	NR	(NA)	(NA)	(NA)	.9131	.9361	.9438	(NA)	.9531
Around Cell	R	.9520 0	.9608 0	.9657 0	.9580 0	.9663 0	.9731 0	.9601 0	.9667 0
	NR	.9520	.9608	.9657	.9580	.9663	.9731	.9601	.9667
NO Diode	R	.8899 5	.8900 0	.9137 0	.8928 4	.9084 1	.9191 0	.8895 0	.9299 0
	NR	.7993	.8900	.9137	.8337	.9011	.9191	.8895	.9299

Note 1: Module diode has no effect on cross strapped modules.

Replacement Strategy

Replacement Fraction	Small Module						Large Module	
	Plain			Cross Strapped (4D)			Plain	Strapped (4D)
	Low	Med	High	Low	Med	High		
1.00 D	1.000 34	.8912 1	.9144 0	1.000 34	1.000 34	.9783 34	.9166 4(16)	.9658 3(12)
ND	.8899 5	.8900 0	.9137 0	.8928 4	.9084 1	.9191 0	.8895 0	.9299 0
.98 D	1.000 34	.8931 2	.9144 0	.9928 32	.9917 32	.9783 17	.8915 1(4)	.9658 3(12)
ND	.8899 5	.8900 0	.9144 0	.8928 8	.9084 1	.9191 0	.8895 0	.9299 0
.95 D	.9711 29	.8931 2	.9144 0	.9505 17	.9516 7	.9632 8	.8915 1(4)	.9531 0
ND	.8879 3	.8900 0	.9137 0	.8793 0	.9084 1	.9191 0	.8895 0	.9299 0
.00 D	.8684 0	.8900 0	.9144 0	.8793 0	.9071 0	.9243 0	.8902 0	.9385 0
ND	.7993	.8900	.9137	.8337	.9011	.9191	.8895	.9299

MODULE DEVELOPMENT AND ENGINEERING SCIENCES

Effect of High-Efficiency Cells

Diode Location	Rep.	Low Redundancy		Large Module			
		STD I-V	HEFF I-V	Plain		Cross-Strapped	
				STD	HEFF	STD	HEFF
No Diode	R	.8899 5	.8572 7	.8895 0	.9030 0	.9299 0	.9493 3(12)
	NR	.7993	.7515	.8895	.9030	.9299	.9241
Around Module	R	1.000 34	1.000 34	.8915 1(4)	.9042 1(4)	(NA)	(NA)
	NR	.8684	.8612	.8902	.9031		
Around Block	R	1.000 34	1.000 34	(NA)	(NA)	.9658 3(12)	.9677 23(92)
	NR	.9131	.9094			.9531	.9445
Around Cell	R	.9520 0	.9512 0	.9601 0	.9537 0	.9667 0	.9657 0
	NR	.9520	.9512	.9601	.9537	.9667	.9657

Conclusions

- PVARRAY could simulate a variety of configurations
- Results were consistent with previous parametric study results

DENDRITIC WEB-TYPE SOLAR CELL MINI-MODULES

WESTINGHOUSE ELECTRIC CORP.

R. B. Campbell

Contract Requirements

- PROVIDE TWENTY-FIVE (25) MINI-MODULES COMPOSED OF DENDRITIC WEB SOLAR CELLS
- NOMINAL GLASS SIZE - 12 CM X 40 CM
- MODULES TO BE IDENTICAL WITH RESPECT TO DESIGN, MATERIALS, AND MANUFACTURING AND ASSEMBLY PROCESSES TO FULL SCALE MODULES
- MODULES TO BE ELECTRICALLY FUNCTIONAL

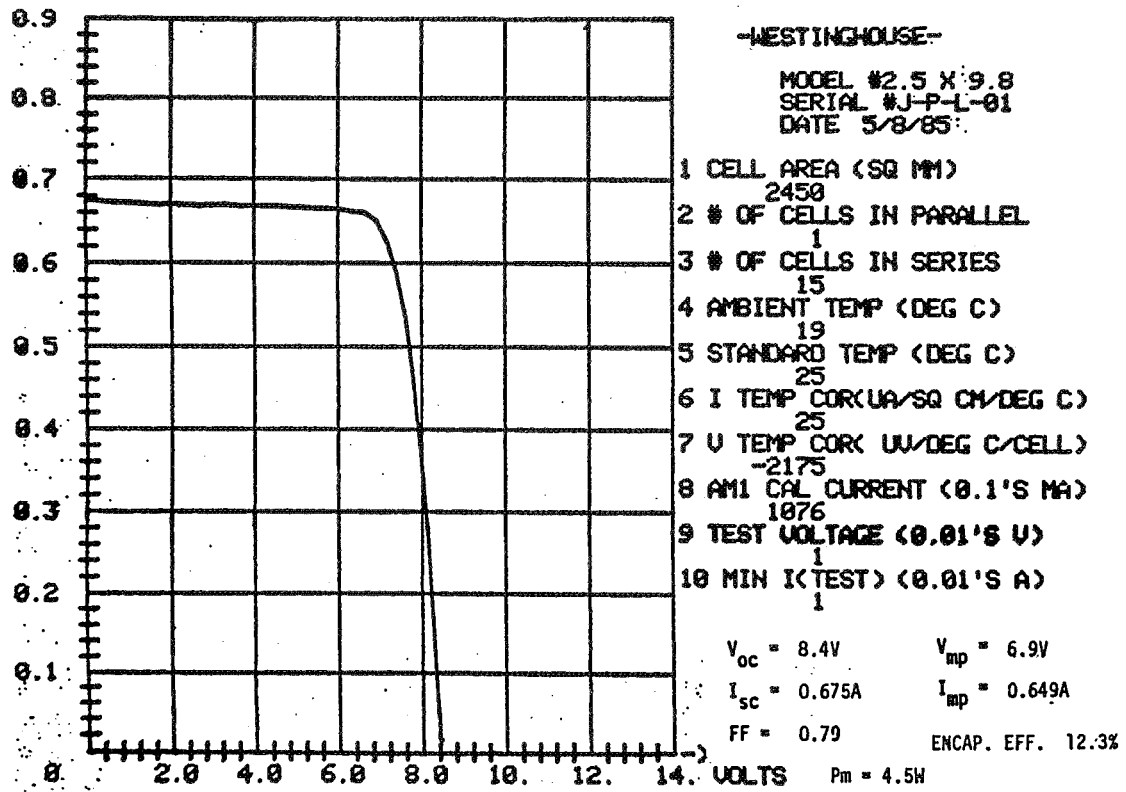
Contract Purpose

- TO PROVIDE TEST VEHICLE FOR ENVIRONMENTAL TESTING
- TO ASSESS RELIABILITY OF PROCESS AND DESIGN

Module Design

- 15 CELLS, EACH 2.5 CM X 9.8 CM; SERIES CONNECTED
- GLASS SIZE - 11.8 CM X 40.8 CM
- MODULE LAYUP: LOW IRON TEMPERED GLASS (1/8" THICK)
CRANE GLASS
EVA
SOLAR CELLS
CRANE GLASS
EVA
TEDLAR (WHITE - 0.002" THICK)
- AMP "SOLARLOK" CONNECTORS

MODULE DEVELOPMENT AND ENGINEERING SCIENCES



Module Performance

- ELECTRICAL OUTPUT - 4.6 WATTS/MODULE (w_p AT $25^{\circ}C$, AM-1, $100 MW/CM^2$)
- ENCAPSULATED EFFICIENCY - 12.3%

ORIGINAL PAGE IS
OF POOR QUALITY

